frontiers | Research Topics

Tunicates in evolutionary developmental biology

Edited by
Paolo Sordino, Lucia Manni, Chiara Anselmi and
Rosa Maria Sepe

Published in
Frontiers in Ecology and Evolution
Frontiers in Cell and Developmental Biology

ISSN 1664-8714
ISBN 978-2-8325-6053-2
DOI 10.3389/978-2-8325-6053-2

About Frontiers

Frontiers is more than just an open access publisher of scholarly articles: it is a pioneering approach to the world of academia, radically improving the way scholarly research is managed. The grand vision of Frontiers is a world where all people have an equal opportunity to seek, share and generate knowledge. Frontiers provides immediate and permanent online open access to all its publications, but this alone is not enough to realize our grand goals.

Frontiers journal series

The Frontiers journal series is a multi-tier and interdisciplinary set of open-access, online journals, promising a paradigm shift from the current review, selection and dissemination processes in academic publishing. All Frontiers journals are driven by researchers for researchers; therefore, they constitute a service to the scholarly community. At the same time, the *Frontiers journal series* operates on a revolutionary invention, the tiered publishing system, initially addressing specific communities of scholars, and gradually climbing up to broader public understanding, thus serving the interests of the lay society, too.

Dedication to quality

Each Frontiers article is a landmark of the highest quality, thanks to genuinely collaborative interactions between authors and review editors, who include some of the world's best academicians. Research must be certified by peers before entering a stream of knowledge that may eventually reach the public - and shape society; therefore, Frontiers only applies the most rigorous and unbiased reviews. Frontiers revolutionizes research publishing by freely delivering the most outstanding research, evaluated with no bias from both the academic and social point of view. By applying the most advanced information technologies, Frontiers is catapulting scholarly publishing into a new generation.

What are Frontiers Research Topics?

Frontiers Research Topics are very popular trademarks of the *Frontiers journals series*: they are collections of at least ten articles, all centered on a particular subject. With their unique mix of varied contributions from Original Research to Review Articles, Frontiers Research Topics unify the most influential researchers, the latest key findings and historical advances in a hot research area.

Find out more on how to host your own Frontiers Research Topic or contribute to one as an author by contacting the Frontiers editorial office: frontiersin.org/about/contact

Tunicates in evolutionary developmental biology

Topic editors

Paolo Sordino — Anton Dohrn Zoological Station Naples, Italy
Lucia Manni — University of Padua, Italy
Chiara Anselmi — Stanford University, United States
Rosa Maria Sepe — Anton Dohrn Zoological Station Naples, Italy

Citation

Sordino, P., Manni, L., Anselmi, C., Sepe, R. M., eds. (2025). *Tunicates in evolutionary developmental biology*. Lausanne: Frontiers Media SA.
doi: 10.3389/978-2-8325-6053-2

Table of contents

frontiers | Frontiers in Ecology and Evolution

TYPE Editorial
PUBLISHED 14 February 2025
DOI 10.3389/fevo.2025.1549081

OPEN ACCESS

EDITED AND REVIEWED BY
Stefano Tiozzo,
UMR7009 Laboratoire de Biologie du Développement de Villefranche sur Mer, France

*CORRESPONDENCE
Paolo Sordino
paolo.sordino@szn.it

RECEIVED 20 December 2024
ACCEPTED 27 January 2025
PUBLISHED 14 February 2025

CITATION
Anselmi C, Sepe RM, Manni L and Sordino P (2025) Editorial: Tunicates in evolutionary developmental biology.
Front. Ecol. Evol. 13:1549081.
doi: 10.3389/fevo.2025.1549081

Editorial: Tunicates in evolutionary developmental biology

Chiara Anselmi[1], Rosa Maria Sepe[2], Lucia Manni[1] and Paolo Sordino[3]*

[1]Department of Biology, University of Padova, Padova, Italy, [2]Department of Biology and Evolution of Marine Organisms, Anton Dohrn Zoological Station, Naples, Italy, [3]Sicily Marine Centre, Anton Dohrn Zoological Station, Messina, Italy

KEYWORDS

sensory inputs, torpor, regeneration, neurotransmitters, lumen formation, oogenesis, asexual reproduction

Editorial on the Research Topic
Tunicates in evolutionary developmental biology

Tunicates, the closest living relatives of vertebrates, offer an extraordinary window into the evolutionary processes that shape animal development (Ferrier, 2011; Johnson et al., 2024; Todorov et al., 2024). These marine invertebrates display remarkably diverse lifestyles (benthic, pelagic, solitary, gregarious, or colonial), life cycles (simple or complex), and development (direct, indirect, sexual, or asexual) (Ricci et al., 2022; Nanglu et al., 2023). This diversity, combined with their genetic similarities to vertebrates, makes tunicates valuable models for understanding how developmental mechanisms contribute to evolutionary novelties (Procaccini et al., 2011; Popsuj et al., 2024).

Recent advancements in tunicate genomics and expression profiling have made it possible to gain a deeper understanding of the molecular underpinnings of tunicate development (Oda and Satou, 2025; Sánchez-Serna et al., 2025). At the same time, there is much we do not yet know about specific research questions within tunicate Evo-Devo, e.g., the evolution of tunicate muscle types or the homology between vertebrate hair cells and tunicate coronal sensory cells. This research is crucial for identifying genes that are conserved between species and those that have diverged, providing insights into the genetic basis of morphological differences across tunicate species or among broader metazoans.

The studies compiled in this Research Topic speak to four major themes, pushing the boundaries of thought at the sub-cellular, cellular, organ, and organism levels. In short, they provide new insights into the molecular networks, cellular behaviors, and developmental processes that underpin the diversification of tunicates and their evolution in the context of chordate development. The Research Topic includes seven publications in *Frontiers in Ecology and Evolution* and four in *Frontiers in Cell and Developmental Biology*. It features a mix of five Original Research articles, one Brief Research Report, four Reviews, and one Perspective article.

The Research Topic showcases original research on a range of tunicate species, including *Ciona robusta*, *Oikopleura dioica*, *Botrylloides leachii*, and *Polyandrocarpa zorritensis*. Together with the tunicate species considered in all 11 publications, they

represent a broad spectrum of developmental biology, from mechanisms of regeneration to the evolution of cellular systems such as stem cells and the immune system. Altogether, these studies deepen our understanding of how morphological and physiological novelties emerge through changes in developmental programs

The Research Topic also dives into the genetic and cellular mechanisms at play in tunicates. Fritzsch and Glover provide a review of the gene networks involved in the development of sensory organs, including the evolution of olfactory receptors, eyes, and hair cells, which are key structures in both tunicates and vertebrates. These studies emphasize the conserved genetic pathways and their divergent roles in the development of sensory organs across chordates.

At the subcellular level, Bi et al. contribute an original research paper that explores the important role of a matrix metalloprotease, Nas15, in the vacuolation in the notochord of ascidians, and the role of tubular organ lumen formation in maintaining hydrostatic pressure, a feature that is conserved across tunicates, amphioxus, and vertebrates. It also serves as a reference for research on human abnormal lumenogenesis diseases. The study by Feng and Thompson focuses on the role of Aurora kinases during oogenesis in *O. dioica*, offering new insights into cell cycle regulation in this emerging model organism. This study highlights how Aurora kinases changed their interaction proteins by independent evolution, leading to a functional separation in spindle and chromosome regulations. Glover et al. further enhance our understanding of calcium signaling in tunicates, highlighting its importance in various developmental processes. What is clear is that, in all questions concerning the universal role of calcium signaling, the small larval size, low cell number, and rapid development of tunicates provide insights of developmental and evolutionary significance.

At the cellular level, Anselmi et al. review two decades of data on mechanoreceptor structures, focusing on the coronal organs of adult tunicates. These organs, located at the base of the oral siphon, detect potentially dangerous particles entering the pharynx, and their sensory cells serve as prime candidates for understanding the evolution of vertebrate hair cells of the inner ear and lateral line organ. Hyams et al. focus on the morphological, cellular, and molecular changes that *B. leachii* hemolymph undergoes under physiological stress in torpor conditions, contributing valuable insights for future studies on hibernation phenomena in other organisms.

At the organ level, Stokes et al. investigate myocardial regeneration in *Ciona* injured hearts, finding gene expression changes that include orthologous genes in vertebrates that are involved in cardiac development and disease processes. Thus, this article provides valuable insights into the conserved molecular mechanisms that facilitate heart tissue repair across chordates.

On a broader organism scale, Nydam et al. examine the evolution of allorecognition in Botryllid ascidians, shedding light on the molecular and ecological mechanisms that govern this process in colonial tunicates. Their research contributes to our understanding of how complex, multi-cellular interactions and immune responses have evolved in these fascinating organisms. Hotta et al. offer a perspective on the evolutionary and developmental biology of organismal transparency in tunicates, particularly in salps, larvaceans, and some ascidian species. The authors propose novel methodologies to evaluate transparency, giving rise to the interdisciplinary field of organismal transparency biology. The review by Pennati et al. highlights serotonin signaling in tunicates, comparing its roles across species and offering a broader evolutionary perspective in chordates. Likely due to events of loss and gain of functions, tunicates exhibit both ancient roles, such as the control of ciliary beating and locomotion coordination, and chordate-specific novelties, such as the modulation of various aspects of intestinal function. Similarly, Tobias-Santos et al. explore how environmental factors such as salinity limit the asexual reproduction of *P. zorritensis*, providing a unique perspective on the evolutionary adaptation of colonial tunicates to varying environmental conditions.

In conclusion, this Research Topic has advanced our understanding of tunicate Evo-Devo, shedding light on some of the molecular, cellular, and developmental processes driving tunicate diversification and evolution in the context of chordate development. Continued exploration of tunicates, alongside new techniques and experimental species (Walters et al., 2019; Daric et al., 2024), promises to deepen our understanding of the relationships between genotype, phenotype, and environment. As we continue to unravel the secrets of tunicate development and evolution, we may gain new insights into fundamental biological processes. We hope this Research Topic serves as a valuable reference and contributes to the evolving field of tunicate Evo-Devo.

Author contributions

CA: Writing – original draft, Writing – review & editing. RS: Writing – original draft, Writing – review & editing. LM: Writing – original draft, Writing – review & editing. PS: Writing – original draft, Writing – review & editing.

Conflict of interest

The authors declare that the research was conducted in the absence of any commercial or financial relationships that could be construed as a potential conflict of interest.

Publisher's note

References

Daric, V., Lanoizelet, M., Mayeur, H., Leblond, C., and Darras, S. (2024). Genomic resources and annotations for a colonial ascidian, the light-bulb sea squirt *Clavelina lepadiformis*. *Genome Biol. Evol.* 16, evae038. doi: 10.1093/gbe/evae038

Ferrier, D. E. (2011). Tunicates push the limits of animal evo-devo. *BMC Biol.* 9, 3. doi: 10.1186/1741-7007-9-3

Johnson, C. J., Zhang, Z., Zhang, H., Shang, R., Piekarz, K. M., Bi, P., et al. (2024). A change in cis-regulatory logic underlying obligate versus facultative muscle multinucleation in chordates. *Development* 151, dev202968. doi: 10.1242/dev.202968

Nanglu, K., Lerosey-Aubril, R., Weaver, J. C., and Ortega-Hernández, J. (2023). Mid-cambrian tunicate and the deep origin of the ascidiacean body plan. *Nat. Commun.* 14, 3832. doi: 10.1038/s41467-023-39012-4

Oda, I., and Satou, Y. (2025). A master regulatory loop that activates genes in a temporally coordinated manner in muscle cells of ascidian embryos. *Development* 152, dev204382. doi: 10.1242/dev.204382

Popsuj, S., Cohen, L., Ward, S., Lewis, A., Yoshida, S., Herrera, R. A., et al. (2024). CRISPR/cas9 protocols for disrupting gene function in the non-vertebrate chordate *Ciona*. *Integr. Comp. Biol.* 64, 1182–1193. doi: 10.1093/icb/icae108

Procaccini, G., Affinito, O., Toscano, F., and Sordino, P. (2011). "A new animal model for merging ecology and evolution," in *Evolutionary Biology – Concepts, Biodiversity, Macroevolution and Genome Evolution*. Ed. P. Pontarotti (Springer, Berlin, Heidelberg, Germany). doi: 10.1007/978-3-642-20763-1_

Ricci, L., Salmon, B., Olivier, C., Andreoni-Pham, R., Chaurasia, A., Alié, A., et al. (2022). The onset of whole-body regeneration in *Botryllus schlosseri*: morphological and molecular characterization. *Front. Cell Dev. Biol.* 10. doi: 10.3389/fcell.2022.843775

Sánchez-Serna, G., Badia-Ramentol, J., Bujosa, P., Ferrández-Roldán, A., Torres-Águila, N. P., Fabregà-Torrus, M., et al. (2025). Less, but more: new insights from appendicularians on chordate fgf evolution and the divergence of tunicate lifestyles. *Mol. Biol. Evol.* 42, msae260. doi: 10.1093/molbev/msae260

Todorov, L. G., Oonuma, K., Kusakabe, T. G., Levine, M. S., and Lemaire, L. A. (2024). Neural crest lineage in the protovertebrate model *Ciona*. *Nature* 635, 912–916. doi: 10.1038/s41586-024-08111-7

Walters, T. L., Gibson, D. M., and Frischer, M. E. (2019). Cultivation of the marine pelagic tunicate *Dolioletta gegenbauri* (Uljanin 1884) for experimental studies. *J. Vis. Exp.* 150, e59832. doi: 10.3791/59832

frontiers | Frontiers in Ecology and Evolution

TYPE Original Research
PUBLISHED 04 December 2023
DOI 10.3389/fevo.2023.1214191

OPEN ACCESS

EDITED BY
Paolo Sordino,
Anton Dohrn Zoological Station Naples, Italy

REVIEWED BY
Tony De Tomaso,
University of California, Santa Barbara, United States
Paul Simion,
University of Namur, Belgium
David Osca,
University of Las Palmas de Gran Canaria, Spain

*CORRESPONDENCE
Marie L. Nydam
mnydam@soka.edu

RECEIVED 11 May 2023
ACCEPTED 09 November 2023
PUBLISHED 04 December 2023

CITATION
Nydam ML, Lemmon AR, Lemmon EM, Ziegler K, Cohen CS, Palomino-Alvarez LA and Gissi C (2023) Phylogenomics and systematics of botryllid ascidians, and implications for the evolution of allorecognition.
Front. Ecol. Evol. 11:1214191.
doi: 10.3389/fevo.2023.1214191

Phylogenomics and systematics of botryllid ascidians, and implications for the evolution of allorecognition

Marie L. Nydam[1]*, Alan R. Lemmon[2], Emily M. Lemmon[3], Kevin Ziegler[3], C. Sarah Cohen[4], Lilian A. Palomino-Alvarez[5,6] and Carmela Gissi[7,8,9]

[1]Life Sciences Concentration, Soka University of America, Aliso Viejo, CA, United States, [2]Department of Scientific Computing, Florida State University, Tallahassee, FL, United States, [3]Department of Biological Science, Florida State University, Tallahassee, FL, United States, [4]Biology Department and Estuary and Ocean Science Center, San Francisco State University, Tiburon, CA, United States, [5]Posgrado en Ciencias del Mar y Limnología, Universidad Nacional Autónoma de México, Ciudad de México, Mexico, [6]Unidad Multidisciplinaria de Docencia e Investigación Sisal (UMDI-Sisal), Facultad de Ciencias Nacional Autónoma de México, Ciudad de México, Mexico, [7]Department of Biosciences, Biotechnologies and Environment, University of Bari "Aldo Moro", Bari, Italy, [8]Institute of Biomembranes, Bioenergetics and Molecular Biotechnologies (IBIOM), Consiglio Nazionale delle Ricerche, Bari, Italy, [9]Consorzio Nazionale Interuniversitario per le Scienze del Mare (CoNISMa), Roma, Italy

Allorecognition, the ability of an organism to distinguish kin from non-kin, or self from non-self, has been studied extensively in a group of invertebrate chordates, the colonial ascidians called botryllids (Subphylum Tunicata, Class Ascidiacea, Family Styelidae). When two conspecific botryllid colonies come in contact, there are two potential outcomes to an allorecognition reaction: fusion or rejection. The rejection outcome of allorecognition varies by species, and has been classified by type (referred to as R-Type). R-Type is defined according to how far the fusion process progresses before the rejection begins, since the rejection reaction appears as an interference of the fusion process. Here, we map the evolution of R-Types onto an extended and robust phylogeny of the botryllids. In this study, we have reconstructed the largest phylogenomic tree of botryllids, including 97 samples and more than 40 different species, and mapped on it nine of the 13 species for which the R-Type is known. Based on the R-Type known in a single outgroup species (*Symplegma reptans*), we infer that at least R-Type B and E-like could be ancestral to the *Botrylloides/Botryllus* group. However, the application of ancestral character state reconstructions does not provide conclusive results since several clades show more than one equiparsimonious R-Type state. Notably, all R-Type A species are clustered together and certainly evolved later than other R-Types. Our phylogenomic tree has been built on 177 nuclear loci and nearly all clades are well supported. Moreover, our phylogenetic analyses also take into account the results of species delimitation analyses based on the mitochondrial COI gene and of careful morphological analyses of the samples. The implementation of this integrated taxonomic approach, combining morphological as well as nuclear and mitochondrial data, has allowed the description of six new species, and the identification of a number of putative unnamed taxa. Thus, our results also demonstrate the existence of an unexplored hidden diversity within botryllids.

KEYWORDS

***Botryllus*, *Botrylloides*, ascidian, allorecognition, histocompatibility, rejection**

Introduction

Allorecognition is the ability of an organism to distinguish kin from non-kin, or self from non-self and is found in all major groups of organisms, from eubacteria to plants (Buss, 1982). It has been studied extensively in a focal group of invertebrate chordates, the colonial ascidians called botryllids (Subphylum Tunicata, Class Ascidiacea, Family Styelidae), also widely used as models in immunobiology, angiogenesis, asexual reproduction and whole body regeneration (Lauzon et al., 2013; Voskoboynik and Weissman, 2015; Blanchoud et al., 2018; Ballarin et al., 2021; Nourizadeh et al., 2021). When two conspecific botryllid colonies come in contact, there are two potential outcomes to an allorecognition reaction: fusion or rejection (the overall phenomenon is called "colony specificity"). In fusion, colonies that share alleles at allorecognition loci physically merge (Saito et al., 1994). In rejection, colonies that do not share these allorecognition alleles undergo cytotoxic reactions and erect borders to prevent further interaction (Saito et al., 1994). In botryllid colonies, zooids (single animals genetically identical to all other zooids in the colony) are covered with a common tunic and are connected to the other zooids by a ramified vascular network (De Tomaso et al., 2005). At the colony edge, the terminals of the vascular vessels form several vascular ampullae (De Tomaso et al., 2005). Fusion and rejection processes mainly involve the ampullae and the tunic covering them, including blood within the ampullae (De Tomaso et al., 2005). Across botryllids, the fusion process is very similar and occurs through five stages, but the rejection processes vary between species (Saito et al., 1994 and references therein). According to Figure 7 of Saito et al. (1994), five types of rejection (R-Type A, R-Type B, R-Type C, R-Type D, and R-Type E) can be recognized: they are classified by how far the fusion process progresses before the rejection begins, since the rejection reaction appears as an interference of the fusion process. A scheme depicting the five R-Types, redrawn from Figure 7 of Saito et al. (1994), is shown in Figure 1.

R-Type A rejection occurs at the first stage of fusion (Saito et al., 1994). In this type of rejection, the outer surface of the animal's body (the tunic) is the site of rejection: fusion of the tunics of the two colonies occurs first, and only at limited points of contact, and the ampullae do not fuse. Then, cytotoxic reactions occur within the tunic between blood cells of the opposing colonies (Saito, 2003). In the final phase of the rejection reaction, a new border composed of a thin, fibrous material is formed between the opposing colonies. R-Type B rejection also occurs at the first stage of fusion, but in its final phase the blood cells become black and necrotic, and are visible without a microscope. R-Type C rejection occurs at the second stage of fusion: as in R-Type A and B, tunic fusion only occurs in small areas around ampullar tips. After blood cells infiltrate around the tips of the penetrating ampullae, these ampullae begin to shrink and withdraw or are amputated. R-Type D rejection occurs during the third stage of fusion, and complete fusion of the outer tunic occurs first. Then, we see penetration of one colony's ampullae into the opposing colony's tunic (but, without fusion between opposing colonies' ampullae). Just like in R-Types A–C, then cytotoxic reactions occur within the tunic between blood cells of the opposing colonies. When the colonies reject, a dark necrotic reaction is observed around the interacting vessels and cells. Vessels are then pinched off and abandoned in a necrotic area that is demarcated by a thick fibrous barrier between the two colonies. This barrier between colonies is not seen in R-Type C rejections. R-Type E is at the most extreme end of the behavioral spectrum of botryllid allorecognition: it consists of the complete membrane fusion of the circulatory systems of opposing colonies and subsequent exchange of blood cells between the two colonies. Cells in the blood interact between the two colonies and these interacting cells turn dark and lyse. Parts of the shared circulatory system and tunic area become necrotic and the two colonies both shrink away from the zone of interaction. Fused circulatory elements may be pinched off from the parent colony and left to degenerate in a necrotic zone (Saito et al., 1994).

The R-Type has been characterized only in some botryllids and current knowledge shows that it is species-specific (Saito et al., 1994; Hirose et al., 2002; Saito, 2003) (Table 1). As an exception to this species-specificity, *Botryllus schlosseri* populations from California, USA, show R-Type B rejection (Saito et al., 1994), as do populations from Venice, Italy (Sabbadin et al., 1992), whereas *B. schlosseri* populations from Massachusetts, USA, show R-Type C rejection (Saito et al., 1994). However, this exception is very probably only ostensible and related to the species-complex status of *B. schlosseri*, discovered and partially solved (Lopez-Legentil et al., 2006; Bock et al., 2012; Yund et al., 2015; Nydam et al., 2017a; Brunetti et al., 2020; Salonna et al., 2021) only after Saito's study on the *B. schlosseri* rejection process. The species-specificity of the R-type suggests that the pathways, gene expression or gene regulatory mechanisms involved in the rejection process are at least partially different between the different botryllids. Therefore, these R-types should be placed in a phylogenetic context, in order to understand the evolution of allorecognition in botryllids. An 18S rDNA (Cohen et al., 1998) and a mitochondrial cytochrome oxidase COI (mtCOI) (Salonna et al., 2021) botryllid phylogeny provide a first foundation to solve this issue. In particular, Cohen et al.'s mapped the allorecognition behavioral variation on an 18S rDNA tree comprising nine botryllids, and found R-Type E species at the base of the botryllid tree, with R-Type D species evolving next, and R-Type A species evolving most recently (Figure 2A, summarizing the results of Figure 3 of Cohen et al., 1998). Thus, Cohen et al. (1998) inferred that more derived species evolved more external allorecognition responses and that the R-Type E, i.e., the most internal form of allorecognition, was the ancestral condition. Their hypothesis does not strictly follow the parsimony criterion and was not made applying a specific "ancestral state reconstruction" analysis, however Cohen et al. underlined that the identification of internal allorecognition as the ancestral state is compatible with observations on the allogeneic blood reactions in solitary ascidians. In Cohen et al.'s tree, the phylogenetic relationship between R-Type E and the other R-Types is supported with a 80% bootstrap confidence value in the Maximum Likelihood tree (Figure 2A), but only with a 60% bootstrap confidence value in the Maximum Parsimony tree (see Cohen et al., 1998, Figure 2). If we map the R-type on the Salonna's mtCOI tree, an R-Type E species is again found to be an early diverging lineage (Figure 2B), evolving just

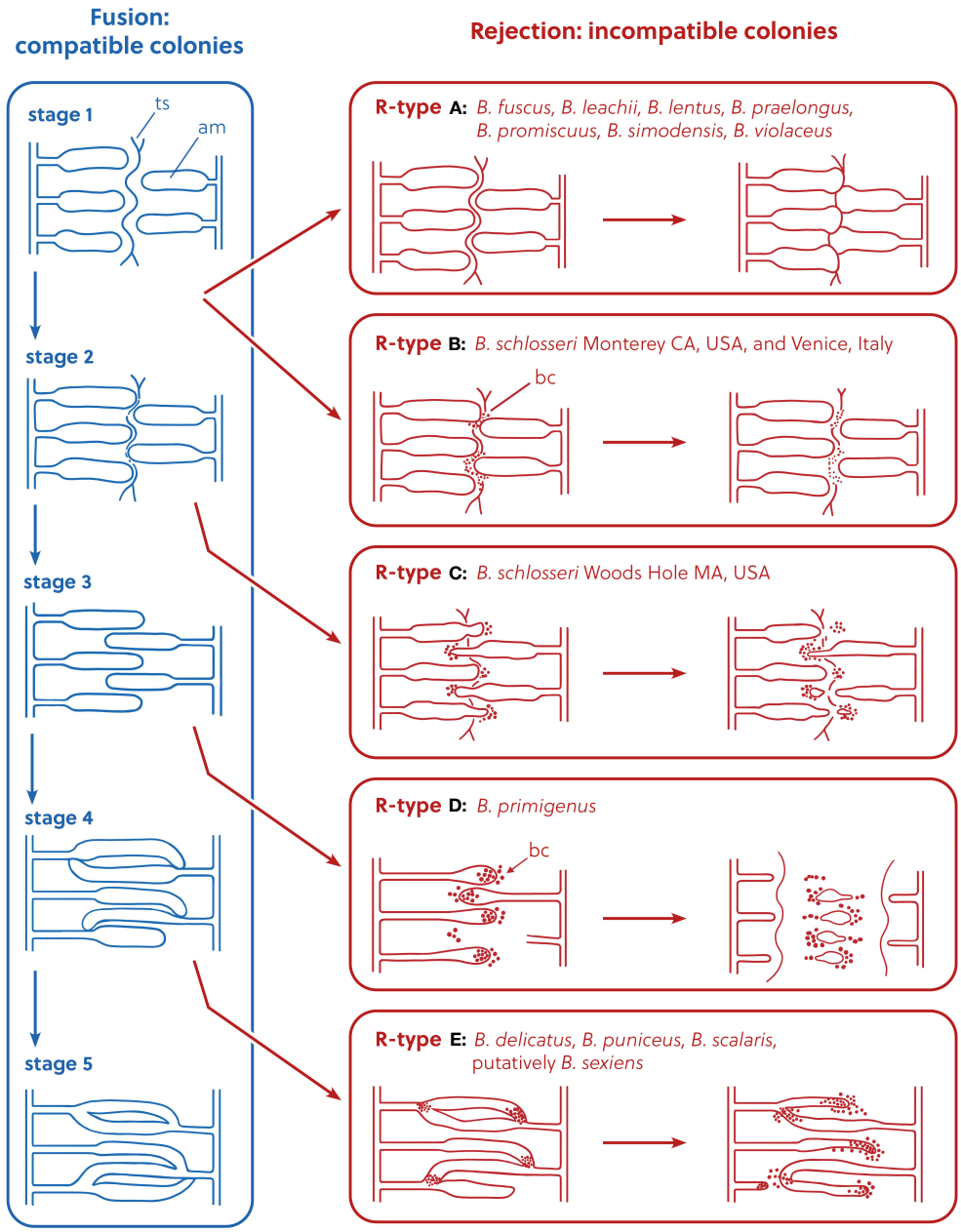

FIGURE 1
Representation of the allorejection process, R-Types A–E, redrawn and modified from Saito et al. (1994), Figure 7. In the rejection panels, the diagram is not intended to show the exact position of the ampullae, but to describe their relative position compared to the stage of origin in the fusion process. ts, tunic surface; am, ampulla; bc, blood cell.

after the node of *Botrylloides conchyliatus* (Salonna et al., 2021) for which there is no allorecognition information. However, the position of this R-Type E species is not well-supported. In general, most nodes of this mtCOI tree remain unresolved. Indeed, even the clade including R-Type A and R-Type D species is not well-supported (Figure 2B). Only R-Type B and C, so far characterized only in the *B. schlosseri* species complex (Table 1), are in a well-supported clade with no other rejection types (Figure 2B).

In this study we have reconstructed the botryllid phylogeny using 177 Anchored Hybrid Enrichment (AHE) nuclear loci selected among the 200 nuclear probes developed in Nydam et al. (2021), in order to resolve the deepest unresolved nodes present in the single-locus botryllid phylogenies based on 18S rRNA and mtCOI. The obtained phylogeny has 97 specimens and includes: 21 samples specifically collected for this study; most of the specimens analyzed in Salonna et al. (2021) and in Palomino-Alvarez et al. (2022); as well as the entire sample dataset of Nydam et al. (2021). Therefore, it represents the largest known botryllid diversity. Since our phylogeny contains nine of the 13 species that have been characterized for rejection type, it is also particularly appropriate for reconstructing the evolutionary history of the allorecognition reaction in botryllids.

TABLE 1 Rejection (R) types of botryllid species from the literature.

Species	Rejection (R) type	Reference for rejection
Botrylloides fuscus	A	Hirose et al., 1988
Botrylloides leachii	A	Zaniolo and Ballarin, 2001; Zaniolo et al., 2006
Botrylloides lentus	A	Okuyama et al., 2002
Botrylloides praelongus	A	Atsumi and Saito, 2011
Botrylloides simodensis	A	Hirose et al., 1990
Botrylloides violaceus	A	Hirose et al., 1988
Botryllus promiscuus	A	Okuyama and Saito, 2002
Botryllus schlosseri from Monterey, California	B	Scofield and Nagashima, 1983; Boyd et al., 1990
Botryllus schlosseri from Venice, Italy	B	Sabbadin et al., 1992
Botryllus schlosseri from Woods Hole, Massachusetts	C	Boyd et al., 1990
Botryllus primigenus	D	Tanaka and Watanabe, 1973
Botryllus delicatus	E	Okuyama and Saito, 2001
Botryllus puniceus	E	Saito and Nagasawa, 2003
Botrylloides scalaris (former *Botryllus scalaris*)*	E	Saito and Watanabe, 1982
Botrylloides sexiens (former *Botryllus sexiens*)*	*Putative* E	Cohen et al., 1998

*: these species have been originally described as belonging to the genus *Botryllus*, but according to the definition of the *Botryllus* and *Botrylloides* genera of Brunetti (2009), they should both be reassigned to the genus *Botrylloides* (see Results and Discussion).

Materials and methods

Sample collection

A total of 21 botryllid samples were collected for this study and analyzed together with 46 samples published in Nydam et al. (2021), 18 samples published in Salonna et al. (2021) and 12 samples published in Palomino-Alvarez et al. (2022). All these samples (total of 97) were used to build the phylogenomic trees described below and they are listed in Supplementary Table 1, together with collection information and the related mtCOI Accession numbers. Photographs and morphological details of the samples that were collected as part of the current study are in Supplementary File 1.

For the 21 new samples, a small piece of colony was removed from each sample in the field, cleaned to remove algae and other contaminants, and preserved in 95% ethanol, RNAlater (ThermoFisher), or a DMSO solution saturated with NaCl. For the species that were morphologically described, a fragment of the colony was also relaxed using menthol crystals and subsequently preserved in 10% formalin in salt water buffered with sodium borate.

Sample identification: DNA barcoding

For 16 of the 21 new samples, we sequenced the mtCOI gene for molecular barcoding purposes. Accession numbers for these 16 sequences are denoted in Supplementary Table 1, with an asterisk. DNA was extracted using the Nucleospin Tissue Kit (Macherey Nagel). PCR was performed using either OneTaq DNA Polymerase (New England Biolabs) or Phusion High-Fidelity DNA Polymerase (New England Biolabs). OneTaq reactions comprised the following ingredients: 25 µl total reaction volume with 16.38 µl of nuclease-free water (New England Biolabs), 5 µl of 5X buffer (New England Biolabs), 0.5 µl of 10 mM dNTPs, 0.5 µl of 10 µM of each primer, 0.12 µl of OneTaq and 2 µl of DNA template (100–500 ng). Phusion reactions were as follows: 20 µl total reaction volume with 10.8 µl of nuclease-free water (New England Biolabs), 4 µl of 5X HF buffer (New England Biolabs), 0.4 µl of 10 mM dNTPs, 0.6 µl of 100% DMSO, 1 µl of 10 µM of each primer, 0.2 µl of Phusion and 2 µl of DNA template (100–500 ng).

Each DNA sample was amplified with one of the following PCR primer pairs: LCO1490/HCO2198 (Folmer et al., 1994) or Tun_forward/Tun_reverse2 (Stefaniak et al., 2009). "Tun" primers were only used with OneTaq polymerase, following this protocol: 94°C for 1 min, 60x (94°C for 10 sec, 50°C for 30 sec, 72°C for 50 sec), 72°C for 10 min. Folmer's primers were only used with Phusion polymerase, following this protocol: 98°C for 30 sec, 35x (98°C for 10 sec, 48°C for 30 sec, 72°C for 30 sec), 72°C for 5 min. Supplementary Table 1 reports the primer pair used for each sample first published in this study.

PCR products were purified through incubation with 1 µl each of Exonuclease I (New England Biolabs) and Antarctic Phosphatase (New England Biolabs) at 37°C for 1 hour, followed by 90°C for 10 min. All PCR products were Sanger sequenced in both directions at Eurofins Genomics (Louisville, KY) using industry standard protocols. Forward and reverse sequences were edited and combined into a consensus sequence using Codon Code Aligner (Codon Code Corporation). Consensus sequences are available on GenBank (Accession Numbers are listed in Supplementary Table 1).

Sample identification: morphological techniques

A formalin-preserved portion was saved for 10 of the 21 botryllid samples specifically collected for this study and used for morphological studies (see column "Morphology" in Supplementary Table 1). These samples were assigned to species using descriptions from the literature (Oka, 1928; Saito et al., 1981a; Saito et al., 1981b; Saito and Watanabe, 1985; Okuyama and Saito, 2001; Saito and Okuyama, 2003; Atsumi and Saito, 2011). A total of 31 morphological characters were analyzed and are summarized as follows: arrangement of systems, position of ovaries and testes, testes morphology, number of stigmatal rows, completeness of the second stigmatal row, arrangement of stigmata, shape of intestine, location of anterior edge of intestinal loop, location of anus, number of stomach folds, appearance of the stomach folds, shape of the

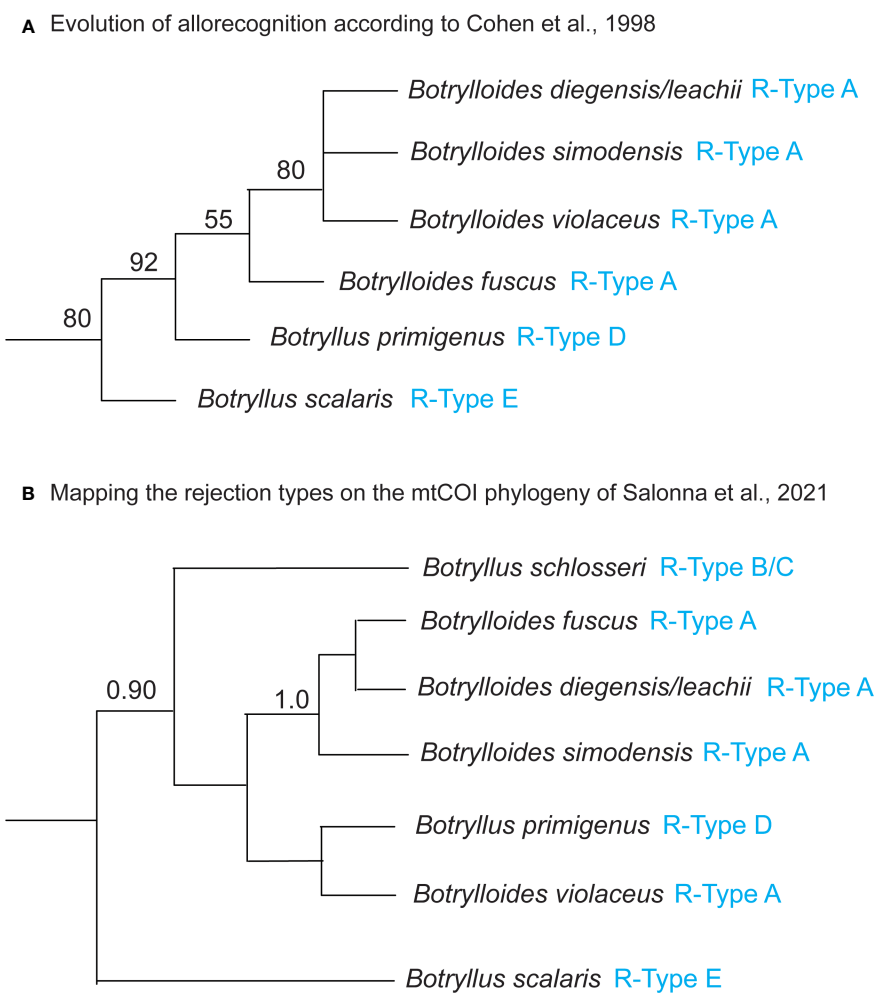

FIGURE 2
(A) Evolution of allorecognition in botryllids according to Cohen et al. (1998). 18S rDNA Maximum Likelihood tree with bootstrap percentage values at the nodes, reproduced from Cohen et al. (1998) Figure 3 and including only species for which the R-type is known. **(B)** Mapping the rejection types on the mtCOI phylogenetic tree of Salonna et al. (2021). Mitochondrial COI Bayesian majority rule consensus tree reconstructed from the "Elongated-856nt" alignment, reproduced from Salonna et al. (2021) Figure 2 and including only species for which the R-type is known. Bayesian posterior probabilities at the nodes are only represented if they are ≥ 0.90. R-types (from Table 1) are indicated in blue. *Botrylloides diegensis/leachii*: based on Viard et al. (2019), all published mtCOI sequences of *Botrylloides leachii* should actually belong to *Botrylloides diegensis*. Waiting for confirmation by more detailed morphological analyses, here we labeled the 18S rDNA and the mtCOI sequences as *Botrylloides diegensis/leachii*. See discussion in the section "Mapping mtCOI Species Delimitation on the Phylogenomic Tree".

stomach, shape and size of the pyloric caecum, number and size orders of the oral tentacles, distribution of pigment cells in the zooid, zooid length, colony color when living and after fixation, and tunic thickness (Saito and Watanabe, 1985; Saito and Okuyama, 2003; Brunetti, 2009). New described species were assigned to the genus *Botryllus* or *Botrylloides* according to the Brunetti's definition of these genera (Brunetti, 2009).

Species delimitation

To determine where botryllid species boundaries lie, species delimitation analyses were conducted on a dataset including:

- 73 of the 77 mtCOI sequences listed in Supplementary Table 1 (the four mtCOI sequences reported with a tilde sign (~) in Supplementary Table 1 were excluded because they were too short to include in the alignment);
- 175 additional mtCOI sequences belonging primarily to the taxa represented in the phylogenetic tree but also to eight additional botryllid species and to five *Symplegma* species (see species with an asterisk in Supplementary Table 2 Column E).

Symplegma (Family Styelidae, Subfamily Polyzoinae) was used as an outgroup since previous morphological and molecular data have identified this genus as sister to botryllids (Berrill, 1950; Ben-Shlomo et al., 2010).

Thus, the whole analyzed mtCOI dataset comprises 248 sequences that were either generated as part of the current study or previously published in Palomino-Alvarez et al. (2022) or Salonna et al. (2021). Supplementary Table 2 reports the results

of the species delimitation analyses, and includes also the GenBank Accession Numbers of the 248 analyzed sequences with the relevant publication information. A 467 bp alignment of 247 mtCOI sequences was created by the Muscle alignment algorithm in CodonCode Aligner v. 10 (CodonCode Corporation, Centerville, MA). This alignment was analyzed using two single-locus methods for species delimitation: ASAP (Puillandre et al., 2021) and bPTP (Zhang et al., 2013). ASAP (Assemble Species by Automatic Partitioning) uses pairwise genetic distances to partition putative species (named OTUs, Operational Taxonomic Unit) by identifying gaps between larger distances (presumed interspecific) and smaller distances (presumed intraspecific) (Puillandre et al., 2021). ASAP builds on the earlier program ABGD (Automatic Barcode Gap Discovery) (Puillandre et al., 2012) by removing the *a priori* defined maximum genetic intraspecific divergence (P) and ranking the partitions (Puillandre et al., 2021). bPTP (Bayesian Poisson Tree Process) is derived from PTP, which analyzes a user-inputed phylogenetic tree to identify regions of the tree that are transition points between branching rates consistent with a speciation model and those consistent with a coalescent model (Zhang et al., 2013). bPTP adds Bayesian support values to the putative species nodes (Zhang et al., 2013). The OTU partitions between ASAP and bPTP can differ (Ducasse et al., 2020), so we employed both methods.

We ran ASAP using all three available substitution models: p-distances, Jukes-Cantor, and Kimura 2P. The analysis was performed using ASAP web server: https://bioinfo.mnhn.fr/abi/public/asap/asapweb.html. A Maximum Likelihood (ML) tree was generated from the same 467 bp alignment of 248 sequences using RAxML HPC BlackBox (Stamatakis, 2014) on CIPRES (Cyberinfrastructure for Phylogenic Research) Science Gateway v. 3.3 (Miller et al., 2010). This ML tree was analyzed with bPTP using the web server: http://species.h-its.org/, and results from both Maximum Likelihood and Bayesian-derived partitions were obtained.

We considered a clade to be a species if at least two of the three analyses (ASAP, bPTP-ML and bPTP-Bayesian) agreed to recover that clade as a single OTU. ASAP and bPTP use different conceptual and algorithmic frameworks, and bPTP-ML and BPTP-Bayesian use different trees. We decided to use results that were supported by at least two of the three methods, as we believe that these results would be more robust than results supported by only one method.

Phylogenomic tree building

DNA extraction, library preparation, anchored hybrid enrichment (AHE), library sequencing, and raw read alignment methods were conducted on 51 samples (i.e., all samples of Supplementary Table 1 not previously published in Nydam et al., 2021) as described in Nydam et al. (2021) aside from three minor changes. All three changes are modifications of parameter values used in the automated procedure described in Hamilton et al. (2016). The changes are outlined below: first, during raw read alignment, consensus sequences were constructed from assembly clusters containing greater than an average of 37 reads (previously-used value: 250). Second, during masking, a 10-base threshold was used for masking misaligned regions (previously-used value: 14). Lastly, during trimming, 49 sequences were required to be present at a site to prevent removal of the site (previously-used value: 25). Only 177 loci were recovered after quality control and filtering. The size of these loci and the correspondence to the AHE nuclear probes and loci used in Nydam et al. (2021) is reported in Supplementary Table 3.

Phylogenomic trees were built on the whole dataset of 97 samples using two different methods. First, using RAxML v. 8.2.12 (Randomized Axelerated Maximum Likelihood) a species tree was estimated based on the sequence data from all loci concatenated together. Although concatenated, alpha-shape parameters, GTR rates, and empirical base frequencies were estimated separately for each "locus" using the -q option in RAxML; GTR Gamma was specified as the model of nucleotide substitution. Bootstrap support values for the best scoring ML tree were calculated from 100 rapid bootstrap replicates. Second, an unrooted species tree was estimated using a coalescent summary method, ASTRAL-II v.5.7.8 (Accurate Species TRee ALgorithm). Individual single-locus trees provided as input into the ASTRAL analysis were constructed in RAxML with 100 rapid bootstrap replicates using the GTR Gamma model of nucleotide substitution. The support values on the ASTRAL tree are automatically generated from quartet frequencies; the authors of ASTRAL recommend using these values instead of bootstrapping. *Symplegma* sp. was forced as an outgroup in both the concatenated RAxML tree and the ASTRAL tree. Additional details of these methods are available in Nydam et al. (2021).

Ancestral state reconstructions

Ancestral character state reconstructions in a parsimony framework were conducted in Mesquite v. 3.8.1 using the RAxML phylogenomic tree as described above (Maddison and Maddison, 2023). The single character "R-Type" was traced across the phylogeny, with the five possible character states being "R-Type A", "R-Type B", "R-Type C", "R-Type D", and "R-Type E". The R-type of the outgroup *Symplegma* sp. can be either similar phenotypically to R-Type B or to R-Type E, although it is not known whether the molecular or mechanistic bases of these types are similar. We therefore ran three analyses: one with *Symplegma* sp. coded as unknown, one with *Symplegma* sp. coded as R-Type B, and one with *Symplegma* sp. coded as R-Type E. When *Symplegma* sp. received an "R-Type", then 26 (26.8%) of the 97 specimens in the analysis received an "R-Type", and 71 were classified as unknown. When *Symplegma* sp. did not receive an "R-Type", then 24 (24.7%) of the 97 specimens in the analysis received an "R-Type" and 73 were classified as unknown. *Botryllus sexiens* is classified in the literature as "putatively" R-Type E, and in this analysis it was coded as R-Type E.

Results and discussion

Sample identification reveals a hidden botryllid diversity

A total of 21 samples were specifically collected for this study in several localities around the world, from Japan to America and Australia (Supplementary Table 1). According to an integrated taxonomy approach, their taxonomic identification was based on morphological examinations and/or mtCOI barcoding followed by species delimitation analyses. Morphological descriptions for each of these samples are in Supplementary File 2, where they are discussed together with the results of the species delimitation analyses. The overall results of species delimitation analyses are summarized with blue circles/rectangles in Figure 3 and shown in detail in Supplementary Table 2 (see also the section "Mapping Species Delimitation on the Phylogenomic Tree").

The specimens from Japan belong to five already-described species (i.e., *Botrylloides lenis, Botrylloides lentus, Botrylloides simodensis, Botryllus scalaris* and *Botryllus sexiens*) and to two new species described here for the first time: *Botrylloides saitoi* n. sp. and *Botryllus watanabei* n. sp.

No formalin-preserved fraction was available for the four new specimens from Heron Island, Australia (*Botrylloides* sp. Aust 7, *Botrylloides* sp. Aust 8, *Botrylloides* sp. Aust 10 and *Botrylloides* sp. Aust 14), and for a specimen from Florida (*Botryllus* sp. Crandon Park Marina, Key Biscayne, FL, USA). Moreover, a mtCOI sequence with a length suitable for species delimitation analyses was obtained only for *Botrylloides* sp. Aust 7 (Supplementary Tables 1 and 2). Thus, these specimens were tentatively identified based on their positions in the phylogenomic trees (Figure 3 and Supplementary File 5):

- *Botrylloides* sp. Aust 7 and *Botrylloides* sp. Aust 8 samples are in the same clade as *Botrylloides leptum* (inside Clade "m") with very little nuclear genetic divergence within this clade, as shown by the very short branches. Although the mtCOI sequence of *Botrylloides* sp. Aust 7 is 98.3% identical to *Botrylloides leptum* and is included in the same OTU of *Botrylloides leptum* by all species delimitation analyses (blue circle in Figure 3 and Supplementary Table 2), conclusive identification will require the comparison of formalin-preserved samples of both the Heron Island species and of *Botrylloides leptum.*
- *Botrylloides* sp. Aust 10 is in the same clade as *Botrylloides conchyliatus* (inside Clade "g") with very little nuclear genetic divergence between the two taxa, so this specimen was assigned to the *Botrylloides* genus (see section: "Phylogenomic tree and the *Botryllus*-only Clade "a""). Confirmation of the taxonomic assignment of this sample awaits a mtCOI barcode sequencing and morphological examination.
- *Botrylloides* sp. Aust 14 clusters together with Australian *Botrylloides* sp. SY24 (inside Clade "l") with little nuclear genetic divergence shown. The lack of formalin-preserved samples for both samples (Supplementary Table 1; Nydam et al., 2021) and of the mtCOI sequence from *Botrylloides* sp. Aust 14 (Supplementary Table 1) prevents a well-defined taxonomic attribution and requires further study.
- *Botryllus* sp. from Crandon Park Marina (Key Biscayne, FL, USA) in a clade including only *Botryllus* species (inside Clade "p" of Figure 3), so it was tentatively assigned to the genus *Botryllus* (hereafter named "*Botryllus* Crandon Park"; one sample). The lack of a formalin-preserved sample and a mtCOI sequence too short for species delimitation analyses means that further study is required for a more reliable taxonomic attribution.

Two distinct new taxa were identified by species delimitation analyses as "unnamed species" since they did not group to mtCOIs associated with a given species. Moreover, they could not be assigned to an already known species, nor described as a new species, because formalin-preserved samples were not available. This is the case for *Botrylloides* sp. SHJ-20.1 from Shikine Island, Izu Islands, Japan (hereafter named "*Botrylloides* SHJ20.1"; one sample; inside Clade "n" and with a blue circle in Figure 3), and the species hereafter named "*Botrylloides* sp. (Atsumi and Saito, 2011)" (two samples; inside Clade "m" and with a blue circle in Figure 3). Although this last species was not formally described in Atsumi and Saito (2011), it was reported in that study as morphologically very similar to *Botrylloides simodensis* and genetically distinguishable using the mitochondrial cytochrome b (cytb) gene (see Supplementary File 2 for our analyses on cytb).

As for *Botryllus* sp. SHJ 5.1 (from Shikine Island, Izu Islands, Japan; in Clade "p" of Figure 3), a formalin-preserved sample was available but the lack of clear diagnostic characters and of the mtCOI sequence necessary to carry out species delimitation analyses led to the assignment of this sample only at genus level (see details in Supplementary File 2).

Updated plates (Supplementary File 3) and morphological descriptions (Supplementary File 4) for four other taxa, originally reported in Nydam et al. (2021) as *Botrylloides* sp. and *Botryllus* sp., allowed their description as new species, named here as:

- *Botrylloides nigerflavus* n. sp. from Panama,
- *Botrylloides frankovichi* n. sp. from Florida and the Bahamas,
- *Botrylloides marikabani* n. sp. from Marikaban Island in the Philippines, and
- *Botryllus bayanani* n. sp. from Catalagan, Marikaban Island, and Puerto Galera in the Philippines.

Species delimitation analyses also support these morphological results (Supplementary Table 2 and blue circle in Figure 3), with the single exception of *Botrylloides marikabani* n. sp., for which the availability of only two mtCOI sequences (Supplementary Tables 1 and 2) could have hindered its identification as a single new species. Indeed, two distinct OTUs were identified in *Botrylloides marikabani* by the mtCOI species delimitation analyses (see also the presence of a blue rectangle in Figure 3).

Botrylloides jacksonianum and *Botrylloides leptum* (inside Clade "o" and "l" of Figure 3, respectively), were already identified as distinct species in the mtCOI botryllid phylogeny of Salonna et al. (2021), but are currently unaccepted as valid species according to the Ascidiacea World Database (Shenkar et al., 2022). Indeed, they were both originally described by Herdman (as *Sarcobotrylloides jacksonianum* and *Botrylloides leptum*) (Herdman, 1891; Herdman, 1899), but were then synonymized with *Botrylloides leachii* (Kott, 1985; Kott, 2005; Shenkar et al., 2022). The mtCOI species delimitation analyses and the phylogenomic trees presented here (Figure 3 and Supplementary File 5) provide further evidence that *Botrylloides jacksonianum* and *Botrylloides leptum* are distinct species, both different from *B. leachii*, and that these Herdman's species should be resurrected, as previously proposed by Salonna et al. (2021).

The *Botrylloides* cf. *pannosum* sample (inside Clade "o"), similar to the original description of *Botrylloides pannosum* (Herdman, 1899), was also here identified as a distinct species by the species delimitation analyses (Supplementary Table 2 and blue circle in Figure 3) but must be compared to Herdman's type specimen of *Botrylloides pannosum* (originally *Sarcobotrylloides pannosum*) to make an unambiguous taxonomic identification (as proposed in Salonna et al., 2021). If *Botrylloides* cf. *pannosum* is indeed *Botrylloides pannosum*, then *Botrylloides pannosum* should also be resurrected since, like *Botrylloides jacksonianum* and *Botrylloides leptum*, even *Botrylloides pannosum* was synonymized with *Botrylloides leachii* (Shenkar et al., 2022). The necessary work to resurrect this additional Herdman's species is ongoing (M. Ekins, unpublished data).

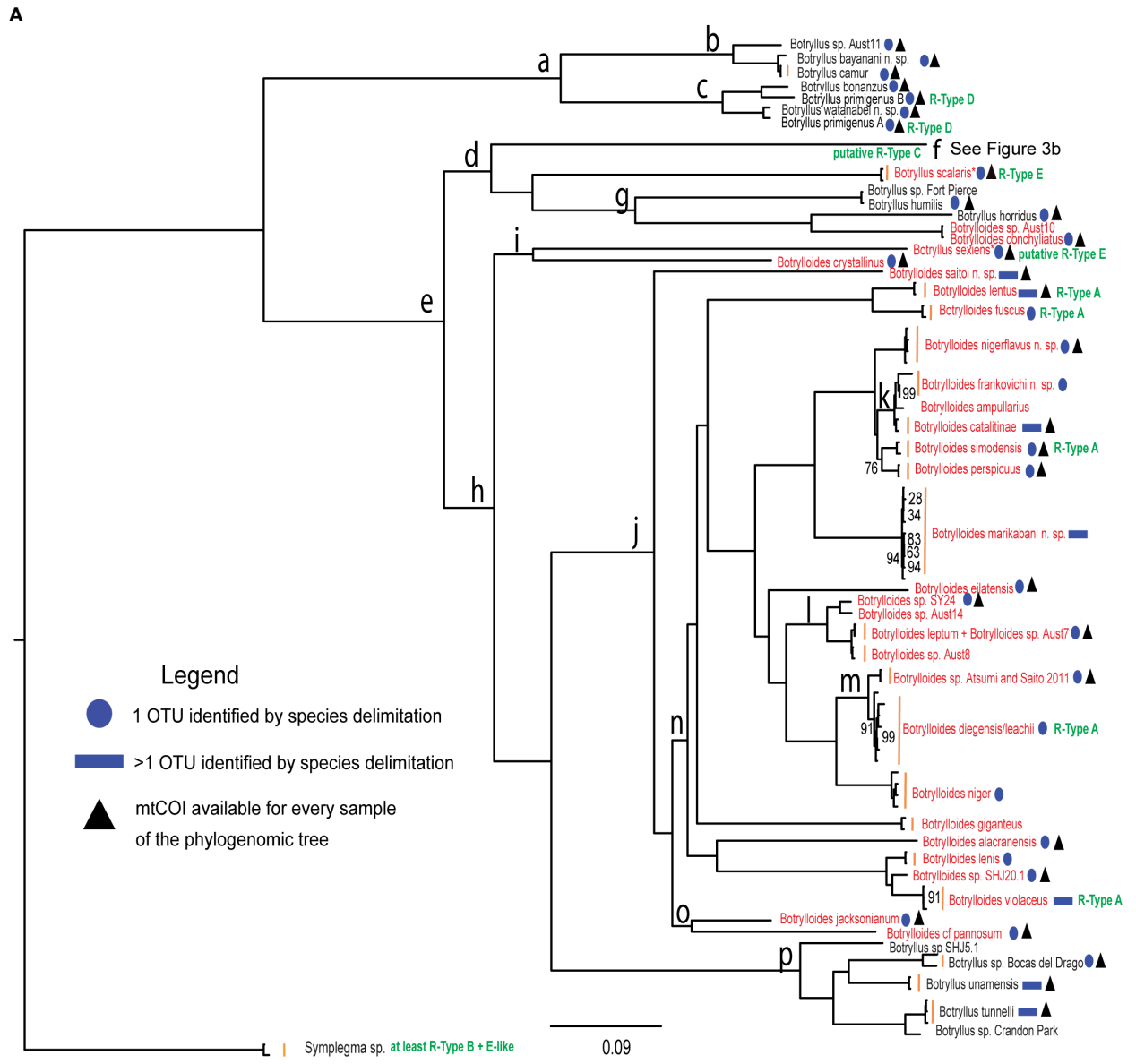

FIGURE 3 (Continued)

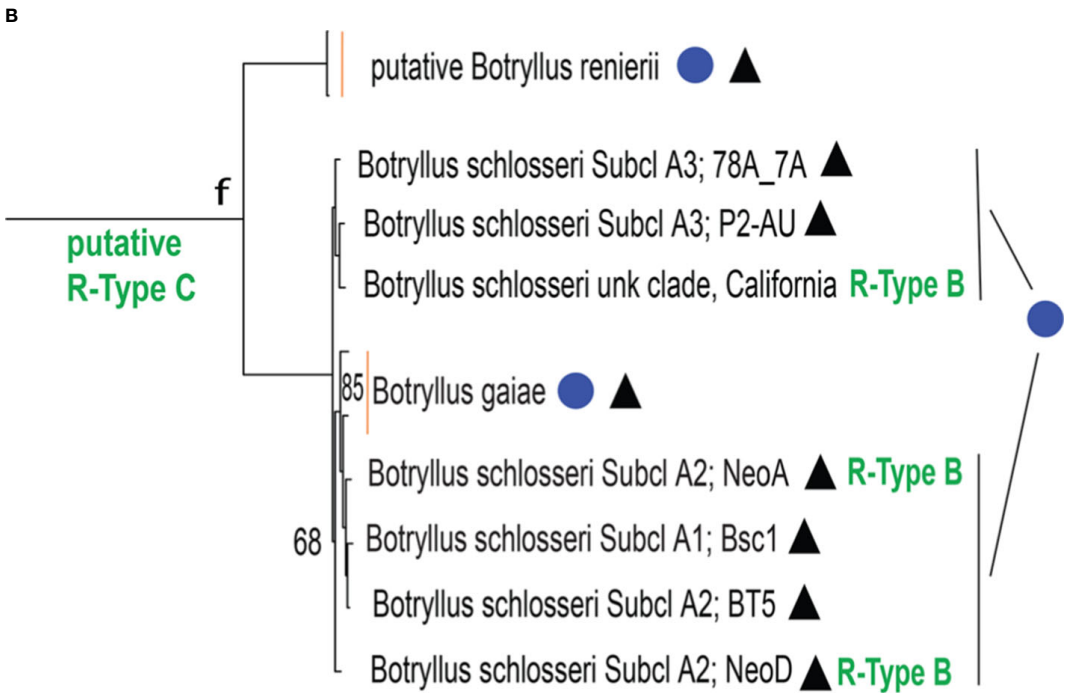

FIGURE 3 (Continued)
Phylogenomic tree of botryllid based on 177 concatenated nuclear loci and generated by RAxML. **(A)** Entire tree excluding clade "f". **(B)** Clade "f" corresponding to the *Botryllus schlosseri* species complex. The scale bar indicates 0.09 substitutions per site. R-types are in green text. *Botrylloides* species and species proposed to be re-assigned to the genus *Botrylloides* are in red text. Blue circles refer to samples identified as belonging to the same OTU in the mtCOI species delimitation results shown in Supplementary Table 2. Blue rectangles refer to samples belonging to more than one OTU as identified in the mtCOI species delimitation results shown in Supplementary Table 2. Black triangles denote OTUs for which the mtCOI sequences used in species delimitation analyses are available for every sample that appears in the phylogenomic tree. Vertical orange bars group leaves of the same species. An asterisk labels *Botryllus* species proposed to be reassigned to the *Botrylloides* genus. "Subcl" indicates subclades as recognized in *Botryllus schlosseri sensu* Brunetti et al. (2017) by the "Elongated-856nt" mtCOI alignment analyzed in Salonna et al. (2021). Bootstrap support values are displayed at each node only when < 100%. The clade "f" branch in panel **(A)** was truncated at level of its internal node.

Overall, the implementation in botryllids of an integrated taxonomy approach, combining morphological as well as nuclear and mitochondrial molecular analyses, allowed us not only to describe six new species but also to identify a number of putative unnamed taxa, for which the examination of additional samples is needed to clarify whether they belong to previously undescribed species. Thus, our results clearly demonstrate the existence of an unexplored hidden diversity within botryllids. This cryptic diversity can be due to factors such as the complexity of morphological analyses, the lack of certain/evident key characters for species discrimination, the paucity of taxonomic experts working in this group, and the historical reliance on morphological characteristics alone for both sample identification and species description.

Phylogenomic tree and the *Botryllus*-only Clade "a"

Figure 3 shows the phylogenomic tree generated by RAxML from the concatenation of the 177 analyzed nuclear loci, while Supplementary File 5 shows the coalescent summary tree generated by ASTRAL from the 177 single-locus trees. Since the topology of the two trees is almost identical, and in both trees nearly all clades are well supported (bootstrap values = 1 in the ASTRAL tree and 100% in the RAxML tree), we will focus only on the RAxML tree of Figure 3. A *Botryllus*-only clade (Clade "a") is the sister clade to the rest of the ingroup, including both *Botryllus* and *Botrylloides* species (Figure 3 and Supplementary Figure 5). We were able to examine and describe the morphological characteristics of 4 of the 7 species forming Clade "a": *Botryllus camur* (Palomino-Alvarez et al., 2022), *Botryllus bonanzus* (Palomino-Alvarez et al., 2022), *Botryllus primigenus* B (Salonna et al., 2021), and *Botryllus watanabei* n. sp. (Supplementary File 2). All of these species have small zooids with four stigmatal rows, a feature neither found in other botryllids included in this phylogeny nor in the outgroup genus *Symplegma*, which is characterized by the presence of 8–13 stigmatal rows (Rocha RM, Montesanto F, Nydam M, unpublished data; Mastrototaro et al., 2019). Moreover *Botryllus watanabei* n. sp. has wide stomach folds, a rectangular stomach shape like *Symplegma* species (Plate 9g in Supplementary Figure 1), and zooids that exhibit a merging of the 1st and 2nd longitudinal vessels on the left side (Plate 9e in Supplementary Figure 1), which is a *Symplegma* character. *B. primigenus*'s species name means "first, primordial, ancestral" in Latin, because it occupies an intermediate position between *Botrylloides*/*Botryllus* and other colonial Styelidae with regard to the structure of its systems (Oka, 1928). Notably, our Clade "a" is in agreement with and retains many characteristics considered ancestral in Saito's botryllid phylogeny

(Saito et al., 2001), a phylogeny based on the combination of 18S rDNA sequences and several other features such as life history, reproductive characters, morphology and allorejection mechanisms. In particular, in Saito's phylogeny (Saito et al., 2001), *B. primigenus* and all other botryllids with 4 stigmatal rows cluster together and are described as unique in their morphology and life history. So, Saito's hypothesis is that these species diverged early in the botryllid evolution, although immediately after a group consisting of *Botryllus scalaris*, *Botryllus horridus* and *Botryllus puniceus*. Even in our phylogenomic tree (Figure 3), *Botryllus scalaris* and *Botryllus horridus* group together (see Clade "d" in Figure 3), however they do not form the earliest diverging botryllid clade. In general, our tree is in good agreement with Saito's phylogeny except for the monophyly of the genus *Botrylloides*, that, remarkably, in our tree become polyphyletic (see red names in Figure 3 and next section). It should be noted that the *Botrylloides* polyphyly here observed could also be due to our taxon sampling, which was much larger than that of Saito, and in particular to the phylogenetic position of species absent in Saito's phylogeny since they were described or genetically identified only after 2001, i.e., after the publication date of Saito et al. (2001) (see for example, Clade "p" and the clade *Botrylloides conchyliatus*/*Botrylloides* sp. Aust10 in Figure 3 were identified after 2001).

Phylogenomic tree and the status of *Botryllus* and *Botrylloides* genera

In Figure 3, both *Botrylloides* and *Botryllus* species are found together within the clade "e", emerging just next to the aforementioned clade "a", but these two genera do not form separate clusters (see the distribution of the red names in Figure 3, labeling original and reassigned *Botrylloides* species). Remarkably, the large Clade "j" includes all the analyzed *Botrylloides* species, except for three species: *Botrylloides* sp. Aust 10, *Botrylloides conchyliatus* and *Botrylloides crystallinus*. The last species forms Clade "i" together with *Botryllus sexiens* (Plate 5 of Supplementary Files 1 and 2). Based on the original morphological description of *Botryllus sexiens* (Saito et al., 1981a), this species has zooids arranged in ladder systems with several common cloacal apertures. Therefore, according to the definition of the *Botryllus* and *Botrylloides* genera reported in Brunetti (2009), it should be moved to the *Botrylloides* genus, and renamed to *Botrylloides sexiens* (hereafter we will refer to this taxon as "*Botryllus*/*Botrylloides*" *sexiens*). This will also keep Clade "i" as *Botrylloides* only. Given the overall topology of Figure 3 and Supplementary File 5, neither of the two genera is monophyletic, and *Botryllus* is paraphyletic with respect to *Botrylloides*. Remarkably, this result was obtained in spite of the fact that the assignment of five specimens was based on the implicit assumption that species of the same genus should cluster together and then that each genus was monophyletic (see previous section "Sample identification reveals a hidden botryllid diversity": this holds for four *Botrylloides* and one *Botryllus* species that were tentatively identified at genus level based just on their positions in the phylogenomic trees, since no formalin-preserved fraction and no suitable mtCOI sequences were available). Overall, the lack of monophyly of both genera aligns with the topologies in previous botryllid phylogenies (Cohen et al., 1998; Nydam et al., 2021).

Assigning a botryllid species to the genus *Botryllus* or *Botrylloides* is not easy, also because the definition of these genera has changed over time and some authors have even synonymized them (Monniot, 1988). In general, only few characters have been used to distinguish these genera (Saito et al., 2001 and references therein; Brunetti, 2009 and references therein): the genus *Botrylloides* has been defined by the presence of zooids arranged in ladder systems, ovary posterior to testis, and embryos developing in a sac-like incubatory pouch forming an outgrowth of the body wall. On the contrary, the genus *Botryllus* has been defined by the presence of zooids arranged in oval or star-shaped systems, ovary anterior or dorsal to testis, and embryos developing in the peribranchial cavity without a brooding organ. However, Saito already observed inconsistencies in these classification criteria since some botryllid species show features not coinciding with neither the definition of *Botryllus* nor that of *Botrylloides*, but have a mixture of the above-mentioned characters (Saito et al., 2001; Okuyama and Saito, 2002). So, he proposed that the definition of the two genera should be amended (Saito et al., 2001). According to Brunetti (2009), who followed the original definition of Milne-Edwards (1841), the two genera differ and should be distinguished by the presence/absence of an atrial siphon and by the consequent structure of the cloaca, which limits the arrangement of the zooids in the systems. Indeed, in *Botryllus* zooids, the atrial opening is located at the distal end of a conical siphon and its anterior rim extends as a small dorsal tongue, thus allowing only the formation of oval or star-shaped systems. On the contrary, in *Botrylloides* zooids, there are no atrial siphons and the atrial opening is wide, usually with a broad dorsal lip extending from its anterior rim, thus producing ladder systems. On this basis, it is not surprising that neither *Botryllus* nor *Botrylloides* appear monophyletic in our phylogenomic reconstruction (Figure 3 and Supplementary File 5): this lack of monophyly could be biologically significant, just related to the different criteria used for the genus assignment of the new species described over time, or a mixture of both factors. For example, according to the genus definition of Brunetti (2009), both *Botryllus sexiens* and *Botryllus scalaris*, described by Saito in 1981, should be moved to the genus *Botrylloides*: their zooids are indeed arranged in ladder systems with several common cloacal apertures. Therefore, both these species await reassignment to the genus *Botrylloides* and we labeled them with an asterisk in our phylogenomic tree (Figure 3). The same fate could probably affect even other botryllids, if a detailed re-analysis of the already described species is carried out.

As for the overall topology of the main *Botrylloides* Clade "j", in the RAxML tree (Figure 3) *Botrylloides saitoi* n. sp. is sister to the remaining taxa, however in the ASTRAL coalescent summary tree (Supplementary File 5), the corresponding branch consists of a subclade of three species: *Botrylloides saitoi* n. sp., *Botrylloides jacksonianum*, and *Botrylloides cf. pannosum* (in the RaxML tree, the last two species are joined in Clade "o" that emerges just after the *Botrylloides saitoi* n. sp. branch). This is the main difference between the RAxML tree from concatenated loci (Figure 3), and the ASTRAL coalescent summary tree from single-locus trees

(Supplementary File 5). Other minor differences are reported in Supplementary File 6. The morphological characteristics of *Botrylloides saitoi* n. sp. place it firmly in the *Botrylloides* genus (see species description in Plate 6 of Supplementary Files 1, and 2), but its phylogenetic position predicts that it could represent a morphological transition between *Botryllus* and *Botrylloides*, alone or together with *Botrylloides jacksonianum* and *Botrylloides cf. pannosum*, depending on the considered phylogenomic tree.

Relationships in the clade of the former *Botryllus schlosseri* complex

In our phylogenetic reconstructions (Figure 3 and Supplementary File 5), Clade "f" encompasses the cryptic species of the former *Botryllus schlosseri* species complex, i.e.:

- The putative *Botryllus renierii*, as proposed in Salonna et al. (2021), corresponding to *Botryllus schlosseri* Clade D *sensu* Bock et al. (2012);
- The recently described *Botryllus gaiae* (Brunetti et al., 2020), corresponding to *Botryllus schlosseri* Clade E *sensu* Bock et al., 2012; and
- *Botryllus schlosseri sensu* Brunetti et al. (2017), corresponding to *Botryllus schlosseri* Clade A *sensu* Bock et al. (2012). The samples of the latter species are reported in Figure 3 also indicating the subclade to which they belong, according to the phylogeny based on an "Elongated-856nt" mtCOI alignment of Salonna et al. (2021) (see "Subcl A1 to A3" in Figure 3).

The putative *Botryllus renierii* forms a monophyletic clade that is a sister group to Clade "f" and is well separated from all other samples of the *B. schlosseri* complex. Noteworthy, *Botryllus gaiae* is nested in a clade containing all *Botryllus schlosseri sensu* Brunetti et al. (2017) samples, moreover samples of subclade A2 do not cluster together (Figure 3). On the contrary, in the ASTRAL coalescent summary tree (Supplementary File 5), most of the corresponding nodes (i.e., those in the cluster including *Botryllus schlosseri sensu* Brunetti et al. (2017) and *Botryllus gaiae*) have unreliable support values < 0.5. Therefore, based on the RAxML phylogenomic tree neither *Botryllus gaiae* nor *Botryllus schlosseri sensu* Brunetti et al. (2017) are monophyletic (Clade "f" in Figure 3), but based on the ASTRAL tree (Supplementary File 5) these relationships are unresolved. Finally, the RAxML result is in disagreement with our mtCOI species delimitation analyses that identify all *Botryllus schlosseri sensu* Brunetti et al. (2017) as belonging to the same OTU, distinct from the OTU of *Botryllus gaiae* (Supplementary Table 2; see also blue circles in Figure 3 for *Botryllus gaiae* and *Botryllus schlosseri*). A clear distinction between *Botryllus gaiae* and *Botryllus schlosseri sensu* Brunetti et al. (2017) was also obtained in all previous mtCOI analyses (Lopez-Legentil et al., 2006; Bock et al., 2012; Yund et al., 2015; Nydam et al., 2021) based on even longer mtCOI alignments (Salonna et al., 2021), as well as by the analysis of the entire mitochondrial genome in several samples (Brunetti et al., 2020).

Overall, these results highlight a possible inconsistency between nuclear and mitochondrial data in the clade of the former *Botryllus schlosseri* species complex, which appear when only the RAxML result is taken into account. There could be several explanations for this inconsistency:

a) The anchored hybrid enrichment here used is designed for capturing orthologous loci characterized by conserved anchor regions plus neighboring variable flanking regions, so in principle it is able to resolve both shallow and deep taxonomic relationships (Hamilton et al., 2016). However, it is still possible that our dataset does not include enough variable informative loci to accurately resolve the short branches inside the former *Botryllus schlosseri* species complex. This explanation is supported by the inconsistency of the results of the RAxML compared to the ASTRAL analyses and by the finding that the nuclear locus 18S rDNA recovered distinct well-supported cryptic species in the *Botryllus schlosseri* species complex (Bock et al., 2012), and between *Botryllus schlosseri* and *Botryllus gaiae* (Nydam et al., 2017b).

b) We cannot exclude the possibility that the inconsistency between the nuclear and the mitochondrial phylogenies (with lack of monophyly of the former cryptic species in our nuclear RAxML tree) could be due to introgression and hybridization between the original cryptic species of the species complex. However, no evidence of gene flow was found between *B. schlosseri* and *B. gaiae* at seven microsatellite loci (Bock et al., 2012), and one of the two *B. gaiae* samples in our nuclear tree came from a population (Falmouth, UK) from which the microsatellite data were obtained.

In conclusion, the current data make it impossible to determine whether the nuclear or mitochondrial phylogeny represents the true evolutionary history of the former *Botryllus schlosseri* species complex. This issue could be solved only by the parallel analyses of a larger dataset of complete mitochondrial genomes including representative of all cryptic species of this taxon, and of a larger dataset of nuclear loci, *ad hoc* designed for the evolutionary distances present within the former *Botryllus schlosseri* species complex.

Mapping mtCOI species delimitation on the phylogenomic tree

The phylogenomic tree of Figure 3 was assembled to cover a broad range of the genetic diversity within the *Botrylloides*/*Botryllus* tree, so it does not allow the species delimitation analyses because it contains insufficient information on the intra-species variability. Therefore, our species delimitation results based on mtCOI sequences (Supplementary Table 2) were mapped on this nuclear phylogenomic tree in order to identify species-level clades. The cross-referencing of these results is particularly important for closely related taxa, i.e., for the sister taxa/clades showing very short internal branch lengths in Figure 3.

In particular, the results of the mtCOI species delimitation analyses (Supplementary Table 2) were summarized in Figure 3 using a blue circle to indicate species consisting of a single OTU and a blue rectangle to indicate species consisting of multiple OTUs. In most cases, the nuclear and the mtCOI data used for the phylogenomic and the species delimitation analyses, respectively, gave congruent results. For example, the two *Botryllus primigenus* samples 1S and 2S, already identified as distinct OTUs in Salonna et al. (2021), were not found to be sister taxa but were placed in separate clades by the nuclear data. In agreement with this result, they were identified as two distinct OTUs by the mtCOI species delimitation analyses (Supplementary Table 2). Therefore, these two samples should be considered as belonging to two different species, named in Figure 3 as "*Botryllus primigenus* A" for sample 1S and "*Botryllus primigenus* B" for sample 2S, although they were morphologically identified and provided by Saito Y. as belonging to the same *Botryllus primigenus* species (personal communication). A partial agreement between nuclear and mtCOI data can be seen in Clade "f", which includes the former *Botryllus schlosseri* species complex (see above section).

A total of eight species are each identified as consisting of multiple OTUs by the mtCOI species delimitation analyses (see species with a blue rectangle in Figure 3), suggesting that additional molecular samples/data are needed to better clarify the taxonomic status of these species or indicating inconsistencies between molecular and morphological data. Some of these cases were already discussed in Nydam et al. (2021) (for *Botrylloides marikabani* n. sp.) and in Palomino-Alvarez et al. (2022) (for *Botrylloides unamensis* and *Botrylloides catalitinae*), while for *Botrylloides violaceus* the lack of morphological information on the samples present in the tree prevents us from formulating hypotheses explaining this result.

Within clade "n", all our *Botrylloides diegensis* samples forms a single OTU together with the *Botrylloides leachii* samples published in Salonna et al. (2021) (Supplementary Table 2): this is in agreement with Viard's proposal that all published mtCOI sequences of *B. leachii* should be re-assigned to *Botrylloides diegensis* (Viard et al., 2019). However, the samples assigned to *Botrylloides diegensis* in Viard et al. (2019) were described only for the colony color pattern, without details on the anatomical traits discriminating *Botrylloides leachii* from *Botrylloides diegensis* (i.e., the number of rows of stigmata, the presence/absence of muscle in the branchial sac, and the number of stomach folds (Brunetti and Mastrototaro, 2017)). Since the absence of these morphological data prevent the evaluation of a possible case of species synonymy, in Figure 3 we have labeled this clade/OTU as "*Botrylloides diegensis/leachii*". Combined morphological and molecular analyses, performed on exactly the same samples, will be necessary to resolve this question.

Additional comments on the mapping of mtCOI species delimitation results on the phylogenomic tree are reported in Supplementary File 6.

Phylogenomic implications for the evolution of allorecognition

Our goal in building the botryllid phylogenomic tree was to document the evolution of allorecognition in the *Botrylloides* and *Botryllus* genera. Allorecognition R-types were therefore mapped on Figure 3 and Supplementary File 5, which was rooted with *Symplegma*, i.e., the sister genus to the *Botrylloides/Botryllus* group. *Symplegma* also has zooids connected via a vascular system with ampullae (Shirae et al., 1999) and can undergo allorecognition. The rejection reaction has so far been studied in a single *Symplegma* species, *S. reptans*, where it has been found that some colonies exhibit only R-Type B and other colonies only R-Type E rejection reactions (Shirae et al., 1999). However, the R-Type E of *S. reptans* differs from R-Type E of *B. scalaris*, since the rejection process is mainly mediated by the activation of morula cells in *S. reptans* and by phagocytes in *B. scalaris* (Shirae et al., 1999). Thus, in these two species, the R-Type E is morphologically similar, since it involves the same allorecognition site, but is characterized by differences in the hemocyte behavior and thus probably in the underlying molecular processes. Remarkably, morula cells, not phagocytes, have been found to be principal "effector cells" in the rejection reaction in the few other botryllids (all R-Type A) in which the hemocyte histochemistry of this process has been investigated (Shirae et al., 1999). With the caveat that this inference is based on a single outgroup species, we can infer that at least R-Type B and an R-Type "E-like" process are ancestral to the entire botryllid group.

Cohen et al. (1998) showed that the allorecognition response involving the most internal tissues (R-Type E) is the ancestral allorecognition condition, thus providing evidence for an evolutionary progression of the allorecognition system from R-Type E to R-Type D and then to R-Type A (Cohen et al., 1998 and Figure 2A). Our phylogenomic trees do not support this finding (Figure 3 and Supplementary File 5) and the application of an ancestral character state reconstruction program does not provide conclusive results (Supplementary Files 7–9 and their detailed description in Supplementary File 6). Indeed, in the ancestral character state reconstructions, several clades show more than one equiparsimonious state, and the results vary considerably depending on the R-Type assigned to the outgroup species, which is not definitely known (indeed *Symplegma* shows at least two different R-Types). Our reconstructions should also be viewed with several caveats since: 1) parsimony is not the only framework in which to conduct these analyses; 2) 73–75% of our specimens have an unknown R-Type, which decreases the robustness of the overall analysis; and 3) the nested position of *B. sexiens* in our phylogeny, inside Clade "h", strongly affects the overall ancestral state reconstructions since its R-type is only putative (it should be R-Type E) and it is the only "not R-Type A" included in the large Clade "h". In our opinion, the preponderance of unknown R-Types and the uncertainty of *B. sexiens*' R-Type are the main reasons leading to view our ancestral reconstructions as provisional.

Our analyses differ from those of Cohen in several aspects, including the usage of an ancestral character state reconstruction software strictly following the parsimony criterion and the outgroup choice. In particular, this last factor can strongly affect the tree topology. Compared to Cohen et al. (1998), our outgroup was more accurately selected since it is the genus phylogenetically nearest to botryllids, and also shows allorejection reactions similar to botryllids. Our overall picture of the evolution of the rejection

reaction in botryllids is much more complex but still not definitive. First of all, we have insufficient data to define the ancestral R-Type in the *Symplegma* outgroup, since the rejection reaction was studied only in one species (*Symplegma reptans*) where both R-Type B and an R-Type "E-like" were observed (Shirae et al., 1999). So, probably many other R-Types are present in the *Symplegma* genus outgroup. Thus, without clear and complete data on the R-Type of the outgroups, several alternative scenarios can be hypothesized for the botryllid allorecognition evolution. For example, R-Type D or E can be considered as the ancestral status of all botryllids if the *Symplegma* R-Types data are not taken into account (Supplementary File 7), while R-Type B, D or E can be the ancestral status of all botryllids if one of the known *Symplegma* R-Types is accepted as ancestral (Supplementary Files 8 and 9). Although the R-Type is missing for many species of our phylogeny, the R-Type A species are all clustered together and certainly evolved later, in Clade "n" at the latest (Supplementary Files 7–9). Finally, to understand the evolution of allorejection in botryllids, this process needs to be investigated also at the level of hemocyte behavior (i.e., cells that recognize self–non-self and effector cells), not only of allorejection sites (Shirae et al., 1999), in order to better classify the different R-Types.

Although we do not obtain conclusive results, our data provide interesting observations. Clade "d" includes all available samples of the former *Botryllus schlosseri* species complex and it displays either R-Type B or R-Type C phenotypes, with the R-Type B observed in populations from California (Pacific Ocean) and from Venice (Mediterranean Sea), and the R-Type C observed in populations from Massachusetts (Atlantic Ocean) (Table 1). At the time the *Botryllus schlosseri* rejection experiments were carried out (Boyd et al., 1990), its status as species complex was unknown, so it is now impossible to unambiguously associate a specific R-Type to each cryptic species without repeating the allorecognition experiments on genetically characterized colonies. However, based on sample geographic origin, we have mapped R-Type B at the level of our sample coming from California (i.e., "*Botryllus schlosseri*, unk. clade" in Figure 3) and from Venice (i.e., "*Botryllus schlosseri*, NeoA and NeoD in Figure 3), while we have not associated R-Type C to any specific *Botryllus schlosseri* sample, since in our tree there are no *Botryllus schlosseri* samples coming from Massachusetts. We have also tentatively mapped R-Type C at the level of the basal node including of the *Botryllus schlosseri* species complex, since California and Massachusetts samples analyzed by Boyd et al. (1990) all certainly belong to the *Botryllus schlosseri* species complex. Moreover, we hypothesize that both R-Type B and R-Type C are present in *Botryllus schlosseri sensu* Brunetti et al. (2017), i.e., in clade A *sensu* Bock et al. (2012), since current cryptic species distribution data shows that *Botryllus schlosseri sensu* Brunetti et al. (2017) is the only species widespread worldwide, while *Botryllus gaiae* (i.e., the former cryptic clade E) is present only in the European waters (including the Mediterranean Sea), and the other cryptic species are geographically restricted to a few localities (see Brunetti et al., 2017; Nydam et al., 2017a; Brunetti et al., 2020 and references therein). *Botryllus scalaris* (which, as previously discussed, should be moved to the genus *Botrylloides*) is the only one of three known R-Type E species (Table 1) present in our tree, and is found in Clade "d", so close to the *Botryllus schlosseri* species complex.

Clade "h" includes all the currently known R-Type A species (Table 1), however we do not know if this clade includes even other R-Types, as many of its species have not been analyzed for R-Types. In support of the presence of species other than R-Type A in Clade "h", *Botryllus sexiens* (that we proposed to move into the *Botrylloides* genus) is thought to be R-Types E (Cohen et al., 1998). It would be interesting to study the R-Types in Clade "p", which is a small *Botryllus* clade in the large Clade "h" consisting mostly of *Botrylloides*.

Botryllus R-Types so far known are B, C, D, and E, while *Botrylloides* are only R-Type A, but they will also include R-Type E if our proposal to reassign both *Botryllus sexiens* and *Botryllus scalaris* to the genus *Botrylloides* is considered valid.

There are six genes present in the *Botrylloides* and *Botryllus* genera that have characteristics consistent with a role in allorecognition: two highly polymorphic genes (fuhc^{sec} and fuhc^{tm}) (Nydam et al., 2013a), two genes encoding for putative receptors (fester and uncle fester) (Nyholm et al., 2006; McKitrick et al., 2011), and two genes which may be involved in generating specificity (Hsp40-L and BHF) (Nydam et al., 2013b; Voskoboynik et al., 2013). Since uncle fester is responsible for the rejection response (McKitrick et al., 2011), we predict that a different expression pattern of this gene could be responsible for the different R-Type reactions. In particular, the presence of this protein only on circulatory cells in R-Type E species would explain the complete membrane fusion of colony circulatory systems prior to rejection. On the contrary, R-Type A–D reactions are likely the result of expressing uncle fester on more external tissues (e.g., on the surface of the tunic cuticle, in the subcuticular region, within the tunic matrix, or at the surface of the ampullar epithelium). This hypothesis needs to be tested by tissue-specific transcriptome analyses.

The results of xenorecognition experiments, wherein colonies from different species interact with each other (Saito, 2003), can also be mapped onto our phylogenomic tree. Unlike the allorejection reaction, in xenorecognition the rejection is the default, and the fusion response is an interruption of that process. There are three outcomes from xenorecognition experiments, which can also vary depending on the conditions (contact at growing edges, at cut surfaces, or blood plasma injection): 1) both species initiated a rejection response, 2) neither species initiated a rejection response, 3) one species initiated a rejection response and the other did not (Saito, 2003). If the loci responsible for initiating the rejection response are species-specific, then the more closely related species pairs would be predicted to initiate rejection responses, while the more distantly related species pairs would not. The three participant species in the Saito's xenorecognition experiments were *Botrylloides simodensis* (R-Type A), *Botryllus primigenus* (R-Type D), and *Botryllus scalaris* (R-Type E) (Saito, 2003). Taking into account the results of both growing-edge and cut surface contacts, *B. primigenus* (R-Type D) initiated a rejection reaction with both *B. simodensis* (R-Type A) and *B. scalaris* (R-Type E) (Saito, 2003). *B. simodensis* (R-Type A) initiated a rejection reaction with both *B. primigenus* (R-Type D) and *B. scalaris* (R-Type E) (Saito, 2003). In

contrast, *B. scalaris* (R-Type E) did not react with either the R-Type A or the R-Type D species in both conditions (Saito, 2003). In the Cohen et al., 1998 phylogeny (Figure 2A), the R-Type E species is sister to the rest of the species and is referred in that paper as emerging early in the tree, so the earlier evolving species could not initiate a rejection response with later evolving species, but the later evolving R-Type A and the R-Type D species had the capacity to initiate a rejection response with the earlier evolving R-Type E species. In the current phylogeny (Figure 3 and Supplementary File 5), the R-Type E species *B. scalaris* is sister group to the former *B. schlosseri* complex, including R-Type B and putative R-Type C species (see Figure 3B; Supplementary File 5B and Clade "d" in Figure 3A and Supplementary File 5A) but, to our knowledge, rejection reactions between R-Type B/C and R-Type E have not been tested. However, it seems that the loci responsible for xenorejection initiation in R-Type E may have evolved in such a way as to be incompatible with R-Type A and R-Type D. This is also in accordance with a greater separation between R-Type E and all other R-Types, due for example to the major involvement of phagocytes instead of morula cells in the R-Type E allorejection reaction (Shirae et al., 1999).

Xenorecognition experiments within R-Type A species (*B. fuscus*, *B. lentus*, *B. simodensis*, and *B. violaceus*) have also been conducted (Hirose et al., 2002). The results of a contact at colony growing edges do not correlate with phylogenetic position. Indeed, *B. violaceus* reacts with *B. fuscus* with an intense hemolytic reaction but not with *B. lentus* or *B. simodensis* (Hirose et al., 2002), although *B. violaceus* is sister to the clade that includes the other three species (Figure 3 and Supplementary File 5). *B. fuscus* and *B. lentus* are sister species in our phylogeny, but they do not react the same way when the growing edges of their colonies contact either *B. simodensis* or *B. violaceus* (Hirose et al., 2002).

Data availability statement

The datasets presented in this study can be found in online repositories. The names of the repository/repositories and accession number(s) can be found in the article/Supplementary Material.

Ethics statement

Ethical review and approval was not required for the study on animals in accordance with the local legislation and institutional requirements.

Author contributions

MN: Project management, sample contribution, DNA barcoding, species delimitation analyses, morphological analyses, manuscript writing. AL: Project management on the genomic work. EL: Project management on the genomic work. KZ: Alignment and assembly of genomic reads, tree creation. CSC: Sample contribution. LP-A: Sample contribution. CG: Sample contribution, manuscript writing. All authors contributed to the article and approved the submitted version.

Funding

The author(s) declare financial support was received for the research, authorship, and/or publication of this article. MN was funded by a Luce Initiative for Asian Studies and the Environment Grant awarded to Centre College, and by Soka University of America. CG acknowledges the Molecular Biodiversity Laboratory of the Italian node of Lifewatch (CNR, Consiglio Nazionale delle Ricerche, Italy), Elixir-IT (the European Research Infrastructure for Life Science), and CNRBiOmics (Infrastructural project PIR01_00017 of MUR – Ministero dell'Università e della Ricerca, Italy). Posgrado en Ciencias del Mar y Limnología, UNAM, and Consejo Nacional de Ciencia y Tecnología (2018-000012-01NACF-08376, CVU 447073) supported LP-A. Grants from the Harte Charitable Foundation and CONABIO-NE018 to Nuno Simoes supported the samples obtained from the Gulf of Mexico and the Caribbean by LP-A.

Acknowledgments

We would like to thank the following people for assistance with sample collection: Sylvain Agostini, Erin Grey-Avis, Tony De Tomaso, Ben Harvey, Morgan Hawkins, Kazuo Inaba, Koetsu Kon, Yukinobu Isowa, Toru Miura, Hitoshi Sawada, Maki Shirae-Kurabayashi, Lauren Stefaniak. We thank Loriano Ballarin and Euichi Hirose for helpful discussions on the details of the rejection reaction in botryllids. We thank Alberto Guerra for drawing Figure 1. The insightful comments of three reviewers improved the manuscript. We also thank the Italian MEDITS survey program, the Steinhardt Museum of Natural History (National Center for Biodiversity Studies, Israel), the Queensland Museum (Australia) and the lamented Yasunori Saito for kindly providing the ascidian samples previously analyzed in Salonna et al. (2021). We acknowledge The Philippines' Bureau of Fisheries and Aquatic Resources and the National Fisheries Research and Development Institute for their role in the 2014–2016 Verde Island Passage (VIP) Expedition. All *B. marikabani* specimens were collected during the NSF Biotic Survey VIP Expedition under Gratuitous Permit # GP-0077-14 from the municipalities of Puerto Galera and Batangas.

Conflict of interest

The authors declare that the research was conducted in the absence of any commercial or financial relationships that could be construed as a potential conflict of interest.

Publisher's note

All claims expressed in this article are solely those of the authors and do not necessarily represent those of their affiliated organizations, or those of the publisher, the editors and the reviewers. Any product that may be evaluated in this article, or claim that may be made by its manufacturer, is not guaranteed or endorsed by the publisher.

Supplementary material

The Supplementary Material for this article can be found online at: https://www.frontiersin.org/articles/10.3389/fevo.2023.1214191/full#supplementary-material

References

Atsumi, M. O., and Saito, Y. (2011). Studies on Japanese botryllid ascidians. V. A new species of the genus *Botrylloides* very similar to *Botrylloides simodensis* in morphology. *Zoological Sci.* 28, 532–542. doi: 10.2108/zsj.28.532

Ballarin, L., Karahan, A., Salvetti, A., Rossi, L., Manni, L., Rinkevich, B., et al. (2021). Stem cells and innate immunity in aquatic invertebrates: bridging two seemingly disparate disciplines for new discoveries in biology. *Front. Immunol.* 12. doi: 10.3389/fimmu.2021.688106

Ben-Shlomo, R., Reem, E., Douek, J., and Rinkevich, B. (2010). Population genetics of the invasive ascidian *Botryllus schlosseri* from South American coasts. *Mar. Ecol. Prog. Ser.* 412, 85–92. doi: 10.3354/meps08688

Berrill, N. J. (1950). The Tunicata with an account of the British species. *Ray Society*. (London: Ray Society, Johnson Reprints).

Blanchoud, S., Rinkevich, B., and Wilson, M. J. (2018). Whole-body regeneration in the colonial tunicate Botrylloides leachii. *Mar. Organisms as Model. Syst. Biol. Med.* 65, 337–355. doi: 10.1007/978-3-319-92486-1_16

Bock, D. G., MacIsaac, H. J., and Cristescu, M. E. (2012). Multilocus genetic analyses differentiate between widespread and spatially restricted cryptic species in a model ascidian. *Proc. R. Soc. B: Biol. Sci.* 279, 2377–2385. doi: 10.1098/rspb.2011.2610

Boyd, H. C., Weissman, I. L., and Saito, Y. (1990). Morphologic and genetic verification that Monterey *Botryllus* and Woods Hole *Botryllus* are the same species. *Biol. Bull.* 178, 239–250. doi: 10.2307/1541825

Brunetti, R. (2009). Botryllid species (Tunicata, Ascidiacea) from the Mediterranean coast of Israel, with some considerations on the systematics of Botryllinae. *Zootaxa* 2289, 18–32. doi: 10.11646/zootaxa.2289.1.2

Brunetti, R., Griggio, F., Mastrototaro, F., Gasparini, F., and Gissi, C. (2020). Toward a resolution of the cosmopolitan *Botryllus schlosseri* species complex (Ascidiacea, Styelidae): mitogenomics and morphology of clade E (*Botryllus gaiae*). *Zoological J. Linn. Soc.* 190, 1175–1192. doi: 10.1093/zoolinnean/zlaa023

Brunetti, R., and Mastrototaro, F. (2017). *Fauna d'Italia. Ediz. Vol. 2: Ascidiacea of the European Waters*. (Milan, Italy: Edagricole-New Business Media II). Vol. 51.

Brunetti, R., and Mastrototaro, F. (2017). "Ascidiacea of the European waters," in *Edagricole - New Business Media II*.

Buss, L. (1982). Somatic cell parasitism and the evolution of somatic tissue compatibility. *Proc. Natl. Acad. Sci.* 79, 5337–5341. doi: 10.1073/pnas.79.17.5337

Cohen, C. S., Saito, Y., and Weissman, I. L. (1998). Evolution of allorecognition in botryllid ascidians inferred from a molecular phylogeny. *Evolution* 52, 746–756. doi: 10.1111/j.1558-5646.1998.tb03699.x

De Tomaso, A., Nyholm, S. V., Palmeri, K. J., Ishizuka, K. J., Ludington, W. B., Mitchel, K., et al. (2005). Isolation and characterization of a protochordate histocompatibility locus. *Nature* 438, 454–459. doi: 10.1038/nature04150

Ducasse, J., Ung, V., Lecointre, G., and Miralles, A. (2020). LIMES: A tool for comparing species partitions. *Bioinformatics* 36, 2282–2283. doi: 10.1093/bioinformatics/btz911

Folmer, O., Black, M., Hoeh, W., Lutz, R., and Vrijenhoek, R. (1994). DNA primers for amplification of mitochondrial cytochrome c oxidase subunit I from diverse metazoan invertebrates. *Mol. Mar. Biol. Biotechnol.* 3, 294–299.

Hamilton, C. A., Lemmon, A. R., Lemmon, E. M., and Bond, J. E. (2016). Expanding anchored hybrid enrichment to resolve both deep and shallow relationships within the spider tree of life. *BMC Evolutionary Biol.* 16, 212. doi: 10.1186/s12862-016-0769-y

Herdman, W. A. (1891). A revised classification of the Tunicata, with definitions of the orders, suborders, families, subfamilies, and genera, and analytical keys to the species. *J. Linn. Soc. London* 23, 558–652.

Herdman, W. A. (1899). *Descriptive catalogue of the Tunicata in the Australian Museum* (Sydney N.S.W. T: Dobb and Company).

Hirose, E., Saito, Y., and Watanabe, H. (1988). A new type of manifestation of colony specificity in the compound ascidian, *Botrylloides violaceus* Oka. *Biol. Bull.* 175, 240–245. doi: 10.2307/1541564

Hirose, E., Saito, Y., and Watanabe, H. (1990). Allogeneic rejection induced by cut surface contact in the compound ascidian, Botrylloides simodensis. *Invertebrate Reprod. Dev.* 17, 159–164. doi: 10.1080/07924259.1990.9672105

Hirose, E., Shirae, M., and Saito, Y. (2002). Colony specificity in the xenogeneic combinations among four *Botrylloides* species (Urochordata, Ascidiacea). *Zoological Sci.* 19, 747–753. doi: 10.2108/zsj.19.747

Kott, P. (1985). The Australian ascidiacea. Part I, phlebobranchia and Stolidobranchia. *Memoirs Queensland Museum* 23, 1–440.

Kott, P. (2005). Catalogue of Tunicata in Australian waters. *Australian Biological Resources Study*. (Queensland Museum, Brisbane: Australia Department of the Environment and Heritage).

Lauzon, R. J., Brown, C., Kerr, L., and Tiozzo, S. (2013). Phagocyte dynamics in a highly regenerative urochordate: insights into development and host defense. *Dev. Biol.* 374, 357–373. doi: 10.1016/j.ydbio.2012.11.006

Lopez-Legentil, S., Turon, X., and Planes, S. (2006). Genetic structure of the star sea squirt, *Botryllus schlosseri*, introduced in southern European harbours. *Mol. Ecol.* 15, 3957–3967. doi: 10.1111/j.1365-294x.2006.03087.x

Maddison, W. P., and Maddison, D. R. (2023) *Mesquite: a modular system for evolutionary analysis. Version 3.81*. Available at: http://www.mesquiteproject.org.

Mastrototaro, F., Montesanto, F., Salonna, M., Grieco, F., Trainito, E., Chimienti, G., et al. (2019). Hitch-hikers of the sea: concurrent morphological and molecular identification of *Symplegma brakenhielmi* (Tunicata: Ascidiacea) in the western Mediterranean Sea. *Mediterr. Mar. Sci.* 20, 197–207. doi: 10.12681/mms.19390

McKitrick, T. R., Muscat, C. C., Pierce, J. D., Bhattacharya, D., and De Tomaso, A. W. (2011). Allorecognition in a basal chordate consists of independent activating and inhibitory pathways. *Immunity* 34, 616–626. doi: 10.1016/j.immuni.2011.01.019

Miller, M. A., Pfeiffer, W., and Schwartz, T. (2010). "Creating the CIPRES Science Gateway for inference of large phylogenetic trees," in *Proceedings of the Gateway Computing Environments Workshop (GCE)*, New Orleans, LA, 14 Nov. 2010 (New York City). 1–8. doi: 10.1109/gce.2010.5676129

Milne-Edwards, H. (1841). Observations sur les ascidies composées des côtes de la Manche. *Chez Fortin-Masson Cie* (Paris, France).

Monniot, C. (1988). Ascidies de nouvelle-caledonie. IV. Styelidae. *Bull. Natl. Museum Natural History Paris* 10, 163–196. doi: 10.5962/p.292203

Nourizadeh, S., Kassmer, S., Rodriguez, D., Hiebert, L. S., and De Tomaso, A. W. (2021). Whole body regeneration and developmental competition in two botryllid ascidians. *Evodevo* 12, 15. doi: 10.1186/s13227-021-00185-y

Nydam, M. L., Giesbrecht, K. B., and Stephenson, E. E. (2017a). Origin and dispersal history of two colonial ascidian clades in the *Botryllus schlosseri* species complex. *PloS One* 12, e0169944. doi: 10.1371/journal.pone.0169944

Nydam, M. L., Hoang, T. A., Shanley, K. M., and De Tomaso, A. W. (2013b). Molecular evolution of a polymorphic HSP40-like protein encoded in the histocompatibility locus of an invertebrate chordate. *Dev. Comp. Immunol.* 41, 128–136. doi: 10.1016/j.dci.2013.03.004

Nydam, M. L., Lemmon, A. R., Cherry, J. R., Kortyna, M. L., Clancy, D. L., Hernandez, C., et al. (2021). Phylogenomic and morphological relationships among the botryllid ascidians (Subphylum Tunicata, Class Ascidiacea, Family Styelidae). *Sci. Rep.* 11, 1–13. doi: 10.1038/s41598-021-87255-2

Nydam, M. L., Neutschil, N., Sanders, E., Langenbacher, A., Lewis, D. L., Marimuthu, A., et al. (2013a). The candidate histocompatibility locus of a basal chordate encodes two highly polymorphic proteins. *PLoS One* 8, e65980. doi: 10.1371/journal.pone.0065980

Nydam, M. L., Stephenson, E. E., Waldman, C. E., and De Tomaso, A. W. (2017b). Balancing selection on allorecognition genes in the colonial ascidian Botryllus schlosseri. *Dev. Comp. Immunol.* 69, 60–74. doi: 10.1016/j.dci.2016.12.006

Nyholm, S. V., Passegue, E., Ludington, W., Voskoboynik, A., Mitchel, K., Weissman, I. L., et al. (2006). fester, a candidate allorecognition receptor from a primitive chordate. *Immunity* 25, 163–173. doi: 10.1016/j.immuni.2006.04.011

Oka, A. (1928). Ueber eine merkwürdige Botryllus-Art, *B. primigenus* nov. sp. *Proc. Imperial Acad.* 4, 303–305.

Okuyama, M., and Saito, Y. (2001). Studies on Japanese botryllid ascidians. I. A new species of the genus *Botryllus* from the Izu Islands. *Zoological Sci.* 18, 261–267. doi: 10.2108/zsj.18.261

Okuyama, M., and Saito, Y. (2002). Studies on Japanese botryllid ascidians. II. A new species of the genus *Botryllus* from the vicinity of Shimoda. *Zoological Sci.* 19, 809–815. doi: 10.2108/zsj.19.809

Okuyama, M., Saito, Y., and Hirose, E. (2002). Fusion between incompatible colonies of a viviparous ascidian. *Botrylloides lentus*. *Invertebrate Biol.* 121, 163–169. doi: 10.1111/j.1744-7410.2002.tb00057.x

Palomino-Alvarez, L. A., Nydam, M. L., Rocha, R. M., and Simoes, N. (2022). New *Botrylloides*, *Botryllus* and *Symplegma* (Ascidiacea: Styelidae) in coral reefs of the southern Gulf of Mexico and Mexican Caribbean Sea. *MDPI Diversity* 14, 977. doi: 10.3390/d14110977

Puillandre, N., Brouillet, S., and Achaz, G. (2021). ASAP: assemble species by automatic partitioning. *Mol. Ecol. Resour.* 21, 609–620. doi: 10.1111/1755-0998.13281

Puillandre, N., Lambert, A., Brouillet, S., and Achaz, G. (2012). ABGD, Automatic Barcode Gap Discovery for primary species delimitation. *Mol. Ecol.* 21, 1864–1877. doi: 10.1111/j.1365-294x.2011.05239.x

Sabbadin, A., Zaniolo, G., and Ballarin, L. (1992). Genetic and cytological aspects of histocompatibility in ascidians. *Bollettino della Società zoologica italiana* 59, 167–173. doi: 10.1080/11250009209386665

Saito, Y. (2003). Xenogeneic rejection among three Botryllids (compound ascidians). *Zoological Sci.* 20, 581–589. doi: 10.2108/zsj.20.581

Saito, Y., Hirose, E., and Watanabe, H. (1994). Allorecognition in compound ascidians. *Int. J. Dev. Biol.* 38, 237–247.

Saito, Y., Mukai, H., and Watanabe, H. (1981a). Studies of Japanese compound styelid ascidians. I. Two new species of *Botryllus* from the vicinity of Shimoda. *Publications Seto Mar. Biol. Lab.* 26, 347–355. doi: 10.5134/176033

Saito, Y., Mukai, H., and Watanabe, H. (1981b). Studies of Japanese compound styelid ascidians. II. A new species of the genus *Botrylloides* and redescription of Botrylloides violaceus. *Publications Seto Mar. Biol. Lab.* 26, 357–368. doi: 10.5134/176032

Saito, Y., and Nagasawa, N. (2003). Studies on Japanese botryllid ascidians. III. A new species of the genus *Botryllus* with a vivid colony color from the vicinity of Shimoda. *Zoological Sci.* 20, 765–771. doi: 10.2108/zsj.20.765

Saito, Y., and Okuyama, M. (2003). Studies on Japanese botryllid ascidians. IV. A new species of the genus *Botryllus* with a unique colony shape, from the vicinity of Shimoda. *Zoological Sci.* 20, 1153–1161. doi: 10.2108/zsj.20.1153

Saito, Y., Shirae, M., Okuyama, M., and Cohen, C. S. (2001). "Phylogeny of botryllid ascidians," in *The Biology of Ascidians*. Eds. H. Sawada, H. Yokosawa and C. C. Lambert (Berlin/Heidelberg: Springer), 315–320. doi: 10.1007/978-4-431-66982-1_50

Saito, Y., and Watanabe, H. (1982). Colony specificity in the compound ascidian, *Botryllus scalaris*. *Proc. Japan Acad. Ser. B*, 58, 105–108. doi: 10.2183/pjab.58.105

Saito, Y., and Watanabe, H. (1985). Studies on Japanese compound styelid ascidians-IV. Three new species of the genus *Botrylloides* from the vicinity of Shimoda. *Publications Seto Mar. Biol. Lab.* 30, 227–240. doi: 10.5134/176112

Salonna, M., Gasparini, F., Huchon, D., Montesanto, F., Haddas-Sasson, M., Ekins, M., et al. (2021). An elongated COI fragment to discriminate botryllid species and as an improved ascidian DNA barcode. *Sci. Rep.* 11, 1–19. doi: 10.1101/2021.01.20.427448

Scofield, V. L., and Nagashima, L. S. (1983). Morphology and genetics of rejection reactions between oozoids from the tunicate Botryllus schlosseri. *Biol. Bull.* 165, 733–744. doi: 10.2307/1541475

Shenkar, N., Gittenberger, A., Lambert, G., Rius, M., Rocha, R. M., Swalla, B. J., et al. (2022) *Ascidiacea World Database*. Available at: https://www.marinespecies.org/ascidiacea (Accessed 2022-10-24).

Shirae, M., Hirose, E., and Saito, Y. (1999). Behavior of hemocytes in the allorecognition reaction in two compound ascidians, *Botryllus scalaris* and Symplegma reptans. *Biol. Bull.* 197, 188–197. doi: 10.2307/1542614

Stamatakis, A. (2014). RAxML version 8: a tool for phylogenetic analysis and post-analysis of large phylogenies. *Bioinformatics* 30, 1312–1313. doi: 10.1093/bioinformatics/btu033

Stefaniak, L., Lambert, G., Gittenberger, A., Zhang, H., Lin, S., and Whitlatch, R. B. (2009). Genetic conspecificity of the worldwide populations of *Didemnum vexillum* Kott 2002. *Aquat. Invasions* 4, 29–44. doi: 10.3391/ai.2009.4.1.3

Tanaka, K., and Watanabe, H. (1973). Allogeneic inhibition in a compound ascidian, *Botryllus primigenus* Oka. I. Processes and features of "Nonfusion" reaction. *Cell. Immunol.* 7, 410–426. doi: 10.1016/0008-8749(73)90206-2

Viard, F., Roby, C., Turon, X., Bouchemousse, S., and Bishop, J. (2019). Cryptic diversity and database errors challenge non-indigenous species surveys: an illustration with Botrylloides spp. in the English Channel and Mediterranean Sea. *Front. Mar. Sci.* 6, 615. doi: 10.3389/fmars.2019.00615

Voskoboynik, A., Newman, A. M., Corey, D. M., Sahoo, D., Pushkarev, D., Neff, N. F., et al. (2013). Identification of a colonial chordate histocompatibility gene. *Science* 341, 384–387. doi: 10.1126/science.1238036

Voskoboynik, A., and Weissman, I. L. (2015). *Botryllus schlosseri*, an emerging model for the study of aging, stem cells, and mechanisms of regeneration. *Invertebrate Reprod. Dev.* 59, 33–38. doi: 10.1080/07924259.2014.944673

Yund, P. O., Collins, C., and Johnson, S. L. (2015). Evidence of a native northwest Atlantic COI haplotype clade in the cryptogenic colonial ascidian *Botryllus schlosseri*. *Biol. Bull.* 228, 201–216. doi: 10.1086/bblv228n3p201

Zaniolo, G., and Ballarin, L. (2001). "Colony specificity in *botrylloides leachi* (Savigny): preliminary reports," in *The Biology of Ascidians*. Eds. H. Sawada, H. Yokosawa and C. C. Lambert (Tokyo: Springer). doi: 10.1007/978-4-431-66982-1_65

Zaniolo, G., Manni, L., and Ballarin, L. (2006). Colony specificity in *Botrylloides leachi*. I. Morphological aspects. *ISJ-Invertebrate Survival J.* 3, 125–136.

Zhang, J., Kapli, P., Pavlidis, P., and Stamatakis, A. (2013). A general species delimitation method with applications to phylogenetic placements. *Bioinformatics* 29, 2869–2876. doi: 10.1093/bioinformatics/btt499

frontiers | Frontiers in Cell and Developmental Biology

TYPE Brief Research Report
PUBLISHED 07 December 2023
DOI 10.3389/fcell.2023.1323378

OPEN ACCESS

EDITED BY
Lucia Manni,
University of Padua, Italy

REVIEWED BY
Alfonso Ferrández Roldán,
University of Barcelona, Spain
William Kinsey,
University of Kansas Medical Center,
United States

*CORRESPONDENCE
Haiyang Feng,
hyfeng@live.cn
Eric M. Thompson,
eric.thompson@uib.no

RECEIVED 17 October 2023
ACCEPTED 21 November 2023
PUBLISHED 07 December 2023

CITATION
Feng H and Thompson EM (2023), Functional specialization of Aurora kinase homologs during oogenic meiosis in the tunicate *Oikopleura dioica*. *Front. Cell Dev. Biol.* 11:1323378. doi: 10.3389/fcell.2023.1323378

Functional specialization of Aurora kinase homologs during oogenic meiosis in the tunicate *Oikopleura dioica*

Haiyang Feng[1,2]* and Eric M. Thompson[2,3]*

[1]Institute of Biological Sciences, Jinzhou Medical University, Jinzhou, China, [2]Sars International Centre for Marine Molecular Biology, University of Bergen, Bergen, Norway, [3]Department of Biological Sciences, University of Bergen, Bergen, Norway

A single Aurora kinase found in non-vertebrate deuterostomes is assumed to represent the ancestor of vertebrate Auroras A/B/C. However, the tunicate *Oikopleura dioica*, a member of the sister group to vertebrates, possesses two Aurora kinases (Aurora1 and Aurora2) that are expressed in proliferative cells and reproductive organs. Previously, we have shown that Aurora kinases relocate from organizing centers to meiotic nuclei and were enriched on centromeric regions as meiosis proceeds to metaphase I. Here, we assessed their respective functions in oogenic meiosis using dsRNA interferences. We found that Aurora1 (Aur1) was involved in meiotic spindle organization and chromosome congression, probably through the regulation of microtubule dynamics, whereas Aurora2 (Aur2) was crucial for chromosome condensation and meiotic spindle assembly. *In vitro* kinase assays showed that Aur1 and Aur2 had comparable levels of kinase activities. Using yeast two-hybrid library screening, we identified a few novel interaction proteins for Aur1, including c-Jun-amino-terminal kinase-interacting protein 4, cohesin loader Scc2, and mitochondrial carrier homolog 2, suggesting that Aur1 may have an altered interaction network and participate in the regulation of microtubule motors and cohesin complexes in *O. dioica*.

KEYWORDS

tunicate, Aurora kinase, INCENP, interaction/scaffolding proteins, oogenic meiosis, molecular evolution

Introduction

The Aurora kinases are a group of evolutionarily conserved serine/threonine protein kinases that regulate diverse cellular events during mitosis and meiosis (Hochegger et al., 2013). Aurora originated as a single gene in the last eukaryotic common ancestor (LECA) and evolved independently in plants, fungi, protists, and metazoans (Brown et al., 2004). However, the Aurora kinase sequences of invertebrates are highly divergent from those of vertebrates and often exhibit long-branch attraction artifacts in phylogenetic analyses (Brown et al., 2004). The single, bifunctional Aurora present in the echinoderm starfish and tunicate ascidians are believed to represent the ancestral kinase that gave rise to Auroras A and B in vertebrates (Abe et al., 2010; Hebras and McDougall, 2012). Whether this scenario is generally applicable in chordates requires stringent functional evidence across closely related phyla, in order to better understand the selection pressures that restrain the concerted functions of Aurora homologs.

In species with a single Aurora, it functions at the spindle poles, chromosomes, and central spindle in mitosis (Li et al., 2008; Abe et al., 2010; Hebras and McDougall, 2012). In metazoans possessing two Aurora kinases, functional studies consistently reveal the division of labor between A- and B-type Aurora kinases at the spindle poles and equator (Hochegger et al., 2013). In contrast, reports on the meiotic functions of Aurora kinases in a few model organisms are sparse and less consistent (Nguyen and Schindler, 2017). Aurora A has a common role in regulating microtubule assembly and maintenance in the meiotic spindle, but this task is carried out at different sites. Aurora A associates with acentriolar microtubule organizing centers (aMTOCs) at the spindle poles in mouse oocytes and induces the fragmentation of aMTOCs through the phosphorylation of polo-like kinase 1 (PLK1) (Blengini et al., 2021), while active Aurora A/AIR-1 is concentrated on chromosomes during prometaphase I and on interchromosomal microtubules during anaphase I in *C. elegans* oocytes (Sumiyoshi et al., 2015). The chromosomal passenger complex (CPC) kinase, Aurora B, is involved in multiple aspects of meiotic division, such as chromosome condensation, cohesion, and error correction in kinetochore-microtubule (KT-MT) attachments. In *C. elegans* oocytes, Aurora B/AIR-2 is localized on the equatorial axis of holocentric bivalents where it provides spatial cues to load condensin I, promotes ring complex (RC) assembly, and releases interhomolog cohesins at the onset of anaphase I (Rogers et al., 2002; Collette et al., 2011; Divekar et al., 2021). In *Drosophila* oocytes, Aurora B/*ial* interacts with non-centromeric chromosomes and regulates spindle bipolarity and chromosome biorientation at the central spindle ring (Radford et al., 2012). In mouse oocytes, Aurora C replaces Aurora B at the interchromatid axis (ICA) and centromeres and also localizes on aMTOCs. Aurora C regulates the loading of condensin, chromosome alignment, correction of erroneous KT-MT attachments, and aMTOC clustering (Balboula and Schindler, 2014; Nguyen et al., 2014; Balboula et al., 2016). Subtle differences in the localizations and catalytic activities of Aurora kinases are imposed by their interacting proteins (Carmena et al., 2009). It remains unclear to what extent the distinct requirements of Aurora kinases in meiotic progression reflect the diversity of their interaction proteins and substrates in different organisms. This is of interest in the context of gene gains and losses during metazoan evolution.

The tunicate, *Oikopleura dioica*, in the sister group to vertebrates, is an emerging model used to study variants in cell cycle regulation (Delsuc et al., 2006; Campsteijn et al., 2012; Ma et al., 2022). It has a compact genome of 70 Mb, accompanied by massive gene losses and lineage-specific gene duplications (Denoeud et al., 2010; Ferrández-Roldán et al., 2021). In contrast to ascidians, appendicularians possess two Aurora kinase homologs. In this study, we assessed the distinct roles of two Aurora kinases during oogenesis in *O. dioica*. We found that Aurora1 regulated microtubule dynamics during meiotic spindle assembly, and Aurora2 was essential for chromosome condensation and meiotic spindle assembly. We also identified some novel interaction proteins for Aurora1, suggesting new avenues for further investigation of the evolutionary trajectory of Aurora kinases in chordates.

Materials and methods

Animal culture and microinjection

Oikopleura dioica culture was carried out as before (Bouquet et al., 2009). dsRNA was synthesized using the T7 RiboMAX™ Express RNAi System (Promega) from a 300–400-bp DNA fragment within the CDS of the target gene as templates. At day 4, females were placed in artificial seawater, removed from their houses, anesthetized in ethyl 3-aminobenzoate methanesulfonate salt (MS-222, 0.125 mg/mL, Sigma), and injected with 400 ng/μL of dsRNA solutions. Shortly before spawning, the injected mature females were individually transferred to artificial seawater in six-well plates coated with 0.1% gelatin. After spawning, oocytes were collected for RT–qPCR or used for phenotypic analyses. Capped Aur1-GFP mRNA was synthesized from a linearized pANZ-OdAur1-GFP fusion construct (IDT) using the mMESSAGE mMACHINE T7 Transcription Kit (Ambion) and was injected into the 1-cell embryos at 400 ng/μL. The injected embryos were collected at 2–8 cell stages for immunostaining using an anti-GFP antibody (AMS Biotechnology, TP401) to detect the localizations of Aurora1.

Antibodies

Primary antibodies include anti-Histone H3-pS10 (Upstate, 06–570), anti-H3-pS28 (Abcam, ab10543), anti-Aurora A (pT288)/Aurora B (pT232)/Aurora C (pT198) (Cell Signaling Technology, D13A11), anti-α-Tubulin (Abcam, ab6161), anti-GFP (AMS Biotechnology, TP401), and anti-His tag (Santa Cruz, sc-8036). Secondary antibodies against rabbit, mouse, or rat IgG (conjugated Alexa Fluor 488, 568 or HRP) were supplied by molecular probes. Primary antibodies were used at 1:100 dilutions, and secondary antibodies were used at 1:300 dilutions for immunofluorescence. Primary and secondary antibodies were used at 1:2000 and 1:5000 dilutions, respectively, in Western blots.

Imaging

Following immunostaining, nuclei were counterstained with 1 μM TO-PRO-3 iodide (Molecular Probes). Fluorescence images were acquired using a Leica SP5 Confocal with 40x/NA1.25 objective. Brightfield images were acquired using a Nikon TE2000-S microscope with 20x/NA0.45 objective. All images were processed using ImageJ.

Protein expression and purification

The coding sequences of OdAur1 or OdAur2 and INbox sequences (residues 493–572) of OdINCENPa were cloned into the first and second cassettes of a bi-cistronic vector pHTvAMP1-SGC (gift from Dr. Jonathan M. Elkins) (Abdul Azeez et al., 2019). The resulting constructs expressed as the complexes of his-tagged Aurora (N-terminal fusion residues:

MGSSHHHHHHSQDPENLYFQGANSSSARLQ for OdAur1 and MGSSHHHHHHSQDPENLYFQGANS for OdAur2) and INboxes with an additional N-terminal methionine. The constructs were transformed into *E. coli* BL21 (DE3)-R3-pRARE2. The resulting colonies were inoculated into the 5-mL SOB media and cultured overnight. These overnight cultures were inoculated into the 1-L SOB media and were grown to OD600 of 0.5 at 37°C. A final concentration of 0.5 mM IPTG was added to induce protein expression, and afterward, the cultures were grown at 20°C overnight. The next day, the bacterial cells were harvested by centrifugation, resuspended in binding buffer (50 mM Tris-HCl pH 7.5, 500 mM NaCl, 20 mM imidazole, 5% glycerol, and protease inhibitor cocktail), and lysed by sonication. After high-speed centrifugation, the supernatant was recovered and passed through a 0.45-μm syringe filter before loading to a column packed with 1 mL of Ni Sepharose resin (GE Healthcare). The resin was washed with an increasing gradient (20 mM–100 mM) of imidazole. The purified proteins were eluted with three bed volumes of 250 mM imidazole and concentrated using an Amicon Ultra-4 10K centrifugal filter device (Millipore). Protein concentrations were determined by the Bradford assay (Thermo Fisher).

Aurora kinase assays

Equal amounts of purified proteins were used in kinase assays with the CycLex Aurora Family Kinase Assay Kit (MBL|Medical & Biological Laboratories), following the manufacturer's instructions. In brief, 10 μL of protein sample and 90 μL of kinase reaction buffer containing 0.125 mM ATP were added to the well that was pre-coated with "Aurora-substrate-1" and were incubated for 30 min at 30°C. After washing the well, 100 μL of HRP-conjugated antibody, recognizing the phosphorylated substrate, was added and incubated for 30 min at 25°C. After another round of washing, 100 μL of chromogenic reagent was added and incubated for 15 min at 25°C. Finally, 100 μL of stop solution was added to terminate the color development reaction. Absorbance was measured at 450 nm with a TECAN microplate reader.

Yeast two-hybrid library screening

Total RNA from mixed samples containing oocytes and early embryos was extracted using the RNAqueous™-Micro Total RNA Isolation Kit (Ambion). A cDNA library was generated and incorporated into the prey vector pGADT7-pla using the all-direct method (Shanghai Biogen Biotechnology Corporation) and then transformed into a yeast strain Y187 following the LiAc transformation procedure (Clontech) and, hereafter, named the prey library as pGADT7-Od-pla. A bait vector pGBKCg containing Aur1 (pGBKCg-Aur1) was transformed into AH109. The autoactivation of the bait vector was tested and confirmed that the bait vector did not activate *HIS3*, *ADE2*, and *LacZ* reporters. Next, prey library cells were incubated with the overnight culture of bait cells for 24 h at 30°C. One aliquot of zygotes was gradient-diluted and plated on SD-TL plates to calculate mating efficiency. The rest were plated on SD-TLH +5 mM 3AT plates and maintained at 30°C for 3–4 days. Positive colonies were further inoculated on SD-TLHA plates to test the *ADE2* reporter. Plasmids were rescued from the colonies that passed both *HIS3* and *ADE2* tests and sequenced. Sequences were blasted against NCBI and OikoBase (http://oikoarrays.biology.uiowa.edu/Oiko/) databases to retrieve their protein identities and mRNA expression profiles at different developmental stages of *O. dioica*.

Results

Identification and functional characterization of Aurora homologs in appendicularians

Appendicularians, also known as larvaceans, include three families: Oikopleuridae, Fritillaridae, and Kowalevskiidae. In the available genome and transcriptome databases of appendicularians, we ran a local tBLASTn search using Aurora ortholog sequences from both invertebrates and vertebrates as queries. We consistently found two Aurora homologs with very significant E-values (2e-066–7e-144) in *Oikopleura dioica*, *Oikopleura albicans*, and *Fritillaria borealis*. Among the vertebrates, phylogenetic trees clearly showed that vertebrate Aurora A formed one orthologous clade. Auroras B and C in mammals and Aurora B in amphibians formed another clade. However, the nodes leading to other invertebrate deuterostomes were not well resolved with high-bootstrap values. The single Aurora observed in amphioxus, hemichordates, and echinoderms was weakly clustered together. Auroras in ascidians have occupied a separate branch. Auroras in appendicularians underwent rapid evolution as witnessed by their long-branch lengths, and they also underwent an independent gene duplication event which generated two lineages: Aurora1 and Aurora2 in *O. dioica*, *O. albicans*, and *F. borealis* (Figure 1A; Supplementary Data S1). OdAur1-capped mRNA with a C-terminal GFP fusion was injected into 1-cell embryos, and the localizations of OdAur1-GFP fusion protein during early embryonic mitoses were analyzed. Aurora1 was localized on centrosomes throughout mitosis. Using a commercial phospho-Aurora antibody that can recognize the phosphorylated forms of both Aurora1 and Aurora2 in *O. dioica*, we assessed the combined signals of the two Aurora kinases. As expected, during early embryonic cleavages, signals were found on centrosomes and chromosomes in prophase and metaphase, and on centrosomes and the central spindle in anaphase (Figure 1B). As such, Aurora2 would occupy the chromosome-central spindle axis. This suggests that Aurora1 and Aurora2 in *O. dioica* represent the polar and equatorial forms of Aurora kinases, respectively, and they are most likely to be functional equivalents of vertebrate Auroras A and B during mitosis.

The expression profiles of the two Aurora kinases during oogenesis were analyzed by RT–qPCR. Their transcripts co-existed during oogenesis, with maximum expression levels at P5 and maturation phases during which nurse nuclei exported RNAs and proteins to rapidly growing pro-oocytes (Figure 1C). Our previous studies have shown that combined Aurora signals were present in meiotic nuclei and organizing centers (OCs) during P3, relocated to selected meiotic nuclei during P4, and enriched toward centromeric regions during prometaphase I. This coincided with the

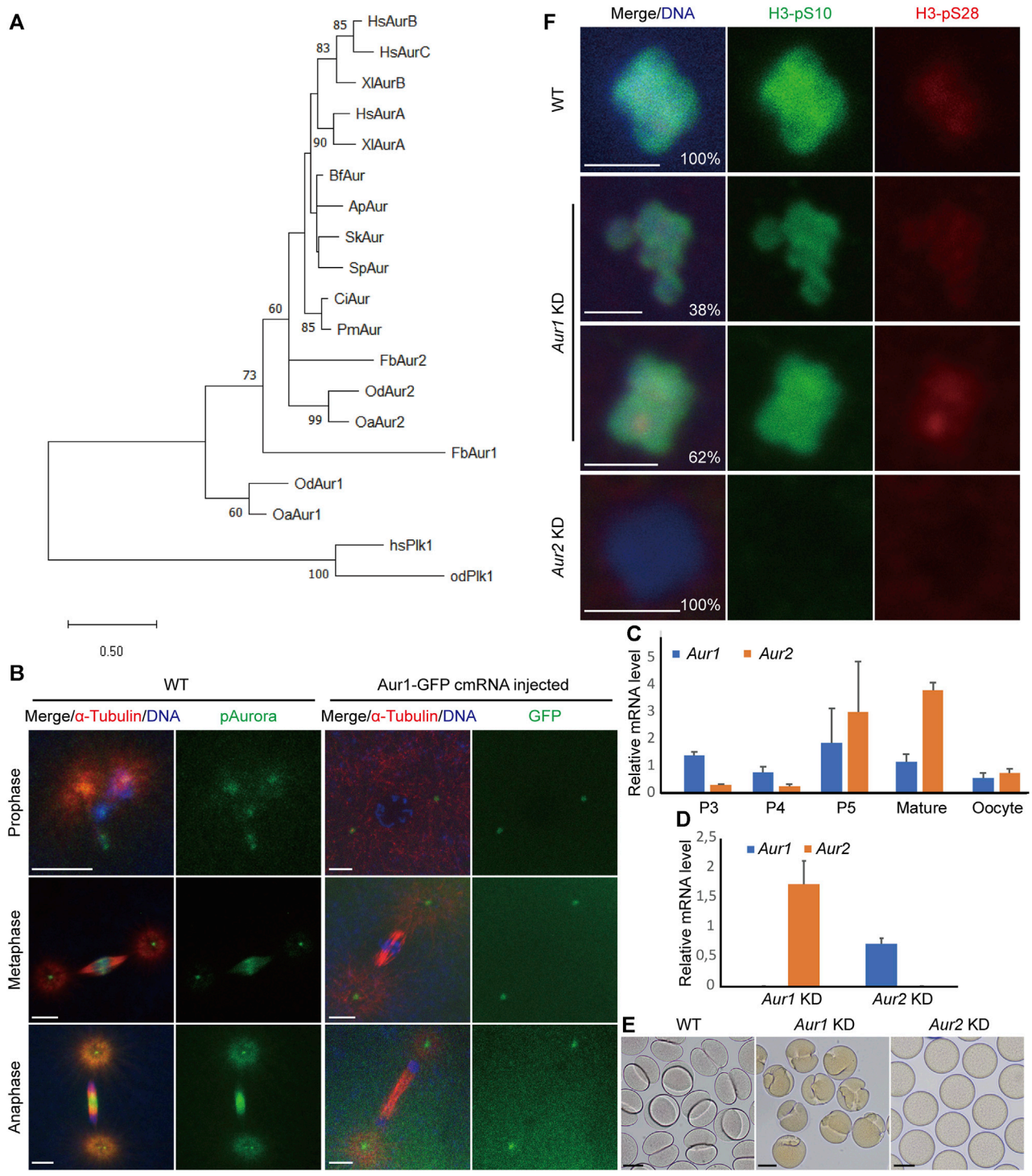

FIGURE 1
Identification, expression profiles, and distinct functions of Aurora1 and Aurora2 kinases during oogenic meiosis in *Oikopleura dioica*. **(A)** Phylogenetic relationships of Aurora kinases of three larvaceans in deuterostomes. The tree was constructed in MEGA11 using the maximum likelihood method based on the alignment of the catalytic domains of Aurora kinases (Supplementary Data S1) (Tamura et al., 2021). An LG + G amino acid substitution model was used in a 1,000-iteration bootstrap test. Only bootstrap percentages >50% are shown on the nodes. Tree was drawn to scale, with branch lengths measured in the expected number of substitutions per site. Plk1 kinases were used as an outgroup to root the tree. The abbreviations of the selected species are as follows: Hs, *Homo sapiens*; Xl, *Xenopus laevis*; Od, *Oikopleura dioica*; Oa, *Oikopleura albicans*; Fb, *Fritillaria borealis*; Ci, *Ciona intestinalis*; Pm, *Phallusia mammillata*; Bf, *Branchiostoma floridae*; Sk, *Saccoglossus kowalevskii*; Ap, *Asterina pectinifera*; and Sp, *Strongylocentrotus purpuratus*. **(B)** Localizations of combined Aurora signals and Aurora1 during embryonic mitoses. Scale bars: 5 μm. **(C)** Relative mRNA levels of *Aur1* and *Aur2* during *O. dioica* oogenesis. Coenocytic oogenesis is subdivided into five phases, P1 to P5 (Ganot et al., 2007). P3 corresponds to pachytene and diplotene, during which the coenocyst grows rapidly. In P4, a subset of pro-oocytes increases in size by cytoplasmic transfer through ring canals and meiotic chromatin condenses. During P5, oocytes attained their full size, and nurse and excess meiotic nuclei underwent apoptosis.
(*Continued*)

FIGURE 1 (Continued)
Subsequently, oocyte maturation is completed, and spawning occurs *via* the rupture of the gonad wall. Mean values normalized to EF1 transcripts are shown with standard error bars (n = 3). **(D)** Knockdown efficiencies of target genes in spawned oocytes were obtained using RT–qPCR after dsRNA-mediated knockdowns of *Aur1* and *Aur2*, respectively. Fold changes of mRNA levels relative to those in wild type are shown with standard error bars (n = 3). **(E)** At 30 min after exposure to wild-type sperm, WT embryos underwent first cleavage (left). *Aur1* KD embryos showed "boxing glove"-like shapes (middle), whereas *Aur2* KD oocytes were non-viable (right). Scale bars: 50 μm. **(F)** Knockdowns of *Aur1* and *Aur2* had distinct effects on histone H3-S10 and H3-S28 phosphorylation on oocyte chromosomes. In WT (top), the H3-pS10 signal was present along the entire chromosomes, and H3-pS28 was enriched at centromeres. In *Aur1* KD (n = 52, middle), although H3-pS10 appeared normal, 38% of oocytes showed faint signals of H3-pS28 spreading along the entire chromosomes, and 62% of oocytes showed enriched signals of H3-pS28 at centromeres. In all *Aur2* KD oocytes (n = 36, bottom), both H3-pS10 and H3-pS28 signals were absent on decondensed chromosomes. Scale bars: 2 μm.

changes of histone H3-S10 and H3-S28 phosphorylation from P3 to P4 in selected meiotic nuclei and acentrosomal spindle assembly during prometaphase I (Øvrebø et al., 2015; Feng and Thompson, 2018).

To explore their potential roles in the aforementioned meiotic features, dsRNA knockdowns (*Aur1* KD or *Aur2* KD) were carried out by gonad injection. Knockdown efficiencies were calculated by RT–qPCR, showing that the mRNAs of target genes dropped to extremely low levels, whereas paralogous genes were not significantly affected (Figure 1D). After exposure to wild-type sperm, some *Aur1* KD oocytes seemed to extrude two polar bodies with normal timing. However, when the first mitotic division started, cleavage furrows emerged from one side of most zygotes and abnormally progressed inwards, appearing as "boxing gloves" at 30 min post-fertilization (Figure 1E). Thereafter, some furrows regressed, whereas others formed one or more furrows from other locations, resulting in two or three cells with unequal sizes or disrupted division axes (Supplementary Figure S1). In contrast, *Aur2* KD oocytes were non-viable, and polar body extrusion was not observed (Figure 1E). We suspect that defective mitotic cleavages in *Aur1* KD might be caused by defects in meiotic progression. We have previously shown that H3-S10 and H3-S28 phosphorylation can indicate the progression of meiosis I. Therefore, we assessed these two histone modifications in *Aur1* KD and *Aur2* KD oocytes (Figure 1F). H3-pS10 was present on the entire chromosomes in all the *Aur1* KD oocytes that have been analyzed, similar to WT, but H3-pS28 was either spread along entire chromosomes in 38% of oocytes or enriched on centromeres in 62% of oocytes. This suggests that Aurora1 is involved in promoting the progression of prometaphase I. In all the *Aur2* KD oocytes, both H3-pS10 and H3-pS28 were absent, and chromosomes were decondensed, reminiscent of *INCENPa* knockdown phenotypes (Feng et al., 2019). This confirms that Aurora2 and INCENPa, as the kinase and scaffold proteins, respectively, in the CPC, are essential for H3-S10 and -S28 phosphorylation and chromosome condensation during oogenic meiosis of *O. dioica*.

Distinct roles of Aurora1 and Aurora2 in regulating acentrosomal spindle assembly

The first meiotic spindle is organized without centrosomes in *O. dioica*, potentially through a chromatin-dependent pathway mainly driven by Aurora kinases. The enrichment of Aurora signals on centromeric regions was concomitant with the establishment of robust microtubules around the chromosomes (Figure 2A). Intriguingly, a variety of defects in meiotic spindle assembly in *Aur1* KD oocytes were observed and classified into 10 categories based on spindle morphology and karyotype (Figure 2B). Among 315 oocytes from six *Aur1* KD females, only 6% had normal-looking spindles. An additional 36% of spindles appeared to be elongated, compact, multi-polar, or rudimentary, with diffuse Aurora signals on most chromosomes. Spindles were absent in the remaining majority, with few, sporadic microtubules in contact with chromosomes. Interestingly, in 6% of oocytes, we also observed homologous chromosomes detached from a partially organized spindle. To assess the extent that these defects can affect chromosome segregation, *Aur1* KD oocytes were fertilized with WT sperm and collected within 5 min post-fertilization to analyze the progression of anaphase I. In WT, Aurora signals relocated to the central spindle and overlapped with fine and robust microtubule fibers which emerged between segregating homologous chromosomes, when thick microtubule fibers at the two poles were degraded (Figure 2A). In contrast, among 245 oocytes from six *Aur1* KD females, 93% of defective spindles were not capable of segregating chromosomes. In rare cases when Aurora signals were enriched on the central spindle and chromosomes managed to segregate, 5% showed less robust microtubule staining in the central spindle, and 2% showed lagging chromosomes along the central spindle (Figure 2C). In all the *Aur2* KD oocytes observed in seven females, neither Aurora signals nor microtubules were detected around decondensed chromosomes (Figure 2D).

In summary, Aurora1 was involved in the enrichment of Aurora2 on centromeres and the regulation of microtubule dynamics to promote acentrosomal spindle assembly that was particularly driven by centromeric Aurora2. The deregulation of Aurora1 can lead to defective chromosome congression during metaphase I and subsequent mis-segregation during anaphase I.

INbox motif of INCENPa activates both Aurora1 and Aurora2

It was observed that Aurora1 can assist Aurora2 in regulating meiotic progression. Then, we assessed whether Aurora1 has any intrinsic enzymatic activity. To make a comparison, the His-tagged full-length proteins of Aurora1 and Aurora2 were expressed and purified in complexes with the INbox motif of INCENPa using a bi-cistronic vector pHTvAMP1-SGC in *E. coli*. Western blot analyses confirmed that the concentrations of purified protein complexes were similar before carrying out the Aurora kinase assay (Figure 3A). Interestingly, *in vitro*, INCENPa activated Aurora1 to similar levels as it activated Aurora2 when provided with a synthetic substrate that

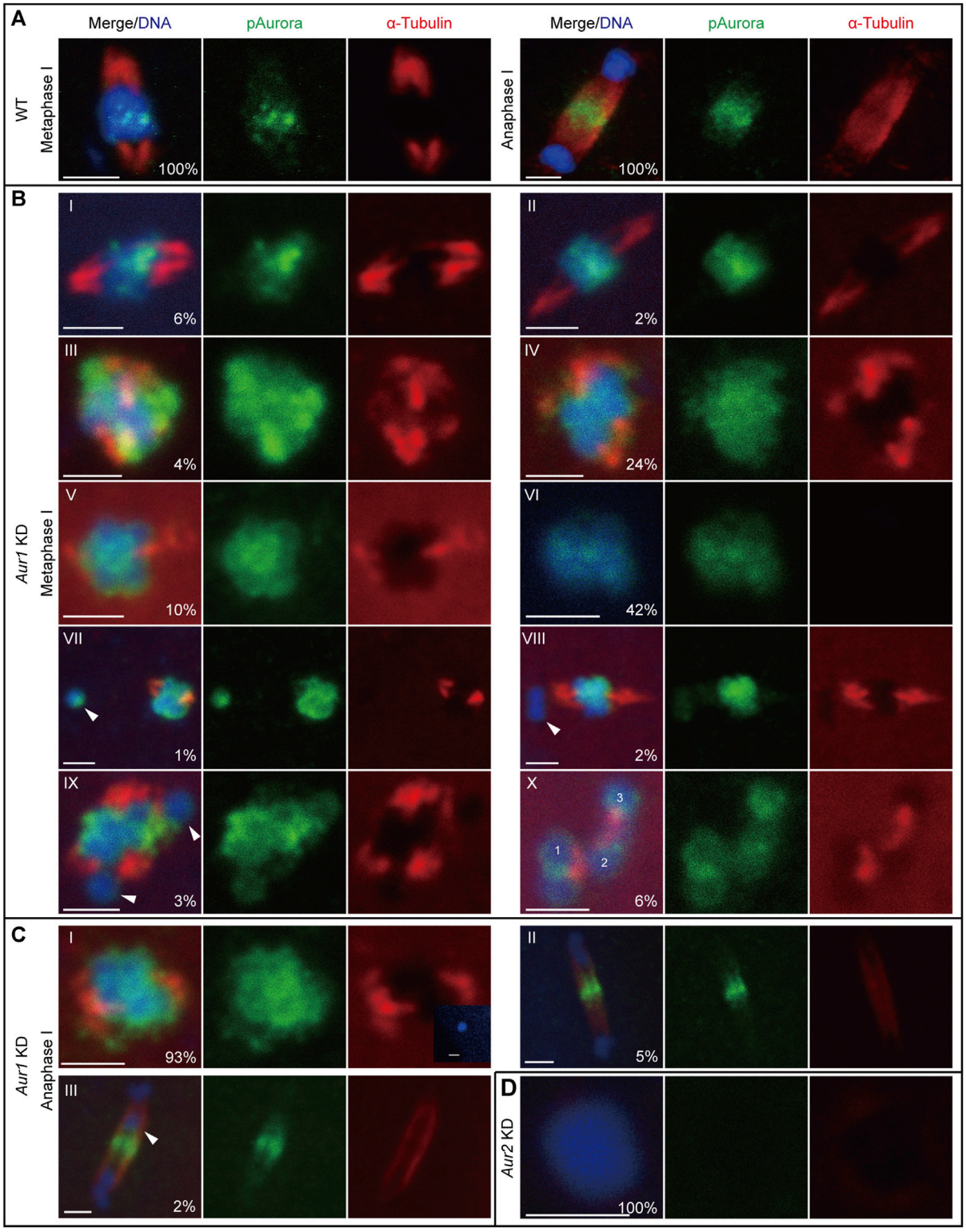

FIGURE 2
Differential requirements of Aurora1 and Aurora2 in meiotic spindle assembly. **(A)** In WT oocytes, phospho-Aurora signals were enriched on centromeres and robust microtubule fibers radiated from opposite poles to form a bipolar spindle at metaphase I (left). During anaphase I (right), phospho-Aurora signals accumulated at the central spindle, and interchromosomal microtubules formed between the two masses of segregating homologous chromosomes. **(B)** *Aur1* KD caused a range of defects in meiotic spindle assembly at metaphase I. These defects were categorized, with proportions labeled in the merge panel (n = 315). (I) 6% showed normal spindles with lengths of 4–5 μm; (II) 2% showed elongated spindles with lengths >6 μm; (III) 4% showed compact spindles with lengths <4 μm, exhibiting delocalized Aurora signals surrounding chromosomes; (IV) 24% showed thick microtubules radiating from opposite poles to form rudimentary spindles; (V) 10% lacked spindles with few microtubules attached to chromosomes; and (VI) 42% lacked spindles and showed no detectable microtubule staining. In categories IV to VI, diffuse Aurora signals were spread along
(*Continued*)

FIGURE 2 (Continued)
chromosomes. In addition, small proportions of defects in homolog chromosome congression were also observed and distributed in the following categories: (VII) 1% showed one homologous chromosome (arrowhead) detached from the spindle; (VIII) 2% showed one bivalent (a pair of homologous chromosomes, arrowhead) detached from the spindle; (IX) 3% showed two separate chromosomes (arrowhead) detached from the spindle, and the spindle seemed to be multi-polar; and (X) 6% showed three separate bivalents with microtubules between them. **(C)** Within 5 min after exposure to WT sperm, the progression of anaphase I in *Aur1* KD oocytes was analyzed (n = 245). (I) 93% showed defective spindles. Insert panel showed a sperm nucleus inside an *Aur1* KD oocyte. (II) 5% showed normal segregating chromosomes with enriched Aurora signals on the central spindle and less robust interchromosomal microtubule fibers. (III) 2% showed lagging chromosomes (arrowhead) along the central spindle. **(D)** In all *Aur2* KD oocytes (n = 26), chromosomes were decondensed, and phospho-Aurora signals and microtubule staining were absent. Scale bars: 2 μm.

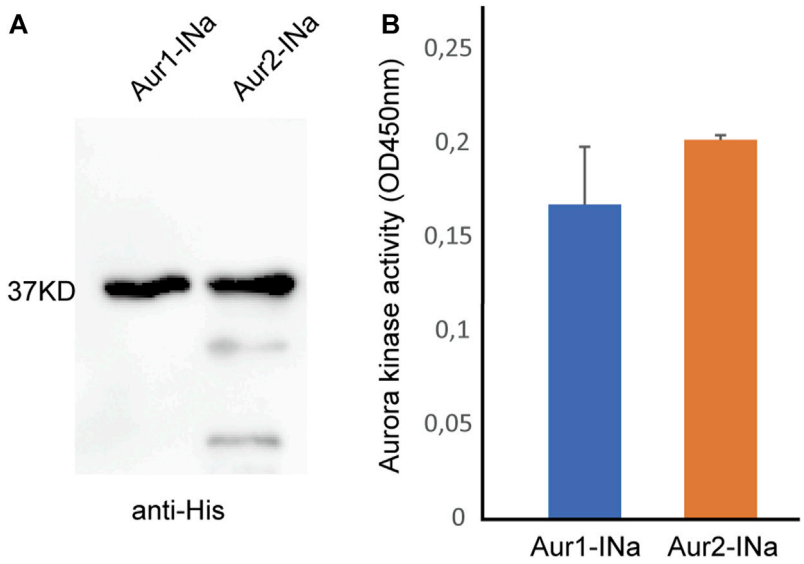

FIGURE 3
Kinase activity assay of Aurora1 or Aurora2 complexed with the INbox motif of INCENPa. **(A)** Western blot of purified Aurora1 and Aurora2 complexed with the INbox of INCENPa (INa) using an anti-His tag antibody. **(B)** INbox motif can stimulate the kinase activities of Aurora1 and Aurora2. Mean values with standard errors were calculated from four independent experiments.

TABLE 1 ***O. dioica*** **Aurora1 interaction proteins identified by a yeast two-hybrid screen.**

Protein name	NCBI accession no.	Expression profile	Function
c-Jun-amino-terminal kinase-interacting protein 4, JIP4	CBY17774.1	All stages	Scaffold protein mediating JNK signaling; spermatozoa–egg interaction; and lysosomal positioning
Nipped-B-like protein, Scc2/Nipbl	GSOIDP00013090001[a]	All stages	Forms Scc2/Scc4 heterodimeric complex that regulates cohesin loading
Mitochondrial carrier homolog 2	CBY22100.1	All stages	Mitochondria fusion
Tetratricopeptide repeat protein 36, Ttc36	CBY23270.1	Tail shift, day 2, testis	Proximal tubule marker in the mouse kidney cortex
Dmx-like protein 1	CBY20658.1	All stages	Contains a large number of WD repeats
Peroxidase-like	CBY07839.1	Somatic cells after the tail shift	Breaks down hydrogen peroxide
Calcium/calmodulin-dependent 3′,5′-cyclic nucleotide phosphodiesterase 1C	CBY23339.1	1hpf; hatched; early tadpole; tail shift; day 1, 2, and 5; and testis	Regulates the intracellular levels of second messengers cAMP and cGMP and controls Ca^{2+} homeostasis
Unnamed protein	CBY11821.1	All stages	—

[a]OikoBase accession number.

contained an Aurora consensus phosphorylation site (Figure 3B). This implies that *O. dioica* Aurora1 is a *bona fide* Aurora kinase and can be activated by a known interaction partner.

Novel interaction proteins of Aurora1 in *O. dioica*

Aurora kinases are organized in regulatory kinase cascades by their interaction/scaffolding proteins that are involved in the activation and spatiotemporal targeting of kinases. Our initial genome-wide search failed to detect TPX2, a microtubule-binding protein that normally localizes Aurora A toward the spindle and the mid-body (Bayliss et al., 2003), implying that the Aurora1-scaffold complement might have changed in *O. dioica*. Considering new interaction proteins of Aurora1, a cDNA prey library (number of independent clones: 9.60×10^6) generated from oocytes and early embryos of *O. dioica* was screened with Aurora1 as bait using a yeast two-hybrid library screening approach. This approach identified eight possible interaction proteins (Table 1). To our knowledge, none of them have been previously reported as Aurora A interaction proteins.

Discussion

O. dioica Aurora1 might have rewired its interaction network

Given the loss of canonical interaction proteins of Aurora A, such as TPX2 in *O. dioica*, it is perhaps not surprising that several new binding partners of Aurora1 may have developed. c-Jun-amino-terminal kinase-interacting protein 4 (JIP4) is the scaffolding protein in the JNK/mitogen-activated protein kinases (MAPK) signaling pathway (Nguyen et al., 2005). JIP4 is involved in the bidirectional transportation of cargos along the microtubules through interaction with kinesin-1 and dynactin/dynein motors (Montagnac et al., 2009). The interface between JIP4 and kinesin-1 lies in the tetratricopeptide repeat (TPR) motif of kinesin-1 light chain (KLC1). Interestingly, we also identified a TPR-containing protein (Ttc36) as an Aurora1 interaction protein. Although Ttc36 is less studied, the TPR motif comprises 3–16 tandem-repeats of 34 amino acid residues and forms an all-helical structure, often mediating protein–protein interactions and cell cycle regulation (D'Andrea and Regan, 2003). Thus, it is tempting to speculate that JIP4 brings Aurora1 in close proximity to microtubule motors, allowing Aurora1 to phosphorylate kinesin-1 or dynactin/dynein subunits and regulate microtubule dynamics. Aurora A phosphorylates dynactin's largest subunit $p150^{glued}$ on its N-terminal microtubule-binding domain (MBD), which regulates the disassociation of the dynactin/dynein complex from the spindle poles after NEBD in *Drosophila* S2 cells (Romé et al., 2010). This phosphorylation is also involved in central spindle assembly at anaphase in human cells (Reboutier et al., 2013). It would be of great interest to test whether Aurora1 regulates microtubule dynamics through the interaction with JIP4.

Scc2/Nipbl regulates the loading of cohesin onto chromatin before the S phase (Mattingly et al., 2022). In addition to cohesin loading, Scc2 can move between cohesin complexes on chromosomes after DNA replication (Rhodes et al., 2017). Its interaction with Aurora1 suggests that Aurora1 might make transient contact with cohesin complexes at crossover sites, where homologous chromosomes are held together, and on centromeres between sister chromatids in meiosis I. Indeed, we observed one or two homologous chromosomes as being detached from the main chromosome mass in a minor proportion of *Aur1* KD oocytes. Further investigation is needed to test whether Aurora1 is involved in the maintenance of cohesion at metaphase I.

Although the function of Aurora in mitochondria is outside the scope of this study, we did identify mitochondrial carrier homolog 2 (MTCH2), a regulator of mitochondrial fusion, as an Aurora1 interaction protein (Bahat et al., 2018). Human Aurora A is transported into mitochondria in the interphase and induces mitochondrial fragmentation (Bertolin et al., 2018). This transport relies on its N-terminal 36 amino acids serving as an atypical mitochondrial targeting sequence (MTS). Once inside the mitochondria, MTS is cleaved off, generating two forms of truncated Aurora A. The N terminal of *O. dioica* Aurora1 is approximately 90 aa shorter than human Aurora A and does not have an MTS motif (Supplementary Data S1). It is possible that MTCH2 might serve as a transporter to import Aurora1 into the mitochondria in *O. dioica*.

It would be of interest to develop specific antibodies for the aforementioned interaction proteins, in order to assess these interactions *in vivo* by Co-IP and colocalization assays. Targeted perturbations would be informative to dissect their roles in the regulation of Aurora1 in more detail.

Evolution of Aurora homologs in appendicularians

Considering their distinct roles in meiotic spindle organization, we argue that the two Aurora kinases co-exist in meiotic nuclei. Aurora1 has opportunities to contact microtubules that are synthesized through an Aurora2-dependent pathway on chromosomes. This proposed pattern is distinct from other invertebrate and vertebrate models reported thus far. Aurora1 in *O. dioica*, or in appendicularians in general, may have evolved to regulate microtubule dynamics during meiotic spindle assembly. The role of *O. dioica* Aurora2 in regulating chromosome condensation and acentrosomal spindle assembly is consistent with the roles in vertebrates. However, a key residue (Gly198 in human Aurora A or Asn142 in human Aurora B) in the catalytic domain that determines the interaction partners, subcellular localizations, and functions of the respective Aurora kinases in vertebrates has been altered to Gly in the two *O. dioica* Aurora kinases (Gly105 in Aurora1 or Gly91 in Aurora2, Supplementary Data S1) (Fu et al., 2009). The two Aurora kinases in *O. dioica* share this feature with the single ancestral Aurora which possesses Gly at the equivalent residue in most invertebrate deuterostomes, social amoeba, and yeast.

A question raised for many years is why independent evolution of Aurora kinases in a few invertebrates has led to a similar functional separation in spindle and chromosome regulations. Although our study cannot definitively respond to this question, we can provide some new insights. As shown in this study, *O. dioica* Aurora1 has substantially changed its interaction proteins and regulated meiotic spindle organization from distinct locations. There is also cross-talk between Aurora1 and Aurora2 in promoting their respective

localizations, along with other signaling cascades that are brought together by novel interaction/scaffolding proteins.

Data availability statement

The datasets presented in this study can be found in online repositories. The names of the repository/repositories and accession number(s) can be found at: https://www.ncbi.nlm.nih.gov/genbank/, SCLG00000000.1 https://www.ncbi.nlm.nih.gov/genbank/, SDII00000000.1.

Ethics statement

This manuscript presents research on animals that do not require ethical approval for their study.

Author contributions

HF: conceptualization, data curation, formal analysis, investigation, methodology, resources, validation, writing–original draft, and writing–review and editing. ET: conceptualization, formal analysis, funding acquisition, project administration, resources, supervision, and writing–review and editing.

Funding

The authors declare financial support was received for the research, authorship, and/or publication of this article. This work was supported by the SARS Centre core budget (EMT).

Acknowledgments

The authors thank Anne E. Aasjord for providing animals from the appendicularian facility and the Chourrout Group at the Michael Sars Centre for access to sequence data from hermaphroditic appendicularian species. They also thank Dr. Jonathan M. Elkins at the University of Oxford for providing the bi-cistronic vector pHTvAMP1-SGC. Yeast two-hybrid library screening was carried out by the Shanghai Biogen Biotechnology Corporation.

Conflict of interest

The authors declare that the research was conducted in the absence of any commercial or financial relationships that could be construed as a potential conflict of interest.

Publisher's note

Supplementary material

The Supplementary Material for this article can be found online at: https://www.frontiersin.org/articles/10.3389/fcell.2023.1323378/full#supplementary-material

References

Abdul Azeez, K. R., Chatterjee, S., Yu, C., Golub, T. R., Sobott, F., and Elkins, J. M. (2019). Structural mechanism of synergistic activation of Aurora kinase B/C by phosphorylated INCENP. *Nat. Commun.* 10, 3166. doi:10.1038/s41467-019-11085-0

Abe, Y., Okumura, E., Hosoya, T., Hirota, T., and Kishimoto, T. (2010). A single starfish Aurora kinase performs the combined functions of Aurora-A and Aurora-B in human cells. *J. Cell Sci.* 123, 3978–3988. doi:10.1242/jcs.076315

Bahat, A., Goldman, A., Zaltsman, Y., Khan, D. H., Halperin, C., Amzallag, E., et al. (2018). MTCH2-mediated mitochondrial fusion drives exit from naïve pluripotency in embryonic stem cells. *Nat. Commun.* 9, 5132. doi:10.1038/s41467-018-07519-w

Balboula, A. Z., Nguyen, A. L., Gentilello, A. S., Quartuccio, S. M., Drutovic, D., Solc, P., et al. (2016). Haspin kinase regulates microtubule-organizing center clustering and stability through Aurora kinase C in mouse oocytes. *J. Cell Sci.* 129, 3648–3660. doi:10.1242/jcs.189340

Balboula, A. Z., and Schindler, K. (2014). Selective disruption of Aurora C kinase reveals distinct functions from Aurora B kinase during meiosis in mouse oocytes. *PLoS Genet.* 10, e1004194. doi:10.1371/journal.pgen.1004194

Bayliss, R., Sardon, T., Vernos, I., and Conti, E. (2003). Structural basis of Aurora-A activation by TPX2 at the mitotic spindle. *Mol. Cell* 12, 851–862. doi:10.1016/S1097-2765(03)00392-7

Bertolin, G., Bulteau, A.-L., Alves-Guerra, M.-C., Burel, A., Lavault, M.-T., Gavard, O., et al. (2018). Aurora kinase A localises to mitochondria to control organelle dynamics and energy production. *Elife* 7, e38111. doi:10.7554/eLife.38111

Blengini, C. S., Ibrahimian, P., Vaskovicova, M., Drutovic, D., Solc, P., and Schindler, K. (2021). Aurora kinase A is essential for meiosis in mouse oocytes. *PLoS Genet.* 17, e1009327. doi:10.1371/journal.pgen.1009327

Bouquet, J.-M., Spriet, E., Troedsson, C., Otterå, H., Chourrout, D., and Thompson, E. M. (2009). Culture optimization for the emergent zooplanktonic model organism *Oikopleura dioica*. *J. Plankton Res.* 31, 359–370. doi:10.1093/plankt/fbn132

Brown, J. R., Koretke, K. K., Birkeland, M. L., Sanseau, P., and Patrick, D. R. (2004). Evolutionary relationships of Aurora kinases: implications for model organism studies and the development of anti-cancer drugs. *BMC Evol. Biol.* 4, 39. doi:10.1186/1471-2148-4-39

Campsteijn, C., Øvrebø, J. I., Karlsen, B. O., and Thompson, E. M. (2012). Expansion of cyclin D and CDK1 paralogs in *Oikopleura dioica*, a chordate employing diverse cell cycle variants. *Mol. Biol. Evol.* 29, 487–502. doi:10.1093/molbev/msr136

Carmena, M., Ruchaud, S., and Earnshaw, W. C. (2009). Making the Auroras glow: regulation of Aurora A and B kinase function by interacting proteins. *Curr. Opin. Cell Biol.* 21, 796–805. doi:10.1016/j.ceb.2009.09.008

D'Andrea, L. D., and Regan, L. (2003). TPR proteins: the versatile helix. *Trends biochem. Sci.* 28, 655–662. doi:10.1016/j.tibs.2003.10.007

Delsuc, F., Brinkmann, H., Chourrout, D., and Philippe, H. (2006). Tunicates and not cephalochordates are the closest living relatives of vertebrates. *Nature* 439, 965–968. doi:10.1038/nature04336

Denoeud, F., Henriet, S., Mungpakdee, S., Aury, J.-M., Da Silva, C., Brinkmann, H., et al. (2010). Plasticity of animal genome architecture unmasked by rapid evolution of a pelagic tunicate. *Science* 330, 1381–1385. doi:10.1126/science.1194167

Divekar, N. S., Davis-Roca, A. C., Zhang, L., Dernburg, A. F., and Wignall, S. M. (2021). A degron-based strategy reveals new insights into Aurora B function in *C. elegans*. *PLoS Genet.* 17, e1009567. doi:10.1371/journal.pgen.1009567

Feng, H., Raasholm, M., Moosmann, A., Campsteijn, C., and Thompson, E. M. (2019). Switching of INCENP paralogs controls transitions in mitotic chromosomal passenger complex functions. *Cell Cycle* 18, 2006–2025. doi:10.1080/15384101.2019.1634954

Feng, H., and Thompson, E. M. (2018). Specialization of CDK1 and cyclin B paralog functions in a coenocystic mode of oogenic meiosis. *Cell Cycle* 17, 1425–1444. doi:10.1080/15384101.2018.1486167

Ferrández-Roldán, A., Fabregà-Torrus, M., Sánchez-Serna, G., Duran-Bello, E., Joaquín-Lluís, M., Bujosa, P., et al. (2021). Cardiopharyngeal deconstruction and ancestral tunicate sessility. *Nature* 599, 431–435. doi:10.1038/s41586-021-04041-w

Fu, J., Bian, M., Liu, J., Jiang, Q., and Zhang, C. (2009). A single amino acid change converts Aurora-A into Aurora-B-like kinase in terms of partner specificity and cellular function. *Proc. Natl. Acad. Sci. U. S. A.* 106, 6939–6944. doi:10.1073/pnas.0900833106

Ganot, P., Kallesøe, T., and Thompson, E. M. (2007). The cytoskeleton organizes germ nuclei with divergent fates and asynchronous cycles in a common cytoplasm during oogenesis in the chordate *Oikopleura*. *Dev. Biol.* 302, 577–590. doi:10.1016/j.ydbio.2006.10.022

Hebras, C., and McDougall, A. (2012). Urochordate ascidians possess a single isoform of Aurora kinase that localizes to the midbody via TPX2 in eggs and cleavage stage embryos. *PLoS One* 7, e45431. doi:10.1371/journal.pone.0045431

Hochegger, H., Hégarat, N., and Pereira-Leal, J. B. (2013). Aurora at the pole and equator: overlapping functions of Aurora kinases in the mitotic spindle. *Open Biol.* 3, 120185. doi:10.1098/rsob.120185

Li, H., Chen, Q., Kaller, M., Nellen, W., Gräf, R., and De Lozanne, A. (2008). *Dictyostelium* Aurora kinase has properties of both Aurora A and Aurora B kinases. *Eukaryot. Cell* 7, 894–905. doi:10.1128/EC.00422-07

Ma, X., Øvrebø, J. I., and Thompson, E. M. (2022). Evolution of CDK1 paralog specializations in a lineage with fast developing planktonic embryos. *Front. Cell Dev. Biol.* 9, 770939. doi:10.3389/fcell.2021.770939

Mattingly, M., Seidel, C., Muñoz, S., Hao, Y., Zhang, Y., Wen, Z., et al. (2022). Mediator recruits the cohesin loader Scc2 to RNA Pol II-transcribed genes and promotes sister chromatid cohesion. *Curr. Biol.* 32, 2884–2896.e6. doi:10.1016/j.cub.2022.05.019

Montagnac, G., Sibarita, J.-B., Loubéry, S., Daviet, L., Romao, M., Raposo, G., et al. (2009). ARF6 interacts with JIP4 to control a motor switch mechanism regulating endosome traffic in cytokinesis. *Curr. Biol.* 19, 184–195. doi:10.1016/j.cub.2008.12.043

Nguyen, A. L., Gentilello, A. S., Balboula, A. Z., Shrivastava, V., Ohring, J., and Schindler, K. (2014). Phosphorylation of threonine 3 on histone H3 by haspin kinase is required for meiosis I in mouse oocytes. *J. Cell Sci.* 127, 5066–5078. doi:10.1242/jcs.158840

Nguyen, A. L., and Schindler, K. (2017). Specialize and divide (twice): functions of three Aurora kinase homologs in mammalian oocyte meiotic maturation. *Trends Genet.* 33, 349–363. doi:10.1016/j.tig.2017.03.005

Nguyen, Q., Lee, C. M., Le, A., and Reddy, E. P. (2005). JLP associates with kinesin light chain 1 through a novel leucine zipper-like domain. *J. Biol. Chem.* 280, 30185–30191. doi:10.1074/jbc.M505499200

Øvrebø, J. I., Campsteijn, C., Kourtesis, I., Hausen, H., Raasholm, M., and Thompson, E. M. (2015). Functional specialization of chordate CDK1 paralogs during oogenic meiosis. *Cell Cycle* 14, 880–893. doi:10.1080/15384101.2015.1006000

Radford, S. J., Jang, J. K., and McKim, K. S. (2012). The chromosomal passenger complex is required for meiotic acentrosomal spindle assembly and chromosome biorientation. *Genetics* 192, 417–429. doi:10.1534/genetics.112.143495

Reboutier, D., Troadec, M.-B., Cremet, J.-Y., Chauvin, L., Guen, V., Salaun, P., et al. (2013). Aurora A is involved in central spindle assembly through phosphorylation of Ser 19 in P150Glued. *J. Cell Biol.* 201, 65–79. doi:10.1083/jcb.201210060

Rhodes, J., Mazza, D., Nasmyth, K., and Uphoff, S. (2017). Scc2/Nipbl hops between chromosomal cohesin rings after loading. *Elife* 6, e30000. doi:10.7554/eLife.30000

Romé, P., Montembault, E., Franck, N., Pascal, A., Glover, D. M., and Giet, R. (2010). Aurora A contributes to $p150^{glued}$ phosphorylation and function during mitosis. *J. Cell Biol.* 189, 651–659. doi:10.1083/jcb.201001144

Sumiyoshi, E., Fukata, Y., Namai, S., and Sugimoto, A. (2015). *Caenorhabditis elegans* Aurora A kinase is required for the formation of spindle microtubules in female meiosis. *Mol. Biol. Cell* 26, 4187–4196. doi:10.1091/mbc.E15-05-0258

Tamura, K., Stecher, G., and Kumar, S. (2021). MEGA11: molecular evolutionary genetics analysis version 11. *Mol. Biol. Evol.* 38, 3022–3027. doi:10.1093/molbev/msab120

frontiers | Frontiers in Ecology and Evolution

TYPE Original Research
PUBLISHED 08 December 2023
DOI 10.3389/fevo.2023.1196859

OPEN ACCESS

EDITED BY
Rosa Maria Sepe,
Anton Dohrn Zoological Station Naples, Italy

REVIEWED BY
Rita Marino,
Anton Dohrn Zoological Station Naples, Italy
Federica Montesanto,
University of Florida, United States

*CORRESPONDENCE
Baruch Rinkevich
buki@ocean.org.il

RECEIVED 30 March 2023
ACCEPTED 06 November 2023
PUBLISHED 08 December 2023

CITATION
Hyams Y, Panov J, Taranenko E, Brodsky L, Rinkevich Y and Rinkevich B (2023) "Keep on rolling": circulating cells in a botryllid ascidian torpor. *Front. Ecol. Evol.* 11:1196859. doi: 10.3389/fevo.2023.1196859

"Keep on rolling": circulating cells in a botryllid ascidian torpor

Yosef Hyams[1,2], Julia Panov[3], Elizaveta Taranenko[3], Leonid Brodsky[3], Yuval Rinkevich[4] and Baruch Rinkevich[1]*

[1]Israel Oceanographic and Limnological Research, National Institute of Oceanography, Haifa, Israel, [2]Marine Biology Department, Leon H. Charney School of Marine Sciences, University of Haifa, Haifa, Israel, [3]Tauber Bioinformatics Research Center, University of Haifa, Haifa, Israel, [4]Comprehensive Pneumology Center, Institute of Lung Biology and Disease, Helmholtz Zentrum Munchen, München, Germany

Hemocytes of the colonial tunicate *Botrylloides leachii* play important roles throughout the animal's life span, including transport and storage of nutrients, respiration, regeneration, budding, sexual reproduction, defense responses, and tunic generation. Nevertheless, very little is known about the involvement of hemocytes or their functions in the remarkable torpor phenomenon characteristic of this species. Changes in water temperature result in rapid and dramatic morphological changes in which the entire colony degenerates, leaving remnants devoid of feeding and reproductive organs that form compacted and opaque masses of lacunae filled with hemocyte cells. Here, we study hemocyte populations in active and hibernating colonies at the morphological, cellular, and molecular levels using histological and transmission electron microscopy observations, primary cell culture observations, and single-cell transcriptomics. This study defines and captures the different cell types in torpor and control stages and further highlights torpor-associated cell types. Multinucleated cells (MNCs) appear only in torpor stages and under *in vitro* conditions and are most likely formed from cell fusions. Bacteria-carrying phagocytes are cells specific to a torpor state with yet unknown function. Single-cell sequencing analysis revealed 14 transcriptionally distinct cell clusters. The hibernating colonies had a low throughput of cells, yet all but two transcriptional clusters were present in hibernating colonies. A comparison of gene expressions in the same cell clusters revealed torpor-specific transcriptional modalities in seven of the cell types. Single-cell sequencing generates an enormous amount of valuable data that can serve researchers in future studies of ascidians and torpor phenomena and provide opportunities for future meta-analysis studies. However, the technical challenges create bottlenecks for the full exploitation of single-cell RNA sequencing (scRNA-seq) data. We developed an interactive, searchable, and intuitive cloud-based database where researchers can easily explore the single-cell transcriptomics data generated by us from active and torpid *B. leachii* colonies. The data can be interrogated and downloaded for further analysis and comparative studies. The Dashboard is available at: http://bleachii.tauberbioinformatics.org/seurat?id=Bleachii-v1. By elucidating hemocyte populations during hibernation, these results provide the basis for future studies of hibernation at the cellular and molecular levels in *B. leachii* and comparative studies of hibernation phenomena in other organisms.

KEYWORDS

***Botrylloides leachii*, hemocytes, torpor, transcriptomics, single cell RNA-seq, cell fusion, multinucleated cells, microbiome**

1 Introduction

Botrylloides aff. leachii (*B. leachii*) are colonial ascidians that reside under rocks in shallow subtidal zones. Each colony consists of genetically identical units, zooids, which are embedded into a semi-translucent gelatinous organic matrix, the tunic. Each zooid has its own heart and hemocoelic circulatory system, which is shared by the whole colony as well as the entire set of zooids and is embedded into a tunic closed by terminal extensions of the vasculature, termed ampullae.

One unique characteristic of ascidians is their remarkable ability to regenerate full-size colonies after a prolonged dormancy state, known as torpor. *B. leachii*, similar to other marine and land-dwelling multicellular organisms, have the ability to enter dormancy states as a response to environmental and biological cues (Hand and Hardewig, 1996; Caceres, 1997; Storey, 2002; Storey, 2010). During dormancy, the organism expresses discreet physiological qualities and behaviors, allowing it to tolerate severe environmental settings through phases of metabolic decline, detained development, and caloric restriction (Storey, 2010). Certain organisms display daily dormancy bouts, while other taxa exhibit seasonal dormancy, termed "hibernation" when developing during the winter months and "aestivation" when taking place throughout summer (Storey and Storey, 2011). While many organisms are able to enter the dormancy state, torpor in *B. leachii* and other colonial ascidians is remarkable. The ascidians are capable of regenerating into a full-size colony from a small fraction intact during dormancy.

Recent studies have shown that torpor in *B. leachii* colonies begins with developmental arrest and is followed by tissue degradation until only remnants of the original size remain (Hyams et al., 2017). During this state, the colony lacks feeding and reproductive organs but is composed of vascular carpets made up of abnormally condensed and twisted masses of lacunae, which are packed with opaque piles of hemocyte cells (Figure 1).

In botryllid ascidians, hemocytes exert a wide range of functions, including transportation and storage of nutrients (Cima et al., 2016), respiration (Ballarin and Cima, 2005), whole-body regeneration (Rinkevich et al., 1995; Rinkevich et al., 2007; Rinkevich et al., 2008), budding (Brunetti, 1976; Voskoboynik et al., 2007; Rinkevich et al., 2013), sexual reproduction (Blanchoud et al., 2018a), defense reactions (Rinkevich and Shapira, 1998; Cima et al., 2016; Ballarin et al., 2021), and tunic generation (Hirose et al., 1995). While *B. leachii* hemocyte compositions and morphologies were investigated previously using cytological, histochemical, and histoenzymatical analyses (Cima et al., 2001; Cima et al., 2016; Blanchoud et al., 2017; Cima, 2022; Zeng et al., 2022), the classification of hemocyte cell types and their functions remains ambiguous (Vanni et al., 2022). The different classification criteria, the lack of unified terminology, the high structural diversity of hemocytes among ascidian species, and poorly documented intermediate stages of differentiation and dissimilarity of identical hemocytes resulting from different fixation methods (Burighel et al., 1997; Cima et al., 2001; Blanchoud et al., 2017) have all contributed to the challenges of cell classification and comparative studies.

Previously, we observed that during torpor, the regular distribution of hemocyte populations is altered, and two new cell types appear (Hyams et al., 2017; Hyams et al., 2022). The multinucleated cells (MNCs), containing 2–11 nuclei each,

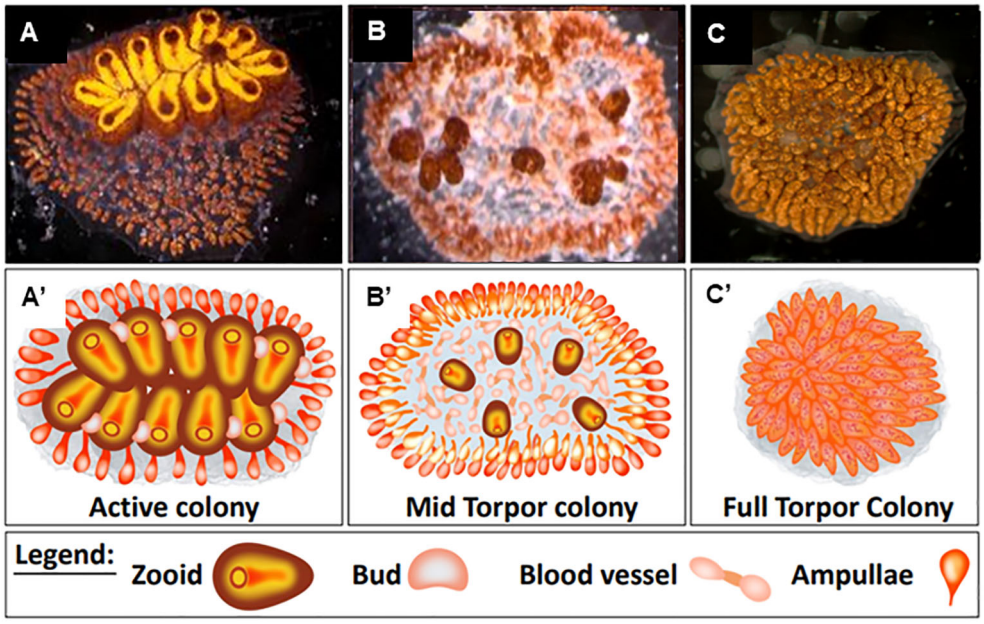

FIGURE 1
Distinct physiological states of *Botrylloides leachii* colony. **(A′–C′)** Schematic illustrations of **(A–C)** physiological states. **(A, A′)** Active colony. All functional zooids are arranged in two parallel chains of colonial systems. Each single zooid contains one functional oral siphon, and 1–4 parallel buds develop on the zooid epithelium walls. **(B, B′)** Mid-torpor colonies, small and less developed round-shaped zooids are detached from each other, and some of the developing buds are further detached from parent zooids. **(C, C′)** Fully torpid colony where the functional zooids and their buds are relapsed within the colony's tunic matrix forming a compacted mass of vasculature. Bars, 2 mm. Illustrations **(A′–C′)** made by Oshrat Ben-Hamo.

express high levels of *Piwi*, a well-characterized and evolutionary conserved stemness marker (Rinkevich et al., 2010), indicating their involvement in the regeneration abilities of *B. leachii*. Thus, we previously suggested that MNCs should be considered as stem cells. Bacteria-bearing phagocytes appeared at full torpor and comprised 1%–5% of the hemolymph cell population. Each cell contained 4–25 bacteria cells sizing 1–2 µm (Hyams et al., 2022).

Furthermore, we previously investigated the gene expression patterns of *B. leachii* colonies during active and torpor states in two colonial compartments, the whole zooid and whole ampullae (Hyams et al., 2022). Our findings showed that gene expression profiles change significantly in the torpor state compared to the active, naive state of the colony in both compartments. Changes in cellular composition during torpor contribute to the observed changes in gene expression profiles. Hemocyte populations have been shown to play a critical role in the ability of *B. leachii* to enter and exit torpor, highlighting the importance of understanding the cellular and molecular changes that occur during this process.

Several methods are available to study cellular populations. To analyze and study morphological structure and characteristics, histological analysis can be used coupled with histochemical staining. Transmission electron microscopy (TEM) is another method of visualizing morphological characteristics coupled with the use of antibodies to highlight proteins of interest. In addition, the development of colonies on the cellular level can be studied in primary cell cultures where the colonies are monitored daily. Finally, single-cell gene expression techniques have been used widely to study complex tissue for identifying transcriptome profiles of different cell populations. In ascidians, single-cell sequencing was previously used to investigate embryonic development (Winkley et al., 2021), as well as the development of the larval nervous system (Sharma et al., 2019).

In this study, we used the above-mentioned techniques to investigate the morphological and physiological changes as well as changes in gene expression patterns in individual cells between active and dormant states of *B. leachii* colonies.

2 Methods

2.1 Animals

Colonies of *B. aff. leachi* (hereby termed *B. leachii*) (Reem et al., 2018) were collected from the undersides of intertidal stones along the Israeli Mediterranean coast at depths ranging from 0.5 to 4 m. The colonies, along with the thin calcareous substrate layer of the stone to which they were attached, were carefully peeled off using industrial razor blades, following the protocol described in Rinkevich et al. (2007). After collection, specimens of *B. leachii* were transported to the seawater system at the National Institute of Oceanography (Haifa). Each colony was then tied onto a single 5 × 7.5 cm glass slide using a thin cotton string. The colonies were maintained in 25-L seawater tanks using established husbandry protocols (Rinkevich and Shapira, 1998). They were fed a varied diet on a daily basis, consisting of commercial powdered plankton, unicellular algae, and freeze-dried rotifers. Within a few days, many of the *B. leachii* specimens had started to glide onto or had completely moved to the glass slides, becoming firmly attached to the glass substrates. All colonies were cleaned once a week using fine brushes and industrial razor blades. Newly developing *B. leachii* colonies were cut by razor blades between systems to form independent fragments (ramets), each containing two to three genetically identical colonial systems (Rinkevich et al., 1996). Each ramet was then transferred to a separate glass slide to allow continual development into a large colony. In this way, 20 genotypes of ramets were developed and underwent further experimental conditioning. The ramets were acclimatized for a period of 2 weeks before any further experimental procedures.

2.2 Experimental assay

The generated 20 genotypes were randomly split into three experimental sets (each set containing at least one ramet of each genotype), reflecting three distinct physiological states: a) “active colonies” cultured in 20°C standing seawater tanks (Figures 1A, A′, n = 10). In these colonies, all functional zooids are arranged in two parallel chains of colonial systems. Each single zooid contains one functional oral siphon, and one to four parallel buds develop on the zooid epithelium walls. b) “Mid torpor” colonies (Hyams et al., 2017) (Figures 1B, B′, n = 10) were cultured for 5 days in 15°C standing seawater tanks. In this state, the zooids become small, round-shaped, and less developed. They detach from each other, and some of the developing buds further detach from the parent zooids. c) “Torpid colonies”, fully hibernating ramets, were maintained for 20 days in 15°C standing seawater tanks (Figures 1C, C′, n = 10). In this state, functional zooids and their buds are relapsed within the colony’s tunic matrix, forming a compacted mass of vasculature. All experimental ramets in the three distinct physiological states were examined daily for morphological changes using a stereomicroscope (Nikon SMZ1000) and photographed using a stereomicroscope camera (Olympus XC 30) to monitor their morphological statuses.

2.3 Histology

Active (n = 6) and torpid (n = 6) ramets were fixed for 1–2 h in Bouin’s solution and dehydrated in a graded series of ethanol and butanol (70%–100%), followed by tissue embedding in paraffin wax. By employing a hand-operated microtome (Leica 2045, Nußloch, Germany), cross serial sections (4–8 µm) were cut. The histological sections were de-waxed and stained with either alum hematoxylin and eosin (H&E) to elucidate morphological details or the reagent Schiff Feulgen reaction to stain DNA (Lillie, 1977).

2.4 Hemocyte characterization along active and torpor states

Histological sections from *B. leachii* colonies in the three distinct physiological states were used for the characterization

ofchanges in hemocyte populations during the transition from active to torpor states: "active" colonies (n = 3), "mid torpor" colonies (n = 6), and "fully torpid" colonies (n = 5). Identifications of the different hemocyte cell populations were performed in an upright microscope (BX-50, Olympus, Hamburg, Germany). Four ampulla sections (10 μm each) from each ramet were photographed through a digital color camera (Olympus DP73, Hamburg, Germany), and the hemocyte populations for each physiological state were documented. Hemocyte descriptions followed the terminologies of Cima et al. (Cima et al., 2001; Cima, 2022), Hirose et al. (2003), and Hyams et al. (2017). The relative abundance of each type of hemocyte was determined by dividing the number of observed cells of a particular type by the total number of cells per square millimeter on the histological slide. Student's t-test was used for statistical analysis.

2.5 Development of primary cell cultures

Whole populations of circulating hemocytes were isolated from the peripheral extended ampullae of six active and six torpid ramets and dispersed among the wells of 96-well plates. The cells were cultured in an incubator as described in Rinkevich and Rabinowitz (1993). Each well was observed under a Nikon inverted phase contrast microscope every day for 30 days. All morphological changes and changes in cell populations were quantified and recorded.

2.6 Transmission electron microscopy

"Active" (n = 4), "mid torpor" (n = 3), and "torpid" (n = 4) ramets were fixed at room temperature in 4% glutaraldehyde (EM grade cat: G 5882, Sigma, Roedermark, Germany), post-fixed in 1% OsO_4 in ddH_2O for 1 h (4°C), then washed (×3) in cold ddH_2O, and inserted for overnight into 1% uranyl acetate diluted in ddH_2O. Dehydration was performed at room temperature in graded ethanol series that included immersion (10 min each) in 50%, 70% and 95%, and then in 100% (×2, 10 min each) and transferred to propylene oxide (PO; 15 min); then, the samples were submerged in 1:1 PO/Epon for 1 h, in 1:2 PO/Epon overnight, and in 100% Epon for 2–3 h. Each ramet was inserted individually in a labeled mold. The mold was filled with 100% Epon and was allowed to polymerize (65°C oven, 24 h). Ultrathin sections (80–90 nm) were cut using an ultramicrotome (Ultracut, Leica) equipped with a diamond knife (Diatome), placed on 300 mesh nickel grids (Polysciences Inc., Warrington, PA, USA), and stained with uranyl acetate and lead citrate. Analyses were performed on a Jeol 1230 TEM at 80 kV. Digital photographs were taken using a Gatan MultiScan 701 camera.

2.7 Immunolocalization in TEM

Colonial ramets were fixed in 4% paraformaldehyde solution (EM grade cat: G 5882, Sigma, Germany) with 0.05% glutaraldehyde in phosphate buffer, washed several times in phosphate-buffered saline (PBS), and embedded into 2.3 M sucrose solution overnight (4°C). Ramets were mounted on pins for cryo-ultramicrotomy and then inserted in liquid nitrogen. Ultrathin cryosections (80–90 nm) were cut using an ultramicrotome machine (Ultracut; Leica) equipped with a diamond knife (Diatome) within a cryo-sectioning chamber. Each individual thawed cryo-section was transferred to a Formvar- and carbon-coated EM grid (Nickel) within a drop of 2.3 M sucrose solution. Non-specific epitopes were blocked with 1% bovine serum albumin (BSA) in PBS (1 h), and sections were then incubated with rabbit anti-*Bl-Piwi* antibodies (2 h, room temperature; Bl-Piwi2: rabbit polyclonal anti-*B. leachii* 1:4,000, Genemed Synthesis Inc., San Antonio, TX, USA) developed in the lab (Rinkevich et al., 2010), followed by incubation (1 h) with protein A gold conjugates (15-nm gold particles). The ultrathin sections were then counterstained (10 min on ice) using 0.5% uranyl acetate in 2% methylcellulose. Immunogold-labeled sections were analyzed in a Jeol 1230 TEM at 80 kV. Digital photographs were taken using a Gatan MultiScan 701 camera. For negative controls, the same protocol as above was used without the primary antibody.

2.8 Single-cell RNA sequencing

Whole hemocyte cells were extracted by puncturing marginal ampullae with a needle (27G) according to the established technique (Rinkevich et al., 2010). The cells of each sample were collected in a 1.5-ml tube, and the number of cells was estimated using a hemocytometer under the microscope. The number of hemocytes was diluted in different samples in order to start with a similar number of cells. Assays were prepared following the Drop-seq protocol (Bageritz and Raddi, 2019). Single cells (100/μl) from hemocyte suspensions of active (n = 3) and torpid (n = 2) colonies were inserted in a droplet containing barcoded beads (120/μl, ChemGenes Corporation, Wilmington, MA, USA) using a microfluidic polydimethylsiloxane device (Nanoshift) at rates of 4,000 μl/h for 15 min each colony. Droplet breakage was then performed using perfluoro octanol (Sigma-Aldrich). Beads were harvested, the hybridized mRNA transcripts were reverse transcribed (Maxima RT, Thermo Fisher, Waltham, MA, USA) and the left primers were digested by exonuclease I (New England Biolabs, Ipswich, MA, USA). After that, the beads were washed, counted, and aliquoted for pre-amplification (2,000 beads/reaction, equals ~100 cells/reaction) using a polymerase chain reaction (PCR) solution (12 cycles; primer: AAGCAGTGGTATCAACGCAGAGT [100 μM], 2× KAPA HiFi Hotstart Readymix [KAPA Biosystems, Woburn, MA, USA]). Cycle conditions: 3 min 95°C, 4 cycles of 20 s 98°C, 45 s 65°C, 3 min 72°C, followed by 8 cycles of 20 s 98°C, 20 s 67°C, 3 min 72°C, and then 5 min at 72°C. The PCR products of all individual cells from each sample were pooled together and purified (×2) by 0.6× clean-up beads (CleanNA, Waddinxveen, Netherlands), according to the manufacturer's instructions. The cDNA quality of pooled samples (n = 5) was employed using Bioanalyzer High Sensitivity DNA Analysis (Agilent, Santa Clara, CA, USA). Then, 1 ng of pre-amplified cDNA from the estimated 1,000 cells in each sample was tagged by Nextera

XT (Illumina, San Diego, CA, USA) with a custom P5 primer (Integrated DNA Technologies, Coralville, IA, USA). Single-cell libraries were sequenced in a 100-bp paired-end run on the Illumina HiSeq4000 using a 0.2 nM denatured sample and 5% PhiX spike-in. For read 1 priming, 0.5 μM Read1CustSeqB (primer sequence: GCCTGTCCGCGGAAGCAGTGGTATCAACGCAGAGTAC) was used.

2.9 Bioinformatics data analyses of scRNA-seq

Reads were mapped to the *B. leachii* reference genome (Blanchoud et al., 2018b) using a Drop-seq alignment pipeline with default parameters (https://github.com/broadinstitute/Drop-seq). The resulting raw expression tables were further analyzed using the Seurat R package (Satija et al., 2015). Due to very low unique molecular identifier (UMI) counts, it was decided not to filter any low-expressing cells in the torpor colonies. The gene expressions across all samples were normalized, and variable genes were selected using the Seurat package (Shalek et al., 2014). Principal component analysis (PCA) was performed on variable genes only. A total of 50 first principal components were used for the non-linear dimensionality reduction using the UMAP algorithm (McInnes et al., 2018). UMAP was performed with default parameters. To eliminate the batch effect after merging the cells from the active and torpid colonies, the Harmony algorithm was utilized (Korsunsky et al., 2019). The clustering of cells in the merged and batch-corrected data was performed using the Seurat implementation of the Louvain algorithm with default parameters (Satija et al., 2015).

To identify the markers of cell clusters, all genes with low variability across clusters were first filtered out. Next, using Seurat's built-in function "FindMarkers", marker genes were assigned for each of the identified clusters of cells. The function compares the expression of genes in cells of a cluster to its expression in all other cells and identifies a gene as a marker for the cluster if the gene's expression has a log2 Fold Change > 1 and a p-value <0.05 using a Wilcoxon rank sum test. Annotation of marker genes was performed using the Aniseed database (Dardaillon et al., 2020) and BLASTx (Boratyn et al., 2013) alignment of sequences converted to protein sequences on all ascidian proteins. Overall functional annotation of the collection of all marker genes for each cluster was performed using the overrepresentation of Gene Ontology (GO) terms based on the ontological data from the Aniseed database (Dardaillon et al., 2020).

The density of expression for each cluster was calculated following Petegrosso and colleagues (Petegrosso et al., 2019). The density of expression was taken as a proxy of the overall activity of the cell cluster and calculated as the sum of expressions of all genes in the cells within a cluster divided by the number of cells in the cluster. Differential gene expression was inferred using the built-in Seurat "FindMarkers" function utilizing the Wilcoxon rank sum test for each cluster separately between active and torpid colonies. The threshold for significance was set as an adjusted p-value <0.05. Genes were annotated using the Aniseed GO terms database (Dardaillon et al., 2020).

All the obtained results have been effectively integrated into an intuitive and interactive Dashboard, providing users with seamless access and a user-friendly interface for convenient referencing and exploration. The Dashboard allows for effortless navigation through the various findings, enabling users to visualize and interpret the data in a comprehensive and efficient manner. Its user-friendly design ensures that accessing and exploring the results are both intuitive and straightforward. The Dashboard can be accessed at the following URL: http://bleachii.tauberbioinformatics.org/seurat?id=Bleachii-v1.

3 Results

The hemocyte populations in naive (active) colonies of *B. leachii* have been previously characterized by us and other laboratories (Rinkevich and Rabinowitz, 1993; Cima et al., 2001; Hirose et al., 2003; Blanchoud et al., 2017; Hyams et al., 2017; Jiménez-Merino et al., 2019; Cima, 2022; Hyams et al., 2022). Furthermore, we previously reported on cellular changes in torpid colonies, including the presence of two cell types that are almost unique to the torpor state: MNCs and bacteria-bearing cells (Hyams et al., 2017; Hyams et al., 2022). In this study, we utilized multiple imaging and sequencing techniques to systematically observe changes in the cellular composition of *B. leachii* colonies in both active and torpid states.

3.1 Morphological observations of *B. leachii* hemocytes in active and torpid colonies

As a first step toward understanding the cellular changes of *B. leachii* colonies in torpor conditions, the hematological properties of active and torpid *B. leachii* colonies were characterized. Hemocytes were collected from ampullae of *B. leachii* colonies under the stereomicroscope, and nine cell types were identified in histological sections. Figure 2 and Table 1 show the nine main types of hemocytes observed in active and torpid colonies of *B. leachii*. Hemoblasts are small, mostly spherical 3–5-μm cells with a high nucleocytoplasmic ratio. The nucleus is round and 2–3 μm in size and occupies most of the cell volume with a central nucleolus, often unrecognizable (Figure 2A). The cytoplasm of the observed cells is basophilic, indicating active biosynthesis. It forms a thin, homogeneous peripheral layer and occasionally exhibits small pseudopodia. MNCs are cells that appear mostly in the torpor state. These cells are spherical and 7–30 μm in size, with a diverse number of nuclei (2–10) that are 2 μm each (Figure 2B). Hyaline amebocytes have diverse ameboid shapes and vary in size, 8–25 μm.

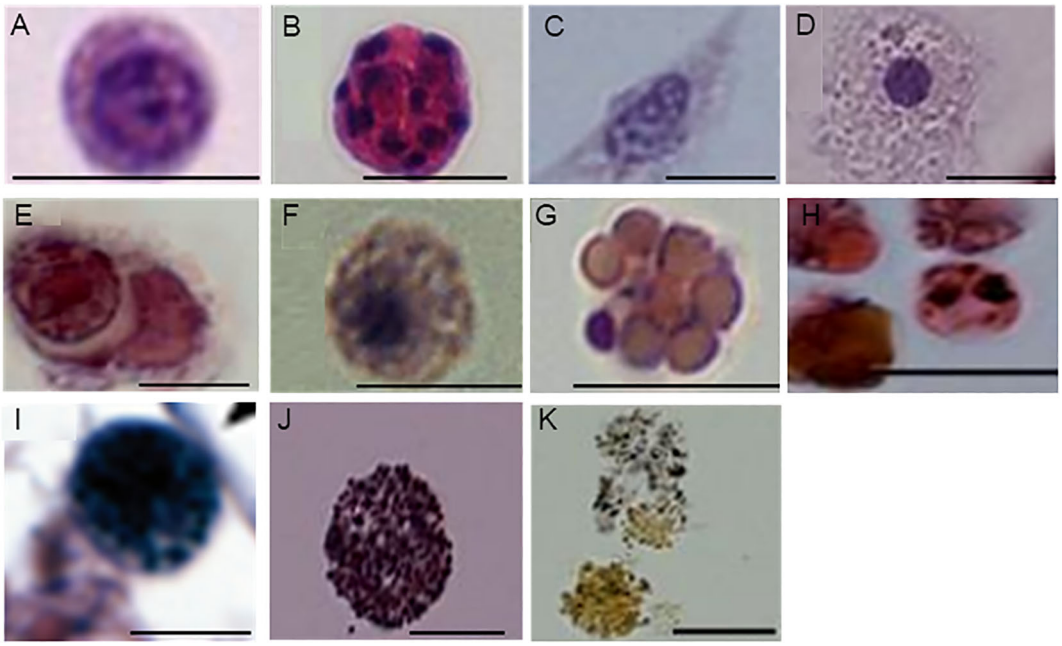

FIGURE 2
Characterization of *Botrylloides leachii* hemocytes. **(A)** Hemoblasts: characterized by a large nucleus, the associated nucleolus, and thin layer of cytoplasm. **(B)** Multinucleated cell (MNC): exhibits 10 nuclei. **(C, D)** Hyaline amebocytes: two representative types. **(C)** Hyaline amebocytes: filopodial cytoplasm, oval grainy nucleus. **(D)** Hyaline amebocytes: spreading cytoplasm that contains clear vacuoles and a spherical nucleus. **(E)** Macrophage-like cells: variable appearance of engulfed material, an elliptic peripheral nucleus (arrows). **(F)** Granular amebocyte: characterized by homogeneous granules and a small spherical nucleus. **(G)** Compartment cell: contains diverse vacuoles and a small peripheral nucleus. **(H)** Morula cells: contain vacuoles and granules in the cytoplasm with various contents. **(I)** Pigment cell: features micro-grainy cytoplasm with granules of different sizes. **(J, K)** Nephrocytes: bright granules, varying in color from brown to yellow. Bars, 10 μm.

The cells often have a fusiform shape (Figures 2C, D). The cytoplasm contains granules (Figure 2C) and/or spherical vacuoles (Figure 2D) and carries lamellipodia and/or filopodia. The nucleus is large, 3–4 μm in size, and spherical or oval and looks grainy due to its highly basophilic content. Macrophage-like cells are large ameboid phagocytes, 10 μm to 25 μm in size, and spherical or oval when empty, mostly with engulfed heterogeneous material that occupies most of the cell volume (Figure 2E). Sometimes, granules and vacuoles are seen. Color morphs: black, brown, yellow colors, orange, pink, red, and blue. The nucleus is elliptic, 3 μm in size, and positioned at the periphery of the cell. Granular amebocyte is an ameboid cell, round or oval in shape, and 5–7 μm in size. These cells contain homogenous granules in the cytoplasm, which are stained gray by alum H&E stain. The nucleus is smooth, round, and 1–2 μm in size and may appear at any position within the cell (Figure 2F). Compartment cells contain clear compartments stained in pink and orange (Figure 2G). The nucleus is smooth and 1 μm in size and may appear in any part of the cell. Morula cells are mostly spherical cells and 8–10 μm in size. The cytoplasm is eosinophilic containing diverse vacuoles and granules, which are stained as pink, orange, and red with black and brown color morphs. The nucleus is located at the periphery and is hardly recognizable (Figure 2H). Pigment cells are spherical, grainy cells and 8 to 13 μm in size containing brown granules (Figure 2I). The nucleus is round, smooth, and 2 μm in size and may appear in any part of the cell. Nephrocytes are very similar to pigment cells with lighter brownish (Figure 2J) or yellow granules (Figure 2K).

3.2 Hemocyte cell type population changes under torpor conditions

We next systematically evaluated four distinct types of cells, namely, hemoblasts, multinucleated cells, macrophage-like cells, and vacuolated cells, in active, mid-torpor, and fully torpid colonies of *B. leachii*. The mid-torpor phase represents the period when the colony is under physiological stress and enters the torpor state (see Methods).

To monitor variations in cell numbers across different physiological states, we selected three *B. leachii* colonies with distinct genotypes. We induced morphological and physiological changes in each colony corresponding to the active, mid-torpor, and full-torpor states using experimental conditioning (see Methods). For each colony and in each of the three states, we randomly selected and examined five ampullae to determine the number of cells of each of the aforementioned cell types. Cells were counted in the H&E-stained histological sections. Figure 3 presents the changes in the distribution of cell number per square millimeter of histological slide across the three physiological states (Supplementary Table 1).

We observed a significant decline in the number of hemoblast cells during the torpor state. Initially, the hemoblasts accounted for

10.3389/fevo.2023.1196859

TABLE 1 Hemocyte populations and their characteristics in *Botrylloides leachii* active and hibernating colonies.

Cell type	Characteristics	Observed in active colony	Observed in torpor colony
Hemoblasts	Small, mostly spherical 3–5 µm cells with high nucleocytoplasmic ratio. The nucleus is round and 2–3 µm in size and occupies most of the cell volume with central nucleolus, often recognizable.	Yes	Low amount
Hyaline amebocytes	Diverse ameboid shapes and vary in size, 8–25 µm. The cells are often fusiform-shaped. The cytoplasm contains granules and/or spherical vacuoles and carries lamellipodia and/or filopodia. The nucleus is large, 3–4 µm in size, spherical or oval, and looks grainy.	Yes	Yes
Macrophage-like cells	Large ameboid phagocytes, 10 µm to 25 µm in size. Spherical or oval when empty, mostly with engulfed heterogeneous material that occupies most of the cell volume.	Yes	High amount
Granular amebocyte	Round or oval in shape, 5–7 µm in size. The cells contain homogenous granules in the cytoplasm, which are stained gray. The nucleus is smooth, round, and 1–2 µm in size and may appear at any position within the cell.	Yes	Yes
Compartment cells	Contains clear compartments staining in pink and orange. The nucleus is smooth and 1 µm in size and may appear in any part of the cell.	Yes	Yes
Morula cells	Cells are mostly spherical and 8–10 µm in size. The cytoplasm is eosinophilic containing diverse vacuoles and granules, which are stained as pink, orange, and red with black and brown color morphs.	Yes	Yes
Pigment cells	Spherical, grainy cells, 8–13 µm in size, containing brown granules. The nucleus is round, smooth, and 2 µm in size and may appear in any part of the cell.	Yes	High amount
Nephrocyte	Cells have very similar features to pigment cells; however, their granules are lighter brownish and yellow.	Yes	High amount
Multinucleated cells (MNCs)	Giant cell 10–30 µm in size containing 2–15 nuclei under the same membrane.	Barely	Yes

approximately 14% of all cells in active colonies. However, their population gradually decreased to approximately 2% during the mid-torpor state and further plummeted to a mere 0.5% of the entire cell population during full torpor (Figure 3; Supplementary Table 1).

Conversely, the number of multinucleated cells exhibited an increase during the mid-torpor and torpor states. These cells were rarely observed in active colonies, constituting less than 0.5% of all observed cells. In contrast, they accounted for over 6% of the cell population in mid-torpor colonies. The number of MNCs slightly declined during full torpor, representing 5% of all observed cells (Figure 3; Supplementary Table 1).

Phagocytes were observed as one of the most abundant cell types in active colonies, comprising more than 18% of the total cell population. Similarly, in mid-torpid colonies, the frequency of phagocytes remained high, constituting 15% of all cells. However, a significant decline in the number of phagocyte cells was observed in torpid colonies, where they accounted for less than 5% of the entire cell population (Figure 3; Supplementary Table 1).

The prevalence of vacuolated cells, which include pigment cells and nephrocyte cells, increased during the torpor state; however, the increase was not statistically significant due to high variation between the observations. Initially, vacuolated cells accounted for just over 32% of all observed cells in active colonies. During the mid-torpor phase, the proportion of vacuolated cells rose to 37%, and in the torpor state, these cells constituted almost 40% of all observed cells (Figure 3; Supplementary Table 1).

3.3 Primary cell cultures

We further validated our histological observations of live active and torpid *B. leachii* colonies using the primary cell cultures of circulating hemocyte cells from active (n = 6) and torpid (n = 6) ramets. We incubated cell cultures derived from both active and torpid colonies under similar conditions (see Methods) and observed them daily for a period of 30 days. By monitoring the cell cultures over time, we were able to investigate the changes that cell cultures from two distinct physiological conditions underwent

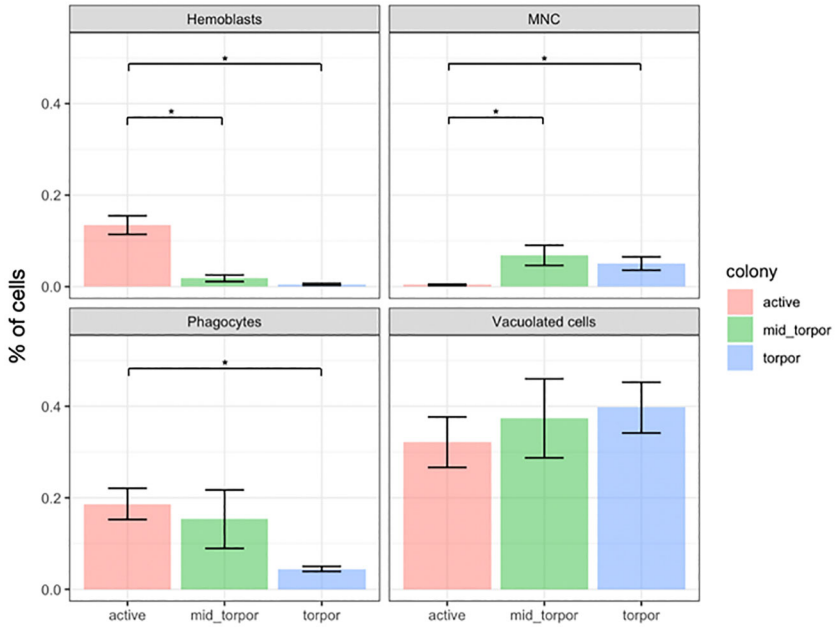

FIGURE 3
Cell frequency variations across physiological states in *Botrylloides leachii* colonies. Changes in percent of four types of hemocytes across three physiological states of *B. leachii* colonies. The number of cells was calculated per square millimeter of histological slide. Asterisk (*) indicates significant change (p-value <0.05) in cell number between physiological states as calculated by Student's t-test.

and assess the effects of these conditions on the cellular behavior of *B. leachii*.

Our observations of the cell cultures from active and torpid colonies at day 0 were consistent with our histological observations of the colonies. Cell cultures prepared from active colonies were dominated by vacuolated cells and hemoblasts with sizes ranging from 3 to 15 μm. At this stage (day 0), MNCs were rarely observed in the active colony cultures (Figure 4A). However, the cell cultures of the hibernating colony at day 0 were dominated by hemocytes with sizes ranging from 8 to 30 μm, with vacuolated cells and MNCs being the most common types (Figures 4D, D1, D2) and hemoblasts being rare. The primary cultures from the hibernating colonies containing many MNCs remained stable over the course of the experimental procedure (30 days) with no significant cellular changes (Figures 4E, F). The cell cultures from active colonies underwent cellular changes during the experiment. On day 3, we observed the initiation of cell aggregations, with 3–25 cells per cell aggregate (Figures 4B, C, cell aggregates are denoted by arrowheads). The cell aggregates became more frequent with the passage of time.

3.4 Ultrastructural analysis of cells unique to the torpor state

To reveal the ultrastructure of cells unique to the torpor state (MNCs and bacteria-bearing cells), we utilized TEM, a high-resolution imaging technique that allows for the visualization of internal cellular structures in great detail.

TEM observations and immunostaining of *Piwi* were performed on two types of MNC morphs and bacteria-carrying cells. The first type of MNC morph denoted by Morph-1 (Figure 5A) is characterized by large cells (10–20 μm), each containing a large vacuole (8 μm in diameter) enclosed within a thin layer of cytoplasm. Each large vacuole typically contained three to eight separated nuclei, each 2 μm, and Golgi (Figure 5A′; nuclei and Golgi bodies are denoted by "nu" for nucleus and "go" for Golgi). An additional separate nucleus (2 μm) that features scattered chromatins (Figure 5A, red arrowhead) and several mitochondria was also observed in Morph-1 MNCs. The second type of MNC morph, denoted by Morph-2 (Figure 5B), has large cells (10–18 μm), multiple vacuoles (5–8 μm each) surrounded by a thin peripheral cytoplasmic layer, and several mitochondria (Figure 5B; mitochondria are denoted by "mt"). Cells of both MNC subpopulations (Morph-1 and Morph-2) expressed *Piwi* stemness marker in all nuclei (Figures 5C–C′). In addition, bacteria-carrying cells were observed in torpid colonies (Figure 5D). These cells were 10–30 μm in size, and each contained 5 to 15 intact bacterial cells.

3.5 Single-cell sequencing

To further characterize the different types of hemocytes in active and torpid colonies of *B. leachii*, we utilized Drop-seq single-cell sequencing technology. Single-cell sequencing allows for the identification of gene expression profiles for individual cells, enabling the differentiation of cell types and subtypes within a heterogeneous tissue.

Whole hemocyte cells from three active and two torpid colonies were extracted from the marginal ampullae and collected in a cell suspension (see Methods). The number of cells was estimated using

10.3389/fevo.2023.1196859

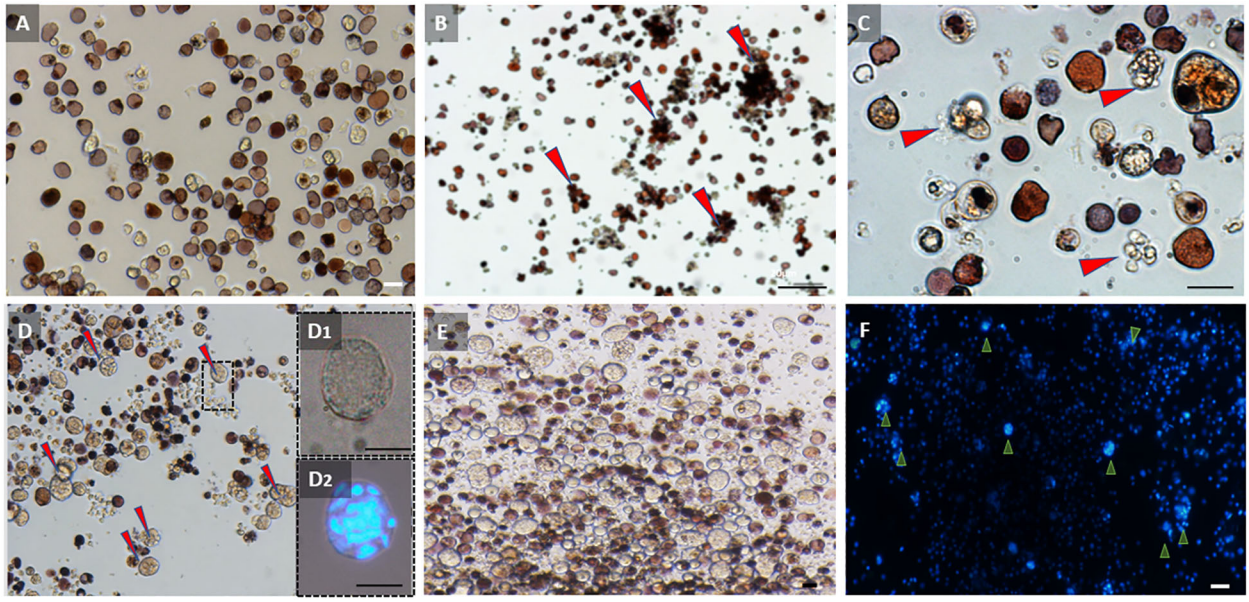

FIGURE 4
Observations of primary cultures of hemocytes from active and torpid *Botrylloides leachii* colonies. **(A)** Hemocytes from an active colony immediately following cell extractions (day 0). Most abundant cells are hemoblasts and vacuolated cells. **(B)** Hemocytes from an active colony 3 days after *in vitro* conditions. Hemocytes begin to aggregate into closely located bundles (red arrowheads). **(C)** Hemoblast aggregations (red arrowheads) from the active colony, 3 days following isolation. **(D)** Hemocytes from torpor colony immediately following cell extractions (day 0). Many multinucleated cells (MNCs) are observed (red arrowheads). (D1) Multinucleated cells (MNCs) in hibernating colony immediately after cell extractions (day 0). (D2) Multinucleated cells (MNCs) immediately after cell extraction (day 0) stained with DAPI. **(E)** Hemocyte cell distribution in torpid colony at day 20 under *in vitro* conditions. Numerous multinucleated cells (MNCs) can be observed, with no significant alterations in cell populations compared to torpid colonies at day 0. **(F)** Hemocyte cell distribution in torpid colony at day 20 under *in vitro* conditions. DAPI-stained image highlighting the presence of numerous multinucleated cells (MNCs) in the observed population (indicated by arrowheads). Bars, 10 µm.

a hemocytometer under a microscope, and samples were diluted in order to initiate the sequencing with a similar number of cells. The cell suspensions were then sequenced using Drop-seq technology (see Methods).

Raw sequencing reads from each active and torpid colony were aligned to the *B. leachii* genome (Blanchoud et al., 2018b), and the number of cells in each colony and the amount of expressed genes in each cell were quantified. It was found that hibernating colonies

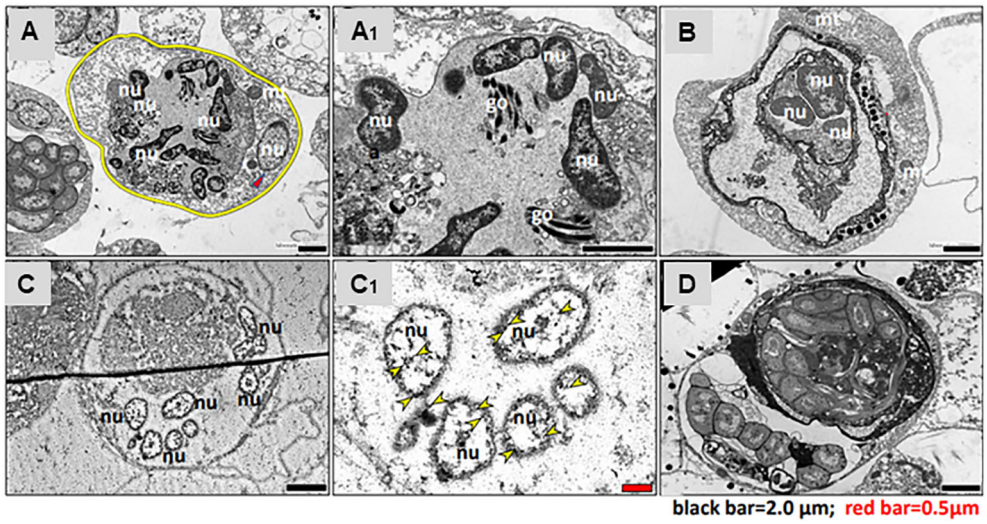

FIGURE 5
Transmission electron microscopy of torpor-specific hemocytes. **(A)** MNC Morph-1: the cell membrane, highlighted with a yellow circle, contains nine nuclei (nu) and a Golgi apparatus (go). (A1) Close-up view of MNC Morph-1, similar to panel **(A)**, showing detailed structure. **(B)** MNC Morph-2: the cell contains three nuclei (nu) and two mitochondria (mt). **(C)** Immunostaining of MNCs for *Piwi*: the cell comprises six nuclei (nu), with each nucleus expressing *Piwi* protein. (C1) Immunostaining of MNC for *Piwi*, similar to panel **(C)**; *Piwi* is indicated by yellow arrowheads. **(D)** Bacteria-bearing cell: the main part of cellular cytoplasm is populated with intact bacteria cells. nu, nuclei; go, Golgi; mt, mitochondria.

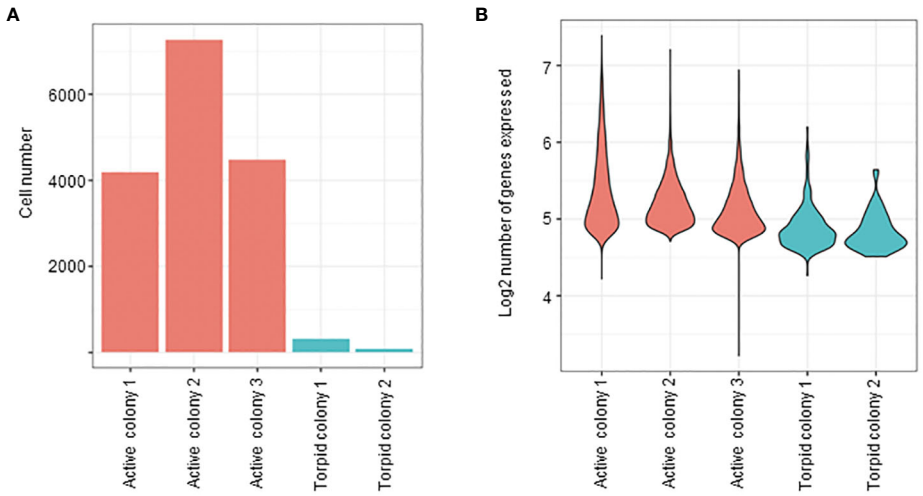

FIGURE 6
Cell abundances based on single-cell analysis. **(A)** Bar plot representing the number of cells in both active and hibernating colonies. **(B)** Violin plots illustrating the distribution of genes per cell (on logarithmic scale) in both active and torpid colonies. The width of the violins represents the density of the gene expression values, with wider sections indicating higher density.

had very low throughput of successfully sequenced cells (Figure 6A). In addition, even when a cell was successfully sequenced, the number of expressed genes in cells of torpid colonies was significantly lower than the number of expressed genes in cells of active colonies (Figure 6B).

Raw expression values across all cells from all colonies were normalized, and cells were embedded into two-dimensional space using UMAP (McInnes et al., 2018), a non-linear embedding algorithm (Figures 7A, B). Each point on the UMAP plot represents a single cell, and the distances between points represent similarities in gene expression across the entire transcriptome. The clustering of the cells was performed separately, and clusters were overimposed on the UMAP (seen as different colors of dots on the UMAP in Figures 7A, B). The distinct clusters represent different cell types with their own distinct transcriptional states. A total of 14 distinct cell clusters were identified in the hemocytes of *B. leachii*. The active colonies expressed cells from all 14 cell clusters, while two of these cell clusters (clusters 11 and 12) were not observed in the torpid colonies (Figures 7C, D).

We next proceeded to identify marker genes for each of the cell clusters, genes that are highly expressed in one cluster and are almost not expressed in cells of all other clusters. We identified several marker genes for each cluster, as detailed in Supplementary Table 2. However, it is important to note that clusters 0 and 10 did not exhibit any significant markers. We then attempted to annotate the cell clusters as known cell types leveraging these found marker genes. However, the ascidian hemocytes are not well characterized, and most of the cell functions and also markers of the cells are not known. For most of the cell clusters, we were not successful in finding their known identity. Thus, we give a detailed review of the cell clusters, their marker genes, and the set of genes with differential expression in active and torpid colonies to assist further investigations into the hemocyte identity, functions, and changes in the torpor state.

In both the active and hibernating colonies, unsupervised cluster 0 was the most abundant cell type and consisted of 26% of cells in active colonies and 23% of cells in hibernating colonies (Figures 7C, D; Supplementary Table 3). Cluster 0, however, did not have a unique expression; i.e., we did not find any genes that had high expression in cells of this cluster and low expression in all other cells. The expression density, used as a proxy for the transcriptional activity of cells, in this cluster, was slightly lower in cells of hibernating colonies compared to cells in active colonies (Figure 7E; Supplementary Table 4). We found 10 significantly downregulated and 24 significantly upregulated genes in cells of cluster 0 in torpid colonies compared to cells of cluster 0 in active colonies (Supplementary Table 5).

Cluster 1 consisted of approximately 14% of cells in active and hibernating colonies (Figures 7C, D; Supplementary Table 3), and we identified three marker genes with high expression in these cells compared to all other cells (Figure 8A; Supplementary Table 2). The genes were not annotated in the Aniseed database and were not successfully aligned with BLASTx on any of the ascidian proteins. Interestingly, cluster 1 cells in active colonies showed high expression density (see Methods), indicating high gene activity in the cluster (Figure 7E; Supplementary Table 4). We found eight downregulated and eight upregulated genes in torpid compared to active colonies in cells of cluster 1 (Supplementary Table 6).

Cluster 2 consisted of 10% of cells in active colonies and 13% in torpid colonies. A total of 20 marker genes were identified in this cluster of cells, and 15 of these markers were well annotated (Figure 8B; Supplementary Table 2). Interestingly, one of the marker genes for cluster 2 was successfully aligned with the allorecognition gene in *Botryllus schlosseri*, a close relative of *B. leachii* (Supplementary Figure 1A). This gene, termed BHF (for *Botryllus* Histocompatibility Factor; Voskoboynik et al., 2013), encodes self/non-self and determines "graft" outcomes in this group of organisms. The BHF is significantly upregulated in colonies poised

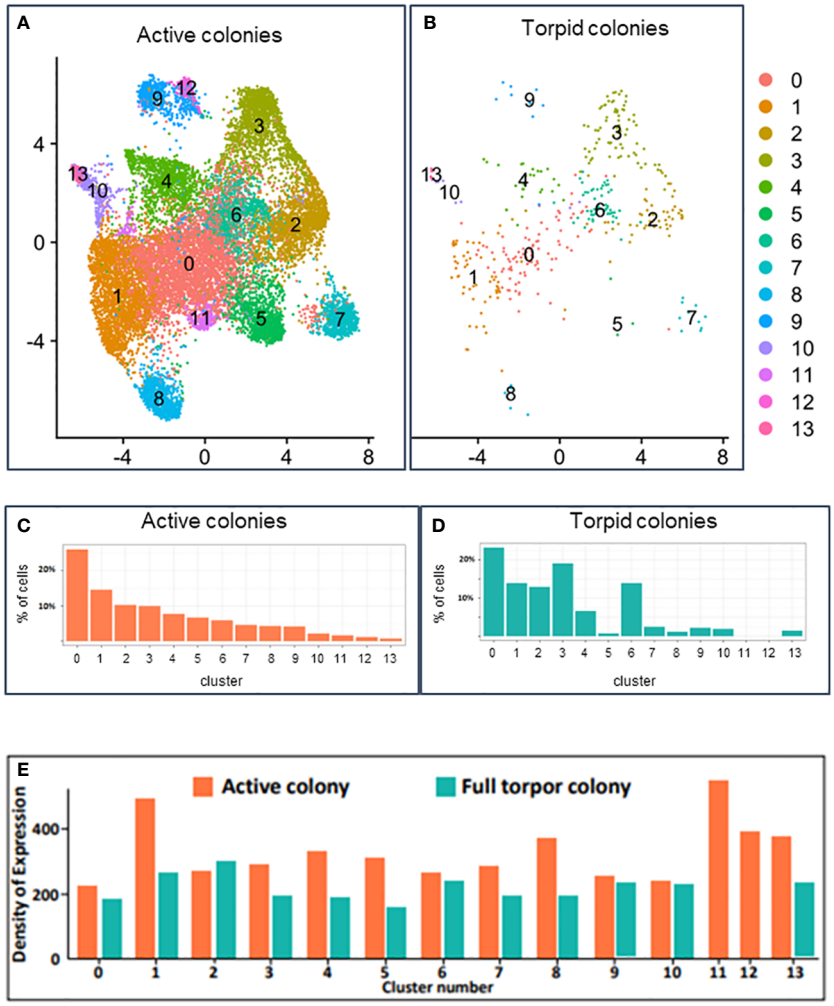

FIGURE 7
Single-cell transcriptomics analysis. **(A)** UMAP plot of unsupervised clustering of cells in active *Botrylloides leachii* colonies based on the expression levels. Each dot represents a cell, and colors indicate the unsupervised cluster assignment. **(B)** UMAP plot of unsupervised clustering of cells in torpid *B. leachii* colonies based on the expression levels. Each dot represents a cell, and colors indicate the unsupervised cluster assignment. **(C)** Percentage of cells in active colonies belonging to each cluster. **(D)** Percentage of cells in torpid colonies belonging to each cluster. **(E)** Expression density: the sum of expressions of all genes in all cells within a specific cluster divided by the number of cells in the cluster. Expression density calculation provides an estimate of the average expression per cell and can be used as a proxy of transcriptional activity of cells. Expression density is shown for active colonies (represented by orange) and torpid colonies (represented by green).

to allorecognition responses and predicts histocompatibility outcomes (fusion and rejection), and by employing whole-mount *in situ* hybridization, it was found to be highly expressed in the vasculature and the animal blood (Voskoboynik et al., 2013) (Supplementary Figure 1B). Cluster 2 cells of torpid colonies had a slightly (10%) higher expression activity than cells of active colonies (Figure 7E; Supplementary Table 4). Interestingly, most of the differentially expressed genes were upregulated in torpid colonies compared to active in cells of this cluster. A total of 32 upregulated and six downregulated genes were found (Supplementary Table 7). Many of the upregulated (in torpid colonies) genes were associated with ribosomal functions and gene translation, further indicating the activity of the cells in cluster 2 of torpid colonies.

Cluster 3 consisted of almost 10% of cells in the active colonies (Figure 7C; Supplementary Table 3). The number of cells in this cluster rose significantly to 19% of all cells (Fold Change = 1.9) in torpid colonies (Figure 7D; Supplementary Table 3). We identified 20 marker genes of this cluster with 15 genes that were well annotated (Figure 8C; Supplementary Table 2). Many of the marker genes were related to the "ferric iron binding" function. Interestingly, even though the cells of cluster 3 were more frequent in torpid colonies than in active colonies, the density of expression of these cells was higher in active colonies (Figure 7E; Supplementary Table 4). This again indicates the overall low transcriptional activity of torpid colonies. Differential expression analysis of genes in cluster 3 yielded seven downregulated and 17 upregulated genes in torpid compared to active colonies (Supplementary Table 8).

Cluster 4 contained 7% of cells in both active and torpid colonies (Figures 7C, D; Supplementary Table 3). Nine gene markers of this cluster were identified with five well-annotated genes (Figure 8D; Supplementary Table 2). As in cluster 3, in this cluster, the density of expression in torpid colonies was significantly

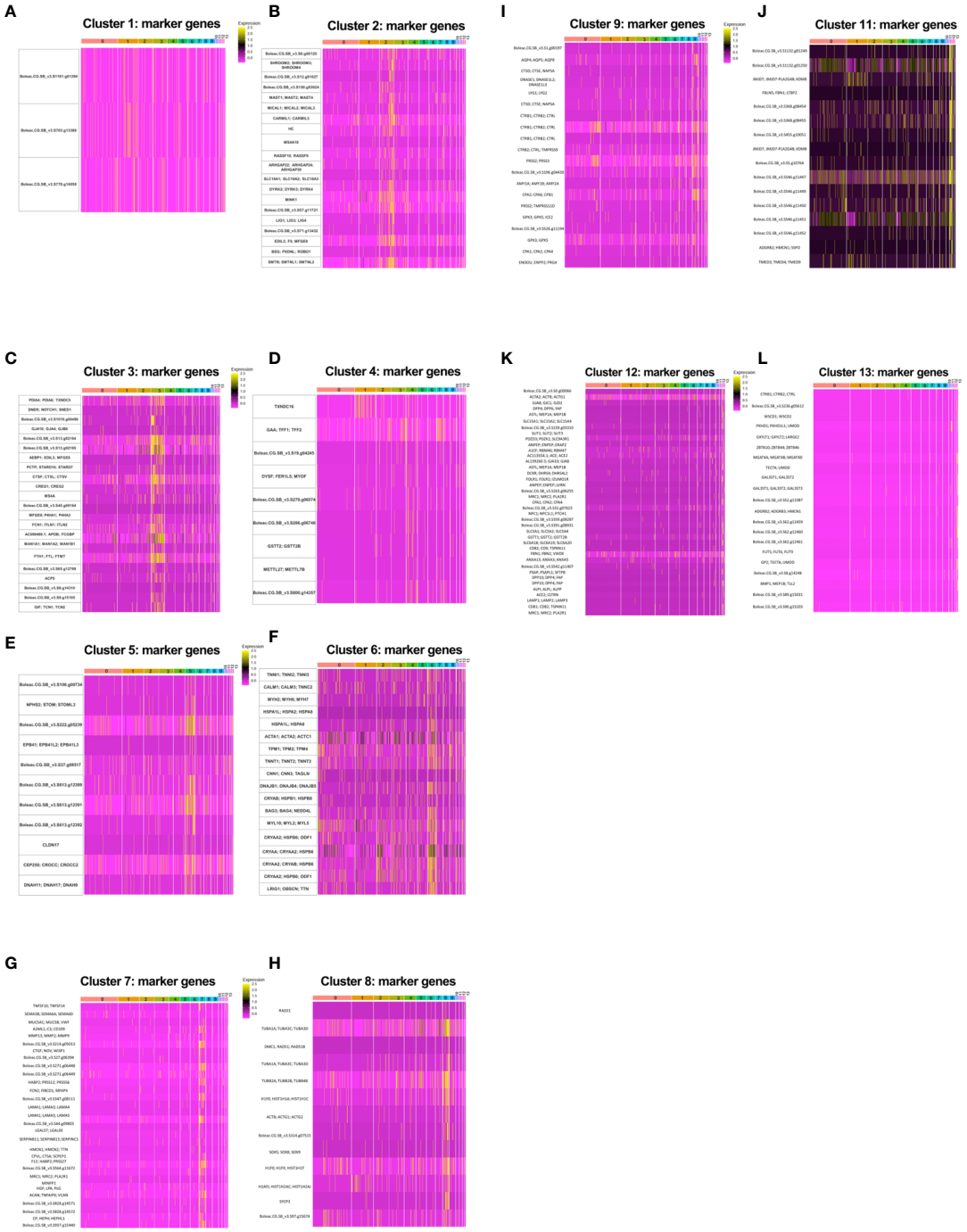

FIGURE 8
Cell cluster gene markers. **(A)** Heat map of gene markers for cells in cluster 1 in active and torpid colonies. **(B)** Heat map of gene markers for cells in cluster 2 in active and torpid colonies. **(C)** Heat map of gene markers for cells in cluster 3 in active and torpid colonies. **(D)** Heat map of gene markers for cells in cluster 4 in active and torpid colonies. **(E)** Heat map of gene markers for cells in cluster 5 in active and torpid colonies. **(F)** Heat map of gene markers for cells in cluster 6 in active and torpid colonies. **(G)** Heat map of gene markers for cells in cluster 7 in active and torpid colonies. **(H)** Heat map of gene markers for cells in cluster 8 in active and torpid colonies. **(I)** Heat map of gene markers for cells in cluster 9 in active and torpid colonies. **(J)** Heat map of gene markers for cells in cluster 11 in active and torpid colonies. **(K)** Heat map of gene markers for cells in cluster 12 in active and torpid colonies. **(L)** Heat map of gene markers for cells in cluster 13 in active and torpid colonies.

lower (Fold Change = 0.58) than in torpid colonies (Figure 7E; Supplementary Table 4), indicating overall low expression activity in torpid cells. In cluster 4, two downregulated and 11 upregulated genes were found in torpid compared to active colonies (Supplementary Table 9).

Cluster 5 of hemocytes in active colonies contained approximately 7% of cells (Figure 7C; Supplementary Table 3). The number of cells in cluster 5 fell dramatically (Fold Change = 0.1) in torpid colonies and equated to only 0.7% of all cells (Figure 7D; Supplementary Table 3). In addition to the drastic

reduction in the number of cells in torpid colonies, their activity levels calculated as expression density also fell by almost half (Fold Change = 0.51) (Figure 7E; Supplementary Table 4). We found 11 marker genes of cells in cluster 5. Five of these genes were successfully annotated with BLASTx alignment on ascidian proteins (Figure 8E; Supplementary Table 2). Interestingly, we found 64 highly upregulated (log2 Fold Change > 3) genes in torpid colonies compared to active colonies (Supplementary Table 10). These genes were mostly related to cation-coupled chloride cotransporters, which modulate the transport of sodium and/or potassium cations coupled with chloride anions across the cell membrane.

Hemocytes of cluster 6 rose significantly in number in torpid colonies compared to active colonies (Fold Change = 2.4), indicating their importance in the torpor state. In active colonies, these cells constituted only 0.5% of all cells, while in torpid colonies, their number rose to more than 1% of all cells (Figures 7C, D; Supplementary Table 3). The transcription activity of cluster 6 cells in torpid colonies was similar to the activity in active colonies (Figure 7E; Supplementary Table 4). We found 18 gene markers of this cell cluster, all of which were annotated with BLASTx (Figure 8F; Supplementary Table 2). The differentially expressed genes included 10 downregulated and 21 upregulated genes in torpid compared to active colonies (Supplementary Table 11).

The number of cells in cluster 7 fell by almost 50% from 4% of all cells in active colonies (Figure 7C; Supplementary Table 3) to 2% of all cells in torpid colonies (Figure 7D; Supplementary Table 3). The expression density of cells in cluster 7 fell in torpid colonies by almost 40% (Figure 7E; Supplementary Table 4). We found 30 gene markers for cluster 7 with 20 genes successfully annotated (Figure 8G; Supplementary Table 2). The differentially expressed genes included 49 genes, all of which were upregulated in torpid compared to active colonies (Supplementary Table 12).

Cluster 8 consisted of 4% of all cells in active colonies and fell to just above 1% of cells in torpor (Figures 7C, D; Supplementary Table 3). The expression density indicating the overall transcriptional activity of cells in cluster 8 was much lower in the torpor state than in active colonies (Fold Change = 0.28) (Figure 7E; Supplementary Table 4). We found 13 gene markers, 11 of which were annotated (Figure 8H; Supplementary Table 2). We found 35 differentially expressed genes, all of which were upregulated in torpid colonies compared to active ones (Supplementary Table 13). We found differentially upregulated genes to be associated with "ER to Golgi transport".

Cluster 9 consisted of 4% of all cells in the active colonies and dropped to 2% of all cells in torpid colonies (Figures 7C, D; Supplementary Table 3). The overall transcriptional activity of cells remained similar in a torpor state (Figure 7E; Supplementary Table 4). We found 20 marker genes of cluster 8, 17 of which were successfully annotated (Figure 8I; Supplementary Table 2). Overall transcriptional activity of cells in cluster 8 fell by almost 50% in the torpor state compared to active colonies (Figure 7E; Supplementary Table 4). Differentially expressed genes of cluster 9 included one downregulated and 59 upregulated genes in torpid colonies compared to active colonies (Supplementary Table 14).

Cluster 10 consisted of close to 2% of all cells in both active and torpid colonies (Figures 7C, D; Supplementary Table 3). The expression density in cluster 10 revealed that the transcription activity of cells in this cluster in torpid colonies remains similar to the active colonies (Figure 7E; Supplementary Table 4). We found no significant gene markers for cells in cluster 10. Differentially expressed genes in cells of cluster 10 in active and torpid colonies included 51 genes, all of which were upregulated in torpid colonies (Supplementary Table 15).

Clusters 11 and 12 were unique to active colonies and consisted of 1.5% and 1.1% of all cells, respectively (Figures 7C, D; Supplementary Table 3). Interestingly, the overall transcriptional activity measured by expression density was higher than average in cluster 11 cells of active colonies (Figure 7E). In cluster 11, we found 16 marker genes, five of which were successfully annotated (Figure 8J; Supplementary Table 2). For cluster 12, we found 39 marker genes, with 32 of these genes successfully annotated (Figure 8K; Supplementary Table 2).

Cluster 13 contained 0.7% of all cells in active colonies. The proportion of cells increased in torpid colonies to constitute 1.5% of all cells (Figures 7C, D; Supplementary Table 3). Even though the proportion of cells increased in torpor, overall transcription activity was decreased in the torpor state (Figure 7E; Supplementary Table 4). We found 21 marker genes of cells in cluster 13 (Figure 8K; Supplementary Table 2). Comparing gene expression in active and torpid cells of cluster 13, we found four upregulated genes in torpid cells (Supplementary Table 16).

4 Discussion

The hemocytes of the colonial tunicate *B. leachii* play significant roles throughout the animal's life cycle, encompassing a variety of crucial functions. These functions include nutrient transport and storage, respiration, regeneration, budding, sexual reproduction, defense responses, and tunic generation (Rinkevich et al., 2007; Rinkevich et al., 2013; Hyams et al., 2017). In this study, we systematically studied hemocyte populations in active and torpid colonies. We identified morphological, cellular, and molecular changes that *B. leachii* hemolymph undergoes under physiological stress in torpor conditions.

As the first step to elucidating the cell populations in the active and torpid colonies, we morphologically characterized nine cell types comprising distinctive cell populations in *B. leachii* hemocytes (Figure 2; Table 1). We did not observe significant variations in cell morphology between the active and torpid colonies. However, similar to our previous observations (Hyams et al., 2017; Hyams et al., 2022), we did identify two distinct cell types exclusive to torpor: MNCs and specialized macrophage-like cells containing intact bacterial cells within their cytoplasm, "bacteria-bearing cells".

In our previous investigations (18), we documented changes in the quantities of hemocyte cells, including hemoblasts, morula cells, and phagocyte cells, between torpid and active colonies of *B. leachii*. Additionally, we reported the presence of MNCs (Hyams et al., 2017) and bacteria-bearing cells (Hyams et al., 2022) specifically in torpid colonies. To validate our earlier findings, we conducted a comprehensive analysis of four specific cell types and examined changes in their abundance during three distinct physiological

states experienced by *B. leachii* colonies: the active state, mid-torpor state, and full torpor state. Our observations revealed notable changes in cell populations within torpid colonies (Figure 3; Supplementary Table 1). Specifically, we observed a significant decrease in the abundance of hemoblasts and phagocytes, whereas in a previous study (Hyams et al., 2017), we documented an increase in phagocytes in torpid colonies, suggesting that the cellular profiles and their changes along various physiological states are intricate and necessitate further experimentation. In contrast to the phagocytes, the number of MNCs exhibited a substantial increase in torpid colonies compared to the active state. We did not observe significant alterations in the quantity of vacuolated cells across the different physiological states.

Utilizing primary cell cultures, we made longitudinal observations of *B. leachii* hemocytes and found that while torpid colonies stayed relatively stable across the 30 days of our observations (Figure 4), the active colonies started changing after 3 days of the experiment. We observed the initiation of cell aggregations with 3–25 cells per cell aggregate and the subsequent formation of MNCs in cell cultures generated from active colonies (Figures 4B, C).

TEM observations further revealed the ultrastructure of MNCs and bacteria-bearing cells. We observed several types of MNC morphs. Some MNC morphs contained vacuoles with separate nuclei and Golgi apparatus in addition to a separate nucleus (Figures 5A–A′) and mitochondria. Other MNC morphs were characterized by large size with many vacuoles surrounded by a thin cytoplasmic layer and several mitochondria (Figure 5B). Cells of both MNC subpopulations expressed *Piwi* in all nuclei (Figures 5C–C′). We also observed torpor-specific cells with intact bacteria (Figure 5D). The potential significant roles of these cells in the animal's biology have been discussed in previous studies (Lauzon et al., 2000; Hyams et al., 2017; Hyams et al., 2022).

Previously, MNCs were sporadically recorded during *B. leachii* development, including whole-body regeneration from minute vasculature fragments (Rinkevich et al., 2007; Rinkevich et al., 2010; Rinkevich et al., 2013), in blastogenic stage D (Alvarez-Dolado et al., 2003; Lauzon et al., 2013), and during colonial dormancy (Rinkevich et al., 2010; Hyams et al., 2017; Hyams et al., 2022). In addition, a wide range of studies have documented cell fusion in mammalian systems during the last two decades (Alvarez-Dolado et al., 2003; Knapp and Tanaka, 2012; Pesaresi et al., 2019; Yao and Wang, 2020), indicating that cellular fusion is a unanimous phenomenon, contributing to a range of repair/stress phenomena. Our observation of the emergence of MNCs at the beginning of dormancy, the display of stem cell marker (*Piwi*) in these highly differentiated sizable cells (ca 20 μm in size, inclusive of 11 nuclei/cell), and the documented appearance of MNCs during blastogenic stage D (Lauzon et al., 2000) suggest that the *B. leachii* MNCs are a fundamental cell type that appears as an outcome of hemoblast fusion (Figure 4) (Hyams et al., 2017). Several types of MNC morphs were documented (Hyams et al., 2017). All of these types of MNCs expressed the stemness marker *Piwi* in all their nuclei, suggesting that these cells may function as a pool of "primed" cells available for emergency needs such as for rapid regeneration at arousal from dormancy or at stage D of blastogenesis, where fast developmental response during reduced cell division cycles is needed. However, it is possible that some MNCs may also be the outcome of uncompleted mitotic cell cycles, yet this less likely option requires further investigation.

It is further unlikely that the *B. leachii* MNCs are phagocytic cells containing apoptotic cells inside the phagosome, as recorded at the take-over phase of blastogenesis (Voskoboynik et al., 2004; Franchi et al., 2016). The MNCs do not exhibit any apoptotic characteristic along torpor in *B. leachii*, and they were documented in dormant colonies for prolonged periods of several months (under our laboratory settings), which would be very unlikely for an apoptotic process.

Further, in order to investigate the molecular mechanisms underlying the cellular changes within torpid colonies, we employed a cutting-edge single-cell sequencing technique. This method allowed us to identify specific gene expression profiles of individual cells, enabling the differentiation of cell types and subtypes within a heterogeneous tissue. Single-cell sequencing is a powerful technology that can provide insights into the transcriptional programs of different cell populations and has been widely used to investigate transcriptional changes during development, disease progression, and cellular responses to external stimuli. The use of single-cell sequencing in our study allowed for a more comprehensive characterization of the different hemocyte types in *B. leachii* and provided new insights into the transcriptional differences between these cells in active and torpid colonies.

Despite the same methodology employed for the preparation of sequencing libraries for active and hibernating colonies, sequencing outcomes were extremely low in hibernating colonies (Figure 6). It could be a result of overall low mRNA expression in hemocytes under torpor conditions, a tenet supported by our recent work (Hyams et al., 2022) where we observed that total RNA is significantly lower in hibernating colonies. A different explanation may be related to the library preparation aspects and Drop-seq technology itself. It has been noted that several of the library preparation steps and the technical aspects of the sequencing process can generate unrepresentative and biased sequencing (Lindenbach and Rice, 1997; Wu et al., 2019; Denisenko et al., 2020; Ke et al., 2022; Oh et al., 2022). It should be taken into consideration that the lower RNA expression in torpid colonies could potentially lead to biases or missed low-abundance transcripts. We also acknowledge that there might be inherent variability in hemocyte populations across different individual colonies, even under the same physiological state, which could impact the results.

Analysis of gene expression profiles of the single-cell sequencing suggested 14 hemocyte types (cell clusters) in active *B. leachii* colonies (Figure 7A). Two of these cell types were not present in the torpid colonies (Figure 7B). In our comprehensive analysis, we thoroughly examined each cluster of cells and investigated their specific characteristics, revealing marker genes associated with each cluster (Figure 8) and comparing the number of cells within each cluster between active and torpid colonies. Additionally, we evaluated the overall transcriptional activity in active and torpid colonies, shedding light on the global gene expression patterns associated with these distinct states. Moreover, we identified differentially expressed genes in cells from active and torpid colonies within each cluster,

uncovering key genes potentially driving the observed physiological differences. The detailed results from the analysis of the single-cell transcriptomics data have been integrated into an interactive Dashboard (http://bleachii.tauberbioinformatics.org/seurat?id=Bleachii-v1), providing a user-friendly platform for easy interrogation and utilization of the findings. The Dashboard allows users to explore the results in a convenient and intuitive manner, enabling them to delve deeper into the transcriptomic profiles of individual cells and gain valuable insights from the data.

This study focused on investigating the hemocyte cell populations within both active and torpid colonies of *B. leachii*. Notably, in torpid colonies, the circulating hemocytes represent the sole bodily compartment that "keeps on rolling" and remains active and functional, enabling the organism to successfully reemerge as a new functional colony when favorable environmental conditions arise. Understanding the cellular dynamics and the transcriptome changes in these circulating hemocytes provides valuable insights into the regenerative capabilities and adaptive strategies employed by *B. leachii*.

Data availability statement

The data presented in the study are deposited in the NCBI repository, accession number PRJNA1045036.

Ethics statement

There is no need for animal AC, since this species is a cosmopolitan invasive species.

Author contributions

BR conceived and designed the experiments. YH performed the experiments. BR, YR, and LB provided the resources. YH, JP, and ET analyzed the data. YH, BR, and JP wrote the manuscript with the contributions of all co-authors. All authors contributed to the article and approved the submitted version.

Funding

The author(s) declare financial support was received for the research, authorship, and/or publication of this article. This work received funding from the Laszlo N. Tauber Family Foundation and was funded by the United States–Israel Binational Science Foundation (BSF No. 2015012; to BR), by the BSF, as part of the joint program with the NSF, the National Science Foundation, USA (NSF/BSF no 2021650; to BR), and the ISF grant No. 172/17 (to BR).

Acknowledgments

We would like to extend our thanks to Dr M. Strunz (Comprehensive Pneumology Center, Helmholtz Zentrum, München) for performing the Drop-seq methodology, G. Paz for assistance in preparing the figures, O. Ben-Hamo (www.oshratbenhamo.wixsite.com/osher) for the artwork, and P. Maishev Tauber Bioinformatics Research Center, University of Haifa for developing the interactive Dashboard.

Conflict of interest

The authors declare that the research was conducted in the absence of any commercial or financial relationships that could be construed as a potential conflict of interest.

Publisher's note

Supplementary material

The Supplementary Material for this article can be found online at: https://www.frontiersin.org/articles/10.3389/fevo.2023.1196859/full#supplementary-material

SUPPLEMENTARY FIGURE 1
Botryllus Histocompatibility Factor. **(A)** BLASTx alignment of amino acid sequence of *B. leachii* gene (Boleac.CG.SB-v3.S222.g05250) on *Botryllus* Histocompatibility Factor (BHF) protein sequence. **(B)** UMAP dot plot of *B. leachii* gene (Boleac.CG.SB-v3.S222.g05250) expression. Colored dots indicate cells with high expression of Boleac.CG.SB-v3.S222.g05250 gene.

References

Alvarez-Dolado, M., Pardal, R., Garcia-Verdugo, J. M., Fike, J. R., Lee, H. O., Pfeffer, K., et al. (2003). Fusion of bone-marrow-derived cells with Purkinje neurons, cardiomyocytes and hepatocytes. *Nature* 425, 968–973. doi: 10.1038/nature02069

Bageritz, J., and Raddi, G. (2019). Single-cell RNA sequencing with drop-seq. *Methods Mol. Biol.* 1979, 73–85. doi: 10.1007/978-1-4939-9240-9_6

Ballarin, L., and Cima, F. (2005). Cytochemical properties of Botryllus schlosseri haemocytes: indications for morpho-functional characterisation. *Eur. J. Histochem.* 49, 255–264. doi: 10.4081/952

Ballarin, L., Karahan, A., Salvetti, A., Rossi, L., Manni, L., Rinkevich, B., et al. (2021). Stem cells and innate immunity in aquatic invertebrates: bridging two seemingly disparate

disciplines for new discoveries in biology. *Front. Immunol.* 12. doi: 10.3389/fimmu.2021.688106

Blanchoud, S., Rinkevich, B., and Wilson, M. J. (2018a). Whole-body regeneration in the colonial tunicate botrylloides leachii. *Results Probl. Cell Differ* 65, 337–355. doi: 10.1007/978-3-319-92486-1_16

Blanchoud, S., Rutherford, K., Zondag, L., Gemmell, N. J., and Wilson, M. J. (2018b). *De novo* draft assembly of the Botrylloides leachii genome provides further insight into tunicate evolution. *Sci. Rep.* 8, 5518. doi: 10.1038/s41598-018-23749-w

Blanchoud, S., Zondag, L., Lamare, M. D., and Wilson, M. J. (2017). Hematological analysis of the ascidian Botrylloides leachii (Savigny, 1816) during whole-body regeneration. *Biol. Bull.* 232, 143–157. doi: 10.1086/692841

Boratyn, G. M., Camacho, C., Cooper, P. S., Coulouris, G., Fong, A., Ma, N., et al. (2013). BLAST: a more efficient report with usability improvements. *Nucleic Acids Res* 41, W29–W33. doi: 10.1093/nar/gkt282

Brunetti, R. (1976) *Biological cycle of Botrylloides leachi (Savigny) (Ascidiacea) in the Venetian lagoon., Vie Milieu*. Available at: https://hal.science/hal-02989323 (Accessed May 26, 2023).

Burighel, B., Cloney, P., and Cloney, R. A. (1997). *Microscopic anatomy of invertebrates*, Vol. 15. (New York: John Wiley and Sons), 221–347.

Caceres, C. E. (1997). Dormancy in invertebrates. *Invertebr. Biol.* 116, 371. doi: 10.2307/3226870

Cima, F. (2022). Searching for the Origin and the Differentiation of Haemocytes before and after Larval Settlement of the Colonial Ascidian Botryllus schlosseri: An Ultrastructural Viewpoint. *J. Mar. Sci. Eng.* 10, 987. doi: 10.3390/jmse10070987

Cima, F., Franchi, N., and Ballarin, L. (2016). "Origin and functions of tunicate hemocytes," in *Evol. Immune Syst. Conserv. Diversif* (London: Elsevier Inc.), 29–49. doi: 10.1016/B978-0-12-801975-7.00002-5

Cima, F., Perin, A., Burighel, P., and Ballarin, L. (2001). Morpho-functional characterization of haemocytes of the compound ascidian *Botrylloides leachi* (Tunicata, Ascidiacea). *Acta Zool* 82, 261–274. doi: 10.1046/j.1463-6395.2001.00087.x

Dardaillon, J., Dauga, D., Simion, P., Faure, E., Onuma, T. A., DeBiasse, M. B., et al. (2020). ANISEED 2019: 4D exploration of genetic data for an extended range of tunicates. *Nucleic Acids Res.* 48, D668–D675. doi: 10.1093/nar/gkz955

Denisenko, E., Guo, B. B., Jones, M., Hou, R., de Kock, L., Lassmann, T., et al. (2020). Systematic assessment of tissue dissociation and storage biases in single-cell and single-nucleus RNA-seq workflows. *Genome Biol.* 21, 130. doi: 10.1186/s13059-020-02048-6

Franchi, N., Ballin, F., Manni, L., Schiavon, F., Basso, G., and Ballarin, L. (2016). Recurrent phagocytosis-induced apoptosis in the cyclical generation change of the compound ascidian Botryllus schlosseri. *Dev. Comp. Immunol.* 62, 8–16. doi: 10.1016/j.dci.2016.04.011

Hand, S. C., and Hardewig, I. (1996). Downregulation of cellular metabolism during environmental stress: Mechanisms and implications. *Annu. Rev. Physiol.* 58, 539–563. doi: 10.1146/annurev.ph.58.030196.002543

Hirose, E., Saito, Y., and Watanabe, H. (1995). Regeneration of the tunic cuticle in the compound ascidian, Botrylloides simodensis. *Dev. Comp. Immunol.* 19, 143–151. doi: 10.1016/0145-305X(94)00062-K

Hirose, E., Shirae, M., and Saito, Y. (2003). Ultrastructures and classification of circulating hemocytes in 9 botryllid ascidians (Chordata: Ascidiacea). *Zoolog. Sci.* 20, 647–656. doi: 10.2108/zsj.20.647

Hyams, Y., Panov, J., Rosner, A., Brodsky, L., Rinkevich, Y., and Rinkevich, B. (2022). Transcriptome landscapes that signify Botrylloides leachi (Ascidiacea) torpor states. *Dev. Biol.* 490, 22–36. doi: 10.1016/j.ydbio.2022.06.005

Hyams, Y., Paz, G., Rabinowitz, C., and Rinkevich, B. (2017). Insights into the unique torpor of Botrylloides leachi, a colonial urochordate. *Dev. Biol.* 428, 101–117. doi: 10.1016/j.ydbio.2017.05.020

Jiménez-Merino, J., Santos De Abreu, I., Hiebert, L. S., Allodi, S., Tiozzo, S., De Barros, C. M., et al. (2019). Putative stem cells in the hemolymph and in the intestinal submucosa of the solitary ascidian Styela plicata. *Evodevo* 10, 1–19. doi: 10.1186/s13227-019-0144-3

Ke, M., Elshenawy, B., Sheldon, H., Arora, A., and Buffa, F. M. (2022). Single cell RNA-sequencing: A powerful yet still challenging technology to study cellular heterogeneity. *BioEssays* 44, 2200084. doi: 10.1002/bies.202200084

Knapp, D., and Tanaka, E. M. (2012). Regeneration and reprogramming. *Curr. Opin. Genet. Dev.* 22, 485–493. doi: 10.1016/j.gde.2012.09.006

Korsunsky, I., Millard, N., Fan, J., Slowikowski, K., Zhang, F., Wei, K., et al. (2019). Raychaudhuri, Fast, sensitive and accurate integration of single-cell data with Harmony. *Nat. Methods* 16, 1289–1296. doi: 10.1038/s41592-019-0619-0

Lauzon, R. J., Brown, C., Kerr, L., and Tiozzo, S. (2013). Phagocyte dynamics in a highly regenerative urochordate: Insights into development and host defense. *Dev. Biol.* 374, 357–373. doi: 10.1016/j.ydbio.2012.11.006

Lauzon, R. J., Rinkevich, B., Patton, C. W., and Weissman, I. L. (2000). A morphological study of nonrandom senescence in a colonial urochordate. *Biol. Bull.* 198, 367–378. doi: 10.2307/1542692

Lillie, R. D. (1977). Histopathologic technic and practical histochemistry. *Ann. Intern. Med.* 86, 376. doi: 10.7326/0003-4819-86-3-376_6

Lindenbach, B. D., and Rice, C. M. (1997). trans-Complementation of yellow fever virus NS1 reveals a role in early RNA replication. *J. Virol.* 71, 9608–9617. doi: 10.1128/jvi.71.12.9608-9617.1997

McInnes, L., Healy, J., Saul, N., and Großberger, L. (2018). UMAP: uniform manifold approximation and projection. *J. Open Source Softw* 3, 861. doi: 10.21105/joss.00861

Oh, J. M., An, M., Son, D. S., Choi, J., Cho, Y. B., Yoo, C. E., et al. (2022). Comparison of cell type distribution between single-cell and single-nucleus RNA sequencing: enrichment of adherent cell types in single-nucleus RNA sequencing. *Exp. Mol. Med.* 54, 2128–2134. doi: 10.1038/s12276-022-00892-z

Pesaresi, M., Sebastian-Perez, R., and Cosma, M. P. (2019). Dedifferentiation, transdifferentiation and cell fusion: in *vivo* reprogramming strategies for regenerative medicine. *FEBS J.* 286, 1074–1093. doi: 10.1111/febs.14633

Petegrosso, R., Li, Z., and Kuang, R. (2019). Machine learning and statistical methods for clustering single-cell RNA-sequencing data. *Brief. Bioinform.* 21, 1209–1223. doi: 10.1093/bib/bbz063

Reem, E., Douek, J., and Rinkevich, B. (2018). Ambiguities in the taxonomic assignment and species delineation of botryllid ascidians from the Israeli Mediterranean and other coastlines, Mitochondrial DNA Part A DNA Mapping. *Seq. Anal.* 29, 1073–1080. doi: 10.1080/24701394.2017.1404047

Rinkevich, B., and Rabinowitz, C. (1993). *In vitro* culture of blood cells from the colonial protochordate Botryllus schlosseri. *Vitr. Cell. Dev. Biol. - Anim.* 29, 79–85. doi: 10.1007/BF02634375

Rinkevich, B., and Shapira, M. (1998). An improved diet for inland broodstock and the establishment of an inbred line from Botryllus schlosseri, a colonial sea squirt (Ascidiacea). *Aquat. Living Resour* 11, 163–171. doi: 10.1016/S0990-7440(98)80113-7

Rinkevich, B., Shlemberg, Z., and Fishelson, L. (1995). Whole-body protochordate regeneration from totipotent blood cells. *Proc. Natl. Acad. Sci. U. S. A.* 92, 7695–7699. doi: 10.1073/pnas.92.17.7695

Rinkevich, B., Shlemberg, Z., and Fishelson, L. (1996). "Survival budding processes in the colonial tunicate Botrylloides from the medeterranean sea: The role of totipotent blood cells," in *Invertebr. Cell Cult. Look. Towar. 21st Century*, 1–9.

Rinkevich, Y., Paz, G., Rinkevich, B., and Reshef, R. (2007). Systemic bud induction and retinoic acid signaling underlie whole body regeneration in the urochordate Botrylloides leachi. *PloS Biol.* 5, 900–913. doi: 10.1371/journal.pbio.0050071

Rinkevich, Y., Rinkevich, B., and Reshef, R. (2008). Cell signaling and transcription factor genes expressed during whole body regeneration in a colonial chordate. *BMC Dev. Biol.* 8, 100. doi: 10.1186/1471-213X-8-100

Rinkevich, Y., Rosner, A., Rabinowitz, C., Lapidot, Z., Moiseeva, E., and Rinkevich, B. (2010). Piwi positive cells that line the vasculature epithelium, underlie whole body regeneration in a basal chordate. *Dev. Biol.* 345, 94–104. doi: 10.1016/j.ydbio.2010.05.500

Rinkevich, Y., Voskoboynik, A., Rosner, A., Rabinowitz, C., Paz, G., Oren, M., et al. (2013). Repeated, long-term cycling of putative stem cells between niches in a basal chordate. *Dev. Cell* 24, 76–88. doi: 10.1016/j.devcel.2012.11.010

Satija, R., Farrell, J. A., Gennert, D., Schier, A. F., and Regev, A. (2015). Spatial reconstruction of single-cell gene expression data. *Nat. Biotechnol.* 33, 495–502. doi: 10.1038/nbt.3192

Shalek, A. K., Satija, R., Shuga, J., Trombetta, J. J., Gennert, D., Lu, D., et al. (2014). Single-cell RNA-seq reveals dynamic paracrine control of cellular variation. *Nature* 510, 363–369. doi: 10.1038/nature13437

Sharma, S., Wang, W., and Stolfi, A. (2019). Single-cell transcriptome profiling of the Ciona larval brain. *Dev. Biol.* 448, 226–236. doi: 10.1016/j.ydbio.2018.09.023

Storey, K. B. (2002). "Life in the slow lane: Molecular mechanisms of estivation," in *Comp. Biochem. Physiol. - A Mol. Integr. Physiol.* (133):733–754. doi: 10.1016/S1095-6433(02)00206-4

Storey, K. B. (2010). Out cold: Biochemical regulation of mammalian hibernation - A mini-review. *Gerontology* 56, 220–230. doi: 10.1159/000228829

Storey, K. B., and Storey, J. M. (2011). *Hibernation: Poikilotherms* (Chichester: ELS, Wiley). doi: 10.1002/9780470015902.a0003214.pub2

Vanni, V., Anselmi, C., Ballarin, L., Drago, L., Gasparini, F., Gordon, T., et al. (2022). Current knowledge on stem cells in ascidians. *Adv. Aquat. Invertebr. Stem Cell Res.* 273. doi: 10.3390/books978-3-0365-1635-6-9

Voskoboynik, A., Newman, A. M., Corey, D. M., Sahoo, D., Pushkarev, D., Neff, N. F., et al. (2013). Identification of a colonial chordate histocompatibility gene. *Sci. (80-.)* 341, 384–387. doi: 10.1126/science.1238036

Voskoboynik, A., Rinkevich, B., Weiss, A., Moiseeva, E., and Reznick, A. Z. (2004). Macrophage involvement for successful degeneration of apoptotic organs in the colonial urochordate Botryllus schlosseri. *J. Exp. Biol.* 207, 2409–2416. doi: 10.1242/jeb.01045

Voskoboynik, A., Simon-Blecher, N., Soen, Y., Rinkevich, B., De Tomaso, A. W., Ishizuka, K. J., et al. (2007). Striving for normality: whole body regeneration through a series of abnormal generations. *FASEB J.* 21, 1335–1344. doi: 10.1096/fj.06-7337com

Winkley, K. M., Reeves, W. M., and Veeman, M. T. (2021). Single-cell analysis of cell fate bifurcation in the chordate Ciona. *BMC Biol.* 19, 1–26. doi: 10.1186/s12915-021-01122-0

Wu, H., Kirita, Y., Donnelly, E. L., and Humphreys, B. D. (2019). Advantages of single-nucleus over single-cell RNA sequencing of adult kidney: Rare cell types and novel cell states revealed in fibrosis. *J. Am. Soc Nephrol.* 30, 23–32. doi: 10.1681/ASN.2018090912

Yao, Y., and Wang, C. (2020). Dedifferentiation: inspiration for devising engineering strategies for regenerative medicine. *NPJ Regen. Med.* 5, 20. doi: 10.1038/s41536-020-00099-8

Zeng, F., Peronato, A., Ballarin, L., and Rothbächer, U. (2022). Sweet tunicate blood cells: A glycan profiling of haemocytes in three ascidian species. *Adv. Aquat. Invertebr. Stem Cell Res. MDPI*. doi: 10.3390/books978-3-0365-1635-6-11

frontiers | Frontiers in Ecology and Evolution

TYPE Original Research
PUBLISHED 15 February 2024
DOI 10.3389/fevo.2024.1332780

OPEN ACCESS

EDITED BY
Paolo Sordino,
Anton Dohrn Zoological Station Naples, Italy

REVIEWED BY
Maria Flavia Gravina,
University of Rome Tor Vergata, Italy
Federica Montesanto,
University of Florida, United States

*CORRESPONDENCE
Alexandre Alié
alexandre.alie@imev-mer.fr

†These authors share first authorship

RECEIVED 03 November 2023
ACCEPTED 24 January 2024
PUBLISHED 15 February 2024

CITATION
Tobias-Santos V, Andreoni-Pham R, El Gharbi D, Lebel M, Tiozzo S and Alié A (2024) Salinity-mediated limitation of asexual reproduction in the colonial ascidian *Polyandrocarpa zorritensis*. *Front. Ecol. Evol.* 12:1332780. doi: 10.3389/fevo.2024.1332780

Salinity-mediated limitation of asexual reproduction in the colonial ascidian *Polyandrocarpa zorritensis*

Vitoria Tobias-Santos[1†], Rita Andreoni-Pham[1,2†], Dany El Gharbi[1], Marie Lebel[1], Stefano Tiozzo[1] and Alexandre Alié[1*]

[1]Laboratoire de Biologie du Développement de Villefranche-sur-Mer (LBDV, UMR 7009), Institut de la Mer de Villefranche (IMEV), Sorbonne Université, Centre National de la Recherche Scientifique (CNRS), Villefranche-sur-Mer, France, [2]Université Côte d'Azur, Centre National de la Recherche Scientifique (CNRS), Institut National de la Santé et de la Recherche Médicale (INSERM), Institute for Research on Cancer and Aging (IRCAN), Nice, France

Ascidians are among the most common invasive marine invertebrates worldwide. Many species of non-indigenous ascidians (NIAs) have successfully colonized the Mediterranean Sea, notably within anthropized coastal lagoons and harbors. Although invasive species are generally characterized by their broad ecological tolerance, different ascidian species exhibit varied responses to biotic and abiotic environmental stressors, including temperature and salinity. Acquiring a better understanding about of the impact of such parameters on ascidian life history is crucial for predicting the invasive potential of NIAs. In this study, we investigated the impact of various salinities on the reproduction of the colonial ascidian *Polyandorcarpa zorritensis*, a species indigenous to Peru and a thriving invader. *P. zorritensis* undergoes asexual reproduction via a peculiar form of budding named vasal budding and produces resistant spherules, which likely facilitated its dissemination over long distances. Despite its widespread distribution along the Pacific and Atlantic coasts, it is only found in a few Mediterranean coastal areas with a low salinity. We tested the impact of different salinity conditions on the sexual and asexual reproduction rates of *P. zorritensis* in a controlled laboratory setting. Our experiments showed that the rate of asexual reproduction in colonies bred at 29 or 36 ppt salinity levels, corresponding to the natural range inhabited by *P. zorritensis*, was higher than those grown in 40 ppt salinity, commonly found in Mediterranean marinas and harbors. The results suggest that, although *P. zorritensis* has been present in the Mediterranean for several decades, its potential for invasion could be constrained by an intolerance to high salinity.

KEYWORDS

tunicate, development, budding, salinity, invasive, non-indigenous species

Introduction

Ascidians are one of the most common invasive marine invertebrates worldwide (Lambert and Lambert, 1998; Izquierdo-Muñoz, 2009; Clarke Murray et al., 2014; Ulman et al., 2017; Cardeccia et al., 2018; Ulman et al., 2019a). When introduced to a new environment, non-indigenous ascidians (NIAs) can propagate on hard substrates, outcompete local species, and alter the native fouling communities (Lambert, 2002; Castilla et al., 2004; Bullard et al., 2007; Dias et al., 2008). Coastal anthropized areas like harbors and lagoons are particularly susceptible to being colonized by NIAs, which are mainly introduced by human-mediated vectors such as hull fouling and aquaculture activities (Lambert and Lambert, 2003; Clarke Murray et al., 2011; López-Legentil et al., 2015; Ulman et al., 2019b; Nichols et al., 2023). In these semi-enclosed habitats, environmental conditions differ from the open sea from which they are separated by natural or artificial barriers, leading to short-scale instability in terms of eutrophication, pollution, temperature, and salinity (Cognetti and Maltagliati, 2000; Gewing et al., 2017). In particular, temperature and salinity have a strong influence on the distribution of marine species, especially ascidians (Dybern, 1967; Dybern, 1969; Sims, 1984; Vázquez and Young, 1996; Vázquez and Young, 2000; Bullard et al., 2007; Epelbaum et al., 2009; Chebbi et al., 2010; Pineda et al., 2012; Gewing et al., 2018). With limited dispersal capacity due to a biphasic life cycle dominated by the sessile adult stage, ascidians' survival is compromised by local unfavorable conditions (Carballo, 2000). Therefore, although successful ascidian invaders are generally recognized for their broad ecological tolerance (Lambert and Lambert, 2003; Gröner et al., 2011; Granot et al., 2017; Rocha et al., 2017; Platin and Shenkar, 2023), NIAs can also display poor survival or reproductive outcomes when exposed to temperature and salinity that differ from their region of origin (Shenkar and Loya, 2008; Nagar and Shenkar, 2016; Gewing et al., 2018). Enhancing our understanding of how environmental factors influence the reproductive strategies of NIAs is essential for more accurately predicting their invasive potential (Rocha et al., 2017; Platin and Shenkar, 2023).

Polyandrocarpa zorritensis (*Stolidobranchia: Styelidae*) is a colonial ascidian that was first described from the coast of Peru (Van Name, 1931). In recent decades *P. zorritensis* has become a prevalent invasive species in temperate coastal areas (Lambert and Lambert, 1998; Brunetti and Mastrototaro, 2004). One of the oldest reports of *P. zorritensis* outside its native range was on the Italian Mediterranean coast (Brunetti, 1978) and the species has recently been reported in several Mediterranean harbors and gulfs (Brunetti and Mastrototaro, 2004; Mastrototaro et al., 2008; Stabili et al., 2015; Tempesti et al., 2022). It was also found in several Pacific and Atlantic regions including Japan (Nishikawa et al., 1993; Otani, 2002; Iwasaki et al., 2004), Southern California (Lambert and Lambert, 1998; Nichols et al., 2023), Hawaii (Abbott et al., 1997), the Galapagos Islands (Lambert, 2019), the Panama Canal (Carman et al., 2011), the Caribbean (Monniot, 2018; Streit et al., 2021), Brazil (Millar, 1958), the Gulf of Mexico (Lambert et al., 2005), Florida (Vázquez and Young, 1996) and North Carolina (Villalobos et al., 2017). From 1994 to 2020, there was a noticeable rise in *P. zorritensis* abundance in Californian marinas, accompanied by a concomitant northward expansion of the species (Nichols et al., 2023). Similarly, subsequent to its initial introduction to Japan in 1991, *P. zorritensis* has emerged as a common NIA detected along the country's coasts (Iwasaki et al., 2004). The successful invasiveness of *P. zorritensis* has been attributed to its apparent tolerance to fluctuations in temperature and salinity (Lambert and Lambert, 1998) and its singular mode of asexual reproduction by vasal budding (Brunetti and Mastrototaro, 2004; Alié et al., 2018; Scelzo et al., 2019). During this process, the species produces resistant dormant forms (spherules) that plausibly allow long-distance human-mediated transport and colony restoration even in the absence of adult individuals and after extensive dormancy (Scelzo et al., 2019; Hiebert et al., 2022). Previous experimental studies demonstrated that larval behavior (Vázquez and Young, 1996) as well as zooid and spherule survival (Hiebert et al., 2022) are impacted by extreme temperature or salinity. However, we still have a poor understanding of the relationship between environmental parameters and asexual and sexual reproduction in *P. zorritensis*.

Coastal lagoons, harbors and marinas of the Mediterranean are known as hotspots for the entry and secondary spread of non-indigenous invasive species, whose diversity and distribution are influenced by environmental factors such as temperature, primary productivity or climate type (Ulman et al., 2017; Ulman et al., 2019a; Ulman et al., 2019b). While some non-indigenous ascidians such as *Ascidiella aspersa, Styela plicata, Ciona robusta*, and *Pyura dura*, are widely distributed throughout the Mediterranean, NIAs from the Red Sea are mostly found in the eastern Mediterranean (e.g. *Microcosmus exasperatus, Herdmania momus*), suggesting that west-east temperature and salinity gradients in the Mediterranean (Coll et al., 2010) may influence the distribution of non-indigenous ascidians, in relation to the species-specific ecological tolerances (Shenkar and Loya, 2008; Platin and Shenkar, 2023). Despite its local abundance, *P. zorritensis* is not among the most widely spread NIAs in the Mediterranean (Izquierdo-Muñoz, 2009; Cardeccia et al., 2018; Ulman et al., 2019a). *P. zorritensis* was not found on the 583 vessel hulls examined by Ulman et al. (2019b), although 71% of these vessels hosted at least one NIA. *P. zorritensis* was only recorded in one out of the 50 marinas analyzed by Ferrario et al. (2017), as well as Ulman et al. (Ulman et al., 2017; Ulman et al., 2019a). Furthermore, it was present in only one of the 32 marinas sampled in northern Spain (López-Legentil et al., 2015) and is absent from NIA-rich areas along the Tunisian and Israeli coasts (Chebbi et al., 2010; Gewing and Shenkar, 2017). Therefore, despite the long-standing observation of *P. zorritensis* in the Mediterranean (Brunetti, 1978), its distribution in the region has remained relatively restricted to the northwestern basins (Figure 1A). While salinity levels in marinas rich in NIAs are frequently higher than those found in surrounding open water (Ulman et al., 2019a), several Mediterranean sites where *P. zorritensis* is found have a salinity below the average 38 ppt of the western Mediterranean. In Taranto harbor's Mare Piccolo in Italy and the Thau lagoon in France, salinity levels have an annual average of 36-37 ppt (Audouin, 1962; Brunetti and Mastrototaro, 2004; André et al., 2021). Additionally, a salinity of 34 ppt was measured at the Santa Carla de la Rapita harbor in the Ebro delta

FIGURE 1
(A) Sites in the Mediterranean Sea where the presence of *Polyandrocarpa zorritensis* was reported. 1: Turon and Perera, 1988; 2: https://doris.ffessm.fr/Especes/Polyandrocarpa-zorritensis-Polyandrocarpe-de-Zorritos-5004; 3: Brunetti, 1978; 4: Tempesti et al., 2022; 5: Virgili et al., 2022; 6: Mastrototaro et al., 2008; 7: Stabili et al., 2015. The yellow spot marks La Spezia, where the samples for this study were collected. **(B)** Satellite view of the Assonautica Marina in La Spezia. Credit: Landsat/Copernicus Data SIO, NOAA, US Navy, NGA, GEBCO Inst. Geogr. Nacional GeoBasis-DE/BKG (©2009) 3D.

(López-Legentil et al., 2015). In La Spezia harbor, the spring salinity fluctuates between 32 and 37 ppt (Brunetti, 1978), while in Livorno harbor, the range spans from 35 to 39 ppt (Tempesti et al., 2022). In this study we investigated the influence of salinity on the reproduction of *P. zorritensis*, with emphasis on asexual reproduction by budding, analyzing in laboratory-controlled conditions the effects of different salinity values reported in regions where the species is found.

Materials and methods

Polyandrocarpa zorritensis collection, identification and husbandry

Colonies of *Polyandrocarpa zorritensis* were collected in the harbor of La Spezia, Italy (Assonautica Benedetti, 44°06′10.7″N, 9° 49′34.5″E) (Figure 1B). The presence of *P. zorritensis* was recorded by visual inspection of the mooring lines along the jetties of the marina on six occasions from May 2016 to February 2023. Salinity and temperature (Supplementary Table) were measured close to the surface, at the depth where *P. zorritensis* colonies were present. Taxonomic identification follows Van Name (1931), and molecular barcoding of colonies from La Spezia was conducted previously (Alié et al., 2018). The spherules were gently separated from the colony and stored in tanks containing seawater at 11°C (at salinity of 38-39ppt) before being used for experiments. To obtain zooids used for the experiments, the spherules were transferred to water tanks containing 12 liters of artificial seawater (ASW) at 24°C, prepared with deionized water and marine salt (Red Sea Salt, Red Sea) at the desired concentration. The spherules were placed on microscope glass slides (5x7cm) on the bottom of the tanks, with 5 to 12 spherules per slide and 3 to 4 slides per tank (see Supplementary Table). Since the number of stolons depends on spherule size (Scelzo et al., 2019), we took care to use spherules of similar sizes. The day-night light cycle was 12:12.

Upon hatching, bubblers were added to oxygenate the water, and animals were fed twice a day with a mix of 15ml of live *Tisochrysis lutea*, 15ml of live *Chaetoceros gracilis*, 250µl ISO800, and 250µl of Shellfish Diet 1800 (Reed Mariculture) per tank. Water was changed every two days, temperature was maintained around 24-24.5°C and colorimetric tests (Ammonia Marine Test Kit and Nitrate\Nitrite Marine Test Kit, Red Sea) were performed on a regular basis to ensure that NH_3/NH_4, NO_2 and NO_3 wastes did not reach toxic values throughout the experiments.

Asexual reproduction monitoring and quantification

Experiments were conducted from spherules collected in the harbor of La Spezia from 2019 to 2022. A first set of experiments was conducted on two different batches of spherules that were collected in autumn (November 5, 2019 and November 10, 2022) and maintained at 11°C for 80 and 99 days, respectively. Results from these two experiments were combined and analyzed as a single experiment (hereafter called "autumn"). Another set of experiments was conducted on a single batch of spherules collected in winter (February 2, 2022, called winter batch) and maintained at 11°C for 73 days and 97 days, respectively. A last experiment was conducted on spherules collected in spring (May 12, 2022, called spring batch) and used immediately after collection. Zooids were cultivated at 22, 29, 36 and 40ppt. Photos of the zooids were taken at regular intervals (see Supplementary Figure 1 as an example), up to 24 days after spherule seeding, from which date image-based quantification of asexual reproduction tends to become complicated due to the high number of overlapping stolons, which makes the individual assignment difficult. Pictures were taken with a Canon EOS 6D camera equipped with a 100mm macro lens. Stolon bases, stolon tips, budding nests, and newly hatched zooids were quantified from pictures of the last day of each experiment, using the Cell Counter plugin on ImageJ.

Quantification of sexual reproduction

Sexual reproduction was evaluated by counting the number of embryos and larvae produced per zooid, which were obtained from one experiment using the autumn 2022 spherules (Supplementary Table). Upon having reached sexual maturity (approximately a month after spherule seeding), zooids were relaxed in seawater with MS-222 (E10521-10G, Sigma Aldrich), then fixed in a solution of 4% paraformaldehyde diluted in ASW according to the salinity of each sample, at room temperature and then kept at 4°C. After several days of fixation, zooids were dissected and the number of gonads and brooded embryos in the atrial chamber was counted for each individual (see Supplementary Figures 2B-B' as an example). The swimming larvae and the embryos accidentally released by the zooids during the 9 days preceding their fixation were also counted, by visually inspecting the tanks every morning (from the time the light goes on, 8 a.m., to early afternoon, when they stopped releasing larvae) and before every water change. In this experiment, we raised 19 spherules at 40ppt, 22 spherules at 36 ppt and 20 spherules at 29 ppt (Supplementary Table).

Morphological measures, heartbeat rate and stolon pulsation period

Zooid size was measured using ImageJ, on the one-month-old animals hatched from spherules of the autumn 2022 batch, relaxed in MS-222 (a pinch of powder in 15 ml of sea water), and before fixing. Size was measured between the tip of the inhalant siphon and the posterior-most point of the body cavity (see Supplementary Figure 2A as an example). Heart and stolon beating rates were measured in an additional experiment using 14-days-old animals from the autumn batch (Supplementary Table). Heart beating rate was measured visually under a stereomicroscope, thanks to the transparency of the tunic, as the number of pulsations per minute. Stolon pulsation period was measured using timelapse imaging taken with a Leica M165-FC stereomicroscope equipped with an MC170-HD camera. One picture was taken every 5 seconds, a pulsation period being the lag time until the beating tip of a stolon comes back to its initial condition (see example movies at https://drive.google.com/drive/folders/1Z522byRFvnHer677YMKoQZMvjaDs6fKX?usp=sharing).

Results

Presence of *Polyandrocarpa zorritensis* coincides with lower salinity in La Spezia marina

In 2016, we investigated several spots in the La Spezia Bay, including marinas (Circolo Velico Palmito 44.086377, 9.878521; Darsena Pagliari 44.104680, 9.859106; Porto La Grazie 44.068307, 9.835713; Assonautica 44.103388, 9.82633) and open water oyster racks (44.071649, 9.857886; 44.057952, 9.842249). We only found *P. zorritensis* in the Assonautica marina (Figure 1B), the innermost investigated spot of the bay. From 2016 to 2023, we regularly found *Polyandrocarpa zorritensis* in this marina, usually as large aggregate colonies and/or as mats of dormant spherules on the immersed boat lines, in the proximity of a freshwater outlet (Figure 2). In May 2016 and 2022, the species was only visible on the proximal-most pontoons of the marina, where the salinity was the lowest, i.e., 29 and 34 ppt respectively (Figures 2A, D). While we cannot totally rule out that small residual colonies were present on the other pontoons, they were likely inconspicuous enough not to be detected. In the autumn and winter seasons, the colonies had a wider distribution, with measured salinities ranging between 36 and 38 ppt (Figures 2B, C, E, F).

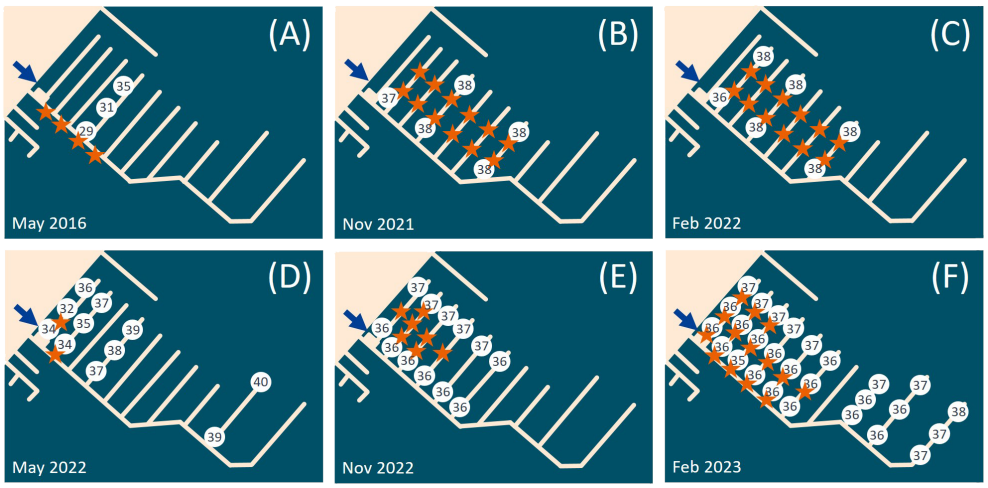

FIGURE 2
Polyandrocarpa zorritensis presence and salinity values observed in **(A)** May 2016, **(B)** May 2021, **(C)** February 2022, **(D)** May 2022, **(E)** November 2022 and **(F)** February 2023. The blue arrow indicates the inflow of fresh water in the marina. The white circles contain the salinity values (in ppt) observed in the different sites of the marina. The orange stars indicate the spots where *P. zorritensis* was found.

High salinity negatively affected the rate of asexual reproduction

To study the effect of the observed salinity on the asexual budding in *P. zorritensis*, we quantified the production of stolons, budding nests (also called buds) and new zooids produced by individual adult zooids (illustrated in Figure 3) cultivated at 22, 29, 36 and 40 ppt (Supplementary Table). These adults were obtained from dormant spherules collected in the field and later placed in experimental conditions in the laboratory. While none of the spherules placed at 22 ppt hatched, nearly every spherule in the other salinity conditions hatched after 5 to 7 days and gave rise to a functional zooid (Supplementary Table). When using spherules collected in autumn (Figures 4A-A") and maintained in dormancy for three months before the experiment, the salinity significantly affected the number of stolonial tips, which was significantly lower at 40 than at 36 ppt (Mann-Whitney p-value = 0.0071) (Figure 4A'), as well as the number of buds and of newly hatched zooids, which was significantly lower at 40 than at 29 (p-value = 0.0099) and 36 ppt (p-value = 6.05e-5) (Figure 4A"). The number of stolon bases was also significantly lower at 40 ppt than at 36 ppt (p-value = 0.014) and did not differ between 29 and the two other conditions (Figure 4A).

Experiments conducted with spherule batches collected in different seasons gave a similar, albeit less pronounced trend. When using spherules collected in winter (Figures 4B-B"), the number of stolon bases and stolon tips did not differ between the three treatments (Figures 4B-B'), but the salinity affected the number of nests and new zooids, which was lower at 40 than at 29 ppt (p-value = 0.011) (Figure 4B"). Finally, for spherules collected in spring (Figures 4C-C"), the number of stolon bases and stolon tips did not differ between the three treatments (Figures 4C-C') but the number of nest and new zooids was lower at 40 than 36 ppt (p-value = 0.037) (Figure 4C").

In order to estimate the yield between the growth of the colony and the actual reproduction via budding, we calculated a budding index, defined as the ratio between the number of nests and new zooids to the number of stolon bases. Regardless of the spherule batch used, as salinity increased, the budding index decreased (Figures 4D-D"). Using autumn and winter spherules, the budding index was significantly lower at 40 ppt when compared to 29 and 36 ppt (Figures 4D, D'). Using spring spherules the index was significantly higher at 29 ppt when compared to 40 and 36 ppt (Figure 4D"). All p-values associated with these experiments are given in the Supplementary Table.

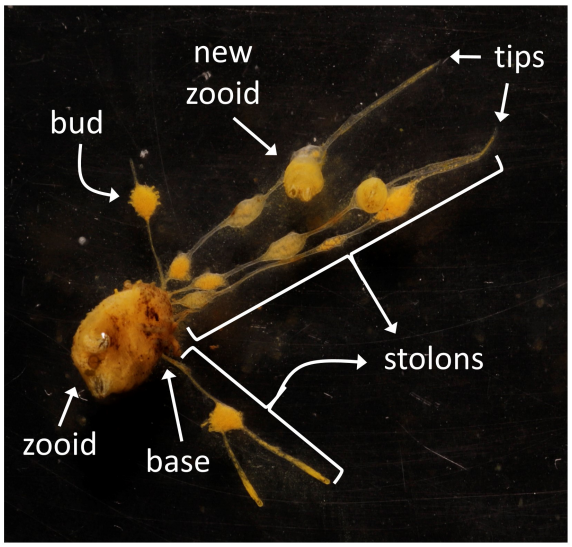

FIGURE 3
Parameters measured for the rate of asexual reproduction. Image showing a zooid originated from a dormant spherule, indicating the base of a stolon, tips of stolons, a bud (or budding nest), and a new zooid formed from a bud.

Salinity did not affect zooid physiology

Physiological variables reflecting the general zooid health (Dijkstra et al., 2008) were measured on the animals exposed to the tested salinities. The average size of the zooids, measured from the tip of the inhalant siphon to the posterior-most point of the body cavity, were 1.14, 1.24 and 1.31 cm for 50 days-old zooids grown at 29, 36 and 40 ppt respectively, with a significant difference between 29 and 40 ppt (p-value = 0.043) (Figure 5A; Supplementary Table). The average heartbeats rate (Figure 5B) did not significantly differ between the three conditions (56, 60 and 57.2 pulsations per minute at 29, 36 and 40 ppt respectively), neither did the period of stolon beating (110, 112 and 107 seconds at 29, 36 and 40 ppt respectively) (Figure 5C). These results suggest that zooids grow slightly slower at 29 ppt but do not experience chronic stress significantly affecting blood circulation in the colony.

Production of embryos and larvae

To assess whether sexual reproduction was equally affected by the salinity, we counted the number of gonads and offspring (larvae and embryos) present in the body cavity of one-month-old zooids obtained from autumn spherules (Figures 5D, E). The number of gonads did not significantly differ between the three conditions (Figure 5E). An average of 0.50 (± 0.82 SD), 2.04 (± 2,76) and 4.42 (± 6,6) offspring per zooid at 29, 36 and 40 ppt, respectively (Figure 5D) was counted, with no statistical difference between the three conditions probably due to high inter-individual variance. Indeed, while some zooids did not contain any offspring, others were bearing up to 19 embryos (Supplementary Table). Thus, we also counted the larvae and embryos present in the tanks during the nine days before the end of the experiment (Supplementary Figure 3). Adding these numbers to the offspring found inside the body cavity, we obtain a total of 11 larva and 23 embryos released by 20 zooids at 29 ppt (0.24 offspring per zooid/day), 112 larvae and 37 embryos released by the zooids at 36 ppt (0.73 offspring per zooid/day), and 104 larvae and 17 embryos released by 19 zooids at 40 ppt (0.70 offspring per zooid/day). Experimental replicates would be necessary to test for statistical significance, yet these results suggest

10.3389/fevo.2024.1332780

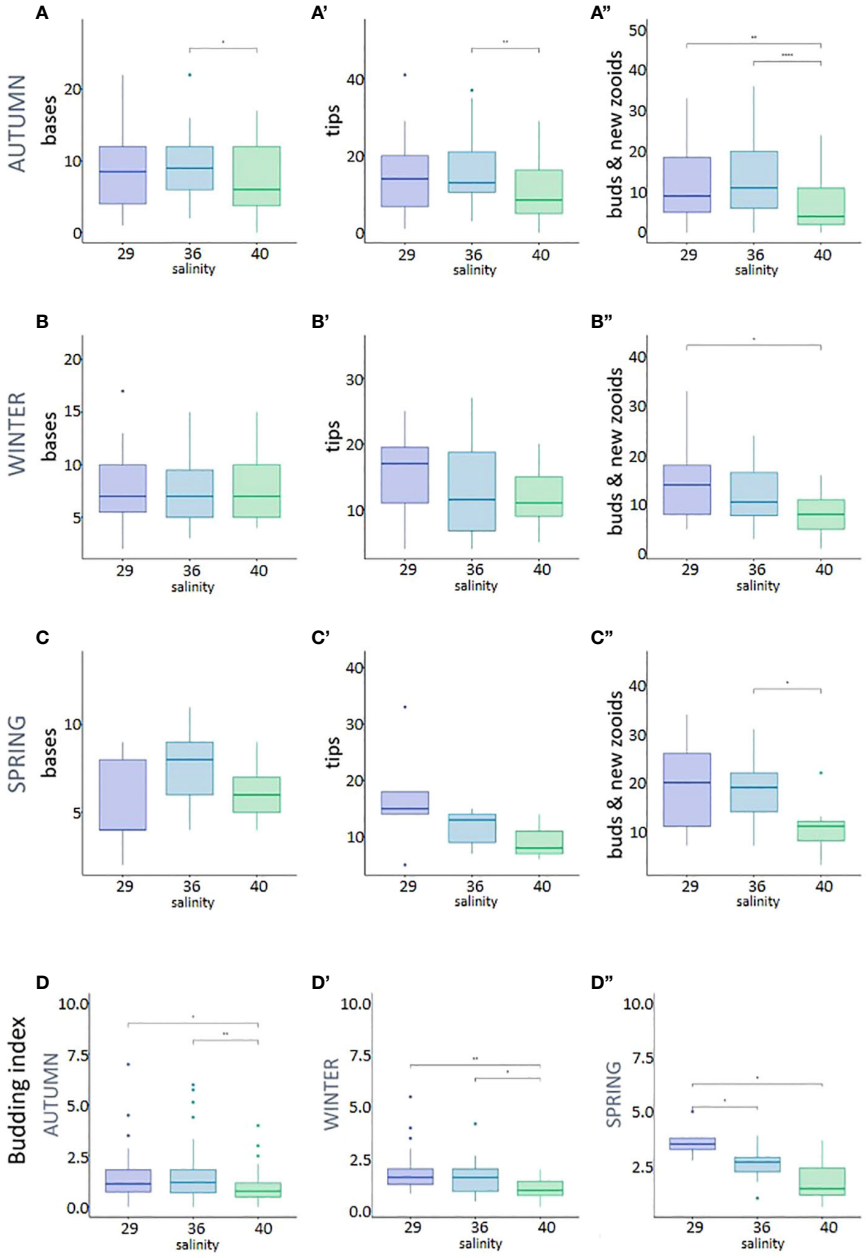

FIGURE 4
Asexual reproduction in the three different salinities: 29, 36 and 40 ppt, measured by the production of stolons bases, stolons tips, buds and new zooids, per adult zooid; **(A**-A") Autumn batch; **(B**-B") Winter batch; **(C**-C") Spring batch; **(D**-D") Budding index, i.e. ratio of buds and new zooids to stolon bases, per adult zooid. Stars correspond to the statistical analysis [Mann-Withney test with *p-value < 0.05, **p-value <0.01, and ****p-value < 0.001; absence of asterisk means no statistical significance (p-value > 0.05)].

that the number of offspring is approximately ten times lower at 29 ppt than at higher salinities.

Discussion

Salinity effect on asexual budding in *P. zorritensis*

Our results suggest that the rate of asexual reproduction in *P. zorritensis*, *i.e.* the number of asexually produced zooids 14 days after hatching of the spherules, is lower at 40 ppt salinity compared to 29 and 36 ppt. The salinity values of this study were selected on the basis of experimental evidence: 29 ppt was selected as it is the minimum level at which *P. zorritensis* was found in the sampling site (La Spezia, Assonautica Marina), while 36 ppt was chosen as it corresponds to the average level in semi-enclosed basins colonized by *P. zorritensis* in the Mediterranean Sea (Audouin, 1962; Brunetti and Mastrototaro, 2004). This salinity level also closely matches the surface salinity in the northern Peruvian coast (Chaigneau et al., 2013), where *P. zorritensis* was originally described. On the other hand, a salinity of 40 ppt is frequently observed in Mediterranean

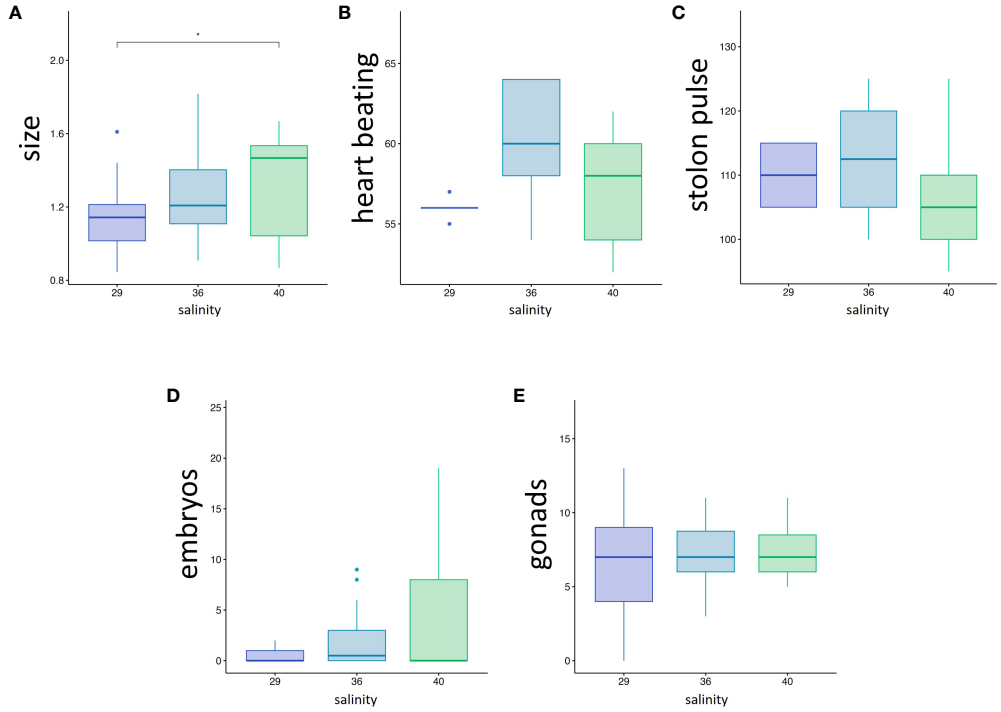

FIGURE 5
(A-C) Colony health parameters, **(A)** zooid size in cm, **(B)** heart beating rate (pulsations.min^{-1}), **(C)** Stolon pulsation period (time between two consecutive pulsation, in seconds). **(D, E)** Influence of salinity on sexual reproduction: **(D)** Number of brooded embryos per 1 month-old zooids. **(E)** Number of gonads per 1 month-old zooid. Stars correspond to the statistical analysis [Mann-Withney test with *p-value < 0.05; absence of asterisk means no statistical significance (p-value > 0.05)].

marinas (Ulman et al., 2019a; present study), which are the primary entry points and habitats for most non-indigenous ascidians (NIAs). Our experiments indicate that the quantity of zooids produced by spherules is smaller at 40 ppt than at lower salinities, indicating a negative impact of relatively high salinity on the asexual propagation of *P. zorritensis*.

Salinity has a notable impact on the budding index, which represents the average number of buds per stolon and which was used as a proxy for the relative energy allocation to colony expansion versus asexual replication (budding). This index was generally lower at 40 ppt, except for the comparisons between 36 and 40 ppt with spring spherules, where the difference is not statistically significant. Yet, while salinity affected the number of buds and zooids in most experiments, a significant effect on stolon bases and tips was only observed between 36 and 40 ppt with the autumn batch. This observation could reflect a different dynamic of colony expansion related to the larger size of autumn spherules (Hiebert et al., 2022). Additionally, it is also important to note that zooids raised at 40 ppt showed a slightly larger size than those raised at lower salinities. Taken as a whole, these results suggest that individuals raised at 40 ppt may prioritize somatic growth and colony expansion over asexual reproduction compared to those at lower salinities.

Overwintering spherules are probably a seasonal population bottleneck for *P. zorritensis*. Notably, in March 2018 and May 2019, *P. zorritensis* appeared to disappear almost completely from the La Spezia site, where only a few scattered resting spherules were found attached to boat mooring lines (Hiebert et al., 2022). Similarly, in May 2022, the animals were confined to the immediate proximity zone. This scenario contrasts sharply with the autumn situation, where *P. zorritensis* extensively dominated the benthic community by forming dense colonies consisting of numerous stolons and buds (see Figure 5 in Hiebert et al., 2022 or Figure 2 in Scelzo et al., 2019). This suggests that only a limited number of spherules are overwintering and that successful hatching in spring may be crucial for replenishing the population of *P. zorritensis*, which mainly relies on budding (Brunetti and Mastrototaro, 2004; Hiebert et al., 2022). Consequently, adverse conditions such as high salinity may significantly decrease the rate of asexual reproduction and greatly impact the fitness of *P. zorritensis*.

The above observations further support that salinity has a pronounced effect on the budding index in colonies originating from spring spherules. Indeed, these spherules were collected when the strongest salinity gradients were observed in the La Spezia marina, together with the lowest salinities recorded (34 to 40 ppt in May 2022 and 29 to 35 ppt in May 2016). In our experiments the spring batch was the only group to show a statistical difference between 29 and 36 ppt, with a budding index that was 2.5 times higher at 29 ppt compared to 40 ppt. This finding may have significant implications for adaptability to salinity gradients,

because spring spherules could be particularly vulnerable to water salinity. Therefore, strong salinity gradients during this critical season may have a significant impact on the reproductive outcomes of *P. zorritensis*, as the overwintering spherules are the ones that replenish the population.

The dispersal of *P. zorritensis* may be limited by extremely low salinities. Previous research has shown that the hatching potential of dormant spherules is halved after exposure to 15 ppt salinity for 48 hours and subsequent return to higher salinity (Hiebert et al., 2022). Thus, spherules are capable to withstand acute hypo-osmotic stress. However, our present findings suggest that spherules are unable to produce zooids when maintained at 22 ppt. In addition, it appears that a low salinity prevents larval recruitment. Indeed, Vázquez and Young (1996) reported that *P. zorritensis* larvae displayed abnormal swimming behavior at 26 ppt or lower, and actively escaped from water at 22 ppt when exposed to vertical haloclines. Taking these findings together with our present results, it is clear that water with a salinity as low as 22 ppt does not facilitate asexual reproduction and hinders larval recruitment, suggesting that *P. zorritensis* may not be able to thrive in brackish environments.

Effect of different salinities on asexual versus sexual reproduction

Although previous work on a colonial stolidobranch showed that temperature and salinity have different effects on sexual and asexual reproduction (Brunetti, 1984), the present study showed no statistically significant difference in the number of gonads and brooded embryos between the different experimental conditions. However, the number of larvae observed swimming in the tanks was approximately ten times lower at 29 ppt when compared to 36 and 40 ppt, suggesting that 36 ppt may be an ideal salinity at which both asexual and sexual reproduction rates are high. Further research into the effects of salinity on sexual reproduction could be carried out using histological analyses to examine gonadal maturity. In addition, other aspects related to sexual reproduction could be studied, such as the age at which zooids reach sexual maturity, or larval swimming behavior and larval recruitment at different salinities.

Coloniality in ascidians is often associated with reduced zooid size, ovoviviparity, and fewer embryos compared to solitary species (Berrill, 1935; Svane and Young, 1989; Zega et al., 2006; Alié et al., 2018). Accordingly, the gonads of *P. zorritensis* contain relatively few eggs, each zooid bearing approximately 20 embryos at different developmental stages (Van Name, 1945; Monniot, 2016; present study), and the embryonic development takes several days (personal observations). Each day a zooid releases only a few larvae (this study), which are lecithotrophic and low-dispersive with swimming times ranging from only a few minutes to a few hours (Vázquez and Young, 1996, personal observations). Therefore, a decrease in asexual reproduction in *P. zorritensis*, as observed at 40 ppt, may severely limit its fitness because sexual reproduction is unlikely to compensate for reproductive success in this species. In contrast, solitary *Polycarpa* species, which are closely related to *P. zorritensis* (Alié et al., 2018), are usually larger and have more and larger gonads (Van Name, 1945; Vazquez et al., 1995). They can spawn several dozens of planktonic eggs per week (Gordon et al., 2020), thus promoting long-distance dispersal by currents (Berrill, 1935; Svane and Young, 1989; Havenhand, 1991). *Styela plicata*, another Stolidobanch that is also very abundant in La Spezia marina, is a broadcast spawner of floating eggs that develop for several hours before metamorphosis (Yamaguchi, 1975; Villa and Patricolo, 2000; Crean and Marshall, 2015). Notably, there are reports of solitary oviparous phlebobranchs whose larvae can survive for ten days or disperse up to 1.5 km away (Svane and Young, 1989; Havenhand, 1991). In conclusion, while the colonial lifestyle is thought to provide competitive advantages over solitary organisms by allowing for indeterminate growth, colonization of complex microhabitats, or high regenerative capacity (Jackson, 1977; Kott, 1989; Dias et al., 2008; Hiebert et al., 2019), when a colonial ascidian such as *P. zorritensis* is in an environment where asexual propagation is hindered, the relatively few poorly dispersing larvae may limit its ability to compete for space with other fouling benthic organisms.

Conclusions

Understanding the ecological tolerance of *P. zorritensis* is crucial for global invasive potential forecasting, aiding targeted conservation efforts in high-priority ecosystems (Locke, 2009; Nichols et al., 2023). Salinity affects sexual and asexual reproduction, while previous research shows its impact on spherule and zooid survival under temperature stress (Hiebert et al., 2022). These findings, coupled with the predicted rise in Mediterranean Sea salinity (Parras-Berrocal et al., 2020), suggest a limited expansion potential of *P. zorritensis*. However, further research is required to characterize its ecological tolerance range, especially regarding the unknown impact of temperature on colony growth.

Data availability statement

The original contributions presented in the study are included in the article/Supplementary Material. Further inquiries can be directed to the corresponding author.

Ethics statement

Ethical approval was not required for the study involving animals in accordance with the local legislation and institutional requirements because the used species is not under restriction for ethical purpose.

Author contributions

VT-S: Conceptualization, Data curation, Formal analysis, Investigation, Writing – original draft, Writing – review & editing. RA-P: Conceptualization, Data curation, Formal analysis, Investigation, Writing – review & editing. DEG: Data curation, Formal analysis, Investigation, Writing – review & editing. ML: Formal analysis, Investigation, Writing – review & editing. ST: Conceptualization, Supervision, Writing – original draft, Writing – review & editing. AA: Conceptualization, Data curation, Formal analysis, Investigation, Supervision, Writing – original draft, Writing – review & editing.

Funding

The author(s) declare financial support was received for the research, authorship, and/or publication of this article. This study was supported by Sorbonne University EMERGENCE 2021/22 and INSB-DBM2021-2024.

Acknowledgments

We would like to thank the "Service Aquariologie" of CRB (IMEV-FR3761) supported by EMBRC-France for the help with the marine-culture facility. We warmly thank Laurent Gilleta for assistance with animal collection and husbandry. We are also grateful to the team of Assonautica marina (La Spezia) and to lab members who helped collecting *P. zorritensis*: Irene Kopelman, Manon Boosten, Marta Scelzo, Laurel Hiebert and Sonia Lotito. We thank Laurel Hiebert and Roland Zimm for advice on the manuscript. Finally, we thank Alexandre Jan and Christian Sardet for their help and advice on the photographic setup.

Conflict of interest

The authors declare that the research was conducted in the absence of any commercial or financial relationships that could be construed as a potential conflict of interest.

Publisher's note

Supplementary material

The Supplementary Material for this article can be found online at: https://www.frontiersin.org/articles/10.3389/fevo.2024.1332780/full#supplementary-material

SUPPLEMENTARY FIGURE 1
Example of asexual reproduction photo documentation; **(A)** First day of image acquisition, when the zooid starts shooting stolons (seven days after the experiment's start); **(B)** Intermediate stage of the experiment; **(C)** Last day of image acquisition, at which the experiment was stopped.

SUPPLEMENTARY FIGURE 2
(A) The zooid size is the result from the sum of two measures: 1. oral siphon length, 2. zooid body (from the base to the region between the two siphons; **(B)** Zooid dissection for embryos and gonads counting. (B') Dissected zooid showing the location of gonads.

SUPPLEMENTARY FIGURE 3
Larvae released by the zooids during the nine days prior sample fixation.

References

Abbott, D. P., Newberry, A. T., and Morris, K. M. (1997). *Section 6B: Ascidians (Urochordata). Reef and Shore Fauna of Hawaii* Vol. 64 (Honolulu, Hawai'i: Bishop Museum Special Publ).

Alié, A., Hiebert, L. S., Simion, P., Scelzo, M., Prünster, M. M., Lotito, S., et al. (2018). Convergent acquisition of nonembryonic development in styelid ascidians. *Mol. Biol. Evol.* 35 (7), 1728–1743. doi: 10.1093/molbev/msy068

André, F., Girard, P., and Alié, A. (2021) *DORIS, 08/07/2021: Polyandrocarpa zorritensis (Van Name 1931)*. Available at: https://doris.ffessm.fr/ref/specie/5004.

Audouin, J. (1962). Hydrologie de l'étang de Thau. *Revue des Travaux de l'Institut des Pêches Maritimes* 26, 5–104.

Berrill, N. J. (1935). Studies in tunicate development. Part IV. Asexual reproduction. *Philos. Trans. R. Soc. London Ser. B Biol. Sci.* 225 (526), 327–379. doi: 10.1098/rstb.1935.0014

Brunetti, R. (1978). *Polyandrocarpa zorritensis* (Van name 1931) A colonial ascidian new to the mediterranean record. *Vie Milieu* XXVIII–XXIX (AB), 647–652.

Brunetti, R. (1984). Combined Effects of Temperature and Salinity on Colonies of Botryllus schlosseri and Botfylloides leachi (Ascidiacea) from the Venetian Lagoon. *Mar. Ecol. Prog. Ser.* 2 (4), 303–314. doi: 10.3354/meps002303

Brunetti, R., and Mastrototaro, F. (2004). The non-indigenous stolidobranch ascidian *Polyandrocarpa zorritensis* in the mediterranean: description, larval morphology and pattern of vascular budding. *Zootaxa* 528 (1), 1. doi: 10.11646/zootaxa.528.1.1

Bullard, S. G., Lambert, G., Carman, M. R., Byrnes, J., Whitlatch, R. B., Ruiz, G., et al. (2007). The colonial ascidian didemnum sp. A: current distribution, basic biology and potential threat to marine communities of the Northeast and West coasts of North America. *J. Exp. Mar. Biol. Ecol.* 342 (1), 99–108. doi: 10.1016/j.jembe.2006.10.020

Carballo, J. L. (2000). Larval ecology of an ascidian tropical population in a mediterranean enclosed ecosystem. *Mar. Ecol. Prog. Ser.* 195, 159–167. doi: 10.3354/meps195159

Cardeccia, A., Marchini, A., Occhipinti-Ambrogi, A., Galil, B., Gollasch, S., Minchin, D., et al. (2018). Assessing biological invasions in European seas: biological traits of the most widespread non-indigenous species. *Estuarine Coast. Shelf Sci.* 201, 17–28. doi: 10.1016/j.ecss.2016.02.014

Carman, M., Bullard, S., Rocha, R., Lambert, G., Dijkstra, J., Roper, J., et al. (2011). Ascidians at the Pacific and Atlantic entrances to the Panama canal. *Aquat. Invasions* 6 (4), 371–380. doi: 10.3391/ai.2011.6.4.02

Castilla, J. C., Guiñez, R., Caro, A. U., and Ortiz, V. (2004). Invasion of a rocky intertidal shore by the tunicate pyura praeputialis in the bay of antofagasta, Chile. *Proc. Natl. Acad. Sci.* 101 (23), 8517–8524. doi: 10.1073/pnas.0401921101

Chaigneau, A., Dominguez, N., Eldin, G., Vasquez, L., Flores, R., Grados, C., et al. (2013). Near-coastal circulation in the Northern humboldt current system from shipboard ADCP data: CIRCULATION OF THE NHCS FROM SADCP DATA. *J. Geophys. Res.: Oceans* 118 (10), 5251–5266. doi: 10.1002/jgrc.20328

Chebbi, N., Mastrototaro, F., and Missaoui, H. (2010). Spatial distribution of ascidians in two Tunisian lagoons of the Mediterranean sea. *Cahiers Biol. Mar.* 51 (2), 117–127.

Clarke Murray, C., Gartner, H., Gregr, E. J., Chan, K., Pakhomov, E., and Therriault, T. W. (2014). Spatial distribution of marine invasive species: environmental, demographic and vector drivers. *Diversity Distrib.* 20 (7), 824–836. doi: 10.1111/ddi.12215

Clarke Murray, C., Pakhomov, E. A., and Therriault, T. W. (2011). Recreational boating: A large unregulated vector transporting marine invasive species: transport of NIS by recreational boats. *Diversity Distrib.* 17 (6), 1161–1172. doi: 10.1111/j.1472-4642.2011.00798.x

Cognetti, G., and Maltagliati, F. (2000). Biodiversity and adaptive mechanisms in brackish water fauna. *Mar. pollut. Bull.* 40 (1), 7–14. doi: 10.1016/S0025-326X(99)00173-3

Coll, M., Piroddi, C., Steenbeek, J., Kaschner, K., Lasram, F. B. R., Aguzzi, J., et al. (2010). The biodiversity of the Mediterranean Sea: estimates, patterns, and threats. *PloS One* 5 (8), e11842. doi: 10.1371/journal.pone.0011842

Crean, A. J., and Marshall, D. J. (2015). Eggs with larger accessory structures are more likely to be fertilized in both low and high sperm concentrations in styela plicata (Ascidiaceae). *Mar. Biol.* 162 (11), 2251–2256. doi: 10.1007/s00227-015-2755-0

Dias, G. M., Delboni, C. G. M., and Duarte, L. F. L. (2008). Effects of competition on sexual and clonal reproduction of a tunicate: the importance of competitor identity. *Mar. Ecol. Prog. Ser.* 362, 149–156. doi: 10.3354/meps07447

Dijkstra, J., Dutton, A., Westerman, E., and Harris, L. (2008). Heart Rate Reflects Osmotic Stress Levels in Two Introduced Colonial Ascidians Botryllus schlosseri and Botrylloides violaceus. *Mar. Biol.* 154 (5), 805–811. doi: 10.1007/s00227-008-0973-4

Dybern, B. I. (1967). The distribution and salinity tolerance of ciona intestinalis (L.) F. Typica with special reference to the waters around Southern Scandinavia. *Ophelia* 4 (2), 207–226. doi: 10.1080/00785326.1967.10409621

Dybern, B. I. (1969). Distribution and ecology of ascidians in kviturdvikpollen and Vågsböpollen on the West coast of Norway. *Sarsia* 37 (1), 21–40. doi: 10.1080/00364827.1969.10411143

Epelbaum, A., Herborg, L. M., Therriault, T. W., and Pearce, C. M. (2009). Temperature and salinity effects on growth, survival, reproduction, and potential distribution of two non-indigenous botryllid ascidians in British Columbia. *J. Exp. Mar. Biol. Ecol.* 369 (1), 43–52. doi: 10.1016/j.jembe.2008.10.028

Ferrario, J., Caronni, S., Occhipinti-Ambrogi, A., and Marchini, A. (2017). Role of commercial harbours and recreational marinas in the spread of non-indigenous fouling species. *Biofouling* 33 (8), 651–660. doi: 10.1080/08927014.2017.1351958

Gewing, M.-T., Goldstein, E., Buba, Y., and Shenkar, N. (2018). Temperature resilience facilitates invasion success of the solitary ascidian herdmania momus. *Biol. Invasions* 21 (2), 349–361. doi: 10.1007/s10530-018-1827-8

Gewing, M.-T., López-Legentil, S., and Shenkar, N. (2017). Anthropogenic factors influencing invasive ascidian establishment in natural environments. *Mar. Environ. Res.* 131, 236–242. doi: 10.1016/j.marenvres.2017.10.001

Gewing, M.-T., and Shenkar, N. (2017). Monitoring the magnitude of marine vessel infestation by non-indigenous ascidians in the Mediterranean. *Mar. pollut. Bull.* 121 (1–2), 52–59. doi: 10.1016/j.marpolbul.2017.05.041

Gordon, T., Roth, L., Caicci, F., Manni, L., and Shenkar, N. (2020). Spawning induction, development and culturing of the solitary ascidian polycarpa mytiligera, an emerging model for regeneration studies. *Front. Zool.* 17 (1), 19. doi: 10.1186/s12983-020-00365-x

Granot, I., Shenkar, N., and Belmaker, J. (2017). Habitat niche breadth predicts invasiveness in solitary ascidians. *Ecol. Evol.* 7 (19), 7838–7847. doi: 10.1002/ece3.3351

Gröner, F., Lenz, M., Wahl, M., and Jenkins, S. R. (2011). Stress resistance in two colonial ascidians from the Irish sea: the recent invader didemnum vexillum is more tolerant to low salinity than the cosmopolitan diplosoma listerianum. *J. Exp. Mar. Biol. Ecol.* 409 (1–2), 48–52. doi: 10.1016/j.jembe.2011.08.002

Havenhand, J. N. (1991). Fertilisation and the potential for dispersal of gametes and larvae in the solitary ascidian ascidia Mentula Müller. *Ophelia* 33 (1), 01–15. doi: 10.1080/00785326.1991.10429738

Hiebert, L. S., Scelzo, M., Alié, A., De Tomaso, A. W., Brown, F. D., and Tiozzo, S. (2022). Comparing dormancy in two distantly related tunicates reveals morphological, molecular, and ecological convergences and repeated co-option. *Sci. Rep.* 12 (1), 12620. doi: 10.1038/s41598-022-16656-8

Hiebert, L. S., Vieira, E. A., Dias, G. M., Tiozzo, S., and Brown, F. D. (2019). Colonial ascidians strongly preyed upon, yet dominate the substrate in a subtropical fouling community. *Proc. R. Soc. B* 286 (1903), 20190396. doi: 10.1098/rspb.2019.0396

Iwasaki, K., Kimura, T., Kinoshita, K., Yamaguchi, T., Nishikawa, T., Nishi, E., et al. (2004). Human-mediated introduction and dispersal of marine organisms in Japan: Results of a questionnaire survey by the Committee for the Preservation of the Natural Environment, the Japanese Association of Benthology. *Japan. J. Benthol.* 59 (1), 22–44. doi: 10.5179/benthos.59.22

Izquierdo-Muñoz, A. (2009). Recent non-indigenous ascidians in the Mediterranean Sea. *Aquat. Invasions* 4 (1), 59–64. doi: 10.3391/ai.2009.4.1.5

Jackson, J. B. C. (1977). Competition on marine hard substrata: The adaptive significance of solitary and colonial strategies. *Am. Nat.* 111, 743–767. doi: 10.1086/283203

Kott, P. (1989). Form and function in the ascidiacea. *Bull. Mar. Sci.* 45, 253–276.

Lambert, C. C., and Lambert, G. (1998). Non-indigenous ascidians in Southern California harbors and marinas. *Mar. Biol.* 130 (4), 675–688. doi: 10.1007/s002270050289

Lambert, C. C., and Lambert, G. (2003). Persistence and differential distribution of nonindigenous ascidians in harbors of the Southern California bight. *Mar. Ecol. Prog. Ser.* 259, 145–161. doi: 10.3354/meps259145

Lambert, G. (2002). Nonindigenous ascidians in tropical waters. *Pacific Sci.* 56 (3), 291–298. doi: 10.1353/psc.2002.0026

Lambert, G. (2019). Fouling ascidians (Chordata: ascidiacea) of the galápagos: Santa Cruz and Baltra Islands. *Aquat. Invasions* 14 (1), 132–149. doi: 10.3391/ai.2019.14.1.05

Lambert, G., Faulkes, Z., Lambert, C. C., and Scofield, V. L. (2005). Ascidians of South Padre Island, Texas, with a key to species. *Texas J. Sci.* 57, 251–262.

Locke, A. (2009). A screening procedure for potential tunicate invaders of Atlantic Canada. *Aquat. Invasions* 4 (1), 71–79. doi: 10.3391/ai.2009.4.1.7

López-Legentil, S., Legentil, M. L., Erwin, P. M., and Turon, X. (2015). Harbor networks as introduction gateways: contrasting distribution patterns of native and introduced ascidians. *Biol. Invasions* 17 (6), 1623–1638. doi: 10.1007/s10530-014-0821-z

Mastrototaro, F., D'Onghia, G., and Tursi, A. (2008). Spatial and seasonal distribution of ascidians in a semi-enclosed basin of the Mediterranean Sea. *J. Mar. Biol. Assoc. United Kingdom* 88 (5), 1053–1061. doi: 10.1017/S0025315408001392

Millar, R. H. (1958). Some ascidians from Brazil. *Ann. Mag. Natural History* 1 (8), 497–514. doi: 10.1080/00222935808650975

Monniot, F. (2016). A new species of Polyandrocarpa (Ascidiacea, styelidae) in the Mediterranean sea. *Zootaxa* 4132 (1), 87. doi: 10.11646/zootaxa.4132.1.7

Monniot, F. (2018). Ascidians collected during the madibenthos expedition in Martinique: 2. Stolidobranchia, *styelidae*. *Zootaxa* 4410 (2), 291. doi: 10.11646/zootaxa.4410.2.3

Nagar, L., and Shenkar, N. (2016). Temperature and salinity sensitivity of the invasive ascidian *microcosmus exasperatus* Helle. *Aquat. Invasions* 11 (1), 33–43. doi: 10.3391/ai.2016.11.1.04

Nichols, C. L., Lambert, G., and Nydam, M. L. (2023). Continued persistence of non-native ascidians in Southern California harbors and marinas. *Aquat. Invasions* 18 (1), 1–22. doi: 10.3391/ai.2023.18.1.101962

Nishikawa, T., Kajiwara, Y., and Kawamura, K. (1993). Probable introduction of *Polyandrocarpa zorritensis* (Van Name) to Kitakyushu and Kochi. Japan. *Zool. Sci. Suppl. Tokyo* 10, 176.

Otani, M. (2002). Appearance and latest trends of introduced marine sessile animals in Japanese waters. *Sessile Org* 19, 69–92. doi: 10.4282/sosj.19.69

Parras-Berrocal, I. M., Vazquez, R., Cabos, W., Sein, D., Mañanes, R., Perez-Sanz, J., et al. (2020). The climate change signal in the Mediterranean Sea in a regionally coupled atmosphere–ocean model. *Ocean Sci.* 16, 743–765. doi: 10.5194/os-16-743-2020

Pineda, M. C., Turon, X., and López-Legentil, S. (2012). Stress levels over time in the introduced ascidian *styela plicata*: the effects of temperature and salinity variations on hsp70 gene expression. *Cell Stress Chaperones* 17 (4), 435–444. doi: 10.1007/s12192-012-0321-y

Platin, R., and Shenkar, N. (2023). Can Stand the Heat – Ecology of the Potentially Invasive Ascidian *Styela plicata* along the Mediterranean Coast of Israel. *Front. Mar. Sci.* 10. doi: 10.3389/fmars.2023.1159231

Rocha, R. M., Castellano, G. C., and Freire, C. A. (2017). Physiological tolerance as a tool to support invasion risk assessment of tropical ascidians. *Mar. Ecol. Prog. Ser.* 577, 105–119. doi: 10.3354/meps12225

Scelzo, M., Alexandre, A., Pagnotta, S., Lejeune, C., Henry, P., Gilletta, L., et al. (2019). Novel budding mode in *Polyandrocarpa zorritensis*: A model for comparative studies on asexual development and whole body regeneration. *EvoDevo* 10 (1), 7. doi: 10.1186/s13227-019-0121-x

Shenkar, N., and Loya, Y. (2008). The solitary ascidian herdmania momus: native (Red sea) versus non-indigenous (Mediterranean) populations. *Biol. Invasions* 10 (8), 1431–1439. doi: 10.1007/s10530-008-9217-2

Sims, L. L. (1984). Osmoregulatory capabilities of three macrosympatric stolidobranch ascidians, *Styela clava* Herdman, *S. plicata* (Lesueur), and *S. montereyensis* (Dall). *J. Exp. Mar. Biol. Ecol.* 82 (2–3), 117–129. doi: 10.1016/0022-0981(84)90098-4

Stabili, L., Licciano, M., Longo, C., Lezzi, M., and Giangrande, A. (2015). The Mediterranean non-indigenous ascidian *Polyandrocarpa zorritensis*: microbiological accumulation capability and environmental implications. *Mar. pollut. Bull.* 101 (1), 146–152. doi: 10.1016/j.marpolbul.2015.11.005

Streit, O. T., Lambert, G., Erwin, P. M., and López-Legentil, S. (2021). Diversity and abundance of native and non-native ascidians in Puerto Rican harbors and marinas. *Mar. pollut. Bull.* 167, 112262. doi: 10.1016/j.marpolbul.2021.112262

Svane, I., and Young, C. M. (1989). The ecology and behaviour of ascidian larvae. *Oceanogr. Mar. Biol.: an Annu. Rev.* 27, 45–90.

Tempesti, J., Langeneck, J., Romani, L., Garrido, M., Lardicci, C., Maltagliati, F., et al. (2022). Harbour type and use destination shape fouling community and non-indigenous species assemblage: A study of three Northern Tyrrhenian port systems (Mediterranean sea). *Mar. pollut. Bull.* 174, 113191. doi: 10.1016/j.marpolbul.2021.113191

Turon, X., and Perera, M. (1988). Las ascidias del Delta del Ebro. Aspectos faunisticos y cuantitativos. *P. Dept. Zool. Barcelona* 14, 81–90.

Ulman, A., Ferrario, J., Forcada, A., Arvanitidis, C., Occhipinti-Ambrogi, A., and Marchini, A. (2019a). A Hitchhiker's guide to Mediterranean marina travel for alien species. *J. Environ. Manage.* 241, 328–339. doi: 10.1016/j.jenvman.2019.04.011

Ulman, A., Ferrario, J., Forcada, A., Seebens, H., Arvanitidis, C., Occhipinti-Ambrogi, A., et al. (2019b). Alien species spreading via biofouling on recreational vessels in the Mediterranean sea. *J. Appl. Ecol.* 56 (12), 2620–2629. doi: 10.1111/1365-2664.13502

Ulman, A., Ferrario, J., Occhipinti-Ambrogi, A., Arvanitidis, C., Bandi, A., Bertolino, M., et al. (2017). A massive update of non-indigenous species records in Mediterranean marinas. *PeerJ* 5, e3954. doi: 10.7717/peerj.3954

Van Name, W. G. (1931). The North and South American ascidians. *Bull. Amer. Mus. Nat. Hist.* 61.

Van Name, W. G. (1945). The North and South American ascidians. *Bull. Amer. Mus. Nat. Hist.* 84.

Vazquez, E., Ramos-Espla, A. A., and Turon, X. (1995). The genus polycarpa (*Ascidiacea*, *styelidae*) on the Atlantic and Mediterranean coasts of the Iberian Peninsula. *J. Zool.* 237 (4), 593–614. doi: 10.1111/j.1469-7998.1995.tb05017.x

Vázquez, E., and Young, C. M. (1996). Responses of compound ascidian larvae to haloclines. *Mar. Ecol. Prog. Ser.* 133, 179–190. doi: 10.3354/meps133179

Vázquez, E., and Young, C. M. (2000). Effects of low salinity on metamorphosis in estuarine colonial ascidians. *Inverteb. Biol.* 119 (4), 433–444. doi: 10.1111/j.1744-7410.2000.tb00113.x

Villa, L. A., and Patricolo, E. (2000). The follicle cells of styela plicata (*Ascidiacea*, tunicata): A sem study. *Zool. Sci.* 17 (8), 1115–1121. doi: 10.2108/zsj.17.1115

Villalobos, S., Lambert, G., Shenkar, N., and López-Legentil, S. (2017). Distribution and population dynamics of key ascidians in North Carolina harbors and marinas. *Aquat. Invasions* 12 (4), 447–458. doi: 10.3391/ai.2017.12.4.03

Virgili, R., Tanduo, V., Katsanevakis, S., Terlizzi, F., Villani, G., Fontana, A., et al. (2022). The miseno lake (Central-Western Mediterranean sea): an overlooked reservoir of non-indigenous and cryptogenic ascidians in a marine reserve. *Front. Mar. Sci.* 9. doi: 10.3389/fmars.2022.866906

Yamaguchi, M. (1975). Growth and reproductive cycles of the marine fouling ascidians *ciona intestinalis*, *styela plicata*, *botrylloides violaceus*, and *leptoclinum mitsukurii* at aburatsubo-moroiso inlet (Central Japan). *Mar. Biol.* 29 (3), 253–259. doi: 10.1007/BF00391851

Zega, G., Thorndyke, M. C., and Brown, E. R. (2006). Development of swimming behaviour in the larva of the ascidian ciona intestinalis. *J. Exp. Biol.* 209 (17), 3405–3412. doi: 10.1242/jeb.02421

frontiers | Frontiers in Cell and Developmental Biology

TYPE Review
PUBLISHED 12 March 2024
DOI 10.3389/fcell.2024.1340157

OPEN ACCESS

EDITED BY
Lucia Manni,
University of Padua, Italy

REVIEWED BY
João E. Carvalho,
UMR7009 Laboratoire de Biologie du Développement de Villefranche sur Mer, France
Gerhard Schlosser,
University of Galway, Ireland

*CORRESPONDENCE
Joel C. Glover,
joel.glover@medisin.uio.no

RECEIVED 17 November 2023
ACCEPTED 26 February 2024
PUBLISHED 12 March 2024

CITATION
Fritzsch B and Glover JC (2024), Gene networks and the evolution of olfactory organs, eyes, hair cells and motoneurons: a view encompassing lancelets, tunicates and vertebrates.
Front. Cell Dev. Biol. 12:1340157.
doi: 10.3389/fcell.2024.1340157

Gene networks and the evolution of olfactory organs, eyes, hair cells and motoneurons: a view encompassing lancelets, tunicates and vertebrates

Bernd Fritzsch[1] and Joel C. Glover[2,3]*

[1]Department of Biological Sciences, University of Nebraska Medical Center, Omaha, NE, United States, [2]Sars International Centre for Marine Molecular Biology, University of Bergen, Bergen, Norway, [3]Laboratory of Neural Development and Optical Recording (NDEVOR), Department of Molecular Medicine, Institute of Basic Medical Sciences, University of Oslo, Oslo, Norway

Key developmental pathways and gene networks underlie the formation of sensory cell types and structures involved in chemosensation, vision and mechanosensation, and of the efferents these sensory inputs can activate. We describe similarities and differences in these pathways and gene networks in selected species of the three main chordate groups, lancelets, tunicates, and vertebrates, leading to divergent development of olfactory receptors, eyes, hair cells and motoneurons. The lack of appropriately posited expression of certain transcription factors in lancelets and tunicates prevents them from developing vertebrate-like olfactory receptors and eyes, although they generate alternative structures for chemosensation and vision. Lancelets and tunicates lack mechanosensory cells associated with the sensation of acoustic stimuli, but have gravisensitive organs and ciliated epidermal sensory cells that may (and in some cases clearly do) provide mechanosensation and thus the capacity to respond to movement relative to surrounding water. Although functionally analogous to the vertebrate vestibular apparatus and lateral line, homology is questionable due to differences in the expression of the key transcription factors *Neurog* and *Atoh1/7,* on which development of vertebrate hair cells depends. The vertebrate hair cell-bearing inner ear and lateral line thus likely represent major evolutionary advances specific to vertebrates. Motoneurons develop in vertebrates under the control of the ventral signaling molecule hedgehog/sonic hedgehog (*Hh,Shh*), against an opposing inhibitory effect mediated by dorsal signaling molecules. Many elements of *Shh*-signaling and downstream genes involved in specifying and differentiating motoneurons are also exhibited by lancelets and tunicates, but the repertoire of MNs in vertebrates is broader, indicating greater diversity in motoneuron differentiation programs.

KEYWORDS

transcription factors, gene networks, motoneurons, hair cells, eyes, olfaction

Introduction

The comparative study of the nervous system and associated sensory structures can provide insight into the evolution of the molecular pathways governing their development and function. Chordates (lancelets, tunicates, and vertebrates) share several key structural features in this regard, including a notochord, a dorsal neural tube, and a dorsal opening of the rostral neural tube that forms the neuropore (Figure 1). Beyond this, there are additional similarities and some significant differences in the organization and development of sensory and efferent systems, which require elucidation at the molecular level. Recent genetic insights are beginning to facilitate evolutionary comparisons of these systems in the three chordate groups (Marlétaz et al., 2018; Poncelet and Shimeld, 2020; Marletaz et al., 2023; Roure et al., 2023).

Lancelets have only two main central nervous system (CNS) divisions, whereas tunicates have up to four (Takahashi and Holland, 2004) and vertebrates have at least five including the unique rostral extension comprising the bipartite telencephalon (Figure 1). The relative lengths of the notochord and neural tube differ; in lancelets the notochord extends beyond the rostral and caudal ends of the neural tube, in tunicates the neural tube extends rostrally beyond the notochord (Miyamoto and Crowther, 1985; Søviknes et al., 2007; Søviknes and Glover, 2008; Dong et al., 2009), and in all vertebrates the notochord ends near the midbrain-hindbrain boundary, so that the entire prosencephalon extends rostrally beyond the notochord (Welsch et al., 1998; Satoh et al.,

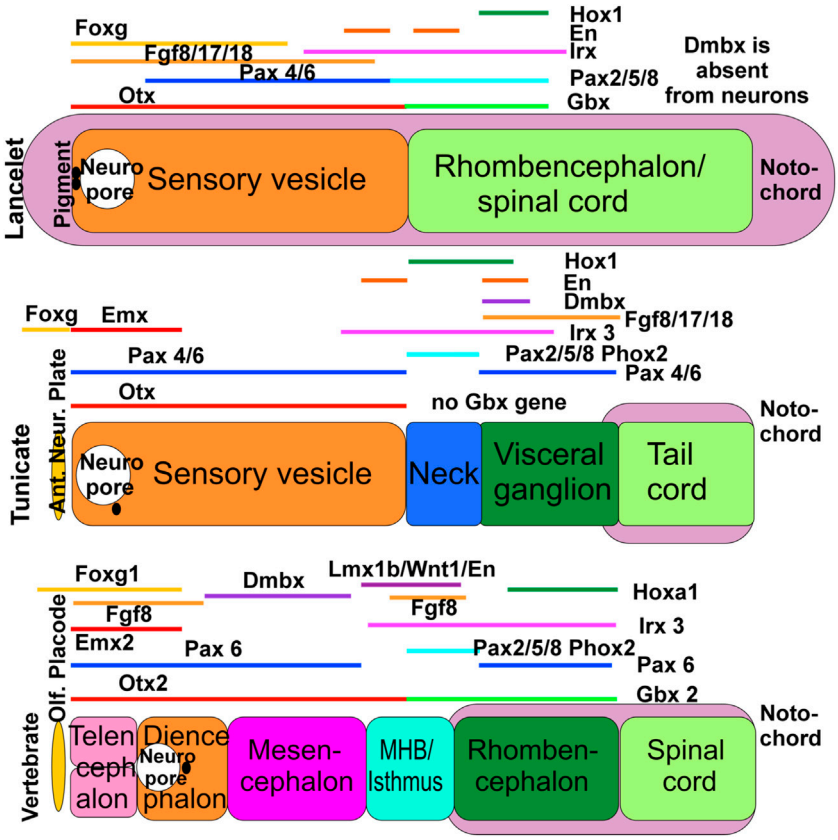

FIGURE 1
The evolution of gene expression in chordates, shown schematically here in lancelets, ascidian tunicates (represented by *Ciona*) and vertebrates. All three chordate groups exhibit partially overlapping expression of *Foxg, Emx, Otx, Irx*, and *Fgf* orthologs. In some cases the vertebrate gene names are used in all 3 panels for comparison, but we emphasize that these represent the corresponding gene orthologs in lancelets and tunicates (which may have different names in these taxa, particularly in cases where multiple orthologs exist in vertebrates). Lancelets do not express a *Dmbx* ortholog in the neural tube. In ascidian tunicates, *Dmbx* ortholog expression coincides with the caudal limit of *Irx3* ortholog expression and *Foxg* ortholog expression extends rostral to the neuropore. In vertebrates, *Dmbx* expression extends rostral to the *Irx3* expression domain to define the midbrain, while the forebrain and the olfactory placode are *Foxg1-positive*. In lancelets, *Gbx* ortholog expression overlaps with *Pax2/5/8* ortholog and most of *Irx3* ortholog expression. Ascidian tunicates have no *Gbx* ortholog but have a relationship between *Pax2/5/8 and Pax4/6* ortholog expression domains comparable to vertebrates. In vertebrates, the *Otx* expression domain abuts the *Gbx* expression domain. Together, these data show that certain gene expression domains are topographically conserved (*Hox, Otx*), whereas others show varying degrees of overlap (*Foxg, Dmbx*). It is conceivable that the evolution of nested expression domains of transcription factors is causally related to the evolution of specific neuronal features around the MHB. In vertebrates, the abutting domains of *Otx2* and *Gbx2* expression at the MHB stabilize the expression of Fgf8 (lower right), which in turn stabilizes the expression of *Wnt1* and engrailed (En1). Mutation of *Otx2, Gbx2, Fgf8, Lmx1b* or *Wnt1* eliminates the MHB. *Pax2/5/8* is also expressed at the MHB, whereas Dmbx expression starts immediately rostral to the MHB (in the midbrain) to later expand into the hindbrain and spinal cord. Experimental work has demonstrated that the development of vertebrate motor centers in the midbrain and upper hindbrain depends on the formation of the MHB. Ant. Neur. Plate; anterior neural plate boundary; MHB, midbrain/hindbrain boundary; Olf. Placode, olfactory placode. Modified after (Takahashi and Holland, 2004; Glover et al., 2018; Liu and Satou, 2019; Benito-Gutiérrez et al., 2021; Roure et al., 2023).

2014; Witten and Hall, 2022; Fritzsch et al., 2023). In addition, distinct developmental lineages generate neural crest, placodes, eyes, and taste buds in vertebrates, but not in lancelets or tunicates (Moody and LaMantia, 2015; Holland, 2020; Elliott et al., 2022; Fritzsch and Martin, 2022; Adameyko, 2023; Zine and Fritzsch, 2023).

In terms of neuron numbers, some tunicates have a greatly miniaturized CNS, containing about 177 neurons in the larva of the ascidian *Ciona* (Ryan et al., 2018; Holland, 2020), and about 130 neurons in the appendicularian *Oikopleura* (Søviknes et al., 2005; Nishida et al., 2021). In contrast, the lancelet has about 20,000 neurons whereas vertebrates have a wide range of neuron numbers [from about 600,000 in lamprey up to 86 billion in humans; (Holland, 2020; Lent et al., 2012; Von Bartheld et al., 2016; von Twickel et al., 2019)].

Vertebrates generate a variety of cranial sensory structures derived from the ectodermal placodes, including (in rough rostro-caudal order) the olfactory, anterior pituitary, lens, trigeminal and otic and epibranchial placodes. In addition, the vertebrate neural crest gives rise to cells that delaminate from the dorsal neural tube to emigrate and establish a range of peripheral cell types and structures including sensory and autonomic ganglia. *Bona fide* placodes and neural crest are not found in lancelets and tunicates, although in tunicates two proto-placodal ectodermal domains have been identified that give rise to some peripheral sensory cells and may be homologous with the vertebrate placodes (Schlosser, 2015).

Tunicates as a group exhibit a wide range of genome sizes, up to 800–900 million base pairs (Mbp) in some species (Naville et al., 2019; Plessy et al., 2023), while other species have remarkably small and compact genomes (as low as 70–170 Mbp) (Denoeud et al., 2010). Lancelets have about 520 Mbp (Miyamoto and Crowther, 1985; Søviknes et al., 2007; Søviknes and Glover, 2008; Dong et al., 2009; Marlétaz et al., 2018) while vertebrates can have up to about 3,000 Mbp (Fodor et al., 2020; Holland, 2020; Marletaz et al., 2023). A major difference between lancelets and tunicates on the one hand and vertebrates on the other is the genome reshaping that followed two rounds of whole genome duplications (WGD) that occurred early in the vertebrate lineage, (Holland and Daza, 2018; Marlétaz et al., 2018; Simakov et al., 2022), with a third WGD having occurred in teleosts (Marletaz et al., 2023).

Many CNS patterning genes are common among chordates (Schlosser, 2015; Glover et al., 2018; Holland, 2020; Liu and Satou, 2020; Holland and Holland, 2021). However, their utilization differs across the chordate lineages. For example, *Otx* and *Gbx* interact to pattern the anteroposterior (AP) axis of the vertebrate CNS, but this interaction is only partly evident in lancelets, and the *Gbx* gene appears to be absent in *Ciona*, the most studied tunicate species (Figure 1). *Dmbx* is central in establishing the midbrain in vertebrates, but evidently plays a different role in lancelets and tunicates [Figure 1; (Takahashi and Holland, 2004; Glover et al., 2018)]. Expression of *Pax4/6* and *Pax2/5/8* and their orthologs in respectively more anterior and more posterior regions of the CNS differs in vertebrates, lancelets and tunicates (Figure 1). In vertebrates, WNT and BMP signaling contributes to anteroposterior patterning during neural induction [Figure 1; (Meinhardt, 2015; Kozmikova and Kozmik, 2020; Chowdhury et al., 2022; Roure et al., 2023)] and is also important for patterning dorsal structures of the brain stem and spinal cord, where it acts in concert with *Lmx1a/b* and *Gdf7* to induce the roof plate and the choroid plexus (Glover et al., 2018; Chizhikov et al., 2021; Elliott et al., 2022). Detailed analysis shows differences in the expression of *Wnt* genes of lancelets, tunicates and vertebrates (Somorjai et al., 2018; Roure et al., 2023), and the existence of a *Gdf7* ortholog is currently unclear in lancelets and tunicates (Kozmikova and Yu, 2017; Winkley et al., 2020; Fodor et al., 2021). The expression of *Fgf8/17/18* and their orthologs also differs markedly across the chordate lineages, relating to the prosencephalon and the midbrain/hindbrain isthmus in vertebrates (Watson et al., 2017; Jahan et al., 2021), to the cerebral vesicle in lancelets and to the visceral/caudal ganglion in tunicates (Figure 1). *Hox* genes have been essential for the evolutionary elaboration of the caudal neural tube that has created the rhombencephalon of vertebrates (Glover et al., 2018; Holland, 2020). Lancelets have a single *Hox* gene cluster, which has been duplicated twice to form 4 clusters in vertebrates (Holland and Holland, 2022), whereas tunicates have lost several *Hox* genes that are otherwise shared by lancelets and the Parahoxazoa [placozoans, cnidarians and bilaterians; (Seo et al., 2004; Ryan et al., 2010; Schultz et al., 2023)]. In vertebrates, *Atoh1* is expressed dorsally from the spinal cord to the brainstem, including the cerebellum (Bermingham et al., 2001). Cross-interaction between *Neurog1/2* and *Atoh1* (Fritzsch et al., 2006) influences development of the otic placode (*Neurog1, Atoh1*) and epibranchial neurons (*Neurog2, Atoh1*) in vertebrates (Fritzsch and Elliott, 2017; Zhang and Xu, 2023; Zine and Fritzsch, 2023). Neither an otic nor an epibranchial placode have been described in lancelets or tunicates, although a potentially homologous posterior proto-placode has been proposed in tunicates. Expression of the lancelet *Atoh1* ortholog has not been described in the CNS [only within mesoderm; (Chowdhury et al., 2022)], whereas expression of the tunicate *Atoh1* ortholog in tunicates is linked to the development of putative hair cells in the circumoral region (Tang et al., 2013) and their associated sensory neurons (Stolfi et al., 2015; Manni et al., 2018).

As in the CNS, the gene regulatory networks (GRN) governing the development of chemosensory, visual and mechanoreceptive cells and structures show some fundamental similarities but also important differences. Despite evidence for similar gene circuits in tunicate and vertebrate neural lineages (Ryan et al., 2018; Liu and Satou, 2020), absence of an early and broad expression of *Foxg* in tunicates contrasts with vertebrates, where *Foxg1* is essential for the development of olfactory organs, eyes, epibranchial neurons, and ears (Ermakova et al., 2019; Liu and Satou, 2019; Dvorakova et al., 2020; Zine and Fritzsch, 2023). Lancelets and tunicates have chemoreceptors, but these are not organized into an olfactory organ as seen in vertebrates. Lancelets, and tunicates that exhibit vision, have photoreceptors (Vopalensky et al., 2012) associated with supporting cells in primitive eye structures, but not a multilayered retina as in vertebrates. Indeed, developing tunicate eyes lack an *Atoh* pro-ortholog expression like the *Atoh7* expression that is critical for creating vertebrate retinal ganglion neurons (Ryan and Meinertzhagen, 2019; Wu et al., 2021; Fritzsch and Martin, 2022). Lancelets have putative mechanosensory cells but evidently none associated with acoustic mechanosensation (Lacalli, 2004; Wicht and Lacalli, 2005), and at least some tunicates develop cells with a morphology similar to vertebrate hair cells and with a distinct

neuronal innervation (Rigon et al., 2013; Manni et al., 2018) (reviewed in Anselmi et al., 2024, in press). In contrast to these overt differences in sensory structures and cells, all three chordate taxa have motoneurons that innervate peripheral muscle used to generate body movements, although the manner in which this innervation is achieved can differ substantially (Søviknes et al., 2007).

In summary, substantial structural and cellular differences among lancelets, tunicates and vertebrates in the sensory systems for olfaction, vision and sensory/hair cell-mediated mechanoreception are beginning to be correlated with differences in the molecular networks governing the respective developmental specification and differentiation processes. On the efferent side, motoneurons are a highly conserved neuron type, yet exhibit a variety of target innervation modes. Lancelets, tunicates and vertebrates may share some elements of a common molecular framework for the generic specification of motoneurons, but this has been elaborated in vertebrates to create additional motoneuron subtypes.

We note that, to ensure distinction between gene and protein abbreviations, we use throughout this review the convention used for rodents (gene abbreviations are italicized with first letter in upper case and subsequent letters in lower case, protein abbreviations are not italicized, and all letters are in upper case).

The olfactory system is prominent in vertebrates but less developed in lancelets and tunicates

The origin of G-protein coupled olfactory receptors (OR) genes can be traced back to the latest common ancestor of chordates, including lancelets, which have over 30 OR genes, comparable to lampreys (Niimura, 2009; Niimura, 2012). No orthologues of OR receptors have been found in tunicates, despite the presence of putative chemoreceptors in the oral region (Veeman et al., 2010; Kaji et al., 2016).

In vertebrates, the olfactory epithelium (OS) contains progenitors that give rise to distinct classes of olfactory sensory neurons (OSN), vomeronasal sensory neurons (VSN) and GnRH (gonadotropin releasing hormone)-expressing neurons that control the hypothalamic-pituitary-gonadal axis (Causeret et al., 2023). ORs are expressed by the OSN, whose axons projection to and establish glomeruli with second order neurons within the olfactory bulbs in the telencephalon (Fritzsch et al., 2019; Poncelet and Shimeld, 2020; Elliott et al., 2022; Zhu et al., 2022). Since their discovery (Buck and Axel, 1991), OR genes have been found in all vertebrates including fish, amphibians, reptiles, birds, and mammals. They comprise the largest vertebrate gene family, with up to 2,000 genes and hundreds of OR pseudogenes (Zhang and Firestein, 2002; Niimura and Nei, 2007; Niimura et al., 2020; Policarpo et al., 2023).

The olfactory epithelia (OE) and the olfactory bulb (OB) develop from the olfactory placode and the telencephalon, respectively (Fritzsch and Elliott, 2022; Imai, 2022). The olfactory placode is one of the cranial sensory placodes that give rise to several specialized sensory organs [OE, auditory and vestibular organs (Moody and LaMantia, 2015; Schlosser, 2021)]. A set of transcription factors, including *Eya/Six, Pitx, Otx2, Pax4/6,* and *Emx2* regulate the induction of the olfactory placode. Additionally, retinoic acid (RA), FGF8, SHH, and BMP4 secreted from adjacent mesenchymal cells define the axes of the OE and induce nasal cavity formation (Moody and LaMantia, 2015; Poncelet and Shimeld, 2020). These factors together trigger the upregulation of specific genes required for the generation of olfactory sensory neurons [e.g., *Sox2*, *Ascl1*, *Neurog1*, *Neurod1*, and *Foxg1*; (Panaliappan et al., 2018; Dvorakova et al., 2020; Bayramov et al., 2022; Roure et al., 2023)]. Specific microRNAs also play a critical role in the differentiation of these neurons (Kersigo et al., 2011).

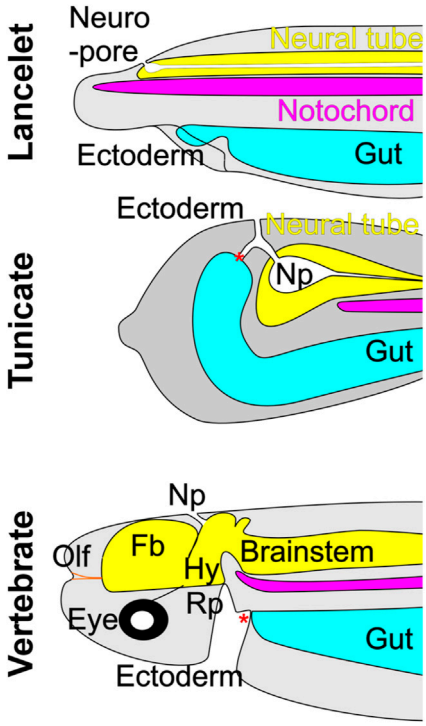

FIGURE 2
The neuropore (Np) in lancelets and tunicates (represented by the ascidian *Ciona*) forms an opening that connects the neurectoderm and the ectoderm. In vertebrates, the neuropore is transient and marks the point at which the neuroectoderm extends rostrally to form the forebrain (Fb), which appears to be unique to vertebrates. The olfactory placode (Olf), another vertebrate invention, develops rostral to the forebrain, and contains primary olfactory neurons that project to the forebrain. Neither lancelets nor tunicates have an olfactory system *per se* but have individual chemosensory cells that in lancelets likely express olfactory receptors. Note that in tunicates the neuropore has a collateral opening to the gut. In lancelets, the extension of the notochord prevents the formation of such a collateral opening. Vertebrates develop a structure in the embryonic oral ectoderm called Rathke's pouch (Rp), which forms the hypophyseal placode (Hy) that exhibits a unique interaction with the CNS at the hypothalamus. * indicates the mouth opening. Modified after (Veeman et al., 2010; Winkley et al., 2020; Schlosser, 2021a).

Detailed analysis in *Ciona* has revealed the origin of the tunicate neuropore [Figure 2; (Veeman and Reeves, 2015)], which becomes confluent with the opening of the gut (Veeman et al., 2010) and is fused with the mouth orifice. This structural arrangement resembles that related to the embryonic origin of olfactory structures in vertebrates. Nevertheless, although tunicates possess oral chemoreceptors, they appear to lack *bona fide* homologs of the OE and OB (Niimura, 2012; Schlosser, 2021a). A similar anatomical

relationship between neuropore and oral cavity is prevented in lancelets by the rostrally extended notochord [Figures 1, 2; (Ota and Kuratani, 2006)]. This structural intervention may be a contributing factor to the lack of a vertebrate-like olfactory system, since it could prevent inductive cell-cell interactions between gut and neural tube (Moody and LaMantia, 2015; Touhara et al., 2016; Schlosser, 2018; Holland, 2020; Poncelet and Shimeld, 2020). Although lancelets have no distinctive olfactory organ (Figure 2), they do have cells expressing OR genes near the mouth and along the lateral body wall (Niimura, 2012; Poncelet and Shimeld, 2020; Schlosser, 2021a).

GnRH is a marker across chordates for the anlage that give rise to the vertebrate adenohypophysis and olfactory structures and their potential homologs in lancelets and tunicates (Bassham and Postlethwait, 2005; Poncelet and Shimeld, 2020). The expression in tunicates of *Eya/Six*, which is necessary for olfactory development in mouse (Xu et al., 1997; Riddiford and Schlosser, 2016; Xu et al., 2021), initially suggested a potential evolutionary link to the vertebrate olfactory system (Bassham and Postlethwait, 2005). However, expression of *Foxg1* suggests that this likely only relates to peripheral olfactory structures. *Foxg1*, which is important for the development of the olfactory neural plate and olfactory bulb in vertebrates (Kersigo et al., 2011; Dvorakova et al., 2020), is only expressed at the anterior margin of the tunicate neural plate, where it is involved in the development of sensory neurons, but does not appear to be involved in the development of second-order neurons [Figure 1; (Panaliappan et al., 2018; Dvorakova et al., 2020; Liu and Satou, 2020; Benito-Gutiérrez et al., 2021; Zhang et al., 2021; Roure et al., 2023)]. Thus, despite some similarity between tunicates and vertebrates in the expression of GnRH, *Eya/Six* and *Foxg* (Roure et al., 2023), and of additional specific genes in GnRH-positive receptor cells (Touhara et al., 2016; Poncelet and Shimeld, 2020), it is unclear whether tunicates develop a homolog of the vertebrate olfactory placode or olfactory bulb (Cao et al., 2019). In this regard lancelets show greater similarity to vertebrates, as *Eya/Six* and *Foxg* are expressed in the lancelet sensory vesicle, part of the CNS (Figure 1).

In summary, neither lancelets nor tunicates possess a vertebrate-like olfactory system, but lancelets have OR-gene expressing receptors that may be homologous to vertebrate olfactory receptors, and tunicates develop GnRH-positive cells that may be homologous to vertebrate vomeronasal receptors. Only vertebrates have the extraordinarily extensive repertoire of OR genes and the elaborate synaptic interactions between olfactory sensory axons and central target neurons that form the glomeruli in the olfactory bulb. A more in-depth comparative review of olfactory system evolution can be found in (Poncelet and Shimeld, 2020).

Evolving the visual system: from primitive photoreceptive structures in lancelets and tunicates to the eyes of vertebrates

Opsins are central to phototransduction and provide one basis for understanding evolution of the visual system in chordates (Lamb, 2020; Moraes et al., 2021; Roberts et al., 2022). Opsins evolved together with the regulatory gene *Pax6,* which drives the development of eyes across animal phyla, in many cases through interaction with retinoic acid (RA) signaling (Fuhrmann, 2010; Lamb, 2013; Schwab, 2018). A total of 21 opsin genes has been identified in lancelets (Pergner and Kozmik, 2017), and these code for highly variable opsin proteins, generating a diversity comparable to that in vertebrates. Comparison to the vertebrate opsin gene family has provided information on duplications and gene loss events in lancelets (Pantzartzi et al., 2018). By contrast, the tunicate *Ciona* has only 3 opsin genes, which have sequence similarity to the vertebrate visual opsins (Kusakabe et al., 2001; Terakita, 2005; Ryan and Meinertzhagen, 2019; Pisani et al., 2020).

Potential evolutionary relationships between vertebrate eyes and pineal gland on the one hand and lancelet photoreceptive organs on the other have been reviewed in some detail recently (Pergner et al., 2020). Lancelets have four photosensitive organs, the frontal eye and the lamellar body (a presumed homolog of the vertebrate pineal gland), both of which contain ciliary photoreceptors, and the Joseph cells and the dorsal ocelli, both of which contain rhabdomeric photoreceptors. The frontal eye exhibits several similarities to the vertebrate retina, including specific gene expression domains comparable to vertebrate counterparts (Pergner and Kozmik, 2017). *Pax6*, considered a master regulator for eye formation, is expressed in the regions giving rise to all four of these photosensitive organs (Glardon et al., 1998). Cells associated with the frontal eye express the photoreceptor- and opsin-related transcription factors *Pax2/5/8*, *Six3/6*, *Otx*, *Mitf* as well as melanin synthesis genes [Figure 3; (Lamb et al., 2007)] and opsins (Vopalensky et al., 2012). Each photoreceptor cell in the frontal eye has a ciliary process that extends out of the neuropore, and an axonal projection to the CNS (Lacalli et al., 1994; Pergner and Kozmik, 2017) that may mediate further synaptic connections to motoneurons (Lacalli, 2018; Schlosser, 2021). In contrast to the frontal eye and lamellar body, the Joseph cells and dorsal ocelli express melanopsin, suggesting homology to vertebrate non-visual circadian photoreceptors (Gomez Mdel et al., 2009). Despite the clear presence of functional photoreceptors in all these structures, none of them approaches the complexity of constituent cell types found in the vertebrate retina and pineal gland. A potential explanation is the duplication of the *Atoh* pro-ortholog to create the *Atoh1 and Atoh7* genes in vertebrates, the latter of which is critical for creating vertebrate retinal ganglion neurons, and the lack of *Neurod* and *Otx* gene expression in the photoreceptive organs of lancelets, which is critical for creating vertebrate rods and cones (Ryan and Meinertzhagen, 2019; Wu et al., 2021; Chowdhury et al., 2022; Fritzsch and Martin, 2022).

In tunicates, ciliated photoreceptors associated with adjacent pigment cells have been described in many species, although appendicularian tunicates such as *Oikopleura* lack a visual organ entirely (Konno et al., 2010; Kourakis et al., 2019; Braun et al., 2020; Glover, 2020; Winkley et al., 2020; Olivo et al., 2021). In *Ciona*, the ocellus is made up of a cup-shaped pigment cell, 3 lens cells (not homologous to the vertebrate lens), and a number of photoreceptor cells that comprise 3 morphologically distinct groups (Olivo et al., 2021). Some of the photoreceptor cells are adjacent to pigment cells such that light detection by these is directional, and some are displaced from the lens cells and thus react primarily to unfocused light. The photoreceptor cells have an outer segment with multiple lamellae and each connects directly to neurons in the adjacent sensory vesicle that mediate photic responses (Lacalli and

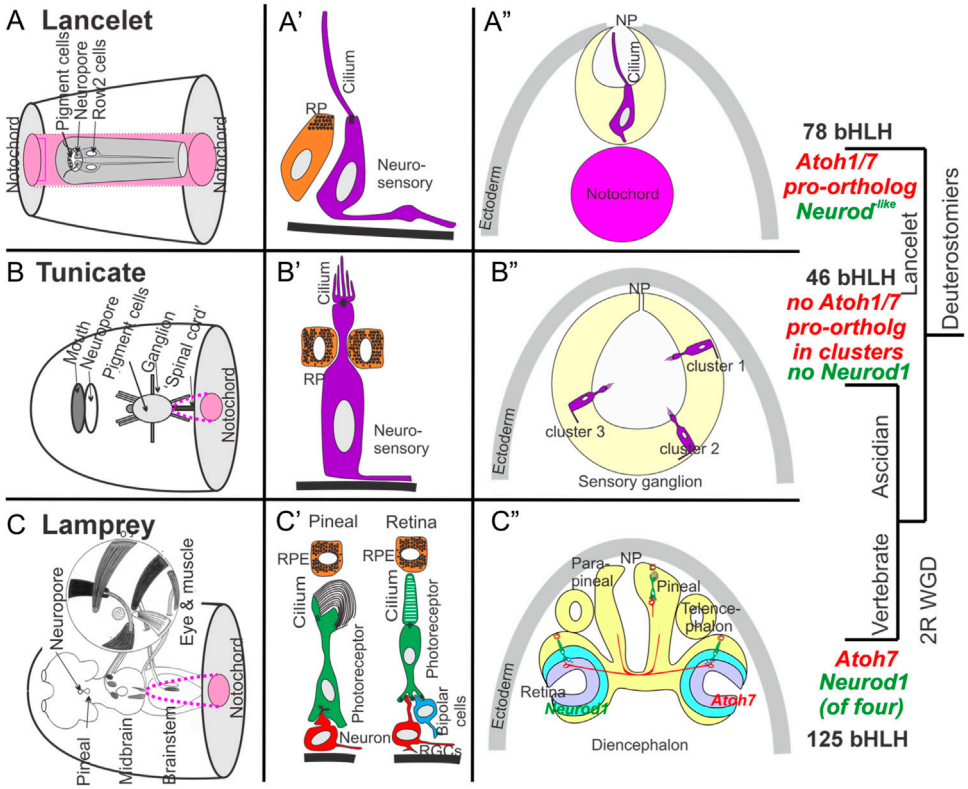

FIGURE 3
Comparison of lancelet, tunicate, and lamprey (vertebrate) photoreceptive organs. **(A)** Lancelets have a frontal eye **(A')** with photoreceptor cells that contain visual pigments and that have a simple cilium but without lamellae. The cilium extends into the central lumen of the terminal sac towards the neuropore (NP) **(A")**. Note that the notochord (pink) extends beyond the rostrum (transverse section view). **(B)** Ascidian tunicates have ciliated photoreceptors with an outer segment of lamellae **(B', B")**. Photoreceptors can be organized into as many as three distinct clusters, some associated with pigment cells in certain species **(B")**. Note that the notochord (pink) does not extend to the level of the transverse section. **(C)** Lampreys have two photoreceptive organs: the pineal/parapineal and the retina **(C)**. Photoreceptor cells in both organs exhibit ribbon synapses **(C)**. Axonal projections to the brain arise either directly (pineal/parapineal) or indirectly via ganglion cells (RGCs) in the retina, which also contains bipolar, horizontal and amacrine cells that process visual inputs. The eye is moved by three sets of extraocular muscles (inset). Note that vertebrates express distinct bHLH genes (Atoh7, Neurod1, **(C')**) in the developing eye. Expression of orthologs of these genes has not been demonstrated near the eyes in lancelets **(A')** or tunicates **(B')**. Atonal is required for eye development in flies and has evolved into multiple distinct Atoh, Neurod and Neurog genes in vertebrates. Modified after (Eakin and Kuda, 1970; Barnes, 1971; Eakin, 1973; Fritzsch and Collin, 1990; Fritzsch et al., 1990; Lacalli et al., 1994; Collin et al., 2009; Braun and Stach, 2017; Marlétaz et al., 2018; Suzuki and Grillner, 2018; Braun and Stach, 2019; Cao et al., 2019; Elliott et al., 2022; Elliott et al., 2021; Martin et al., 2021; Baker and Brown, 2018).

Holland, 1998; Konno et al., 2010; Razy-Krajka et al., 2012; Braun and Stach, 2019; Ryan and Meinertzhagen, 2019). In addition to opsins, *Ciona* also expresses the protein arrestin, a homolog of vertebrate β-arrestin which regulates opsin-based G-protein signaling to temporally curtail photoreceptor responses, suggesting that this function may be conserved from tunicates to vertebrates (Nakagawa et al., 2002; Kawano-Yamashita et al., 2011). In the salp *Thalia*, the blastozooid stage has a horseshoe-shaped set of pigmented cells adjacent to photoreceptor cells that are split among three cups that contain transparent transient lens cells and point in different directions (Barnes, 1971; Lacalli and Holland, 1998; Konno et al., 2010; Braun and Stach, 2017; Winkley et al., 2020). Small nerve branches connect these primitive eyes to the brain (Ryan et al., 2018; Braun and Stach, 2019).

Pax6 is expressed in the ocellus of *Ciona* (Irvine et al., 2008), but as in lancelets, other genes associated with vertebrate retinal neuron specification are not, including *Atoh7*, *Neurod1 and Otx2* (Ryan and Meinertzhagen, 2019; Wu et al., 2021; Fritzsch and Martin, 2022). Another bHLH gene important for retinal development in vertebrates, *Atoh8* (Cao et al., 2019) is expressed in the sensory ganglion domain of *Ciona,* but is not clear whether it is eventually expressed in the ocellus [*Atoh8* is not expressed in the brain, only the retina, in vertebrates; (Negrón-Piñeiro et al., 2020a; Rawnsley et al., 2013; Divvela et al., 2022)]. It may be that the larger repertoire within certain key gene families generated through WGD in vertebrates (for example, duplication of an *Atoh* pro-ortholog to generate *Atoh1* and *Atoh7*) may have facilitated an increase in cell type and photoreceptive organ diversity (Fritzsch et al., 2010; Holland and Daza, 2018). A more limited gene repertoire might thus explain the less elaborate differentiation of eye-related cells and structures in tunicates.

Pax6 is also expressed in the rostral CNS of appendicularian tunicates like *Oikopleura* (Cañestro and Postlethwait, 2007), but does not drive the formation of photoreceptors or any eye-like organ. Since retinoid signaling is an important factor promoting eye development in vertebrates (Cvekl and Wang, 2009), the evolutionary loss of all components of the retinoid signaling system in *Oikopleura* (Cañestro and Postlethwait, 2007) might

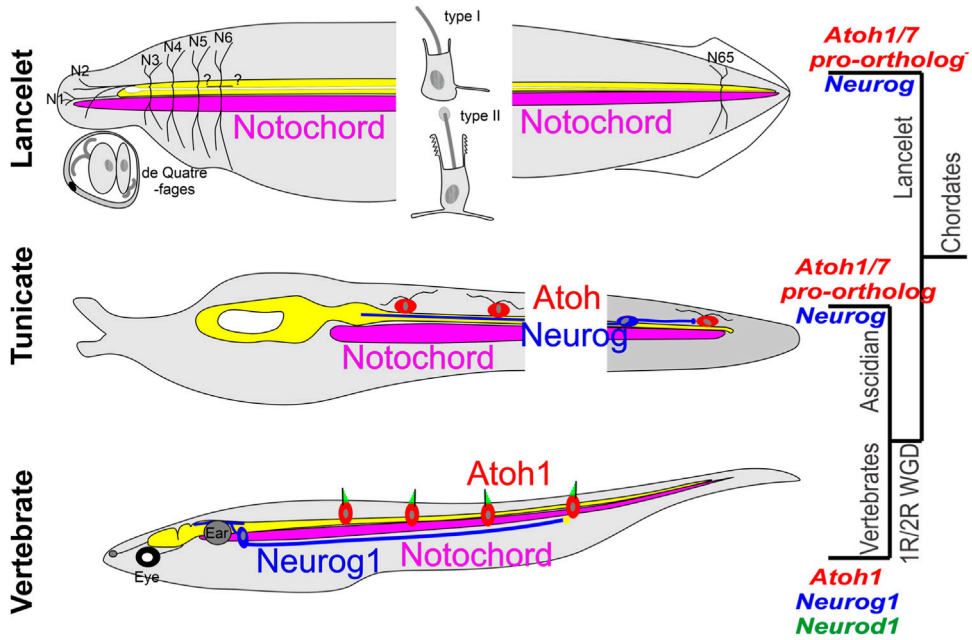

FIGURE 4
Comparison of some lancelet, tunicate, and vertebrate mechanosensory receptors. Lancelets have three types of ectodermally derived putative mechanosensory cells: the cells of the corpuscles de Quatrefages (associated with nerves 1 and 2), the type I epidermal sensory cell, which is a primary sensory cell with an axonal extension into the CNS, and the type II epidermal sensory cell, which is likely a secondary sensory cell that may be innervated by central neurons that have widespread axon terminations in the skin. Neither Neurog nor the Atoh1/7 pro-ortholog (NeuroD/Atonal-related gehe) have been linked to development of these cells (Neurog is only expressed in the notochord, expression of NeuroD/Atonal-related has not been described in the CNS). The ascidian tunicate Ciona has putative mechanosensory cells in the epidermis that have axons that can extend into the CNS (and thus appear to be primary sensory cells) or are innervated by bipolar tail neurons with central axons that extend to reach the visceral ganglion. Expression of Neurog and of the Atoh1/7-pro-ortholog (Atonal) is involved in the development of these cells. Vertebrates have sensory neurons located in peripheral sensory ganglia whose development depends on the expression of Neurog1 followed by Neurod1; these have peripheral axons that either may or may not contact secondary sensory cells, and central axons that project into the spinal cord and the brainstem. The brainstem receives afferent input from electroreceptor (ELL) and lateral line (LL) sensory neurons that connect peripherally to Atoh1+ secondary sensory (hair) cells in the body wall, and from auditory and vestibular sensory neurons that contact hair cells in the inner ear (gray), which is unique to vertebrates. Modified after (Tang et al., 2013; Stolfi et al., 2015; Holland and Daza, 2018; Manni et al., 2018; Holland, 2020; Zhao et al., 2020; Elliott et al., 2021; Fritzsch, 2021).

explain the absence of photoreceptors in appendicularian tunicates despite expression of *Pax6*.

In summary, although lancelets, tunicates and vertebrates share opsins and arrestins as basic molecular components for phototransduction, and *Pax6* appears to be a common driver of photoreceptor development in all three (except for appendicularian tunicates), we lack enough information to relate the lancelet frontal eye and the multiple tunicate eyes to the bilateral eyes and pineal gland of vertebrates [Figure 3; (Lamb, 2013; Lamb, 2020; Fritzsch and Martin, 2022)]. The main difference is the absence of certain genes, particularly *Atoh7* and *Neurod1*, which are required for eye and pineal gland development in vertebrates. Moreover, the complete lack of photoreceptors despite *Pax6* expression in appendicularian tunicates requires a molecular explanation.

Evolving hair cells and connecting them to the CNS

Hair cells are believed to have evolved as a retained phenotype from the common ancestor of choanoflagellates and metazoans. In this idea, the motility-enabling flagellum-microvilli complex has been converted to a mechanosensory device and the basic choanoflagellate cell type has given rise to a sensory cell within a synaptically-coupled neural circuit (Caicci et al., 2013; Fritzsch and Straka, 2014; Fritzsch and Elliott, 2017; Colgren and Burkhardt, 2022; Van Le et al., 2023). An important line of inquiry has been to determine whether lancelets and tunicates have hair cells that are homologous to the hair cells of vertebrates, which are found in the vestibular and cochlear sensory organs and in the lateral line neuromasts of vertebrates. For such homology to hold, it should be possible to find ciliated secondary sensory cells (sensory cells that do not have an axon, but receive synapses from primary sensory cells) in lancelets and tunicates.

Lancelets have primary sensory cells (sensory cells with axons that project to the CNS) widely distributed in the skin (Poncelet and Shimeld, 2020; Holland and Holland, 2022). Among these, a unique group in the corpuscles de Quatrefages extend neurites into the dorsal entry points of the first and second nerves (Fritzsch, 1996; Wicht and Lacalli, 2005). In addition, there are two types of widely distributed solitary sensory cells in the skin, type I and type II [Figure 4; (Wicht and Lacalli, 2005; Schlosser, 2021a)], each with a central kinocilium surrounded by microvilli, which are branched in the type II sensory cells. The type I sensory cells are primary sensory cells. The type II sensory cells have been suggested to be secondary sensory cells (sensory cells that do not have a centrally projecting

axon) with short basal processes (Wicht and Lacalli, 2005) (Figure 3). Although the type II sensory cells are well positioned for mechanoreception and on morphological grounds have the appearance of hair cells, it is not yet clear whether they function as hair cells. Extensive RNA sequencing characterization has shown that the origin of the lancelet epidermal sensory cells is inconsistent with homology to neural crest-derived sensory ganglion neurons of vertebrates (Schlosser, 2021; Chowdhury et al., 2022; Zine and Fritzsch, 2023); indeed, there are no overt ganglia associated with lancelet afferent nerves (Fritzsch and Northcutt, 1993). Further work is needed to assess whether the origin of the type II sensory cells is homologous to the vertebrate placodes that give rise to the vestibular, auditory or lateral line hair cells.

In tunicates, peripheral ciliated sensory neurons have been described at larval and adult stages in ascidians (such as *Ciona*), thaliaceans and appendicularians (such as *Oikopleura*). In *Ciona*, these include the larval caudal and trunk epidermal neurons (CENs and TENs) and the papilla neurons (PNs). CENs and TENs are ciliated and have axons extending to the nerve cord, and thus appear to be primary sensory cells. CEN and TEN axons contact each other and/or central bipolar relay neurons in the CNS [Figure 4; (Tang et al., 2013; Stolfi et al., 2015; Manni et al., 2018; Ryan et al., 2018; Piekarz and Stolfi, 2023)]. In ascidians the CENs and TENs are positioned peripherally along the length of the body in a way that is reminiscent of the vertebrate lateral line, and they originate from neurogenic regions of the ectoderm (the neurogenic midlines) that are reminiscent of the postotic placodes that give rise to lateral line neuromasts and sensory neurons in teleosts. However, since they appear to be primary sensory cells, the potential homology would be to the sensory neurons in the lateral line ganglia, not to the hair cells of the lateral line neuromasts.

Despite the connectional similarity between the central bipolar neurons in *Ciona* (that synapse with the CENs and TENs) and vertebrate sensory neurons in dorsal root, vestibular and cochlear ganglia, it is unclear whether these are homologous [Figure 4; (Schlosser, 2021a; Fritzsch, 2021)]. Moreover, a developmental origin in tunicates homologous to the otic placode that gives rise to the vertebrate inner ear and most of the neurons in its associated ganglia (Schlosser, 2021; Zine and Fritzsch, 2023) has not been demonstrated.

The PNs are ciliated peripheral neurons that extend axons towards the sensory vesicle. At early larval stages some PNs synapse onto RTENs peripheral to the sensory vesicle; it is unclear whether later growing PN axons do the same or extend into the sensory vesicle (reviewed in Anselmi et al., 2024, in press). PNs have a combined chemosensory and mechanosensory function, responding to chemical cues that are known to promote substrate attachment, and to mechanical stimulation which upon substrate contact triggers metamorphosis to the adult sessile stage (Hoyer et al., 2024). The PNs develop from the anterior neurogenic zone.

The appendicularian tunicate *Oikopleura* bears a bilateral pair of secondary sensory cells (the Langerhans receptors) each with a long, modified ciliary structure. These have been shown to have a mechanosensory function (Bone and Ryan, 1979; Holmberg, 1986), and are therefore potentially homologous to vertebrate hair cells. But their embryonic origin and molecular patterning have not been assessed.

Ascidian, thaliacean and appendicularian tunicates also have ciliated secondary sensory cells in the circumoral region in free-swimming forms (larval ascidians and thaliaceans and larval and adult appendicularians), and in the coronal organ in both free-swimming (appendicularian) and sessile and pelagic (ascidian and thaliacean) adult forms (Engelmann and Fritzsch, 2022) (reviewed in Anselmi et al., 2024, in press). These are potentially homologous to vertebrate hair cells. However, there is great diversity among tunicate species in the organization of cilia in these cells, which is different from that of vertebrate hair cells in the inner ear and lateral line. The secondary sensory cells of the tunicate coronal organ have a central kinocilium with surrounding stereocilia, whereas the cilia bundle of vertebrate hair cells has a distinct axis with the kinocilium at one extreme and stereocilia arrayed in decreasing lengths towards the other extreme (the kinocilium subsequently degenerates in mammalian cochlear hair cells, but the axis of graded stereocilia height remains). In both tunicates and vertebrates the cilia are bound to each other by link proteins, strongly indicative of a similar mechanosensory function. Indeed, in some tunicate species, the secondary sensory cells in the coronal organ have been demonstrated physiologically to have a mechanoreceptive function, but it is unclear whether all are mechanoreceptive or alternatively chemoreceptive (or both) (Caicci et al., 2013; Manni et al., 2018; Poncelet and Shimeld, 2020; Engelmann and Fritzsch, 2022; Van Le et al., 2023) (reviewed in Anselmi et al., 2024, in press). A cladistic analysis has suggested a monociliated cell as the ancestral form giving rise to the diverse forms exhibited in tunicate coronal organs (Rigon et al., 2013).

The coronal organ derives from the stomodeal portion of the anterior proto-placode in tunicates, a structure that has been suggested to be potentially homologous to one or more of the posterior vertebrate placodes (otic and/or lateral line) that give rise to hair cells. However, this potential homology remains to be proven, as there are some discrepancies in gene expression relative to vertebrate placodes during their development (reviewed in Anselmi et al., 2024, in press).

In vertebrates, the *Atoh1* gene plays a pivotal role in specifying the hair cell phenotype. A single *atonal/lin-32/Atoh* bHLH gene is found in Protostomia (fly, *D. melanogaster;* nematode, *C elegans*). This gene has been conserved in Deuterostomia, and duplicated in vertebrates to generate the genes *Atoh1* and *Atoh7*. In lancelets and tunicates, potential orthologs are the *NeuroD/Atonal-related* gene and the single *Atonal* gene, respectively. *Atonal* is expressed in the coronal organ of tunicates (Rigon et al., 2018). Of additional relevance with respect to sensory cell and neuron diversity are the genes *Neurod* (4 in vertebrates, 1 *NeuroD/Atonal-related* in lancelets, two potential orthologs in *Ciona*), *Neurog* (3 in vertebrates, 1 in lancelets, 1 in *Ciona*), and *Olig* (3 in vertebrates, 2 in lancelets, evidently absent in *Ciona*) (Simionato et al., 2007; Negrón-Piñeiro et al., 2020b). In vertebrates, *Neurog1/2* and *Neurod1* are associated with the emergence of distinct peripheral sensory cells (under the control of *Atoh1*) and of sensory neurons in sensory ganglia (direct action of *Neurog1/2 and Neurod1*) (Fritzsch, 2021).

Expression of *NeuroD/Atonal-related* in the lancelet nervous system has not been described (Simionato et al., 2007; Holland et al., 2008; Holland, 2020; Zhao et al., 2020; Chowdhury et al., 2022). In tunicates, *Neurog* and *Atonal* are expressed in the nerve cord and peripheral sensory cells (Tang et al., 2013; Stolfi et al., 2015; Cao

et al., 2019; Ryan and Meinertzhagen, 2019). It is currently not known whether the specification of secondary mechanosensory cells (both putative and definitive) in tunicates depends on expression of *Atonal* in the way the specification of hair cells depends on *Atoh1* in vertebrates.

In summary, there are clear distinctions among putative mechanosensory cells and their sources of innervation in lancelets (epidermally derived primary sensory cells that project to the CNS), tunicates (epidermally derived primary sensory cells that project to the CNS and epidermally derived secondary sensory cells innervated by neurons in the CNS), and vertebrates (placode-derived secondary sensory cells that are innervated by placode- and neural crest-derived sensory neurons within sensory ganglia). *Atoh* gene ortholog expression appears to be a common feature in tunicate and vertebrate mechanosensory cells (*Atonal* in tunicates, *Atoh1* in vertebrates), but it is unclear if this is shared by lancelets. The recruitment (in some cases preceded by duplications) of additional genes governing differentiation of mechanoreceptors and associated sensory neurons is related to the more complex organization of mechanosensory systems in vertebrates, exemplified by the highly specialized vestibular and cochlear organs and their ganglia (Figure 4). A central element in this evolutionary elaboration has been the creation in vertebrates of dedicated placodal anlage (otic placode for auditory and vestibular, post-otic for lateral line) that give rise to peripheral mechanosensory structures bearing hair cells.

Molecular specification of motoneurons and diversity of neuromuscular organization

In the vertebrate posterior neural tube, sonic hedgehog (SHH) acts as a graded morphogen emanating from the notochord and floor plate to promote the formation of ventral progenitor domains, one of which (pMN) gives rise to all motoneurons. WNT proteins and bone morphogenetic proteins (BMPs) emanating from the dorsal neural tube generate an opposing gradient that inhibits ventral progenitor formation and MN differentiation (Roure et al., 2023). The action of these opposing gradients, coupled with reciprocal repressive interactions between progenitor domain-defining transcription factors, leads to well defined and restricted progenitor populations, and is the basis for the localization of MNs in the ventral neural tube [later migrations can posit some MNs more dorsally; (Briscoe and Novitch, 2008)]. Except for the p3 ventral progenitor domain (which gives rise to V3 interneurons), the action of SHH is not a direct induction of ventral progenitor fates, but rather inhibition of the intracellular protein GLI3, which acts to repress ventral progenitor fates. It has been shown that MNs can still be generated in the absence of SHH and GLI3, indicating that MNs can be specified through another pathway that is normally repressed by GLI3. In this case, however, MNs and other (interneuronal) cell type precursors are intermingled instead of being organized into discrete anatomical populations. It has been proposed that the SHH signaling pathway has achieved a necessary status during vertebrate evolution to ensure that ventral progenitor domains are properly patterned in the face of increasing neuronal numbers.

Once specified, differentiation of MNs in vertebrates involves the expression of several genes, including the transcription factor genes *Nkx6.2*, *Olig*, *Isl1*, and *Mnx*, and culminating in the expression of choline acetyltransferase (ChAT) and the vesicular acetylcholine (ACh) transporter (vAChT), key components of the machinery for synthesizing and utilizing ACh as a neurotransmitter.

Lancelets and tunicates express hedgehog (*Hh*) genes homologous to vertebrate *Shh* (1 gene in lancelets, 2 in *Ciona*), as well as *Wnt* and *Bmp* genes dorsally (Shimeld, 1999; Lin et al., 2009; Hudson et al., 2011; Ryan et al., 2018; Benito-Gutiérrez et al., 2021). In both lancelets and vertebrates, HH/SHH is expressed ventrally (in both notochord and floor plate) together with *Patched* (PTC) and *Smoothened* (SMO), transmembrane proteins that transduce the HH/SHH signal, and with GLI and SUFU proteins that mediate SHH-elicited transcriptional events. However, in *Ciona* expression of *Hh1* and *Hh2* is spatially limited to the ventral nerve cord (absent in the notochord) and temporally limited there to early (pre-hatching) stages. PTC, SMO and GLI are also expressed, indicating that the main components of the HH-signaling pathway are present during the generation of MNs (Imai et al., 2009; Islam et al., 2010). However, MNs are still generated in the absence of *Hh* expression, suggesting that MN specification relies on a non-HH-mediated removal (spatially or temporally) of *Gli* expression (Hudson et al., 2011; Di Gregorio, 2020; Ren et al., 2020). This is similar to the situation created by double knockout of *Shh* and *Gli3* in vertebrates. Since only a handful of MNs are generated in tunicates, the role of *Shh/Hh* in creating a dorsoventrally restricted domain of MN progenitors may not be as important in tunicates as in vertebrates, and therefore may have been relaxed to the point that HH-signaling has been eliminated as a necessary factor for MN specification.

Lancelets have two types of motoneurons, dorsal (branchial) and ventral (somatic) (Fritzsch and Northcutt, 1993; Lacalli and Kelly, 2003; Wicht and Lacalli, 2005). There is a noticeable left/right asymmetry and an incomplete overlap of most rostral motoneurons (Ren et al., 2020). Lancelets have a single *Nkx6* gene, two *Olig* genes and a single *Islet* gene (Jackman et al., 2000; Ren et al., 2020), which probably have comparable functions to the mammalian orthologues (Delás and Briscoe, 2020). Both MN types express *Nkx6, OligA* and *Islet*, but the latter does not appear to be expressed in more posterior MNs (Jackman et al., 2000; Ren et al., 2020). As in vertebrates, MN specification in lancelets also involves *Hox* and *bHLH* genes, although the relevant interactions among these have not been well characterized in lancelets (Ferrier et al., 2001; Langeland et al., 2006; Leung and Shimeld, 2019; Dasen, 2022). In tunicates, which lack an *Olig* gene, the expression patterns and functional roles of *Nkx6*, *Islet*, and *Hox* orthologs in the context of MN differentiation have yet to be elucidated (Roure et al., 2023). Thus, it remains to be seen how similar this process is molecularly in the three chordate groups.

In lancelets, innervation of muscle is unusual, in that MNs do not project axons out of the spinal cord, but rather make contacts with muscle cells that appose the ventrolateral margin of the spinal cord (Flood, 1966; Wicht and Lacalli, 2005; Fritzsch et al., 2017). In tunicate larvae, MNs send axons into the periphery from the nerve

cord. The ascidian tunicates *Ciona* and *Halocynthia* have at larval stages respectively 5 pairs of MNs and 3 pairs of MNs in the visceral ganglion, considered to be homologous to the posterior part of the vertebrate hindbrain (Dufour et al., 2006; Stolfi et al., 2015; Ryan and Meinertzhagen, 2019; Fritzsch and Martin, 2022). Since most of the tail musculature is located well caudal to these MNs, activation of the musculature requires that MN axons descend for multiple segments along the nerve cord prior to exiting into the periphery, and that more rostral muscle cells transmit depolarization to more caudal muscle cells via gap junctions (Okada et al., 2002). By contrast, in the appendicularian tunicate *Oikopleura*, there are 10 pairs of MNs corresponding to the 10 pairs of muscle cells, 3 in the caudal ganglion (roughly homologous to the visceral ganglion of ascidian tunicates) and 7 in the caudal nerve cord. Most of the MNs innervate a muscle cell at the same or next caudal segmental level. This near co-distribution of MNs and muscle cells along the rostrocaudal axis is more similar to the situation in vertebrates (Søviknes et al., 2007).

Extraocular muscles (EOMs) are in many ways unique compared to other skeletal muscles in vertebrates (Noden and Francis-West, 2006; Spencer and Porter, 2006; Fritzsch et al., 2017; Ziermann et al., 2018). They derive from epithelial mesodermal coeloms termed head cavities. Three pairs of head cavities form from the pharyngeal pouches, thereby exhibiting a metameric arrangement that has prompted the notion of three cranial somites (Bjerring, 1978; Gilland and Baker, 2005; Kuratani and Adachi, 2016). Extraocular muscles thus form relatively near the midbrain (near the source of cranial nerve III, the oculomotor nerve), the midbrain-hindbrain transition (near the source of cranial nerve IV, the trochlear nerve) and the hindbrain (the source of cranial nerve VI, the abducens nerve). Oculomotor and trochlear MNs are special somatic motoneurons (SSM, whose specification require expression of *Phox2a*), whereas abducens MNs are somatic motor neurons (SM, specification independent of *Phox2a*) (Epstein et al., 1999; Brunet and Pattyn, 2002; Litingtung et al., 2002; Fritzsch et al., 2017; Delás and Briscoe, 2020). Along with most (but not all) MNs in the hindbrain, differentiation of the SSM in the oculomotor and trochlear nuclei depends on the expression of *Phox2* transcription factors [reviewed in (Fritzsch et al., 2017)].

The development of extraocular muscles and their innervating MNs is a vertebrate innovation, arising through the need to mobilize the eye to create a more flexible and powerful visual system [reviewed in Fritzsch et al., 2024 in press]. Neither extraocular muscles nor MNs to innervate them are present in lancelets or tunicates. It is unclear whether lancelets express *Phox2* genes in the nervous system. Although *Phox2* is expressed in the ciliomotor neurons that control branchial ciliary flow in the sessile adult *Ciona* (which derive from the larval "neck" region), it is unclear which brain stem neurons these might correspond to in vertebrates. It is also unclear whether *Phox2* expression is involved in the differentiation of the larval MNs in the visceral ganglion, which also corresponds to part of the vertebrate brain stem (Gigante et al., 2023; preprint). Thus, SSM in general may be a vertebrate invention, beyond the specific lack of extraocular MNs in lancelets and tunicates (Fritzsch et al., 2017).

In summary, the different chordate taxa share many elements of a common molecular program for specifying generic MNs, but differences exist in the way specific genes and signaling pathways are utilized. In addition, a variety of neuromuscular organization patterns, including the direct apposition of muscle to the ventrolateral spinal cord obviating the need for peripheral MN axons in lancelets, and the rostrally restricted MN localization with activation of muscle by descending MN axons combined with sequential activation of more caudal muscle cells via gap junctions in ascidian tunicates, deviate substantially from the vertebrate pattern. On the other hand, the numerical equivalence and co-distribution along the anteroposterior axis of MNs, muscle cells and neuromuscular junctions in the appendicularian *Oikopleura* bears a close resemblance to the vertebrate organization, in which MNs are distributed along the entire anteroposterior axis of the brain stem and spinal cord in rough alignment with the skeletal musculature they innervate. The difference between ascidian and appendicularian tunicate patterns is almost certainly related to the rapid metamorphosis of ascidians into sessile adults contrasting with the continuous free-swimming lifestyle of the appendicularians. A major evolutionary advance in vertebrates has been the elaboration of MN subtypes generated by the incorporation of additional MN-specifying genes including the *Phox2* genes. This has clearly involved a co-evolution of more diverse skeletal muscle functions in vertebrates such as the deployment of extraocular muscles to generate eye movements.

Summary and conclusion

Despite their differences in neural architecture, and the evolutionary distance separating them (about 600 million years), the three main chordate taxa should exhibit some degree of homology in the development and organization of major sensory and motor cell types. Current knowledge regarding the molecular underpinnings of chemo-, photo- and mechanosensitive cells and organs, and of motoneurons, indeed reveals common genetic elements in lancelets, tunicates, and vertebrates. These include the expression of a family of diverse OR genes in lancelet chemosensory cells and the vertebrate olfactory epithelium, the link between *Pax4/6* and photoreceptive cells in lancelets, tunicates and vertebrates, the utilization of *Atoh1/7* genes in specifying ciliated secondary sensory cells in tunicates and hair cells in vertebrates, and the pivotal role of the SHH-signaling pathway in generating MN progenitors in all three taxa. On the other side of the coin, significant differences in the presence or utilization (expression pattern) of specific genes in lancelets and tunicates are related to an unelaborated olfactory system (lack of *Foxg1* expression in CNS of tunicates), the primitive nature of their eyes (lack of expression of *Atoh1/7*-like genes in lancelets and tunicates), the less elaborate organization of their mechanosensory systems (lack of an otic placode in lancelets and tunicates) and less MN diversity (lack of *Phox2* recruitment into MN differentiation in lancelets and tunicates). Two major innovations that likely have been major drivers of the differences

between the protochordate taxa and vertebrates are the extended repertoire of transcription factors (enabled by WGD) employed in specifying sensory and neuronal cell types, and the introduction of placodal anlage that elaborated the peripheral structures associated with olfaction, vision and mechanoreception.

Further study of the gene networks responsible for protochordate sensory and motor development should gradually fill in the many gaps that remain in the comparative assessment of homology and diversity of protochordates relative to vertebrates. In this regard, it is important to point out that our current knowledge is based on the investigation of only a handful of the 30 or so extant species of lancelets (which have similar body plans and lifestyles) and the approximately 3,000 extant species of tunicates (which have quite diverse body plans and lifestyles). The far greater number of vertebrate species (about 60,000) are arguably better represented by the relatively few model organisms that have been investigated extensively, but also here there are likely to be interesting examples of diversity not yet revealed, which will necessitate explanation at the molecular level.

Author contributions

BF: Writing–original draft, Writing–review and editing. JG: Writing–original draft, Writing–review and editing.

Funding

The author(s) declare that financial support was received for the research, authorship, and/or publication of this article. Funded by NIA (AG060504) to BF was obtained through a grant from the Norwegian Research Council to the Sars International Centre for Marine Molecular Biology.

Conflict of interest

The authors declare that the research was conducted in the absence of any commercial or financial relationships that could be construed as a potential conflict of interest.

The author(s) declared that they were an editorial board member of Frontiers, at the time of submission. This had no impact on the peer review process and the final decision.

Publisher's note

References

Adameyko, I. (2023). Evolutionary origin of the neural tube in basal deuterostomes. *Curr. Biol.* 33, R319–R331. doi:10.1016/j.cub.2023.03.045

Anselmi, C., Fuller, G. K., Stolfi, A., Groves, A., and Manni, L. (2024). Sensory cells in tunicates: insights into mechanoreceptor evolution. *J. Comp. Neurol.* in press 531, 1229–1243. doi:10.1002/cne.25492

Baker, N. E., and Brown, N. L. (2018). All in the family: proneural bHLH genes and neuronal diversity. *Development* 145, dev159426. doi:10.1242/dev.159426

Barnes, S. N. (1971). Fine structure of the photoreceptor and cerebral ganglion of the tadpole larva of Amaroucium constellatum (Verril) (subphylum: urochordata; class: ascidiacea). *Z. für Zellforsch. Mikrosk. Anat.* 117, 1–16. doi:10.1007/BF00331097

Bassham, S., and Postlethwait, J. H. (2005). The evolutionary history of placodes: a molecular genetic investigation of the larvacean urochordate *Oikopleura dioica*. *Development* 132, 4259–4272. doi:10.1242/dev.01973

Bayramov, A., Ermakova, G., Kucheryavyy, A., Meintser, I., and Zaraisky, A. (2022). Lamprey as laboratory model for study of molecular bases of ontogenesis and evolutionary history of vertebrata. *J. Ichthyology* 62, 1213–1229. doi:10.1134/s0032945222060029

Benito-Gutiérrez, È., Gattoni, G., Stemmer, M., Rohr, S. D., Schuhmacher, L. N., Tang, J., et al. (2021). The dorsoanterior brain of adult amphioxus shares similarities in expression profile and neuronal composition with the vertebrate telencephalon. *BMC Biol.* 19, 110–119. doi:10.1186/s12915-021-01045-w

Bermingham, N. A., Hassan, B. A., Wang, V. Y., Fernandez, M., Banfi, S., Bellen, H. J., et al. (2001). Proprioceptor pathway development is dependent on Math1. *Neuron* 30, 411–422. doi:10.1016/s0896-6273(01)00305-1

Bjerring, H. C. (1978). A Contribution to Structural Analysis of the Head of Craniate Animals the orbit and its contents in 20-22-mm embryos of the North American actinopterygian *Amia calva* L., with particular reference to the evolutionary significance of an aberrant, nonocular, orbital muscle innervated by the oculomotor nerve and notes on the metameric character of the head in craniates. *Zool. Scr.* 6, 127–183. doi:10.1111/j.1463-6409.1978.tb00768.x

Bone, Q., and Ryan, K. P. (1979). The Langerhans receptor of Oikopleura (tunicata: larvacea). *J. Mar. Biol. Assoc. U. K.* 59, 69–75. doi:10.1017/s002531540004618x

Braun, K., Leubner, F., and Stach, T. (2020). Phylogenetic analysis of phenotypic characters of Tunicata supports basal Appendicularia and monophyletic Ascidiacea. *Cladistics* 36, 259–300. doi:10.1111/cla.12405

Braun, K., and Stach, T. (2017). Structure and ultrastructure of eyes and brains of Thalia democratica (thaliacea, tunicata, chordata). *J. Morphol.* 278, 1421–1437. doi:10.1002/jmor.20722

Braun, K., and Stach, T. (2019). Morphology and evolution of the central nervous system in adult tunicates. *J. Zoological Syst. Evol. Res.* 57, 323–344. doi:10.1111/jzs.12246

Briscoe, J., and Novitch, B. G. (2008). Regulatory pathways linking progenitor patterning, cell fates and neurogenesis in the ventral neural tube. *Philos. Trans. R. Soc. Lond B Biol. Sci.* 363, 57–70. doi:10.1098/rstb.2006.2012

Brunet, J.-F., and Pattyn, A. (2002). Phox2 genes—from patterning to connectivity. *Curr. Opin. Genet. Dev.* 12, 435–440. doi:10.1016/s0959-437x(02)00322-2

Buck, L., and Axel, R. (1991). A novel multigene family may encode odorant receptors: a molecular basis for odor recognition. *Cell* 65, 175–187. doi:10.1016/0092-8674(91)90418-x

Caicci, F., Gasparini, F., Rigon, F., Zaniolo, G., Burighel, P., and Manni, L. (2013). The oral sensory structures of Thaliacea (Tunicata) and consideration of the evolution of hair cells in Chordata. *J. Comp. Neurology* 521, 2756–2771. doi:10.1002/cne.23313

Cañestro, C., and Postlethwait, J. H. (2007). Development of a chordate anterior-posterior axis without classical retinoic acid signaling. *Dev. Biol.* 305, 522–538. doi:10.1016/j.ydbio.2007.02.032

Cao, C., Lemaire, L. A., Wang, W., Yoon, P. H., Choi, Y. A., Parsons, L. R., et al. (2019). Comprehensive single-cell transcriptome lineages of a proto-vertebrate. *Nature* 571, 349–354. doi:10.1038/s41586-019-1385-y

Causeret, F., Fayon, M., Moreau, M. X., Ne, E., Oleari, R., Parras, C., et al. (2023). Diversity within olfactory sensory derivatives revealed by the contribution of Dbx1 lineages. bioRxiv.

Chizhikov, V. V., Iskusnykh, I. Y., Fattakhov, N., and Fritzsch, B. (2021). Lmx1a and Lmx1b are redundantly required for the development of multiple components of the mammalian auditory system. *Neuroscience* 452, 247–264. doi:10.1016/j.neuroscience.2020.11.013

Chowdhury, R., Roure, A., le Pétillon, Y., Mayeur, H., Daric, V., and Darras, S. (2022). Highly distinct genetic programs for peripheral nervous system formation in chordates. *BMC Biol.* 20, 152. doi:10.1186/s12915-022-01355-7

Colgren, J., and Burkhardt, P. (2022). The premetazoan ancestry of the synaptic toolkit and appearance of first neurons. *Essays Biochem.* 66, 781–795. doi:10.1042/EBC20220042

Collin, S. P., Davies, W. L., Hart, N. S., and Hunt, D. M. (2009). The evolution of early vertebrate photoreceptors. *Philosophical Trans. R. Soc. B Biol. Sci.* 364, 2925–2940. doi:10.1098/rstb.2009.0099

Cvekl, A., and Wang, W. L. (2009). Retinoic acid signaling in mammalian eye development. *Exp. Eye Res.* 89, 280–291. doi:10.1016/j.exer.2009.04.012

Dasen, J. S. (2022). Establishing the molecular and functional diversity of spinal motoneurons. *Adv. Neurobiol.* 28, 3–44. doi:10.1007/978-3-031-07167-6_1

Delás, M. J., and Briscoe, J. (2020). Repressive interactions in gene regulatory networks: when you have no other choice. *Curr. Top. Dev. Biol.* 139, 239–266. doi:10.1016/bs.ctdb.2020.03.003

Denoeud, F., Henriet, S., Mungpakdee, S., Aury, J. M., Da Silva, C., Brinkmann, H., et al. (2010). Plasticity of animal genome architecture unmasked by rapid evolution of a pelagic tunicate. *Science* 330, 1381–1385. doi:10.1126/science.1194167

Di Gregorio, A. (2020). The notochord gene regulatory network in chordate evolution: conservation and divergence from Ciona to vertebrates. *Curr. Top. Dev. Biol.* 139, 325–374. doi:10.1016/bs.ctdb.2020.01.002

Divvela, S. S. K., Saberi, D., and Brand-Saberi, B. (2022). Atoh8 in development and disease. *Biology* 11, 136. doi:10.3390/biology11010136

Dong, B., Horie, T., Denker, E., Kusakabe, T., Tsuda, M., Smith, W. C., et al. (2009). Tube formation by complex cellular processes in *Ciona intestinalis* notochord. *Dev. Biol.* 330, 237–249. doi:10.1016/j.ydbio.2009.03.015

Dufour, H. D., Chettouh, Z., Deyts, C., de Rosa, R., Goridis, C., Joly, J. S., et al. (2006). Precraniate origin of cranial motoneurons. *Proc. Natl. Acad. Sci. U. S. A.* 103, 8727–8732. doi:10.1073/pnas.0600805103

Dvorakova, M., Macova, I., Bohuslavova, R., Anderova, M., Fritzsch, B., and Pavlinkova, G. (2020). Early ear neuronal development, but not olfactory or lens development, can proceed without SOX2. *Dev. Biol.* 457, 43–56. doi:10.1016/j.ydbio.2019.09.003

Eakin, R. M. (1973). *The third eye*. Univ of California Press.

Eakin, R. M., and Kuda, A. (1970). Ultrastructure of sensory receptors in ascidian tadpoles. *Z. für Zellforsch. Mikrosk. Anat.* 112, 287–312. doi:10.1007/BF02584045

Elliott, K. L., Pavlínková, G., Chizhikov, V. V., Yamoah, E. N., and Fritzsch, B. (2021). Development in the mammalian auditory system depends on transcription factors. *Int. J. Mol. Sci.* 22, 4189. doi:10.3390/ijms22084189

Elliott, K. L., Sokolowski, B., Yamoah, E. N., and Fritzsch, B. (2022). "An integrated perspective of communalities and difference across sensory receptors and their distinct central input," in *The evolution of sensory system revealed: gene regulation, cellular networks and processes*. Editors B. Fritzsch and K. Elliott (Wiley).

Elliott, K. L., Sokolowski, B., Yamoah, E. N., and Fritzsch, B. (2022). "An integrated perspective of commonalities and differences across sensory receptors and their distinct central inputs," in *Evolution of neurosensory cells and systems* (CRC Press), 255–290. doi:10.1201/9781003092810.10

Engelmann, J., and Fritzsch, B. (2022). "Lateral line input to 'almost'all vertebrates shares a common organization with different distinct connections, Evolution of Neurosensory Cells and Systems," in *Evolution of neurosensory cells and systems*. CRC Press, 201–222. doi:10.1201/9781003092810.8

Epstein, D. J., McMahon, A. P., and Joyner, A. L. (1999). Regionalization of Sonic hedgehog transcription along the anteroposterior axis of the mouse central nervous system is regulated by Hnf3-dependent and -independent mechanisms. *Development* 126, 281–292. doi:10.1242/dev.126.2.281

Ermakova, G. V., Kucheryavyy, A. V., Zaraisky, A. G., and Bayramov, A. V. (2019). The expression of FoxG1 in the early development of the European river lamprey *Lampetra fluviatilis* demonstrates significant heterochrony with that in other vertebrates. *Gene Expr. patterns* 34, 119073. doi:10.1016/j.gep.2019.119073

Ferrier, D. E., Brooke, N. M., Panopoulou, G., and Holland, P. W. (2001). The Mnx homeobox gene class defined by HB9, MNR2 and amphioxus AmphiMnx. *Dev. Genes Evol.* 211, 103–107. doi:10.1007/s004270000124

Flood, P. R. (1966). A peculiar mode of muscular innervation in amphioxus. Light and electron microscopic studies of the so-called ventral roots. *J. Comp. Neurology* 126, 181–217. doi:10.1002/cne.901260204

Fodor, A., Liu, J., Turner, L., and Swalla, B. J. (2020). Transitional chordates and vertebrate origins: tunicates. *Curr. Top. Dev. Biol.* 141, 149–171. doi:10.1016/bs.ctdb.2020.10.001

Fodor, A., Liu, J., Turner, L., and Swalla, B. J. (2021). Transitional chordates and vertebrate origins: tunicates. *Curr. Top. Dev. Biol.* 141, 149–171. doi:10.1016/bs.ctdb.2020.10.001

Fritzsch, B. (1996). Similarities and differences in lancelet and craniate nervous systems. *Israel J. Zoology* 42, S147–S160.

Fritzsch, B. (2021). An integrated perspective of evolution and development: from genes to function to ear, lateral line and electroreception. *Diversity* 13, 364. doi:10.3390/d13080364

Fritzsch, B. (2024). Evolution and development of extraocular motor neurons, nerves and muscles in vertebrates. *Ann Anat.* 53, 152225. doi:10.1016/j.aanat.2024.152225

Fritzsch, B., and Collin, S. P. (1990). Dendritic distribution of two populations of ganglion cells and the retinopetal fibers in the retina of the silver lamprey (Ichthyomyzon unicuspis). *Vis. Neurosci.* 4, 533–545. doi:10.1017/s0952523800005745

Fritzsch, B., Eberl, D. F., and Beisel, K. W. (2010). The role of bHLH genes in ear development and evolution: revisiting a 10-year-old hypothesis. *Cell. Mol. life Sci.* 67, 3089–3099. doi:10.1007/s00018-010-0403-x

Fritzsch, B., and Elliott, K. L. (2017). Gene, cell, and organ multiplication drives inner ear evolution. *Dev. Biol.* 431, 3–15. doi:10.1016/j.ydbio.2017.08.034

Fritzsch, B., and Elliott, K. L. (2022). "The senses: perspectives from brain, sensory ganglia, and sensory cell development in vertebrates," in *Evolution of neurosensory cells and systems*. CRC Press, 1–28. doi:10.1201/9781003092810.1

Fritzsch, B., Elliott, K. L., and Glover, J. C. (2017). Gaskell revisited: new insights into spinal autonomics necessitate a revised motor neuron nomenclature. *Cell Tissue Res.* 370, 195–209. doi:10.1007/s00441-017-2676-y

Fritzsch, B., Elliott, K. L., and Pavlinkova, G. (2019). Primary sensory map formations reflect unique needs and molecular cues specific to each sensory system. *F1000Research* 8, F1000 Faculty Rev-345. doi:10.12688/f1000research.17717.1

Fritzsch, B., and Martin, P. R. (2022). *Vision and retina evolution: how to develop a retina*. IBRO neuroscience reports 12, 240–248. doi:10.1016/j.ibneur.2022.03.008

Fritzsch, B., and Northcutt, G. (1993). Cranial and spinal nerve organization in amphioxus and lampreys: evidence for an ancestral craniate pattern. *Cells Tissues Organs* 148, 96–109. doi:10.1159/000147529

Fritzsch, B., Pauley, S., Feng, F., Matei, V., and Nichols, D. (2006). The molecular and developmental basis of the evolution of the vertebrate auditory system. *Int. J. Comp. Psychol.* 19, 1–25. doi:10.46867/ijcp.2006.19.01.06

Fritzsch, B., Schultze, H.-P., and Elliott, K. L. (2023). The evolution of the various structures required for hearing in Latimeria and tetrapods. *IBRO Neurosci. Rep.* 14, 325–341. doi:10.1016/j.ibneur.2023.03.007

Fritzsch, B., Sonntag, R., Dubuc, R., Ohta, Y., and Grillner, S. (1990). Organization of the six motor nuclei innervating the ocular muscles in lamprey. *J. Comp. Neurology* 294, 491–506. doi:10.1002/cne.902940402

Fritzsch, B., and Straka, H. (2014). Evolution of vertebrate mechanosensory hair cells and inner ears: toward identifying stimuli that select mutation driven altered morphologies. *J. Comp. Physiology A* 200, 5–18. doi:10.1007/s00359-013-0865-z

Fuhrmann, S. (2010). "Eye morphogenesis and patterning of the optic vesicle," in *Curr. Top. Dev Biol*. Elsevier 93, 61–84. doi:10.1016/B978-0-12-385044-7.00003-5

Gilland, E., and Baker, R. G. (2005). Evolutionary patterns of cranial nerve efferent nuclei in vertebrates. *Brain, Behav. Evol* 66, 234–254. doi:10.1159/000088128

Gigante, E. D., Piekarz, K. M., Gurgis, A., Cohen, L., Razy-Krajka, F., Popsuj, S., et al. (2023). Specification and survival of post-metamorphic branchiomeric neurons in the hindbrain of a non-vertebrate chordate. *bioRxiv [Preprint]*. doi:10.1101/2023.06.16.545305

Glardon, S., Holland, L. Z., Gehring, W. J., and Holland, N. D. (1998). Isolation and developmental expression of the amphioxus Pax-6 gene (AmphiPax-6): insights into eye and photoreceptor evolution. *Development* 125, 2701–2710. doi:10.1242/dev.125.14.2701

Glover, J. C. (2020). *Oikopleura. Curr. Biol.* 30, R1243–R1245. doi:10.1016/j.cub.2020.07.075

Glover, J. C., Elliott, K. L., Erives, A., Chizhikov, V. V., and Fritzsch, B. (2018). Wilhelm His' lasting insights into hindbrain and cranial ganglia development and evolution. *Dev. Biol.* 444, S14–S24. doi:10.1016/j.ydbio.2018.02.001

Gomez Mdel, P., Angueyra, J. M., and Nasi, E. (2009). Light-transduction in melanopsin-expressing photoreceptors of Amphioxus. *Proc. Natl. Acad. Sci. U. S. A.* 106, 9081–9086. doi:10.1073/pnas.0900708106

Holland, L. (2020). *Invertebrate origins of vertebrate nervous systems, Evolutionary Neuroscience*. Elsevier, 51–73.

Holland, L. Z., Albalat, R., Azumi, K., Benito-Gutiérrez, È., Blow, M. J., Bronner-Fraser, M., et al. (2008). The amphioxus genome illuminates vertebrate origins and cephalochordate biology. *Genome Res.* 18, 1100–1111. doi:10.1101/gr.073676.107

Holland, L. Z., and Daza, D. O. (2018). A new look at an old question: when did the second whole genome duplication occur in vertebrate evolution? *Genome Biol.* 19, 1–4. doi:10.1186/s13059-018-1592-0

Holland, L. Z., and Holland, N. D. (2021). Cephalochordates: a window into vertebrate origins. *Curr. Top. Dev. Biol.* 141, 119–147. doi:10.1016/bs.ctdb.2020.07.001

Holland, L. Z., and Holland, N. D. (2022). The invertebrate chordate amphioxus gives clues to vertebrate origins. *Curr. Top. Dev. Biol.* 147, 563–594. doi:10.1016/bs.ctdb.2021.12.011

Holmberg, K. (1986). The neural connection between the Langerhans receptor cells and the central nervous system in *Oikopleura dioica* (Appendicularia). *Zoomorphol* 106, 31–34. doi:10.1007/bf00311944

Hudson, C., Ba, M., Rouvière, C., and Yasuo, H. (2011). Divergent mechanisms specify chordate motoneurons: evidence from ascidians. *Development* 138, 1643–1652. doi:10.1242/dev.055426

Hoyer, J., Kolar, K., Athira, A., van den Burgh, M., Dondorp, D., Liang, Z., et al. (2024). Polymodal sensory perception drives settlement and metamorphosis of Ciona larvae. *Curr. Biol.* doi:10.1016/j.cub.2024.01.041

Imai, T. (2022). "Development of the olfactory system: from sensory neurons to cortical projections," in *Evolution of neurosensory cells and systems*. CRC Press, 21–60. doi:10.1201/9781003092810.2

Imai, T., Yamazaki, T., Kobayakawa, R., Kobayakawa, K., Abe, T., Suzuki, M., et al. (2009). Pre-target axon sorting establishes the neural map topography. *Science* 325, 585–590. doi:10.1126/science.1173596

Irvine, S. Q., Fonseca, V. C., Zompa, M. A., and Antony, R. (2008). Cis-regulatory organization of the Pax6 gene in the ascidian *Ciona intestinalis*. *Dev. Biol.* 317, 649–659. doi:10.1016/j.ydbio.2008.01.036

Islam, A. F., Moly, P. K., Miyamoto, Y., and Kusakabe, T. G. (2010). Distinctive expression patterns of Hedgehog pathway genes in the *Ciona intestinalis* larva: implications for a role of Hedgehog signaling in postembryonic development and chordate evolution. *Zool. Sci.* 27, 84–90. doi:10.2108/zsj.27.84

Jackman, W. R., Langeland, J. A., and Kimmel, C. B. (2000). Islet reveals segmentation in the Amphioxus hindbrain homolog. *Dev. Biol.* 220, 16–26. doi:10.1006/dbio.2000.9630

Jahan, I., Kersigo, J., Elliott, K. L., and Fritzsch, B. (2021). Smoothened overexpression causes trochlear motoneurons to reroute and innervate ipsilateral eyes. *Cell tissue Res.* 384, 59–72. doi:10.1007/s00441-020-03352-0

Kaji, T., Reimer, J. D., Morov, A. R., Kuratani, S., and Yasui, K. (2016). Amphioxus mouth after dorso-ventral inversion. *Zool. Lett.* 2, 2–14. doi:10.1186/s40851-016-0038-3

Kawano-Yamashita, E., Koyanagi, M., Shichida, Y., Oishi, T., Tamotsu, S., and Terakita, A. (2011). β-arrestin functionally regulates the non-bleaching pigment parapinopsin in lamprey pineal. *PloS one* 6, e16402. doi:10.1371/journal.pone.0016402

Kersigo, J., D'Angelo, A., Gray, B. D., Soukup, G. A., and Fritzsch, B. (2011). The role of sensory organs and the forebrain for the development of the craniofacial shape as revealed by Foxg1-cre-mediated microRNA loss. *Genesis* 49, 326–341. doi:10.1002/dvg.20714

Konno, A., Kaizu, M., Hotta, K., Horie, T., Sasakura, Y., Ikeo, K., et al. (2010). Distribution and structural diversity of cilia in tadpole larvae of the ascidian *Ciona intestinalis*. *Dev. Biol.* 337, 42–62. doi:10.1016/j.ydbio.2009.10.012

Kourakis, M. J., Borba, C., Zhang, A., Newman-Smith, E., Salas, P., Manjunath, B., et al. (2019). Parallel visual circuitry in a basal chordate. *Elife* 8, e44753. doi:10.7554/eLife.44753

Kozmikova, I., and Kozmik, Z. (2020). Wnt/β-catenin signaling is an evolutionarily conserved determinant of chordate dorsal organizer. *eLife* 9, e56817. doi:10.7554/eLife.56817

Kozmikova, I., and Yu, J.-K. (2017). Dorsal-ventral patterning in amphioxus: current understanding, unresolved issues, and future directions. *Int. J. Dev. Biol.* 61, 601–610. doi:10.1387/ijdb.170236ik

Kuratani, S., and Adachi, N. (2016). What are head cavities?a history of studies on vertebrate head segmentation. *Zoological Sci.* 33, 213–228. doi:10.2108/zs150181

Kusakabe, T., Kusakabe, R., Kawakami, I., Satou, Y., Satoh, N., and Tsuda, M. (2001). Ci-opsin1, a vertebrate-type opsin gene, expressed in the larval ocellus of the ascidian *Ciona intestinalis*. *FEBS Lett.* 506, 69–72. doi:10.1016/s0014-5793(01)02877-0

Lacalli, T. (2018). Amphioxus, motion detection, and the evolutionary origin of the vertebrate retinotectal map. *EvoDevo* 9, 6–5. doi:10.1186/s13227-018-0093-2

Lacalli, T., and Holland, L. (1998). The developing dorsal ganglion of the salp Thalia democratica, and the nature of the ancestral chordate brain. *Philosophical Trans. R. Soc. Lond. Ser. B Biol. Sci.* 353, 1943–1967. doi:10.1098/rstb.1998.0347

Lacalli, T. C. (2004). Sensory systems in amphioxus: a window on the ancestral chordate condition. *Brain, Behav. Evol.* 64, 148–162. doi:10.1159/000079744

Lacalli, T. C., Holland, N., and West, J. (1994). Landmarks in the anterior central nervous system of amphioxus larvae. *Philosophical Trans. R. Soc. Lond. Ser. B Biol. Sci.* 344, 165–185.

Lacalli, T. C., and Kelly, S. J. (2003). Ventral neurons in the anterior nerve cord of amphioxus larvae. I. An inventory of cell types and synaptic patterns. *J. Morphol.* 257, 190–211. doi:10.1002/jmor.10114

Lamb, T. D. (2013). Evolution of phototransduction, vertebrate photoreceptors and retina. *Prog. Retin. eye Res.* 36, 52–119. doi:10.1016/j.preteyeres.2013.06.001

Lamb, T. D. (2020). Evolution of the genes mediating phototransduction in rod and cone photoreceptors. *Prog. Retin. eye Res.* 76, 100823. doi:10.1016/j.preteyeres.2019.100823

Lamb, T. D., Collin, S. P., and Pugh, E. N. (2007). Evolution of the vertebrate eye: opsins, photoreceptors, retina and eye cup. *Nat. Rev. Neurosci.* 8, 960–976. doi:10.1038/nrn2283

Langeland, J. A., Holland, L. Z., Chastain, R. A., and Holland, N. D. (2006). An amphioxus LIM-homeobox gene, AmphiLim1/5, expressed early in the invaginating organizer region and later in differentiating cells of the kidney and central nervous system. *Int. J. Biol. Sci.* 2, 110–116. doi:10.7150/ijbs.2.110

Lent, R., Azevedo, F. A., Andrade-Moraes, C. H., and Pinto, A. V. (2012). How many neurons do you have? Some dogmas of quantitative neuroscience under revision. *Eur. J. Neurosci.* 35, 1–9. doi:10.1111/j.1460-9568.2011.07923.x

Leung, B., and Shimeld, S. M. (2019). Evolution of vertebrate spinal cord patterning. *Dev. Dyn.* 248, 1028–1043. doi:10.1002/dvdy.77

Lin, Y., Cai, Z., Huang, S., Yang, L., Wang, C., Liu, Z., et al. (2009). Ptc, smo, sufu, and the hedgehog signaling pathway in amphioxus. *Evol. Dev.* 11, 710–718. doi:10.1111/j.1525-142X.2009.00378.x

Litingtung, Y., Dahn, R. D., Li, Y., Fallon, J. F., and Chiang, C. (2002). Shh and Gli3 are dispensable for limb skeleton formation but regulate digit number and identity. *Nature* 418, 979–983. doi:10.1038/nature01033

Liu, B., and Satou, Y. (2019). Foxg specifies sensory neurons in the anterior neural plate border of the ascidian embryo. *Nat. Commun.* 10, 4911–5010. doi:10.1038/s41467-019-12839-6

Liu, B., and Satou, Y. (2020). The genetic program to specify ectodermal cells in ascidian embryos. *Dev. growth & Differ.* 62, 301–310. doi:10.1111/dgd.12660

Manni, L., Anselmi, C., Burighel, P., Martini, M., and Gasparini, F. (2018). Differentiation and induced sensorial alteration of the coronal organ in the asexual life of a tunicate. *Integr. Comp. Biol.* 58, 317–328. doi:10.1093/icb/icy044

Marlétaz, F., Firbas, P. N., Maeso, I., Tena, J. J., Bogdanovic, O., Perry, M., et al. (2018). Amphioxus functional genomics and the origins of vertebrate gene regulation. *Nature* 564, 64–70. doi:10.1038/s41586-018-0734-6

Marletaz, F., Timoshevskaya, N., Timoshevskiy, V., Simakov, O., Parey, E., Gavriouchkina, D., et al. (2023). The hagfish genome and the evolution of vertebrates. bioRxiv

Martin, P. R., and Fritzsch, B. (2021)."Vision and retina information processing: from opsins to the visual cortex," in *Evolution of neurosensory cells and systems* (CRC Press), 61–88. doi:10.1201/9781003092810.3

Meinhardt, H. (2015). "Models for patterning primary embryonic body axes: the role of space and time," in *Seminars in cell & developmental biology* (Elsevier), 103–117.

Miyamoto, D. M., and Crowther, R. J. (1985). Formation of the notochord in living ascidian embryos. *J. Embryol. Exp. Morphol.* 86, 1–17. doi:10.1242/dev.86.1.1

Moody, S. A., and LaMantia, A.-S. (2015). "Transcriptional regulation of cranial sensory placode development," in *Current topics in developmental biology* (Elsevier), 301–350.

Moraes, M. N., de Assis, L. V. M., Provencio, I., and Castrucci, A. M. d.L. (2021). Opsins outside the eye and the skin: a more complex scenario than originally thought for a classical light sensor. *Cell tissue Res.* 385, 519–538. doi:10.1007/s00441-021-03500-0

Nakagawa, M., Orii, H., Yoshida, N., Jojima, E., Horie, T., Yoshida, R., et al. (2002). Ascidian arrestin (Ci-arr), the origin of the visual and nonvisual arrestins of vertebrate. *Eur. J. Biochem.* 269, 5112–5118. doi:10.1046/j.1432-1033.2002.03240.x

Naville, M., Henriet, S., Warren, I., Sumic, S., Reeve, M., Volff, J.-N., et al. (2019). Massive changes of genome size driven by expansions of non-autonomous transposable elements. *Curr. Biol.* 29, 1161–1168. doi:10.1016/j.cub.2019.01.080

Negrón-Piñeiro, L. J., Wu, Y., and Di Gregorio, A. (2020a). Transcription factors of the bHLH family delineate vertebrate landmarks in the nervous system of a simple chordate. *Genes* 11, 1262. doi:10.3390/genes11111262

Negrón-Piñeiro, L. J., Wu, Y., and Di Gregorio, A. (2020b). Transcription factors of the bHLH family delineate vertebrate landmarks in the nervous system of a simple chordate. *Genes* 11, 1262. doi:10.3390/genes11111262

Niimura, Y. (2009). On the origin and evolution of vertebrate olfactory receptor genes: comparative genome analysis among 23 chordate species. *Genome Biol. Evol.* 1, 34–44. doi:10.1093/gbe/evp003

Niimura, Y. (2012). Olfactory receptor multigene family in vertebrates: from the viewpoint of evolutionary genomics. *Curr. genomics* 13, 103–114. doi:10.2174/138920212799860706

Niimura, Y., Ihara, S., and Touhara, K. (2020). "Mammalian olfactory and vomeronasal receptor families," in *The senses*. Editor B. Fritzsch (Elsevier), 516–535.

Niimura, Y., and Nei, M. (2007). Extensive gains and losses of olfactory receptor genes in mammalian evolution. *PloS one* 2, e708. doi:10.1371/journal.pone.0000708

Nishida, H., Ohno, N., Caicci, F., and Manni, L. (2021). 3D reconstruction of structures of hatched larva and young juvenile of the larvacean *Oikopleura dioica* using SBF-SEM. *Sci. Rep.* 11, 4833. doi:10.1038/s41598-021-83706-y

Noden, D. M., and Francis-West, P. (2006). The differentiation and morphogenesis of craniofacial muscles. *Dev. Dyn. official Publ. Am. Assoc. Anatomists* 235, 1194–1218. doi:10.1002/dvdy.20697

Okada, T., Katsuyama, Y., Ono, F., and Okamura, Y. (2002). The development of three identified motor neurons in the larva of an ascidian, Halocynthia roretzi. *Dev. Biol.* 244, 278–292. doi:10.1006/dbio.2002.0585

Olivo, P., Palladino, A., Ristoratore, F., and Spagnuolo, A. (2021). Brain sensory organs of the ascidian Ciona robusta: structure, function and developmental mechanisms. *Front. Cell Dev. Biol.* 9, 701779. doi:10.3389/fcell.2021.701779

Ota, K. G., and Kuratani, S. (2006). The history of scientific endeavors towards understanding hagfish embryology. *Zoological Sci.* 23, 403–418. doi:10.2108/zsj.23.403

Panaliappan, T. K., Wittmann, W., Jidigam, V. K., Mercurio, S., Bertolini, J. A., Sghari, S., et al. (2018). Sox2 is required for olfactory pit formation and olfactory neurogenesis through BMP restriction and Hes5 upregulation. *Development* 145, dev153791. doi:10.1242/dev.153791

Pantzartzi, C. N., Pergner, J., and Kozmik, Z. (2018). The role of transposable elements in functional evolution of amphioxus genome: the case of opsin gene family. *Sci. Rep.* 8, 2506–2511. doi:10.1038/s41598-018-20683-9

Pergner, J., and Kozmik, Z. (2017). Amphioxus photoreceptors-insights into the evolution of vertebrate opsins, vision and circadian rhythmicity. *Int. J. Dev. Biol.* 61, 665–681. doi:10.1387/ijdb.170230zk

Pergner, J., Vavrova, A., Kozmikova, I., and Kozmik, Z. (2020). Molecular fingerprint of amphioxus frontal eye illuminates the evolution of homologous cell types in the chordate retina. *Front. Cell Dev. Biol.* 8, 705. doi:10.3389/fcell.2020.00705

Piekarz, K. M., and Stolfi, A. (2023). Development and circuitry of the tunicate larval Motor Ganglion, a putative hindbrain/spinal cord homolog. *J. Exp. Zoology Part B Mol. Dev. Evol.* doi:10.1002/jez.b.23221

Pisani, D., Rota-Stabelli, O., and Feuda, R. (2020). Sensory neuroscience: a taste for light and the origin of animal vision. *Curr. Biol. CB* 30, R773–r775. doi:10.1016/j.cub.2020.05.009

Plessy, C., Mansfield, M. J., Bliznina, A., Masunaga, A., West, C., Tan, Y., et al. (2023). Extreme genome scrambling in cryptic *Oikopleura dioica* species. bioRxiv

Policarpo, M., Baldwin, M., Casane, D., and Salzburger, W. (2023). Diversity and evolution of the vertebrate chemoreceptor gene repertoire. *Nat Commun*. doi:10.1038/s41467-024-45500-y

Poncelet, G., and Shimeld, S. M. (2020). The evolutionary origins of the vertebrate olfactory system. *Open Biol.* 10, 200330. doi:10.1098/rsob.200330

Rawnsley, D. R., Xiao, J., Lee, J. S., Liu, X., Mericko-Ishizuka, P., Kumar, V., et al. (2013). The transcription factor Atonal homolog 8 regulates Gata4 and Friend of Gata-2 during vertebrate development. *J. Biol. Chem.* 288, 24429–24440. doi:10.1074/jbc.M113.463083

Razy-Krajka, F., Brown, E. R., Horie, T., Callebert, J., Sasakura, Y., Joly, J. S., et al. (2012). Monoaminergic modulation of photoreception in ascidian: evidence for a proto-hypothalamo-retinal territory. *BMC Biol.* 10, 45. doi:10.1186/1741-7007-10-45

Ren, Q., Zhong, Y., Huang, X., Leung, B., Xing, C., Wang, H., et al. (2020). Step-wise evolution of neural patterning by Hedgehog signalling in chordates. *Nat. Ecol. Evol.* 4, 1247–1255. doi:10.1038/s41559-020-1248-9

Riddiford, N., and Schlosser, G. (2016). Dissecting the pre-placodal transcriptome to reveal presumptive direct targets of Six1 and Eya1 in cranial placodes. *Elife* 5, e17666. doi:10.7554/eLife.17666

Rigon, F., Gasparini, F., Shimeld, S. M., Candiani, S., and Manni, L. (2018). Developmental signature, synaptic connectivity and neurotransmission are conserved between vertebrate hair cells and tunicate coronal cells. *J. Comp. Neurol.* 526, 957–971. doi:10.1002/cne.24382

Rigon, F., Stach, T., Caicci, F., Gasparini, F., Burighel, P., and Manni, L. (2013). Evolutionary diversification of secondary mechanoreceptor cells in tunicata. *BMC Evol. Biol.* 13, 112. doi:10.1186/1471-2148-13-112

Roberts, N. S., Hagen, J. F., and Johnston, R. J., Jr (2022). The diversity of invertebrate visual opsins spanning Protostomia, Deuterostomia, and Cnidaria. *Dev. Biol.* 492, 187–199. doi:10.1016/j.ydbio.2022.10.011

Roure, A., Chowdhury, R., and Darras, S. (2023). Regulation of anterior neurectoderm specification and differentiation by BMP signaling in ascidians. *Development* 150, dev201575. doi:10.1242/dev.201575

Ryan, J. F., Pang, K., Mullikin, J. C., Martindale, M. Q., and Baxevanis, A. D. (2010). The homeodomain complement of the ctenophore *Mnemiopsis leidyi* suggests that Ctenophora and Porifera diverged prior to the ParaHoxozoa. *Evodevo* 1, 9. doi:10.1186/2041-9139-1-9

Ryan, K., Lu, Z., and Meinertzhagen, I. A. (2018). The peripheral nervous system of the ascidian tadpole larva: types of neurons and their synaptic networks. *J. Comp. Neurology* 526, 583–608. doi:10.1002/cne.24353

Ryan, K., and Meinertzhagen, I. A. (2019). Neuronal identity: the neuron types of a simple chordate sibling, the tadpole larva of *Ciona intestinalis*. *Curr. Opin. Neurobiol.* 56, 47–60. doi:10.1016/j.conb.2018.10.015

Satoh, N., Rokhsar, D., and Nishikawa, T. (2014). Chordate evolution and the three-phylum system. *Proc. R. Soc. B Biol. Sci.* 281, 20141729. doi:10.1098/rspb.2014.1729

Schlosser, G. (2015). *Vertebrate cranial placodes as evolutionary innovations—the ancestor's tale, Current topics in developmental biology*. Elsevier, 235–300.

Schlosser, G. (2018). A short history of nearly every sense—the evolutionary history of vertebrate sensory cell types. *Integr. Comp. Biol.* 58, 301–316. doi:10.1093/icb/icy024

Schlosser, G. (2021). *Development of sensory and neurosecretory cell types: vertebrate cranial placodes, volume 1*. CRC Press.

Schlosser, G. (2021a). *Evolutionary origin of sensory and neurosecretory cell types: vertebrate cranial placodes, volume 2*. CRC Press.

Schultz, D. T., Haddock, S. H. D., Bredeson, J. V., Green, R. E., Simakov, O., and Rokhsar, D. S. (2023). Ancient gene linkages support ctenophores as sister to other animals. *Nature* 618, 110–117. doi:10.1038/s41586-023-05936-6

Schwab, I. (2018). The evolution of eyes: major steps. The Keeler lecture 2017: centenary of Keeler Ltd. *Eye* 32, 302–313. doi:10.1038/eye.2017.226

Seo, H. C., Edvardsen, R. B., Maeland, A. D., Bjordal, M., Jensen, M. F., Hansen, A., et al. (2004). Hox cluster disintegration with persistent anteroposterior order of expression in *Oikopleura dioica*. *Nature* 431, 67–71. doi:10.1038/nature02709

Shimeld, S. M. (1999). The evolution of the hedgehog gene family in chordates: insights from amphioxus hedgehog. *Dev. Genes Evol.* 209, 40–47. doi:10.1007/s004270050225

Simakov, O., Bredeson, J., Berkoff, K., Marletaz, F., Mitros, T., Schultz, D. T., et al. (2022). Deeply conserved synteny and the evolution of metazoan chromosomes. *Sci. Adv.* 8, eabi5884. doi:10.1126/sciadv.abi5884

Simionato, E., Ledent, V., Richards, G., Thomas-Chollier, M., Kerner, P., Coornaert, D., et al. (2007). Origin and diversification of the basic helix-loop-helix gene family in metazoans: insights from comparative genomics. *BMC Evol. Biol.* 7, 33–18. doi:10.1186/1471-2148-7-33

Somorjai, I. M., Martí-Solans, J., Diaz-Gracia, M., Nishida, H., Imai, K. S., Escrivà, H., et al. (2018). Wnt evolution and function shuffling in liberal and conservative chordate genomes. *Genome Biol.* 19, 98. doi:10.1186/s13059-018-1468-3

Søviknes, A. M., Chourrout, D., and Glover, J. C. (2005). Development of putative GABAergic neurons in the appendicularian urochordate *Oikopleura dioica*. *J. Comp. Neurol.* 490, 12–28. doi:10.1002/cne.20629

Søviknes, A. M., Chourrout, D., and Glover, J. C. (2007). Development of the caudal nerve cord, motoneurons, and muscle innervation in the appendicularian urochordate *Oikopleura dioica*. *J. Comp. Neurol.* 503, 224–243. doi:10.1002/cne.21376

Søviknes, A. M., and Glover, J. C. (2008). Continued growth and cell proliferation into adulthood in the notochord of the appendicularian *Oikopleura dioica*. *Biol. Bull.* 214, 17–28. doi:10.2307/25066656

Spencer, R. F., and Porter, J. D. (2006). Biological organization of the extraocular muscles. *Prog. Brain Res.* 151, 43–80. doi:10.1016/S0079-6123(05)51002-1

Stolfi, A., Ryan, K., Meinertzhagen, I. A., and Christiaen, L. (2015). Migratory neuronal progenitors arise from the neural plate borders in tunicates. *Nature* 527, 371–374. doi:10.1038/nature15758

Suzuki, D. G., and Grillner, S. (2018). The stepwise development of the lamprey visual system and its evolutionary implications. *Biol. Rev.* 93, 1461–1477. doi:10.1111/brv.12403

Takahashi, T., and Holland, P. W. (2004). Amphioxus and ascidian Dmbx homeobox genes give clues to the vertebrate origins of midbrain development. *Development* 131, 3285–3294. doi:10.1242/dev.01201

Tang, W. J., Chen, J. S., and Zeller, R. W. (2013). Transcriptional regulation of the peripheral nervous system in *Ciona intestinalis*. *Dev. Biol.* 378, 183–193. doi:10.1016/j.ydbio.2013.03.016

Terakita, A. (2005). The opsins. *Genome Biol.* 6, 213. doi:10.1186/gb-2005-6-3-213

Touhara, K., Niimura, Y., and Ihara, S. (2016). *Vertebrate odorant receptors, chemosensory transduction*. Academice Press, 49–66. doi:10.1016/B978-0-12-801694-7.00003.2

Van Le, M.-L., Müller, L.-M., and Stach, T. (2023). The oral sensory organs in Bathochordaeus stygius (Tunicata Appendicularia) are unique in structure and homologous to the coronal organ. *Front. Zool.* 20, 40. doi:10.1186/s12983-023-00518-8

Veeman, M., and Reeves, W. (2015). Quantitative and *in toto* imaging in ascidians: working toward an image-centric systems biology of chordate morphogenesis. *genesis* 53, 143–159. doi:10.1002/dvg.22828

Veeman, M. T., Newman-Smith, E., El-Nachef, D., and Smith, W. C. (2010). The ascidian mouth opening is derived from the anterior neuropore: reassessing the mouth/neural tube relationship in chordate evolution. *Dev. Biol.* 344, 138–149. doi:10.1016/j.ydbio.2010.04.028

Von Bartheld, C. S., Bahney, J., and Herculano-Houzel, S. (2016). The search for true numbers of neurons and glial cells in the human brain: a review of 150 years of cell counting. *J. Comp. Neurology* 524, 3865–3895. doi:10.1002/cne.24040

von Twickel, A., Kowatschew, D., Saltürk, M., Schauer, M., Robertson, B., Korsching, S., et al. (2019). Individual dopaminergic neurons of lamprey SNc/VTA project to both the striatum and optic tectum but restrict Co-release of glutamate to striatum only. *Curr. Biol. CB* 29, 677–685. doi:10.1016/j.cub.2019.01.004

Vopalensky, P., Pergner, J., Liegertova, M., Benito-Gutierrez, E., Arendt, D., and Kozmik, Z. (2012). Molecular analysis of the amphioxus frontal eye unravels the evolutionary origin of the retina and pigment cells of the vertebrate eye. *Proc. Natl. Acad. Sci.* 109, 15383–15388. doi:10.1073/pnas.1207580109

Watson, C., Shimogori, T., and Puelles, L. (2017). Mouse Fgf8-Cre-LacZ lineage analysis defines the territory of the postnatal mammalian isthmus. *J. Comp. Neurology* 525, 2782–2799. doi:10.1002/cne.24242

Welsch, U., Chiba, A., and Honma, Y. (1998). *The notochord*. The biology of hagfishes, 145–149.

Wicht, H., and Lacalli, T. C. (2005). The nervous system of amphioxus: structure, development, and evolutionary significance. *Can. J. Zoology* 83, 122–150. doi:10.1139/z04-163

Winkley, K. M., Kourakis, M. J., DeTomaso, A. W., Veeman, M. T., and Smith, W. C. (2020). *Tunicate gastrulation, Current topics in developmental biology*. Elsevier, 219–242.

Witten, P. E., and Hall, B. K. (2022). *The Notochord: development, Evolution and contributions to the vertebral column*. CRC Press. doi:10.1201/9781315155975

Wu, F., Bard, J. E., Kann, J., Yergeau, D., Sapkota, D., Ge, Y., et al. (2021). Single cell transcriptomics reveals lineage trajectory of retinal ganglion cells in wild-type and Atoh7-null retinas. *Nat. Commun.* 12, 1465–1520. doi:10.1038/s41467-021-21704-4

Xu, J., Li, J., Zhang, T., Jiang, H., Ramakrishnan, A., Fritzsch, B., et al. (2021). Chromatin remodelers and lineage-specific factors interact to target enhancers to establish proneurosensory fate within otic ectoderm. *Proc. Natl. Acad. Sci.* 118, e2025196118. doi:10.1073/pnas.2025196118

Xu, P.-X., Woo, I., Her, H., Beier, D. R., and Maas, R. L. (1997). Mouse Eya homologues of the Drosophila eyes absent gene require Pax6 for expression in lens and nasal placode. *Development* 124, 219–231. doi:10.1242/dev.124.1.219

Zhang, T., Xu, J., and Xu, P. X. (2021). Eya2 expression during mouse embryonic development revealed by Eya2(lacZ) knockin reporter and homozygous mice show mild hearing loss. *Dev. Dyn.* 250, 1450–1462. doi:10.1002/dvdy.326

Zhang, T., and Xu, P.-X. (2023). The role of Eya1 and Eya2 in the taste system of mice from embryonic stage to adulthood. *Front. Cell Dev. Biol.* 11, 1126968. doi:10.3389/fcell.2023.1126968

Zhang, X. M., and Firestein, S. (2002). The olfactory receptor gene superfamily of the mouse. *Nat. Neurosci.* 5, 124–133. doi:10.1038/nn800

Zhao, D., Chen, S., Horie, T., Gao, Y., Bao, H., and Liu, X. (2020). Comparison of differentiation gene batteries for migratory mechanosensory neurons across bilaterians. *Evol. Dev.* 22, 438–450. doi:10.1111/ede.12331

Zhu, K. W., Burton, S. D., Nagai, M. H., Silverman, J. D., de March, C. A., Wachowiak, M., et al. (2022). Decoding the olfactory map through targeted transcriptomics links murine olfactory receptors to glomeruli. *Nat. Commun.* 13, 5137. doi:10.1038/s41467-022-32267-3

Ziermann, J. M., Diogo, R., and Noden, D. M. (2018). Neural crest and the patterning of vertebrate craniofacial muscles. *Genesis* 56, e23097. doi:10.1002/dvg.23097

Zine, A., and Fritzsch, B. (2023). Early steps towards hearing: placodes and sensory development. *Int. J. Mol. Sci.* 24, 6994. doi:10.3390/ijms24086994

frontiers | Frontiers in Cell and Developmental Biology

TYPE Brief Research Report
PUBLISHED 13 March 2024
DOI 10.3389/fcell.2024.1304755

OPEN ACCESS

EDITED BY
Rosa Maria Sepe,
Anton Dohrn Zoological Station Naples, Italy

REVIEWED BY
Honoo Satake,
Suntory Foundation for Life Sciences, Japan
Ugo Coppola,
Cincinnati Children's Hospital Medical Center, United States
Michael Veeman,
Kansas State University, United States

*CORRESPONDENCE
Heather J. Evans Anderson,
heather.evansanderson@ahu.edu

RECEIVED 29 September 2023
ACCEPTED 31 January 2024
PUBLISHED 13 March 2024

CITATION
Stokes S, Palmer PP, Barth JL, Price RL, Parker BG and Evans Anderson HJ (2024), Gene expression and cellular changes in injured myocardium of *Ciona intestinalis*. *Front. Cell Dev. Biol.* 12:1304755. doi: 10.3389/fcell.2024.1304755

Gene expression and cellular changes in injured myocardium of *Ciona intestinalis*

Serenity Stokes[1], Pooja Pardhanani Palmer[2], Jeremy L. Barth[3], Robert L. Price[4], Bella G. Parker[5] and Heather J. Evans Anderson[6]*

[1]Central Piedmont Community College, Natural Sciences Division, Charlotte, NC, United States, [2]Atrium Health, Division of Community and Social Impact, Department of Community Health, Charlotte, NC, United States, [3]Department of Regenerative Medicine and Cell Biology, Medical University of South Carolina Proteogenomics Facility, Charleston, SC, United States, [4]Department of Cell Biology and Anatomy, University of South Carolina School of Medicine, Columbia, SC, United States, [5]Department of Biology, Stetson University, DeLand, FL, United States, [6]Department of Health and Biomedical Sciences, Advent Health University, Orlando, FL, United States

Ciona intestinalis is an invertebrate animal model system that is well characterized and has many advantages for the study of cardiovascular biology. The regulatory mechanisms of cardiac myocyte proliferation in *Ciona* are intriguing since regeneration of functional tissue has been demonstrated in other organs of *Ciona* in response to injury. To identify genes that are differentially expressed in response to *Ciona* cardiac injury, microarray analysis was conducted on RNA from adult *Ciona* hearts with normal or damaged myocardium. After a 24- or 48-h recovery period, total RNA was isolated from damaged and control hearts. Initial results indicate significant changes in gene expression in hearts damaged by ligation in comparison to control hearts. Ligation injury shows differential expression of 223 genes as compared to control with limited false discovery (5.8%). Among these 223 genes, 117 have known human orthologs of which 68 were upregulated and 49 were downregulated. Notably, *Fgf9/16/20*, insulin-like growth factor binding protein and Ras-related protein *Rab11b* were significantly upregulated in injured hearts, whereas expression of a junctophilin ortholog was decreased. Histological analyses of injured myocardium were conducted in parallel to the microarray study which revealed thickened myocardium in injured hearts. Taken together, these studies will connect differences in gene expression to cellular changes in the myocardium of *Ciona*, which will help to promote further investigations into the regulatory mechanisms of cardiac myocyte proliferation across chordates.

KEYWORDS

***Ciona intestinalis*, myocardium, gene expression, cardiac myocyte, microarray**

Introduction

As a tunicate, *Ciona intestinalis* is part of the group of invertebrate chordates that are most closely related to vertebrates (Delsuc et al., 2006). Molecular phylogenetic analyses indicate that much of the *Ciona* protein-encoding genome is conserved when compared to vertebrates, but with reduced genetic redundancy (Dehal et al., 2002). Current literature and database resources such as Aniseed (https://www.aniseed.cnrs.fr/) provide extensive information on the *Ciona* genome annotations, gene expression patterns and developmental lineages of major cell types,

including central and peripheral nervous system and the cardiopharyngeal lineage (Stolfi et al., 2010; Abitua et al., 2012; Stolfi et al., 2015; Brozovic et al., 2018; Horie et al., 2018). Moreover, *Ciona* embryos develop rapidly and are easily manipulated with molecular tools (Davidson, B. 2007; Cota et al., 2017). Thus, *Ciona* as part of the closest invertebrate outgroup to the vertebrates is an excellent animal model for the analysis of gene function and developmental processes.

While most studies investigating *Ciona* have examined embryonic and larval phases, few studies have examined mature adults. The adult *Ciona* is a sessile marine organism whose average size varies from 12 to 20 cm in length with the major organs located in the caudal region and the heart lying adjacent to the stomach. While the cardiac cells are specified during embryonic development, the heart forms post-metamorphosis during the juvenile phase (Davidson, 2007; Cota et al., 2017). Cardiac myocytes in *Ciona* share many of the same structural features as other chordates; however, the myocardium of *Ciona* is comprised of a single layer of cardiac myocytes *versus* the trabeculated myocardium of more complex chordates (Evans Anderson and Christiaen, 2016). The ultrastructure of the adult *Ciona* myocardium was described previously (Evans Anderson and Christiaen, 2016). This review suggests that the *Ciona* heart retains the genetic underpinnings of cardiac cell specification and basic cellular organization for all chordates. Of note, cardiac myocytes in *Ciona* are mononuclear and have less sarcomeric organization than mature mammalian cardiac myocytes. Instead, the ultrastructure of *Ciona* cardiac myocytes is more similar to embryonic or neonatal cardiac myocytes in mammals (Goldstein and Traeger, 1984; Evans Anderson and Christiaen, 2016; Guo and Pu, 2020). This is interesting since mononuclear cardiomyocytes in mammals have been shown to retain proliferative abilities, whereas mature polyploid cardiac myocytes lose proliferative capacity (Shen et al., 2020).

Regeneration of functional tissue has been characterized in *Ciona*. Studies have shown complete regeneration of siphons and neural complex (Dahlberg et al., 2009; Jeffery, 2015). However, regeneration of the *Ciona* heart has not been demonstrated yet, but it remains likely given that other solitary ascidians are capable of complete regeneration of tissues, including the heart (Gordon et al., 2021). In this study we examine altered gene expression and cellular changes to injured myocardium of *Ciona*. Very few studies have been conducted on the *C. intestinalis* heart and no previous studies have detailed the effects of cellular injury to the *C. intestinalis* heart. As the most closely related group to vertebrates with orthologous genes and conserved cell lineage specification mechanisms, *Ciona* can provide important insights into cardiac gene regulation, as well as cardiac myocyte biology.

Materials and methods

Animal husbandry

Ciona intestinalis adults (7–12 cm) were obtained by M-REP (San Diego, CA). The animals were maintained in a 65-gallon saltwater tank equipped with appropriate water circulation and filtration system.

Injury model

Adult *Ciona* hearts were subjected to injury via ligation. To set up ligations, hearts were exposed via a 3 cm incision in the animal's tunic and body wall muscle. Surgical silk (4 cm pieces of 000 gauge (Ethicon, NJ)) was tied around the exposed heart apex and tightened to restrict fluid flow but allow peristaltic contractions to continue. Animals were placed in separate baskets for a 24- or 48-h recovery period. At the end of each of these periods, hearts that were still visibly beating were processed for analysis. Control groups consisted of exposed but non-ligated hearts for each treatment group (24- and 48-h). A minimum of 4 hearts per group was done for each experiment, which were repeated at least three times for each group.

Histology

Ligated and control hearts were fixed in 4% paraformaldehyde (Electron Microscopy Sciences, PA) and stored at 4°C. Heart tissues were placed in a tissue processor, dehydrated in a graded ethanol series and embedded in Paraplast Xtra (Electron Microscopy Sciences, PA). Sections were cut at 5 mm and stained with Harris hematoxylin, immunofluorescence or Modified Russell-Movat Pentachrome staining. For immunostaining, slides were rehydrated through a graded series of MeOH/PBS. (75%, 50%, 25%) for 15 min each and then washed twice with PBS. PBSBT1 (1%–5% BSA, 1% Triton X-100 in PBS) was used to block for 1 h at RT twice. Diluted primary antibody (1:100 MF20) in PBST2 (1% BSA, 0.5% Triton X-100 in PBS) was applied and slides were incubated at 4°C for 16 h and then washed in PBST for 30 min five times. Secondary antibody with fluor was diluted in PBST2 and incubated for 4 h at RT then washed in PBST for 30 min five times. DAPI was included in mounting media. Slides were imaged using confocal microscopy.

Modified Russell-Movat Pentachrome staining

Modified Russell-Movat Pentachrome Stain (ScyTek Laboratories, UT) was used to histologically visualize the presence of muscle, mucin, collagen, elastin, and fibrin in *Ciona* heart sections. Staining incubations were performed at room temperature. A working elastic stain solution (ESS) was prepared using 2 parts hematoxylin solution (5%), 1-part ferric chloride solution (10%), and 1 part Lugol's Iodine solution. For 10 slides, 20 drops of hematoxylin, 10 drops of ferric chloride, and 10 drops of Lugol's Iodine were, and sections stained for 20 min. Slides were rinsed in running tap water until no excess stain remained. The slides were laid in the staining tray at an angle, and 15 drops of ferric chloride (2%) differentiating solution were applied and allowed to run off the slides. The slides were rinsed in running tap water, and then checked with a light microscope for differentiation of the tissue. If differentiation was not seen, the ferric chloride (2%) differentiation solution was applied again and allowed to run off the slides. The slides were then rinsed in two changes of distilled water. Next, 10 drops of sodium thiosulfate solution (5%) were applied to slides and incubated for 1 min. The slides were then rinsed in tap water for 2 min followed by 2 successive 1-min rinses in

distilled water. 10 drops of acetic acid solution (3%) were applied, and the slides were incubated for 2 min to equilibrate the tissue for alcian blue staining. The acetic acid solution was shaken off, and without rinsing, 10 drops of alcian blue solution, pH 2.5, were applied. The slides were incubated for 25 min, rinsed in tap water for 2 min followed by 2 successive 1-min changes in distilled water. 10 drops of Biebrich Scarlet/Acid Fuschin solution were applied. The slides were incubated for 10 min, and then rinsed in two 1-min changes of distilled water. Next, the tissue was equilibrated with a 10 s application of acetic acid (1%) with agitation and rinsed quickly in distilled water. Slides were then differentiated in 2 changes of 10 drops of phosphotungstic acid (5%) for 3 min each. The slides were then analyzed microscopically for proper differentiation of elastic fibers (collagen fibers remained clear at this checkpoint); if this was not achieved, the differentiation process was repeated. The slides were then placed back in a tray at an angle, and 10 drops of acetic acid (1%) were applied and allowed to run over the sections and off the slides. The slides were laid flat again, and without rinsing, 10 drops of tartrazine were applied. The slides were incubated for 1 minute and then rinsed in three 1-min changes of absolute alcohol.

Microarray

RNA was isolated by RNeasy Mini Kit (Qiagen) from injured and control hearts at 24 h or 48 h following treatment. Biological replicates were prepared for each sample type (control 24 h $n = 3$; control 48 h $n = 2$; injured 24 h $n = 4$; injured 48 h $n = 3$). A custom *Ciona* microarray A-AFFY-106 (CINT06a520380F; Affymetrix, Affymetrix, Santa Clara, CA) was obtained in collaboration with L. Christiaen (New York University). RNA samples were processed for Affymetrix microarray analysis at the Medical University of South Carolina Proteogenomics Facility as previously described (Lang et al., 2015). Briefly, total RNA samples were evaluated by Bioanalyzer 2100 (Agilent) to ensure integrity of ribosomal peaks and absence of degradation products. RNA was converted to biotin-labeled, fragmented cRNA using the 3′ IVT Express Kit (Affymetrix) according to manufacturer recommendations. Labeled cRNA was hybridized to GeneChips overnight at 45°C in a rotating oven. Post hybridization washing, staining and fluorescence scanning were performed with Affymetrix instrumentation and reagents as directed. Hybridization data (CEL files) were imported into Affymetrix Expression Console software and intensity values normalized by robust multi-array average (RMA) (Irizarry et al., 2003). Comparative analysis was done with dChip software (Li and Wong, 2001). Criteria for differential expression were absolute fold change greater >2 and $p < 0.01$ (Student's t-test). False discovery was estimated based on the number of genes discovered by iterative comparison with permuted sample assignments. Annotations for differentially expressed genes were accessed via the Aniseed Database. Raw microarray data (CEL files) are deposited at NCBI Gene Expression Omnibus (Accession # GSE244713).

Reverse transcription quantitative PCR (RT-qPCR)

RNA isolated from embryos, larvae, and juvenile *Ciona* as well as control ($n = 4$) and injured adult *Ciona* hearts ($n = 6$) was converted to cDNA using iScript™ cDNA Synthesis Kit (Bio-Rad) following manufacturer's protocol, then stored at −80°C until qPCR analysis. Primers were selected using Primer3 program (http://frodo.wi.mit.edu/) for *Ciona* Fgf9/16/20 (GenBank: AB086097.1) and *Ciona* FoxP genes (GenBank: NM_001078471.1) (Table 1). *Ciona* β-actin (CLSTR00046) expression was used as an internal control to normalize expression data. Serial dilutions of cDNA were used to evaluate primer efficiency. *Ciona* cDNA was diluted 1:10 for use in qPCR reaction. The reaction mix was 2 µL diluted cDNA; 5 µL L 2x SyBr Green PCR mix (iTaq universal SYBR green supermix, Bio-Rad); 0.05 µL 10 mM forward primer; 0.05 µL 10 mM reverse primer; and 2.9 µL nuclease free water. Reactions were run using Bio-rad CFX384 qPCR machine with the following protocol: 95°C 30 s; then 40 cycles of 95°C 5 s; 60°C 1 min. Amplifications were performed in triplicate. The average Ct value for β-actin was used to normalize the Ct values for FGF and FoxP genes. Each assay included a no-template control and a reverse transcription negative control for each primer pair. Data were analyzed using Bio-Rad CFX Maestro Software.

TABLE 1 Primer sets.

Primer	Sequence
FGF 131	Left: TCAATACGCCGTCCTTGAAT
	Right: ACTCGCGATTGAATGTTTC
FGF 113	Left: GGTACCCAAGAAAGCCACAA
	Right: TTGCTGTTCATTGCCAGGTA
FoxP 148	Left: TAGCCCAGAAGAGGACGGTA
	Right: CTGTTGCCGGTAAAATCCGT
FoxP 165	Left: CATGGAAGAACGCTGTGAGA
	Right: ACGGAGTTTCGATACGGTTG

Results

To elucidate genes that might be involved in induction of cardiac myocyte proliferation and myocardial regeneration, a microarray was conducted on control *versus* injured *Ciona* heart in to examine gene expression changes. To induce cardiac injury, adult *Ciona* hearts were exposed from the tunic. Injury to the hearts was done by ligation in which a surgical thread was tied around the heart to restrict flow for periods of 24- or 48-h (Figure 1). The contraction of the myocardium was used to confirm the animal was still alive post-injury. Several methods of injury to the *Ciona* hearts were attempted and ligation was the injury that allowed the animals to live for 48–72 h post injury and also produced results that were evident histologically and replicable. Ligation has been used as a form of myocardial injury in other animal models (Abarbanell et al., 2010). Injured and control hearts were then dissected and used to isolate RNA or fixed for further histological analyses.

RNA isolated from control *versus* injured hearts was subjected to microarray analysis via custom Affymetrix GeneChips. Comparisons restricted to 24 or 48-h time points did not yield significant genes. Therefore the 24- and 48-h samples within each

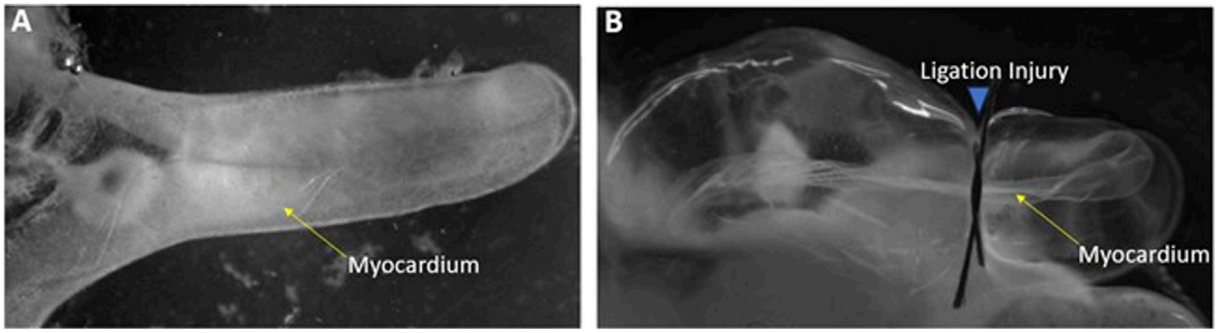

FIGURE 1
Ligation injury model of Ciona heart **(A)** Control heart exposed from *Ciona*. **(B)** Injured heart following 24-h of ligation.

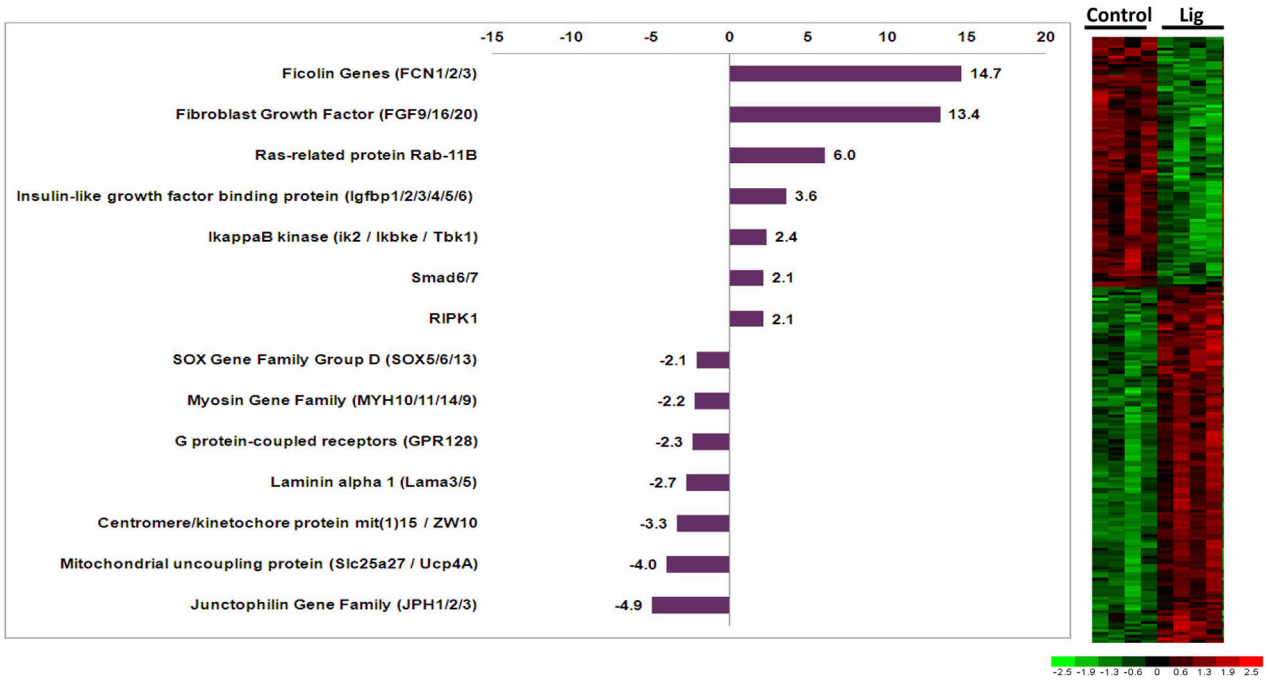

FIGURE 2
Altered gene expression in injured *Ciona* hearts. Comparison of ligated *versus* control hearts identified 223 differentially expressed genes. Fold changes for select orthologous genes are shown in the graph. Expression profiles for all differentially expressed genes are illustrated in the adjacent heatmap.

group were treated as the same sample type. Results of differential expression analysis are illustrated in the adjacent heatmap (Figure 2). Analysis of ligated hearts *versus* control yielded 223 differentially expressed genes (fold change >2, $p < 0.01$, Student's t-test) with limited false discovery (5.8%). Among these 223 genes, 117 have known human orthologs of which 68 were upregulated and 49 were downregulated. The annotations for the differentially expressed genes were accessed via the Aniseed Database (http://www.aniseed.cnrs.fr/). Expression changes for genes of interest are shown in the graph below (Figure 2). *Fgf9/16/20* is of particular interest, along with other proliferation related genes such as *Rab11b* and insulin like growth factor binding protein.

The full data set is accessible via Gene Expression Omnibus (GEO) – NCBI, to review GEO data, use accession GSE244713: Go to: https://nam10.safelinks.protection.outlook.com/?url=%3A%2F%2Furldefense.com%2Fv3%2F__%3A%2F%2Fwww.ncbi.nlm.nih.gov%2Fgeo%2Fquery%2Facc.cgi%3Facc%3DGSE244713__%3B!!Ab1_Rw!Fm1KQOqKhUyHpx-ej14R43nOCMBeCjIXhLQRxlrqMdwvV1j4UOc4s7_tEVpsxcIpIhjLdFqeIoQ_98XWpg%24&data=05%7C01%7Chevansanderson%40stetson.edu%7C99b4895e5b9d443e0c8408dbc9ad6557%7C7d854659421348c180cadf7831c02e6d%7C0%7C0%7C638325518791474686%7CUnknown%7CTWFpbGZsb3d8eyJWIjoiMC4wLjAwMDAiLCJQIjoiV2luMzIiLCJBTiI6Ik1haWwiLCJXVCI6Mn0%3D%7C3000%7C%7C%7C&sdata=XS1LE4cBd02SmDPJ7qfKRhU%2FPeehACqPJA9ZV9Tv2CY%3D&reserved=0. Enter token ipwhooiexjmhvgp into the box.

To confirm microarray analysis results, select genes of interest were subjected to reverse transcription quantitative PCR. *Fgf9/16/20* gene

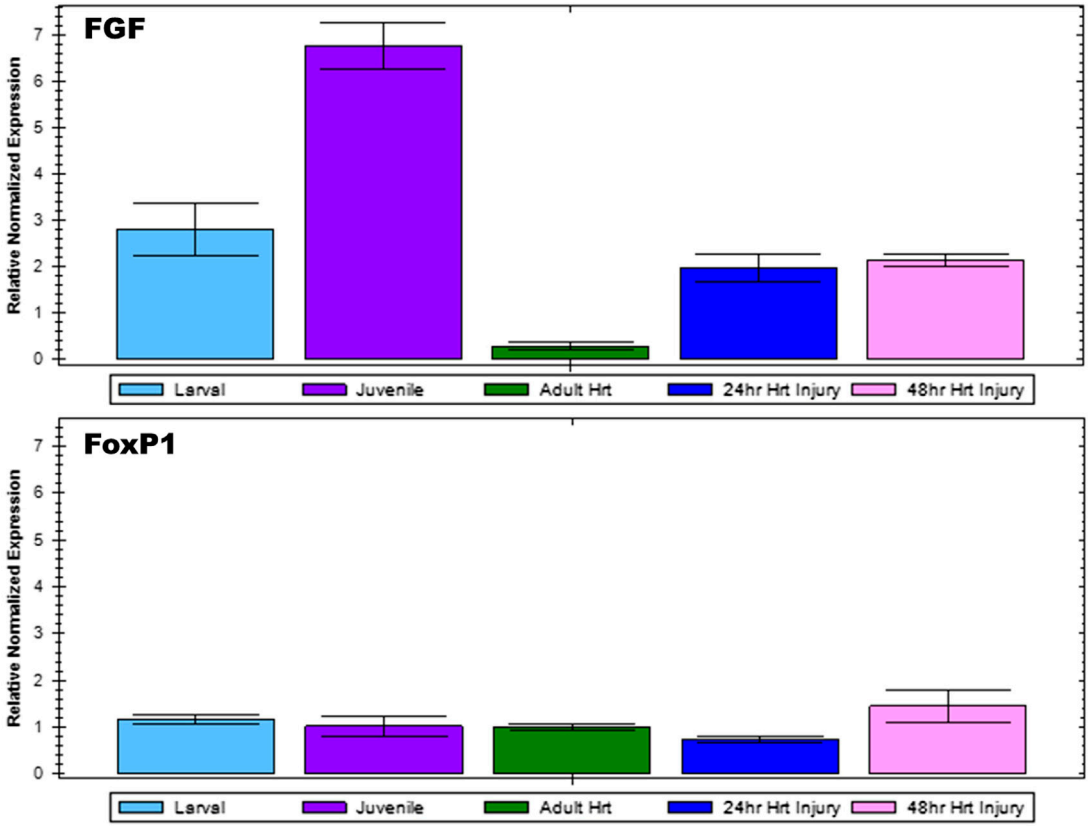

FIGURE 3
qPCR analysis to confirm microarray results. Relative normalized expression levels of *Fgf9/16/20* and *FoxP1* for *Ciona* larval, juvenile, and adult heart as well as injured adult heart at 24 and 48-h post-injury were analyzed by RT-qPCR. Results are normalized relative to *β-Actin*. Error bars represent standard error of the mean.

expression was analyzed for *Ciona* larval, juvenile, and adult hearts as well as injured adult hearts at 24 and 48 h post injury (Figure 3). Gene expression levels were normalized using β-Actin expression for each sample. *Fgf9/16/20* expression was found to be lowest in the adult heart; however, during the juvenile stage when the heart is forming, *Fgf9/16/20* is most highly expressed. When the heart is injured, *Fgf9/16/20* expression increased compared to adult heart samples in both 24- and 48-h ligation injury time points. In comparison, expression of *FoxP1* was examined across all samples. *FoxP1* did not significantly change across developmental timepoints or with injured hearts.

In order to examine the cellular changes that occurred after cardiac injury in *Ciona*, histological analyses were conducted. Immunofluorescence was performed using MF20 antibody to detect myosin heavy chain in cardiac myocytes (Bader et al., 1982) and DAPI to visualize nuclei (Figure 4). After injury, the myocardium thickens as visualized by increased MF20 expression (Figure 4B). This result was consistent in sections stained with Movats Pentachrome stain, which identifies collagen, elastin, muscle, mucin and fibrin in tissue sections (Figure 4D). These histological assays also revealed punctate bodies in the pericardium of *Ciona* hearts that were labeled by both MF20 and as muscle in Movats Pentachrome staining. These bodies were most defined in the control sections (Figures 4A,C). Further analysis is required in order to understand what these punctate bodies are and how the structural changes observed in the myocardium compare to responses to cardiac injury in other species.

Discussion

The *Ciona* model system presents an interesting opportunity to study cellular structure and gene expression changes in an adult myocardium. *Ciona* Comparison of the gene changes observed in *Ciona versus* gene expression changes that occur in experiments with more complex hearts might reveal interesting results. Moreover, *Ciona* may provide a chance to delineate the cellular and molecular requirements for cardiac regeneration with two distinct advantages: a chance to track cellular origins back to early progenitors and the genetic and cellular simplicity of an invertebrate chordate.

Here, we utilized a microarray study to analyze gene expression changes that occurred after injury to the adult heart. One of the most upregulated genes Fgf9/16/20, which increased 13.4 fold in injured hearts, has been shown in vertebrates to be an important regulator of cardiac myocyte proliferation (Itoh et al., 2016; Khosravi et al., 2021; Tahara et al., 2021). Interestingly, Fgf16/20 in mice regulates proliferation via cell signaling from the endocardium and cell signaling from the epicardium in other vertebrates (Lavine et al., 2005; Smith and Bader, 2007). However, *Ciona* do not have a discernable endocardium or epicardium but might retain some of the cell signaling mechanisms from Fgf 9/16/20 that promote cardiac myocyte proliferation. Furthermore, it has been shown that the FGF pathway is critical in the specification of progenitor cells to the cardiac lineage in *Ciona* as well as vertebrates (Davidson et al., 2006; Woznica

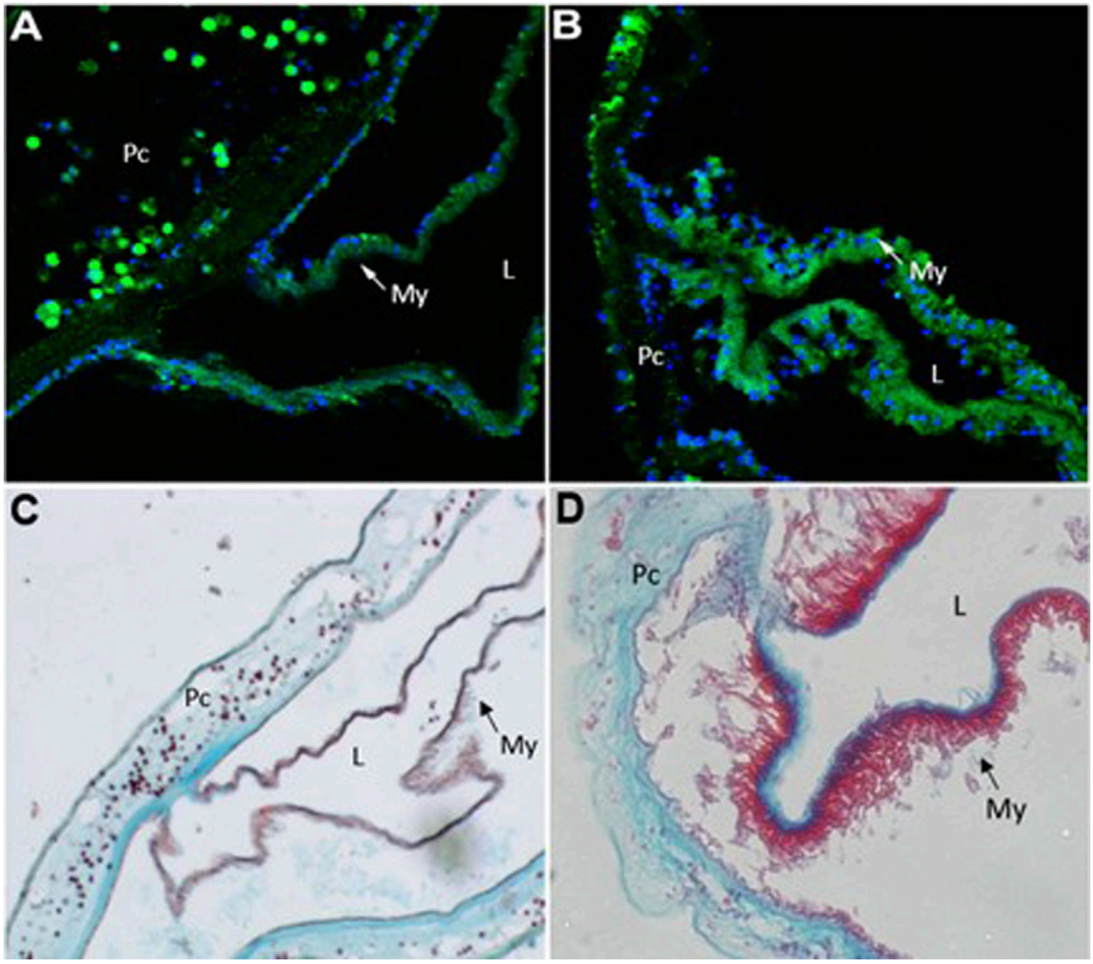

FIGURE 4
Injury to heart results in cellular changes to myocardium. Representative images of control **(A and C)** *versus* injured **(B and D)** *Ciona* hearts. **(A)** section of control heart showing the myocardium (My,green) where it transitions to the pericardium (Pc). Punctate green bodies were observed in the pericardial space. Cardiac myocyte nuclei (blue) are seen at the basal side of the myocardium opposite of the lumen (L). **(B)** injured myocardium (green) increases sarcomeric myosin expression after 48 h of injury. **(C)** control heart stained with Movat's Pentachrome (Muscle–RED, Mucins–BLUE, Elastin–BLACK/BLUE, Collagen–YELLOW, Fibrin–intense Red) shows where the myocardium (My, red) joins the pericardium (Pc). Punctate red bodies were observed in the pericardial space **(D)** injured myocardium (red) appears thickened 48 h post injury.

et al., 2012; Razy-Krajka et al., 2018; Tahara et al., 2021). Fgf 9/16/20 has been reported to be part of the subfamily E, which shows clear evolutionary relationship that is shared among chordates (Oulion et al., 2012). Other notable genes included insulin-like growth factor binding protein (IGFbp) and Rab11b (3.6-fold and 6-fold upregulated, respectively) since these genes are also involved in cardiac development, regeneration, and induction of pluripotent stem cells to cardiac myocytes (Sugden, 2003; Díaz del Moral et al., 2021). IGFbp has also been implicated in the inhibition of apoptosis in cardiac myocytes (Tang et al., 2021). The IGFbp gene family has a complex evolution where current evidence suggests that these genes evolved distinct functions early in vertebrate evolution (Daza et al., 2011). Additional characterization of IGFbp ortholog functions across chordate species would help elucidate how specific functions arose. Rab proteins are known to regulate vesicular transport in mammalian cardiac myocytes which are important in cell signaling mechanisms related to cardiac hypertrophy (Wu et al., 2001; Elias et al., 2012). Specifically, Rab11 is involved with GLUT4 glucose transporter in response to insulin in vertebrates (Kessler et al., 2000). The *Rab* family is well conserved across all chordates and is thought to have a predominant role in molecular communication between cells (Coppola et al., 2019). Notable genes that were found to be downregulated include the junctophilin gene family ortholog, which decreased 4.9-fold in ligated hearts. Decreased junctophilin expression in mice and humans has been found to cause cardiac hypertrophy (Landstrom et al., 2011; Beavers et al., 2014). Thus, the observed gene expression changes in injured *Ciona* hearts include orthologous genes in vertebrates that are known to have important roles in cardiac development and disease processes.

As part of the closest invertebrate outgroup to the vertebrates with a conserved genetic, the Ciona heart provides a useful model system to further elucidate the blueprint of cardiac myocyte proliferation and potentially provide insights into conserved cardiac regeneration mechanisms. Genetic manipulation or alteration of cell signaling mechanisms could be used in Ciona to promote cardiac myocyte proliferation or myocardial growth using conserved signaling pathway components and/or growth factors. The easily accessible Ciona heart

could be used to study effects of flow and mechanotransduction on cardiac myocytes. The possibilities using modern techniques to further characterize the Ciona heart are vast and these studies may provide important insights into cardiac myocyte biology.

Data availability statement

The original contributions presented in the study are publicly available. This data can be found here: GSE244713.

Ethics statement

The studies involving animals were reviewed and approved by Winthrop University Institutional Biosafety Committee (#B13001.R2).

Author contributions

SS: Conceptualization, Data curation, Formal Analysis, Investigation, Methodology, Writing–original draft. PP: Data curation, Formal Analysis, Investigation, Methodology, Validation, Writing–original draft. JB: Formal Analysis, Methodology, Resources, Software, Writing–review and editing. RP: Methodology, Resources, Supervision, Writing–review and editing. BP: Writing–review and editing, Validation. HA: Conceptualization, Data curation, Formal Analysis, Funding acquisition, Investigation, Project administration, Resources, Supervision, Writing–original draft, Writing–review and editing.

Funding

The author(s) declare financial support was received for the research, authorship, and/or publication of this article. The project was supported by NIH Grant Number 1R15HL104587-01 from the National Heart, Lung, and Blood Institute and NIH Grant Number P20 RR-16461 from the National Center for Research Resources for support of the program entitled "South Carolina IDeA Networks of Biomedical Research Excellence." Microarray analysis was conducted at the Medical University of South Carolina Proteogenomics Facility, which is supported by NIGMS P20 GM103499 as well as the Medical University of South Carolina Office of the Vice President for Research.

Acknowledgments

Microscopy analyses were assisted by Jeff Davis and RP, Director of the Instrument Resource Facility (IRF) at the University of South Carolina School of Medicine (USC SOM). The ligation model was developed with the help of Dr. Jay Potts (USC SOM). Dr. Brad Davidson (Swarthmore College, PA) served as a mentor for this project.

Conflict of interest

The authors declare that the research was conducted in the absence of any commercial or financial relationships that could be construed as a potential conflict of interest.

Publisher's note

References

Abarbanell, A. M., Herrmann, J. L., Weil, B. R., Wang, Y., Tan, J., Moberly, S. P., et al. (2010). Animal models of myocardial and vascular injury. *J. Surg. Res.* 162 (2), 239–249. doi:10.1016/j.jss.2009.06.021

Abitua, P. B., Wagner, E., Navarrete, I. A., and Levine, M. (2012). Identification of a rudimentary neural crest in a non-vertebrate chordate. *Nature* 492 (7427), 104–107. doi:10.1038/nature11589

Bader, D., Masaki, T., and Fischman, D. A. (1982). Immunochemical analysis of myosin heavy chain during avian myogenesis *in vivo* and *in vitro*. *J. Cell Biol.* 95 (3), 763–770. doi:10.1083/jcb.95.3.763

Beavers, D. L., Landstrom, A. P., Chiang, D. Y., and Wehrens, X. H. T. (2014). Emerging roles of junctophilin-2 in the heart and implications for cardiac diseases. *Cardiovasc. Res.* 103 (2), 198–205. doi:10.1093/cvr/cvu151

Brozovic, M., Dantec, C., Dardaillon, J., Dauga, D., Faure, E., Gineste, M., et al. (2018). ANISEED 2017: extending the integrated ascidian database to the exploration and evolutionary comparison of genome-scale datasets. *Nucleic Acids Res.* 46 (D1), D718–D725. doi:10.1093/nar/gkx1108

Coppola, U., Ristoratore, F., Albalat, R., and D'Aniello, S. (2019). The evolutionary landscape of the Rab family in chordates. *Cell. Mol. Life Sci.* 76, 4117–4130. doi:10.1007/s00018-019-03103-7

Cota, C. D., Palmquist, K., and Davidson, B. (2017). *Heart development in Ciona*. Reference Module in Life Sciences. Elsevier.

Dahlberg, C., Auger, H., Dupont, S., Sasakura, Y., Thorndyke, M., and Joly, J. (2009). Refining the *Ciona intestinalis* model of central nervous system regeneration. *PloS one* 4 (2), e4458. doi:10.1371/journal.pone.0004458

Davidson, B. (2007). *Ciona intestinalis* as a model for cardiac development. *Seminars Cell and Dev. Biol.* 18 (1), 16–26. doi:10.1016/j.semcdb.2006.12.007

Davidson, B., Shi, W., Beh, J., Christiaen, L., and Levine, M. (2006). FGF signaling delineates the cardiac progenitor field in the simple chordate, *Ciona intestinalis*. *Genes and Dev.* 20 (19), 2728–2738. doi:10.1101/gad.1467706

Daza, D. O., Sundström, G., Bergqvist, C. A., Duan, C., and Larhammar, D. (2011). Evolution of the insulin-like growth factor binding protein (IGFBP) family. *Endocrinology* 152 (6), 2278–2289. doi:10.1210/en.2011-0047

Dehal, P., Satou, Y., Campbell, R. K., Chapman, J., Degnan, B., De Tomaso, A., et al. (2002). The draft genome of *Ciona intestinalis*: insights into chordate and vertebrate origins. *Sci. (New York, N.Y.)* 298 (5601), 2157–2167. doi:10.1126/science.1080049

Delsuc, F., Brinkmann, H., Chourrout, D., and Philippe, H. (2006). Tunicates and not cephalochordates are the closest living relatives of vertebrates. *Nature* 439 (7079), 965–968. doi:10.1038/nature04336

Díaz Del Moral, S., Benaouicha, M., Muñoz-Chápuli, R., and Carmona, R. (2021). The insulin-like growth factor signalling pathway in cardiac development and regeneration. *Int. J. Mol. Sci.* 23 (1), 234. doi:10.3390/ijms23010234

Elias, M., Brighouse, A., Gabernet-Castello, C., Field, M. C., and Dacks, J. B. (2012). Sculpting the endomembrane system in deep time: high resolution phylogenetics of Rab GTPases. *J. Cell Sci.* 125 (10), 2500–2508. doi:10.1242/jcs.101378

Evans Anderson, H., and Christiaen, L. (2016). Ciona as a simple chordate model for heart development and regeneration. *J. Cardiovasc Dev. Dis.* 3, 25. doi:10.3390/jcdd3030025

Goldstein, M. A., and Traeger, L. (1984). "Ultrastructural changes in postnatal development of the cardiac myocyte," in *The developing heart: clinical implications of its molecular biology and physiology* (Springer), 1–20.

Gordon, T., Upadhyay, A. K., Manni, L., Huchon, D., and Shenkar, N. (2021). And then there were three extreme regeneration ability of the solitary chordate *Polycarpa mytiligera*. *Front. Cell Dev. Biol.* 9, 652466. doi:10.3389/fcell.2021.652466

Guo, Y., and Pu, W. T. (2020). Cardiomyocyte maturation: new phase in development. *Circulation Res.* 126 (8), 1086–1106. doi:10.1161/CIRCRESAHA.119.315862

Horie, R., Hazbun, A., Chen, K., Cao, C., Levine, M., and Horie, T. (2018). Shared evolutionary origin of vertebrate neural crest and cranial placodes. *Nature* 560 (7717), 228–232. doi:10.1038/s41586-018-0385-7

Irizarry, R. A., Hobbs, B., Collin, F., Beazer-Barclay, Y. D., Antonellis, K. J., Scherf, U., et al. (2003). Exploration, normalization, and summaries of high density oligonucleotide array probe level data. *Biostatistics* 4 (2), 249–264. doi:10.1093/biostatistics/4.2.249

Itoh, N., Ohta, H., Nakayama, Y., and Konishi, M. (2016). Roles of FGF signals in heart development, health, and disease. *Front. Cell Dev. Biol.* 4, 110. doi:10.3389/fcell.2016.00110

Jeffery, W. R. (2015). Closing the wounds: one hundred and twenty five years of regenerative biology in the ascidian C iona intestinalis. *Genesis* 53 (1), 48–65. doi:10.1002/dvg.22799

Kessler, A., Tomas, E., Immler, D., Meyer, H. E., Zorzano, A., and Eckel, J. (2000). Rab11 is associated with GLUT4-containing vesicles and redistributes in response to insulin. *Diabetologia* 43, 1518–1527. doi:10.1007/s001250051563

Khosravi, F., Ahmadvand, N., Bellusci, S., and Sauer, H. (2021). The multifunctional contribution of FGF signaling to cardiac development, homeostasis, disease and repair. *Front. Cell Dev. Biol.* 9, 672935. doi:10.3389/fcell.2021.672935

Landstrom, A. P., Kellen, C. A., Dixit, S. S., Van Oort, R. J., Garbino, A., Weisleder, N., et al. (2011). Junctophilin-2 expression silencing causes cardiocyte hypertrophy and abnormal intracellular calcium-handling. *Circ. Heart Fail.* 4 (2), 214–223. doi:10.1161/CIRCHEARTFAILURE.110.958694

Lang, H., Xing, Y., Brown, L. N., Samuvel, D. J., Panganiban, C. H., Havens, L. T., et al. (2015). Neural stem/progenitor cell properties of glial cells in the adult mouse auditory nerve. *Sci. Rep.* 5 (1), 13383. doi:10.1038/srep13383

Lavine, K. J., Yu, K., White, A. C., Zhang, X., Smith, C., Partanen, J., et al. (2005). Endocardial and epicardial derived FGF signals regulate myocardial proliferation and differentiation *in vivo*. *Dev. Cell* 8 (1), 85–95. doi:10.1016/j.devcel.2004.12.002

Li, C., and Wong, W. H. (2001). Model-based analysis of oligonucleotide arrays: expression index computation and outlier detection. *Proc. Natl. Acad. Sci.* 98 (1), 31–36. doi:10.1073/pnas.011404098

Oulion, S., Bertrand, S., and Escriva, H. (2012). Evolution of the FGF gene family. *Int. J. Evol. Biol.* 2012, 298147. doi:10.1155/2012/298147

Razy-Krajka, F., Gravez, B., Kaplan, N., Racioppi, C., Wang, W., and Christiaen, L. (2018). An FGF-driven feed-forward circuit patterns the cardiopharyngeal mesoderm in space and time. *eLife* 7, e29656. doi:10.7554/eLife.29656

Shen, H., Gan, P., Wang, K., Darehzereshki, A., Wang, K., Kumar, S. R., et al. (2020). Mononuclear diploid cardiomyocytes support neonatal mouse heart regeneration in response to paracrine IGF2 signaling. *Elife* 9, e53071. doi:10.7554/eLife.53071

Smith, T. K., and Bader, D. M. (2007). Signals from both sides: control of cardiac development by the endocardium and epicardium. *Seminars Cell and Dev. Biol.* 18 (1), 84–89. doi:10.1016/j.semcdb.2006.12.013

Stolfi, A., Gainous, T. B., Young, J. J., Mori, A., Levine, M., and Christiaen, L. (2010). Early chordate origins of the vertebrate second heart field. *Science* 329 (5991), 565–568. doi:10.1126/science.1190181

Stolfi, A., Ryan, K., Meinertzhagen, I. A., and Christiaen, L. (2015). Migratory neuronal progenitors arise from the neural plate borders in tunicates. *Nature* 527 (7578), 371–374. doi:10.1038/nature15758

Sugden, P. H. (2003). Ras, Akt, and mechanotransduction in the cardiac myocyte. *Circulation Res.* 93 (12), 1179–1192. doi:10.1161/01.RES.0000106132.04301.F5

Tahara, N., Akiyama, R., Wang, J., Kawakami, H., Bessho, Y., and Kawakami, Y. (2021). The FGF-AKT pathway is necessary for cardiomyocyte survival for heart regeneration in zebrafish. *Dev. Biol.* 472, 30–37. doi:10.1016/j.ydbio.2020.12.019

Tang, X., Jiang, H., Lin, P., Zhang, Z., Chen, M., Zhang, Y., et al. (2021). Insulin-like growth factor binding protein-1 regulates HIF-1α degradation to inhibit apoptosis in hypoxic cardiomyocytes. *Cell Death Discov.* 7, 242. doi:10.1038/s41420-021-00629-3

Woznica, A., Haeussler, M., Starobinska, E., Jemmett, J., Li, Y., Mount, D., et al. (2012). Initial deployment of the cardiogenic gene regulatory network in the basal chordate, *Ciona intestinalis*. *Dev. Biol.* 368 (1), 127–139. doi:10.1016/j.ydbio.2012.05.002

Wu, G., Yussman, M. G., Barrett, T. J., Hahn, H. S., Osinska, H., Hilliard, G. M., et al. (2001). Increased myocardial Rab GTPase expression: a consequence and cause of cardiomyopathy. *Circulation Res.* 89 (12), 1130–1137. doi:10.1161/hh2401.100427

frontiers | Frontiers in Cell and Developmental Biology

TYPE Review
PUBLISHED 14 March 2024
DOI 10.3389/fcell.2024.1359207

OPEN ACCESS

EDITED BY
Ebenezer N. Yamoah,
University of Nevada, Reno, United States

REVIEWED BY
Joel C. Glover,
University of Oslo, Norway
Cedric Patthey,
Umeå University, Sweden

*CORRESPONDENCE
Chiara Anselmi,
chiara90@stanford.edu
Lucia Manni,
lucia.manni@unipd.it

RECEIVED 21 December 2023
ACCEPTED 04 March 2024
PUBLISHED 14 March 2024

CITATION
Anselmi C, Fuller GK, Stolfi A, Groves AK and Manni L (2024), Sensory cells in tunicates: insights into mechanoreceptor evolution. *Front. Cell Dev. Biol.* 12:1359207. doi: 10.3389/fcell.2024.1359207

Sensory cells in tunicates: insights into mechanoreceptor evolution

Chiara Anselmi[1,2]*, Gwynna K. Fuller[3], Alberto Stolfi[4], Andrew K. Groves[3,5] and Lucia Manni[6]*

[1]Hopkins Marine Station, Institute for Stem Cell Biology and Regenerative Medicine, Stanford University, Pacific Grove, CA, United States, [2]Wu Tsai Neurosciences Institute, Stanford University, Stanford, CA, United States, [3]Department of Molecular and Human Genetics, Baylor College of Medicine, Houston, TX, United States, [4]School of Biological Sciences, Georgia Institute of Technology, Atlanta, GA, United States, [5]Department of Neuroscience, Baylor College of Medicine, Houston, TX, United States, [6]Dipartimento di Biologia, Università degli Studi di Padova, Padova, Italy

Tunicates, the sister group of vertebrates, offer a unique perspective for evolutionary developmental studies (Evo-Devo) due to their simple anatomical organization. Moreover, the separation of tunicates from vertebrates predated the vertebrate-specific genome duplications. As adults, they include both sessile and pelagic species, with very limited mobility requirements related mainly to water filtration. In sessile species, larvae exhibit simple swimming behaviors that are required for the selection of a suitable substrate on which to metamorphose. Despite their apparent simplicity, tunicates display a variety of mechanoreceptor structures involving both primary and secondary sensory cells (*i.e.*, coronal sensory cells). This review encapsulates two decades of research on tunicate mechanoreception focusing on the coronal organ's sensory cells as prime candidates for understanding the evolution of vertebrate hair cells of the inner ear and the lateral line organ. The review spans anatomical, cellular and molecular levels emphasizing both similarity and differences between tunicate and vertebrate mechanoreception strategies. The evolutionary significance of mechanoreception is discussed within the broader context of Evo-Devo studies, shedding light on the intricate pathways that have shaped the sensory system in chordates.

KEYWORDS

mechanoreceptor, evolution, placode, chordates, hair cells, primary sensory cells, secondary sensory cells

1 Introduction

Twenty years ago, a paper provocatively titled "Novel, secondary sensory cell organ in ascidians: in search of the ancestor of the vertebrate lateral line" by Burighel and others (Burighel et al., 2003), provided evidence that the tunicate ascidian *Botryllus schlosseri* possessed a complex mechanosensory organ, the coronal organ. Unlike the previously characterized multicellular mechanoreceptor organs of adult tunicates (Manni and Pennati, 2015), this novel organ was not composed of peripheral neurons (*i.e.*, primary sensory cells) but showed dedicated axonless secondary receptor cells. These secondary receptor cells were contacted at their base by neurites coming from brain neurons, forming both afferent and efferent synapses with the sensory cells (Figure 1A). This discovery also revealed that the adult tunicate brain possessed sensory neurons, since then not considered, for the elaboration of afferent information from the coronal sensory cells and their control by means of efferent inputs. Moreover, in *B. schlosseri*, coronal sensory cells showed an apical bundle with a cilium accompanied by microvilli and/or stereovilli. They were aligned on the

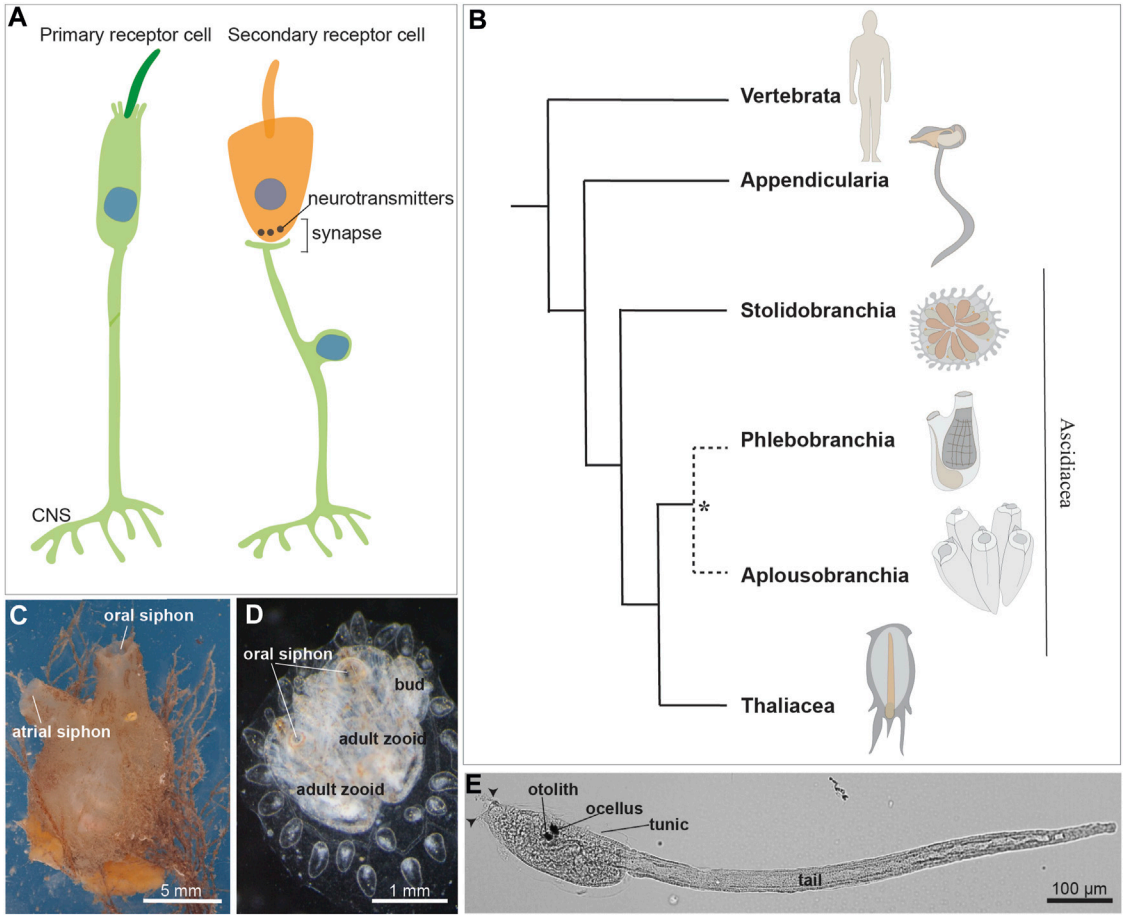

FIGURE 1
(A) Illustration of a primary and a secondary receptor cell in tunicates. The primary receptor is a peripheral neuron, whose soma (indicated by the blue nucleus) is in the epidermis. The secondary receptor (orange) is, *vice versa*, a dedicated receptor that transmits its input to a brain sensory neuron. **(B)** Chordate evolutionary tree. * The monophyly of Phlebobranchia is disputed [see (DeBiasse et al., 2020)]. Stolidobranchia species are defined as Pleurogona (with gonads in the lateral body wall), whereas Phlebobranchia and Aplousobranchia are defined as Enterogona (with gonads close to the gut). **(C)** Adult individual of the ascidian *Molgula socialis* (right view). **(D)** Young colony of *Botryllus schlosseri* composed by two adult zooids and their buds. Dorsal view. **(E)** *Ciona robusta* larva at stage 28, 18 h post fertilization at 20°. Arrowheads: two anterior papillae. Ascidian larvae are composed of an anterior cephalenteron, *i.e.*, a body part including both head structures (such as the brain) and trunk structures (such as the gut), and a posterior tail. The cephalenteron is usually called a "trunk".

oral siphon tentacles and exposed to the incoming seawater. In many aspects, these cells resembled vertebrate hair cells of lateral line organs (Manni et al., 2004). These features, combined with the evolutionary proximity between tunicates and vertebrates, considered sister groups (Delsuc et al., 2018), initiated a controversial yet exciting debate on the homology of coronal sensory cells and hair cells. This discussion extended to the homology of the embryonic territories from which they originate. Vertebrate hair cells derive from neurogenic placodes (namely, from the otic and the lateral line placodes) that, together with the neural crest, were at that time considered exclusive to vertebrates (Manni et al., 2001; 2004). Therefore, the discovery of the coronal organ (with sensory cells hypothesized homologous to vertebrate hair cells), together with the publication of the first data on the presence of placodal area and neural crest-like cells in tunicates (Manni et al., 2001; Jeffery et al., 2004; Mazet and Shimeld, 2005), challenged the foundation of the main theory of vertebrate evolution, the so-called "New head hypothesis" (Gans and Northcutt, 1983). This theory proposed that neurogenic placodes and neural crest cells were, with respect to non-vertebrate chordates, novel cell populations that contributed to the success of vertebrates and their development of complex nervous systems.

In the past 20 years since the discovery of the coronal organ, numerous aspects of its morphology, physiology, and development have been elucidated (Burighel et al., 2011; Manni and Pennati, 2015). The organ has been found in all the tunicate taxa (except for Salps, see below) so far examined. Its mechanoreceptive function and synaptic connectivity has been established and some key developmental genes studied. Nevertheless, many questions remain unanswered, making the investigation of tunicate mechanoreception an intriguing question in evolutionary developmental biology research.

Tunicates constitute a diverse group of marine invertebrates, including both pelagic and sessile animals with different behavior and motility, thus having varied sensory requirements. Traditionally, tunicates were classified into three classes: the sessile Ascidiacea and

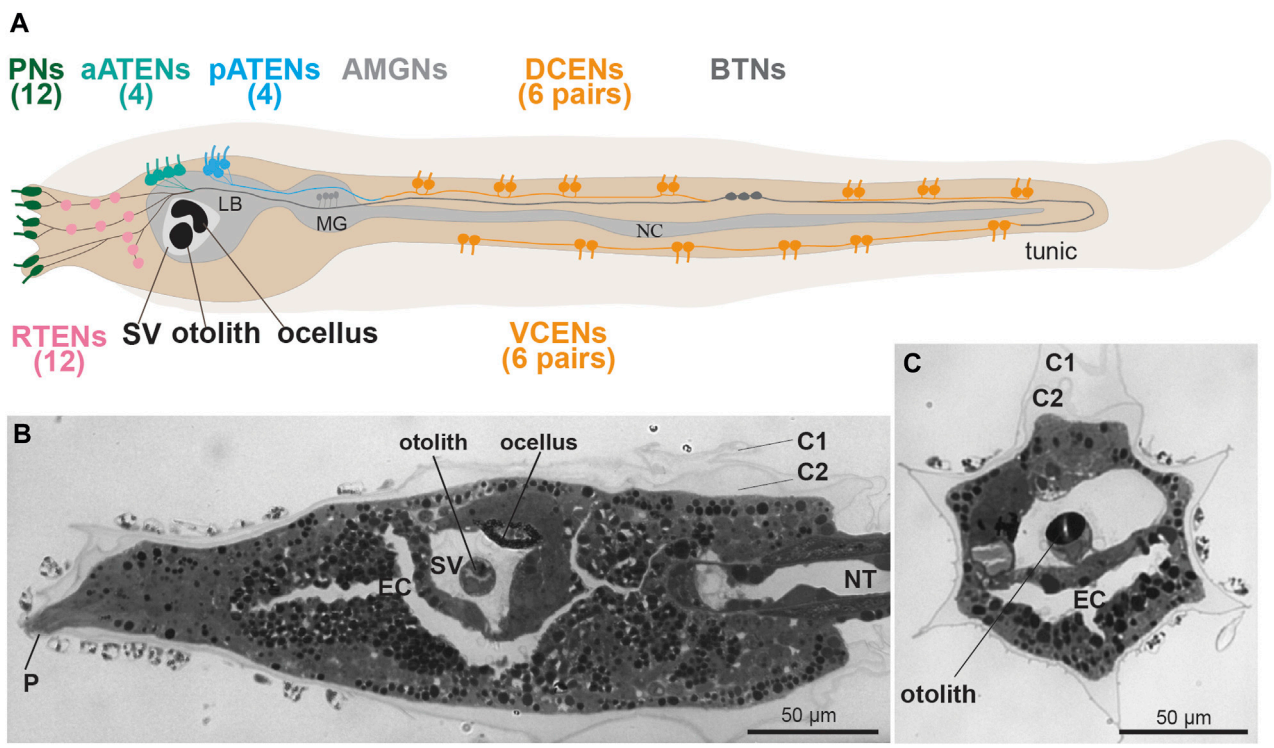

FIGURE 2
(A) Larval sensory neurons in *Ciona robusta* (see Ryan et al., 2017). Left lateral view. In the tail there are two groups of caudal epidermal neurons, 12 dorsal (DCENs) and 12 ventral (VCENs). There are three groups of Trunk Epidermal Neurons, 12 rostral (RTEN), four anterior (aATENs) and four posterior (pATENs). There are three rostral papillae with two pairs of sensory neurons (Pns) each. **(B,C)** frontal and cross sections of *C. robusta*, showing some sensory structures: the anterior dorsal papilla (P), and the sensory vesicle (SV) with the otolith and the ocellus, Toluidine blue. C1-C2: tunic cuticular layer; EC: endodermal cavity; LB: larval brain; MG: motor ganglion; NC: nerve cord; NT: notochord; SV: sensory vesicle.

the pelagic Thaliacea and Larvacea. However, molecular phylogenies suggest that ascidians are a paraphyletic group and support the monophyly of thaliaceans (Delsuc et al., 2018; Kocot et al., 2018; DeBiasse et al., 2020) (Figures 1B–D). The tunicate tadpole swimming larva exhibits a typical chordate body plan which is lost during metamorphosis in ascidians and thaliaceans. At this stage the latter adopts a sac-like body with two apertures, the oral and the atrial siphons, for seawater circulation and filtration. The sessile ascidians, the most extensively studied group, exhibit a larva with a tripartite brain derived from the dorsal nerve tube. The larva also possesses numerous primary mechanosensory cells scattered in the monolayered epidermis, allowing the detection of a suitable substrate for metamorphosis (Wakai et al., 2021; Sakamoto et al., 2022). The sessile adult has a ganglionic brain, and its mobility is limited to the siphon and body wall contraction as defensive responses (Mackie and Burighel, 2005).

Here we review research on mechanoreception in tunicates. We begin by examining mechanoreceptor cells and organs based on primary receptors in the ascidian larva (Section 2). Then, we describe the diversity of mechanoreception structures (including both single or clustered cells and multicellular organs) based on primary receptors exhibited by adult tunicates (Section 3). Lastly, we consider 20 years of research on the coronal organ from a morphological, physiological and developmental point of view, describing similarities and differences between coronal sensory cells and vertebrate hair cells (Section 4).

2 Putative mechanosensory cells of the ascidian larva

As the larvae are primarily responsible for ascidian dispersal, their simple swimming behavior is modified by environmental stimuli. This is likely to increase the odds of escaping predation and settling in a suitable location for metamorphosis. For instance, mechanical stimulation of the adhesive/sensory papillae, the three sensory organs (two dorsal and one ventral) located in the anterior larval region (Figures 1E, 2A–B) is sufficient and necessary to trigger metamorphosis in *Ciona* (Wakai et al., 2021; Sakamoto et al., 2022). While mechanosensitive modulation of swimming has yet to be definitively shown in ascidian larvae, startle-like behaviors have been described in *Ciona* (Athira et al., 2022). Here we discuss what is known about the development and function of the candidate primary mechanosensory cell types that have been identified in these larvae.

2.1 Caudal epidermal neurons

Sometimes referred to as Caudal Epidermal Sensory Neurons, these primary receptors are a subset of a broader class of tail epidermal neurons and were initially described in *Diplosoma listerianum* (previously named *D. macdonaldi*) (Torrence and Cloney, 1982). They have since been reported in numerous other

species spread across both enterogonid (e.g., *Ciona, Phallusia*) and stolidobranch (e.g., *Halocynthia, Molgula*) ascidians (Torrence and Cloney, 1982; Takamura, 1998; Imai and Meinertzhagen, 2007; Terakubo et al., 2010; Ohtsuka et al., 2014; Ryan et al., 2018). Although the CENs have yet to be conclusively shown to be mechanosensory, Torrence and Cloney proposed this based on ultrastructural similarities to cupular organ mechanoreceptors of the adult (Torrence and Cloney, 1982). (Figure 1E) CENs are found embedded in the epidermis of the larval tail, along both the dorsal and ventral midlines (Figure 1E). Therefore they are sometimes divided into Dorsal CEN (DCEN) and Ventral CEN (VCEN) subtypes (Ryan et al., 2018) (Figure 2A). CENs occur in regularly interspersed pairs, but their number is variable, with an average of 14 pairs per larva reported in *Ciona* (Pasini et al., 2006). Each neuron bears a single cilium that projects into the overlying extracellular tunic. In the tunic these cilia form a branched network termed the ASNET (Ascidian Dendritic Network In Tunic) (Torrence and Cloney, 1982; Konno et al., 2010; Terakubo et al., 2010; Yokoyama et al., 2014). While the base of the cilia are formed by microtubules and are clearly stained by anti-acetylated tubulin immunofluorescence, their distal portions in the tunic do not contain ordered microtubule arrays (Torrence and Cloney, 1982; Terakubo et al., 2010). CENs possess short axons that form contacts primarily between each other and a few putative relay neurons, such as the Bipolar Tail Neurons (BTNs) (Stolfi et al., 2015; Ryan et al., 2018). The BTNs have been proposed to be homologous to vertebrate cranial sensory neurons (Papadogiannis et al., 2022), though their sensory capabilities are entirely unknown. Like all epidermal neurons, CENs express *Slc17a6/7/8,* encoding Vesicular glutamate transporter (Vglut) and are therefore likely glutamatergic (Horie et al., 2008).

Extensive work in *Ciona* has revealed the embryonic origins of the CENs and the molecular pathways regulating their specification. CENs arise from neurogenic midlines of the tail epidermis, both dorsally and ventrally. Both midlines are derived from b-lineage blastomeres that also give rise to epidermal cells and BTNs (Pasini et al., 2006). While induction of the dorsal and ventral neurogenic midlines occurs independently through different signals, they converge on a shared gene regulatory network for sensory neurogenesis (Pasini et al., 2006; 2012; Tang et al., 2013; Waki et al., 2015). Both midlines express Msx, which in turn activates the expression of the proneural bHLH gene, *Achaete-Scute-like.a* (*Ascl.a,* though sometimes referred to as *Ascl2* or *Ascl.b* previously). However, in the dorsal midline, *Msx* is activated by Otx and Nodal, while in the ventral midline it is activated instead by Tbx2/3 (Pasini et al., 2006; Waki et al., 2015). Otx and Nodal expression in the dorsal midline in turn depends on FGF signaling, while Tbx2/3 expression in the ventral midline is induced by ADMP/BMP signaling instead (Pasini et al., 2006; Waki et al., 2015). Downstream of Ascl.a, both dorsal and ventral networks appear to function through a series of transcription factors, especially conserved neuronal selectors such as Pou4 and Myt1 (Tang et al., 2013). While all the cells in these neurogenic midlines express Ascl.a and thus likely have the potential to give rise to CENs, the final number of neurons is limited by typical lateral inhibition via the Delta/Notch pathway and the microRNA miR-124 (Chen et al., 2011; Tang et al., 2013).

Given that the dorsal and ventral neurogenic midlines are induced by different mechanisms, it has been proposed that one may have evolved as a co-option of the other (Waki et al., 2015). More specifically, it was proposed that the ventral midline is the ancestral one, as induction of ventrolateral sensory neurons by BMP is observed in cephalochordates as well (Lu et al., 2012). The neurogenic dorsal midline of tunicates and vertebrates would therefore represent a co-option of this neurogenic program in the last common olfactorian ancestor (last common ancestor of tunicates and vertebrates). In vertebrates, the dorsal neurogenic domain would have allowed for the emergence of neural crest-derived neurons and other sensory neuron types, like Rohon-Beard cells of anamniote larvae. Alternatively, the ventral midline may have evolved specifically in tunicates as a co-option of an ancestral Msx-dependent neural plate border program for sensory neuron specification. Complementary to these scenarios, it has also been suggested that both dorsal and ventral midlines were neurogenic in the chordate ancestor, and that vertebrates lost the ventral one (Pasini et al., 2006). However, it was reported that another tunicate species, *Halocynthia roretzi,* has only a small number of ventral CENs near the tail tip, and that its dorsal neurogenic midline depends on FGF, Nodal, and BMP combined, along with yet-undiscovered inductive signals (Ohtsuka et al., 2014). Although the midline neurogenic programs are deeply conserved across tunicates (Coulcher et al., 2020), it is clear that additional work on diverse tunicate species will be required to better refine our evolutionary models.

2.2 Trunk epidermal neurons (RTENs, aATENs, and pATENs)

In addition to putative mechanosensory neurons of the tail, there are three epidermal neuron subtypes found in the dorsal areas of the epidermis of the larval "trunk". These primary receptors were defined as Trunk Epidermal Neurons. These are, from anterior to posterior, Rostral Trunk Epidermal Neurons (RTENs), Anterior Apical Trunk Epidermal Neurons (aATENs), and Posterior Trunk Epidermal Neurons (pATENs) (Imai and Meinertzhagen, 2007; Ryan et al., 2018) (Figure 2A). In *Ciona*, there are 7 RTENs on either left/right side (14 total neurons) of the dorsolateral epidermis between the papillae and the sensory vesicle (Ryan et al., 2018). The aATENs occur as two left/right pairs on either side of the dorsal midline (4 total neurons), while the four pATENs appear to lie directly on the midline (Ryan et al., 2018). Although all trunk epidermal neurons contribute to the larval ASNET, like CENs their mechanosensory abilities have never been tested (Abitua et al., 2015; Poncelet et al., 2022; Hoyer et al., 2024). The three subtypes all have well-developed axons but show different connectivity within the PNS network, hinting at distinct functions. RTENs form extensive chemical synapses onto a few different interneurons in the larval brain including the Eminens cells, which are GABAergic (Cao et al., 2019). pATENs on the other hand form extensive inputs onto the Ascending Motor Ganglion (AMG) complex, especially the sole cholinergic (i.e., excitatory) AMG neuron, AMG5 (Ryan et al., 2018; Ryan et al., 2016; Ryan et al., 2017; Kourakis et al., 2019; Popsuj and Stolfi, 2021). Downstream connections even suggest opposite effects on swimming behavior,

either arresting swimming (RTENs) or triggering swimming (pATENs). In contrast, the aATENs do not appear to form very many chemical synapses, at least at the relatively early larval stage documented by the connectome studies (Ryan et al., 2018). This may support its proposed role as a neurosecretory cell, and potentially homologous to both olfactory neurons and Gonadotropin-releasing hormone (GnRH) neurons in vertebrates (Abitua et al., 2015; Okawa et al., 2020).

Much less is known about the development of the different Trunk Epidermal Neurons, compared to the CE Ns. In *Halocynthia,* RTENs are specified from anterior neural plate lateral border cells by FGF, Nodal, and BMP signaling (Ohtsuka et al., 2014), while excess BMP signaling appears to suppress the formation of the oral siphon placode, or stomodeum, which gives rise to the aATENs in Ciona (Abitua et al., 2015). A similar FGF/Nodal/BMP combination is required for CEN specification in Halocynthia (see above), though this may be different in *Ciona* and other tunicate families. This suggests that a common gene regulatory network might be shared between Trunk and Caudal subsets of ESNs. The development of the pATENs has not been studied at all, to our knowledge. In sum, much work remains to be done on both the function and development of these different Trunk Epidermal Neurons.

2.3 Papilla neurons

Despite our current knowledge of the *Ciona* larval connectome and the regulation of caudal and Trunk Epidermal Neuron development, there is little direct evidence supporting their mechanosensitive nature. There is no evidence directly refuting that CENs and assorted Trunk Epidermal Neurons are mechanosensory cells, either. However, the larval neuron most widely accepted as a mechanosensitive cell type is the Papilla Neuron (PN) (Figure 2A) (Manni et al., 2021). In *Ciona,* PNs (sometimes called Papilla Sensory Neurons or Primary Sensory Neurons of the Papillae) are found surrounding the three adhesive/sensory papillae at the very anterior end of the larva (Zeng et al., 2019). There are two dorsal papillae (one left, one right) and one medial ventral papilla (Figures 2A, B). Each papilla contains exactly 4 PNs, and additional cell types with proposed adhesive and/or sensory functions (Zeng et al., 2019; Johnson et al., 2023b). PNs are also found in species with complex eversible papillae (e.g., *Diplosoma* spp.) and even in those without overtly protrusive papillae, (e.g., *Molgula* spp) (Torrence and Cloney, 1982; Vorontsova et al., 1997). Larval metamorphosis in *Ciona* depends on mechanosensation, as larvae attach to a solid substrate to initiate tail regression and the transition to the post-metamorphic, sessile stage. Mechanical stimulation of the papillae were shown to be sufficient and necessary for triggering metamorphosis, while impairing PN development or function can block metamorphosis (Wakai et al., 2021; Sakamoto et al., 2022; Hoyer et al., 2024).

Like all epidermal neurons in the *Ciona* larva, PNs have apical cilia and axons. Their axons continue to extend posteriorly towards the larval brain during the swimming period, and these potentially late connections coincide with the competence period (Johnson et al., 2023b). Swimming larvae are not immediately competent to initiate tail regression and metamorphosis immediately after hatching, and competence to settle is acquired only after a few hours of swimming (Nakayama-Ishimura et al., 2009), presumably while PN axons are still growing. Unfortunately, the *Ciona* larva connectome was described in a relatively early larval specimen, and these later connections have not been documented at the synaptic level (Ryan et al., 2016). Little else is known about how PNs might regulate tail regression and metamorphosis downstream of mechanical stimulation. It is known that GnRH is important for tail regression, while GABA appears to regulate GnRH release and other processes in metamorphosis, such as body rotation (Hozumi et al., 2020). However, it is unclear where and how these neurotransmitters act, in the absence of PN synaptic connectivity data.

The PNs develop from an anterior neurogenic territory surrounding the central cells of the papillae that shows many similarities to the neurogenic midlines of the tail (Johnson et al., 2023b; Roure et al., 2023). This territory expresses *Ascl.a,* and later on Delta/Notch signaling limits the number of *Pou4*+ cells that will differentiate into PNs (Johnson et al., 2023b). The papilla territory in turn is specified by *Foxc* and *Foxg* orthologs (Horie et al., 2018; Liu and Satou, 2019), which suggests an evolutionary connection to anterior placodes of vertebrate embryos. However, the cells that give rise to PNs appear to downregulate *Foxg,* while sustained *Foxg* expression is associated with the more central papilla cell types, like the Axial Columnar Cells (ACCs) (Johnson et al., 2023b). Knocking out *Pou4* blocks PN differentiation and metamorphosis (Sakamoto et al., 2022; Johnson et al., 2023b). Similarly, using chemogenetics to inhibit PN function also inhibits metamorphosis (Hoyer et al., 2024). Candidate effectors of PN functions have also been knocked down/out, resulting in similar loss of metamorphosis. For instance, morpholino knockdown and TALEN-mediated knockout of a gene encoding the TRP channel family member PKD2 reduced the incidence of mechanically-induced Ca^{2+} transients in PNs and moderately inhibited metamorphosis (Sakamoto et al., 2022). Similarly, CRISPR/Cas9-mediated knockout of *Vamp1/2/3,* encoding synaptic vesicle protein Synaptobrevin, also modestly inhibited metamorphosis (Johnson et al., 2023a). However, the exact mechanotransduction channel in the PNs has yet to be identified. Based on Ca^{2+} imaging, PNs also respond to chemical cues, suggesting they may be polymodal sensory cells (Hoyer et al., 2024). Certain chemicals can promote or inhibit tunicate settlement and metamorphosis, suggesting that the larvae rely on both biotic and abiotic cues for optimal settlement site selection (Durante, 1991; Rae Flores and Faulkes, 2008; Hoyer et al., 2024). Interestingly, the ACCs at the very center of the papillae also respond to mechanical stimuli (Hoyer et al., 2024), which may reflect independent mechanosensory ability, or local communication between PNs and ACCs. In sum, although substantial work is still needed to better understand the development and function of the PNs, they represent a promising model for the study of tunicate mechanosensation thanks to the clear metamorphosis defects associated with their loss or perturbation.

2.4 Otolith and antenna cells

Most ascidian larvae have an otolith/statocyst, which is most frequently a single, rounded melanin-containing cell suspended in the lumen of the sensory vesicle (Torrence, 1986; Jiang et al., 2005) (Figures 2A–C). *Ciona* larvae exhibit strong geotactic behavior, preferring to settle on the dark underside of obstacles in the

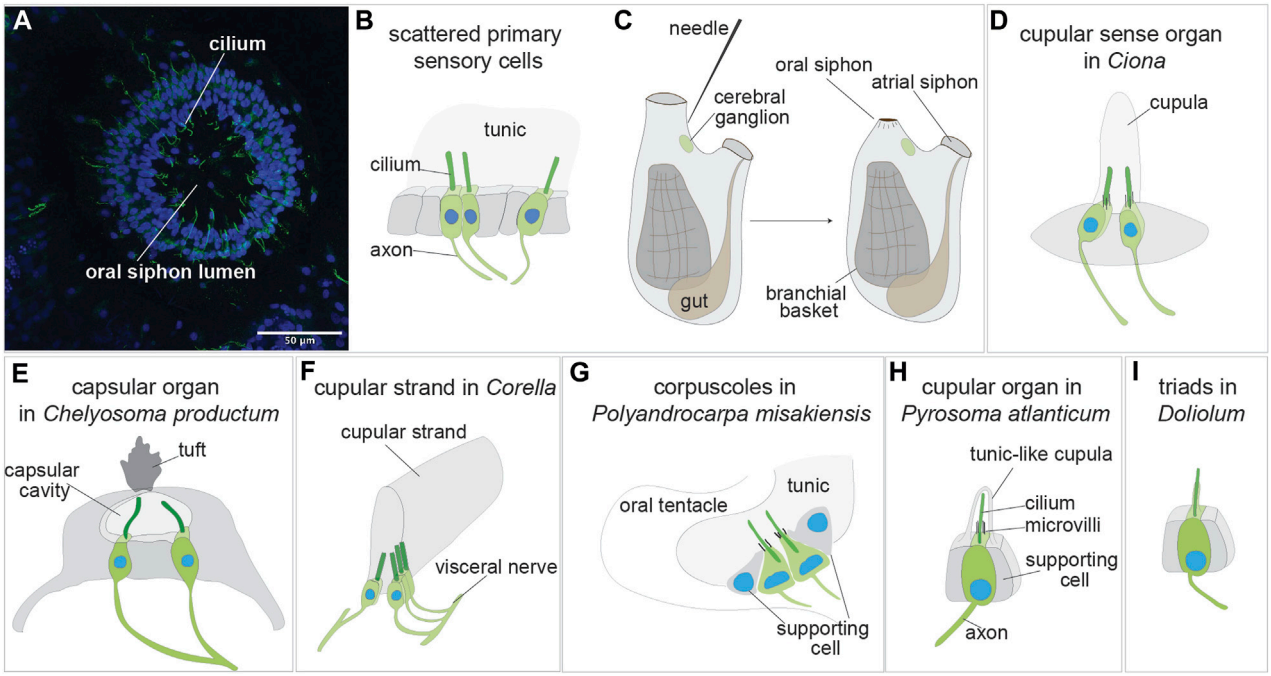

FIGURE 3
Sensory organs based on primary sensory cells in adult tunicate (see Caicci et al., 2013; Manni and Pennati, 2015; Anselmi et al., 2022). **(A)** Confocal imaging of the primary sensory cells stained with anti-alpha tubulin (green) labelling nerves and Hoechst (blue) in the oral siphon of *B. schlosseri*. **(B)** Scattered primary sensory cells.) **(C)** Illustration of the primary sensory cell stimulation in the "siphon stimulation test". **(D)** Cupular sense organ in *Ciona*. **(E)** Capsular organ in *Cheliosoma productum*. **(F)** Cupular strand in *Corella*. **(G)** Corpuscles in *Polyandrocarpa misakiensis*. **(H)** Cupular organ in *Pyrosoma atlanticum*. **(I)** Triads in *Doliolum nationalis*.

water (Jiang et al., 2005), such as floating docks and ship hulls. A light- and gravity-dependent circuit has been proposed for ensuring such behavior, as larvae will swim up (or position themselves upwards if facing down) when drifting under a shaded area (Bostwick et al., 2020). Key to this behavior are the Antenna Cells, a pair of neurons that make contact with the otolith and presumably detect its displacement in the sensory vesicle via mechanotransduction (Torrence, 1986; Sakurai et al., 2004). However, little is known about these neurons aside from their characterization by the connectome studies, in which they were shown to make extensive synapses onto a handful of relay neurons in the larval brain (Ryan et al., 2016). Therefore, their mechanosensory nature is by far the most speculative and poorly documented out of all the candidate mechanoreceptors of the tunicate larva. A variant of the typical larvae of some colonial species belonging to the taxon Styelidae have only one sensory organ, the photolith, which is thought to function in both gravity and light reception (Sorrentino et al., 2001). In *B. schlosseri*, it consists of a unicellular statocyst, formed by an expanded pigment cup, which receives extensions from six photoreceptor cells (Sorrentino et al., 2001).

3 Mechanosensation in adult tunicates

Mechanoreception in adult tunicates is well developed, relying on both primary sensory cells, which are either scattered, organized in small clusters, or in specific organs (Figure 3), and the secondary sensory cells of the coronal organ (as discussed in Section 3.3). However, information on primary sensory cells and/or organs containing primary sensory cells in adult tunicates is quite limited in comparison to that regarding the ascidian larva. In most cases only morphological data are available with occasional supplementation from the results obtained by neurophysiologists who worked in the field in the 70–90 s of the last century. Even though no developmental data are currently available for these primary sensory cells, developmental data is available for the oral siphons, a very sensitive region where many primary sensory cells are located. Specifically, the oral siphon primordium expresses anterior placode markers Pitx and Dlx, indicating that oral siphon primordia express genes shared with vertebrate placodes (Boorman and Shimeld, 2002; Irvine et al., 2007; Graham and Shimeld, 2013). The comparative morphology of the coronal organ has been deeply analyzed in several tunicate species and some aspects of its development and physiology have been studied in a select few ascidians.

3.1 Scattered or clustered primary mechanoreceptor cells in adult tunicates

Isolated primary cells (or small clusters of 2-3 primary sensory cells) have been described in the vicinity of the siphons, the most responsive regions of adult ascidian and thaliaean tunicates [reviewed in (Mackie and Burighel, 2005; Manni and Pennati, 2015)] (Figures 3A, B). These cells are peripheral neurons whose

somata are in the monolayered epidermis that both delimits the animal body and descends into the siphons. A long axon extends from the soma base to the central nervous system, whereas a dendrite, represented by a single cilium, projects apically. Since the epidermis is covered by the tunic, these intraepithelial sensory cells are not directly exposed to the external seawater. They react to stimuli through the tunic, which has a different thickness and elasticity depending on species and body region. In the ascidians *Corella inflata* and *Corella eumyota*, each siphon has approximately 8,000 primary sensory neurons that have been revealed by immunohistochemical labeling (Mackie et al., 2006). Physiological tests have shown that these cells are tactile and vibration sensors. In the same siphon region, rounded, axonless cells were also frequently seen, along with cells with very short axons; both have been suggested to be early stages in the formation of the sensory neurons. In the colonial ascidian *B. schlosseri*, the oral siphon primary sensory cells have been analyzed in relation to the blastogenetic cycle and to colony aging (Anselmi et al., 2022) (Figure 3B). The number of these mechanoreceptor cells varies along the cycle, increasing from early-to mid-cycle, before decreasing in late-cycle. This dynamic pattern parallels zooid sensitivity to stimuli, which is greatest when the number of mechanoreceptors is highest. Similarly, both the number of oral siphon primary sensory cells and zooid sensitivity to stimulation are higher in zooids belonging to young colonies than in those belonging to old colonies. In *B. schlosseri*, the ability of these mechanoreceptors to respond to stimuli has been detected using a sensitive behavioral test, the siphon stimulation test (Anselmi et al., 2022) (Figure 3C). This test assesses the ability of the oral siphon to close after stimulation with a waterjet whose pressure is controlled by a microinjector. The waterjet pressure is increased progressively, and the minimum pressure needed to induce a siphon contraction is recorded as a parameter indicating zooid sensitivity.

Primary ciliated sensory neurons, presumed mechanoreceptors, have also been reported in thaliaceans and appendicularians and were described using conventional light microscope staining techniques or Nomarski microscopy [reviewed in (Bone, 1998)]. Unfortunately, detailed morphological observations from transmission electron microscopy (TEM) are not available for these sensory cells. In *Pyrosoma*, those around the inhalant siphon were investigated experimentally, finding that their delicate touch evokes siphon contraction, whereas a stronger stimulation evokes a siphon contraction by branchial ciliary arrest (Mackie and Bone, 1978). In salps, sensory cells with a long cilium were also reported on the mouth lips, sometimes also organized in small groups. However, no detailed or physiological information is available on them (Bone, 1998).

3.2 Multicellular mechanoreceptor organs based on primary sensory cells in adult tunicates

A number of multicellular organs with putative mechanoreceptive function have been described morphologically in tunicates, both at light and electron microscopy [reviewed in (Bone, 1998; Mackie and Burighel, 2005; Caicci et al., 2013; Manni and Pennati, 2015)]. In some cases, their mechanoreceptive function has been determined by means of experimental studies; in other cases, it has been inferred on the basis of organ morphology and position. No data are available on their development. Among tunicates, ascidians have been more extensively studied than thaliaceans and larvaceans. The variety of multicellular organs, probably evolved from clusters of simple ciliated mechanoreceptors (Mackie and Singla, 2003), underlines the importance of mechanoreception and its behavioral integration.

The first organs to be described using scanning and transmission electron microscopy were the cupular sense organs (75–100 per individual) located in the atrial mantle epithelium of the adult ascidian *Ciona intestinalis* (Bone and Ryan, 1978) (Figure 3D). They are composed of groups of supporting cells flanking 15–20 ciliated neurons whose sensorial cilia are embedded in a gelatinous cupula, probably produced by the supporting cells. The cupula gives the name to the organs. These organs are able to detect near field vibrations as well as local water movements that displace the cupula and the cilia within it, resulting in electrical responses in the sensory cells. For their overall morphology and physiology, shared with the neuromasts of the lateral line organ and the hair cells of the vertebrate inner ear, the cupular sense organs were suggested by the authors to be evolutionarily linked to the vertebrate mechanosensory organs. From a cellular point of view, however, the cupular sense organs comprise primary sensory cells, whereas the vertebrate counterparts comprise secondary sensory cells, making the hypothesized homology inconsistent.

For many years the cupular sense organs were the only multicellular mechanoreceptor organs known in adult ascidians, until Mackie and Singla described in the atrial wall of the branchial sac of the solitary ascidian *Chelyosoma productum* the capsular organs at light and electron microscopy (Mackie and Singla, 2003) (Figure 3E). In the latter, the sensory cells are grouped in a macula and are characterized by a group of short microvilli surrounding a long cilium projecting into a small cavity (the “capsule”). The capsule cavity is delimited by supporting cells, is filled with a fluid and has an acellular diaphragm spanning an opening in the top. Each sensory cell has an axon reaching the brain via the visceral nerve, the nerve connecting the brain to the visceral organ (branchial sac, gut and heart). By means of electrophysiological recordings and tests aimed to determine their sensitivity, the authors concluded that these organs are vibrational-sensing and are adaptive in detecting the movements of objects in the vicinity.

The same authors described also in the genus *Corella* other organs based on primary sensory cells (Mackie and Singla, 2005). Using immunocytochemical analyses, they found in *C. eumyota* structures resembling the cupular sense organs of *C. intestinalis*, but located on the atrial surface of the branchial sac. Moreover, they recognized in *C. inflata*, using both immunocytochemistry and electron microscopy, a novel sense organ, the cupular strand (Figure 3F) which is a very elongated cupular organ located in the atrial surface of the branchial sac. Axons from the sensory cells enter the cerebral ganglion through the visceral nerve. Neither the cupular sense organs nor the cupular strand have been studied physiologically. However, by analogy with such structures in other metazoans, cupular organs were supposed to be hydrodynamic sensors registering local disturbances or changes in water flow through the atrial cavity.

A similar function was hypothesized for primary sensory cells of the colonial ascidian *Polyandrocarpa misakiensis* (Koyama, 2008). These cells form small corpuscles located in epidermal pockets filled with tunic at the base of the oral and atrial siphons and have been called "oral tentacular sensory cells" and "atrial tentacular sensory cells", respectively. The sensory cells, both isolated and forming small clusters, have axons joining a nearby nerve located at the base of the siphons (Figure 3G). Their apical apparatus is composed of a long, modified cilium projecting into the tunic, accompanied by a ring of microvilli of equal length. Supporting cells delimit the small cluster of sensory cells or are located between the isolated sensory cells. Some oral tentacular sensory cells are also found associated with neurosecretory cells.

Cupular sense organs have also been described in the thaliacean *Pyrosoma atlanticum* (Pyrosomatida), in a study aimed at describing at electron transmission microscopy the oral sensory structures of this tunicate (Caicci et al., 2013). The organs, previously mentioned by (Fedele, 1923), are scattered on the rounded flaps of the oral siphon and are composed of pyriform sensory cells accompanied by supporting cells (Figure 3H). The sensory cell apical plasmalemma exhibits a long cilium surrounded by 50–60 microvilli and is embedded in a tunic-like cupula secreted by supporting cells. An axon emerges from the sensory cell basal side. The organ function has not been investigated. However, displaying strong morphological resemblance with the ascidian cupular organs, it was supposed they play a similar mechanosensory role, probably in relation to reflex patterns involved in swimming control. Indeed, when the oral siphon is stimulated by touching, or by the collision of large particles or their entry into the gill, the animal responds by arresting ciliary beating and contracting the siphon (Bone and Ryan, 1978). It has been suggested that ascidian and thaliacean cupular organs are the result of evolutionary convergence (Caicci et al., 2013).

In the thaliacean *Doliolum nationalis* (Doliolida), triads of sensory cells, have been described in whole mount preparations (Bone, 1959) and by transmission electron microscopy (Caicci et al., 2013). These are a dozen groups of three sensory cells (supporting cells are not present) regularly arranged around the oral siphon, covered by the tunic. Each sensory cell has an apical long cilium projecting into the tunic and extends an axon from its base (Figure 3I). The triads are stimulated by the deformation of their apical cilia when water flows through the oral siphon as the animal swims (Bone, 1959). The oozooid stage of doliolids displays also an otocyst, but no detailed information is available on its morphology (Bone, 1998).

Apart from a statocyst containing a statolith, located on the left part of the Oikopleuridae brain, whose mechanosensory function has not been studied (Bone, 1998), no other multicellular mechanosensory organs based on primary sensory cells have been found in larvaceans. The ventral organ, a sensory structure below the mouth constituted of about 30 primary ciliated receptors, is considered a chemosensor (Bollner et al., 1986).

3.3 Secondary sensory cells in tunicates

The coronal organ has been found in all examined tunicates except salps (see paragraph 4.1) (Burighel et al., 2011; Caicci et al., 2013; Rigon et al., 2013). Positioned at the outer edge of the velum and the tentacles, at the base of the oral siphon, this organ comprises a continuous row of secondary sensory cells (Figure 4A). These cells are characterized by the presence of numerous stereovilli or microvilli and nonmotile cilia (a single cilium or multiple cilia) composed of 9 + 2 microtubules. The secondary sensory cells form a ring at the base of the oral siphon exposed to incoming water. Indeed, they function as mechanoreceptors involved in detecting variation in water flowing inside the oral siphon and possibly dangerous particles (Mackie et al., 2006).

Both afferent and efferent synapses are found between the base of coronal sensory cells and the peripheral axons of sensory neurons whose cell bodies lie on the brain (Burighel et al., 2003). The innervation pattern of the coronal organ has been studied through immunochemistry (Mackie et al., 2006; Gasparini et al., 2013a; Anselmi et al., 2022), and synaptic connectivity has been established using transmission electron microscopy (Burighel et al., 2003; Manni et al., 2004; 2006; Caicci et al., 2010b; Caicci et al., 2013) and *in situ* hybridization (ISH) experiments (Rigon et al., 2018). Each tentacle contains nerve fibers (from the subcoronal nerve) located at the base of the ciliated cells branching from the pericoronal nerve (Figures 4A, 5A, B), a nerve that encircles the oral siphon and originates from the anterior nerve brain. Synaptic contacts have been identified, using TEM, based on the presence of small presynaptic vesicles on one or both sides of the synaptic cleft and the characteristic thickening of the postsynaptic membrane. Frequently, sensory coronal cells make synapses with multiple neurites (Burighel et al., 2011). Glutamate (which mediates afferent hair cell inputs), acetylcholine, GABA and serotonin (which is involved in efferent stimulation to hair cells) are expressed in the coronal organ (Rigon et al., 2018).

The sensory cells are flanked on both sides by supporting cells and, in some species, by secretory cells. Typically, supporting cells extend apically a cytoplasmic crest delimiting the nearby sensory bundle (Figure 4A) and are connected to neighboring cells through tight junctions. There is no gap junction: signal transmission to the central nervous system is solely mediated by neurons located in the brain (Burighel et al., 2011). Secretory cells, when present, face towards the middle of the tentacles and do not form synapses with the nerve that contacts the sensory cells. Their function is not known, however the abundance of ER and the extended Golgi apparatus suggest that they are involved in protein synthesis. Their vicinity to the sensory cells suggests a secretory mechanism activated by the stimulation of the sensory cells (Manni et al., 2006). Sensory cells, supporting cells and, if present, secretory cells are all supported by a basal lamina that consists of a layer of fibers that merge and surround with the nerve fibers.

3.4 Variability of coronal sensory cells

The coronal organ exhibits a remarkable degree of diversity among the different tunicate species and even within the same species (Table 1). The diversity of the coronal organ is correlated to the variability of the apical structure and the presence or absence of secretory cells (Figure 4B). In Stolidobranch ascidians, three types of sensory cells have been identified based on the organization of their apical structure: a central cilium surrounded by microvilli (type 1),

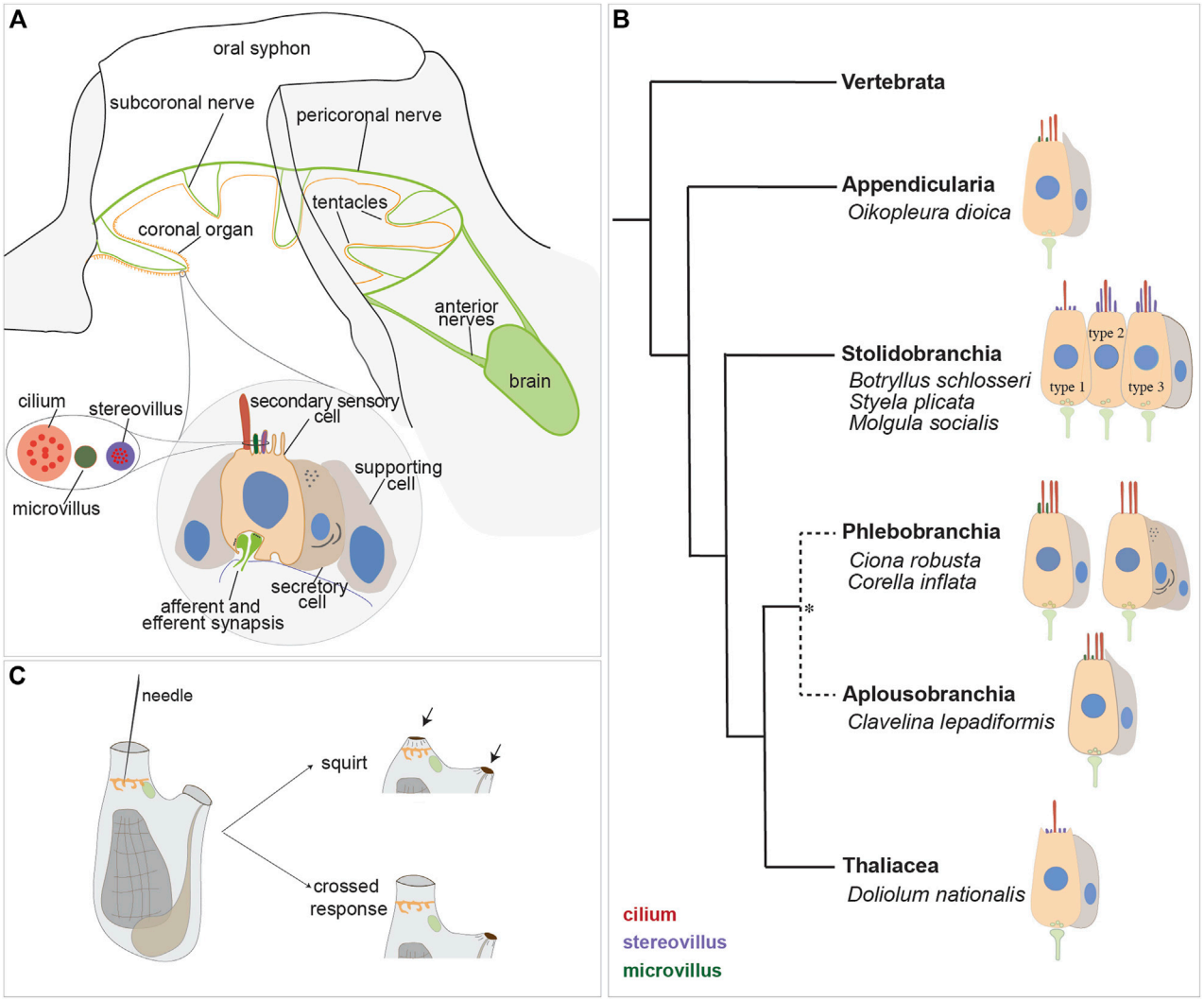

FIGURE 4
Secondary sensory cells in the adult tunicates. **(A)** Location and main features of the coronal organ in tunicates. The organ is composed of a continuous row of cells on the oral tentacles and the velum (orange). Each sensory cell makes synapses with the subcoronal nerves (two per tentacle, close to the coronal organ) that are branches of the pericoronal nerve (green). The latter is a mixed nerve, connected to the brain through the anterior nerves. Sensory cells (pink) are flanked by supporting cells (grey); in some enterogona species, also secretory cells (violet) can be recognised. Stereovilli are apical, finger-like, long structures, composed of parallel actin filaments connected to the cell cytoskeleton; microvilli are thinner than stereovilli, with less abundant actin microfilaments. **(B)** Comparative schematic illustration showing the coronal organ variability in some representatives of tunicate groups. Stolidobranchia ascidians display the greatest complexity in the sensory apical bundle, which can be composed of microvilli or stereovilli, the latter also graded in length. * The monophyly of Phlebobranchia is disputed [see (DeBiasse et al., 2020)]. **(C)** Responses obtained after a strong (upper) and a light (bottom) stimulation of the coronal cells. The latter response is detected in the "tentacle stimulation test".

two long cilia and graded-height stereovilli (type 2), a complete ring of stereovilli surrounding two cilia (type 3). Interestingly, some species like *Styela plicata* can exhibit both type 1 and type 2 sensory cells (Manni et al., 2004). *Molgula socialis* presents a particularly complex condition since displaying all three types of sensory cells with types 2 and 3 predominantly located towards the proximal side of tentacles where they are exposed to inflowing water, while type 1 is located more peripherally (Figures 5C–F). It is worth noting that in Stolidobranch ascidians, extracellular radial filaments connecting the cilia to the surrounding stereovilli have been described (Burighel et al., 2003; Caicci et al., 2010a), even though the precise mechanism of signal transduction is not yet fully understood. In Phlebobranchiata and Aplusobranchiata some species have short microvilli (*Ciona robusta*), while others lack them (*Phallusia mammillata*). Additionally, some species such as *Ascidiella aspersa* and *C. inflata* possess secretory cells. Secretory granules have been found not only in both type 2 and type 3 sensory cells of Pleurogona (Manni et al., 2004; Manni et al., 2006; Caicci et al., 2007) but also in some sensory cells of Enterogona species (Manni et al., 2006).

In larvaceans the ultrastructure of the coronal organ was studied in two species of *Oikopleura* (Rigon et al., 2013). These animals have a single type of secondary sensory cells with numerous cilia of the same length, microvilli in multiple lines. They are flanked by non-ciliated supporting cells forming a crest alongside the coronal organ. A recent study on the mesopelagic giant appendicularian

TABLE 1 Table summarizing the principal findings on the tunicate secondary sensory cells.

Taxon	Species	Location	Proposed function	Behavioural test	Hair bundles	Cytoplasm of sensory cell	Radial filament connecting the cilia	Supporting cells	Accessory secretory cells	References
Pleurogona stolidobranchia	Botryllus schlosseri	tentacles of oral siphon	Sensitivity to contact of inflowing particles	Tentacle stimulation test	Single cilium and stereovilli	Accessory centriole	Loose fibrillar matrix generally present among microvilli and cilia	Supporting cells form a wall or crest		Burighel et al. (2003)
	Botrylloides leachi, B. violaceus	tentacles of oral siphon	Sensitivity to contact of inflowing particles		Single cilium and stereovilli	Accessory centriole	Loose fibrillar matrix generally present among microvilli and cilia	Supporting cells form a wall or crest		Burighel et al. (2003), Burighel et al. (2008)
	Molgula socialis	tentacles of oral siphon	Sensitivity to contact of inflowing particles		Three types (type 1,2 and 3). Stereovilli	Electron dense granules, accessory centriole in sensory cells	Extracellular radial filaments connecting the cilium or cilia to the surrounding stereovilli	Supporting cells form a wall or crest		Caicci et al. (2007)
	Pyura stolonifera, P.haustor	tentacles of oral siphon	Sensitivity to contact of inflowing particles		A pair of cilia surrounded by a crescent ring of stereovilli graded in length	Accessory centriole in sensory cells, electron dense granules	Extracellular radial filaments connecting the cilium or cilia to the surrounding stereovilli	Supporting cells form a wall or crest		Caicci et al. (2010a)
	Styela plicata. S. montereyensis, S. gibsi	tentacles of oral siphon	Sensitivity to contact of inflowing particles		A pair of cilia surrounded by a crescent ring of stereovilli graded in length	Accessory centriole in sensory cells, electron dense granules	Extracellular radial filaments connecting the cilium or cilia to the surrounding stereovilli	Supporting cells form a wall or crest		Manni et al. (2004), Caicci et al. (2010a)
	Polyandrocarpa zorritensis	tentacles of oral siphon	Sensitivity to contact of inflowing particles		A pair of cilia surrounded by a crescent ring of stereovilli graded in length	Accessory centriole in sensory cells, electron dense granules	Extracellular radial filaments connecting the cilium or cilia to the surrounding stereovilli	Supporting cells form a wall or crest		Caicci et al. (2010a)
Enterogona aplousobranchia	Clavelina lepadiformis	tentacles of oral siphon	Sensitivity to contact of inflowing particles		More than two cilia of same length that constitute an oriented rows parallel to coronal organ; microvilli			Supporting cells form a wall or crest		Manni et al. (2006)
	Diplosoma listerianum	tentacles of oral siphon	Sensitivity to contact of inflowing particles		More than two cilia of same length that constitute an oriented rows parallel to coronal organ; microvilli			Supporting cells form a wall or crest		Manni et al. (2006)

(Continued on following page)

10.3389/fcell.2024.1359207

TABLE 1 (*Continued*) Table summarizing the principal findings on the tunicate secondary sensory cells.

Taxon	Species	Location	Proposed function	Behavioural test	Hair bundles	Cytoplasm of sensory cell	Radial filament connecting the cilia	Supporting cells	Accessory secretory cells	References
Enterogona phlebobranchia	Ciona robusta	tentacles of oral siphon	Sensitivity to contact of inflowing particles	Tentacle stimulation test	More than two cilia of same length that constitute an oriented rows parallel to coronal organ; microvilli	Accessory centriole in sensory cells				Mackie et al. (2006), Manni et al. (2006)
	Ascidiella aspersa	tentacles of oral siphon	Sensitivity to contact of inflowing particles		More than two cilia of same length that constitute an oriented rows parallel to coronal organ; microvilli				Accessory secretory cells	Mackie et al. (2006), Manni et al. (2006)
	Phallusia mammillata	tentacles of oral siphon	Sensitivity to contact of inflowing particles		More than two cilia of same length that constitute an oriented rows parallel to coronal organ, no microvilli/stereovilli	Electron dense granules in sensory cells				Mackie et al. (2006), Manni et al. (2006)
	Chelyosoma productum	tentacles of oral siphon	Sensitivity to contact of inflowing particles		More than two cilia of same length that constitute an oriented rows parallel to coronal organ; microvilli				Accessory secretory cells	Mackie et al. (2006), Manni et al. (2006)
	Corella inflata, C. willmeriana	tentacles of oral siphon	Sensitivity to contact of inflowing particles	Tentacle stimulation test	More than two cilia of same length that constitute an oriented rows parallel to coronal organ; no microvilli/stereovilli				Accessory secretory cells	Mackie et al. (2006), Manni et al. (2006)
Appendicularia	Okopleura dioica, O. albicans	lower lip and pharynx	Monitoring particle flow into pharynx		More than two cilia different in lengths and shorter toward the cell edges; microvilli			Supporting cells form a wall or crest		Bone, 1998; Rigon et al. (2013)
Thaliacea	Pyrosoma atlanticum	flaps and a single ventral tentacle	Sensitivity to contact of inflowing particles		Single cilium, stereovilli					Caicci et al. (2013)
	Doliolum nationalis	flaps	Sensitivity to contact of inflowing particles		Single cilium, stereovilli					Caicci et al. (2013)
Salpe	Thalia democratica	absent								Rigon et al. (2013)

10.3389/fcell.2024.1359207

Bathchordeaus stygius has revealed the presence of three pairs of oral sensory organs within the mouth cavity, hypothesized to be homologous to the coronal organ. Each of these organs is composed of sensory cells with an apical cilium, innervated by brain nerves and surrounded by non-ciliated epidermal cells that nearly cover the organ (Le et al., 2023). In addition to the coronal organ, appendicularians possess the so-called Langerhans cells, which are secondary mechanoreceptors located in the posterior of the "trunk" epidermis and connected with afferent neurites through gap junctions. When stimulated, Langerhans cells trigger the escape response of the animal (Bone and Ryan, 1978).

In thaliaceans, the coronal organ has been studied in *Pyrosoma atanticum* and *D. nationalis* (Caicci et al., 2013). These animals have a single type of secondary sensory cell possessing a cilium accompanied by microvilli. Instead of tentacles, at the base of the oral siphon thaliaceans have flaps (*D. nationalis*), or single ventral tentacles with dozens of flaps (*P. atlanticum*). Notably, the coronal organ is absent in *Thalia democratica*, a salp. This absence is likely a derived condition evolved in parallel with the different feeding system adopted by this group of animals. Indeed a cladistic analysis, performed using 19 morphological characters in 16 tunicates species, and a cephalochordate and three vertebrate species as outgroups, revealed that the putative ancestral coronal cell in tunicates was a simple monociliated cell, that successively differentiated into the current variety of oral mechanoreceptors in the various tunicate lineages. The evolutionary changes in sensory cells may correspond to different feeding strategies (Rigon et al., 2013).

3.5 Physiology of the coronal organ

Studies aimed to elucidate the function of the coronal organ have primarily focused on two species: the solitary ascidian *C. inflata* (Mackie et al., 2006) and more recently the colonial ascidian *B. schlosseri* (Manni et al., 2018; Anselmi et al., 2022; Thompson et al., 2022). Behavioral experiments aimed to manipulate water flow patterns and observe siphon closure responses demonstrated that the secondary sensory cells are mechanoreceptors (Mackie et al., 2006). In *C. inflata,* a pioneering study showed that stimulating the oral tentacles with a glass needle caused the atrial siphon to contract to less than half its resting diameter, with no change in the diameter of the oral siphon. This response was named "crossed response" (Figure 4C). Depending on the stimulus strength and duration, the degree of atrial siphon closure during the crossed response varied. While gentle stimulation of the inner surfaces of the siphon or oral tentacles elicited varying degrees of the crossed response, stronger stimulation induced "squirts", characterized by a robust, synchronous contraction of both siphons and adjacent regions of the body wall (Figure 4C). This was accompanied by arrest of the cilia activity in the branchial stigmata responsible for creating the water current. Notably, a single stimulation could evoke not just one but a series of contractions suggesting coordination through a pacemaker (Mackie et al., 2006). These responses were lost after tentacle amputation. Electrophysiological recordings on the oral siphon were conducted to measure the electrical activity of the secondary sensory cells when exposed to specific stimuli in order to understand how sensory cells are activated and transmit signals. The results confirmed that crossed responses and squirts are centrally mediated reflexes but local conduction pathways also exist and persist after brain removal (Mackie et al., 2006).

Further insights have emerged from a different type of behavioral experiment, the tentacle stimulation test, conducted in *B. schlosseri* to assess animal performance under different conditions (Manni et al., 2018; Anselmi et al., 2022). This test aims to record the minimum pressure applied to the tentacle required to trigger the crossed reflex. Controlled and quantifiable pressure was applied through a water jet flow directly to the tentacles. Results showed that stage of adult individuals, the age of the colonies, and their overall condition (*e.g.*, exposure to drug) significatively influence the zooids performance. Specifically, a higher threshold for response is observed in case of lower numbers of brain neurons, as in old colonies and zooids approaching their resorption, or in case of coronal organ impairment following drug treatment. In this regard, is it important to mention that the coronal sensory cells, like vertebrate hair cells, are damaged by gentamicin (an ototoxic drug) treatment resulting in a loss of coronal sensory cell continuity along the organ (Manni et al., 2018). This leads to a significant decrease in the percentage of responsive zooids to the tentacle stimulation test compared to the same colonies before treatment. Interestingly, fenofibrate has been found to have a strong protective effect on coronal sensory cells against the gentamicin-induced toxicity, similar to what occurs in vertebrate hair cells (Park et al., 2017; Manni et al., 2018).

Additionally, experiments involving stimulation of the oral siphon with ultrasound were conducted on three solitary ascidians. These experiments revealed that the coronal organ plays a role in perceiving ultrasounds, exhibiting a frequency-dependent behavioral response. Higher sensitivity was observed at the highest frequency tested (Varello et al., 2023).

3.6 Secondary sensory cell development

In tunicates, the coronal organ develops during embryogenesis from a thickened ectodermal epithelium known as the "anterior proto-placode". This tissue eventually gives rise to the oral siphon, tentacles and velum (Manni et al., 2004; Gasparini et al., 2013a; Manni et al., 2018). Importantly, the anterior proto-placode expresses homologues of some placodal genes (Patthey et al., 2014), (Figure 6).

The development of the coronal organ has been studied using TEM in *C. robusta* and *B. schlosseri* (Manni et al., 2004; Gasparini et al., 2013a). In *Ciona,* coronal cells become morphologically recognizable during the early juvenile stage when they appear as cells with short cilia and occasional microvilli. Over time, these cells progressively develop hair cell-like features, including microvilli containing actin and myosin, and associated with supporting cells. Importantly, the coronal organ continues to grow throughout the entire lifespan of the animal, parallel to the growth of the tentacles. Immunohistochemistry has revealed higher mitotic activity in the coronal organ of adults, with proliferating coronal sensory cells and supporting cells detected using Histone H3 antibody (Gasparini et al., 2013a). ISH has shown that orthologs of genes such as *Atoh1*, *Notch*, *Delta-like*, *HES,* and *Musashi* are expressed during the development of the coronal organ

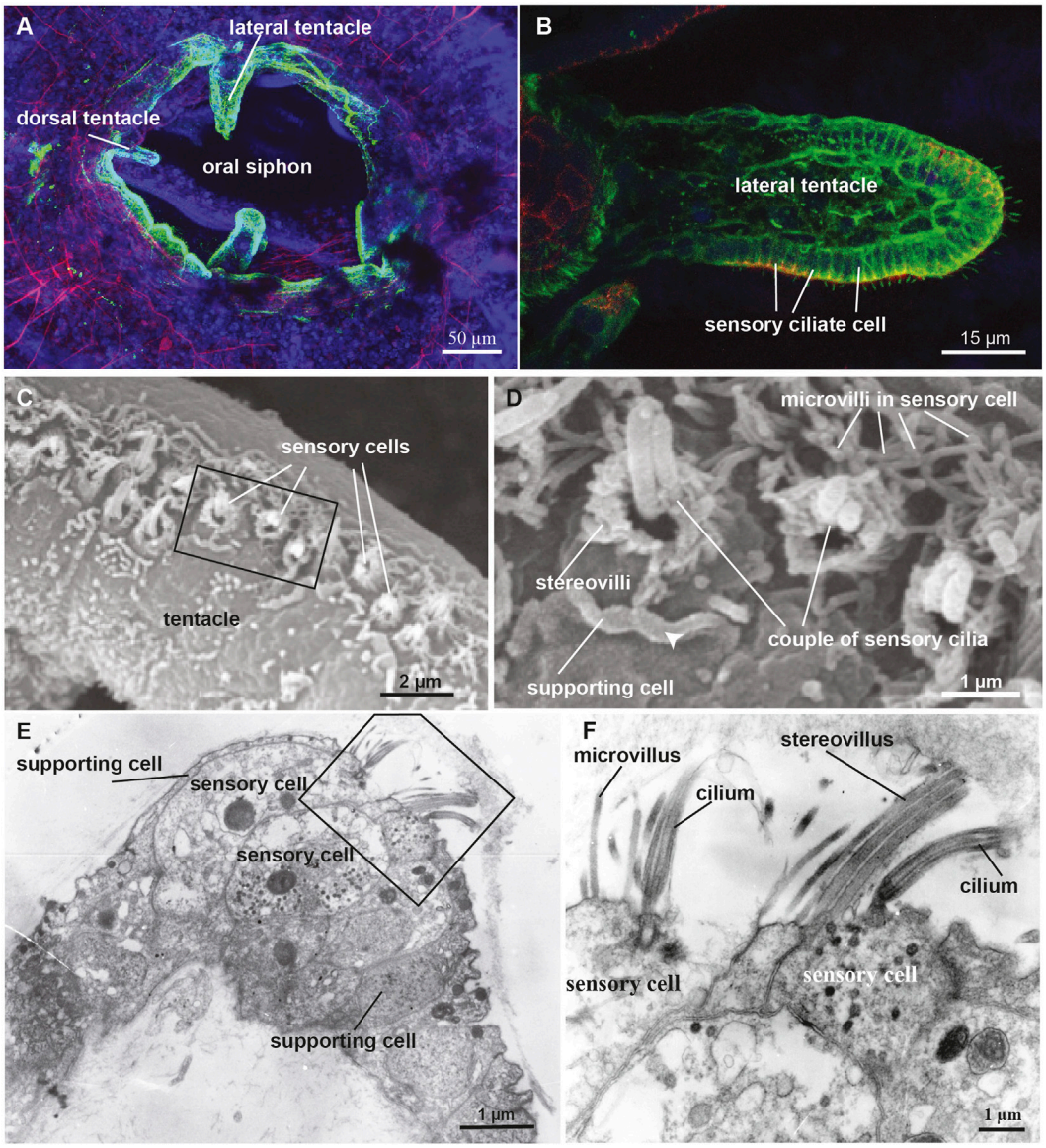

FIGURE 5
(A,B) Confocal pictures of the *B. schlosseri* oral siphon and tentacles stained with anti-alpha tubulin (green) labelling nerves, phalloidin (red) labelling cytoplasmatic actin and dapi (blue) labelling cell nuclei. **(C,D)** Scanning electron microscopy showing the coronal organ of *Molgula socialis*. Squared area in C is enlarged in D. The organ is composed of a row of 1-2 sensory cells (recognisable by their hair bundle) flanked by supporting cells characterized by an apical cytoplasmic crista (arrowhead). Two types of sensory cells can be recognised: with a couple of cilia surrounded by graded stereovilli (type 3), and with a single cilium surrounded by microvilli (type 1). **(E,F)** Transmission electron microscopy showing a transverse section of the coronal organ of *M. socialis*. Squared area in E is enlarged in F to show the different apical bundle structure: two sensory cells at left display microvilli (type 1), whereas the sensory cell at right possesses stereovilli (type 2 or 3).

(Rigon et al., 2018) mirroring gene expression patterns seen in vertebrate neural and hair cell differentiation (Fritzsch and Elliott, 2017).

The development of the coronal organ during asexual reproduction has been investigated *in B. schlosseri* (Manni et al., 2018). The coronal cells undergo cyclical development on a weekly basis becoming first recognizable in the buds during mid-cycle due to the differentiation of their apical bundle and basal synapses. Their definitive configuration is reached when their parents are in late-cycle which coincides with the degeneration of both the parent brain and sensory system.

4 Evolutionary relationships between vertebrate and invertebrate mechanoreceptor cells

In addition to primary mechanosensitive sensory neurons, vertebrates possess specialized secondary mechanosensory cells, including the hair cells of the inner ear and lateral line and Merkel cells of the skin. Vertebrate hair cells share several developmental, morphological, and functional similarities with tunicate primary and secondary mechanoreceptor cells. These similarities and differences are discussed below.

4.1 The development of vertebrate hair cells from cranial placodes

Towards the end of gastrulation, the vertebrate neural plate arises from the most dorsal population of embryonic ectoderm in response to a variety of organizing signals (Grocott et al., 2012; Groves and LaBonne, 2014; Thawani and Groves, 2020). The border between the developing neural plate and the future epidermis gives rise to two distinct multipotential lineages - neural crest cells and cranial placodes. The cranial placodes are ectodermal thickenings that give rise to (1) cranial sensory neurons of the trigeminal ganglia, (2) cranial sensory neurons of the epibranchial ganglia, (3) the otic placode which will form the entire inner ear including hair cells and sensory neurons, (4) the olfactory epithelium, (5) the lens of the eye, and (6) the anterior pituitary gland (Singh and Groves, 2016; Streit, 2018); (Figure 6A). In aquatic vertebrates, lateral line placodes will give rise to the hair cell-bearing neuromasts located along the head and trunk of the animal. The anterior and posterior lateral line neuromasts of teleosts, named for the direction in which their cells migrate, arise from a lateral line placode in the vicinity of the otic placode. Some aquatic species, like axolotls and paddlefish, have ampullary organs containing specialized electroreceptor cells that also arise from a lateral line placode (Baker et al., 2013; Modrell et al., 2017).

Cells destined to give rise to cranial placodes first express members of the AP2a and FoxI families, which distinguish non-neural ectoderm from the adjacent neural ectoderm (Ohyama and Groves, 2004; Grocott et al., 2012; Khatri et al., 2014; Pla and Monsoro-Burq, 2018); (Figure 6B). Some cells within this region then express both Six homeobox transcription factors and Eya co-regulators in what has been termed the pre-placodal domain (Streit, 2004; 2007; Sato et al., 2010). *Six1* is expressed throughout the pre-placodal domain, posterior placodes like the otic placode express *Eya1* and *Six4*, and anterior placodes like the olfactory placode express *Eya2* and *Six3* (Streit, 2004; 2018; Sato et al., 2010). Locally acting signals then divide this pre-placodal region into distinct placodal territories along its anterior-posterior axis. Members of the Pax gene family play an important role in this process: *Pax6*-expressing progenitors give rise to the olfactory and lens placodes, *Pax3*-expressing progenitors give rise to the trigeminal placode, and *Pax2/8*-expressing progenitors give rise to the otic placode and the epibranchial placodes (Baker and Bronner-Fraser, 2001); (Figure 6B).

Once the otic placode has formed, the tissue transforms by invagination into the otic vesicle or otocyst. The otocyst co-opts dorso-ventral and anterior-posterior signals used to pattern the central nervous system (Groves and Fekete, 2012; Wu and Kelley, 2012) to form a series of prosensory patches expressing the *Sox2* transcription factor (Raft and Groves, 2015). These prosensory patches will give rise to the auditory and vestibular epithelium containing hair cells and supporting cells. The surrounding non-sensory epithelium of the ear expresses the transcription factor *Lmx1a* and will give rise to structures such as the semicircular canals of the vestibular system (Gu et al., 2016; Żak and Daudet, 2021). Mutual antagonism between *Sox2* and *Lmx1a*, driven in part by Notch pathway signaling, leads to the correct positioning and distribution of the prosensory patches (Mann et al., 2017). Hair cells and supporting cells develop from each sensory patch through a process of Notch-mediated lateral inhibition. Differentiating hair cells express Notch ligands to suppress a hair cell fate in neighboring cells, which then differentiate as supporting cells (Basch et al., 2016; Brown and Groves, 2020). Below, we discuss evidence for conservation of these developmental events in the formation of coronal sensory cells in tunicates.

4.2 What elements of vertebrate placode development are shared in tunicates?

The presence of thickened, placode-like structures in tunicates was first suggested by a study of the neurohypophysial duct, which generates the neural gland rudiment and migratory cells that contribute to the cerebral ganglion (Manni et al., 2005; 2001; 1999). The discovery of secondary hair cell-like cells in the coronal organs of *Botryllus* and *Ciona* (Burighel et al., 2003; Manni et al., 2005) suggested they may also derive from placodal structures. Subsequent analyses identified four thickened placodal-like structures or "proto-placodes" in tunicate larvae: (1) the rostral proto-placode which will form the larval adhesive organ and its associated sensory neurons, and the adult stolon (Section 2.4), (2) the stomodeal proto-placode that will give rise to the oral siphon including the coronal organ, (3) the afore-mentioned neurohypophysial proto-placode, and (4) the atrial proto-placode which will form the atrial siphon and atrial chamber wall, containing primary mechanosensory cells of the cupular organs (Manni et al., 2004; Gasparini et al., 2013b); (Figure 6A). Subsequent studies analyzed the expression of vertebrate placodal patterning gene orthologues in the developing tunicate proto-placodes at the embryonic, larval, and juvenile stages of *Ciona* and *Botryllus* (Mazet and Shimeld, 2005; Gasparini et al., 2013b). The *Ciona* orthologs of *AP2a* and *Sox2/3*, *Tfap2-r.b* and *Sox1/2/3*, respectively promoted epidermal and neural fate of ectoderm cells (Imai et al., 2017). Members of the Six and Eya families were expressed in both the anterior (stomodeal/neurohypophysial) and posterior (atrial) proto-placodes, with *Six1/2* marking both structure placodes and *Six3/6* being confined to the anterior proto-placode. Tunicate *FoxI* orthologues were expressed in the posterior atrial proto-placode (Mazet and Shimeld, 2005; Gasparini et al., 2013b); (Figure 6B).

Based on these studies of two evolutionarily distant tunicate species, it has been proposed that the tunicate anterior proto-placodes resemble the vertebrate olfactory/lens/hypophyseal placodes, and the tunicate posterior proto-placode resembles the vertebrate otic/epibranchial/lateral line placodes (Gasparini et al., 2013b). However, in vertebrates only the *posterior* otic and lateral line placodes produce hair cells (Groves and LaBonne, 2014; Piotrowski and Baker, 2014), whereas in tunicates coronal sensory cells that most closely resemble vertebrate hair cells are derived from the *anterior* proto-placode. Only the primary mechanosensory cells of the cupular organs are derived from the posterior placode (Gasparini et al., 2013b). Since Six and Eya genes are initially expressed throughout the vertebrate pre-placodal domain (Streit, 2007; Schlosser, 2014), it is likely that additional transcription factor combinations are required to divide this domain more precisely into individual placodes, or that individual placodes are specified at different times. In this regard, it is interesting to note that vertebrate Foxi1/3 genes are initially expressed throughout the

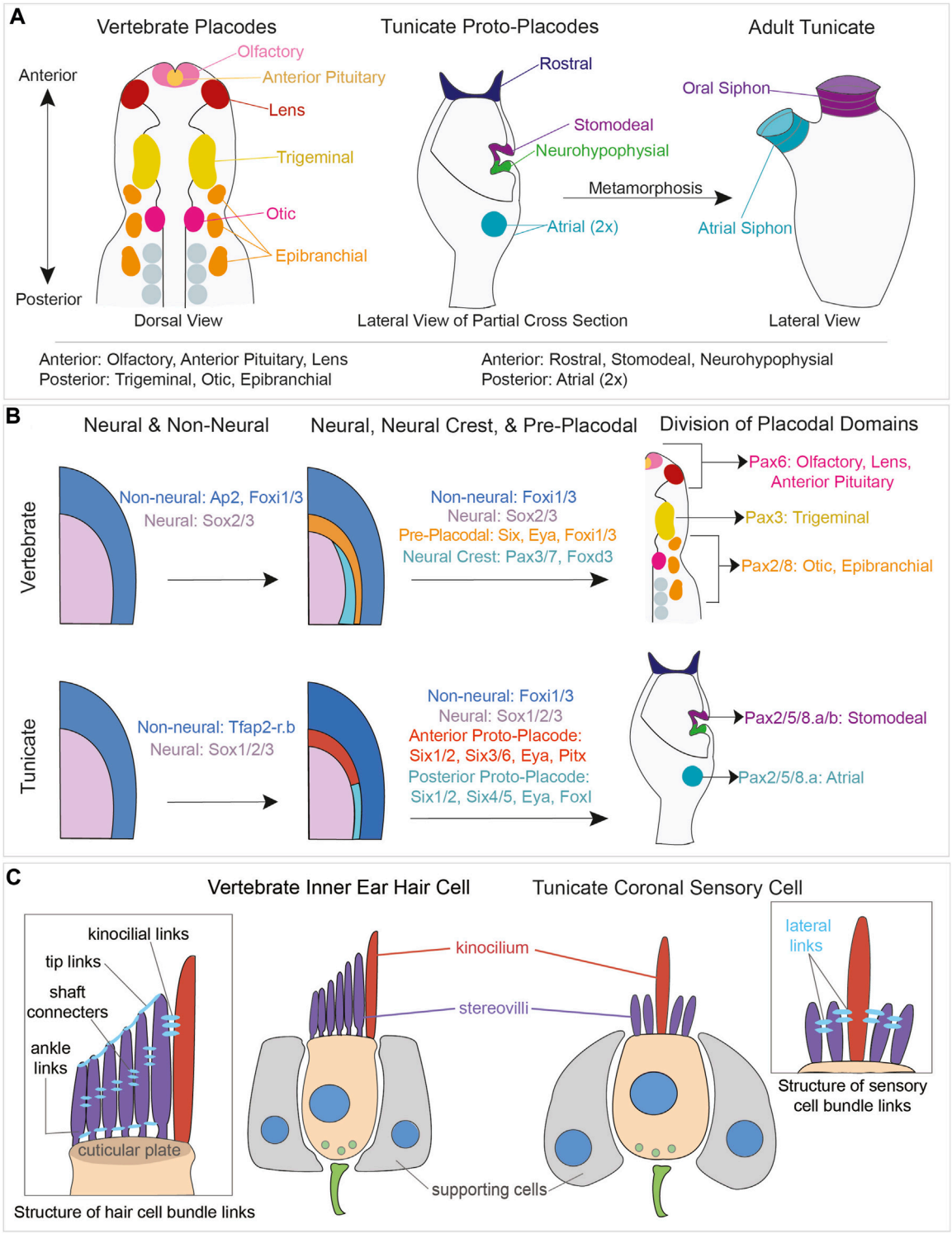

FIGURE 6
Comparison of vertebrate placodal and tunicate proto-placodal development and vertebrate hair cell and tunicate coronal sensory cell structures. **(A)** Schematic of vertebrate placodes compared to tunicate proto-placodes. The anterior placodes include the olfactory, anterior pituitary, and lens placodes. The posterior placodes include the trigeminal, epibranchial, and otic placodes. Tunicates have three anterior proto-placodes:, the rostral, stomodeal, and neurohypophysial placodes. Tunicates have two posterior atrial proto-placodes. Following metamorphosis, the stomodeal proto-placode will give rise to the oral siphon and the atrial proto-placodes will fuse to form the atrial siphon. **(B)** Conservation of genes expressed during vertebrate placodal and tunicate proto-placodal development. Several key genes involved in placode development appear to be conserved. **(C)** Comparison of hair cells from vertebrates and coronal sensory cells from tunicates. Vertebrate hHair cells (tan) are flanked by supporting cells (gray). Sensory cells possess kinocilium (red) and stereovili (purple) that are connected together by different links.

pre-placodal domain, at a time when all parts of the pre-placodal domain are competent to generate the otic placode (Solomon et al., 2003a; 2003b; Ohyama and Groves, 2004; Birol et al., 2016) and are gradually downregulated in an anterior-posterior direction (Khatri et al., 2014; Birol et al., 2016). However, Foxi1/3 appear to be required for the development of only the posterior otic, epibranchial and lateral line placodes in vertebrates (Solomon et al., 2003a; Hans et al., 2004; Birol et al., 2016). Rigon and others (Rigon et al., 2018) speculated that the common ancestor of vertebrates and tunicates may have generated mechanosensory cells from both anterior and posterior placode-like structures, with the ability to generate such cells being lost from the anterior placodes in vertebrates and from the posterior ptoto-placodes in tunicates. One possible explanation for this difference is that the evolution of the tunic covering the exterior surface of the animal placed constraints on where mechanosensory cells could function, restricting them to oral structures on the interior of the body that do not have a tunic covering (Manni et al., 2006).

It should be stressed that the putative homology between a Foxi1/3 and Pax2/8-expressing atrial primordium and the vertebrate "otic-epibranchial progenitor domain" is still far from settled (Graham and Shimeld, 2013; Patthey et al., 2014). A n alternative explanation for this paradox is that the posterior region of the tunicate larval head that expresses Six and FoxI genes does not give rise to sensory structures at all. Vertebrate Six and Foxi1/3 genes are also expressed in the developing pharyngeal arch region of vertebrates at a slightly later stage than their expression in the pre-placodal domain (Ohyama and Groves, 2004; Khatri and Groves, 2013; Edlund et al., 2014; Birol et al., 2016; Ankamreddy et al., 2023), and they are required for correct formation of the pharyngeal arch structures (Solomon et al., 2003a; Nissen et al., 2003; Edlund et al., 2014). Interestingly, FoxI and Six orthologues are also expressed in the branchial fissures (stigmata) of the tunicate atrium where peribranchial and branchial epithelium contact each other and fuse (Gasparini et al., 2013b). This expression pattern is reminiscent of the requirement for Foxi1/3 in the vertebrate pharyngeal pouches and clefts that form by fusion of pharyngeal ectoderm and endoderm (Edlund et al., 2014; Hasten and Morrow, 2019). Thus, while Six and FoxI genes mark the posterior atrial proto-placode in both *Ciona* and *Botryllus*, it is possible that these genes are acting to regulate formation of the atrium itself, rather than the cupular mechanosensory cells in the atrial walls. It may be possible to test the function of tunicate Six and FoxI orthologues by CRISPR-based loss-of-function studies to determine if they are necessary for the formation of primary cupular mechanosensory cells in the atrium or only for the formation of the branchial fissures.

As discussed above, vertebrate placodes acquire their unique identity by expression of different Pax family genes. *Ciona* has six Pax family genes, and, although several are expressed in regions of the larval central nervous system, most do not appear to be expressed in any of the proposed proto-placode structures identified in tunicate larvae (Mazet et al., 2003; Imai et al., 2004; Hudson and Yasuo, 2005). Of the Pax genes in *Ciona*, *Pax2/5/8.a* is expressed in the larval atria and stomodeum cavities, and *Pax2/5/8.b* is expressed weakly in the invaginating stomodeum (Mazet et al., 2003; Mazet and Shimeld, 2005). It remains an open question whether any other Pax genes play a role in the formation or patterning of other placode-like structures in tunicates. For example, *Pax6* gene family members are well known to regulate eye development across most animal phyla (Kozmik, 2008). In vertebrates, *Pax6* has also been co-opted to regulate the formation of the lens through its expression in the lens placode (Cvekl and Ashery-Padan, 2014). Ciona *Pax6* is expressed in parts of the brain associated with the photoreceptive ocellus and has the three "lens" cells lying above the ocellus, although they are not believed to be homologous to vertebrate lens cells. These "lens" cells do not express *Pax6*, nor do they express beta-crystallin (Shimeld et al., 2005). Moreover, vertebrate *Pax6* genes have a lens-specific enhancer that is not present in tunicates (Irvine et al., 2008), suggesting that the co-option of *Pax6* to regulate development of a lens structure occurred after vertebrates and tunicates diverged. Clarification of the role of other Pax genes in tunicate placode derivatives will require more sensitive tools to localize their transcripts, such as single cell RNA-seq and *in situ* hybridization, and to test gene function using loss of function approaches such as CRISPR-Cas9.

4.3 What elements of vertebrate hair cell development are shared in tunicates?

As described above, vertebrate inner ear and lateral line hair cells develop from patches of prosensory tissue marked by *Sox2*, a member of the SoxB transcription family (Neves et al., 2013). SoxC family members, such as *Sox4* and *Sox11* then act within these patches to provide competence for differentiation of hair cells and supporting cells (Gnedeva and Hudspeth, 2015; Wang et al., 2023). Cells within this expression domain upregulate the proneural transcription factor *Atoh1*, which initially marks the progenitors of both hair cells and supporting cells (Yang et al., 2010; Li et al., 2022). ATOH1, which is both necessary and sufficient for hair cell fate, is quickly restricted to differentiating hair cells through Notch-mediated lateral inhibition (Jarman and Groves, 2013; Cai and Groves, 2015). ATOH1 regulates other transcription factors, such as GFI1 and POU4F3, to establish a hair cell gene regulatory network (Iyer and Groves, 2021; Iyer and Groves, 2021). GFI1 can act with ATOH1 to positively promote the expression of hair cell genes and can also act alone to inhibit expression of neuronal genes (Jen et al., 2022; Jen et al., 2022). Since ATOH1 is also responsible for the differentiation of neurons in the cerebellum, brainstem, and spinal cord (Ben-Arie et al., 1997; Lai et al., 2011; Wu et al., 2023), it is possible that secondary mechanosensory receptor cells co-opted *Gfi1* to repress neuronal gene networks during evolution. POU4F3 also promotes hair cell differentiation by acting as a feed-forward pioneer factor: it is first induced by ATOH1 and then binds to many other ATOH1 target genes to make them transcriptionally accessible (Yu et al., 2021). The combined action of ATOH1, GFI1, and POU4F3 promotes a hair cell fate, and these transcription factors are also capable of reprogramming embryonic stem cells, fibroblasts, or non-sensory cells of the ear to a hair cell fate (Costa et al., 2015; Menendez et al., 2020; Iyer et al., 2022).

Several lines of evidence suggest that these three transcription factors have an evolutionarily conserved role in the differentiation of mechanosensory cells. *Drosophila* orthologues of *Atoh1*, *Gfi1,* and *Pou4f3* (*atonal*, *senseless* and *acj6* respectively) are expressed in

developing chordotonal organs that have mechanosensory functions in proprioception, hearing, and balance (Jarman et al., 1993; 1995; Nolo et al., 2000; Lee and Salvaterra, 2002). Significantly, *Atoh1* and *Gfi1* can functionally replace *atonal* and *senseless* in *Drosophila,* and *atonal* can functionally replace *Atoh1* in mice (Ben-Arie et al., 2000; Wang et al., 2002; Acar et al., 2006). Orthologues of *Atoh1*, *Gfi1* and *Pou4f3* have also been identified in *Caenorhabditis elegans* (*Atonh1/lin-32, Gfi1/pag-3,* and *Pou4/unc-86*) and are necessary for the formation of AVM/PVM mechanosensory neurons (Baumeister et al., 1996; Zhao et al., 2020). A Class IV POU gene orthologue has also been shown to be necessary for the development of cnidarian (sea anemone) hair cell-like cells, although it is not known whether *atonal*-like factors regulate this gene in sea anemones (Ozment et al., 2021). Finally, *Atoh1*, *Gfi1,* and *Pou4f3* are all expressed in the touch-sensitive Merkel cells of the skin (Lumpkin et al., 2003; Haeberle et al., 2004; Yu et al., 2021), and *Atoh1* and *Pou4f3* are both necessary for the differentiation of these cells (Maricich et al., 2009; Yu et al., 2021). Significantly, the inductive and pioneer feed-forward relationship between *Atoh1* and *Pou4f3* seen in hair cells is also conserved in Merkel cells, even though they regulate overlapping but distinct sets of genes in these two different mechanosensory cell types (Yu et al., 2021).

It is interesting to speculate on what gene networks are regulated by *Atoh1*, *Gfi1,* and *Pou4f3* orthologues in the different kinds of mechanosensory cells described in the previous paragraph. In a very simplified view, a mechanosensory cell requires (1) membrane specializations to detect mechanical force (such as vertebrate stereovilli or arthropod ciliated dendrites); (2) membrane components to develop a receptor or axon potential; (3) a synaptic apparatus to allow propagation of the mechanosensory stimulus to downstream neurons. These functional modules are created by gene networks expressed during development and then homeostasis. When comparing the molecular identity of cell types, it is important to functionally contextualize homologous genes across species. For example, gene networks regulating synaptic specializations are likely to be more highly conserved between different mechanosensory cells compared to networks regulating the more varied types of force-detecting machinery in these different cell types. Supporting this idea, a recent study comparing vertebrate hair cells and Merkel cells found that genes directly regulated by ATOH1 and POU4F3 in both cell types tended to be associated with synapses, cation channels and potassium channels (Yu et al., 2021). While some modules expressed by an ancestral mechanosensitive cell type may have been conserved, it is also possible that comparable modules were convergently evolved. At present, we have little information on how the development of tunicate mechanosensory cells is regulated. There is currently no evidence that the coronal sensory cellscells and supporting cells of the coronal organ derive from a *SoxB/SoxC*-expressing domain analogous to the prosensory patches of vertebrates. *Atonal* and *Pou4* orthologues are present in *Ciona* and are expressed in larval ciliated epidermal sensory neurons; in these cells *CiAtonal* has been reported to be epistatic to *CiPouf4* (Tang et al., 2013). The coronal organs of *Ciona* express an *Atonal* orthologue, as well as members of the Notch pathway (Rigon et al., 2018), but these genes have yet to be definitively localized to coronal sensory cells or supporting cells. With the advent of molecular techniques such as single cell RNA-seq and CUT&RUN/CUT&Tag, it will become feasible to identify gene networks expressed in mechanosensory cells of different species and to identify the direct targets of transcription factors such as ATOH1, GFI1, and POU4F3 within these networks.

As discussed above, the development of tunicate coronal organ sensory cells from the anterior, stomodeal proto-placode differs from that of hair cells of the vertebrate inner ear and lateral line, which develop from posterior (otic and lateral line) placodes. Although evolutionary scenarios have been proposed to account for this difference (Rigon et al., 2018), the limited data on expression of downstream placodal and prosensory genes in tunicates makes it hard to define the pathways by which coronal sensory cells form in the developing coronal organ. Indeed, it is possible that expression of *Atonal* orthologues in the coronal organ epithelium is sufficient to generate coronal sensory cells and supporting cells without the need to pass through a pre-placodal, placodal or prosensory state. In support of this idea, the chordotonal organs of *Drosophila* are generated by upregulation of *atonal* in embryonic ectoderm to form sensory organ precursors, and over-expression of *atonal* or *Atoh1* is sufficient to generate ectopic chordotonal organs in embryonic ectoderm (Jarman et al., 1993; 1995; Ben-Arie et al., 2000). Merkel cells of the vertebrate skin are generated directly from keratin-expressing epidermis without passing through a *Sox2*+ prosensory phase; here SOX2 appears to control the maturation of Merkel cells, rather than their specification (Lesko et al., 2013; Perdigoto et al., 2014). Finally, activation of *Atoh1*, *Gfi1,* and *Pou4f3* in primary mouse fibroblasts is sufficient to induce many aspects of the hair cell gene regulatory network without prior activation of *SoxB* or *SoxC* factors (Menendez et al., 2020). Localization of *Atoh1* and *Sox2/SoxB* orthologues in developing and mature coronal organ tentacles may help to address some of these questions and to more accurately identify the stages of differentiation of these cells.

4.4 What elements of vertebrate hair cell regeneration are shared in tunicates?

Many vertebrate inner ear and lateral line hair cells undergo gradual turnover and replacement in mature animals, and non-mammalian vertebrates can also robustly regenerate new hair cells after the endogenous hair cells are killed (Stone and Cotanche, 2007; Kniss et al., 2016). In non-mammalian vertebrates, new hair cells are generated by the upregulation of *Atoh1* in supporting cells, which then trans-differentiate to a hair cell fate (Stone and Cotanche, 2007). This can occur with or without supporting cell division, but ultimately leads to full replacement of hair cells and functional recovery. The one exception to this is mammals, where the cochlea is unable to regenerate new hair cells after the onset of hearing and the vestibular system is capable of only a modest amount of turnover and regeneration (Groves, 2010; Bucks et al., 2017). Given the ability of other vertebrates to regenerate hair cells, it is possible that with the ancestral form that gave rise to hair cells also had the capacity to regenerate. If tunicate coronal sensory cells and vertebrate hair cells have a shared evolutionary origin, do tunicate coronal sensory cells regenerate? As adult tunicates mature, the tentacles of the oral siphon continue to grow, implying that there must be some post-metamorphic mechanism to generate new coronal sensory cells and supporting cells. Transmission electron microscopy has revealed rare instances of apparently dividing sensory cells in *Pyura haustor*

(Caicci et al., 2007), and analysis of mitosis by PH3 staining in the coronal organs of adult and juvenile *C. intestinalis* indicates that both supporting cells and coronal sensory cells are capable of creating new coronal sensory cells (Gasparini et al., 2013a). Recent work suggests that exposure of tunicate coronal sensory cells to the ototoxic aminoglycoside gentamicin leads to an apparent loss of some sensory cells from the tentacles and impairs responsiveness of the coronal organ tentacles to touch (Manni et al., 2018). However, it is not known whether coronal sensory cells can be regenerated after such damage, nor whether any new coronal sensory cells are generated by neighboring supporting cells. Further studies are required to explore the potential for tunicate coronal sensory cell regeneration, and whether genes associated with hair cell regeneration in vertebrates like *Atoh1* play a role in this process.

4.5 A consideration of mechanotransduction in vertebrate hair sells and tunicate coronal sensory cells

Vertebrate hair cells are exquisitely sensitive mechanoreceptors; the human ear can detect sounds that vibrate the eardrum by one picometer. Hair cells have a hair bundle protruding from their apical surface consisting of a graded, stair-case-like array of long modified microvilli termed stereocilia or stereovilli (Vélez-Ortega and Frolenkov, 2019); (Figure 6C). Vertebrate hair cells develop with a single true cilium or kinocilium that migrates to an eccentric position on one side of the apical surface of the hair cell as the hair bundle develops (Frolenkov et al., 2004). The kinocilium persists in most mature vertebrate hair cells but degenerates in mammalian cochlear hair cells prior to the onset of hearing (Wang and Zhou, 2021). The apical tips of all but the longest stereovilli are joined to the next tallest stereovillus by a tip link consisting of a heterodimer of a protocadherin, PCDH15, and a cadherin, CDH23 (Vollrath et al., 2007). A mechanotransduction complex (Qiu and Müller, 2018; Holt et al., 2021), is present in all but the tallest stereovilli and this complex consists of pore-forming cation channels, TMC1 and/or TMC2, and two other membrane proteins, TMIE and TMHS/LHFPL5 which help modulate the pore properties of the channel [TMIE; (Zhao et al., 2014; Cunningham et al., 2020)] and bind to PCDH15 [TMHS; (Xiong et al., 2012; Zhao et al., 2014; Ge et al., 2018)]. Loss of any of these proteins compromises hair cell function and causes severe hearing loss. Deflection of the hair bundle applies force to each tip link, leading to an extremely fast (~10 μs) gating of the mechanotransduction channel (Gillespie and Müller, 2009). An array of accessory proteins (such as MYOSIN7A, harmonin, and sans) inside the stereovilli anchors the mechanotransduction complex to the actin core of each stereovillus (Schwander et al., 2010), and mutations in these proteins, or in CDH23 or PCDH15, lead to hereditary deaf-blindness known as Usher syndrome (Cosgrove and Zallocchi, 2014; Whatley et al., 2020). In addition, a second mechanosensitive ion channel, PIEZO2, lies at the base of the hair bundle and is responsible for what have been termed reverse-polarity currents (Beurg and Fettiplace, 2017; Wu et al., 2017), although precise function of PIEZO2 in hair cell mechanotransduction and bundle integrity is still unclear (Qiu and Müller, 2018).

As discussed in Section 3.4, the coronal sensory cells of tunicates show a far greater degree of diversity in different taxa than those of vertebrates (Manni et al., 2006; Caicci et al., 2010a; Rigon et al., 2013). This diversity is seen in the number of cilia, which can vary from just one or two in some groups, to multiple cilia that can be present in single or multiple rows (Table 1; Figure 4B; Figure 6C). The cilia can be located centrally or eccentrically as in vertebrates. Short microvilli can be present or can be elongated to appear more like stereovilli. In most tunicate taxa the stereovilli are of the same length, but in some groups the stereovilli have a more graded morphology reminiscent of a vertebrate hair bundle. Multiple different morphologies of sensory cells can occur in the coronal organs of some taxa, again reminiscent of the different hair cell types seen in vertebrate sensory organs, such as inner and outer hair cells of the mammalian cochlea, type I or type II vestibular hair cells, or the tall and short hair cells of the bird hearing organ, the basilar papilla. Unlike vertebrates, tunicate sensory cells do not appear to have clear tip links connecting their stereovilli, but some taxa show evidence of lateral connections between stereovilli, or between stereovilli and cilia (Burighel et al., 2003; Caicci et al., 2007; Rigon et al., 2013); (Table 1). Such links have some resemblance to the side links, ankle links, shaft connectors and top connectors that are present between stereovilli and between stereovilli and the kinocilium (Richardson and Petit, 2019).

What types of stimulus gate tunicate sensory cells? As discussed in Section 3.5 above, gentle stimulation of the oral tentacles by direct touch, vibration, or electrical shocks can lead to contractions of the atrial and oral siphons known as the crossed response, with stronger stimuli evoking a squirt response caused by strong contractions of both siphons and the body wall (Mackie et al., 2006; Manni et al., 2018). Similar responses can be evoked by particulate matter such as polystyrene beads or ground vegetable matter (Mackie et al., 2006), suggesting that at least one function of the coronal organ is to mediate particle expulsion in response to direct mechanical stimulation. This does not preclude other functions for sensory cells; in this regard it is intriguing that the bundle morphology of some tunicate sensory cells resembles that of electroreceptors seen in many fish and some amphibians (Baker, 2019). Elucidating the types of stimuli that tunicate coronal sensory cells respond to requires more electrophysiology studies such as whole-cell voltage clamp recordings from sensory cells or using fluid jet stimulation to evoke and measure mechanotransduction currents. Additionally, CRISPR may be used to create transgenic tunicates expressing a membrane-localized calcium sensor to detect mechanotransduction and presynaptic activity in hair cells.

It is currently unknown how coronal sensory cells respond to mechanical force, nor the range of forces that can evoke synaptic release. The wide variety of tunicate sensory bundle types, together with the absence of apical tip links in coronal sensory cells suggests it is unlikely that CDH23/PCDH15-mediated gating of a mechanotransduction channel of the sort seen in vertebrates is occurring in tunicates. However, the presence of side links between stereovilli and between stereovilli and cilia suggest an alternative method of mechanoreceptor gating. Indeed, such kinociliary links have been shown to mediate mechanotransduction in developing zebrafish hair cells before being replaced by stereovilli-based mechanotransduction in mature hair cells (Kindt et al., 2012). Insect chordotonal organs

facilitate mechanotransduction with members of the TrpN and TrpV channel family (Li et al., 2018). Although vertebrate hair cells seem to use TMC and PIEZO2 channels for mechanotransduction (see above), TrpN channels may also be required for mechanosensation in some cases (Sidi et al., 2003). The TRPA1 channel was originally proposed as candidates for the vertebrate mechanotransduction channel (Corey et al., 2004), but data from knockout mice suggests that neither TRPA1 nor 32 other Trp channels are necessary for mechanotransduction in mouse hair cells (Kwan et al., 2006; Wu et al., 2016). A Ciona orthologue of *TrpA1* is expressed in coronal sensory cells (Rigon et al., 2018), but its role in mechanotransduction has yet to be tested. PIEZO2 is another possible candidate for the tunicate mechanotransduction channel; it is located at the base of the hair bundle in vertebrate hair cells (Wu et al., 2017) and therefore does not require tip-link based mechanotransduction. PIEZO2 also mediates Merkel cell mechanotransduction without the need for elaborate stereovilli or tip link-based machinery (Maksimovic et al., 2014; Woo et al., 2014; Nakatani et al., 2015).

4.6 Are vertebrate hair cells and tunicate coronal sensory cells homologous?

During chordate evolution, some cell types remain tightly conserved while others have been either lost or convergently evolved across different species. The concept of a "core regulatory complex" (CoRC) of transcription factors has been useful in devising evolutionary scenarios for cell types (Arendt et al., 2016) and as discussed above, mechanosensory cells across vertebrate and invertebrate taxa appear to share factors such as atonal/Atoh1, senseless/Gfi and Pou4 factors. Several models for the evolution of chordate mechanosensory cells have been proposed (for example, Schlosser, 2021). These models propose some form of basal primary sensory cell giving rise to two distinct cell types: a primary sensory neuron that is not mechanosensitive and defined by neurogenin-like transcription factors, and a mechanosensitive cell defined by atonal-like transcription factors and which either lacked an axon altogether (hair cells and coronal sensory cells) or just a short axon (caudal epidermal neurons; see 2.1 above).

At present, only atonal/Atoh1 expression has been characterized in the tunicate coronal organ and has not yet been localized to the coronal sensory cells. Nevertheless, the presence of both hair cell-like cells adjacent to supporting cells, the expression of Notch pathway genes in these cell types and their derivation from proto-placodal structures make a reasonable case for homology between these cell types. However, this conclusion is complicated by the fact that tunicates undergo metamorphosis, which prevents a clear visualization of the transition from tunicate "proto-placodal" structures to a sensory organ. This transition can be readily observed in vertebrates as the pre-placodal domain gives rise to individual placodes, some of which produce hair cells.

Resolving the question of homology between vertebrate hair cells and tunicate coronal sensory cells will be helped by three recent technical advances. First, single cell transcriptional analysis will be able to determine whether the CoRC transcription factors present in vertebrate hair cells and supporting cells are also expressed in coronal sensory cells and their associated supporting/accessory cells. Second, the advent of CRISPR has facilitated loss-of-function studies in many new model and non-model organisms, and disruption of tunicate CoRC mechanosensory transcription factors will allow testing of their necessity for coronal sensory cell differentiation. Finally, it may be possible to perform lineage tracing experiments to determine tunicate proto-placodal cells do indeed contribute to coronal sensory cells following metamorphosis. Resolving these questions could elucidate the ancestral mechanosensory hair cell gene regulatory network or could uncover novel mechanisms of creating mechanosensitive hair cell-like cells in different species.

Author contributions

CA: Conceptualization, Data curation, Investigation, Writing–original draft, Writing–review and editing. GF: Data curation, Investigation, Writing–original draft, Writing–review and editing. AS: Investigation, Writing–original draft, Writing–review and editing. AG: Investigation, Writing–original draft, Writing–review and editing. LM: Conceptualization, Investigation, Supervision, Writing–original draft, Writing–review and editing.

Funding

The author(s) declare that financial support was received for the research, authorship, and/or publication of this article. CA is supported by the Knight Initiative for Brain Resilience Scholar Award, Wu Tsai Neurosciences Institute, Stanford University. GF and AG are supported in part by the Vivian L. Smith Endowed Chair in Neuroscience at Baylor College of Medicine. GF is supported in part by T32GM139534. AS is supported by NIH award R01HD104825. LM is supported by JPI Oceans, Project NoiseInTheSea-2022–0011 DeuteroNoise.

Acknowledgments

AS would like to thank Florian Razy-Krajka and members of the lab for insightful discussions.

Conflict of interest

The authors declare that the research was conducted in the absence of any commercial or financial relationships that could be construed as a potential conflict of interest.

Publisher's note

References

Abitua, P. B., Gainous, T. B., Kaczmarczyk, A. N., Winchell, C. J., Hudson, C., Kamata, K., et al. (2015). The pre-vertebrate origins of neurogenic placodes. *Nature* 524, 462–465. doi:10.1038/nature14657

Acar, M., Jafar-Nejad, H., Giagtzoglou, N., Yallampalli, S., David, G., He, Y., et al. (2006). Senseless physically interacts with proneural proteins and functions as a transcriptional co-activator. *Development* 133, 1979–1989. doi:10.1242/dev.02372

Ankamreddy, H., Thawani, A., Birol, O., Zhang, H., and Groves, A. K. (2023). Foxi3GFP and Foxi3CreER mice allow identification and lineage labeling of pharyngeal arch ectoderm and endoderm, and tooth and hair placodes. *Dev. Dyn.* 252, 1462–1470. doi:10.1002/dvdy.645

Anselmi, C., Kowarsky, M., Gasparini, F., Caicci, F., Ishizuka, K. J., Palmeri, K. J., et al. (2022). Two distinct evolutionary conserved neural degeneration pathways characterized in a colonial chordate. *Proc. Natl. Acad. Sci. U. S. A.* 119, e2203032119. doi:10.1073/pnas.2203032119

Arendt, D., Musser, J. M., Baker, C. V. H., Bergman, A., Cepko, C., Erwin, D. H., et al. (2016). The origin and evolution of cell types. *Nat. Rev. Genet.* 17, 744–757. doi:10.1038/nrg.2016.127

Athira, A., Dondorp, D., Rudolf, J., Peytral, O., and Chatzigeorgiou, M. (2022). Comprehensive analysis of locomotion dynamics in the protochordate *Ciona intestinalis* reveals how neuromodulators flexibly shape its behavioral repertoire. *PLoS Biol.* 20, e3001744. doi:10.1371/journal.pbio.3001744

Baker, C. V., and Bronner-Fraser, M. (2001). Vertebrate cranial placodes I. Embryonic induction. *Dev. Biol.* 232, 1–61. doi:10.1006/dbio.2001.0156

Baker, C. V. H. (2019). "The development and evolution of lateral line electroreceptors: insights from comparative molecular approaches," in Electroreception: fundamental Insights from comparative approaches *springer handbook of auditory research*. Editors B. A. Carlson, J. A. Sisneros, A. N. Popper, and R. R. Fay (Cham: Springer International Publishing), 25–62. doi:10.1007/978-3-030-29105-1_2

Baker, C. V. H., Modrell, M. S., and Gillis, J. A. (2013). The evolution and development of vertebrate lateral line electroreceptors. *J. Exp. Biol.* 216, 2515–2522. doi:10.1242/jeb.082362

Basch, M. L., Brown, R. M., Jen, H.-I., and Groves, A. K. (2016). Where hearing starts: the development of the mammalian cochlea. *J. Anat.* 228, 233–254. doi:10.1111/joa.12314

Baumeister, R., Liu, Y., and Ruvkun, G. (1996). Lineage-specific regulators couple cell lineage asymmetry to the transcription of the *Caenorhabditis elegans* POU gene unc-86 during neurogenesis. *Genes Dev.* 10, 1395–1410. doi:10.1101/gad.10.11.1395

Ben-Arie, N., Bellen, H. J., Armstrong, D. L., McCall, A. E., Gordadze, P. R., Guo, Q., et al. (1997). Math1 is essential for genesis of cerebellar granule neurons. *Nature* 390, 169–172. doi:10.1038/36579

Ben-Arie, N., Hassan, B. A., Bermingham, N. A., Malicki, D. M., Armstrong, D., Matzuk, M., et al. (2000). Functional conservation of atonal and Math1 in the CNS and PNS. *Development* 127, 1039–1048. doi:10.1242/dev.127.5.1039

Beurg, M., and Fettiplace, R. (2017). PIEZO2 as the anomalous mechanotransducer channel in auditory hair cells. *J. Physiol. (Lond)* 595, 7039–7048. doi:10.1113/JP274996

Birol, O., Ohyama, T., Edlund, R. K., Drakou, K., Georgiades, P., and Groves, A. K. (2016). The mouse Foxi3 transcription factor is necessary for the development of posterior placodes. *Dev. Biol.* 409, 139–151. doi:10.1016/j.ydbio.2015.09.022

Bollner, T., Holmberg, K., and Olsson, R. (1986). A rostral sensory mechanism in *Oikopleura dioica* (appendicularia). *Acta Zool.* 67, 235–241. doi:10.1111/j.1463-6395.1986.tb00868.x

Bone, Q. (1959). Observations upon the nervous systems of pelagic tunicates. *J. Cell Sci.* S3-100, 167–181. doi:10.1242/jcs.s3-100.50.167

Bone, Q. (1998). *The biology of pelagic tunicates* (Oxford University PressOxford). doi:10.1093/oso/9780198540243.001.0001

Bone, Q., and Ryan, K. P. (1978). Cupular sense organs in ciona (tunicata: Ascidiacea). *J. Zool.* 186, 417–429. doi:10.1111/j.1469-7998.1978.tb03931.x

Boorman, C. J., and Shimeld, S. M. (2002). Pitx homeobox genes in Ciona and amphioxus show left–right asymmetry is a conserved chordate character and define the ascidian adenohypophysis. *Evol. Dev.* 4 (5), 354–365. doi:10.1046/j.1525-142X.2002.02021.x

Bostwick, M., Smith, E. L., Borba, C., Newman-Smith, E., Guleria, I., Kourakis, M. J., et al. (2020). Antagonistic inhibitory circuits integrate visual and gravitactic behaviors. *Curr. Biol.* 30, 600–609. doi:10.1016/j.cub.2019.12.017

Brown, R., and Groves, A. K. (2020). Hear, hear for notch: control of cell fates in the inner ear by notch signaling. *Biomolecules* 10, 370. doi:10.3390/biom10030370

Bucks, S. A., Cox, B. C., Vlosich, B. A., Manning, J. P., Nguyen, T. B., and Stone, J. S. (2017). Supporting cells remove and replace sensory receptor hair cells in a balance organ of adult mice. *eLife* 6, e18128. doi:10.7554/eLife.18128

Burighel, P., Caicci, F., and Manni, L. (2011). Hair cells in non-vertebrate models: lower chordates and molluscs. *Hear. Res.* 273, 14–24. doi:10.1016/j.heares.2010.03.087

Burighel, P., Caicci, F., Zaniolo, G., Gasparini, F., Degasperi, V., and Manni, L. (2008). Does hair cell differentiation predate the vertebrate appearance? *Brain Res. Bull.* 75, 331–334. doi:10.1016/j.brainresbull.2007.10.012

Burighel, P., Lane, N. J., Fabio, G., Stefano, T., Zaniolo, G., Carnevali, M. D. C., et al. (2003). Novel, secondary sensory cell organ in ascidians: in search of the ancestor of the vertebrate lateral line. *J. Comp. Neurol.* 461, 236–249. doi:10.1002/cne.10666

Cai, T., and Groves, A. K. (2015). The role of atonal factors in mechanosensory cell specification and function. *Mol. Neurobiol.* 52, 1315–1329. doi:10.1007/s12035-014-8925-0

Caicci, F., Burighel, P., and Manni, L. (2007). Hair cells in an ascidian (Tunicata) and their evolution in chordates. *Hear. Res.* 231, 63–72. doi:10.1016/j.heares.2007.05.007

Caicci, F., Degasperi, V., Gasparini, F., Zaniolo, G., Del Favero, M., Burighel, P., et al. (2010a). Variability of hair cells in the coronal organ of ascidians (Chordata, Tunicata). *Can. J. Zool.* 88, 567–578. doi:10.1139/z10-036

Caicci, F., Gasparini, F., Rigon, F., Zaniolo, G., Burighel, P., and Manni, L. (2013). The oral sensory structures of Thaliacea (Tunicata) and consideration of the evolution of hair cells in Chordata. *J. Comp. Neurol.* 521, 2756–2771. doi:10.1002/cne.23313

Caicci, F., Zaniolo, G., Burighel, P., Degasperi, V., Gasparini, F., and Manni, L. (2010b). Differentiation of papillae and rostral sensory neurons in the larva of the ascidian Botryllus schlosseri (Tunicata). *J. Comp. Neurol.* 518, 547–566. doi:10.1002/cne.22222

Cao, C., Lemaire, L. A., Wang, W., Yoon, P. H., Choi, Y. A., Parsons, L. R., et al. (2019). Comprehensive single-cell transcriptome lineages of a proto-vertebrate. *Nature* 571, 349–354. doi:10.1038/s41586-019-1385-y

Chen, J. S., Pedro, M. S., and Zeller, R. W. (2011). miR-124 function during *Ciona intestinalis* neuronal development includes extensive interaction with the Notch signaling pathway. *Development* 138, 4943–4953. doi:10.1242/dev.068049

Corey, D. P., García-Añoveros, J., Holt, J. R., Kwan, K. Y., Lin, S.-Y., Vollrath, M. A., et al. (2004). TRPA1 is a candidate for the mechanosensitive transduction channel of vertebrate hair cells. *Nature* 432, 723–730. doi:10.1038/nature03066

Cosgrove, D., and Zallocchi, M. (2014). Usher protein functions in hair cells and photoreceptors. *Int. J. Biochem. Cell Biol.* 46, 80–89. doi:10.1016/j.biocel.2013.11.001

Costa, A., Sanchez-Guardado, L., Juniat, S., Gale, J. E., Daudet, N., and Henrique, D. (2015). Generation of sensory hair cells by genetic programming with a combination of transcription factors. *Development* 142, 1948–1959. doi:10.1242/dev.119149

Coulcher, J. F., Roure, A., Chowdhury, R., Robert, M., Lescat, L., Bouin, A., et al. (2020). Conservation of peripheral nervous system formation mechanisms in divergent ascidian embryos. *Elife* 9, e59157. doi:10.7554/eLife.59157

Cunningham, C. L., Qiu, X., Wu, Z., Zhao, B., Peng, G., Kim, Y.-H., et al. (2020). TMIE defines pore and gating properties of the mechanotransduction channel of mammalian cochlear hair cells. *Neuron* 107, 126–143. doi:10.1016/j.neuron.2020.03.033

Cvekl, A., and Ashery-Padan, R. (2014). The cellular and molecular mechanisms of vertebrate lens development. *Development* 141, 4432–4447. doi:10.1242/dev.107953

DeBiasse, M. B., Colgan, W. N., Harris, L., Davidson, B., and Ryan, J. F. (2020). Inferring tunicate relationships and the evolution of the tunicate hox cluster with the genome of Corella inflata. *Genome Biol. Evol.* 12, 948–964. doi:10.1093/gbe/evaa060

Delsuc, F., Philippe, H., Tsagkogeorga, G., Simion, P., Tilak, M.-K., Turon, X., et al. (2018). A phylogenomic framework and timescale for comparative studies of tunicates. *BMC Biol.* 16, 39. doi:10.1186/s12915-018-0499-2

Durante, K. M. (1991). Larval behavior, settlement preference, and induction of metamorphosis in the temperate solitary ascidian Molgula citrina Alder and Hancock. *J. Exp. Mar. Biol. Ecol.* 145, 175–187. doi:10.1016/0022-0981(91)90174-U

Edlund, R. K., Ohyama, T., Kantarci, H., Riley, B. B., and Groves, A. K. (2014). Foxi transcription factors promote pharyngeal arch development by regulating formation of FGF signaling centers. *Dev. Biol.* 390, 1–13. doi:10.1016/j.ydbio.2014.03.004

Fedele, M. (1923). Le attivitá dinamiche ed i rapporti nervosi nella vita dei Dolioli. *Pubbl Staz Zool. Napoli* 4, 129–240.

Fritzsch, B., and Elliott, K. L. (2017). Gene, cell, and organ multiplication drives inner ear evolution. *Dev. Biol.* 431, 3–15. doi:10.1016/j.ydbio.2017.08.034

Frolenkov, G. I., Belyantseva, I. A., Friedman, T. B., and Griffith, A. J. (2004). Genetic insights into the morphogenesis of inner ear hair cells. *Nat. Rev. Genet.* 5, 489–498. doi:10.1038/nrg1377

Gans, C., and Northcutt, R. G. (1983). Neural crest and the origin of vertebrates: a new head. *Science* 220, 268–273. doi:10.1126/science.220.4594.268

Gasparini, F., Caicci, F., Rigon, F., Zaniolo, G., Burighel, P., and Manni, L. (2013a). Cytodifferentiation of hair cells during the development of a basal chordate. *Hear. Res.* 304, 188–199. doi:10.1016/j.heares.2013.07.006

Gasparini, F., Degasperi, V., Shimeld, S. M., Burighel, P., and Manni, L. (2013b). Evolutionary conservation of the placodal transcriptional network during sexual and asexual development in chordates. *Dev. Dyn.* 242, 752–766. doi:10.1002/dvdy.23957

Ge, J., Elferich, J., Goehring, A., Zhao, H., Schuck, P., and Gouaux, E. (2018). Structure of mouse protocadherin 15 of the stereocilia tip link in complex with LHFPL5. *eLife* 7, e38770. doi:10.7554/eLife.38770

Gillespie, P. G., and Müller, U. (2009). Mechanotransduction by hair cells: models, molecules, and mechanisms. *Cell* 139, 33–44. doi:10.1016/j.cell.2009.09.010

Gnedeva, K., and Hudspeth, A. J. (2015). SoxC transcription factors are essential for the development of the inner ear. *Proc. Natl. Acad. Sci. U. S. A.* 112, 14066–14071. doi:10.1073/pnas.1517371112

Graham, A., and Shimeld, S. M. (2013). The origin and evolution of the ectodermal placodes. *J. Anat.* 222 (1), 32–40. doi:10.1111/j.1469-7580.2012.01506.x

Grocott, T., Tambalo, M., and Streit, A. (2012). The peripheral sensory nervous system in the vertebrate head: a gene regulatory perspective. *Dev. Biol.* 370, 3–23. doi:10.1016/j.ydbio.2012.06.028

Groves, A. K. (2010). The challenge of hair cell regeneration. *Exp. Biol. Med. (Maywood)* 235, 434–446. doi:10.1258/ebm.2009.009281

Groves, A. K., and Fekete, D. M. (2012). Shaping sound in space: the regulation of inner ear patterning. *Development* 139, 245–257. doi:10.1242/dev.067074

Groves, A. K., and LaBonne, C. (2014). Setting appropriate boundaries: fate, patterning and competence at the neural plate border. *Dev. Biol.* 389, 2–12. doi:10.1016/j.ydbio.2013.11.027

Gu, R., Brown, R. M., Hsu, C.-W., Cai, T., Crowder, A. L., Piazza, V. G., et al. (2016). Lineage tracing of Sox2-expressing progenitor cells in the mouse inner ear reveals a broad contribution to non-sensory tissues and insights into the origin of the organ of Corti. *Dev. Biol.* 414, 72–84. doi:10.1016/j.ydbio.2016.03.027

Haeberle, H., Fujiwara, M., Chuang, J., Medina, M. M., Panditrao, M. V., Bechstedt, S., et al. (2004). Molecular profiling reveals synaptic release machinery in Merkel cells. *Proc. Natl. Acad. Sci. U. S. A.* 101, 14503–14508. doi:10.1073/pnas.0406308101

Hans, S., Liu, D., and Westerfield, M. (2004). Pax8 and Pax2a function synergistically in otic specification, downstream of the Foxi1 and Dlx3b transcription factors. *Development* 131, 5091–5102. doi:10.1242/dev.01346

Hasten, E., and Morrow, B. E. (2019). Tbx1 and Foxi3 genetically interact in the pharyngeal pouch endoderm in a mouse model for 22q11.2 deletion syndrome. *PLoS Genet.* 15, e1008301. doi:10.1371/journal.pgen.1008301

Holt, J. R., Tobin, M., Elferich, J., Gouaux, E., Ballesteros, A., Yan, Z., et al. (2021). Putting the pieces together: the hair cell transduction complex. *J. Assoc. Res. Otolaryngol.* 22, 601–608. doi:10.1007/s10162-021-00808-0

Horie, R., Hazbun, A., Chen, K., Cao, C., Levine, M., and Horie, T. (2018). Shared evolutionary origin of vertebrate neural crest and cranial placodes. *Nature* 560, 228–232. doi:10.1038/s41586-018-0385-7

Horie, T., Kusakabe, T., and Tsuda, M. (2008). Glutamatergic networks in the *Ciona intestinalis* larva. *J. Comp. Neurol.* 508, 249–263. doi:10.1002/cne.21678

Hoyer, J., Kolar, K., Athira, A., van den Burgh, M., Dondorp, D., Liang, Z., et al. (2024). Polymodal sensory perception drives settlement and metamorphosis of Ciona larvae. *Curr. Biol.* doi:10.1016/j.cub.2024.01.041

Hozumi, A., Matsunobu, S., Mita, K., Treen, N., Sugihara, T., Horie, T., et al. (2020). GABA-induced GnRH release triggers chordate metamorphosis. *Curr. Biol.* 30, 1555–1561. doi:10.1016/j.cub.2020.02.003

Hudson, C., and Yasuo, H. (2005). Patterning across the ascidian neural plate by lateral Nodal signalling sources. *Development* 132, 1199–1210. doi:10.1242/dev.01688

Imai, J. H., and Meinertzhagen, I. A. (2007). Neurons of the ascidian larval nervous system in *Ciona intestinalis*: II. Peripheral nervous system. *J. Comp. Neurol.* 501, 335–352. doi:10.1002/cne.21247

Imai, K. S., Hikawa, H., Kobayashi, K., and Satou, Y. (2017). Tfap2 and Sox1/2/3 cooperatively specify ectodermal fates in ascidian embryos. *Development* 144, 33–37. doi:10.1242/dev.142109

Imai, K. S., Hino, K., Yagi, K., Satoh, N., and Satou, Y. (2004). Gene expression profiles of transcription factors and signaling molecules in the ascidian embryo: towards a comprehensive understanding of gene networks. *Development* 131, 4047–4058. doi:10.1242/dev.01270

Irvine, S. Q., Cangiano, M. C., Millette, B. J., and Gutter, E. S. (2007). Non-overlapping expression patterns of the clustered Dll-A/B genes in the ascidian Ciona Intestinalis. *J. Exp. Zool Part B Mol. Dev. Evol.* 308 (4), 428–441. doi:10.1002/jez.b.21169

Irvine, S. Q., Fonseca, V. C., Zompa, M. A., and Antony, R. (2008). Cis-regulatory organization of the Pax6 gene in the ascidian *Ciona intestinalis*. *Dev. Biol.* 317, 649–659. doi:10.1016/j.ydbio.2008.01.036

Iyer, A. A., and Groves, A. K. (2021). Transcription factor reprogramming in the inner ear: turning on cell fate switches to regenerate sensory hair cells. *Front. Cell. Neurosci.* 15, 660748. doi:10.3389/fncel.2021.660748

Iyer, A. A., Hosamani, I., Nguyen, J. D., Cai, T., Singh, S., McGovern, M. M., et al. (2022). Cellular reprogramming with ATOH1, GFI1, and POU4F3 implicate epigenetic changes and cell-cell signaling as obstacles to hair cell regeneration in mature mammals. *eLife* 11, e79712. doi:10.7554/eLife.79712

Jarman, A. P., Grau, Y., Jan, L. Y., and Jan, Y. N. (1993). Atonal is a proneural gene that directs chordotonal organ formation in the Drosophila peripheral nervous system. *Cell* 73, 1307–1321. doi:10.1016/0092-8674(93)90358-w

Jarman, A. P., and Groves, A. K. (2013). The role of Atonal transcription factors in the development of mechanosensitive cells. *Semin. Cell Dev. Biol.* 24, 438–447. doi:10.1016/j.semcdb.2013.03.010

Jarman, A. P., Sun, Y., Jan, L. Y., and Jan, Y. N. (1995). Role of the proneural gene, atonal, in formation of Drosophila chordotonal organs and photoreceptors. *Development* 121, 2019–2030. doi:10.1242/dev.121.7.2019

Jeffery, W. R., Strickler, A. G., and Yamamoto, Y. (2004). Migratory neural crest-like cells form body pigmentation in a urochordate embryo. *Nature* 431, 696–699. doi:10.1038/nature02975

Jen, H.-I., Singh, S., Tao, L., Maunsell, H. R., Segil, N., and Groves, A. K. (2022). GFI1 regulates hair cell differentiation by acting as an off-DNA transcriptional co-activator of ATOH1, and a DNA-binding repressor. *Sci. Rep.* 12, 7793. doi:10.1038/s41598-022-11931-0

Jiang, D., Tresser, J. W., Horie, T., Tsuda, M., and Smith, W. C. (2005). Pigmentation in the sensory organs of the ascidian larva is essential for normal behavior. *J. Exp. Biol.* 208, 433–438. doi:10.1242/jeb.01420

Johnson, C. J., Kulkarni, A., Buxton, W. J., Hui, T. Y., Kayastha, A., Khoja, A. A., et al. (2023a). Using CRISPR/Cas9 to identify genes required for mechanosensory neuron development and function. *Biol. Open* 12, bio060002. doi:10.1242/bio.060002

Johnson, C. J., Razy-Krajka, F., Zeng, F., Piekarz, K. M., Biliya, S., Rothbächer, U., et al. (2023b). Specification of distinct cell types in a sensory-adhesive organ for metamorphosis in the *Ciona* larva. *BioRxiv*. doi:10.1101/2023.05.02.539060

Khatri, S. B., Edlund, R. K., and Groves, A. K. (2014). Foxi3 is necessary for the induction of the chick otic placode in response to FGF signaling. *Dev. Biol.* 391, 158–169. doi:10.1016/j.ydbio.2014.04.014

Khatri, S. B., and Groves, A. K. (2013). Expression of the Foxi2 and Foxi3 transcription factors during development of chicken sensory placodes and pharyngeal arches. *Gene Expr. Patterns* 13, 38–42. doi:10.1016/j.gep.2012.10.001

Kindt, K. S., Finch, G., and Nicolson, T. (2012). Kinocilia mediate mechanosensitivity in developing zebrafish hair cells. *Dev. Cell* 23, 329–341. doi:10.1016/j.devcel.2012.05.022

Kniss, J. S., Jiang, L., and Piotrowski, T. (2016). Insights into sensory hair cell regeneration from the zebrafish lateral line. *Curr. Opin. Genet. Dev.* 40, 32–40. doi:10.1016/j.gde.2016.05.012

Kocot, K. M., Tassia, M. G., Halanych, K. M., and Swalla, B. J. (2018). Phylogenomics offers resolution of major tunicate relationships. *Mol. Phylogenet. Evol.* 121, 166–173. doi:10.1016/j.ympev.2018.01.005

Konno, A., Kaizu, M., Hotta, K., Horie, T., Sasakura, Y., Ikeo, K., et al. (2010). Distribution and structural diversity of cilia in tadpole larvae of the ascidian *Ciona intestinalis*. *Dev. Biol.* 337, 42–62. doi:10.1016/j.ydbio.2009.10.012

Kourakis, M. J., Borba, C., Zhang, A., Newman-Smith, E., Salas, P., Manjunath, B., et al. (2019). Parallel visual circuitry in a basal chordate. *eLife* 8, e44753. doi:10.7554/eLife.44753

Koyama, H. (2008). Sensory cells associated with the tentacular tunic of the ascidian Polyandrocarpa misakiensis (Tunicata: Ascidiacea). *Zool. Sci.* 25, 919–930. doi:10.2108/zsj.25.919

Kozmik, Z. (2008). The role of Pax genes in eye evolution. *Brain Res. Bull.* 75, 335–339. doi:10.1016/j.brainresbull.2007.10.046

Kwan, K. Y., Allchorne, A. J., Vollrath, M. A., Christensen, A. P., Zhang, D.-S., Woolf, C. J., et al. (2006). TRPA1 contributes to cold, mechanical, and chemical nociception but is not essential for hair-cell transduction. *Neuron* 50, 277–289. doi:10.1016/j.neuron.2006.03.042

Lai, H. C., Klisch, T. J., Roberts, R., Zoghbi, H. Y., and Johnson, J. E. (2011). *In vivo* neuronal subtype-specific targets of Atoh1 (Math1) in dorsal spinal cord. *J. Neurosci.* 31, 10859–10871. doi:10.1523/JNEUROSCI.0445-11.2011

Le, M.-L. V., Müller, L.-M., and Stach, T. (2023). The oral sensory organs in Bathochordaeus stygius (Tunicata Appendicularia) are unique in structure and homologous to the coronal organ. *Res. Sq.* doi:10.21203/rs.3.rs-3167810/v1

Lee, M.-H., and Salvaterra, P. M. (2002). Abnormal chemosensory jump 6 is a positive transcriptional regulator of the cholinergic gene locus in Drosophila olfactory neurons. *J. Neurosci.* 22, 5291–5299. doi:10.1523/JNEUROSCI.22-13-05291.2002

Lesko, M. H., Driskell, R. R., Kretzschmar, K., Goldie, S. J., and Watt, F. M. (2013). Sox2 modulates the function of two distinct cell lineages in mouse skin. *Dev. Biol.* 382, 15–26. doi:10.1016/j.ydbio.2013.08.004

Li, S., Fan, T., Li, C., Wang, Y., Li, J., and Liu, Z. (2022). Fate-mapping analysis of cochlear cells expressing Atoh1 mRNA via a new Atoh13*HA-P2A-Cre knockin mouse strain. *Dev. Dyn.* 251, 1156–1174. doi:10.1002/dvdy.453

Li, T., Bellen, H. J., and Groves, A. K. (2018). Using Drosophila to study mechanisms of hereditary hearing loss. *Dis. Model. Mech.* 11, dmm031492. doi:10.1242/dmm.031492

Liu, B., and Satou, Y. (2019). Foxg specifies sensory neurons in the anterior neural plate border of the ascidian embryo. *Nat. Commun.* 10, 4911. doi:10.1038/s41467-019-12839-6

Lu, T.-M., Luo, Y.-J., and Yu, J.-K. (2012). BMP and Delta/Notch signaling control the development of amphioxus epidermal sensory neurons: insights into the evolution of the peripheral sensory system. *Development* 139, 2020–2030. doi:10.1242/dev.073833

Lumpkin, E. A., Collisson, T., Parab, P., Omer-Abdalla, A., Haeberle, H., Chen, P., et al. (2003). Math1-driven GFP expression in the developing nervous system of transgenic mice. *Gene Expr. Patterns* 3, 389–395. doi:10.1016/s1567-133x(03)00089-9

Mackie, G. O., and Bone, Q. (1978). Luminescence and associated effector activity in pyrosoma (tunicata: pyrosomida). *Proc. R. Soc. B Biol. Sci.* 202, 483–495. doi:10.1098/rspb.1978.0081

Mackie, G. O., and Burighel, P. (2005). The nervous system in adult tunicates: current research directions. *Can. J. Zool.* 83, 151–183. doi:10.1139/z04-177

Mackie, G. O., Burighel, P., Caicci, F., and Manni, L. (2006). Innervation of ascidian siphons and their responses to stimulation. *Can. J. Zool.* 84, 1146–1162. doi:10.1139/z06-106

Mackie, G. O., and Singla, C. L. (2003). The capsular organ of Chelyosoma productum (Ascidiacea: corellidae): a new tunicate hydrodynamic sense organ. *Brain Behav. Evol.* 61, 45–58. doi:10.1159/000068878

Mackie, G. O., and Singla, C. L. (2005). Cupular organs in two species of Corella (tunicata: Ascidiacea). *Invertebr. Biol.* 123, 269–281. doi:10.1111/j.1744-7410.2004.tb00161.x

Maksimovic, S., Nakatani, M., Baba, Y., Nelson, A. M., Marshall, K. L., Wellnitz, S. A., et al. (2014). Epidermal Merkel cells are mechanosensory cells that tune mammalian touch receptors. *Nature* 509, 617–621. doi:10.1038/nature13250

Mann, Z. F., Gálvez, H., Pedreno, D., Chen, Z., Chrysostomou, E., Żak, M., et al. (2017). Shaping of inner ear sensory organs through antagonistic interactions between Notch signalling and Lmx1a. *eLife* 6, e33323. doi:10.7554/eLife.33323

Manni, L., Agnoletto, A., Zaniolo, G., and Burighel, P. (2005). Stomodeal and neurohypophysial placodes in *Ciona intestinalis*: insights into the origin of the pituitary gland. *J. Exp. Zool. B Mol. Dev. Evol.* 304, 324–339. doi:10.1002/jez.b.21039

Manni, L., Anselmi, C., Burighel, P., Martini, M., and Gasparini, F. (2018). Differentiation and induced sensorial alteration of the coronal organ in the asexual life of a tunicate. *Integr. Comp. Biol.* 58, 317–328. doi:10.1093/icb/icy044

Manni, L., Caicci, F., Anselmi, C., Vanni, V., Mercurio, S., and Pennati, R. (2021). Morphological study and 3D reconstruction of the larva of the ascidian Halocynthia roretzi. *JMSE* 10, 11. doi:10.3390/jmse10010011

Manni, L., Caicci, F., Gasparini, F., Zaniolo, G., and Burighel, P. (2004). Hair cells in ascidians and the evolution of lateral line placodes. *Evol. Dev.* 6, 379–381. doi:10.1111/j.1525-142X.2004.04046.x

Manni, L., Lane, N. J., Burighel, P., and Zaniolo, G. (2001). Are neural crest and placodes exclusive to vertebrates? *Evol. Dev.* 3, 297–298. doi:10.1046/j.1525-142x.2001.01040.x

Manni, L., Lane, N. J., Sorrentino, M., Zaniolo, G., and Burighel, P. (1999). Mechanism of neurogenesis during the embryonic development of a tunicate. *J. Comp. Neurol.* 412, 527–541. doi:10.1002/(sici)1096-9861(19990927)412:3<527::aid-cne11>3.0.co;2-u

Manni, L., Mackie, G. O., Caicci, F., Zaniolo, G., and Burighel, P. (2006). Coronal organ of ascidians and the evolutionary significance of secondary sensory cells in chordates. *J. Comp. Neurol.* 495, 363–373. doi:10.1002/cne.20867

Manni, L., and Pennati, R. (2015). "Tunicata," in *Structure and evolution of invertebrate nervous systems* (Oxford University Press), 699–718. Available at: https://doi.org/10.1093/acprof:oso/9780199682201.003.0031 (Accessed May 25, 2021).

Maricich, S. M., Wellnitz, S. A., Nelson, A. M., Lesniak, D. R., Gerling, G. J., Lumpkin, E. A., et al. (2009). Merkel cells are essential for light-touch responses. *Science* 324, 1580–1582. doi:10.1126/science.1172890

Mazet, F., Hutt, J. A., Millard, J., and Shimeld, S. M. (2003). Pax gene expression in the developing central nervous system of *Ciona intestinalis*. *Gene Expr. Patterns* 3, 743–745. doi:10.1016/s1567-133x(03)00137-6

Mazet, F., and Shimeld, S. M. (2005). Molecular evidence from ascidians for the evolutionary origin of vertebrate cranial sensory placodes. *J. Exp. Zool. B Mol. Dev. Evol.* 304, 340–346. doi:10.1002/jez.b.21054

Menendez, L., Trecek, T., Gopalakrishnan, S., Tao, L., Markowitz, A. L., Yu, H. V., et al. (2020). Generation of inner ear hair cells by direct lineage conversion of primary somatic cells. *eLife* 9, e55249. doi:10.7554/eLife.55249

Modrell, M. S., Lyne, M., Carr, A. R., Zakon, H. H., Buckley, D., Campbell, A. S., et al. (2017). Insights into electrosensory organ development, physiology and evolution from a lateral line-enriched transcriptome. *eLife* 6, e24197. doi:10.7554/eLife.24197

Nakatani, M., Maksimovic, S., Baba, Y., and Lumpkin, E. A. (2015). Mechanotransduction in epidermal Merkel cells. *Pflugers Arch.* 467, 101–108. doi:10.1007/s00424-014-1569-0

Nakayama-Ishimura, A., Chambon, J., Horie, T., Satoh, N., and Sasakura, Y. (2009). Delineating metamorphic pathways in the ascidian *Ciona intestinalis*. *Dev. Biol.* 326, 357–367. doi:10.1016/j.ydbio.2008.11.026

Neves, J., Vachkov, I., and Giraldez, F. (2013). Sox2 regulation of hair cell development: incoherence makes sense. *Hear. Res.* 297, 20–29. doi:10.1016/j.heares.2012.11.003

Nissen, R. M., Yan, J., Amsterdam, A., Hopkins, N., and Burgess, S. M. (2003). Zebrafish foxi one modulates cellular responses to Fgf signaling required for the integrity of ear and jaw patterning. *Development* 130, 2543–2554. doi:10.1242/dev.00455

Nolo, R., Abbott, L. A., and Bellen, H. J. (2000). Senseless, a Zn finger transcription factor, is necessary and sufficient for sensory organ development in Drosophila. *Cell* 102, 349–362. doi:10.1016/s0092-8674(00)00040-4

Ohtsuka, Y., Matsumoto, J., Katsuyama, Y., and Okamura, Y. (2014). Nodal signaling regulates specification of ascidian peripheral neurons through control of the BMP signal. *Development* 141, 3889–3899. doi:10.1242/dev.110213

Ohyama, T., and Groves, A. K. (2004). Expression of mouse Foxi class genes in early craniofacial development. *Dev. Dyn.* 231, 640–646. doi:10.1002/dvdy.20160

Okawa, N., Shimai, K., Ohnishi, K., Ohkura, M., Nakai, J., Horie, T., et al. (2020). Cellular identity and Ca2+ signaling activity of the non-reproductive GnRH system in the *Ciona intestinalis* type A (Ciona robusta) larva. *Sci. Rep.* 10, 18590. doi:10.1038/s41598-020-75344-7

Ozment, E., Tamvacakis, A. N., Zhou, J., Rosiles-Loeza, P. Y., Escobar-Hernandez, E. E., Fernandez-Valverde, S. L., et al. (2021). Cnidarian hair cell development illuminates an ancient role for the class IV POU transcription factor in defining mechanoreceptor identity. *eLife* 10, e74336. doi:10.7554/eLife.74336

Papadogiannis, V., Pennati, A., Parker, H. J., Rothbächer, U., Patthey, C., Bronner, M. E., et al. (2022). Hmx gene conservation identifies the origin of vertebrate cranial ganglia. *Nature* 605 (7911), 701–705. doi:10.1038/s41586-022-04742-w

Park, C., Ji, H.-M., Kim, S.-J., Kil, S.-H., Lee, J. N., Kwak, S., et al. (2017). Fenofibrate exerts protective effects against gentamicin-induced toxicity in cochlear hair cells by activating antioxidant enzymes. *Int. J. Mol. Med.* 39, 960–968. doi:10.3892/ijmm.2017.2916

Pasini, A., Amiel, A., Rothbächer, U., Roure, A., Lemaire, P., and Darras, S. (2006). Formation of the ascidian epidermal sensory neurons: insights into the origin of the chordate peripheral nervous system. *PLoS Biol.* 4, e225. doi:10.1371/journal.pbio.0040225

Pasini, A., Manenti, R., Rothbächer, U., and Lemaire, P. (2012). Antagonizing retinoic acid and FGF/MAPK pathways control posterior body patterning in the invertebrate chordate *Ciona intestinalis*. *PLoS ONE* 7, e46193. doi:10.1371/journal.pone.0046193

Patthey, C., Schlosser, G., and Shimeld, S. M. (2014). The evolutionary history of vertebrate cranial placodes--I: cell type evolution. *Dev. Biol.* 389, 82–97. doi:10.1016/j.ydbio.2014.01.017

Perdigoto, C. N., Bardot, E. S., Valdes, V. J., Santoriello, F. J., and Ezhkova, E. (2014). Embryonic maturation of epidermal Merkel cells is controlled by a redundant transcription factor network. *Development* 141, 4690–4696. doi:10.1242/dev.112169

Piotrowski, T., and Baker, C. V. H. (2014). The development of lateral line placodes: taking a broader view. *Dev. Biol.* 389, 68–81. doi:10.1016/j.ydbio.2014.02.016

Pla, P., and Monsoro-Burq, A. H. (2018). The neural border: induction, specification and maturation of the territory that generates neural crest cells. *Dev. Biol.* 444 (Suppl. 1), S36–S46. doi:10.1016/j.ydbio.2018.05.018

Poncelet, G., Parolini, L., and Shimeld, S. M. (2022). A microfluidic device for controlled exposure of transgenic *Ciona intestinalis* larvae to chemical stimuli demonstrates they can respond to carbon dioxide. *BioRxiv*. doi:10.1101/2022.08.15.492342

Popsuj, S., and Stolfi, A. (2021). Ebf activates expression of a cholinergic locus in a multipolar motor ganglion interneuron subtype in ciona. *Front. Neurosci.* 15, 784649. doi:10.3389/fnins.2021.784649

Qiu, X., and Müller, U. (2018). Mechanically gated ion channels in mammalian hair cells. *Front. Cell. Neurosci.* 12, 100. doi:10.3389/fncel.2018.00100

Rae Flores, A., and Faulkes, Z. (2008). Texture preferences of ascidian tadpole larvae during settlement. *Mar. Freshw. Behav. Physiol.* 41, 155–159. doi:10.1080/10236240802360914

Raft, S., and Groves, A. K. (2015). Segregating neural and mechanosensory fates in the developing ear: patterning, signaling, and transcriptional control. *Cell Tissue Res.* 359, 315–332. doi:10.1007/s00441-014-1917-6

Richardson, G. P., and Petit, C. (2019). Hair-bundle links: genetics as the gateway to function. *Cold Spring Harb. Perspect. Med.* 9, a033142. doi:10.1101/cshperspect.a033142

Rigon, F., Gasparini, F., Shimeld, S. M., Candiani, S., and Manni, L. (2018). Developmental signature, synaptic connectivity and neurotransmission are conserved between vertebrate hair cells and tunicate coronal cells. *J. Comp. Neurol.* 526, 957–971. doi:10.1002/cne.24382

Rigon, F., Stach, T., Caicci, F., Gasparini, F., Burighel, P., and Manni, L. (2013). Evolutionary diversification of secondary mechanoreceptor cells in tunicata. *BMC Evol. Biol.* 13, 112. doi:10.1186/1471-2148-13-112

Roure, A., Chowdhury, R., and Darras, S. (2023). Regulation of anterior neurectoderm specification and differentiation by BMP signaling in ascidians. *Development* 150, dev201575. doi:10.1242/dev.201575

Ryan, K., Lu, Z., and Meinertzhagen, I. A. (2016). The CNS connectome of a tadpole larva of *Ciona intestinalis* (L.) highlights sidedness in the brain of a chordate sibling. *eLife* 5, e16962. doi:10.7554/eLife.16962

Ryan, K., Lu, Z., and Meinertzhagen, I. A. (2017). Circuit homology between decussating pathways in the ciona larval CNS and the vertebrate startle-response pathway. *Curr. Biol.* 27, 721–728. doi:10.1016/j.cub.2017.01.026

Ryan, K., Lu, Z., and Meinertzhagen, I. A. (2018). The peripheral nervous system of the ascidian tadpole larva: types of neurons and their synaptic networks. *J. Comp. Neurol.* 526, 583–608. doi:10.1002/cne.24353

Sakamoto, A., Hozumi, A., Shiraishi, A., Satake, H., Horie, T., and Sasakura, Y. (2022). The TRP channel PKD2 is involved in sensing the mechanical stimulus of adhesion for initiating metamorphosis in the chordate Ciona. *Dev. Growth Differ.* 64, 395–408. doi:10.1111/dgd.12801

Sakurai, D., Goda, M., Kohmura, Y., Horie, T., Iwamoto, H., Ohtsuki, H., et al. (2004). The role of pigment cells in the brain of ascidian larva. *J. Comp. Neurol.* 475, 70–82. doi:10.1002/cne.20142

Sato, S., Ikeda, K., Shioi, G., Ochi, H., Ogino, H., Yajima, H., et al. (2010). Conserved expression of mouse Six1 in the pre-placodal region (PPR) and identification of an enhancer for the rostral PPR. *Dev. Biol.* 344, 158–171. doi:10.1016/j.ydbio.2010.04.029

Schlosser, G. (2014). Early embryonic specification of vertebrate cranial placodes. *Wiley Interdiscip. Rev. Dev. Biol.* 3, 349–363. doi:10.1002/wdev.142

Schlosser, G. (2021). *Evolutionary origin of sensory and neurosecretory cell types: vertebrate cranial placodes, volume 2*. 1st Edn. Boca Raton: CRC Press. doi:10.1201/9781003160625

Schwander, M., Kachar, B., and Müller, U. (2010). Review series: the cell biology of hearing. *J. Cell Biol.* 190, 9–20. doi:10.1083/jcb.201001138

Shimeld, S. M., Purkiss, A. G., Dirks, R. P. H., Bateman, O. A., Slingsby, C., and Lubsen, N. H. (2005). Urochordate betagamma-crystallin and the evolutionary origin of the vertebrate eye lens. *Curr. Biol.* 15, 1684–1689. doi:10.1016/j.cub.2005.08.046

Sidi, S., Friedrich, R. W., and Nicolson, T. (2003). NompC TRP channel required for vertebrate sensory hair cell mechanotransduction. *Science* 301, 96–99. doi:10.1126/science.1084370

Singh, S., and Groves, A. K. (2016). The molecular basis of craniofacial placode development. *Wiley Interdiscip. Rev. Dev. Biol.* 5, 363–376. doi:10.1002/wdev.226

Solomon, K. S., Kudoh, T., Dawid, I. B., and Fritz, A. (2003a). Zebrafish foxi1 mediates otic placode formation and jaw development. *Development* 130, 929–940. doi:10.1242/dev.00308

Solomon, K. S., Logsdon, J. M., and Fritz, A. (2003b). Expression and phylogenetic analyses of three zebrafish FoxI class genes. *Dev. Dyn.* 228, 301–307. doi:10.1002/dvdy.10373

Sorrentino, M., Manni, L., Lane, N. J., and Burighel, P. (2001). Evolution of cerebral vesicles and their sensory organs in an ascidian larva. *Acta Zool.* 81, 243–258. doi:10.1046/j.1463-6395.2000.00054.x

Stolfi, A., Ryan, K., Meinertzhagen, I. A., and Christiaen, L. (2015). Migratory neuronal progenitors arise from the neural plate borders in tunicates. *Nature* 527, 371–374. doi:10.1038/nature15758

Stone, J. S., and Cotanche, D. A. (2007). Hair cell regeneration in the avian auditory epithelium. *Int. J. Dev. Biol.* 51, 633–647. doi:10.1387/ijdb.072408js

Streit, A. (2004). Early development of the cranial sensory nervous system: from a common field to individual placodes. *Dev. Biol.* 276, 1–15. doi:10.1016/j.ydbio.2004.08.037

Streit, A. (2007). The preplacodal region: an ectodermal domain with multipotential progenitors that contribute to sense organs and cranial sensory ganglia. *Int. J. Dev. Biol.* 51, 447–461. doi:10.1387/ijdb.072327as

Streit, A. (2018). Specification of sensory placode progenitors: signals and transcription factor networks. *Int. J. Dev. Biol.* 62, 195–205. doi:10.1387/ijdb.170298as

Takamura, K. (1998). Nervous network in larvae of the ascidian *Ciona intestinalis*. *Dev. Genes Evol.* 208, 1–8. doi:10.1007/s004270050147

Tang, W., Chen, J. S., and Zeller, R. W. (2013). Transcriptional regulation of the peripheral nervous system in *Ciona intestinalis*. *Dev. Biol.* 378, 183–193. doi:10.1016/j.ydbio.2013.03.016

Terakubo, H. Q., Nakajima, Y., Sasakura, Y., Horie, T., Konno, A., Takahashi, H., et al. (2010). Network structure of projections extending from peripheral neurons in the tunic of ascidian larva. *Dev. Dyn.* 239, 2278–2287. doi:10.1002/dvdy.22361

Thawani, A., and Groves, A. K. (2020). Building the border: development of the chordate neural plate border region and its derivatives. *Front. Physiol.* 11, 608880. doi:10.3389/fphys.2020.608880

Thompson, S. H., Anselmi, C., Ishizuka, K. J., Palmeri, K. J., and Voskoboynik, A. (2022). Contributions from both the brain and the vascular network guide behavior in the colonial tunicate Botryllus schlosseri. *J. Exp. Biol.* 225, jeb244491. doi:10.1242/jeb.244491

Torrence, S. A. (1986). Sensory endings of the ascidian static organ (Chordata, Ascidiacea). *Zoomorphology* 106, 61–66. doi:10.1007/BF00312108

Torrence, S. A., and Cloney, R. A. (1982). Nervous system of ascidian larvae: caudal primary sensory neurons. *Zoomorphology* 99, 103–115. doi:10.1007/BF00310303

Varello, R., Asnicar, D., Boaga, J., and Cima, F. (2023). Behavioural responses to ultrasound antifouling systems by adult solitary ascidians. *JMSE* 11, 1115. doi:10.3390/jmse11061115

Vélez-Ortega, A. C., and Frolenkov, G. I. (2019). Building and repairing the stereocilia cytoskeleton in mammalian auditory hair cells. *Hear. Res.* 376, 47–57. doi:10.1016/j.heares.2018.12.012

Vollrath, M. A., Kwan, K. Y., and Corey, D. P. (2007). The micromachinery of mechanotransduction in hair cells. *Annu. Rev. Neurosci.* 30, 339–365. doi:10.1146/annurev.neuro.29.051605.112917

Vorontsova, M. N., Nezlin, L. P., and Meinertzhagen, I. A. (1997). Nervous system of the larva of the ascidian *Molgula citrina* (alder and hancock, 1848). *Acta Zool.* 78, 177–185. doi:10.1111/j.1463-6395.1997.tb01004.x

Wakai, M. K., Nakamura, M. J., Sawai, S., Hotta, K., and Oka, K. (2021). Two-Round Ca2+ transient in papillae by mechanical stimulation induces metamorphosis in the ascidian *Ciona intestinalis* type A. *Proc. Biol. Sci.* 288, 20203207. doi:10.1098/rspb.2020.3207

Waki, K., Imai, K. S., and Satou, Y. (2015). Genetic pathways for differentiation of the peripheral nervous system in ascidians. *Nat. Commun.* 6, 8719. doi:10.1038/ncomms9719

Wang, D., and Zhou, J. (2021). The kinocilia of cochlear hair cells: structures, functions, and diseases. *Front. Cell Dev. Biol.* 9, 715037. doi:10.3389/fcell.2021.715037

Wang, V. Y., Hassan, B. A., Bellen, H. J., and Zoghbi, H. Y. (2002). Drosophila atonal fully rescues the phenotype of Math1 null mice: new functions evolve in new cellular contexts. *Curr. Biol.* 12, 1611–1616. doi:10.1016/s0960-9822(02)01144-2

Wang, X., Llamas, J., Trecek, T., Shi, T., Tao, L., Makmura, W., et al. (2023). SoxC transcription factors shape the epigenetic landscape to establish competence for sensory differentiation in the mammalian organ of Corti. *Proc. Natl. Acad. Sci. U. S. A.* 120, e2301301120. doi:10.1073/pnas.2301301120

Whatley, M., Francis, A., Ng, Z. Y., Khoh, X. E., Atlas, M. D., Dilley, R. J., et al. (2020). Usher syndrome: genetics and molecular links of hearing loss and directions for therapy. *Front. Genet.* 11, 565216. doi:10.3389/fgene.2020.565216

Woo, S.-H., Ranade, S., Weyer, A. D., Dubin, A. E., Baba, Y., Qiu, Z., et al. (2014). Piezo2 is required for Merkel-cell mechanotransduction. *Nature* 509, 622–626. doi:10.1038/nature13251

Wu, D. K., and Kelley, M. W. (2012). Molecular mechanisms of inner ear development. *Cold Spring Harb. Perspect. Biol.* 4, a008409. doi:10.1101/cshperspect.a008409

Wu, S.-R., Butts, J. C., Caudill, M. S., Revelli, J.-P., Dhindsa, R. S., Durham, M. A., et al. (2023). Atoh1 drives the heterogeneity of the pontine nuclei neurons and promotes their differentiation. *Sci. Adv.* 9, eadg1671. doi:10.1126/sciadv.adg1671

Wu, X., Indzhykulian, A. A., Niksch, P. D., Webber, R. M., Garcia-Gonzalez, M., Watnick, T., et al. (2016). Hair-cell mechanotransduction persists in TRP channel knockout mice. *PLoS ONE* 11, e0155577. doi:10.1371/journal.pone.0155577

Wu, Z., Grillet, N., Zhao, B., Cunningham, C., Harkins-Perry, S., Coste, B., et al. (2017). Mechanosensory hair cells express two molecularly distinct mechanotransduction channels. *Nat. Neurosci.* 20, 24–33. doi:10.1038/nn.4449

Xiong, W., Grillet, N., Elledge, H. M., Wagner, T. F. J., Zhao, B., Johnson, K. R., et al. (2012). TMHS is an integral component of the mechanotransduction machinery of cochlear hair cells. *Cell* 151, 1283–1295. doi:10.1016/j.cell.2012.10.041

Yang, H., Xie, X., Deng, M., Chen, X., and Gan, L. (2010). Generation and characterization of Atoh1-Cre knock-in mouse line. *Genesis* 48, 407–413. doi:10.1002/dvg.20633

Yokoyama, T. D., Hotta, K., and Oka, K. (2014). Comprehensive morphological analysis of individual peripheral neuron dendritic arbors in ascidian larvae using the photoconvertible protein Kaede. *Dev. Dyn.* 243, 1362–1373. doi:10.1002/dvdy.24169

Yu, H. V., Tao, L., Llamas, J., Wang, X., Nguyen, J. D., Trecek, T., et al. (2021). POU4F3 pioneer activity enables ATOH1 to drive diverse mechanoreceptor differentiation through a feed-forward epigenetic mechanism. *Proc. Natl. Acad. Sci. U. S. A.* 118, e2105137118. doi:10.1073/pnas.2105137118

Żak, M., and Daudet, N. (2021). A gradient of Wnt activity positions the neurosensory domains of the inner ear. *eLife* 10, e59540. doi:10.7554/eLife.59540

Zeng, F., Wunderer, J., Salvenmoser, W., Hess, M. W., Ladurner, P., and Rothbächer, U. (2019). Papillae revisited and the nature of the adhesive secreting collocytes. *Dev. Biol.* 448, 183–198. doi:10.1016/j.ydbio.2018.11.012

Zhao, B., Wu, Z., Grillet, N., Yan, L., Xiong, W., Harkins-Perry, S., et al. (2014). TMIE is an essential component of the mechanotransduction machinery of cochlear hair cells. *Neuron* 84, 954–967. doi:10.1016/j.neuron.2014.10.041

Zhao, D., Chen, S., Horie, T., Gao, Y., Bao, H., and Liu, X. (2020). Comparison of differentiation gene batteries for migratory mechanosensory neurons across bilaterians. *Evol. Dev.* 22, 438–450. doi:10.1111/ede.12331

frontiers | Frontiers in Ecology and Evolution

TYPE Review
PUBLISHED 18 April 2024
DOI 10.3389/fevo.2024.1378927

OPEN ACCESS

EDITED BY
Paolo Sordino,
Anton Dohrn Zoological Station Naples, Italy

REVIEWED BY
Graziano Fiorito,
Stazione Zoologica Anton Dohrn, Italy
Shunsuke Yaguchi,
University of Tsukuba, Japan

*CORRESPONDENCE
Silvia Mercurio
silvia.mercurio@unimi.it;
sil.mercurio@gmail.com

RECEIVED 30 January 2024
ACCEPTED 05 April 2024
PUBLISHED 18 April 2024

CITATION
Pennati R, Blumer G, Mercurio S and Scarì G (2024) Serotonin system in tunicates: insight from morphological and molecular approaches.
Front. Ecol. Evol. 12:1378927.
doi: 10.3389/fevo.2024.1378927

Serotonin system in tunicates: insight from morphological and molecular approaches

Roberta Pennati[1], Giorgio Blumer[1], Silvia Mercurio[1]* and Giorgio Scarì[2]

[1]Department of Environmental Science and Policy, Università degli Studi di Milano, Milan, Italy, [2]Department of Biosciences, Università degli Studi di Milano, Milan, Italy

Serotonin (5 hydroxytryptamine, 5-HT) is a biogenic amine of ancient origin that is widespread among animals. It plays multiple roles during development and in adults as neurotransmitter at synaptic level and neuro hormone controlling complex behaviors in both vertebrates and invertebrates. Tunicates occupy a key phylogenetic position to understand the evolution of serotonin functions since they are the sister group of vertebrates. The presence of serotonin in tunicates was first reported in adults of the ascidian *Ciona robusta* (formerly *Ciona intestinalis*) in the 1946. Since then, serotonin systems have been in many tunicate species and its functions during embryogenesis and metamorphosis explored. We reviewed the current knowledge about serotonin in these animals first by comparing its presence and localization in larvae and adults of different species. Then, we focused on the model organism *Ciona* for which data regarding sequences and expression patterns of genes involved in serotonin synthesis and function have been reported. Overall, we provided a comprehensive overview of serotonergic machinery in tunicates and gave hints for future studies in this field.

KEYWORDS

neurotransmitter, ascidian, serotonin receptor, serotonin transporter, 5-HT, development

Introduction

Serotonin [5-hydroxytryptamine (5-HT)] is a biogenic amine of ancient origin that dates back at least 600 million years. It can be found in various unicellular eukaryotes and nearly all metazoans. Its origin clearly predates the emergence of a centralized nervous system, playing a key role in chemotaxis and chemo-signaling in unicellular organisms and functioning as intracellular regulator in multicellular animals (Greczek-Stachura, 2002; Azmitia, 2007; Nichols and Nichols, 2008; Berger et al., 2009; Lv and Liu, 2017). Very early in evolution, 5-HT acquired the additional function as a morphogenetic factor, controlling the proliferation and differentiation of various cell types, including those of the enteric

nervous system (Fiorica-Howells et al., 2000; Azmitia, 2001; Najjar et al., 2023). Its morphogenetic role is also prominent during animal development. In sea urchin and *Drosophila*, 5-HT is involved in early embryogenesis, acting as modulator of gastrulation (Colas et al., 1995; Buznikov et al., 2005). In mammalian and avian development, 5-HT regulates cardiac morphogenesis and neural crest cell migration (Yavarone et al., 1993a, 1993b; Moiseiwitsch and Lauder, 1995; Choi et al., 1997; Neumann et al., 2023).

Later, while maintaining this variety of developmental roles, 5-HT also began to function as neuromodulator. In many invertebrates, 5-HT neurons are primary sensory neurons modulating food intake, defense and locomotor behavior. 5-HT-synthetizing cells are involved in defense mechanisms in both cnidarians and insects (Horen, 1972; Weiger, 1997); in leech and in sea urchin they regulate swimming activity (Kristan and Nusbaum, 1982; Yaguchi and Katow, 2003) while in lobsters they control complex social behavior (Kravitz, 2000). In vertebrates, 5-HT role as modulator of sleep, mood, appetite, and temperature is also well-known (Azmitia, 2007).

5-HT neurons and their organization are completely different among animals reaching the higher complexity in vertebrates. Heterogeneity of 5-HT neurons concerns both their number, varying from hundreds in mollusks to several thousands in mammals, and their localization. In invertebrates, serotonergic system is often associated with sensory organs, and different type of neurotransmission have been described (Bacqué-Cazenave et al., 2020). In humans, 5-HT producing cells are found in brainstem, in the enteric nervous system and in mast cells and modulate the activity of a variety of other neurons or even of the entire neural circuits (Azmitia, 2007).

Tunicates have been recognized as the sister group of vertebrates (Delsuc et al., 2006). Along with cephalochordates and vertebrates, they form the group of chordates, whose common body plan is clearly demonstrated by their larvae. Tunicate larva consists of a trunk that houses the rudiments of the digestive tract and the anterior part of the central nervous system (CNS), and a locomotory tail flanked by muscle cells. The tail contains the neural tube running dorsally to the chord, which is an apomorphy of the chordate clade. The swimming larva undergoes a deep metamorphosis that transforms it, in most cases, into a sessile adult. Additionally, several tunicates exhibit a colonial lifestyle, making them the only chordates to have evolved this particular way of life. As a result, these animals possess a combination of both conserved and derived traits, with the formers mainly displayed by the larva, the latter mainly found in the adult form (Lemaire, 2011).

Traditionally tunicates include three classes, the pelagic appendicularians and thaliaceans and the sessile ascidians, with the last encompassing three orders: Aplousobranchia, Phlebobranchia and Stolidobranchia, identified mainly by gill features. Recent phylogenetic analysis has revisited the phylogeny of tunicates, revealing that the traditionally recognized ascidian group is indeed paraphyletic, with the thaliaceans being the sister group of Aplousobranchia plus Phlebobranchia (Delsuc et al., 2018; Kocot et al., 2018). For the aims of this review, we used the term "ascidian" to indicate a sessile species and maintained the traditional subdivisions for comparative purposes, being well aware that thaliaceans are derived and nested in the ascidian group.

Considering tunicate peculiar features and their key evolutionary position, 5-HT role and localization have been explored in different species, applying both morphological and molecular approaches. The evolution of this ancient and widespread monoamine represents indeed an intriguing topic with still many unsolved questions. Defining its role in tunicates may thus contribute to unveil which aspects are conserved and which are unique to this group.

In this review, we thoroughly examined the existing literature of 5-HT in tunicates to gather information and provide a comprehensive overview of its localization in both larvae and adults. We focused on *Ciona robusta* and *Ciona intestinalis* (from here on *Ciona*) (Brunetti et al., 2015; Pennati et al., 2015), well-established ascidian model systems in many research fields (Dehal et al., 2002; Satoh, 2013; Mercurio et al., 2019a, 2021). Our aim was to identify both novel and conserved features in comparison to phylogenetically related organisms. Furthermore, we documented the current knowledge regarding the genes involved in the synthesis and functioning of 5-HT, as well as the functional characterization of the serotonergic system.

Localization in ascidian larvae

5-HT localization by immunohistochemistry proved to be quite challenging in ascidian larvae, likely due to the low levels of this molecule. In fact, in *Ciona*, even if localization in larvae by means of anti 5-HT antibodies failed, 5-HT was detected by fluorometry after HPLC from early embryonic stages. In the egg, the reported concentration was 3.5 ± 2.9 fmoles/individual, and fell to 1.8 ± 1.5 fmoles/individual in the larva and the authors suggested a maternal origin of 5-HT throughout embryogenesis even if they did not investigate any enzyme expressions or activities (Razy-Krajka et al., 2012). 5-HT concentration increased again in the post-metamorphic stages and these findings align with De Bernardi's study, which reported 5-HT immunolocalization in the *Ciona* visceral ganglion only in individuals at the onset of metamorphosis (De Bernardi et al., 2006). To partially overcome this obstacle and clearly visualize at least the 5-HT-accumulating cells, larvae were treated with exogenous 5-HT before immunostaining experiments. In this condition, 5-HT positive cells were easily observed in the dopaminergic neurons of the ventral sensory vesicle, further suggesting that results were affected by the low sensitivity of the technique (Razy-Krajka et al., 2012).

Staining experiments with antibodies against 5-HT in the larvae of *Eudistoma olivaceum* (Clavelinidae), *Aplidium stellatum* (Polyclinidae), and *Didemnum candidum* (Didemnidae) yielded similar negative results. Conversely, immunohistochemistry analysis reported the presence of a 5-HT-like signal in 20 neural cells of the *Herdmania momus* (Stolidobranchia) and several of these neurons showed fibers projecting posteriorly forming a distinct network. 5-HT immunostaining signal close to the sensory vesicle was reported also in other Stolidobranchia larvae, such as *Microcosmus exasperatus* (Pyuridae), *Styela plicata*

(Styelidae), and *Molgula occidentalis* (Molgulidae), and in the larva of the Phlebobranchia *Ascidia interrupta* (Stach, 2005). In *Styela plicata* larva, De Bernardi and colleagues detected 5-HT in some cells of the sensory vesicle surrounding the single sensory organ, the photolith, and in the adhesive papillae. Similarly, in the larva of *Microcosmus vulgaris* (Pyuridae) 5-HT was found in a few cells close to the gravity sensing otolith (De Bernardi et al., 2006). In *Phallusia mammillata* swimming larvae, 5-HT was detected in the sensory vesicle, adhesive papillae, epidermal trunk neurons, and epidermal tail neurons (Pennati et al., 2001) while in the larvae of *Botrylloides leachi* (Aplousobranchia), 5-HT signal was observed only in peripheral neurons of the papillae (Pennati et al., 2007b).

The larvae of Aplousobranchia species often exhibit partially differentiated adult tracts and organs, a phenomenon known as adultation (Jeffery and Swalla, 1992). In the larvae of these species, 5-HT could be detected both in larval typical organs and in differentiating adult ones. In the *Clavelina oblunga* (Aplouosobranchia) 5-HT immunoreactivity was found in cells close to the statocyte complex, a larval organ, and in the branchial basket, an adult organ (Stach, 2005). Similar findings were observed in *C. lepadiformis* and *C. phlegraea* where 5-HT was immunolocalized in same adult territories as in *C. oblunga* and in few marginal neurons of the adhesive papillae (Pennati et al., 2009).

The larva of *Diplosoma listenarium* revealed serotonin in several neurons of the complex papillae and in the posterior region of the cerebral vesicle, while differentiating zooids display adult-like localization (De Bernardi et al., 2006). Although 5-HT levels can vary among species, its presence remains widespread in tunicate nervous system and often associated with larval sensory activity. Moreover, the presence of serotonergic neurons in the adhesive papillae is a recurrent feature in most of the analyzed ascidian species. It has been suggested that 5-HT release by these neurons may play a role in the signaling cascade that triggers metamorphosis (Pennati and Rothbächer, 2015).

Localization in ascidian adults

Erspamer (1946) was the first to report the presence of 5-HT in adult tunicates. Since then, 5-HT has been found in adults of a variety of solitary ascidian including *Ciona intestinalis*, *Ascidiella aspersa*, *Ascidia mentula*, *Styela plicata*, and *Phallusia mammillata* (Erspamer, 1946; Welsh and Loveland, 1968; Pestarino, 1982; Sakharov and Salimova, 1982; Georges, 1985). More recently, immunolocalization experiments confirmed these results. In adults of *Ciona*, 5-HT containing cells were reported in the pharyngeal bands, in the esophagus and in the stomach; some of them were also aligned in a band extending from the peripharyngeal band of the branchial basket to the endostyle (Braun and Stach, 2016). In juvenile of *P. mammillata*, 5-HT-positive cells were found in the peripharyngeal band, in the gut and two bilaterally symmetric rows of cells between bands 7 and 8 of the endostyle (Pennati et al., 2001). This area also contains cells capable of fixing iodine (Nilsson et al., 1988) and calcitonin-like cells (Thorndyke and Probert, 1979). A similar localization pattern was also observed in adults of other ascidian species: *Clavelina lepadiformis Diplosoma listerianum*, *Ascidiella scabra*, *Perophora japonica* (Braun and Stach, 2016), *Corella parallelogramma* (Nilsson et al., 1988; Braun and Stach, 2016), *Botryllus schlosseri* (Tiozzo et al., 2009; Braun and Stach, 2016). Moreover, in the model organism *B. schlosseri*, 5-HT–positive cells were found in the buds during blastogenic development starting from early stages of bud differentiation, suggesting that 5-HT may play a role in controlling the morphogenetic processes (Tiozzo et al., 2009) (Figure 1).

It has been proposed that 5-HT occurrence in the pharyngeal bands of the branchial basket of these filter feeder animals may serve to control mucus secretion and ciliary beating (Braun and Stach, 2016). In fact, the branchial basket is bordered by a ciliated epithelium and covered by mucus secreted by the endostyle. A role of 5-HT in ciliary beating control was also reported in several invertebrates as well as in numerous larval forms (Hay-Schmidt, 2000). As an alternative hypothesis, serotonin in peripharingeal band may serves in mechanosensory neurons (Valero-Gracia et al., 2016).

The tunicate endostyle is a ventral organ made by folds of the branchial basket epithelium that displays five/nine zones of specialized cells, comprising supporting and glandular cells and cells with iodinating capacity. Serotonin positive cells of the endostyle are innervated by the subendostylar nerve (Braun and Stach, 2016). The endostyle is considered homologous to the vertebrate thyroids due to its capability to produce iodinated molecules (Godeaux, 1989). Interestingly, 5-HT is also found in the parafollicular cells of the thyroid, further supporting the hypothesis of homology between the two organs (Barasch et al., 1987).

In vertebrates, it is known that 95% of the 5-HT is produced in the intestine (Banskota et al., 2019). Actually, this was first noted by Erspamer who discovered “enteramine” in gastrointestinal in a rabbit (Erspamer and Asero, 1952). Intestinal 5-HT has been found to modulate various aspects of intestinal function, including enteric nervous system development, motility, secretion, inflammation, sensation, and epithelial development (Banskota et al., 2019; Najjar et al., 2023).

Based on the detailed morphological description provided by Burighel and Milanesi, the serotonergic cells described in the digestive system of ascidians may be identified as endocrine cells (Burighel and Milanesi, 1975), and considered homolog to the vertebrate enterochromaffin cells (Gershon, 2004). 5-HT-positive cells are also present in the enteric system of cephalochordates (Candiani et al., 2001) but not in hemichordates or echinoderms (Strano et al., 2019; Mercurio et al., 2019b), suggesting that enteric 5-HT may be a novel feature of chordate evolution.

Noteworthy, in all the analyzed species, 5-HT was not detected in the neural ganglion of the adults. It has been proposed that, after metamorphosis, which leads to a reduction of the sense organs and a sessile life style, the function of 5-HT as a neurotransmitter in the CNS were reduced and could even disappear altogether (Braun and Stach, 2018).

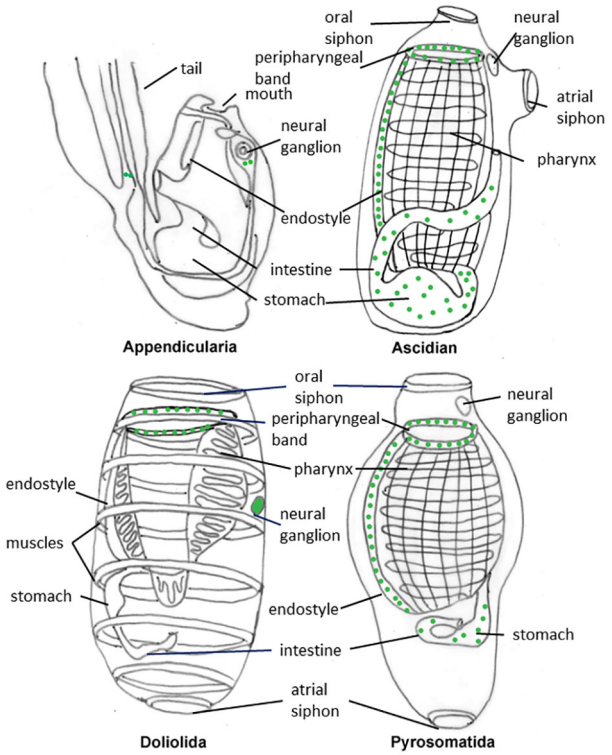

FIGURE 1
Schematic representation of the distribution pattern of serotonin positive cells (green dots) in adults of representative tunicates.

Localization in other tunicates

Tunicates also include free-living thaliaceans encompassing three clades, Doliolida, Salpida and Pyrosomatida, of holoplanktonic organisms with diverse and complex life cycles. Doliolida and Salpida present two different forms, the blastozooid generation, which is produced through asexual reproduction, and the oozooid generation, which is derived from zygote development. Pysosomatida are colonial animals with direct development.

5-HT-positive cells have been reported in many thaliacean species: *Thalia democratica* (Pennati et al., 2012; Braun and Stach, 2016, 2018; Valero-Gracia et al., 2016); *Doliolum nationalis* (Stach, 2005; Braun and Stach, 2018); *Pyrosomella verticillata* (Valero-Gracia et al., 2016; Braun and Stach, 2018), *Salpa fusiformis*, *Iasis cylindrical*, *Pyrosoma atlanticum*, *Pyrostremma agassizi* (Braun and Stach, 2018); *Doliolina muelleri* and *Ihlea punctate* (Valero-Gracia et al., 2016) (Figure 1).

In Salpida and Doliolida species, similar to adult ascidians, serotonergic cells were found in the peripharyngeal band of the digestive tract. However, unlike ascidians, 5-HT immunolabelling was not detected in the endostyle but was instead present in the cerebral ganglion. It has been proposed that the absence of 5-HT in the endostyle of salpids and doliolids could be a character associated with changes in the control of thyroid hormone production (Valero-Gracia et al., 2016). In Pyrosomatida, 5-HT localization appears more comparable to that of adult ascidians: in *Pyrosoma agassizi*, for example, 5-HT-positive cells were found in the peripharyngeal band, endostyle, and intestine, but not in the central nervous system (Braun and Stach, 2018). As Pyrosomatida are basal thaliaceans (Delsuc et al., 2018; Kocot et al., 2018), they may have retained plesiomorphyc characters from their sessile ancestor. It has been proposed that serotonergic neurons might have a locomotory function by controlling body muscles that have been lost in sessile ascidians and retained or re-acquired in free living thaliaceans. 5-HT absence in the CNS of planktonic pyrosomes could be attributed to their reliance on water flow generated by ciliary beating, rather than muscle movement, for locomotion (Braun and Stach, 2018).

Since the complex life cycles of salps and doliolids, the pattern of distribution of 5-HT-containing cells can differ between oozooid and blastozooid stages (Braun and Stach, 2018). In salps, fertilization occurs internally and the zygote develops inside the blastozooid, in close contact with maternal tissues where a placenta forms. 5-HT immunolocalization has been observed in placenta of *T. democratica* (Pennati et al., 2012), but, as viviparity is a derived tract in salps, serotonin presence in the placenta should be considered a derived tract not inherited by the common ancestor of tunicates. Interestingly, 5-HT and its receptors has also been reported in the mammalian placenta, where they are believed to play a role not only in placental development and pregnancy maintenance, but also in fetal development (Yavarone et al., 1993a; Huang et al., 1998). This should be considered a homoplasy, most probably due to a conserved and ancient role of serotonin in embryos development.

In the case of appendicularians, the third and most basal group of tunicates, only two cells in the posterior part of the neural ganglion of *Oikopleura fusiformis* show positive staining against 5-HT antibodies (Stach, 2005), while no 5-HT-like signal has been detected in *Oikopleura dioica* (Braun and Stach, 2016).

A complete overview of serotonin localization in tunicates is provided in Table 1.

The serotonin machinery

5-HT synthesis pathway involved two fundamental enzymes: tryptophan hydroxylase (TPH) and 5-hydroxytryptophan decarboxylase, an aromatic amino acid decarboxylase (AADC). Moreover, 5-HT concentration in extracellular fluid is regulated by selective membrane serotonin transporter (SERT) and 5-HT can be further transported into storage vesicles via a vesicular mono amine transporter (VMAT). The molecular machinery of serotonin system has been extensively studied in *Ciona*.

TPH is the rate limiting enzyme in the biosynthesis of serotonin and is considered a good marker of serotonergic neurons (Goridis and Rohrer, 2002). In the genome of *Ciona* a single gene coding for a TPH (*Ci-TPH*) is present and its sequence shares a high similarity level with those of vertebrates' ones (Pennati et al., 2007a). In posterior larval trunk, *Ci-TPH* expression is restricted to a few cells grouped into two distinct clusters (Pennati et al., 2007a; Razy-Krajka et al., 2012) and in posterior muscle cells of the tail (Pennati et al., 2007a). One gene encoding a vesicular monoamine transporter (*Ci-VMAT*) is expressed specifically in the TPH domain of the trunk (Razy-Krajka et al., 2012).

10.3389/fevo.2024.1378927

TABLE 1 Distribution of serotonin in diverse tunicate species based on current literature.

class, order	family	species	stage	localization	method	reference
appendicularia, copelata	oikopleuridae	*Oikopleura fusiformis*	juvenile, adult	cerebral ganglion	immunohist	Stach, 2005
appendicularia, copelata	oikopleuridae	*Oikopleura dioica*	adult	not detected	immunohist	Braun and Stach, 2016
appendicularia, copelata	oikopleuridae	*Oikopleura rufescens*	adult	not detected	immunohist	Stach, 2005
appendicularia, copelata	oikopleuridae	*Fritillaria sp*	adult	not detected	immunohist	Stach, 2005
ascidiacea, aplousobranchia	polyclinidae	*Aplidium constellatum*	larva	non detected	immunohist	Stach, 2005
ascidiacea, aplousobranchia	styelidae	*Botrylloides leachi*	larva	peripheral neurons of the papillae	immunohist	Pennati et al., 2007b
ascidiacea, aplousobranchia	styelidae	*Botryllus schlosseri*	adult	peripharyngeal band, endostyle, esophagus, stomach, intestine, buds	immunohist	Tiozzo et al., 2009; Braun and Stach, 2016
ascidiacea, aplousobranchia	clavelinidae	*Clavelina lepadiformis*	larva	statocyte complex, branchial basket, adhesive papillae	immunohist	Pennati et al., 2009
ascidiacea, aplousobranchia	clavelinidae	*Clavelina lepadiformis*	adult	peripharyngeal band, endostyle, esophagus, stomach, intestine	immunohist	Braun and Stach, 2016
ascidiacea, aplousobranchia	clavelinidae	*Clavelina oblunga*	larva	statocyte complex, two cells next to sensory vesicles, branchial basket	immunohist	Stach, 2005
ascidiacea, aplousobranchia	clavelinidae	*Clavelina phlegraea*	larva	statocyte complex, the branchial basket, adhesive papillae	immunohist.	Pennati et al., 2009
ascidiacea, aplousobranchia	didemnidae	*Didemnum candidum*	larva	non detected	immunohist.	Stach, 2005
ascidiacea, aplousobranchia	didemnidae	*Diplosoma listenarium*	larva	neurons of the papillae, CNS, developing adult organs	immunohist.	De Bernardi et al., 2006
ascidiacea, aplousobranchia	didemnidae	*Diplosoma listerianum*	adult	peripharyngeal band, endostyle, stomach,	immunohist.	Braun and Stach, 2016
ascidiacea, aplousobranchia	polycitoridae	*Eudistoma olivaceum*	larva	non detected	immunohist.	Stach, 2005
ascidiacea, phlebobranchia	ascidiidae	*Ascidia interrupta*	larva	CNS	immunohist.	Stach, 2005
ascidiacea, phlebobranchia	ascidiidae	*Ascidia mentula*	adult	intestine	histochem., immunohist.	Erspamer, 1946
ascidiacea, phlebobranchia	ascidiidae	*Ascidiella aspersa*	adult	intestine	histochem.	Erspamer, 1946
ascidiacea, phlebobranchia	ascidiidae	*Ascidiella scabra*	adult	peripharyngeal band, endostyle, esophagus, stomach, intestine	immunohist.	Braun and Stach, 2016
ascidiacea, phlebobranchia	cionidae	*Ciona intestinalis*	egg, embryos, post-metamorphic stages	not specified	fluorometry after HPLC	Razy-Krajka et al., 2012
ascidiacea, phlebobranchia	cionidae	*Ciona intestinalis*	pre-metamorphic larva	viscerall ganglion	immunohist.	De Bernardi et al., 2006
ascidiacea, phlebobranchia	cionidae	*Ciona intestinalis*	adult	peripharyngeal band, endostyle, esophagus, stomach, intestine	histochem., immunohist.	Erspamer, 1946; Welsh and Loveland, 1968; Braun and Stach, 2016
ascidiacea, phlebobranchia	corellidae	*Corella parallelogramma*	adult	peripharyngeal band, endostyle, esophagus, stomach,	immunohist.	Nilsson et al., 1988; Braun and Stach, 2016

(Continued)

TABLE 1 Continued

class, order	family	species	stage	localization	method	reference
ascidiacea, phlebobranchia	perphoridae	*Perophora japonica*	adult	peripharyngeal band, endostyle, esophagus, stomach, intestine	immunohist.	Braun and Stach, 2016
ascidiacea, phlebobranchia	ascidiidae	*Phallusia mammillata*	larva	sensory vesicle, adhesive papillae, epidermal trunk neurons, and epidermal tail neurons	immunohist.	Pennati et al., 2001
ascidiacea, phlebobranchia	ascidiidae	*Phallusia mammillata*	adult	peripharyngeal band, endostyle, stomach, intestine	immunohist.	Pennati et al., 2001
ascidiacea, stolidobranchia	pyuridae	*Herdmania momus*	larva	CNS cells and fibers	immunohist.	Stach, 2005
ascidiacea, stolidobranchia	pyuridae	*Microcosmus exasperatus*	larva	CNS	immunohist.	Stach, 2005
ascidiacea, stolidobranchia	molgulidae	*Molgula occidentalis*	larva	CNS	immunohist.	Stach, 2005
ascidiacea, stolidobranchia	styelidae	*Styela plicata*	adult	esophagus, stomach and intestine	immunohist.	Pestarino, 1982
ascidiacea, stolidobranchia	styelidae	*Styela plicata*	larva	CNS, adhesive papillae	immunohist.	Stach, 2005; De Bernardi et al., 2006
thaliacea, doliolida	doliolidae	*Doliolum nationalis*	oozooid and blastozooid	dorsal ganglion, ciliated funnel, intestinal tract	immunohist.	Stach, 2005; Braun and Stach, 2018
thaliacea, doliolida	doliolidae	*Doliolina muelleri*	phorozooid	cerebral ganglion, ciliated funnel, esophagus	immunohist.	Valero-Gracia et al., 2016
thaliacea, doliolida	doliolidae	*Doliolina muelleri*	larva	not detected	immunohist.	Valero-Gracia et al., 2016
thaliacea, pyrosomatida	pyrosomatidae	*Pyrosoma atlanticum*	adult zooid	peripharyngeal band, endostyle, esophagus	immunohist.	Braun and Stach, 2018
thaliacea, pyrosomatida	pyrosomatidae	*Pyrosomella verticillata*	adult zooid	peripharyngeal band, endostyle, esophagus, buds	immunohist.	Valero-Gracia et al., 2016; Braun and Stach, 2018
thaliacea, pyrosomatida	pyrosomatidae	*Pyrostremma agassizi*	adult zooid	peripharyngeal band, endostyle, esophagus	immunohist.	Braun and Stach, 2018
thaliacea, salpida	salpidae	*Iasis cylindrical*	oozoid	cerebral ganglion, peripharyngeal band, esophagus	immunohist.	Braun and Stach, 2018
thaliacea, salpida	salpidae	*Ihlea punctata*	oozooid	cerebral ganglio, peripharyngeal band, esophagus	immunohist.	Valero-Gracia et al., 2016
thaliacea, salpida	salpidae	*Salpa fusiformis*	oozooid and blastozooid	cerebral ganglion, peripharyngeal band, esophagus	immunohist.	Braun and Stach, 2018
thaliacea, salpida	salpidae	*Thalia democratica*	oozoid and blastozooid	cerebral ganglion, peripharyngeal band, esophagus, intestine, placenta	immunohist.	Braun and Stach, 2016, 2018; Pennati et al., 2012; Valero-Gracia et al., 2016

Serotonin transporters (SERTs) are plasma membrane transporters involved in neurotransmitter re-uptake. They are Na^+-dependent transporters belonging to the solute-linked carrier family 6 (SLC6) of membrane co-transporters. *SERTs* are present in the genomes of practically all Metazoa (Caveney et al., 2006). In *Ciona*, *Ci-SERT* transcripts were detected in the territory of *Ci-Tyrosine hydroxylase*, the gene coding for the rate-limiting enzyme of dopamine, but not in the *Ci-TPH* domains of the tail-bud embryos and larvae. It has been proposed that 5-HT could be stored together with dopamine in the *Ci-TH*-expressing cells of the sensory vesicle, a property shared by some vertebrate amacrine cells of the retina. Although there is no evidence that *TPH*-positive cells express any of the two genes encoding aromatic amino acid decarboxylase (*Ci-AADC*) described in *Ciona*, in both *TPH* and *TH* domains the transcripts of GTP cyclohydrolase I (*Ci-GCH*) are present. This latter is the enzyme responsible for the synthesis of tetrahydrobiopterin, an essential cofactor of serotonin and dopamine synthesis (Razy-Krajka et al., 2012). The absence of recognized *AADC* genes expression in TPH positive cells needs to be further investigated, also exploring the possibility of a maternal origin of the protein. Interestingly, *TPH* expression in *Ciona* adults indicates that serotonergic neurons are present also in the tentacle of coronal cells in the oral siphon, considered homologous to vertebrate hair cells (Rigon et al., 2018).

5-HT exerts its function by binding to different types of receptors that in human have been classified into seven families (5HT 1-7) (Pytliak et al., 2011). With the exception of 5HTR3s, that are ligand-gated ion channels, all the other serotonin receptors (5HTRs) are G-protein coupled receptors.

In the genome of *Ciona*, five genes corresponding to serotonin receptors have been identified (Mercurio et al., 2023). The phylogenetic analysis showed that two sequences, *5HT1.1* and *5HT1.2*, are basal to all *5HT1* paralogs of vertebrates. One sequence is ortholog to *5HT2* and has five protein isoforms, one is an ortholog of *5HT7s*, and the last one, *5HT-like*, is highly divergent and basal to all G-coupled *5HT* classes. In *Ciona savigny*, the coding region of *5-HT2* is included in the largest intron of the *Psmd1-like* gene that encodes the non-ATP regulatory subunit 1 (*RPN2*) of the 26S proteasome. The 26S proteasome is a highly conserved multicatalytic protease from yeast to mammals, which functions to degrade proteins following ubiquitination. None of the other 5-HT receptor genes show a similar genomic localization while this organization is shared with the *5-HT2B* gene of all mammals, that are encoded in a large intron of the proteasome *Psmd1* too (Moutkine et al., 2019). Interestingly, it was suggested that this genomic arrangement may outcome in a conserved co-regulatory relationship (Assis et al., 2008).

During development, by *in situ* hybridization, it was possible to identify the territories of expression of four out of the five identified *5HTRs*, with the exception of *Ci-5HT2*. All analyzed genes showed an early expression starting from early gastrula. *Ci-5HT-like* transcripts were identified with strong signal mainly in territories of presumptive nervous system, in precursors of the anterior sensory vesicle and pigment cells, in cells that will contribute to form larval visceral ganglion and in posterior precursors of the bipolar tail neurons. The other identified *Ci-5HTR* genes showed a broader expression, mainly in mesenchyme cells with a sharp anterior limit of expression. *Ci-5HT7* expression was observed in cells of the anterior most row of neural plate progenitors including palp neuron progenitors. The expression of all genes decreased or were no longer detectable at larva stage (Mercurio et al., 2023). Importantly, all the *Ci-5HTRs* were expressed in some territories of CNS lineage, suggesting their contribution in neural development, as reported in vertebrates (Romero-Reyes et al., 2021).

Functional evidence

5-HT is a multifaceted molecule that plays many diverse roles (Berger et al., 2009). Its functions in tunicates are still largely to be elucidated. Some hints come from pharmacological inhibition/stimulation of its receptors and transporter (Pennati et al., 2001, 2003; Mercurio et al., 2023). 5-HT involvement in ascidian embryogenesis has been suggested by the early expression of *5HTRs* genes in *Ciona*, and it was confirmed by treatments with 5-HT active drugs. *P. mammillata* larvae developed by embryos exposed at gastrula stage to Ritanserin, a selective 5HT2 antagonist, showed a roundish head and flat papillae. Juveniles exposed to the same drug had an enlarged heart with blood cells accumulating in it (Pennati et al., 2001). Interestingly, in mouse embryos exposure to Ritanserin induced morphological defects in the head, neural tube and heart, probably by preventing the differentiation of cranial neural crest cells and myocardial precursor cells (Choi et al., 1997). Exposure WAY-100635, an antagonist of 5-HT1 receptors, caused an impairment on anterior trunk with malformed palps and a curved tail both in *P. mammillata* and *Ciona* larvae (Pennati et al., 2001; Mercurio et al., 2023). In treated *Ciona* embryos, the expression of *Ci-Pou IV*, a specific marker of sensory neurons, indicated that the deactivation of 5HTRs disrupted the development of neurons of palps and tail. Is has been suggested that the lack of most of the sensory neurons detected in WAY-100635-treated embryos could be related to drug interference with the complex interactions between diffusible molecules involved in sensory neuron specification such as retinoic acid, FGF/MAPK signal, and the Wnt pathway (Mercurio et al., 2023). Moreover, larvae exposed to WAY-100635 showed a reduction of pigment in otolith and ocellus, the sensory organs of the sensory vesicle. The pigment organs were recognizable by their shape but melanin content was drastically reduced (Pennati et al., 2003; Mercurio et al., 2023). It was demonstrated that WAY- 100635 treated embryos displayed a drastic decrease in expression of *Ci-Tcf*. This gene is specifically expressed in the precursor cells of the ocellus and otolith and its perturbation led to larval sensory organs being only partially melanized, suggesting a role in pigment cell terminal differentiation (Squarzoni et al., 2011). 5-HT involvement in melanin synthesis has been reported in different animals. Disrupting the serotonin synthesis impaired pigment synthesis in eyes of Platyhelminthes (Lambrus et al., 2015). Stress conditions and alterations of 5-HT levels can reduce the production of melanin in humans as in mouse. Agonists of 5-HT_{1A} and 5-HT_{1B} receptors proved to be efficient at restoring pigmentation (Wu et al., 2014). In zebrafish, fluoxetine, a selective inhibitor of serotonin reuptake, increases melanin synthesis via 5-HT_{1A} receptor (Liu et al., 2019).

Fluoxetine is a selective blocker of SERT that generate an increase in extracellular 5-HT. In *Ciona* larvae, exposure to Fluoxetine reduced spontaneous swimming and the shadow response that is a light-triggered bout of high-speed swimming. It was suggested that the DA-synthesizing/5-HT accumulating cells of the ascidian sensory vesicle play a role in controlling the swimming behavior in response to light, strengthening the hypothesis of their homology with the amacrine cells of vertebrates (Razy-Krajka et al., 2012). The function of 5-HT in modulating swimming behavior is further supported by *Ci-TPH* expression in some *Ciona* muscle cells of the larval tail, probably at neuro-muscular junctions, suggesting that 5-HT may regulates the left-right alternate tail contractions during larval swimming (Pennati et al., 2007a).

The blocking of SERT have effects also on ascidian metamorphosis. Larvae of *P. mammillata* exposed to Fluoxetine exhibited an early onset of metamorphosis. A similar stimulating effect was obtained exposing competent larvae to an agonist of 5-HT_1 receptor, 8-OH-DPAT. Conversely, 5-HT depletion, by means of antagonists and by antibody incubation, delayed tail resorption and the onset of metamorphosis. Therefore, it is likely that 5-HT plays a key role in the mechanism triggering metamorphosis in *P. mammillata* larvae (Pennati et al., 2001). 5-HT role in modulating the metamorphosis has been assessed in many different pelagic

larvae of marine animals such as barnacles, cnidarians and mollusks (Barlow and Truman, 1992; Couper and Leise, 1996; McCauley, 1997; Zega et al., 2007a, 2007b), suggesting that this could be a conserved and probably ancient role of 5-HT (Zega et al., 2007b).

Discussion

Serotonin is an ancient molecule that plays crucial roles in tunicates. Due to their phylogenetic position, tunicates are pivotal in understanding at least part of the evolutionary history of this eclectic molecule. They preserved some ancient 5-HT roles, such as control of ciliary beating and locomotion coordination, which are also evident in cnidarians (Mayorova and Kosevich, 2013) and the larvae of various invertebrates (Hay-Schmidt, 2000). 5-HT roles as neurotransmitter, in morphogenesis and melanogenesis, are likely to be ancient ones since they have been described also in platyhelminthes (Lambrus et al., 2015). Conversely, the presence of 5-HT positive cells in the intestine in tunicates (Pennati et al., 2001; Tiozzo et al., 2009; Braun and Stach, 2016, 2018), cephalochordates (Candiani et al., 2001) and vertebrates (Gershon, 2004) could be a chordate specific novelty, since it has never been described in other groups (Strano et al., 2019; Mercurio et al., 2019b). Within the tunicate clade, several events of loss and gain of function might have occurred in relation to the evolution of different life cycles. Some of these functions have been probably lost in appendicularians, the clade for which many details are still in need of exploration. Swimming larvae of sessile forms use 5-HT to control locomotion in response to perception of light stimuli and keep 5-HT role in controlling the timing of metamorphosis. Adults of these sessile forms might have lost 5-HT in CNS consequently to loss of locomotion control. Presence of serotonergic neurons in CNS were regained in doliolids and salps that derive from sessile forms but that have reconquered a pelagic life style, with locomotion driven by muscle contractions. An alternative less parsimonious scenario presumes that Stolidobranchia and the clade of Phlebobranchia plus Aplousobranchia have lost 5-HT in adult CNS independently and the sessile ancestor of Doliolida and Salpida retained it as a plesiomorphic character. The absence of 5-HT containing cells in the endostyle of salps and doliolids compared to pyrosomes may result from a secondary loss of serotonin control over ciliary beating and mucus secretion, as suggested by Valero-Gracia et al. (2016).

Overall, the multifaceted roles of 5-HT in tunicates underscore its importance and versatility, prompting further questions about its evolutionary journey. Despite significant advancements, many aspects remain unresolved with functional studies often fragmentary and focused on a few ascidian species. Moreover, molecular characterization of the serotonergic system has only been accomplished in *Ciona*. Future research should aim to fill these knowledge gaps and better delineate the specific roles of 5-HT in these animals, thus providing valuable insight into its conserved functions and lineage-specific traits.

Author contributions

RP: Conceptualization, Writing – original draft. GB: Data curation, Writing – review & editing. SM: Conceptualization, Supervision, Writing – review & editing. GS: Resources, Supervision, Writing – review & editing.

Funding

The author(s) declare that no financial support was received for the research, authorship, and/or publication of this article.

Acknowledgments

The authors acknowledge the support of the APC central fund of the University of Milan.

Conflict of interest

The authors declare that the research was conducted in the absence of any commercial or financial relationships that could be construed as a potential conflict of interest.

Publisher's note

References

Assis, R., Kondrashov, A. S., Koonin, E. V., and Kondrashov, F. A. (2008). Nested genes and increasing organizational complexity of metazoan genomes. *Trends Genet.* 24, 475–478. doi: 10.1016/j.tig.2008.08.003

Azmitia, E. C. (2001). Modern views on an ancient chemical: serotonin effects on cell proliferation, maturation, and apoptosis. *Brain Res. Bull.* 56, 413–424. doi: 10.1016/S0361-9230(01)00614-1

Azmitia, E. C. (2007). Serotonin and brain: evolution, neuroplasticity, and homeostasis. *Int. Rev. Neurobiol.* 77, 31–56. doi: 10.1016/S0074-7742(06)77002-7

Bacqué-Cazenave, J., Bharatiya, R., Barrière, G., Delbecque, J.-P., Bouguiyoud, N., Di Giovanni, G., et al. (2020). Serotonin in animal cognition and behavior. *Int. J. Mol. Sci.* 21, 1649. doi: 10.3390/ijms21051649

Banskota, S., Ghia, J.-E., and Khan, W. I. (2019). Serotonin in the gut: blessing or a curse. *Biochimie* 161, 56–64. doi: 10.1016/j.biochi.2018.06.008

Barasch, J. M., Tamir, H., Nunez, E. A., and Gershon, M. D. (1987). Serotonin-storing secretory granules from thyroid parafollicular cells. *J. Neurosci.* 7, 4017–4033. doi: 10.1523/JNEUROSCI.07-12-04017.1987

Barlow, L. A., and Truman, J. W. (1992). Patterns of serotonin and SCP immunoreactivity during metamorphosis of the nervous system of the red abalone, *Haliotis rufescens*. *J. Neurobiol.* 23, 829–844. doi: 10.1002/neu.480230705

Berger, M., Gray, J. A., and Roth, B. L. (2009). The expanded biology of serotonin. *Annu. Rev. Med.* 60, 355–366. doi: 10.1146/annurev.med.60.042307.110802

Braun, K., and Stach, T. (2016). Comparative study of serotonin-like immunoreactivity in the branchial basket, digestive tract, and nervous system in tunicates. *Zoomorphology* 135, 351–366. doi: 10.1007/s00435-016-0317-8

Braun, K., and Stach, T. (2018). Distribution and evolution of serotonin-like immunoreactive cells in Thaliacea (Tunicata). *Zoomorphology* 137, 565–578. doi: 10.1007/s00435-018-0416-9

Brunetti, R., Gissi, C., Pennati, R., Caicci, F., Gasparini, F., and Manni, L. (2015). Morphological evidence that the molecularly determined *Ciona intestinalis* type A and type B are different species: *Ciona robusta* and Ciona intestinalis. *J. Zoolog Syst. Evol. Res.* 53, 186–193. doi: 10.1111/jzs.12101

Burighel, P., and Milanesi, C. (1975). Fine structure of the gastric epithelium of the ascidian Botryllus schlosseri. Mucous, endocrine and plicated cells. *Cell Tissue Res.* 158, 481–496. doi: 10.1007/BF00220214

Buznikov, G. A., Peterson, R. E., Nikitina, L. A., Bezuglov, V. V., and Lauder, J. M. (2005). The pre-nervous serotonergic system of developing sea urchin embryos and larvae: pharmacologic and immunocytochemical evidence. *Neurochem. Res.* 30, 825–837. doi: 10.1007/s11064-005-6876-6

Candiani, S., Augello, A., Oliveri, D., Passalacqua, M., Pennati, R., De Bernardi, F., et al. (2001). Immunocytochemical localization of serotonin in embryos, larvae and adults of the lancelet, *branchiostoma floridae*. *Histochem. J.* 33, 413–420. doi: 10.1023/A:1013775927978

Caveney, S., Cladman, W., Verellen, L., and Donly, C. (2006). Ancestry of neuronal monoamine transporters in the Metazoa. *J. Exp. Biol.* 209, 4858–4868. doi: 10.1242/jeb.02607

Choi, D.-S., Ward, S. J., Messaddeq, N., Launay, J.-M., and Maroteaux, L. (1997). 5-HT2B receptor-mediated serotonin morphogenetic functions in mouse cranial neural crest and myocardiac cells. *Dev. Camb. Engl.* 124, 1745–1755. doi: 10.1242/dev.124.9.1745

Colas, J. F., Launay, J. M., Kellermann, O., Rosay, P., and Maroteaux, L. (1995). Drosophila 5-HT2 serotonin receptor: coexpression with fushi-tarazu during segmentation. *Proc. Natl. Acad. Sci.* 92, 5441–5445. doi: 10.1073/pnas.92.12.5441

Couper, J. M., and Leise, E. M. (1996). Serotonin injections induce metamorphosis in larvae of the gastropod mollusc *ilyanassa obsoleta*. *Biol. Bull.* 191, 178–186. doi: 10.2307/1542921

De Bernardi, F., Pennati, R., Candiani, S., Biggiogero, M., Zega, G., Groppelli, S., et al. (2006). Serotonin in the morphogenesis of ascidian nervous system. *Caryologia* 59, 379–383.

Dehal, P., Satou, Y., Campbell, R. K., Chapman, J., Degnan, B., De Tomaso, A., et al. (2002). The draft genome of *Ciona intestinalis*: insights into chordate and vertebrate origins. *Science* 298, 2157–2167. doi: 10.1126/science.1080049

Delsuc, F., Brinkmann, H., Chourrout, D., and Philippe, H. (2006). Tunicates and not cephalochordates are the closest living relatives of vertebrates. *Nature* 439, 965–968. doi: 10.1038/nature04336

Delsuc, F., Philippe, H., Tsagkogeorga, G., Simion, P., Tilak, M.-K., Turon, X., et al. (2018). A phylogenomic framework and timescale for comparative studies of tunicates. *BMC Biol.* 16, 39. doi: 10.1186/s12915-018-0499-2

Erspamer, V. (1946). Presence of enteramine or an enteraminosimilar substance in the gastrointestinal and splenic extracts of fish and in the gastroenteric extracts of ascidians. *Experientia* 2, 369–371. doi: 10.1007/BF02163944

Erspamer, V., and Asero, B. (1952). Identification of Enteramine, the specific hormone of the enterochromaffin cell system, as 5-Hydroxytryptamine. *Nature* 169, 800–801. doi: 10.1038/169800b0

Fiorica-Howells, E., Maroteaux, L., and Gershon, M. D. (2000). Serotonin and the 5-HT2B receptor in the development of enteric neurons. *J. Neurosci.* 20, 294–305. doi: 10.1523/JNEUROSCI.20-01-00294.2000

Georges, D. (1985). Presence of cells resembling serotonergic elements in four species of tunicates. *Cell Tissue Res.* 242, 341–348. doi: 10.1007/BF00214546

Gershon, M. D. (2004). Review article: serotonin receptors and transporters — roles in normal and abnormal gastrointestinal motility. *Aliment. Pharmacol. Ther.* 20, 3–14. doi: 10.1111/j.1365-2036.2004.02180.x

Godeaux, J. E. A. (1989). Functions of the endostyle in the tunicates. *Bull. Mar. Sci.* 45, 228–242.

Goridis, C., and Rohrer, H. (2002). Specification of catecholaminergic and serotonergic neurons. *Nat. Rev. Neurosci.* 3, 531–541. doi: 10.1038/nrn871

Greczek-Stachura, M. (2002). The regulation of swimming speed and the rate of cell division by serotonin in *Paramecium aurelia*. *Cell. Mol. Biol. Lett.* 07.

Hay-Schmidt, A. (2000). The evolution of the serotonergic nervous system. *Proc. R. Soc B Biol. Sci.* 267, 1071. doi: 10.1098/rspb.2000.1111

Horen, W. P. (1972). Insect and scorpion sting. *JAMA* 221, 894–898. doi: 10.1001/jama.1972.03200210038009

Huang, W. Q., Zhang, C. L., Di, X. Y., and Zhang, R. Q. (1998). Studies on the localization of 5-hydroxytryptamine and its receptors in human placenta. *Placenta* 19, 655–661. doi: 10.1016/S0143-4004(98)90027-3

Jeffery, W. R., and Swalla, B. J. (1992). Evolution of alternate modes of development in ascidians. *BioEssays* 14, 219–226. doi: 10.1002/bies.950140404

Kocot, K. M., Tassia, M. G., Halanych, K. M., and Swalla, B. J. (2018). Phylogenomics offers resolution of major tunicate relationships. *Mol. Phylogenet. Evol.* 121, 166–173. doi: 10.1016/j.ympev.2018.01.005

Kravitz, E. A. (2000). Serotonin and aggression: insights gained from a lobster model system and speculations on the role of amine neurons in a complex behavior. *J. Comp. Physiol. A* 186, 221–238. doi: 10.1007/s003590050423

Kristan, W. B., and Nusbaum, M. P. (1982). The dual role of serotonin in leech swimming. *J. Physiol.* 78, 743–747.

Lambrus, B. G., Cochet-Escartin, O., Gao, J., Newmark, P. A., Collins, E.-M. S., and Iii, J. J. C. (2015). Tryptophan hydroxylase is required for eye melanogenesis in the planarian *Schmidtea mediterranea*. *PloS One* 10, e0127074. doi: 10.1371/journal.pone.0127074

Lemaire, P. (2011). Evolutionary crossroads in developmental biology: the tunicates. *Development* 138, 2143–2152. doi: 10.1242/dev.048975

Liu, L., Fu, M., Pei, S., Zhou, L., and Shang, J. (2019). R-fluoxetine increases melanin synthesis through a 5-HT1A/2A receptor and p38 MAPK signaling pathways. *Int. J. Mol. Sci.* 20, 80. doi: 10.3390/ijms20010080

Lv, J., and Liu, F. (2017). The Role of Serotonin beyond the Central Nervous System during Embryogenesis. *Front. Cell. Neurosci.* 11. doi: 10.3389/fncel.2017.00074

Mayorova, T. D., and Kosevich, I. A. (2013). Serotonin-immunoreactive neural system and contractile system in the hydroid *Cladonema* (Cnidaria, Hydrozoa). *Invert. Neurosci.* 13, 99–106. doi: 10.1007/s10158-013-0152-2

McCauley, D. W. (1997). Serotonin plays an early role in the metamorphosis of the hydrozoan *phialidium gregarium*. *Dev. Biol.* 190, 229–240. doi: 10.1006/dbio.1997.8698

Mercurio, S., Bozzo, M., Pennati, A., Candiani, S., and Pennati, R. (2023). Serotonin receptors and their involvement in melanization of sensory cells in *ciona intestinalis*. *Cells* 12, 1150. doi: 10.3390/cells12081150

Mercurio, S., Cauteruccio, S., Manenti, R., Candiani, S., Scarì, G., Licandro, E., et al. (2019a). miR-7 knockdown by peptide nucleic acids in the ascidian *ciona intestinalis*. *Int. J. Mol. Sci.* 20, 5127. doi: 10.3390/ijms20205127

Mercurio, S., Gattoni, G., Messinetti, S., Sugni, M., and Pennati, R. (2019b). Nervous system characterization during the development of a basal echinoderm, the feather star *Antedon mediterranea*. *J. Comp. Neurol.* 527, 1127–1139. doi: 10.1002/cne.24596

Mercurio, S., Messinetti, S., Manenti, R., Ficetola, G. F., and Pennati, R. (2021). Embryotoxicity characterization of the flame retardant tris(1-chloro-2-propyl) phosphate (TCPP) in the invertebrate chordate Ciona intestinalis. *J. Exp. Zool. Part Ecol. Integr. Physiol.* 335, 339–347. doi: 10.1002/jez.2446

Moiseiwitsch, J. R., and Lauder, J. M. (1995). Serotonin regulates mouse cranial neural crest migration. *Proc. Natl. Acad. Sci. U.S.A.* 92, 7182–7186. doi: 10.1073/pnas.92.16.7182

Moutkine, I., Collins, E. L., BéChade, C., and Maroteaux, L. (2019). Evolutionary considerations on 5-HT2 receptors. *Pharmacol. Res.* 140, 14–20. doi: 10.1016/j.phrs.2018.09.014

Najjar, S. A., Hung, L. Y., and Margolis, K. G. (2023). Serotonergic control of gastrointestinal development, motility, and inflammation. *Compr. Physiol.* 13, 4851–4868. doi: 10.1002/cphy.c220024

Neumann, J., Hofmann, B., Dhein, S., and Gergs, U. (2023). Cardiac roles of serotonin (5-HT) and 5-HT-receptors in health and disease. *Int. J. Mol. Sci.* 24, 4765. doi: 10.3390/ijms24054765

Nichols, D. E., and Nichols, C. D. (2008). Serotonin receptors. *Chem. Rev.* 108, 1614–1641. doi: 10.1021/cr078224o

Nilsson, O., Fredriksson, G., Öfverholm, T., and Ericson, L. E. (1988). Electron-microscopic immunocytochemistry of 5-hydroxytryptamine in the ascidian endostyle. *Cell Tissue Res.* 253, 137–143. doi: 10.1007/BF00221748

Pennati, R., Candiani, S., Biggiogero, M., Zega, G., Groppelli, S., Oliveri, D., et al. (2007a). Developmental expression of tryptophan hydroxylase gene in *Ciona intestinalis*. *Dev. Genes Evol.* 217, 307–313. doi: 10.1007/s00427-007-0138-3

Pennati, R., Dell'Anna, A., Zega, G., and De Bernardi, F. (2012). Immunohistochemical study of the nervous system of the tunicate *Thalia democratica* (Forsskal 1775). *Eur. J. Histochem. EJH* 56, e16. doi: 10.4081/ejh.2012.16

Pennati, R., Ficetola, G. F., Brunetti, R., Caicci, F., Gasparini, F., Griggio, F., et al. (2015). Morphological differences between larvae of the *Ciona intestinalis* species complex: hints for a valid taxonomic definition of distinct species. *PloS One* 10, e0122879. doi: 10.1371/journal.pone.0122879

Pennati, R., Groppelli, S., De Bernardi, F., Mastrototaro, F., and Zega, G. (2009). Immunohistochemical analysis of adhesive papillae of *Clavelina lepadiformis* (Müller 1776) and *Clavelina phlegraea* (Salfi 1929) (Tunicata, Ascidiacea). *Eur. J. Histochem. EJH* 53, e4. doi: 10.4081/ejh.2009.e4

Pennati, R., Groppelli, S., Sotgia, C., Candiani, S., Pestarino, M., and De Bernardi, F. (2001). Serotonin localization in *Phallusia mammillata* larvae and effects of 5-HT

antagonists during larval development. *Dev. Growth Differ.* 43, 647–656. doi: 10.1046/j.1440-169X.2001.00608.x

Pennati, R., Groppelli, S., Sotgia, C., Zega, G., Pestarino, M., and De Bernardi, F. (2003). WAY-100635, an antagonist of 5-HT1A receptor, causes malformations of the CNS in ascidian embryos. *Dev. Genes Evol.* 213, 187–192. doi: 10.1007/s00427-003-0311-2

Pennati, R., and Rothbächer, U. (2015). Bioadhesion in ascidians: a developmental and functional genomics perspective. *Interface Focus* 5, 20140061. doi: 10.1098/rsfs.2014.0061

Pennati, R., Zega, G., Groppelli, S., and De Bernardi, F. (2007b). Immunohistochemical analysis of the adhesive papillae of *Botrylloides leachi* (Chordata, Tunicata, Ascidiacea): Implications for their sensory function. *Ital. J. Zool* 74, 325–329. doi: 10.1080/11250000701562229

Pestarino, M. (1982). Occurrence of different secretin-like cells in the digestive tract of the ascidian *Styela plicata* (Urochordata, Ascidiacea). *Cell Tissue Res.* 226, 231–235. doi: 10.1007/BF00217097

Pytliak, M., Vargová, V., Mechírová, V., and Felšöci, M. (2011). Serotonin receptors - from molecular biology to clinical applications. *Physiol. Res.* 60, 15–25. doi: 10.33549/physiolres.931903

Razy-Krajka, F., Brown, E. R., Horie, T., Callebert, J., Sasakura, Y., Joly, J.-S., et al. (2012). Monoaminergic modulation of photoreception in ascidian: evidence for a proto-hypothalamo-retinal territory. *BMC Biol.* 10, 45. doi: 10.1186/1741-7007-10-45

Rigon, F., Gasparini, F., Shimeld, S. M., Candiani, S., and Manni, L. (2018). Developmental signature, synaptic connectivity and neurotransmission are conserved between vertebrate hair cells and tunicate coronal cells. *J. Comp. Neurol.* 526, 957–971. doi: 10.1002/cne.24382

Romero-Reyes, J., Molina-Hernández, A., Díaz, N. F., and Camacho-Arroyo, I. (2021). Role of serotonin in vertebrate embryo development. *Reprod. Biol.* 21, 100475. doi: 10.1016/j.repbio.2020.100475

Sakharov, D. A., and Salimova, N. (1982). Serotonin-containing cells in the ascidian endostyle. *Experientia* 38, 802–803. doi: 10.1007/BF01972280

Satoh, N. (2013). "*Ciona*: A Model for Developmental Genomics," in *Encyclopedia of Life Sciences* (Chichester: John Wiley & Sons, Ltd). doi: 10.1002/9780470015902.a0021411

Squarzoni, P., Parveen, F., Zanetti, L., Ristoratore, F., and Spagnuolo, A. (2011). FGF/MAPK/Ets signaling renders pigment cell precursors competent to respond to Wnt signal by directly controlling Ci-Tcf transcription. *Development* 138, 1421–1432. doi: 10.1242/dev.057323

Stach, T. (2005). Comparison of the serotonergic nervous system among Tunicata: implications for its evolution within Chordata. *Org. Divers. Evol.* 5, 15–24. doi: 10.1016/j.ode.2004.05.004

Strano, F., Micaroni, V., Beli, E., Mercurio, S., Scarì, G., Pennati, R., et al. (2019). On the larva and the zooid of the pterobranch *Rhabdopleura recondita* Beli, Cameron and Piraino 2018 (Hemichordata, graptolithina). *Mar. Biodivers* 49, 1657–1666. doi: 10.1007/s12526-018-0933-2

Thorndyke, M. C., and Probert, L. (1979). Calcitonin-like cells in the pharynx of the ascidian *Styela clava*. *Cell Tissue Res.* 203, 301–309. doi: 10.1007/BF00237244

Tiozzo, S., Murray, M., Degnan, B. M., De Tomaso, A. W., and Croll, R. P. (2009). Development of the neuromuscular system during asexual propagation in an invertebrate chordate. *Dev. Dyn* 238, 2081–2094. doi: 10.1002/dvdy.22023

Valero-Gracia, A., Marino, R., Crocetta, F., Nittoli, V., Tiozzo, S., and Sordino, P. (2016). Comparative localization of serotonin-like immunoreactive cells in Thaliacea informs tunicate phylogeny. *Front. Zool* 13, 45. doi: 10.1186/s12983-016-0177-6

Weiger, W. A. (1997). Serotonergic modulation of behaviour: A phylogenetic overview. *Biol. Rev.* 72, 61–95. doi: 10.1111/j.1469-185X.1997.tb00010.x

Welsh, J. H., and Loveland, R. E. (1968). 5-Hydroxytryptamine in the ascidian, *Ciona intestinalis* L. *Comp. Biochem. Physiol.* 27, 719–722. doi: 10.1016/0010-406X(68)90613-0

Wu, H.-L., Pang, S.-L., Liu, Q.-Z., Wang, Q., Cai, M.-X., and Shang, J. (2014). 5-HT1A/1B receptors as targets for optimizing pigmentary responses in C57BL/6 mouse skin to stress. *PloS One* 9, e89663. doi: 10.1371/journal.pone.0089663

Yaguchi, S., and Katow, H. (2003). Expression of tryptophan 5-hydroxylase gene during sea urchin neurogenesis and role of serotonergic nervous system in larval behavior. *J. Comp. Neurol.* 466, 219–229. doi: 10.1002/cne.10865

Yavarone, M. S., Shuey, D. L., Sadler, T. W., and Lauder, J. M. (1993a). Serotonin uptake in the ectoplacental cone and placenta of the mouse. *Placenta* 14, 149–161. doi: 10.1016/S0143-4004(05)80257-7

Yavarone, M. S., Shuey, D. L., Tamir, H., Sadler, T. W., and Lauder, J. M. (1993b). Serotonin and cardiac morphogenesis in the mouse embryo. *Teratology* 47, 573–584. doi: 10.1002/tera.1420470609

Zega, G., Pennati, R., Dahlström, M., Berntsson, K., Sotgia, C., and De Bernardi, F. (2007a). Settlement of the barnacle *Balanus improvisus*: The roles of dopamine and serotonin. *Ital. J. Zool* 74, 351–361. doi: 10.1080/11250000701631594

Zega, G., Pennati, R., Fanzago, A., and De Bernardi, F. (2007b). Serotonin involvement in the metamorphosis of the hydroid *Eudendrium racemosum*. *Int. J. Dev. Biol.* 51, 307–313. doi: 10.1387/ijdb.062195gz

frontiers | Frontiers in Ecology and Evolution

TYPE Original Research
PUBLISHED 03 May 2024
DOI 10.3389/fevo.2024.1385516

OPEN ACCESS

EDITED BY
Paolo Sordino,
Anton Dohrn Zoological Station Naples, Italy

REVIEWED BY
Ugo Coppola,
Cincinnati Children's Hospital Medical Center, United States
Marios Chatzigeorgiou,
University of Bergen, Norway
Salvatore D'Aniello,
Zoological Station Anton Dohrn, Italy

*CORRESPONDENCE
Hongzhe Peng
penghongzhe@stu.ouc.edu.cn

†These authors have contributed equally to this work

RECEIVED 13 February 2024
ACCEPTED 22 April 2024
PUBLISHED 03 May 2024

CITATION
Bi J, Ge Y, Wang Z, Peng H and Dong B (2024) Matrix metalloproteinase Nas15 regulates the lumen formation and expansion in *Ciona* notochord. *Front. Ecol. Evol.* 12:1385516. doi: 10.3389/fevo.2024.1385516

Matrix metalloproteinase Nas15 regulates the lumen formation and expansion in *Ciona* notochord

Jianqing Bi[1†], Yonghang Ge[1†], Zhuqing Wang[1], Hongzhe Peng[1*] and Bo Dong[1,2,3]

[1]Fang Zongxi Center for Marine EvoDevo, MoE Key Laboratory of Marine Genetics and Breeding, College of Marine Life Sciences, Ocean University of China, Qingdao, China, [2]Laboratory for Marine Biology and Biotechnology, Qingdao Marine Science and Technology Center, Qingdao, China, [3]MoE Key Laboratory of Evolution and Marine Biodiversity, Institute of Evolution and Marine Biodiversity, Ocean University of China, Qingdao, China

Lumen formation, as a key process of biological tube construction, is essential in various physiological processes such as nutrient and waste transporting, gas exchanging, and structural supporting. However, the mechanisms underlying tubular lumen development are still not fully understood. In the present study, we identified a matrix metalloproteinase, Nas15, which is enriched in the apical domain of the *Ciona* embryonic notochord. The expression level of the *Nas15* gene significantly increased during notochord lumen formation and expansion. Nas15 loss-of-function resulted in abnormal notochord lumen expansion in *Ciona* embryos. Besides, yeast two-hybrid screening and CO-IP results indicated a Phosphatase 2 Catalytic Subunit Alpha (PPP2CA) physically interacted with Nas15. PPP2CA also involved in notochord lumen formation via localizing Nas15. Furthermore, we investigated the distribution of laminin in Nas15 disrupted embryos. In conclusion, our results revealed a mechanisms of how notochord cells regulating lumen expansion via metalloproteinase-mediated ECM localization. This findings provide insight into the mechanisms of tubular organ lumen formation and serve as a reference for research on human abnormal lumenogenesis diseases.

KEYWORDS

Nas15, notochord, lumen expansion, ECM, ciona, tunicates

Introduction

Tubular structures play essential roles in various organs, such as the lung, kidney, intestine, and vasculature. Due to their unique structure, biological tubes are responsible for transporting and absorbing materials (Lubarsky and Krasnow, 2003). For instance, arteries facilitate the delivery of blood throughout the body and organs, while the intestinal tube is responsible for

nutrient absorption. Recent research suggests that tube structures also participate in regulating the mechanical properties of tissues (Yasuoka, 2020). In the case of the notochord, the pressure within the notochord lumen is controlled by the secretion of matrix components from notochord cells, which contributes to overall tissue stiffness regulation (Yasuoka, 2020). The vacuole of the notochord is an evolutionally conserved structure, from *Amphioxus*, *Ciona* to vertebrate (Annona et al., 2015). The proper formation of tube lumens is crucial, as any abnormalities in size or shape will lead to various diseases. For example, polycystic kidney disease (Simons and Walz, 2006) and atherosclerotic heart disease (Sarraju and Nissen, 2024) have been identified to be associated with abnormal lumen formation. Tubulogenesis is a critical process in many physiological activities, yet the underlying mechanism of lumen formation remains unclear. Multiple cellular behaviors have been identified as involved in lumen construction, including wrapping, budding, cavitation, cord vacuolation, and cell vacuolation (Lubarsky and Krasnow, 2003). *Ciona* notochord constructs an extracellular lumen via a complicated cell behavior, including cell intercalation, elongation, lumen initial formation/expansion, and bi-directional migration (Dong et al., 2011; Lu et al., 2019), resulting in a flattened endothelial cells covered, connected extracellular lumen, a process known as mesenchymal-epithelial transition (Dong et al., 2009; Ouyang et al., 2023).

Regarding the regulatory mechanism of lumen localization and size, numerous studies have indicated that the secretion of extracellular matrix (ECM) by *Ciona* notochord cells plays a crucial role in the feedback regulation of notochord morphogenesis. The ECM of *Ciona* notochord comprises two distinct types: the basal ECM (notochord sheath) and the apical ECM (Wei et al., 2017). The notochord sheath refers to a layer of basal lamina that covers the surface of the notochord, composed of various components such as collagen, laminin, fibronectin, and other components (Veeman et al., 2008; Segade et al., 2016; Peng et al., 2023). These ECM components are indispensable for notochord morphogenesis. Fibronectin contributes to notochord intercalation (Segade et al., 2016), whereas laminin is involved in notochord boundary formation and convergence extension (Veeman et al., 2008). The collagen surrounding the notochord forms a supracellular arch, facilitating notochord elongation and coordinated movement with multiple tissues (Peng et al., 2023). In addition to the basal notochord sheath, the apical ECM secreted into the lumen also plays a vital role in the initial construction and expansion of the lumen. Extensive research has demonstrated that vesicular trafficking is a critical factor driving lumen expansion (Dong et al., 2011; Bhattachan et al., 2020). The 14-3-3 epsilon protein mediates material transport from the basal membrane to the apical side, which is essential for lumen expansion (Mizotani et al., 2018).

Tissue morphogenesis is a highly dynamic process, necessitating constant reshaping, rebuilding, and recycling of the ECM to maintain an appropriate quantity and quality conducive to development (Bonnans et al., 2014). The proteomic analysis of *Ciona* notochord revealed a diverse array of vesicle transport-related proteins and ECM components (Wang et al., 2023). The DYRK1-endophilin-mediated endocytosis occurs actively in close proximity to the apical membrane of the *Ciona* notochord, thereby implicating the role of ECM dynamic turnover in lumen formation (Ouyang et al., 2023), which highlights the significance of the continuous remodeling of ECM in the process of lumen formation.

So, an interesting question of ECM mediated morphogenesis is how the cells regulate the ECM to feedback influence the tissue reshaping. Matrix metalloproteinase (MMPs) have been identified as key players in this process. MMPs constitute a family of calcium-dependent zinc-containing endopeptidases (Verma and Hansch, 2007) that facilitate the remodeling and degradation of various ECM components (Nagase et al., 2006). Notably, some studies have suggested the involvement of membrane-type matrix metalloproteinase in vascular lumen formation through its regulation of ECM remodeling. These findings shed light on the intricate interplay between cells and the ECM during tissue morphogenesis (Senger and Davis, 2011; Sacharidou et al., 2012).

However, the specific involvement of MMPs in apical ECM remodeling and their regulatory role in lumen formation in the *Ciona* notochord remains elusive. Within the astacin metalloproteinase family, nematode astacins-15 (Nas-15) emerges as a potential candidate component involved in *Ciona* notochord lumen formation, which has been identified in proteomic analysis of *Ciona* notochord (Wang et al., 2023). Previous studies have demonstrated the participation of astacin metalloproteinases in diverse developmental processes, including food digestion, early embryonic development, tissue remodeling, and differentiation (Baumann et al., 1993; Sterchi et al., 2008; Park et al., 2010; Calabria et al., 2019). By analyzing single-cell transcriptome data in the Single Cell Portal (SCP) database, it was observed that the homologous protein of Nas-15 in *Ciona robusta* (*Cr*-Nas15) exhibits high expression levels during the stages of lumen formation in the notochord of *Ciona* embryos (Tarhan et al., 2023). Moreover, the Ghost database revealed specific enrichment of *Cr-Nas15* mRNA surrounding the apical membrane of the notochord lumen (Kusakabe et al., 2002; Satou et al., 2005). Taken together, these clues suggest that *Cr*-Nas15 is a promising candidate MMP involved in *Ciona* notochord lumen formation.

In this study, we initially identified *Cr*-Nas15, which features a typical ZnMc-astacin-like domain and Zinc-binding metalloprotease motif. Subsequently, using qPCR, promoter analysis, and immunofluorescence techniques, we confirmed the specific localization of *Cr-Nas15* at the apical domain of notochord cells during the late tail bud stage of *Ciona* embryos, which overlaps spatially and temporally with notochord lumen formation. We then investigated the functional role of *Cr*-Nas15 in this process. Treatment with the inhibitor actinonin, overexpression of a dominant negative version of Nas-15, and tissue-specific knock-out experiments all resulted in similar lumen formation failure phenotypes, further supporting the involvement of *Cr*-Nas15 in *Ciona* notochord lumen formation. Additionally, we demonstrated that Protein Phosphatase 2 Catalytic Subunit Alpha (PPP2CA) interacts with Nas15, and the PPP2CA is also essential for lumen formation in *Ciona* notochord.

Materials and methods

Animals and electroporation

Adult *Ciona robusta* was collected from Rongcheng and Qingdao in Shandong Province, China. Following collection, the animals were temporarily housed in laboratory artificial seawater tanks, which were carefully maintained at a temperature range of 17°C to 19°C and a salinity level of 30-32‰. Sperm and eggs were obtained separately from different adult *Ciona* individuals. The sperm and eggs were mixed in sea water over 5 minutes for fertilization. Then, the fertilized eggs underwent a dechorionation process before proceeding with electroporation. The electroporation method for *Ciona* embryos was performed based on previously reported techniques (Stolfi and Christiaen, 2012). 40 μg of each plasmid was dissolved in sterile ddH_2O, reaching a total volume of 80 μl. This plasmid solution was then mixed with 420 μl of electroporation buffer. The resultant mixture was transferred into a 4 mm electroporation cuvette. Subsequently, 300 μl of sea water together with dechorionated *Ciona* fertilized eggs were added to the cuvette. Electroporation was carried out using a pulse generator, employing a voltage of 50V and a capacitance of 1500/2000 μF. Following the electroporation step, the embryos were placed into a constant temperature incubator set at 16° C for further incubation.

Plasmid construction

In the promoter analysis experiment, the upstream 3 kb DNA sequence of Nas15 was amplified by PCR using genomic DNA from *C. robusta* as a template with primers Nas*15 (3 k) -F* and *Nas15 (3k) -R*. The PCR product was then inserted into the pEGFP-N1 vector to construct the *Cr-Nas15 (3 kb) > GFP* fusion construct.

The *Ciona* notochord specific expressed vector was constructed via replacing the CMV promoter of pEGFP-N1 with *Ciona savignyi (Cs) brachyury* upsteam 3kb promoter. Using *C. robusta* cDNA as a template, full-length coding sequences (CDS) of Nas15 and PPP2CA were amplified via PCR with primers *Bra > Nas15-F* and *Bra > Nas15-R* and *Bra>PPP2CA-F* and *Bra>PPP2CA-R*, respectively. The PCR products were then inserted into *Brachyury (3 kb) > EGFP-N1* vector, leading to the construction of the expression plasmids *Brachyury (3 kb) > Nas15-EGFP* and *Brachyury (3 kb) > PPP2CA-EGFP*, and the construction of mutant plasmids were generated introducing mutated bases for overexpression experiments. Further, the PCR product was cloned into the linearized vectors *CMV > GFP* and *CMV > HA*, generating the expression plasmids *CMV > Nas15-GFP* and *CMV > PPP2CA-HA* for cell experiments. Additionally, the PCR product was cloned into the linearized vectors *pGBKT7* and *pGADT7* to construct the expression plasmids *pGBKT7-Nas15* and *pGADT7-PPP2CA* for yeast two-hybrid assays. Finally, the CDS of Nas15 was ligated to the *pET-30a* vector for prokaryotic expression of Nas15 protein.

The ClonExpress II one-step cloning kit (Vazyme, Nanjing, China) was utilized to generate all constructs, and their accuracy was verified through sequencing analysis. All the PCR primers are listed in the Supplementary Table S1.

Quantitative PCR

The qPCR was performed based on the previously reported techniques (Livak and Schmittgen, 2001). *Nas15* qPCR primers were designed using Beacon Designer 7 software. Total RNA was extracted from various developmental stages (8, 12, 13, 15, 16, 17, 20, 22, and 24 hours post fertilization, hpf) of *C. robusta* embryos/larvae using RNAiso plus (TAKARA, Japan). The extracted RNA was reverse transcribed into cDNA using the HiScript II Q RT SuperMix for qPCR kit (Novogene, Nanjing, China). Quantitative PCR amplification was performed using the ChamQTM SYBR Color qPCR Master Mix kit (Novogene, Nanjing, China). Data analysis was carried out using the $2^{-\Delta\Delta Ct}$ method, and graphical representation was created using Excel software. The primers are listed in the Supplementary Table S1.

Western Blot

23 hpf (late tailbud stage) *Ciona* embryos were collected and lysed in loading buffer at 100°C for 10 minutes to denature the proteins. The samples were then loaded onto an SDS-PAGE gel for electrophoresis. After electrophoresis, the protein was transferred to a polyvinylidene fluoride (PVDF) membrane. Following membrane transfer, the PVDF membrane was blocked with 5% skimmed milk at room temperature for 2 hours. Primary antibody (Nas15 1:300) was diluted in 10% goat serum and incubated with PVDF membrane for overnight at 4°C. After completion of the primary antibody incubation, the PVDF membrane was washed three times with 0.05% TBST solution for 15 minutes each time. Secondary antibody Goat Anti-Mouse IgG, HRP Conjugate (TransGen, 1:2000, HS201–01) was diluted in 10% goat serum and incubated with PVDF membrane at room temperature for 2 hours. After the secondary antibody incubation, the PVDF membrane was washed three times with 0.05% TBST solution for 15 minutes each time. Once the washing was completed, the membrane was subjected to staining and photographed.

Immunofluorescence staining

Embryos were fixed with 4% paraformaldehyde at room temperature for 2 hours, followed by permeabilization with PBS solution containing 0.1% Triton X-100 (permeabilization was performed three times for a total of 8 hours). Blocking was carried out with 10% goat serum at room temperature for 1 hour. Incubation with the primary antibody (Nas15 1:100) was performed overnight at 4°C. Washing was performed three times with PBS solution containing 0.1% Triton X-100 (a total of 8 hours). Incubation with Alexa Fluor 488-conjugated phalloidin (Invitrogen) and the secondary antibody Goat Anti-Mouse IgG, HRP Conjugate (TransGen, 1:2000, HS201–01) was carried out overnight at 4°C. Washing was performed three times with PBS solution containing 0.1% Triton X-100 (a total of 8 hours). Finally, the embryos were mounted with DAPI for confocal microscopy observation.

Drug treatment

14 hpf (early tailbud stage) *Ciona* embryos was collected and cultured into the 48-well plate (about 200 embryos per well with 2 ml filtered seawater until 16 hpf (mid tailbud stage). Then, Actinonin dissolved in DMSO (MedChemExpress) was added to a final concentration of 1.2 μm in the inhibitor treated group, and the control group was added an equal amount of DMSO. Three repeated experiments were set for each group. Then, the embryos were cultured in 18°C until 23 hpf (late tailbud stage) and collected respectively. The embryos were fixed with 4% paraformaldehyde. Following the staining with phalloidin, the embryos were mounted with DAPI for confocal microscopy observation and imaging.

CRISPR/Cas9

The genome editing in *Ciona* embryos by CRISPR/Cas9 was performed based on the previously reported techniques (Stolfi et al., 2014). Using the CRISPRdi-rect (http://crispr.dbcls.jp), three Nas15 sgRNA sequences were designed and subsequently sent to Shanghai Biotechnology Company for synthesis. Then, two single strands of sgRNAs were mixed respectively and subjected to a 5-minute treatment at 100°C to ensure complete denaturing, followed by a cooling to room temperature for annealing. Subsequently, the annealed primers were ligated to the linearized *Cr-U6 > sgRNA (F+E)* (Addgene number: 59 986) for sgRNAs transcription *in vivo*. Then the constructed sgRNA expression transcription vector was then used as a template for PCR amplification of the U6>sgRNA fragment. After that, the *Cr-EF1α > NLS:: Cas9::NLS::P2A-mCherry* plasmid and the sgRNA PCR product was co-electroporated into *Ciona* embyros. Then, the embryos were cultured in 18°C until 18hpf, and the embryos with red fluorescence were sorted and collected. Genomic DNA extracted from the collected embryos was used for efficiency test using *T7 endonuclease* I digestion. Additionally, the *Cs-Brachyury (1 kb) > NLS::Cas9::NLS::P2A::mCherry* and the sgRNA PCR product was co-electroporated into *Ciona* embryos for phenotype observation. The sequences of sgRNAs were listed in the Supplementary Table S2.

Yeast two-hybrid assay

The yeast two-hybrid experiment was performed following the protocol provided by Matchmaker GAL4-based two-hybrid system (Clontech) (Hu et al., 2021).

Co-immunoprecipitation

HEK293T cells were cultured in DMEM medium supplemented with 10% FBS, 100 U/mL penicillin, and 100 mg/mL streptomycin. The cells were maintained at 37°C in a 5% CO2 atmosphere. After reaching 80-90% confluency, the transfection was carried out using Lipofectamine 3000 Invitrogen (Thermo Fisher) according to the manufacturer's instructions. 48 hours post-transfection, cells were collected and lysed in a buffer containing 50 mM Tris-HCl (pH 8), 75 mM NaCl, 1 mM $MgCl_2$, 0.05% NP-40, 100 mM sucrose, 1 mM DTT, and 1x Protease Cocktail inhibitors (Roche) at 4°C for 30 minutes. Centrifuge at 12000 rpm for 10 minutes to remove cellular debris. Afterward, the supernatant was subjected to overnight incubation with GFP-tap beads (gta 20, chromotek, Germany) on a rotator at 4°C. The immunoprecipitated samples were washed three times with lysis buffer, and then directly boiled at 95°C for 10 minutes in 2×SDS loading buffer. Subsequently, these samples were loaded into 10% SDS-PAGE gels and separated via electrophoresis.

Database searching and analysis

A phylogenetic tree for Nas15 was constructed using MEGA11 software (Tamura et al., 2021). The Conserved Domains Database tool provided by the NCBI website was utilized for protein domain prediction. Multiple sequence alignment was conducted using DNAMAN software (Lynnon Biosoft Bioinformatic Solutions, San Ramon, CA, USA), and the resulting alignments were visually represented. The diameter of the lumen was measured using the software ImageJ. All Significance statistical analysis was preformed using unpaired two-tailed t test. * represents $p<0.05$. ** represents $p<0.01$. *** represents $p<0.001$. **** represents $p<0.0001$. The colocalization of Nas15::tdTomato and PPP2CA::eGFP was analyzed with ImageJ. The phosphorylation sites in Nas15 were predicted using NetPhos - 3.1 (https://services.healthtech.dtu.dk/) website. The single cell sequencing data in different tissues and stages of *Cr-Nas15* were downloaded from Single Cell Portal (SCP) database (https://singlecell.broadinstitute.org/single_cell/study/SCP454/comprehensive-single-cell-transcriptome-lineages-of-a-proto-vertebrate#study-summary) (Tarhan et al., 2023). The *in situ* hybridization result of *Cr-Nas15* were identified on Ghost database (http://ghost.zool.kyoto-u.ac.jp/cgi-bin/photogetkh.cgi?inkey=CLSTR07818&source=kh2013) (Kusakabe et al., 2002; Satou et al., 2005).

Results

The Nas15 is evolutionary conserved in *Ciona*

The sequence of *Cr*-Nas15 was downloaded from the Ghost database. The *Cr*-Nas15 is a 44.2 KDa protein and the *in situ* hybridization data demonstrated its expression in the larval notochord of *Ciona* (Kusakabe et al., 2002; Satou et al., 2005; Tassy et al., 2010). Meanwhile, the single-cell transcriptome sequencing data showed that the *Cr-Nas15* was recognized in larval notochord cells at the lumen formation stage (Tarhan et al., 2023). To explore the evolution of *Cr*-Nas15, a group of *Cr*-Nas15 homologous sequences in other species was identified and then a phylogenetic tree constructed using full-length sequences revealed that *Cr*-Nas15 clustered with proteins from vertebrates, such as *Homo sapiens* MeprinA and *Mus musculus* MeprinA, suggesting its

10.3389/fevo.2024.1385516

evolutionary conservation from invertebrates to chordates (Figure 1A). We also compared the *Cr*-Nas15 domain structure with homologous proteins in other species using the online tool NCBI Conserved Domain Search. The results showed that they both had conserved ZnMc-astacin-like domain and Zinc-binding metalloprotease motif (Figure 1B). Because of the key function of Zinc-binding metalloprotease motif, we analyzed the primary structure of this motif. The results showed that the *Cr*-Nas15 together with the homologous proteins in other species had a conserved motif HEXXHXXGXXH, which was the core structure for Zinc-binding metalloprotease catalytic activity (Bond and Beynon, 1995; Trevisan-Silva et al., 2010) (Figure 1C). In summary, the *Cr*-Nas15 sequence structure is evolutionary conserved including a typical ZnMc-astacin-like domain and Zinc-binding metalloprotease motif, suggesting that the *Cr*-Nas15 may has the similar catalytic activity with that in other species.

The expression of *Cr*-Nas15 has a spatial and temporal overlap with notochord lumen formation

To confirm the temporal expression of *Cr-Nas15* from single-cell transcriptome sequencing dataset, we performed a qRT-polymerase chain reaction (PCR) analysis of *Cr-Nas15* using different developmental-staged embryos. The result shows that the expression level is increasing from 8 hpf (mid gastrula stage) to 24 hpf (hatching larva stage), and highly expressed during 20 hpf (late tailbud stage) to 24 hpf (Figure 2A), which is consistent with the single-cell transcriptome sequencing data. To further explore the expression level of *Cr-Nas15* in different tissues, we built a UMAP plot based on the single cell sequencing data of *Ciona* early embryos. The result indicated that *Cr-Nas15* was expressed in many different tissues, such as the notochord, epidermis, muscle, and endoderm

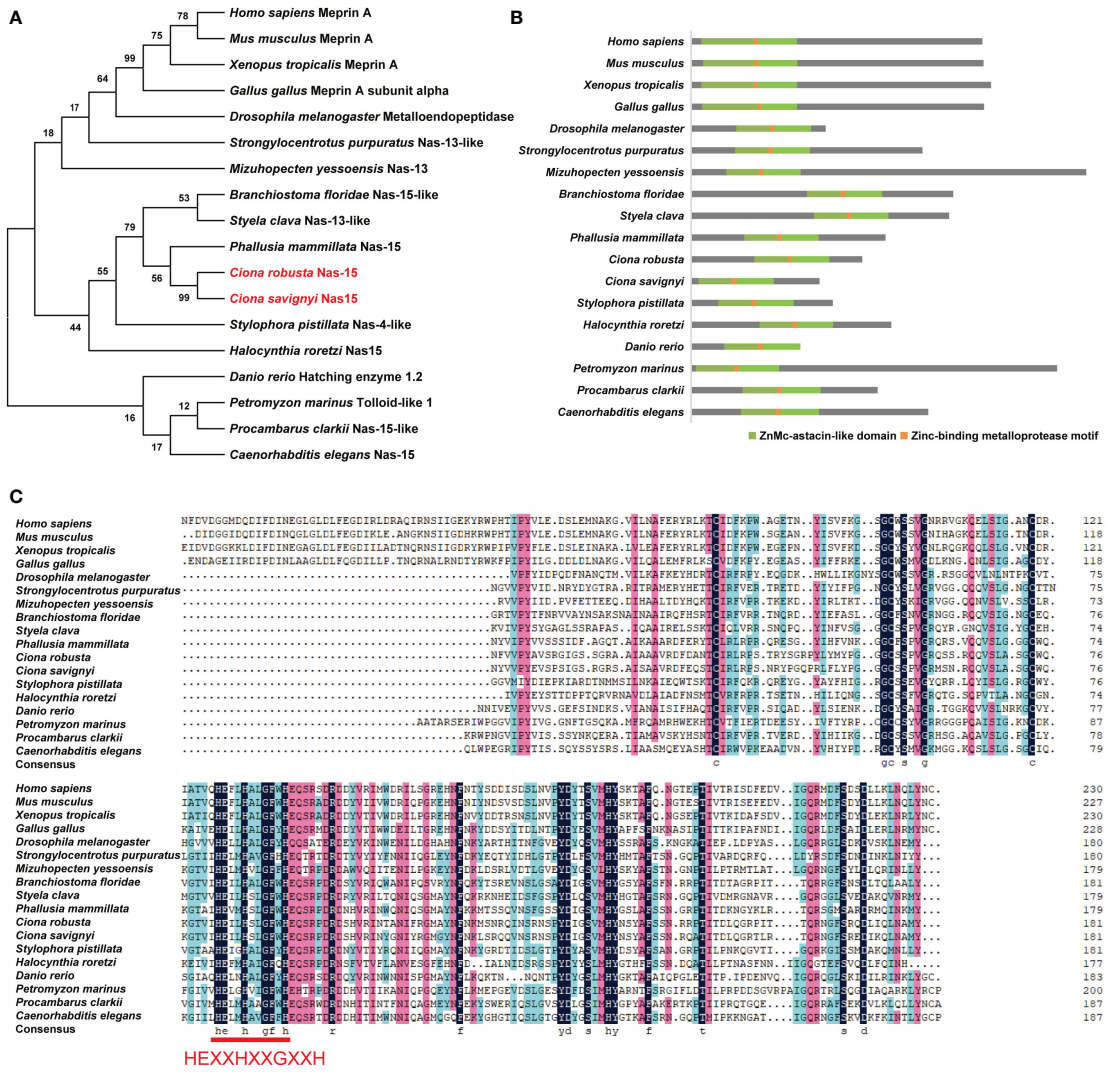

FIGURE 1
Phylogenetic analysis and domain composition of Nas15 in different species. **(A)** Phylogenetic tree analysis of Nas15 in different species. Red font indicates *Ciona robusta* Nas15 and *C. savignyi* Nas15. **(B)** Schematic diagram of Nas15 structure composition in diverse species. ZnMc-astacin-like domain (green) and Zinc-binding metalloprotease motif (orange) are presented in Nas15 in diverse species. **(C)** Protein sequence alignment of Nas15 ZnMc-astacin-like domain from diverse species. In the Zinc-binding metalloprotease motif region of Nas15 from diverse species, the amino acid sequence HEXXHXXGXXH is highly conserved.

10.3389/fevo.2024.1385516

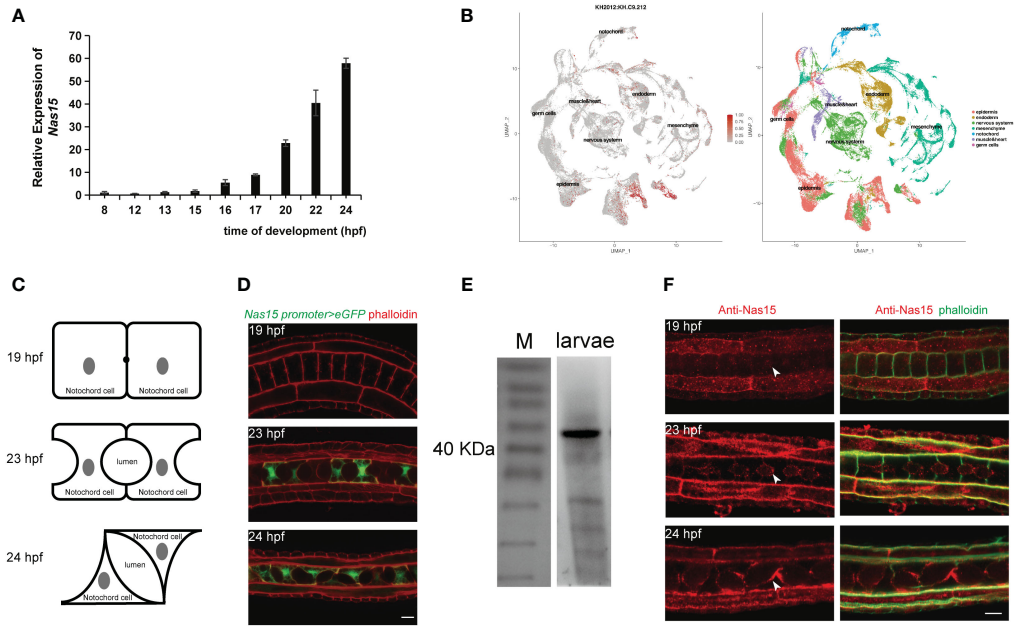

FIGURE 2
Expression pattern and subcellular localization of Nas15. **(A)** *Cr-Nas15* mRNA expression levels at different developmental stages of *Ciona* embryo. **(B)** The UMAP plot displaying the expression of *Cr-Nas15* in different tissues. **(C)** The illustration of *Ciona* notochord lumen in different developmental stages. **(D)** Expression pattern of *Cr-Nas15* promotor-driven GFP in notochord tissue at diverse developmental stages of *Ciona*. **(E)** Western Blot with self-prepared *Cr*-Nas15 murine polyclonal antibody **(F)** *Cr*-Nas15 Immunofluorescence in *Ciona* embryos at different developmental stages. The white arrows represent the signal of *Cr*-Nas15. All scale bars represent 10 μm.

(Cao et al., 2019; Tarhan et al., 2023) (Figure 2B). Together with the qPCR (Figure 2A) and *in situ* hybridization data (Kusakabe et al., 2002; Satou et al., 2005), we inferred that *Cr-Nas15* was expressed in notochord in lumen expansion stages. To confirm this spatial and temporal overlap between *Cr-Nas15* expression and notochord lumen formation, we investigated the *Cr-Nas15* expression level in notochord during entire lumen formation process by the promoter analysis. At 19 hpf (mid gastrula stage), an extracellular lumen initial formed between two adjacent notochord cells, while at 23 hpf and 24 hpf, the lumen undergoes continuous expansion and tilts (Figure 2C). The upstream 3,000 bps were cloned and fused with eGFP and electroporated into the *Ciona* fertilized eggs. Before the lumen formation (19 hpf), we did not observe any fluorescent signal in the notochord. But at 21 hpf (late tailbud stage) and 23 hpf, corresponding to the lumen formation and expansion phase, the eGFP signal was observed in the notochord (Figure 2D). Furthermore, to explore the subcellular localization of *Cr*-Nas15, we prepared a Murine polyclonal antibody with the full length of *Cr*-Nas15 as antigen. To validate the specificity of the antibody, the 23 hpf staged *Ciona* larvae were collected to preform total protein extraction. The western blot with *Cr*-Nas15 antibody showed a band at expected size over 40 KDa, suggesting the high efficacy of self-prepared *Cr*-Nas15 antibody (Figure 2E). We thus performed the *Cr*-Nas15 immunofluorescence experiment with *Ciona* larva at different developmental stages. In 19 hpf embryos before the extracellular lumen formation, the *Cr*-Nas15 has a low signal density in notochord, and localized at the pre-apical membrane of each notochord cells. Then, the *Cr*-Nas15 signal was increased and localized at the apical domain with the lumen formation in 23 hpf. In 24 hpf, in which stage the notochord cells starting a bi-directional migration, *Cr*-Nas15 also enriched at the apical membrane of each notochord cells (Figure 2F). The *Cr*-Nas15 immunofluorescence results confirmed that the *Cr*-Nas15 expression is increasing with the lumen formation, and indicated a special localization at the apical domain near the extracellular lumen. Together with the results of RT-qPCR, promoter analysis and immunofluorescence, we described the *Cr*-Nas15 spatio-temporal expression profile. The *Cr*-Nas15 was expressed at the notochord in lumen formation stages from 19 to 24 hpf, and localized at the apical domain, spatial closing to the extracellular lumen, suggesting a potential function of *Cr*-Nas15 in lumen formation.

The *Cr*-Nas15 is essential for *Ciona* notochord lumen formation

To explore the function of *Cr*-Nas15, actinonin, which binds at the catalytic site of astacin metalloproteinase as a competitive inhibitor (Talantikite et al., 2018). was used to block the function of all astacin metalloproteinase. In the actinonin-treated group, the embryos were cultured in sea water containing 1.2 μM DMSO dissolved actinonin from 16 hpf, while the control group was cultured in sea water with the same dose of DMSO. Then, the embryos were collected and fixed at 21 and 23 hpf stages, respectively. After dying with phalloidin to visualize the cell boundary, we observed the shape of extracellular lumen. In both 21 and 23 hpf, the lumen size in the actinonin-treated embryos obviously smaller than the control group (Figure 3A). So, we

10.3389/fevo.2024.1385516

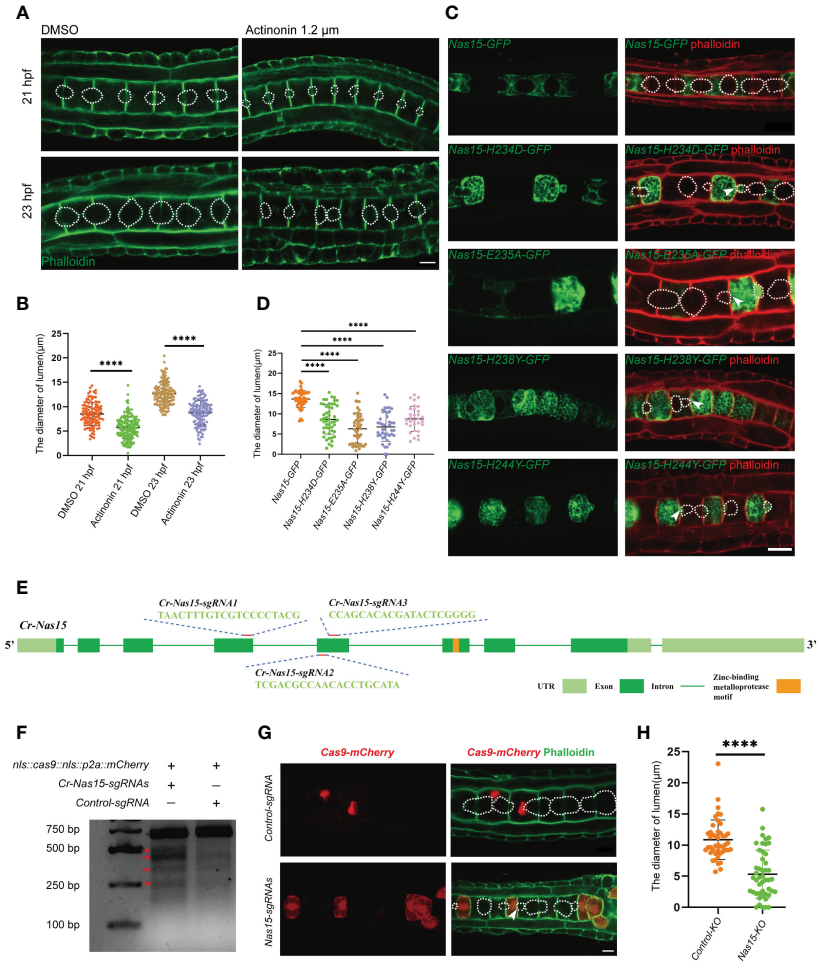

FIGURE 3
Cr-Nas15 loss-of-function disrupted lumen formation and expansion. **(A)** The phenotype of Astacin zinc metalloproteinase inhibitor Actinonin treated embryos. The dashed lines indicate the boundary of lumen. **(B)** Quantification of the lumen diameter of DMSO ($n_{21\ hpf}$ = 112、$n_{23\ hpf}$ = 136) and Actinonin ($n_{21\ hpf}$ = 157、$n_{23\ hpf}$ = 127) treated embryos at 21 and 23 hpf at 16 °C in A. **(C)** Overexpression of dominant negative *Cr-Nas15* results in abnormal formation and expansion of lumen. **(D)** Quantification of the lumen diameter of overexpressing *Nas15* CDS ($n_{Nas15\text{-}GFP}$ = 45) and *Nas15* dominant negative ($n_{Nas15\text{-}H234D\text{-}GFP}$=71、$n_{Nas15\text{-}E235A\text{-}GFP}$= 29、$n_{Nas15\text{-}H238Y\text{-}GFP}$ = 39、$n_{Nas15\text{-}H244Y\text{-}GFP}$ = 29) in C. **(E)** *Cr-Nas15* gene Structure and sgRNAs design. Light green squares represent UTRs, dark green squares represent Exons, green lines represent Introns, and orange square represents Zinc-binding metalloprotease motif. **(F)** *T7 endonuclease* I test results of *Cr-Nas15* knock out embryos. The red arrows show the different bands produced by the *T7 endonuclease* cleavage in the knockout group compared to the control group. **(G)** *Nas15* notochord tissue specific knockout results. After the knock-out of *Nas15*, the formation and expansion of the notochord lumens were abnormal. **(H)** Quantification of the lumen diameter of *Nas15-KO* (n = 47) and *Control-KO* (n = 45) in G. All Significance statistical analysis was preformed using unpaired two-tailed *t* test. ****p < 0.0001. All scale bars represent 10 μm.

measured the diameter of the lumen in 23 hpf. Compared with the control group, the lumen diameter in actinonin-treated group was significantly smaller, both in 21hpf and 23 hpf (Figure 3B). Besides, the lumen shape was also abnormal in actinonin -treated embryos. Compared with the control group, the lumen in actinonin-treated embryos was not homogeneous growing, but expanded bialy towards one neighbor notochord cell (Figure 3A). These results indicate that the astacin metalloproteinase malfunction not only influence the *Ciona* notochord lumen formation, but also inhibit the lumen expansion process.

To further confirm the function of *Cr*-Nas15 involved in the notochord lumen formation, we constructed several dominant negative (DN) versions of *Cr-Nas15* driven by brachyury promoter, which drives the constructs to specifically express in notochord tissue in *Ciona* larvae. According to previous studies, the *Cr-Nas15-H234D*, *H238Y* and *H244Y* lead to Nas15 loss of function by blocking the Zn binding, and the *E235A* lead to the Nas15 catalytic activity malfunction without influencing the Zn and substrate binding (Franco et al., 2005). The *Cr-Nas15-DN* and *wild type (WT)* expression plasmids were electroporated into the *Ciona* embryo, respectively. The results showed that the *Cr-Nas15-WT* was enriched at the notochord apical domain. However, some signals also appeared in the cytoplasm and around the contractile ring, which may be the mis-localization because of the overexpression. The notochord lumen in *Cr-Nas15-WT* overexpression group expanded normally, but all four DN versions led to abnormal lumen formation (Figure 3C). We measured the lumen diameter in all four DN version groups and the *Cr-Nas15-WT* group. The statistical results showed that the volume of lumen in each DN

groups were significantly smaller than which in *Cr-Nas15-WT* group, phenocopying the inhibitor treatment (Figure 3D). Interestingly, the lumen shape in DN overexpression groups also different from the WT group. All four DN versions led to an asymmetrical lumen expansion. Due to the mosaic expression of *Ciona*, the *Cr-Nas15-DN* only expressed in several notochord cells. The lumen between a *Cr-Nas15-DN* overexpression positive cell and a negative cell always asymmetrically expanded into the negative cell (Figure 3C). These results reveal the essential function of *Cr*-Nas15 in *Ciona* notochord lumen expansion.

However, because of the side effect of dominant negative overexpression, we decided to perform a *Cr-Nas15* knock out (KO) using the CRISPR/Cas9 system. Due to the important function of Zinc-binding metalloprotease motif, we designed three guiding RNA around this motif area (Figure 3E). To improve the KO efficacy, all the three guiding RNA plasmids were mixed to electroporate together with Cas9 expression plasmid. We also electroporated the control guiding RNA plasmid together with Cas9 expression plasmid as a control group. Then, the genomic DNA of KO group and control group, respectively were extracted for *T7 Endonuclease* I efficacy test. The knockout efficiency was determined to be approximately 16.37% by calculating the stripe grayscale values, confirming the efficiency of *Cr-Nas15* gene KO (Figure 3F). So, we collected the *Cr-Nas15* notochord specific KO embryos and control embryos. After the phalloidin staining, we observed the phenotype of notochord lumen formation. In *Cr-Nas15* gene KO, 23 of 26 embryos have an abnormal lumen formation, while in control group, there are only 3 of 15 embryos have an abnormal lumen formation (Figure 3G). We also measured the diameter of the lumen in both *Cr-Nas15* gene KO group and control group. The statistical analysis showed that the lumen in *Cr-Nas15* gene KO group were significantly smaller than control group, phenocopying the inhibitor treatment and dominant negative overexpression results (Figure 3H). This result confirms that the *Cr*-Nas15 is an important factor regulating the *Ciona* notochord lumen formation.

Cr-Nas15 interacts with PPP2CA involving in lumen formation

To further find out the working mechanism of *Cr*-Nas15, we performed a yeast two-hybrid (Y2H) screening assay. The Protein Phosphatase 2 Catalytic Subunit Alpha (PPP2CA) was found as a candidate protein interacting with *Cr*-Nas15 (Figure 4A). To confirm the interaction between *Cr*-Nas15 and the PPP2CA, we carried out the CO-IP experiments. When the Nas15-GFP and PPP2CA-HA both existed, a band could be found in the IP group (Figure 4B). These results indicate the interaction between *Cr*-Nas15 and PPP2CA, suggesting the *Cr*-Nas15 and PPP2CA may form a complex functioning together. To confirm the *Cr*-Nas15 and PPP2CA formed a complex intracellular, we co-expressed the *PPP2CA-eGFP* and *Cr-Nas15-tdTomato* in *Ciona* notochord. The imaging data showed that the *PPP2CA-eGFP* and *Cr-Nas15-tdTomato* significantly co-localized together at the apical domain of notochord cell (Figure 4C). Together with these data, the PPP2CA and *Cr*-Nas15 formed a complex around the notochord apical domain. Then, we performed a co-electroporation of *PPP2CA-C201R* or PPP2CA WT with *Cr*-Nas15 fusion protein. The *Cr*-Nas15 showed a lower enrichment on apical membrane in *PPP2CA-C201R* group, suggesting the PPP2CA involved in Nas15 apical localization (Figures 4D, E). To test if the interaction between the PPP2CA and *Cr*-Nas15 is essential for the lumen formation, we constructed the *PPP2CA-C201R* as a dominant negative and overexpressed it in *Ciona* notochord, to observe if it can lead to same phenotype with *Cr*-Nas15 loss-of-function. The result showed that the lumen in *PPP2CA-C201R* overexpressed group is significantly smaller than the control group (Figure 4F), phenocopying the *Cr*-Nas15 loss-of-function. The measurement of lumen diameter also confirmed the smaller lumen phenotype of *PPP2CA-C201R* overexpression (Figure 4G). The identification of multiple phosphorylation sites within Nas15 implies a potential regulatory role of PPP2CA in modulating the phosphorylation levels of Nas15 (Figure 4H). In conclusion, the PPP2CA is an interaction protein of *Cr*-Nas15, which is essential for *Ciona* notochord lumen formation.

Discussion

In our research, we identified a *Ciona* matrix metalloproteinase, *Cr*-Nas15. Through phylogenetic and domain analysis, we confirmed that *Cr*-Nas15 is conserved, including the typical ZnMc-astacin-like domain and Zinc-binding metalloprotease motif. These findings suggest that *Ciona* Nas15 may share a conserved function with Nas proteins in vertebrates. Additionally, employing qPCR, promoter analysis, and immunofluorescence techniques, we have demonstrated the expression of *Cr*-Nas15 in the larval notochord of *Ciona* during lumen formation stages, where it is enriched at the apical domain of *Ciona* notochord cells.

Subsequently, we conducted experiments involving the inhibitor actinonin treatment, dominant negative overexpression, and gene knockout using the CRISPR/Cas9 system. These experiments further confirmed the involvement of *Cr*-Nas15 in notochord lumen formation and expansion. Moreover, we have discovered an interaction between PPP2CA and *Cr*-Nas15, which stabilizes the localization of *Cr*-Nas15 to the notochord apical domain.

The Nas15 belongs to the astacins family, together with the Meprin, BMP1/Tolloid etc (Huxley-Jones et al., 2007), which is a large family of zinc metalloproteases in bacteria and animals (Park et al., 2010). Previous studies have demonstrated that astacin family metalloproteases play crucial roles in various biological processes, including digestion, hatching, peptide processing, morphogenesis, and pattern formation. For example, the Meprins are involved in the base membrane protein hydrolyzing, such as the collagen IV, nidogen and fibronectin, which is essential for ECM remodeling (Kruse et al., 2004). Besides, the Meprin and BMP-1/Tolloid have been found to promote the collagen maturation and assembly by digesting the procollagen (Hopkins et al., 2007; Broder et al., 2013). The HCH-1, another member of BMP-1/tolloid family, participates in the hatching of *C. elegans* by digesting the eggshell. Astacus embryonic astacin (AEA) is highly expressed shortly before hatching, suggesting its function in eggshell degradation (Geier and Zwilling, 1998). Importantly, the functional roles of

10.3389/fevo.2024.1385516

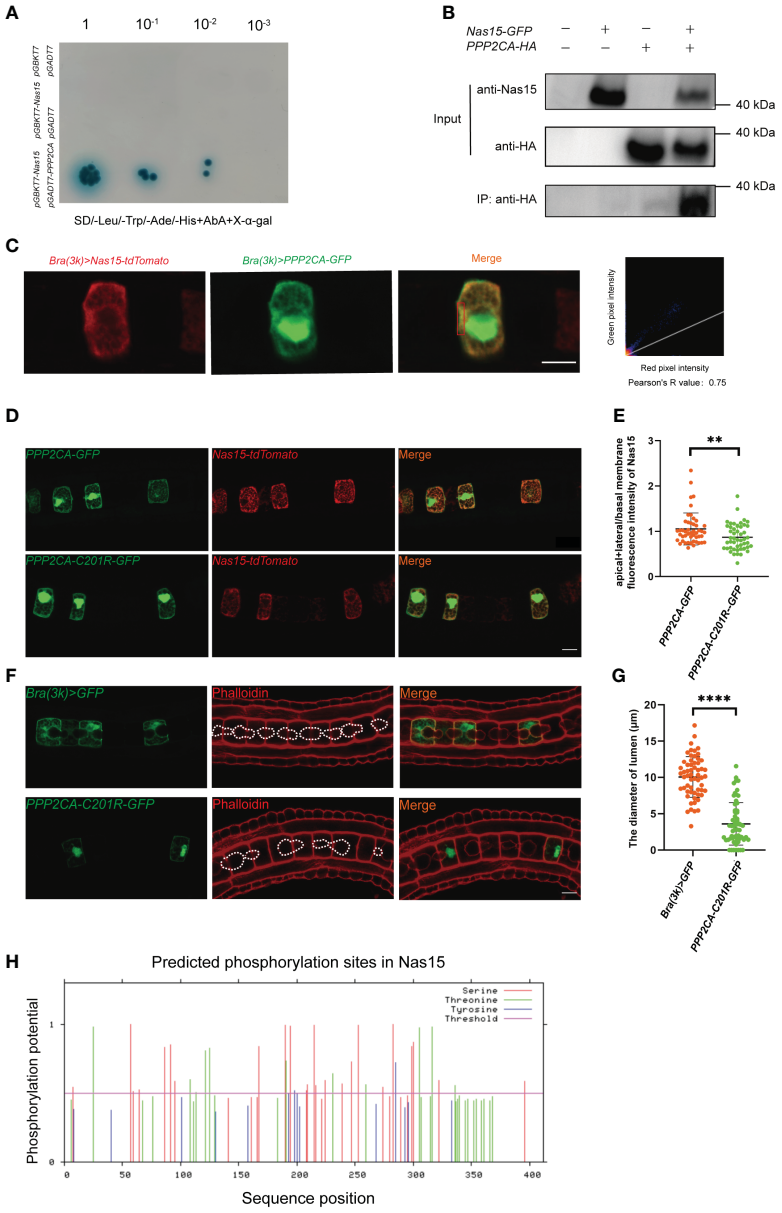

FIGURE 4
Cr-Nas15 interact with PPP2CA involving in lumen formation. **(A)** Interaction assays between Nas15 and PPP2CA by Y2H. **(B)** Co-IP validation of Nas15 interaction with PPP2CA in the HEK293T cell line. **(C)** Co-localization of Nas15 and PPP2CA in the apical domain of notochord cells. Red rectangle indicates the image area preforming colocalization test. **(D)** Co-electroporation of *PPP2CA-C201R* or PPP2CA WT with *Cr*-Nas15 fusion protein marker. **(E)** Quantification of the (apical+lateral)/basal membrane fluorescence intensity of Nas15 of overexpressing PPP2CA ($n_{Brachyury\ (3k)\ >PPP2CA::GFP}$ = 48) and PPP2CA dominant negative ($n_{Brachyury\ (3k)\ >\ PPP2CA\text{-}C201R::GFP}$ = 48) in D. **(F)** Phenotype of PPP2CA dominant negative overexpression in *Ciona* notochord. The dashed lines indicate the boundary of lumen. **(G)** Quantification of the lumen diameter of overexpressing *Brachyury (3k) > GFP* ($n_{Brachyury\ (3k)\ >\ GFP}$ = 59) and *PPP2CA* dominant negative ($n_{Brachyury\ (3k)\ >\ PPP2CA\text{-}C201R::GFP}$ = 61) in F. **(H)** Prediction of phosphorylation sites in Nas15. All Significance statistical analysis was preformed using unpaired two-tailed t test. **p < 0.01 and ****p < 0.0001. All scale bars represent 10 μm.

astacin metalloproteases primarily rely on their ability to digest stable ECM complex structures, facilitating their assembly or remodeling. Interestingly, in our study, Nas15 was found to be enriched on the apical membrane near the extracellular lumen, whereas most of the stable ECM components are localized in the notochord sheath covering the basal side of notochord cells. Both the laminin, fibronectin and collagen are secreted in a polarized manner, leading to the accumulation of the basal membrane in the notochord sheath at the basal domain of the notochord (Veeman3et al., 2008; Segade et al., 2016; Peng et al., 2023). On the contrary, the ECM in the notochord lumen exhibits low density and consists of short fibers, indicating the presence of a viscous fluid composed of dissolved ECM components (Hunziker and Schenk, 1984; Dong et al., 2009; Wei et al., 2017). Therefore, it's worth investigating why the Nas15 localizes to the apical domain instead of basal membrane. One possibility is it interacts with the dissolved ECM to contribute to lumen formation. This observation may suggest a potential novel mechanism of

how matrix metalloproteases regulate morphogenesis. The astacin family proteins have been found to localize to the apical membrane in some special models. For example, Meprin is localized to the apical membranes (brush-border) of renal proximal tubules (Herzog et al., 2014). Initially, Meprin anchors to the apical domain as a transmembrane metalloprotease (TMP), and subsequently, it is released as a secreted MMP through the digestion of ADAM10 (Herzog et al., 2014). However, in our study, we didn't find any *Cr*-Nas15 signal in the lumen space neither in immunofluorescence nor in fluorescence protein fusion protein marker overexpression. *Cr*-Nas15 specifically anchors to the apical membrane of the notochord lumen. Since the immobile *Cr*-Nas15 can only contact with a low-density ECM close to the apical membrane, how can the *Cr*-Nas15 influence the lumen formation?

One possible mechanism is keeping the apical ECM soluble. Around the notochord cells, the ECM exhibits different properties in different area. On the basal side, most of ECM component are made up by long fiber as a basement membrane. But there is no basement membrane ECM can be found but only short fiber ECM instead in the extracellular lumen (Wei et al., 2017), which suggesting a degradation mechanism may exist on the initial apical domain. During the expansion of the *Ciona* notochord lumen, a hydrostatic pressure is generated within the lumen space, driving its expansion (He et al., 2022). In this mechanism, the apical ECM need to be soluble. We propose that *Cr*-Nas15, enriched on the apical membrane, degrades the long ECM fiber to maintain a liquid lumen fluid. Therefore, *Cr*-Nas15 may serve as an protecting potential mechanism to prevent the accumulation of long fiber ECM in the apical domain. So, the ECM components in the initial lumen can act as a "sponge" to facilitate fluid influx (Denker and Jiang, 2012). The ECM degradation activity of *Cr*-Nas15 can increasing the osmotic pressure in the lumen space.

Another possible mechanism by which *Cr*-Nas15 influences lumen formation is by aiding in the maintenance of apical-basal (A-B) polarity. Many studies have shown that the ECM serves as a directional signal that helps cells establish A-B polarity. For example, the basement membrane interacts with integrin, providing an extracellular signal for epithelial cell A-B polarity (Manninen, 2015). In the *Ciona* notochord, the ECM also plays an important role in polarity maintenance (Peng et al., 2020). Thus, the specific apically localized *Cr*-Nas15 may influence the polarized distribution of the basement membrane ECM around notochord cells, which could in turn affect A-B polarity maintenance. In our study, loss-of-function of *Cr*-Nas15 delayed the initial formation of the lumen, suggesting a blocking of A-B polarity establishment. Another interesting phenotype was the asymmetrical expansion of the lumen in *Cr*-Nas15, indicating a decrease in the surface area of the apical membrane. Since apical membrane delivery is provided by polarized vesicle transport, we propose that the disruption of A-B polarity in *Cr*-Nas15 loss-of-function cells could lead to a decrease of apical domain targeting vesicles.

The interaction between cells and ECM plays a crucial role in the regulation of morphogenesis. However, it is still unclear how cells can dynamically regulate the quantity, location, and properties of the ECM to provide feedback control of tissue morphogenesis. In our study, we discovered that *Cr*-Nas15 has the potential ability to degrade ECM within the lumen, which can influence lumen formation. This finding provides a new and possible mechanism for how matrix metalloproteinases may be involved in tubulogenesis.

In this study, the interaction between PPP2CA and *Cr*-Nas15 was identified, and the dominant negative versions of PPP2CA show phenocopy with the *Cr*-Nas15. As PPP2CA functions as the catalytic subunit of a phosphatase, we hypothesize that the phosphorylation of *Cr*-Nas15 plays a crucial role in its function. While *Cr*-Nas15 exhibits numerous potential phosphorylation sites, the specific mechanism remains unclear. Phosphorylation is an important form of post-translational modification that can affect protein localization or activity. Therefore, we propose that PPP2CA may regulate lumen formation indirectly by modulating the function of *Cr*-Nas15.

The notochord is a special mid-line organ of all Chordates, acting as a trunk supporting structure and developmental signaling center (Corallo et al., 2015). As a supporting structure, the mechanical stiffness of notochord is an important factor to provide a basis of controlled and rapid movement and protection of neural tube (Sui et al., 2021). During the notochord evolution, there are two events leading to remarkable stiffness increase. The turgid rod structure appearance constructed with a ECM sheath outside and vacuolated notochord cells inside (Yasuoka, 2020), and the spine formation in which the notochord cells forming the nucleus pulposus of the intervertebral discs (Smits and Lefebvre, 2003; Raghavan et al., 2023). Before the emergence of chordates, some cells or tissues present gene expression pattern similar to that in notochord such as expression of Brachyury in the stomodeum and proctdaeumin of *Polychaete* or hindgut and anal pads of *Drosophila* (Satoh et al., 2012). A notochord-like muscle structure called axochord was reported in *annelid* (Lauri et al., 2014; Brunet et al., 2015), which was considered as a primitive form of notochord. These tissues be known as notochord ancestor both lack observable vacuoles. The notochord in ascidian, *amphioxus* and chordate both have a vacuolation which making up a turgor pressure sheath structure together with the ECM notochord sheath (Yasuoka, 2020), which structure improving the notochord stiffness by sealing a hydrostatic pressure. Interestingly, the notochord vacuolation in *Ciona* is special. The notochord lumen in the *Amphioxus* (Eakin and Westfall, 1962) and chordate such as the *zebrafish*, *chick* and *mice* (Choi et al., 2008; Ellis et al., 2013; Ward et al., 2018) are intercellular vacuole. However, the *Ciona* larval notochord construct an extracellular connected lumen (Dong et al., 2009), which is a special notochord structure in notochord evolution. Previous researches showed that the *Ciona* notochord expressed some evolutionarily conserved key molecule regulating notochord specific gene expression (Maguire et al., 2018; Raghavan et al., 2023), which suggests a key phylogenetic position of *Ciona* as a notochord origin class. Therefore, the notochord extracellular lumen may show the early form of vacuolate notochord. Compared with the intracellular vacuole inflation, the extracellular lumen formation needs some different cell behavior regulation such as the A-B polarity establishing, cell junction remodeling, apical ECM secretion and processing, etc., but the mechanism still remains unclear. Here, we found the MMP family protein *Cr*-Nas15 specific localized at the membrane of extracellular

lumen which is essential for lumen expansion, suggesting that some pre-existing extracellular ingredient degradation such as the ECM may help the extracellular lumen formation. This study suggested that the mechanism that MMP mediated extracellular lumen opening may play as a functional replacement before intracellular notochord vacuole appeared in evolution. So, the *Cr*-Nas15 may play as a clue for further study of the vacuolation of notochord.

Data availability statement

The original contributions presented in the study are included in the article/Supplementary Material, further inquiries can be directed to the corresponding author/s.

Author contributions

JB: Data curation, Formal analysis, Investigation, Methodology, Writing – original draft, Writing – review & editing. YG: Investigation, Visualization, Writing – review & editing. ZW: Investigation, Writing – review & editing. HP: Validation, Visualization, Writing – original draft, Writing – review & editing. BD: Funding acquisition, Methodology, Project administration, Supervision, Validation, Writing – original draft, Writing – review & editing.

Funding

The author(s) declare financial support was received for the research, authorship, and/or publication of this article. This research was funded by the Science & Technology Innovation Project of Laoshan Laboratory (No. LSKJ202203204).

Acknowledgments

We thank members of Dong laboratory for experimental technical guidance. We are very grateful to Guo huarong's lab for sharing the HEK293 T cell lines.

Conflict of interest

The authors declare that the research was conducted in the absence of any commercial or financial relationships that could be construed as a potential conflict of interest.

Publisher's note

Supplementary material

The Supplementary Material for this article can be found online at: https://www.frontiersin.org/articles/10.3389/fevo.2024.1385516/full#supplementary-material

References

Annona, G., Holland, N. D., and D'Aniello, S. (2015). Evolution of the notochord. *EvoDevo* 6, 1–13. doi: 10.1186/s13227-015-0025-3

Baumann, U., Wu, S., Flaherty, K. M., and McKay, D. B. (1993). Three-dimensional structure of the alkaline protease of Pseudomonas aeruginosa: a two-domain protein with a calcium binding parallel beta roll motif. *EMBO J.* 12, 3357–3364. doi: 10.1002/embj.1993.12.issue-9

Bhattachan, P., Rae, J., Yu, H., Jung, W., Wei, J., Parton, R. G., et al. (2020). Ascidian caveolin induces membrane curvature and protects tissue integrity and morphology during embryogenesis. *FASEB J.* 34, 1345–1361. doi: 10.1096/fj.201901281R

Bond, J. S., and Beynon, R. J. (1995). The astacin family of metalloendopeptidases. *Protein Sci.* 4, 1247–1261. doi: 10.1002/pro.5560040701

Bonnans, C., Chou, J., and Werb, Z. (2014). Remodelling the extracellular matrix in development and disease. *Nat. Rev. Mol. Cell Biol.* 15, 786–801. doi: 10.1038/nrm3904

Broder, C., Arnold, P., Vadon-Le Goff, S., Konerding, M. A., Bahr, K., Muller, S., et al. (2013). Metalloproteases meprin alpha and meprin beta are C- and N-procollagen proteinases important for collagen assembly and tensile strength. *Proc. Natl. Acad. Sci. U.S.A.* 110, 14219–14224. doi: 10.1073/pnas.1305464110

Brunet, T., Lauri, A., and Arendt, D. (2015). Did the notochord evolve from an ancient axial muscle? The axochord hypothesis. *Bioessays* 37, 836–850. doi: 10.1002/bies.201500027

Calabria, P. A., Shimokawa-Falcão, L. H. A., Colombini, M., Moura-da-Silva, A. M., Barbaro, K. C., Faquim-Mauro, E. L., et al. (2019). Design and production of a recombinant hybrid toxin to raise protective antibodies against Loxosceles spider venom. *Toxins* 11, 108. doi: 10.3390/toxins11020108

Cao, C., Lemaire, L. A., Wang, W., Yoon, P. H., Choi, Y. A., Parsons, L. R., et al. (2019). Comprehensive single-cell transcriptome lineages of a proto-vertebrate. *Nature* 571, 349–354. doi: 10.1038/s41586-019-1385-y

Choi, K. S., Cohn, M. J., and Harfe, B. D. (2008). Identification of nucleus pulposus precursor cells and notochordal remnants in the mouse: implications for disk degeneration and chordoma formation. *Dev. Dyn.* 237, 3953–3958. doi: 10.1002/dvdy.21805

Corallo, D., Trapani, V., and Bonaldo, P. (2015). The notochord: structure and functions. *Cell Mol. Life Sci.* 72, 2989–3008. doi: 10.1007/s00018-015-1897-z

Denker, E., and Jiang, D. (2012). Ciona intestinalis notochord as a new model to investigate the cellular and molecular mechanisms of tubulogenesis. *Semin. Cell Dev. Biol.* 23, 308–319. doi: 10.1016/j.semcdb.2012.03.004

Dong, B., Deng, W., and Jiang, D. (2011). Distinct cytoskeleton populations and extensive crosstalk control Ciona notochord tubulogenesis. *Development* 138, 1631–1641. doi: 10.1242/dev.057208

Dong, B., Horie, T., Denker, E., Kusakabe, T., Tsuda, M., Smith, W. C., et al. (2009). Tube formation by complex cellular processes in Ciona intestinalis notochord. *Dev. Biol.* 330, 237–249. doi: 10.1016/j.ydbio.2009.03.015

Eakin, R. M., and Westfall, J. A. (1962). Fine structure of the notochord of amphioxus. *J. Cell Biol.* 12, 646–651. doi: 10.1083/jcb.12.3.646

Ellis, K., Bagwell, J., and Bagnat, M. (2013). Notochord vacuoles are lysosome-related organelles that function in axis and spine morphogenesis. *J. Cell Biol.* 200, 667–679. doi: 10.1083/jcb.201212095

Franco, A. A., Buckwold, S. L., Shin, J. W., Ascon, M., and Sears, C. L. (2005). Mutation of the Zinc-Binding Metalloprotease Motif AffectsBacteroides fragilisToxin Activity but Does Not Affect Propeptide Processing. *Infection Immunity.* 73, 5273–5277. doi: 10.1128/IAI.73.8.5273-5277.2005

Geier, G., and Zwilling, R. (1998). Cloning and characterization of a cDNA coding for Astacus embryonic astacin, a member of the astacin family of metalloproteases from

the crayfish Astacus astacus. *Eur. J. Biochem.* 253, 796–803. doi: 10.1046/j.1432-1327.1998.2530796.x

He, M., Wei, J., Li, Y., and Dong, B. (2022). Nuclear factor of activated T cells-5 regulates notochord lumenogenesis in chordate larval development. *Int. J. Mol. Sci.* 23 (22), 14407. doi: 10.3390/ijms232214407

Herzog, C., Haun, R. S., Ludwig, A., Shah, S. V., and Kaushal, G. P. (2014). ADAM10 is the major sheddase responsible for the release of membrane-associated meprin A. *J. Biol. Chem.* 289, 13308–13322. doi: 10.1074/jbc.M114.559088

Hopkins, D. R., Keles, S., and Greenspan, D. S. (2007). The bone morphogenetic protein 1/Tolloid-like metalloproteinases. *Matrix Biol.* 26, 508–523. doi: 10.1016/j.matbio.2007.05.004

Hu, J., Gao, Y., Huang, Q., Wang, Y., Mo, X., Wang, P., et al. (2021). Flotillin-1 interacts with and sustains the surface levels of TRPV2 channel. *Front. Cell Dev. Biol.* 9. doi: 10.3389/fcell.2021.634160

Hunziker, E. B., and Schenk, R. K. (1984). Cartilage ultrastructure after high pressure freezing, freeze substitution, and low temperature embedding. II. Intercellular matrix ultrastructure - preservation of proteoglycans in their native state. *J. Cell Biol.* 98, 277–282. doi: 10.1083/jcb.98.1.277

Huxley-Jones, J., Clarke, T.-K., Beck, C., Toubaris, G., Robertson, D. L., and Boot-Handford, R. P. (2007). The evolution of the vertebrate metzincins; insights from Ciona intestinalis and Danio rerio. *BMC Evolution Biol.* 7, 1–20. doi: 10.1186/1471-2148-7-63

Kruse, M. N., Becker, C., Lottaz, D., Kohler, D., Yiallouros, I., Krell, H. W., et al. (2004). Human meprin alpha and beta homo-oligomers: cleavage of basement membrane proteins and sensitivity to metalloprotease inhibitors. *Biochem. J.* 378, 383–389. doi: 10.1042/bj20031163

Kusakabe, T., Yoshida, R., Kawakami, I., Kusakabe, R., Mochizuki, Y., Yamada, L., et al. (2002). Gene expression profiles in tadpole larvae of Ciona intestinalis. *Dev. Biol.* 242, 188–203. doi: 10.1006/dbio.2002.0538

Lauri, A., Brunet, T., Handberg-Thorsager, M., Fischer, A. H., Simakov, O., Steinmetz, P. R., et al. (2014). Development of the annelid axochord: insights into notochord evolution. *Science* 345, 1365–1368. doi: 10.1126/science.1253396

Livak, K. J., and Schmittgen, T. D. (2001). Analysis of relative gene expression data using real-time quantitative PCR and the 2–ΔΔCT method. *Methods* 25, 402–408. doi: 10.1006/meth.2001.1262

Lu, Q., Bhattachan, P., and Dong, B. (2019). Ascidian notochord elongation. *Dev. Biol.* 448, 147–153. doi: 10.1016/j.ydbio.2018.11.009

Lubarsky, B., and Krasnow, M. A. (2003). Tube morphogenesis: making and shaping biological tubes. *Cell* 112, 19–28. doi: 10.1016/S0092-8674(02)01283-7

Maguire, J. E., Pandey, A., Wu, Y., and Di Gregorio, A. (2018). Investigating evolutionarily conserved molecular mechanisms controlling gene expression in the notochord. *Transgenic Ascidians.* p, 81–99.

Manninen, A. (2015). Epithelial polarity–generating and integrating signals from the ECM with integrins. *Exp. Cell Res.* 334, 337–349. doi: 10.1016/j.yexcr.2015.01.003

Mizotani, Y., Suzuki, M., Hotta, K., Watanabe, H., Shiba, K., Inaba, K., et al. (2018). 14-3-3epsilona directs the pulsatile transport of basal factors toward the apical domain for lumen growth in tubulogenesis. *Proc. Natl. Acad. Sci. U.S.A.* 115, E8873–E8881. doi: 10.1073/pnas.1808756115

Nagase, H., Visse, R., and Murphy, G. (2006). Structure and function of matrix metalloproteinases and TIMPs. *Cardiovasc. Res.* 69, 562–573. doi: 10.1016/j.cardiores.2005.12.002

Ouyang, X., Wu, B., Yu, H., and Dong, B. (2023). DYRK1-mediated phosphorylation of endocytic components is required for extracellular lumen expansion in ascidian notochord. *Biol. Res.* 56, 10. doi: 10.1186/s40659-023-00422-9

Park, J. O., Pan, J., Mohrlen, F., Schupp, M. O., Johnsen, R., Baillie, D. L., et al. (2010). Characterization of the astacin family of metalloproteases in C. elegans. *BMC Dev. Biol.* . 10, 14. doi: 10.1186/1471-213X-10-14

Peng, H., Qiao, R., and Dong, B. (2020). Polarity establishment and maintenance in ascidian notochord. *Front. Cell Dev. Biol.* 8. doi: 10.3389/fcell.2020.597446

Peng, H., Qiao, J., Wang, G., Shi, W., Xia, F., Qiao, R., et al. (2023). A collagen-rich arch in the urochordate notochord coordinates cell shaping and multi-tissue elongation. *Curr. Biol.* 33, 5390–5403 e5393. doi: 10.1016/j.cub.2023.11.001

Raghavan, R., Coppola, U., Wu, Y., Ihewulezi, C., Negrón-Piñeiro, L. J., Maguire, J. E., et al. (2023). Gene expression in notochord and nuclei pulposi: a study of gene families across the chordate phylum. *BMC Ecol. Evol.* 23, 63. doi: 10.1186/s12862-023-02167-1

Sacharidou, A., Stratman, A. N., and Davis, G. E. (2012). Molecular mechanisms controlling vascular lumen formation in three-dimensional extracellular matrices. *Cells Tissues Organs* 195, 122–143. doi: 10.1159/000331410

Sarraju, A., and Nissen, S. E. (2024). Atherosclerotic plaque stabilization and regression: a review of clinical evidence. *Nat. Rev. Cardiol.* 1–11. doi: 10.1038/s41569-023-00979-8

Satoh, N., Tagawa, K., and Takahashi, H. (2012). How was the notochord born? *Evol. Dev.* 14, 56–75. doi: 10.1111/j.1525-142X.2011.00522.x

Satou, Y., Kawashima, T., Shoguchi, E., Nakayama, A., and Satoh, N. (2005). An integrated database of the ascidian, Ciona intestinalis: towards functional genomics. *Zoological science.* 22, 837–843. doi: 10.2108/zsj.22.837

Segade, F., Cota, C., Famiglietti, A., Cha, A., and Davidson, B. (2016). Fibronectin contributes to notochord intercalation in the invertebrate chordate, Ciona intestinalis. *Evodevo* 7, 21. doi: 10.1186/s13227-016-0056-4

Senger, D. R., and Davis, G. E. (2011). Angiogenesis. *Cold Spring Harbor Perspect. Biol.* 3, a005090–a005090. doi: 10.1101/cshperspect.a005090

Simons, M., and Walz, G. (2006). Polycystic kidney disease: cell division without a c (l)ue? *Kidney Int.* 70, 854–864. doi: 10.1038/sj.ki.5001534

Smits, P., and Lefebvre, V. r. (2003). Sox5 and Sox6 are required for notochord extracellular matrix sheath formation, notochord cell survival and development of the nucleus pulposus of intervertebral discs. *Development* 130, 1135–1148. doi: 10.1242/dev.00331

Sterchi, E., Stocker, W., and Bond, J. (2008). Meprins, membrane-bound and secreted astacin metalloproteinases. *Mol. Aspects Med.* 29, 309–328. doi: 10.1016/j.mam.2008.08.002

Stolfi, A., and Christiaen, L. (2012). Genetic and genomic toolbox of the chordate Ciona intestinalis. *Genetics* 192, 55–66. doi: 10.1534/genetics.112.140590

Stolfi, A., Gandhi, S., Salek, F., and Christiaen, L. (2014). Tissue-specific genome editing in Ciona embryos by CRISPR/Cas9. *Development* 141, 4115–4120. doi: 10.1242/dev.114488

Sui, Z., Zhao, Z., and Dong, B. (2021). Origin of the chordate notochord. *Diversity* 13 (10), 462. doi: 10.3390/d13100462

Talantikite, M., Lecorche, P., Beau, F., Damour, O., Becker-Pauly, C., Ho, W. B., et al. (2018). Inhibitors of BMP-1/tolloid-like proteinases: efficacy, selectivity and cellular toxicity. *FEBS Open Bio.* 8, 2011–2021. doi: 10.1002/2211-5463.12540

Tamura, K., Stecher, G., and Kumar, S. (2021). MEGA11: molecular evolutionary genetics analysis version 11. *Mol. Biol. Evolution* . 38, 3022–3027. doi: 10.1093/molbev/msab120

Tarhan, L., Bistline, J., Chang, J., Galloway, B., Hanna, E., and Weitz, E. (2023). Single Cell Portal: an interactive home for single-cell genomics data. *bioRxiv*. doi: 10.1101/2023.07.13.548886

Tassy, O., Dauga, D., Daian, F., Sobral, D., Robin, F., Khoueiry, P., et al. (2010). The ANISEED database: digital representation, formalization, and elucidation of a chordate developmental program. *Genome Res.* 20, 1459–1468. doi: 10.1101/gr.108175.110

Trevisan-Silva, D., Gremski, L. H., Chaim, O. M., da Silveira, R. B., Meissner, G. O., Mangili, O. C., et al. (2010). Astacin-like metalloproteases are a gene family of toxins present in the venom of different species of the brown spider (genus Loxosceles). *Biochimie* 92, 21–32. doi: 10.1016/j.biochi.2009.10.003

Veeman, M. T., Nakatani, Y., Hendrickson, C., Ericson, V., Lin, C., and Smith, W. C. (2008). Chongmague reveals an essential role for laminin-mediated boundary formation in chordate convergence and extension movements. *Development* 135, 33–41. doi: 10.1242/dev.010892

Verma, R. P., and Hansch, C. (2007). Matrix metalloproteinases (MMPs): chemical-biological functions and (Q)SARs. *Bioorg Med. Chem.* 15, 2223–2268. doi: 10.1016/j.bmc.2007.01.011

Wang, Z., Tan, Z., Bi, J., Liu, A., Jiang, A., and Dong, B. (2023). Proteomic identification of intracellular vesicle trafficking and protein glycosylation requirements for lumen inflation in Ciona notochord. *Proteomics*, 23 (10), 2200460. doi: 10.1002/pmic.202200460

Ward, L., Pang, A. S. W., Evans, S. E., and Stern, C. D. (2018). The role of the notochord in amniote vertebral column segmentation. *Dev. Biol.* 439, 3–18. doi: 10.1016/j.ydbio.2018.04.005

Wei, J., Wang, G., Li, X., Ren, P., Yu, H., and Dong, B. (2017). Architectural delineation and molecular identification of extracellular matrix in ascidian embryos and larvae. *Biol. Open* 6, 1383–1390. doi: 10.1242/bio.026336

Yasuoka, Y. (2020). Morphogenetic mechanisms forming the notochord rod: The turgor pressure-sheath strength model. *Dev. Growth Differ.* 62, 379–390. doi: 10.1111/dgd.12665

frontiers | Frontiers in Ecology and Evolution

TYPE Perspective
PUBLISHED 15 November 2024
DOI 10.3389/fevo.2024.1428976

OPEN ACCESS

EDITED BY
Maria Ina Arnone,
Stazione Zoologica Anton Dohrn, Italy

REVIEWED BY
Filomena Ristoratore,
Zoological Station Anton Dohrn, Italy
Yiyang Yuan,
Shandong Academy of Agricultural Sciences, China

*CORRESPONDENCE
Kohji Hotta
khotta@keio.jp

RECEIVED 07 May 2024
ACCEPTED 22 October 2024
PUBLISHED 15 November 2024

CITATION
Hotta K, Miyasaka SO, Oka K and Shito TT (2024) Staring into a crystal ball: understanding evolution and development of *in vivo* aquatic organismal transparency. *Front. Ecol. Evol.* 12:1428976. doi: 10.3389/fevo.2024.1428976

Staring into a crystal ball: understanding evolution and development of *in vivo* aquatic organismal transparency

Kohji Hotta[1]*, Shunsuke O. Miyasaka[1], Kotaro Oka[1,2] and Takumi T. Shito[1]

[1]Department of Bioscience and Informatics, Faculty of Science and Technology, Keio University, Yokohama, Japan, [2]School of Frontier Engineering, Kitasato University, Sagamihara, Japan

Organismal transparency is an ecologically important trait that can provide camouflage advantages to diverse organisms. Transparent organisms are quite common—especially in oceans. Organismal transparency requires low absorption and scattering of light in the body across multi-scale levels. However, it is still not fully understood how such organisms achieve these requirements. Understanding this process requires multiple approaches from various fields and methods. Here, we offer recent insights on this topic from the viewpoints of evolution, developmental biology, and evaluation methodologies of organismal transparency. We also propose "organismal transparency biology" as a new interdisciplinary field of study. Furthermore, we suggest that tunicates are an ideal model animal for studying *in vivo* organismal transparency.

KEYWORDS

bio-transparency, eco-evo-devo, hyperspectral imaging, tunicate, Ascidiidae, Ascidiella aspersa

1 Introduction

Organismal transparency is an important camouflage strategy that aids in defense against visual predators. Organismal transparency is commonly seen in aquatic animals such as jellyfish, siphonophores, some crustaceans, pteropods, some squids, fish larvae and tunicates (McFall-Ngai, 1990; Johnsen, 2001, 2014; Kakiuchida et al., 2017; Bagge, 2019; Shito et al., 2020). Transparency requires that the species minimize both light absorption and scattering (Kerker, 1969). This involves equalizing the refractive index inside and outside the organism, altering its physical surface properties, and avoiding the creation of opaque organic molecules like pigments. Here, we introduce how light scattering, reflection, and absorption relate to organismal transparency and then describe the factors that contribute to improving transparency—namely optical cleaning agents (OCA).

1.1 Light absorption

As incident light passes through the interior of the organism, its intensity decreases due to light absorption. Most organic molecules in organisms do not absorb visible light except for pigments (Inyushin et al., 2019). Natural pigments and other molecules found in marine organisms have specific absorption wavelengths (Pettersen et al., 2014). Pigments absorb the light, and this feature protects animals from harmful UV radiation, transport oxygen by blood cells, and facilitating optical sensation. There are many different strategies to reduce light absorption of pigments. For example, icefish eliminate their own hemoglobin and have transparent blood cells (Ruud, 1954). Transparent glass frogs conceal their body by relocating approximately 89% of the red blood cells to the liver during sleep. Relocation of red blood cells to liver minimizes light absorption and scattering in other tissues, thus enhancing transparency at the whole-body level. Thus, transparency in this species increases by two- to three-fold due to the inability to see red blood cells (Taboada et al., 2022).

Transparency is not only achieved via the absence of pigmentation as in some albino mutants. A relatively transparent mutant lacking pigment (Wakamatsu et al., 2001) was created in medaka leading to transparency. Even in such cases, achieving perfect transparency is limited due to optical scattering. Transparency is also immediately opaque after the death of an transparent oocyte (Shito et al., 2023). This means that not having pigmentation is a minimum requirement for organismal transparency which is not an active strategy for organismal transparency (Bhandiwad and Johnsen, 2011).

The light absorption of living organisms also changes with metabolism (Table 1). For example, in anemone shrimp, the hemolymph penetrates the muscle fibers more when metabolic activity is high due to exercise, thus disrupting the uniformity of the refractive index of the tissue and making the muscle appear opaque (Bagge et al., 2017).

1.2 Light reflection

Light reflection arises at the interface between two optical media with different refractive indices. The main focus in this perspective is marine organismal transparency, which requires the organisms' refractive index to be near seawater's refractive index of 1.33. To achieve optimal transparency, the organism's media should have uniform refractive indices across multiple scales (tissue, cell/Extracelllar Matrix (ECM), and organelles) (Figure 1). For example, the gelatinous body of transparent marine animals such as jellyfish and leptocephalus contains a lot of water, which allows their refractive index to remain transparent in seawater because it is not very different from seawater's reflective index 1.33 (Pfeiler et al., 2002; Warrant and Locket, 2004). In the highly hydrated extracellular gelatinous body matrix of leptocephalus, the body water content is approximately 92% (Pfeiler and Govoni, 1993; Bishop et al., 2000). However, during metamorphosis to the adult eel, approximately 80% of the total body water content is lost (Pfeiler, 1984).

TABLE 1 Inhibiting factors challenging organismal transparency.

Inhibiting factor		Reasons why transparency is inhibited
Structural	Structural Complexity	The presence of complex organs and tissues that are not optically homogeneous can hinder transparency. (cf. nanostructure in 1.3, 1.4)
Physiological	Metabolic Requirements	The need for blood cells and other opaque structures to support metabolism. (1.1)
	Cellular Processes	The presence of cellular organelles and other intracellular structures derived from various cellular processes that scatter light. (cf. organelle degradation by PLAAT in 1.3)
Environmental	External Conditions	Variations in osmotic pressure, pH, and temperature that influence the efficiency of transparency. (2.3)
Above factors influence on		
Optical	Light Absorption	Pigmentation is necessary for UV protection and camouflage, but it reduces transparency. (cf. pigmentation in 1.1)
	Light Scattering	The surface and the internal structure of biological tissues can reflect or scatter light thus reducing transparency. (e.g. 1.2 and 1.3)

1.3 Light scattering

Light scattering is divided into surface scattering (Bagge et al., 2016) on the cell surface for incident light, and internal scattering (Marina et al., 2012; Bagge et al., 2017) that occurs in the presence of various organelles inside the cell. In multicellular organisms, surface scattering occurs at the interface between cells, the cell membrane, and the ECM (Figure 1).

In surface scattering, certain organisms have reduced or eliminated this reflection through the array of sub-microscopic projections (Miller and Autrum, 1979; Wilson and Hutley, 1982; Kakiuchida et al., 2017). This structure does not scatter light but rather mimics a material with a graded reflective index (Johnsen, 2003). In the hyperiid *Cystisoma*, the leg surfaces are covered with tiny nanostructures, thus making the surface resemble long-pile carpet, thus weakening and softening surface light scattering at the interface (Bagge et al., 2016).

Many reports have suggested that transparent organisms employ various strategies to mitigate light absorption and scattering—these are crucial optical factors that facilitate their transparency (Bagge, 2019). Many animals are opaque because the density and refractive index of biological media vary at different spatial scales, i.e., individual, tissue/organ, cell, and organelle levels (Johnsen and Widder, 1999; Johnsen, 2014; Tarique et al., 2023). At the cellular level, the cornea and lens in the eye develop via degradation of organelles by autophagy (Brennan et al., 2023). In the lens cells, organelles such as mitochondria and the endoplasmic reticulum are degraded by a lipid-degrading enzyme from the PLAAT family. Inhibiting this process leads to lens transparency (Morishita et al., 2021).

10.3389/fevo.2024.1428976

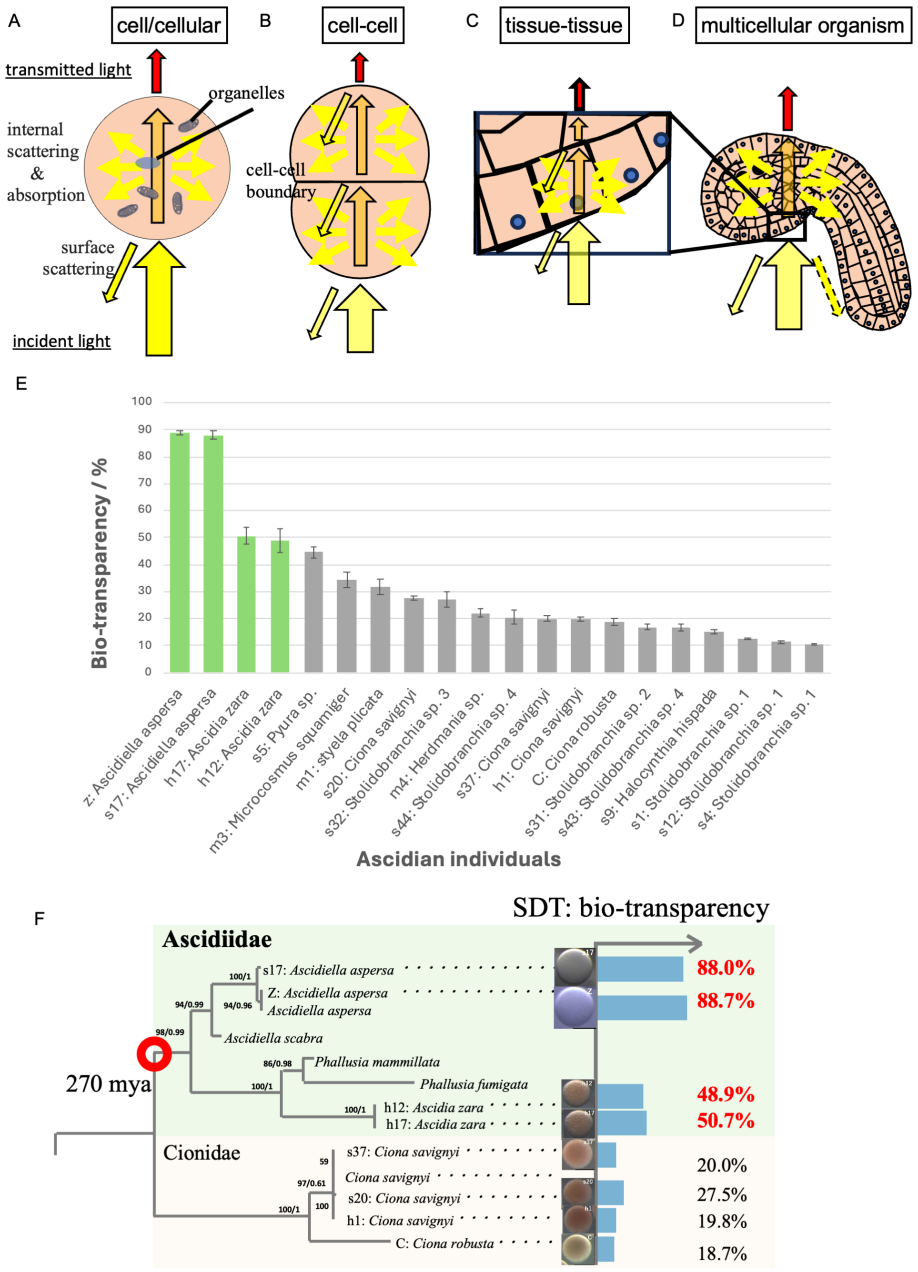

FIGURE 1
Possible multi-scale factors that inhibit organismal transparency in ascidian eggs. **(A)** In a single cell (oocyte in this case), light scattering within the cell is the surface scattering of the cell surface for incident light (black frame with yellow arrow), and the internal scattering in the presence of various organelles inside the cell. Due to the absorption and the internal scattering, the transmitted light (red arrow) is attenuated (orange arrow) when passing through the inside of the organism. **(B)** At the cell-cell boundary, surface scattering occurs due to the cell membrane and the ECM between the cells. **(C)** Similar to cells, surface scattering occurs between tissues with different refractive indexes. **(D)** There are ways to attenuate the surface scattering in some organisms by changing the surface ultra-structure (ex: nipple array). **(E)** Ascidian eggs have a variety of organismal transparency ranging from 10% to 90%, which is comparable to window glass. Green bars indicate species belonging to the Ascidiidae family. **(F)** Ascidiidae, generally characterized by high egg transparency, is believed to have diverged from Cionidae in ascidians approximately 270 million years ago (marked with red circle). This figure was modified from Shito et al. (2020).

It is necessary to devise ways to suppress light scattering at each boundary region between cells, tissues, and organs as described in Section 2.2. At this time, surface scattering on the cell surface is treated as internal scattering at the higher tissue level. In other words, what is treated as surface scattering at a lower level is regarded as internal scattering at higher level (Figure 1A).

1.4 Optical clearing agents

The presence of cellular organelles within the cells (Figure 1A) is thus a factor contributing to tissue opacification. Crystallins have a structure in which specific amino acid residues are arranged regularly, which suppresses light scattering and enhances

transparency. The α-crystallin exhibits chaperone-like functions and solubilizes denatured βγ-crystallin (Rao et al., 1995). α-Crystallin prevents the aggregation of denatured βγ-crystallins by solubilizing them. Aggregated proteins scatter light within the lens, thus reducing transparency. α-Crystallin helps maintain a uniform refractive index within the lens by solubilizing denatured βγ-crystallins and preventing their aggregation, which can reduce light scattering and preserve lens transparency (Horwitz, 1992; Rao et al., 1995). In other words, crystallin molecules in the eye serve as natural endogenous optical clearing agents (OCA). Here, we defined OCA as materials—such as chemical substances, proteins, ECMs, or enzymes—that reduce light scattering and improve optical transparency in biological structures.

Endogenous OCAs have been reported in other transparent animal tissues as well, e.g., fish glycosaminoglycans and antifreeze proteins (see review (Inyushin et al., 2019).

1.5 The inhibiting factors challenging organismal transparency

Many animals are opaque due to the necessity of pigments for UV protection, thus illustrating a delicate balance in their survival (Hansson, 2000). However, as described previously, transparent organisms have a remarkable ability to overcome multiple inhibiting factors that challenge transparency. These factors include structural, physiological, and environmental aspects and cause optically reduces organismal transparency by light absorption and/or light scattering (Table 1).

Despite understanding of the inhibiting factors against organismal transparency, further research is needed to address the following questions: How has transparency evolved in specific lineages? How have organisms acquired transparency during development? What are the specific molecular mechanisms that enable transparency?

These answers require research in various fields and various scientific methods. Here, we discuss new perspectives: evolutionary genomics, developmental biology, and quantification and evaluation methodologies of organismal transparency. These areas have not received sufficient attention and should be studied further in the future.

2 Areas that should be enhanced to understand organismal transparency

2.1 Evolutionary genomics

Formal phylogenetic analysis with a quantitative measurement of transparency has only been performed in a few taxa such as lepidopterans (Gomez et al., 2021) and ascidians (Shito et al., 2020), but the results show that animal transparency is polyphyletic. In lepidopterans, transparent or translucent wings were found across 31 families suggesting that transparency evolved multiple times independently and is due to a massive diversity of structural strategies (Gomez et al., 2021).

Variability in the transparency of ascidian eggs ranges from 10% to 90% across different species (Figure 1E). Interestingly, species within the Ascidiidae family have highly transparent eggs. One hypothesis is that they evolved to enhance their transparency from an opaque ancestor 270 mya (Figure 1F). This suggests the presence of shared genetic changes within this family as shared derived traits (SDTs). Focusing on such animal groups with transparency as a SDT —rather than solely as individual convergent evolution cases—could be an important taxa for elucidating the genetic mechanism of acquiring transparency. Comparative genomics of the Ascidiidae family and other relatives might elucidate the shared genetic mutation among Ascidiidae for organismal transparency that might identify the natural OCAs in transparent tissues of ascidians.

2.2 Developmental biology

The absence of pigments is a prerequisite for organismal transparency as described in 1.1. There is currently no research on how transparency is acquired during the developmental process. We measured bio-transparency (Shito et al., 2020) of developing oocytes according to the oogenesis period of *Ciona robusta* (also called *Ciona intestinalis* type A) (Sakai et al., 2023). The results showed that *Ascidiella aspersa* maintains transparency throughout oogenesis stages I to III, while oocytes of *Ciona robusta* are initially transparent but rapidly become opaque during stage II (Figure 2A) (Satake et al., 2024). These results indicate that oocytes in ascidians are originally transparent, and *A. aspersa* maintains its transparency throughout oogenesis. Additionally, the transmittance spectrum of *A. aspersa* oocyte is maintained during subsequent embryonic development (Figure 2B). Therefore, oocyte transparency has a significant impact on the transparency acquisition of embryos as seen by the consistent transparency from the oogenesis stages (Figure 2A).

Hence, we propose that exploring the mechanism of maintaining oocyte transparency to later developmental stages can help answer more general questions about why the organism body is transparent. This phenomenon may result from the absence or suppression of specific genes involved in pigment synthesis within yolk granules as well as the presence of OCAs that maintain the properties of cellular components responsible for low light scattering. These findings suggest the need to understand the temporal expression of such components via a developmental biology approach.

We also found interesting phenomena about the transparency of *A. aspersa* during the cleavage period. There are changes in the transparency of the cell-cell boundary region. Transparency requires a constant refractive index at the internal and external boundaries. Immediately after cell division, the cell boundaries are observable in both *A. aspersa* and *C. robusta*. However, only the cell-cell boundary in *A. aspersa* becomes transparent after subsequent compaction (Supplementary Video 1; Figures 2C, D). The exact mechanism responsible for this optical property is not known, but the finding suggests that the region of cell-cell boundary (the cell membrane or ECM) in *A. aspersa* uses different properties

10.3389/fevo.2024.1428976

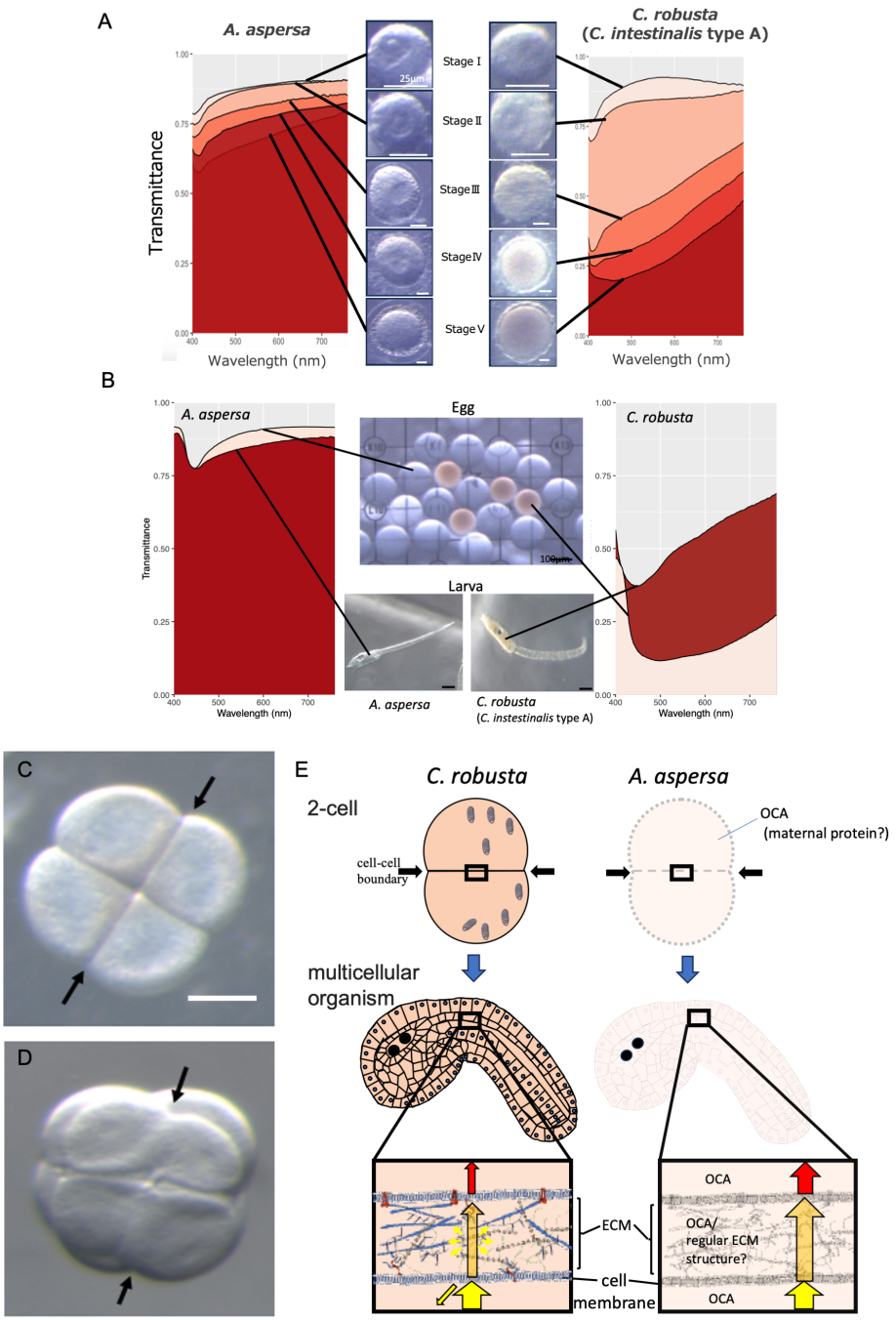

FIGURE 2
Comparison of egg transparency between *A. aspersa* from the Ascidiidae family and opaque species of ascidians, *C. robusta*. **(A)** Quantitative comparison of organismal transparency spectra from Stage I to Stage V during the oocyte maturation process in different ascidian species: *A. aspersa* and *C. robusta*. Spectre data were obtained via a hyperspectral camera (custom model NH-KO, EBA JAPAN, Tokyo, Japan). **(B)** Quantitative comparison of organismal transparency spectra between eggs and larvae in different ascidian species: *A. aspersa* and *C. robusta*. **(C)** Microscopic images of four-cell stage embryos after compaction in *C. robusta* embryo. **(D)** Microscopic images of four-cell stage embryos after compaction in *A. aspersa* embryo. Distinct boundaries are discernible in *C. robusta* at the newly formed cleavage planes in the 4-cell stage, but not in *A. aspersa* embryo (arrows). **(E)** Schematic representation of opaque *C. robusta* and transparent *A. aspersa* embryos. In the cleavage period (two-cell stage), there is no pigment accumulation in the cytoplasm after oogenesis. This suggests the possibility of the presence of some OCAs preventing the internal scattering of transmitted light in *A. aspersa*. *A. aspersa* minimizes light scattering despite the presence of diverse ECM at cell-cell boundary regions even in the multicellular stage. *A. aspersa* likely possesses special factors, e.g., regular ECM structures as well as the presence of OCA with both hydrophilic and hydrophobic properties in the ECM.

with that of *C. robusta*. The ECM is generally hydrophilic, and a difference in the refractive index may occur at the boundary with lipophilic cell membranes. Therefore, OCA with both hydrophilic and lipophilic properties might exist in the transparent ECM of *A. aspersa*. Another possibility is that the structural proteins present in the ECM, such as collagen and keratin, are often transparent if these proteins have a regular structure (Poole and Mostaço-Guidolin, 2021), which results in less light scattering. Studies into whether the ultrastructure of ECM would be regular or not is one of the key factors in the organismal transparency of *A. aspersa* (Figure 2E).

Transparency is physiologically affected (Table 1). We found that actinomycin D transcription inhibitor did not change transparency, but cycloheximide translation inhibitor significantly decreased egg transparency (Shito et al., 2023). Considering the differences between the two inhibitors, we propose that the transparency does not require the expression of new genes but rather relies on the function, metabolism, or enzymatic reactions of already transcribed proteins (maternal proteins). This is consistent with the importance of lipid metabolism in maintaining the optical transparency of the vertebrate lens (Borchman and Yappert, 2010).

2.3 Quantification and evaluation methods of organismal transparency

Advancements in measurement systems are crucial to elucidating the mechanisms of organismal transparency. Recently, Taboada et al. discovered that glass frogs enhance transparency by redistributing 89% of their red blood cells to the liver during sleep as tracked through photoacoustic imaging of glass frog erythrocyte dynamics (Taboada et al., 2022). Concurrently, the reflective indices of a salp were measured by an Abbe refractometer, and the values were slightly greater than seawater (Kakiuchida et al., 2017).

Several other methods have been used to quantify the organismal transparency. A spectrometer can calculate light transmission in one or several spectra (Johnsen and Widder, 1999). Hyperspectral imaging can measure transmittance at various wavelengths from the ultraviolet to the infrared with high resolution (Velasco-Hogan et al., 2019; Shito et al., 2020, 2023). The transmittance differs depending on each spectrum, and different factors such as environmental changes like pH, temperature and salinity, or bioactive substances should influence each spectrum. For instance, higher acidity (lower pH) and temperature variations can alter the protein structures within the organism potentially leading to changes in light scattering and transparency (Surewicz and Olesen, 1995).

There is a need for an evaluation system that can understand the correspondence between these different factors and transmittance for each spectrum. Combining a hyperspectral camera with analytical methods like principal component analysis (PCA) can evaluate the organismal transparency in a multi-dimensional way (Shito et al., 2023). By compressing multidimensional spectral data, information on organismal transparency can be mapped onto two- or three-dimensional space, thus enabling evaluation with higher resolution than before. With this evaluation system, one can clearly see that there are multiple states based on the differences in spectra even though the transparency has the same value.

Raman microscopy is also a powerful tool that potentially can link intrinsic molecular states and transparency over the entire wavelength range (Nakamura et al., 2013). Raman microscopy uses Raman scattering to analyze the molecular vibrations and rotations of materials within a sample. The spectral features of corneal collagen change due to heating and aging are detected using Raman microscopy (Goheen et al., 1978).

Analysis based on these spectral data allows for precise and detailed analysis of transparency by wavelength. For example, by detecting specific wavelengths that are affected by various environmental factors or inhibitors on transparency, we can further understand the mechanism of organismal transparency. Furthermore, such analysis may enable us to identify OCAs present in transparent organisms.

2.4 Implications for biological and medical studies

The fields of biology and medical research have shown that transparency techniques are critical for high-resolution optical imaging of tissues. Deep imaging is hindered by the opacity of tissues, and thus techniques are being developed to make tissue specimens almost transparent by matching the refractive indices of fixed specimens and media to the refractive index of lipid layers or by removing lipids (Hama et al., 2015; Zheng and Rinaman, 2016; Murakami et al., 2018; Umezawa et al., 2019; Tian et al., 2021). This allows for applications such as constructing a 3D atlas of the brain by making tissues and organs transparent (Murakami et al., 2018) or detecting micrometastases of cancer cells (Kingston et al., 2019). However, these specimens are derived from deceased and chemically fixed tissues. Alternatively, we can learn from transparent organisms how they make *in vivo* tissues transparent. Research that learns the molecular mechanisms of making or maintaining transparency from living transparent organisms, rather than focusing on fixed specimens, is a completely different approach. Therefore, the study of organismal transparency can lead to the development of new technologies for *in vivo* imaging of living tissues.

3 Ideal model for unravelling the mechanism of organismal transparency

Tunicates are marine invertebrate chordates and are most closely related to vertebrates. The salps, larvaceans, and some ascidian species are known to be highly transparent. They are classified into three classes: Ascidiacea, Thaliacea and Appendicularia. Some species of Ascidiacea are used as model organisms for the study of developmental biology. They have the following advantages as a model for unravelling the mechanism of organismal transparency.

3.1 Ease of comparative analysis of transparency

As mentioned earlier, the transparency of the egg is a significant factor that determines the subsequent transparency of the embryo. Therefore, ascidians, which facilitate the measurement and comparison of various egg transparencies (Figure 1F), provide an unparalleled simplest experimental system for organismal transparency.

Compared to tissues, organs, or individuals that have different and complex shapes across species, ascidian eggs are simply spherical thus normalizing the effects of differences in thickness and surface structure on transparency (Shito et al., 2020). This in turn facilitates comparative analysis of organism transparency between different species.

Furthermore, both eggs and ascidian cleavage patterns are conserved across species (Dumollard et al., 2017), and thus differences in transparency between internal scattering in the cytoplasm and external scattering at cell boundaries can be easily distinguished at homologous locations at the cellular level for comparative analysis between species (Figure 2E).

3.2 The Ascidiidae family is an ideal experimental resource

The Ascidiidae family showed high eggs transparency (*Ascidiella aspersa*: 88.7% and *Ascidia zara*: 50.7% (Shito et al., 2020)) including *Phallusia mammillata*, *Phallusia nigra*, and *Ascidia ahodori* (Sardet et al., 2011; Yasuo and McDougall, 2018). The Ascidiidae family is thought to have branched off from ascidians, which have a wide variety of transparency (Figure 1F; ranging from 10% to 90%) (Shito et al., 2020). The Ascidiidae family provides an ideal resource for exploring common genetic alterations within the family during the evolution of transparency (e.g., genetic mutations that suppress pigmentation, the mutations in structural proteins such as α-crystallin and water-rich proteoglycans, and mutations in genes involved in the synthesis of ECM at cell-cell boundaries that may suppress light scattering). Thus, a cohort of the Ascidiidae family is an ideal experimental resource to identify the genetic factors underlying the previously enigmatic evolution of transparency in aquatic organisms.

3.3 Convenience of molecular verification experiments

Family Ascidiidae has five genera (*Ascidia, Ascidiella, Fimbrora, Phallusia, Psammascidia*) and is distributed worldwide in seas with various temperatures. The ANISEED database has genome and gene annotations of 11 ascidians containing two Ascidiid species (*Phallusia mammillata* and *Phallusia fumigata*) (Dardaillon et al., 2020). *Phallusia mammillata* is known for its transparent eggs and is used in live imaging studies (Yasuo and McDougall, 2018). Genome sequence of *Ascidia mentula* was recently published (Bishop et al., 2023). *Ascidiella aspersa* is distributed worldwide and has well-defined developmental stages that facilitates gene transfer experiments (Funakoshi et al., 2021). Genome sequencing of *A. apersa* from different habitats including in Japan and Europe are underway. *Ciona* species are already used as model organisms for developmental biology. The abundance of genome data including those from Ascidiidae as well as opaque species (De Thier et al., 2024) allow for genome-wide comparative analysis of gene models and further validation experiments through functional analysis of candidate genes. In this way, ascidians provide a useful environment for elucidating the molecular mechanisms of organismal transparency.

4 Conclusion

Organismal transparency needs to be analyzed by at least separating internal and external scattering. Furthermore, by incorporating the perspectives of development and evolution, we have derived the view that maternal proteins during oogenesis in internal scattering. There is also an unknown mechanism that makes cell boundaries transparent during cleavage in external scattering. Both are important for the organismal transparency of early Ascidiidae embryos.

Future work should study maternally conserved proteins through proteomics and should study the ultrastructure of cell boundaries by electron microscopy or Raman microscopy. This in turn will lead to the discovery of new OCAs that are evolutionarily conserved among Ascidiidae.

Research into the mechanism of organismal transparency is becoming increasingly important and gives rise to the interdisciplinary field of "organismal transparency biology." This is a challenge, and the scientific community should tackle this challenge together.

Data availability statement

The original contributions presented in the study are included in the article/Supplementary Material. Further inquiries can be directed to the corresponding author.

Ethics statement

The manuscript presents research on animals that do not require ethical approval for their study.

Author contributions

KH: Conceptualization, Funding acquisition, Methodology, Project administration, Resources, Supervision, Visualization, Writing – original draft, Writing – review & editing. SM: Data curation, Formal analysis, Investigation, Visualization, Writing – review & editing. KO: Supervision, Writing – review & editing. TS: Data curation, Formal analysis, Funding acquisition, Investigation,

Methodology, Resources, Software, Validation, Visualization, Writing – review & editing.

Funding

The author(s) declare financial support was received for the research, authorship, and/or publication of this article. This study was supported in part by JSPS KAKENHI (21H00440, 23H04717, 24K02038), Keio University Research and Education Centre for Natural Sciences Budget, and KLL Keio Leading Program to KH. The Research Institute of Marine Invertebrates (IKU2021-02) supported TS. The Keio University Doctorate Student Grant-in-Aid Program from Ushioda Memorial Fund supported TS. JSPS KAKENHI Grant Number JP 22J22628 supported TS.

Acknowledgments

Dr. Minoru Ikeda and Captain Toyokazu Hiratsuka (Onagawa Field Center of Tohoku University), Dr. Makoto Kanamori, Dr. Masafumi Natsuike, and Takuya Mizukami (Hokkaido Research Organization, Hakodate Fisheries Research Institute), Dr. Gaku Kumano (Graduate School of Life Sciences, Tohoku University), Mr. Akio Takiya, Dr. Tatsunari Mori, Dr. Takaaki Kayaba, and Dr. Motohito Yamaguchi (Hokkaido Research Organization, Central Fisheries Research Institute) for their help in collecting the samples. We thank Yuki S. Kogure for giving us critical comments for preparing this manuscript. We thank Haruka Miyama Funakoshi and Shimon Kawai for handling *A. aspersa*. EBA JAPAN (Tokyo, Japan) provided a custom model hyperspectral camera (NH-KO) for our study. The *Ciona* individuals were provided by Dr. Yutaka Satou (Kyoto University), Dr. Manabu Yoshida (The University of Tokyo) and Dr. Yasunori Sasakura (University of Tsukuba) with support from the NBRP of AMED, Japan.

Conflict of interest

The authors declare that the research was conducted in the absence of any commercial or financial relationships that could be construed as a potential conflict of interest.

The author(s) declared that they were an editorial board member of Frontiers, at the time of submission. This had no impact on the peer review process and the final decision.

Publisher's note

Supplementary material

The Supplementary Material for this article can be found online at: https://www.frontiersin.org/articles/10.3389/fevo.2024.1428976/full#supplementary-material

SUPPLEMENTARY VIDEO 1
Timelapse movie of the early cleavage of *A. aspersa* from two-cell stage to 32-cell stage. The visibility of cell boundaries decreases at compaction after each cleavage event.

References

Bagge, L. E. (2019). Not as clear as it may appear: challenges associated with transparent camouflage in the ocean. *Integr. Comp. Biol.* 59, 1653–1663. doi: 10.1093/icb/icz066

Bagge, L. E., Kinsey, S. T., Gladman, J., and Johnsen, S. (2017). Transparent anemone shrimp (Ancylomenes pedersoni) become opaque after exercise and physiological stress in correlation with increased hemolymph perfusion. *J. Exp. Biol.* 220, 4225–4233. doi: 10.1242/jeb.162362

Bagge, L. E., Osborn, K. J., and Johnsen, S. (2016). Nanostructures and monolayers of spheres reduce surface reflections in Hyperiid amphipods. *Curr. Biol.* 26, 3071–3076. doi: 10.1016/j.cub.2016.09.033

Bhandiwad, A., and Johnsen, S. (2011). The effects of salinity and temperature on the transparency of the grass shrimp Palaemonetes pugio. *J. Exp. Biol.* 214, 709–716. doi: 10.1242/jeb.049296

Bishop, J., Wood, C., Marine Biological Association Genome Acquisition Lab, Darwin Tree of Life Barcoding collective, Wellcome Sanger Institute Tree of Life Management, Samples and Laboratory team and Wellcome Sanger Institute Scientific Operations: Sequencing Operations, et al. (2023). The genome sequence of a solitary sea squirt, Ascidia mentula (Müller 1776). *Wellcome Open Res.* 8, 583. doi: 10.12688/wellcomeopenres

Bishop, R. E., Torres, J. J., and Crabtree, R. E. (2000). Chemical composition and growth indices in leptocephalus larvae. *Mar. Biol.* 137, 205–214. doi: 10.1007/s002270000362

Borchman, D., and Yappert, M. C. (2010). Lipids and the ocular lens. *J. Lipid Res.* 51, 2473–2488. doi: 10.1194/jlr.R004119

Brennan, L., Costello, M. J., Hejtmancik, J. F., Menko, A. S., Riazuddin, S. A., Shiels, A., et al. (2023). Autophagy requirements for eye lens differentiation and transparency. *Cells* 12. doi: 10.3390/cells12030475

Dardaillon, J., Dauga, D., Simion, P., Faure, E., Onuma, T. A., DeBiasse, M. B., et al. (2020). ANISEED 2019: 4D exploration of genetic data for an extended range of tunicates. *Nucleic Acids Res.* 48, D668–D675. doi: 10.1093/nar/gkz955

De Thier, O., Tawfeeq, M. M., Faure, R., Lebel, M., Dru, P., Blanchoud, S., et al. (2024). First chromosome-level genome assembly of the colonial tunicate Botryllus schlosseri. *bioRxiv* 2024, 5.29.594498. doi: 10.1101/2024.05.29.594498

Dumollard, R., Minc, N., Salez, G., Aicha, S. B., Bekkouche, F., Hebras, C., et al. (2017). The invariant cleavage pattern displayed by ascidian embryos depends on spindle positioning along the cell's longest axis in the apical plane and relies on asynchronous cell divisions. *Elife* 6. doi: 10.7554/elife.19290

Funakoshi, H. M., Shito, T. T., Oka, K., and Hotta, K. (2021). Developmental table and three-dimensional embryological image resource of the ascidian Ascidiella aspersa. *Front. Cell Dev. Biol.* 9. doi: 10.3389/fcell.2021.789046

Goheen, S. C., Lis, L. J., and Kauffman, J. W. (1978). Raman spectroscopy of intact feline corneal collagen. *Biochim. Biophys. Acta* 536, 197–204. doi: 10.1016/0005-2795(78)90065-X

Gomez, D., Pinna, C., Pairraire, J., Arias, M., Barbut, J., Pomerantz, A., et al. (2021). Wing transparency in butterflies and moths: structural diversity, optical properties, and ecological relevance. *Ecol. Monogr.* 91. doi: 10.1002/ecm.1475

Hama, H., Hioki, H., Namiki, K., Hoshida, T., Kurokawa, H., Ishidate, F., et al. (2015). ScaleS: an optical clearing palette for biological imaging. *Nat. Neurosci.* 18, 1518–1529. doi: 10.1038/nn.4107

Hansson, L. A. (2000). Induced pigmentation in zooplankton: a trade-off between threats from predation and ultraviolet radiation. *Proc. Biol. Sci.* 267, 2327–2331. doi: 10.1098/rspb.2000.1287

Horwitz, J. (1992). Alpha-crystallin can function as a molecular chaperone. *Proc. Natl. Acad. Sci. U. S. A.* 89, 10449–10453. doi: 10.1073/pnas.89.21.10449

Inyushin, M., Meshalkina, D., Zueva, L., and Zayas-Santiago, A. (2019). Tissue transparency *in vivo*. *Molecules* 24. doi: 10.3390/molecules24132388

Johnsen, S. (2001). Hidden in plain sight: the ecology and physiology of organismal transparency. *Biol. Bull.* 201, 301–318. doi: 10.2307/1543609

Johnsen, S. (2003). Lifting the cloak of invisibility: the effects of changing optical conditions on pelagic crypsis1. *Integr. Comp. Biol.* 43, 580–590. doi: 10.1093/icb/43.4.580

Johnsen, S. (2014). Hide and seek in the open sea: pelagic camouflage and visual countermeasures. *Ann. Rev. Mar. Sci.* 6, 369–392. doi: 10.1146/annurev-marine-010213-135018

Johnsen, S., and Widder, E. A. (1999). The physical basis of transparency in biological tissue: ultrastructure and the minimization of light scattering. *J. Theor. Biol.* 199, 181–198. doi: 10.1006/jtbi.1999.0948

Kakiuchida, H., Sakai, D., Nishikawa, J., and Hirose, E. (2017). Measurement of refractive indices of tunicates' tunics: light reflection of the transparent integuments in an ascidian Rhopalaea sp. and a salp Thetys vagina. *Zoological Lett.* 3, 7. doi: 10.1186/s40851-017-0067-6

Kerker, M. (1969). *The scattering of light and other electromagnetic radiation* (Academic press). Available online at: https://www.abebooks.com/scattering-light-electromagnetic-radiation-Kerker-Milton/31404218033/bd (Accessed March 21, 2024).

Kingston, B. R., Syed, A. M., Ngai, J., Sindhwani, S., and Chan, W. C. W. (2019). Assessing micrometastases as a target for nanoparticles using 3D microscopy and machine learning. *Proc. Natl. Acad. Sci. U. S. A.* 116, 14937–14946.

Marina, O. C., Sanders, C. K., and Mourant, J. R. (2012). Correlating light scattering with internal cellular structures. *Biomed. Opt. Express* 3, 296–312. doi: 10.1364/BOE.3.000296

McFall-Ngai, M. J. (1990). Crypsis in the pelagic environment. *Am. Zool.* 30, 175–188. doi: 10.1093/icb/30.1.175

Miller, W. H., and Autrum, H. (1979). *Handbook of sensory physiology*, Vol. VII A 6. 69–143.New York: Springer.

Morishita, H., Eguchi, T., Tsukamoto, S., Sakamaki, Y., Takahashi, S., Saito, C., et al. (2021). Organelle degradation in the lens by PLAAT phospholipases. *Nature* 592, 634–638. doi: 10.1038/s41586-021-03439-w

Murakami, T. C., Mano, T., Saikawa, S., Horiguchi, S. A., Shigeta, D., Baba, K., et al. (2018). A three-dimensional single-cell-resolution whole-brain atlas using CUBIC-X expansion microscopy and tissue clearing. *Nat. Neurosci.* 21, 625–637. doi: 10.1038/s41593-018-0109-1

Nakamura, M. J., Hotta, K., and Oka, K. (2013). Raman spectroscopic imaging of the whole Ciona intestinalis embryo during development. *PloS One* 8, e71739. doi: 10.1371/journal.pone.0071739

Pettersen, R., Johnsen, G., Bruheim, P., and Andreassen, T. (2014). Development of hyperspectral imaging as a bio-optical taxonomic tool for pigmented marine organisms. *Org. Divers. Evol.* 14, 237–246. doi: 10.1007/s13127-013-0163-1

Pfeiler, E. (1984). Glycosaminoglycan breakdown during metamorphosis of larval bonefish albula. *Mar. Biol. Lett.* 5, 241–250.

Pfeiler, E., and Govoni, J. J. (1993). Metabolic rates in early life history stages of elopomorph fishes. *Biol. Bull.* 185, 277–283. doi: 10.2307/1542007

Pfeiler, E., Toyoda, H., Williams, M. D., and Nieman, R. A. (2002). Identification, structural analysis and function of hyaluronan in developing fish larvae (leptocephali). *Comp. Biochem. Physiol. B Biochem. Mol. Biol.* 132, 443–451. doi: 10.1016/S1096-4959(02)00060-X

Poole, J. J. A., and Mostaço-Guidolin, L. B. (2021). Optical microscopy and the extracellular matrix structure: A review. *Cells* 10. doi: 10.3390/cells10071760

Rao, P. V., Huang, Q. L., Horwitz, J., and Zigler, J. S. Jr (1995). Evidence that alpha-crystallin prevents non-specific protein aggregation in the intact eye lens. *Biochim. Biophys. Acta* 1245, 439–447. doi: 10.1016/0304-4165(95)00125-5

Ruud, J. T. (1954). Vertebrates without erythrocytes and blood pigment. *Nature* 173, 848–850. doi: 10.1038/173848a0

Sakai, T., Yamamoto, T., Watanabe, T., Hozumi, A., Shiraishi, A., Osugi, T., et al. (2023). Characterization of a novel species-specific 51-amino acid peptide, PEP51, as a caspase-3/7 activator in ovarian follicles of the ascidian, Ciona intestinalis Type A. *Front. Endocrinol.* 14, 1260600. doi: 10.3389/fendo.2023.1260600

Sardet, C., McDougall, A., Yasuo, H., Chenevert, J., Pruliere, G., Dumollard, R., et al. (2011). Embryological methods in ascidians: the Villefranche-sur-Mer protocols. *Methods Mol. Biol.* 770, 365–400. doi: 10.1007/978-1-61779-210-6_14

Satake, H., Kawada, T., Osugi, T., Sakai, T., Shiraishi, A., Yamamoto, T., et al. (2024). Ovarian follicle development in ascidians. *Zoolog. Sci.* 41, 60–67. doi: 10.2108/zs230054

Shito, T. T., Hasegawa, N., Oka, K., and Hotta, K. (2020). Phylogenetic comparison of egg transparency in ascidians by hyperspectral imaging. *Sci. Rep.* 10, 20829. doi: 10.1038/s41598-020-77585-y

Shito, T. T., Oka, K., and Hotta, K. (2023). Multimodal factor evaluation system for organismal transparency by hyperspectral imaging. *PloS One* 18, e0292524. doi: 10.1371/journal.pone.0292524

Surewicz, W. K., and Olesen, P. R. (1995). On the thermal stability of alpha-crystallin: a new insight from infrared spectroscopy. *Biochemistry* 34, 9655–9660. doi: 10.1021/bi00030a001

Taboada, C., Delia, J., Chen, M., Ma, C., Peng, X., Zhu, X., et al. (2022). Glassfrogs conceal blood in their liver to maintain transparency. *Science* 378, 1315–1320. doi: 10.1126/science.abl6620

Tarique, I., Lu, T., and Tariq, M. (2023). Cellular activity of autophagy and multivesicular bodies in lens fiber cells during early lens development in rbm24a mutant of zebrafish: Ultrastructure analysis. *Micron* 169, 103446. doi: 10.1016/j.micron.2023.103446

Tian, T., Yang, Z., and Li, X. (2021). Tissue clearing technique: Recent progress and biomedical applications. *J. Anat.* 238, 489–507. doi: 10.1111/joa.v238.2

Umezawa, M., Haruguchi, S., Fukushima, R., Sekiyama, S., Kamimura, M., and Soga, K. (2019). Rapid increase in transparency of biological organs by matching refractive index of medium to cell membrane using phosphoric acid. *RSC Adv.* 9, 15269–15276. doi: 10.1039/C9RA01445D

Velasco-Hogan, A., Deheyn, D. D., Koch, M., Nothdurft, B., Arzt, E., and Meyers, M. A. (2019). On the nature of the transparent teeth of the deep-sea dragonfish, Aristostomias scintillans. *Matter* 1, 235–249. doi: 10.1016/j.matt.2019.05.010

Wakamatsu, Y., Pristyazhnyuk, S., Kinoshita, M., Tanaka, M., and Ozato, K. (2001). The see-through medaka: a fish model that is transparent throughout life. *Proc. Natl. Acad. Sci. U. S. A.* 98, 10046–10050. doi: 10.1073/pnas.181204298

Warrant, E. J., and Locket, N. A. (2004). Vision in the deep sea. *Biol. Rev. Camb. Philos. Soc* 79, 671–712. doi: 10.1017/S1464793103006420

Wilson, S. J., and Hutley, M. C. (1982). The optical properties of "Moth eye" Antireflection surfaces. *Optica Acta: Int. J. Optics* 29, 993–1009. doi: 10.1080/713820946

Yasuo, H., and McDougall, A. (2018). Practical guide for ascidian microinjection: Phallusia mammillata. *Adv. Exp. Med. Biol.* 1029, 15–24. doi: 10.1007/978-981-10-7545-2_3

Zheng, H., and Rinaman, L. (2016). Simplified CLARITY for visualizing immunofluorescence labeling in the developing rat brain. *Brain Struct. Funct.* 221, 2375–2383. doi: 10.1007/s00429-015-1020-0

frontiers | Frontiers in Ecology and Evolution

TYPE Review
PUBLISHED 03 December 2024
DOI 10.3389/fevo.2024.1470671

OPEN ACCESS

EDITED BY
Lucia Manni,
University of Padua, Italy

REVIEWED BY
Nathalie Oulhen,
Brown University, United States
Ugo Coppola,
Florida Gulf Coast University, United States

*CORRESPONDENCE
Joel C. Glover
joel.glover@medisin.uio.no

RECEIVED 25 July 2024
ACCEPTED 12 November 2024
PUBLISHED 03 December 2024

CITATION
Glover JC, Tolstenkov O and Mikhaleva Y (2024) Calcium signaling in tunicate development.
Front. Ecol. Evol. 12:1470671.
doi: 10.3389/fevo.2024.1470671

Calcium signaling in tunicate development

Joel C. Glover[1,2]*, Oleg Tolstenkov[1] and Yana Mikhaleva[1]

[1]Michael Sars Centre, University of Bergen, Bergen, Norway, [2]Department of Molecular Medicine, Institute of Basic Medical Sciences, University of Oslo, Oslo, Norway

A comparative overview is provided of Ca2+ signaling and its potential mechanistic roles during development in tunicates. As background, the review presents an introduction to tunicate taxonomy, and then a general overview of Ca2+ signaling and methods for recording and measuring Ca2+ signals. It then covers the dynamics and implicated mechanisms of Ca2+ signals during different phases of development from oocyte to larva. These include signals arising in the unfertilized oocyte, signals associated with fertilization and meiosis, intercellular signals occurring from early cleavage stages through gastrulation, intercellular signals during organogenesis, and signals associated with early behavior. Comparisons are made among different tunicate species and where relevant to other chordate species. In many tunicate species, Ca2+ currents across the oocyte membrane are present prior to fertilization, and in the appendicularian *Oikopleura dioica* regular Ca2+ transients have been recorded optically prior to fertilization. Ca2+ signals at this stage have been implicated in pre-fertilization oocyte maturation events. The fertilization transient is the most well-studied Ca2+ signal and is triggered by factors from the sperm, including pivotally a phospholipase C (PLC) isoform that catalyzes the generation of IP3, which elicits release of Ca2+ from the endoplasmic reticulum. Post-fertilization signals are similarly dependent on IP3 signaling and are regulated by cyclin-dependent kinase 1 (Cdk1), and thereby linked to the meiotic divisions required for zygote formation. Ca2+ signals associated with early cleavages through gastrulation arise in blastomeres of the muscle lineage and spread from these in a coordinated fashion to other blastomeres through gap junctions. Post-gastrulation Ca2+ signals begin to show tissue-specificity in their temporal pattern as organogenesis proceeds, likely associated with loss of general gap junction transmission. Once neurulation has occurred, Ca2+ signals arise first in the nervous system and are transmitted synaptically to muscle, while Ca2+ signals arising spontaneously in the epidermis follow a separate temporal pattern. Species differences in the spatiotemporal characteristics of pre- and postgastrulation Ca+2 signals are discussed.

KEYWORDS

oocyte, blastula, gastrula, neurulation, *Oikopleura*, *Ciona*, ascidian, appendicularian

Introduction

Calcium signaling is a universal feature of animal development and influences many developmental processes starting from oocyte maturation and fertilization and extending through organogenesis and cell differentiation. It has been investigated extensively in several chordate species at various development stages (reviewed in Webb and Miller, 2003; Whitaker, 2008).

As the invertebrate chordate clade most closely related phylogenetically to vertebrates (Delsuc et al., 2006, 2008), and with a relatively small number of constituent cells, tunicates provide a favorable model for studies of calcium signaling during development (McDougall et al., 2012). Indeed, some of the early studies of calcium signaling during development were carried out in tunicates (Block and Moody, 1987; Bosma and Moody, 1990; Speksnijder et al., 1990; Dale et al., 1991; Coombs et al., 1992; Arnoult and Villaz, 1994). This review provides an overview of current knowledge about the developmental dynamics and function of calcium signaling in tunicates.

Tunicate diversity

Tunicates are highly diverse in morphology, ecology and behavior, and encompass both sessile and pelagic forms (reviewed in Holland, 2016). They are commonly categorized into three classes, the sessile Ascidiacea and the pelagic Thaliacea and Larvacea (the latter also termed Appendicularia), although more robust cladistic groupings based on large-scale genomic analyses are now recognized (Appendicularia, Stolidobranchia, and Thaliacea + Phlebobranchia + Aplousobranchia, with the Ascidiacea being paraphyletic; Delsuc et al., 2018). Pending a more thorough resolution of evolutionary relationships, we use here the traditional (but admittedly outdated) taxonomic designations to illustrate general variations in developmental features. In ascidian, appendicularian and some thaliacean species, early development generates a free-swimming larval stage that exhibits the typical chordate body plan with a motile tail (some thaliaceans also employ sexual reproduction or an asexual budding reproductive mode that lacks a free-swimming larval stage). In appendicularians, the larval body plan is maintained in the adult (hence the name Larvacea), which remains individually mobile throughout life. Thaliaceans generally form pelagic colonies of tail-less adults, whereas ascidian larvae metamorphose into sessile bottom-dwelling adults with a sac-like body plan. Of relevance to the Ca2+ signaling events to be presented below, model tunicate species across taxa exhibit invariant cell lineages, most have a well-developed notochord, and a muscular tail is the main mode of locomotion.

Sources of Ca2+ signals

Intracellular Ca2+ signals (reviewed in Clapham, 2007) derive from two sources: 1) influx through the cell membrane mediated by Ca2+ channels, driven by the large electrochemical gradient for Ca2+, and 2) release from intracellular Ca2+ stores, principally the endoplasmic/sarcoplasmic reticulum but extending to other compartments such as mitochondria and lysosomes (Figure 1). Cell membrane influx can be mediated by voltage-gated Ca2+ channels (VGCs), mechanosensitive cation channels (MCCs, which pass both Ca2+ and other cations), ligand-gated Ca2+

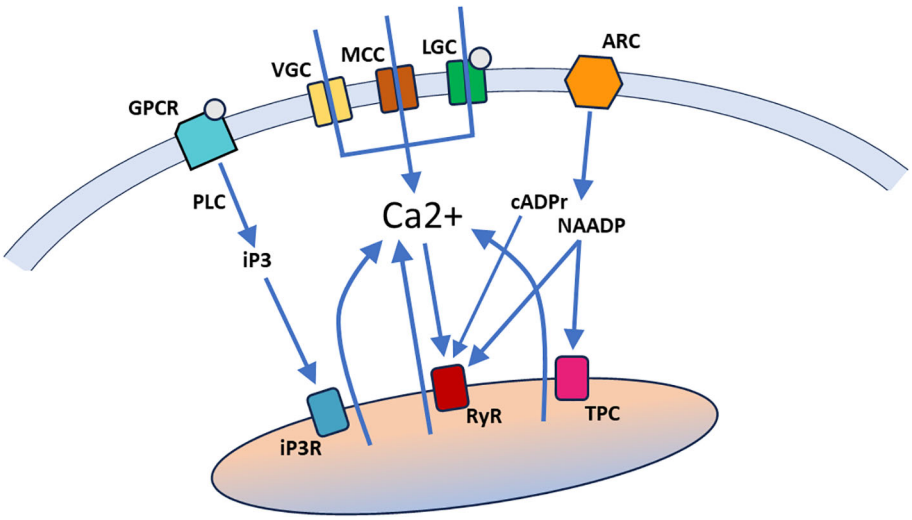

FIGURE 1
A general overview of Ca2+ signaling pathways. Ca2+ can enter the cell through ion channels in the cell membrane, including voltage-gated Ca2+ channels (VGC), mechanosensitive cation channels (MCC), and ligand-gated Ca2+ channels (LGC). Ca2+ can also be released from intracellular stores (indicated by a single organelle here that encompasses the various Ca2+ storing organelles), through binding of second messengers (iP3, cADPr, NAADP and Ca2+ itself) to specific receptors in the organelle membrane. Ligand binding by G-protein coupled receptors in the cell membrane (GPCR) activate phospholipase C (PLC) to generate iP3, which can bind to iP3 receptors (iP3R) in the endoplasmic/sarcoplasmic reticulum. Activation of ADP-ribosyl cyclases (ARC) in the cell membrane generates cADPr and NAADP, both of which bind to ryanodine receptors (RyR) in the endoplasmic/sarcoplasmic reticulum. NAADP also binds to two-pore channels (TPC) in acidic lysosomes.

channels (LGCs), and second messenger-activated Ca2+ channels, of which G-protein coupled receptors (GPCR) and calcium-activated Ca2+ channels are subcategories. Voltage-gated, mechanosensitive and ligand-gated Ca2+ channels have fast opening kinetics and generate inward Ca2+ currents of abrupt onset, variable duration (depending on the channel closing mechanisms) and localized action (since the Ca2+ concentration falls markedly within a few tens of nanometers from the inner surface of the cell membrane). Second messenger-activated Ca2+ channels are slower to open and close and typically generate more protracted Ca2+ signals.

Release from intracellular Ca2+ stores depends on second messenger systems and thus generates Ca2+ signals with a more gradual onset and relatively long durations. In addition, these signals can spread through a larger cytoplasmic volume due to the extent of the storage organelle(s) and the amplifying nature of the second messenger systems. The principal second messengers are inositol trisphosphate (IP3), generated by different isoforms of phospholipase C (PLC), cyclic ADP-ribose (cADPr) and nicotinic acid adenine dinucleotide phosphate (NAADP), generated by ADP-ribosyl cyclases (ARCs), and Ca2+ itself (Galione, 2019; Shah et al., 2022; Kim, 2022; Guse, 2023). To effect Ca2+ release, IP3 binds to IP3 receptors (IP3Rs) on the endoplasmic/sarcoplasmic reticulum, cADPr, NAADP and Ca2+ bind to ryanodine receptors (RYRs) on the endoplasmic/sarcoplasmic reticulum, and NAADP also binds to two-pore channels on acidic lysosomes (Figure 1). The full picture of regulated release from intracellular Ca2+ stores is more complex, but the general overview in Figure 1 provides sufficient context for the discussion of Ca2+ signal mechanisms in tunicate embryos below.

Methods for studying calcium signaling

Calcium signals involve the movement of Ca2+ ions across organelle and cell membranes by dint of calcium channels, pumps and antiporters, the diffusion of Ca2+ ions through gap junctions and over limited distances within the cytoplasm, and the binding of Ca2+ ions to specific calcium buffer and signaling proteins. Because Ca2+ is a universal intra- and intercellular signaling molecule, involved in a myriad of cell functions including cytoskeletal dynamics, cell adhesion, synaptic transmission and muscle contraction, its movement and distribution is highly regulated.

Methods for registering and measuring calcium signals take advantage of either the ionic charge of Ca2+ or the binding of Ca2+ to specific calcium-binding fluorophores or fluorescent proteins. In the former case, electrodes can be used to measure Ca2+ currents and/or resultant membrane potential changes with very high temporal resolution (limited by the electronics used, typically at sub-microsecond levels). A commonly used technique is patch clamp recording, which can measure Ca2+ currents through large populations of Ca2+ channels (as in whole cell recordings) and down to single channels (if only a single or a very few channels are opened or closed within the patch of membrane recorded from) (Cuomo et al., 2006; Gallo et al., 2013; Carvacho et al., 2018). Other types of electrode-based recording can also be used. For example, a vibrating probe system was developed to measure Ca2+ current densities across cell membranes (Jaffe and Nuccitelli, 1974), including associated with the activation current following fertilization of fish oocytes (Nuccitelli, 1987).

Calcium binding to calcium-sensitive fluorophores and fluorescent proteins has been utilized to transform Ca2+ signals into fluorescent signals that can be captured optically (Paredes et al., 2008; de Melo Reis et al., 2020). Calcium-sensitive fluorophores such as Fura-2, Fluo-4 and Calcium Green are organic molecules which, when photo-excited, emit fluorescence of specific wavelengths in a manner that is calcium-dependent. The kinetics of their response to changes in Ca2+ levels vary over a domain spanning milliseconds, limiting the temporal resolution obtainable relative to electrophysiological measurements, but still capable of discriminating signals such as broad calcium action potentials or protracted synaptic potentials. Most calcium-sensitive fluorophores (and fluorescent proteins, see below) only report relative changes in Ca2+ concentration. Fura-2 is an example of a calcium-sensitive fluorophore with a bimodal excitation spectrum, which permits ratiometric measurements that can be used to quantitate the concentration of Ca2+ ions at a given time point (Paredes et al., 2008).

Calcium-sensitive fluorescent proteins exist in nature and are intrinsically fluorescent or bioluminescent with an intensity that is dependent on Ca2+ concentration. Aequorin was the first such protein to be used for imaging Ca2+ signals, particularly in connection with the fertilization of oocytes (Ridgway et al., 1977; Steinhardt et al., 1977). More recently, genetic engineering has been used to create specially designed calcium-sensitive fluorescent proteins through combination of calcium-binding protein domains with an intrinsically fluorescent protein (Zhang et al., 2002). The advantage of engineered calcium-sensitive fluorescent proteins is that their expression can be genetically targeted to specific cell types. The GCaMP family of calcium-sensitive fluorescent proteins has become a particularly popular tool for imaging Ca2+ signals in a variety of organisms and cells (Kettunen, 2020; Shemesh et al., 2020) and encompasses variants of different sensitivities and kinetics. In particular, GCaMP has been used to assess Ca2+ signals during early embryogenesis in both vertebrates (Chen et al., 2017) and tunicates (Akahoshi et al., 2017; Mikhaleva et al., 2019; Tolstenkov et al., 2022). As is the case for calcium-sensitive fluorophores, calcium-sensitive fluorescent proteins have much slower kinetics than electrophysiological measurements but nevertheless can in many cases discriminate individual Ca2+ signals, especially when combined with temporal deconvolution methods (de Melo Reis et al., 2020).

Calcium signaling from oocyte to first cleavage

Pre-fertilization

Calcium is known to play an important role in oocyte maturation and the progression through meiotic arrest (Whitaker, 2008; Gallo et al., 2013). In line with this, Ca2+ currents and signals have been detected in ascidian and appendicularian oocytes prior to

fertilization (Block and Moody, 1987; Moody and Bosma, 1989; Bosma and Moody, 1990; Dale et al., 1991; Coombs et al., 1992; Arnoult and Villaz, 1994; Silvestre et al., 2009; Tosti et al., 2011; Gallo et al., 2013; Mikhaleva et al., 2019). All but the most recent of these studies employed electrophysiological measurements to demonstrate the presence in the oocyte membrane of either mechanosensitive non-selective cation channels (which pass Ca2+ in addition to Na+ and K+) or voltage-sensitive Ca2+ channels, as well as other voltage-sensitive monovalent cation channels. These studies characterized channel types and kinetics and showed that Ca2+ currents depended on extracellular Ca2+ but did not describe the developmental dynamics of pre-fertilization calcium signals. Mikhaleva et al. (2019) employed Fluo-4 or GCaMP6 to visualize these signals in unfertilized oocytes of the appendicularian *Oikopleura dioica* and showed that regularly repetitive Ca2+ transients occur at a frequency of about one every 2-3 minutes. The transients have a stereotypical double-peaked waveform consisting of a minor peak lasting about 3 sec followed after a delay of 10-15 sec by a 20-fold higher amplitude major peak lasting 8-10 sec. They are always initiated at a focal point near the inner surface of the oocyte and spread from there throughout the oocyte as a wave.

It is unclear what initiates these pre-fertilization signals in *Oikopleura*, in particular whether the trigger is intrinsic or extrinsic, such as mechanical or chemical stimulation associated with spawning. In this context it is of interest to compare how appendicularian and ascidian oocytes are obtained experimentally prior to calcium imaging. In *Oikopleura*, natural spawning in free-swimming adults involves wholescale rupture of the gonads, a traumatic and life-terminating event. In the lab this can be induced by mechanical agitation. In both cases, oocytes are violently released en masse, likely resulting in substantial mechanical stimulation, although some protection of the oocyte membrane is afforded by the chorion. By contrast, in ascidians, natural and laboratory-based spawning involves a gradual, enzyme-mediated release of individual follicles from the ovary of sessile adults (Matsubara et al., 2019), which likely has a much milder mechanical impact on the oocytes. Mikhaleva et al. (2019) discuss the possibility that mechanical stimulation of oocytes arising from induced spawning, impalement with the electrodes used to inject GCaMP6 mRNA or the dechorionation necessary to allow loading with Fluo-4 might be stimuli that initiate pre-fertilization signals in *Oikopleura*. Irrespective of how these signals are initiated in the experimental context, it is clear that they do not depend on fertilization and exhibit regular, clock-like dynamics and a stereotypical waveform that are not disrupted by the fertilization transient (although there may be a resetting of the clock; Figure 2; Mikhaleva et al., 2019).

Fertilization transient

Calcium plays a major role in polyspermy block at fertilization, by dint of the generation of a large, global Ca2+ transient that arises shortly after sperm contact, which initiates a chain of events that creates a barrier to penetration by later-arriving sperm. The fertilization transient is arguably the most studied Ca2+ signal in development and has been characterized in many invertebrate and vertebrate species (reviewed in Stricker, 1999; Nixon et al., 2000; Runft et al., 2002; Whitaker, 2006; Carvacho et al., 2018). In tunicates, the fertilization transient has been studied extensively in ascidians, including *Ciona robusta (Ciona intestinalis type A)*, *Ciona intestinalis (Ciona intestinalis type B)*, *Ciona savignyi*, *Ascidiella aspersa* and *Phallusia mamillata* (Hirano and

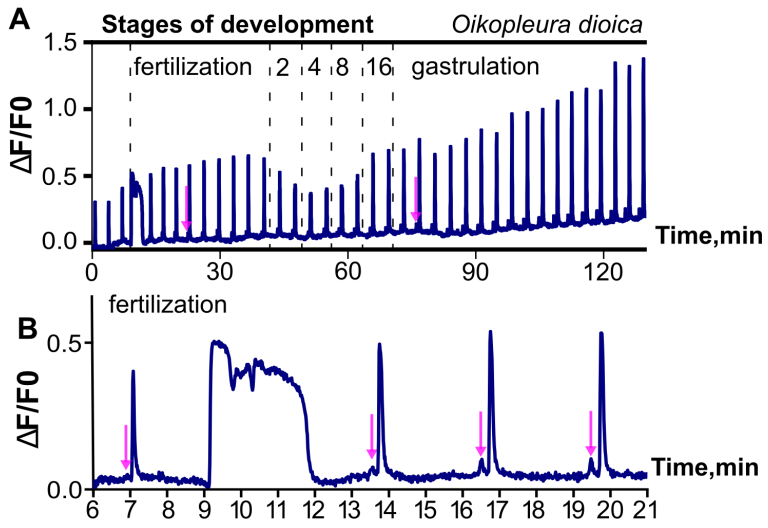

FIGURE 2
Illustration of ongoing, regular Ca2+ signals from pre-fertilization to gastrula stages of *Oikopleura dioica*. Ca2+ signals are represented as fractional changes of fluorescence (F) over a baseline (deltaF/F_0). **(A)** Note the highly regular, repetitive nature of the signals, which begin in the unfertilized oocyte and continue as coordinated intercellular signals as the embryo develops, interrupted only by the fertilization transient. **(B)** Higher magnification highlights the much longer time course of the fertilization transient, and the double-peak waveform of the regular calcium signals, which begin with a small "mini-peak" (indicated by arrows in both **A, B**) followed by a main peak. Modified from Mikhaleva et al. (2019).

Takahashi, 1984; Dale and DeFelice, 1984; Speksnijder et al., 1989; Brownlee and Dale, 1990; Speksnijder, 1992; Goudeau and Goudeau, 1993; Goudeau et al., 1994; Lambert et al., 1994; McDougall et al., 1995; Cuomo et al., 2006; Tosti et al., 2011; reviewed in Dumollard et al., 2004). It has the following general features conserved across tunicate species: 1) it is initiated at the site of sperm entry; 2) it involves multiple sources of Ca2+, including influx of extracellular Ca2+ through voltage-gated and potentially other types of Ca2+ channels in the oocyte membrane and a primary IP3-mediated release of Ca2+ from the endoplasmic reticulum triggered by sperm-derived factors introduced into the egg cytoplasm; 3) it lasts for about 3-5 min (reviewed in Dumollard et al., 2004; Whitaker, 2008). The rise of Ca2+ concentration during the fertilization transient is necessary for subsequent events that prevent polyspermy, such as the release of N-acetylglycosiminidase, which inactivates sperm receptors in the vitelline coat (Lambert et al., 1994; McDougall et al., 1995). In addition, ion depletion experiments show that an inward Na+ current contributes to the fertilization transient in *Ciona*, and that when Na+ is removed extracellularly the transient is diminished and development is defective (Tosti et al., 2011).

As in other species (both vertebrate and invertebrate), the fertilization transient in ascidians is triggered by the PLC-mediated generation of IP3 and binding of IP3 to IP3Rs on the endoplasmic reticulum (reviewed in Runft et al., 2002; Dumollard et al., 2004). In mouse and human, injection of the PLC zeta 1 isoform (PLCζ1), triggers the fertilization transient, and genetic knockout of PLCζ1 in mouse sperm prevents it (reviewed in Carvacho et al., 2018). It has been speculated that PLCζ1 is also the relevant sperm factor in tunicates (Dale et al., 2010), but this has not yet been confirmed. In ascidian oocytes, injection of IP3 is sufficient to initiate a fertilization transient, and specific blockade of PLC gamma (PLCγ) or Src protein tyrosine kinases prevents the fertilization transient, implicating these enzymes in the IP3 transduction signal (Runft and Jaffe, 2000). By contrast, inhibition of RyR does not prevent the fertilization transient (reviewed in Runft et al., 2002). Thus, the primacy of the IP3 pathway evidently is conserved in tunicates and non-tunicate species, although the PLC isoforms involved differ.

Post-fertilization signals prior to first cleavage

Most studies that have characterized the fertilization transient in tunicates note that it is followed by a series of highly regular Ca2+ signals during ensuing meiosis and cleavage (Figure 3, Speksnijder et al., 1989; Speksnijder, 1992; Mikhaleva et al., 2019: Matsuo et al., 2020). In the appendicularian *Oikopleura*, the regular post-fertilization signals are indistinguishable in frequency and waveform from the pre-fertilization signals (Figure 1; Mikhaleva et al., 2019). Moreover, in ascidians, the post-fertilization signals are similar to the pre- and post-fertilization signals in *Oikopleura* in that they are regular and have a much shorter time-course than the fertilization transient (reviewed in Dumollard et al., 2004). However, they appear to lack the doublet waveform seen in *Oikopleura* (Mikhaleva et al., 2019; an absence that may be artefactual depending on the temporal resolution of the Ca2+ recording used). The similarity of pre- and post-fertilization transients across tunicate classes suggests that they represent the same phenomenon and may occur independently of the fertilization transient rather than being necessarily triggered by it. Indeed, it is clear in *Oikopleura* that the fertilization transient arises on a background of regular signals that spans from pre- to post-

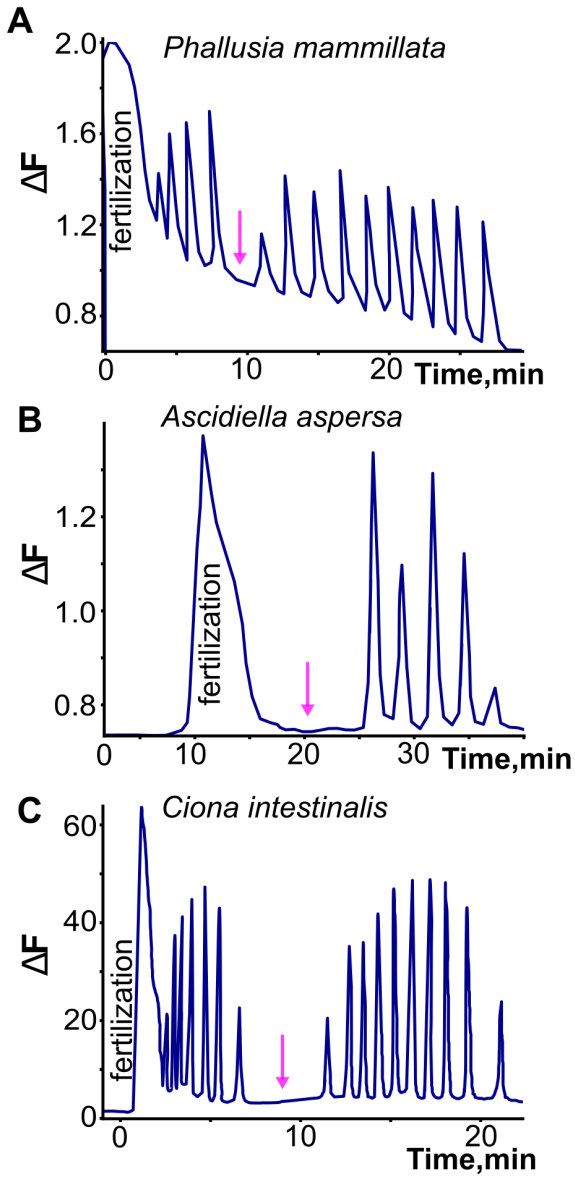

FIGURE 3
Illustration of the fertilization transient and subsequent post-fertilization signals in three ascidian species. Note the longer time course of the fertilization transient, and the regularity of the post-fertilization signals. In contrast to what has been observed in the appendicularian *Oikopleura dioica*, the post-fertilization signals are interrupted by a pause (indicated by arrows) to form two separate trains, related respectively to the two meiotic divisions that occur after the fertilization transient. Adapted and redrawn from Dumollard et al. (2004).

fertilization, and neither initiates these nor alters their character once it has occurred (Mikhaleva et al., 2019).

In ascidians, the post-fertilization signals have been discriminated into two different series separated by a pause, with different pacemakers, related respectively to the first and second meiotic divisions (reviewed extensively in Dumollard et al., 2004). They are reported to cease after the second meiotic division. These temporal features differ from the unabated continuation of the post-fertilization signals into subsequent cleavage stages in the appendicularian *Oikopleura* (Mikhaleva et al., 2019, see below). Whereas the first series of post-fertilization signals in ascidians originate like the fertilization transient from the sperm entry site, the second series shifts to a different origin, within the cortex of the vegetal contraction pole. This region is rich in mitochondria and contains the so-called myoplasm, where maternal determinants of muscle and endoderm are concentrated. Both origins contain endoplasmic reticulum that provide the source of Ca2+ released by IP3 (reviewed in Dumollard et al., 2004).

The molecular mechanisms underlying the post-fertilization signals that regulate meiosis have been studied extensively in ascidians (McDougall and Sardet, 1995; Albrieux et al., 1997, 1998; Albrieux and Villaz, 2000; Levasseur and McDougall, 2000; Wilding et al., 2000; Carroll et al., 2003; Levasseur et al., 2007, 2013; Lambert, 2011), less so in appendicularians (Matsuo et al., 2020). Pharmacological block of IP3Rs using the competitive inhibitor heparin prevents the post-fertilization signals, and UV-stimulated release of caged IP3 is sufficient to trigger similar series of signals and the associated meiotic divisions, with a single large UV pulse sufficient for the first series and additional pulses necessary for the second (McDougall and Sardet, 1995). Direct injection of IP3 through a patch pipette also elicits similar series of signals (Albrieux et al., 1997), whereas injection of NAADP can inhibit them, presumably through depletion of the NAADP-dependent Ca2+ store (Albrieux et al., 1998). Neither injection of ryanodine nor of cADPr elicits the series, corroborating the primacy of IP3 signaling underlying them (Albrieux et al., 1997). The durations of the series are correlated with and regulated by cyclin-dependent kinase 1 (Cdk1) activity, underscoring their tight relationship to the meiotic cell cycle, and possibly extending that relationship to mitotic divisions (McDougall and Levasseur, 1998; Levasseur and McDougall, 2000). Inhibiting Cdk1 eliminates the Ca2+ signals, but not the ability of IP3R agonists to elicit them (Levasseur et al., 2007). Evidently, Cdk1 promotes IP3 formation rather than acting directly on IP3R-mediated Ca2+ release.

The results of these mechanistic studies have in several instances informed similar studies in vertebrates. The study of Ca2+ signaling in tunicates have thus contributed significantly to the overall view of the role of calcium in the early embryo (reviewed in Whitaker, 2008).

Calcium signaling from first cleavage to gastrulation

Although post-fertilization Ca2+ signals have been reported to cease after the second meiosis in several studies of ascidians, Ca2+ is known to play a pivotal role in mitosis (reviewed in Nugues et al., 2022), and calcium signaling elements, including voltage-sensitive Ca2+ channels and ryanodine receptor-sensitive and IP3-sensitive internal release, have been demonstrated in 2-cell embryos of the ascidians *Boltenia villosa* and *Phallusia mammillata* (Coombs et al., 1992; Albrieux and Villaz, 2000). Oscillating Ca2+ currents carried by T-type Ca2+ channels in the cell membranes have been recorded during early cleavage stages of *Styela plicata*, and pharmacological blockade of these channels reduces the rate of cleavage and disrupts normal embryonic development (Gallo et al., 2013). As noted above, in the appendicularian *Oikopleura dioica* post-fertilization calcium signals continue throughout the mitotic divisions that generate the blastula and gastrula (Mikhaleva et al., 2019). These are not linked temporally to cleavages but follow rather the distinctly different clock already established prior to fertilization (once every 2-3 min, as opposed to mitotic cleavages occurring once every 13 min). They exhibit a stereotyped, sequential pattern related to stage and tissue lineage (Figure 4). At the 2-cell stage, a Ca2+ signal is first generated in one blastomere and then spreads to the other. The order is not obligatory, as the two blastomeres can switch in taking the lead. At the 4-cell stage, a Ca2+ signal is first generated in one blastomere before spreading into a neighboring blastomere (either a sister or a non-sister blastomere), before spreading from these into the other pair of blastomeres in sequence. At the 8-cell stage, Ca2+ signals arise in two of the posterior blastomeres and spread from these in a coordinated manner to the other blastomeres. By the 16-cell stage, this temporal pattern achieves a clear tissue type relationship, as the initiation is always in the blastomeres giving rise to the muscle cell lineage (Mikhaleva et al., 2019). This may be related to the shift in post-fertilization Ca2+ signal origin to the myoplasm of the uncleaved ascidian oocyte, suggesting a link between early Ca2+ signaling and body pattern that begins already when ooplasm is reorganized prior to the first cleavage. During subsequent divisions up to gastrulation, the muscle lineage-specific origin is maintained in *Oikopleura* (Mikhaleva et al., 2019). The muscle cell lineage is also where Ca2+ signals are initiated in gastrulae of *Ciona* (Akahoshi et al., 2017), is where a coupling of voltage-gated Ca2+ channels to ryanodine receptors has been characterized in *Halocynthia roretzi* (Nakajo et al., 1999) and is the specific site of voltage-gated Ca2+ currents recorded electrophysiologically after gastrulation in *Boltenia villosa* (Simoncini et al., 1988). Thus, the muscle cell lineage as the origin of whole-embryo Ca2+ signals through gastrulation appears to be a conserved feature in tunicates.

Contrasting with the description in *Oikopleura*, Ca2+ signals in gastrulae of *Ciona* were not reported to follow a patterned sequence, but rather to arise in separate, independent cells (Akahoshi et al., 2017). This is likely due to a lower temporal resolution in the *Ciona* study (0.5-1 frames/second, as opposed to 4 frames/second used by Mikhaleva et al., 2019).

Throughout development to gastrulation in *Oikopleura*, the regular, spontaneous Ca2+ signals exhibit the same waveform as first seen pre-fertilization, with a small "mini-peak" followed by a larger, main peak (Mikhaleva et al., 2019). Pharmacological blockade of Ca2+ channels (using divalent cations or the more specific T-type Ca2+ channel blocker mibefradil) has various effects on the amplitude and shape of the signals, and in the case of the divalent cations Cd2+ and Ni2+ disrupts the

10.3389/fevo.2024.1470671

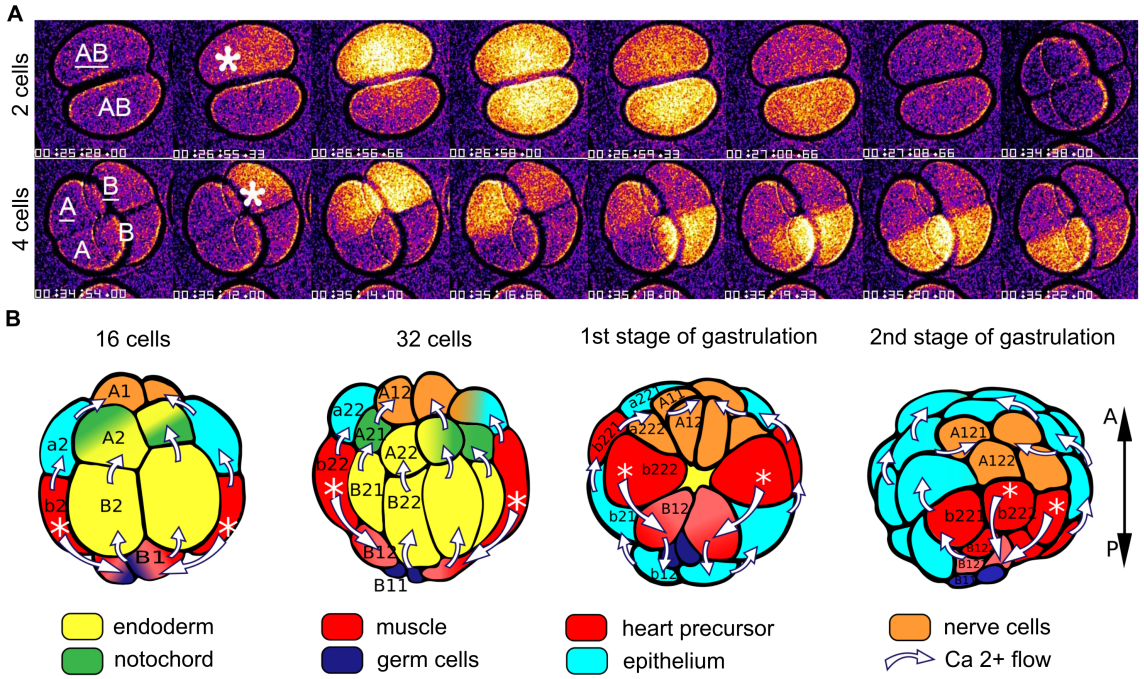

FIGURE 4
Illustration of intercellular Ca2+ signals in *Oikopleura dioica*. **(A)** Video recordings of Ca2+ signals in 2- and 4-cell embryos, showing the spread from the single blastomere of origin (indicated by asterisk) to the other blastromeres. **(B)** Diagrammatic representation of the intercellular spread of Ca2+ signals at later stages, oriented according to the anteroposterior (A-P) axis at the right. The white asterisks indicate the origin of the signals (in cells that give rise to the muscle cell lineage) and the white arrows indicate the trajectory of the signals among the cells. Tissue types are color coded as shown. Modified from Mikhaleva et al. (2019), Figures 2, 3.

coordinated progression of the Ca2+ signals among the blastomeres. Ca2+ channel blockade also leads to perturbed and arrested development, underscoring the importance of Ca2+ signaling in regulating early developmental processes. A similar effect of mibefradil has been reported in *Styela plicata*, in which it diminishes voltage gated Ca2+ currents recorded electrophysiologically, slows the cleavage rate and disrupts larval development (Gallo et al., 2013).

The stereotyped pattern of Ca2+ signal progression, always starting in cells of the muscle lineage and spreading from these throughout the embryo in a choreographed sequence, suggests a selective intercellular communication, and prompted Mikhaleva et al. (2019) to test whether gap junctional signaling is involved. This they did by knocking down the expression of the two (of 29 total) connexin genes that are expressed at early developmental stages in *Oikopleura*, Od-CxA and Od-CxB, through injection of inhibitory dsRNA into oocytes prior to fertilization. No effects were seen through the 32-cell stage, as prior to this the embryo is still supplied by maternally derived transcripts. But by gastrulation, Od-CxA and Od-CxB transcripts were diminished to 20-50% of normal levels. The effect was a severe disruption of Ca2+ signal progression from cell to cell, which was slowed by a factor of 10, and perturbed development (failure of ingression and epiboly at gastrulation, and later tail structure defects in embryos that succeeded to gastrulate). Thus, the patterned intercellular spread of Ca2+ signals depends on the presence of gap junctions, and its disruption is paralleled by abnormal development.

Calcium signaling post-gastrulation

The characteristics and functions of Ca2+ signaling at post-gastrulation stages are less well studied and understood than at earlier stages, particularly in a comparative context (reviewed in Slusarski and Pelegri, 2007; Webb et al., 2005). In vertebrates, Ca2+ transients have been shown to be associated with, and in some cases mechanistically linked to, convergent extension of the body axis (Créton et al., 2000; Prudent et al., 2013; Wallingford et al., 2001; Whitaker, 2006), the establishment of left-right asymmetry (Chuang et al., 2007; Kreiling et al., 2008; Onuma et al., 2020), neural induction and neurulation (Abdul-Wajid et al., 2015; Christodoulou and Skourides, 2015; Créton et al., 1998; Gilland et al., 1999; Leclerc et al., 2000; Moreau et al., 1994; Smedley and Stanisstreet, 1985), somitogenesis (Cheung et al., 2011; Webb et al., 2012; Webb and Miller, 2011) and muscle cell differentiation (Ferrari and Spitzer, 1999; Ohtsuka and Okamura, 2007; Webb et al., 2012).

Calcium signaling during neurulation

The role of Ca2+ signaling during the process of neurulation has been studied in *Ciona* (Abdul-Wajid et al., 2015; Hackley et al., 2013). Abdul-Wajid et al. (2015) have demonstrated a requirement for Ca2+ currents mediated by a T-type calcium channel (coded by the CAV3 gene) for proper closure of the anterior neural tube.

When expression of CAV3 is prevented by the *bugeye* mutation, the normal downregulation of the *ephrinA-d* gene at the end of neurulation is prevented. This disrupts EphrinA-EphA-mediated cell-cell interactions, which are pivotal for neural tube closure. Inhibition of EphrinA activity rescues the *bugeye* phenotype. Treatment of embryos with mibefradil phenocopies the *bugeye* mutation, supporting the importance of T-type Ca2+ channels in mediating *ephrinA-d* downregulation. Using morpholino-based knockdown of CAV3 homologues in *Xenopus laevis* embryos, Abdul-Wajid et al. (2015) showed that the dependence of anterior neural tube closure on T-type Ca2+ channel activity is conserved from tunicates to vertebrates.

Another mutation in *Ciona intestinalis*, *frimousse*, leads to abnormal specification of anterior neural plate cells, which adopt an epidermal rather than a neural fate. The *frimousse* mutation lies in a connexin gene (*cx11*) and abolishes Ca2+ signals in the anterior neural plate (Hackley et al., 2013). Pharmacological blockade of gap junctions and exposure to low-Ca2+ sea water phenocopy the mutation, underscoring the essential role of gap junction-mediated intercellular Ca2+ signals in core developmental processes.

Calcium signaling during general organogenesis

A complete assessment of the roles of Ca2+ during post-gastrulation development requires the recording of Ca2+ signals throughout the organism. Only a few studies have characterized whole-body Ca2+ signaling spanning extended periods of post-gastrulation development, and in only a few species (zebrafish: Créton et al., 1998; Gilland et al., 1999; Cheung et al., 2011; Webb et al., 2012; Tsuruwaka et al., 2017; *Xenopus*: Leclerc et al., 2000; *Ciona*: Abdul-Wajid et al., 2015; Akahoshi et al., 2017; *Oikopleura*: Tolstenkov et al., 2022).

Whole-embryo Ca2+ signals have been characterized in various tissues including the epidermis, palps, central nervous system, peripheral nervous system, muscle, heart, and notochord of *Ciona*, through expression of the genetically encoded Ca2+ indicator GCaMP (Abdul-Wajid et al., 2015; Akahoshi et al., 2017). At the early tailbud stage, oscillating Ca2+ signals have been observed at the midbrain-hindbrain boundary, in differentiating neuronal precursors in the neural plate and nerve cord, and in a rhythmic pattern in a small population of neurons in the visceral ganglion, an activity suggestive of the central pattern generator for swimming (Abdul-Wajid et al., 2015; Akahoshi et al., 2017). At the mid-tailbud stage, Ca2+ signals have been observed in epidermal cells and in posterior notochord cells. Starting at the late tailbud stage, frequent Ca2+ signals have been observed in the tail musculature during maturation of the muscle cells, corroborating an earlier study that showed that Ca2+ influx through voltage-gated Ca2+ channels was associated with muscle cell development (Ohtsuka and Okamura, 2007).

In *Oikopleura*, whole-embryo signals have been characterized using GCaMP6 expressed throughout the body (Tolstenkov et al., 2022). Initially, Ca2+ signals originate in the muscle cells and spread from these into other tissues (Figures 5, 6), continuing the situation through gastrulation in which Ca2+ signals originate from blastomeres of the muscle lineage and spread from these to other blastomeres. The similar spread of Ca2+ signals from differentiated muscle cells to other parts of the body is likely the result of gap junction-mediated coupling across tissue types, although this has not been tested directly by connexin gene knockdown as it has at pre-gastrulation and gastrulation stages (Tolstenkov et al., 2022; Mikhaleva et al., 2019). However, as organogenesis proceeds, Ca2+ signals begin to originate instead in the central nervous system and then spread from there to the muscle cells (Figures 5, 6). At the same time, Ca2+ signals in the epithelium are no longer temporally coupled with the signals in the CNS-muscle axis. Tolstenkov et al. (2022) have proposed that this transition from a muscle origin to separate origins in the CNS and epithelium involves the selective loss of general gap junction-mediated coupling across different tissue types, supplanted by more tissue-specific coupling, perhaps mediated by tissue-specific connexin expression. This hypothesis will require extensive investigation to test, since the number of connexin genes expressed increases as different tissues develop.

With respect to the CNS-muscle axis, the reversal of direction evidently relates to the development of neuromuscular synapse function. The transition is temporally linked to the developmental appearance of neuromuscular junctions (Søviknes et al., 2007), and the spread from CNS to muscle involves a much shorter temporal delay, consistent with neuromuscular synaptic transmission, and is prevented by pharmacological agents that block that transmission (Tolstenkov et al., 2022).

Calcium signals in the nervous system and relationship to early behavior patterns

In the neural plate of *Ciona*, Ca2+ signals appear in specific neural progenitor/neuronal precursor cells that evidently correspond to future motoneurons (MNs) and inhibitory interneurons (Akahoshi et al., 2017). Once the late tailbud stage is reached, repetitive Ca2+ signals appear in the visceral ganglion where MNs reside (Akahoshi et al., 2017), and Ca2+ signals also re-appear (after a period of quiescence at early tailbud stages) in the tail musculature. In *Oikopleura dioica*, the repetitive, neurally driven Ca2+ signals in the tail musculature are correlated with tail movements, and the signal in the muscle cells is protracted relative to the CNS signal, suggesting a link to excitation-contraction coupling, which lasts substantially longer than nerve impulse conduction and synaptic transmission. Tolstenkov et al. (2022) observed an interesting correlation between a given tail muscle contraction and the next initiating Ca2+ signal in the CNS: a new CNS signal arises shortly after and never before the cessation of the muscle signal and associated tail movement. A similar relationship has been observed in *Ciona* between Ca2+ signals recorded in a subpopulation of central neurons (GnRH+ neurons) and tail movements: a new signal in the neurons does

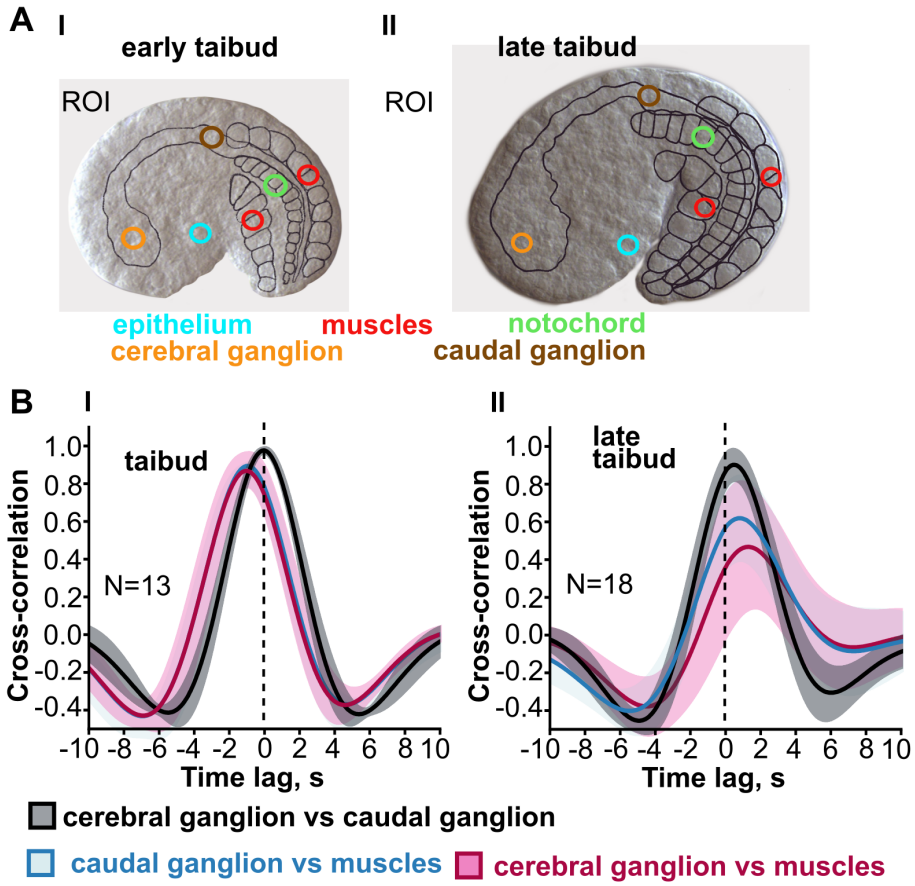

FIGURE 5
Transition from muscle lineage driven intercellular Ca2+ signals to neurally driven signals in *Oikopleura dioica*. **(A)** Signals were recorded from tissue-specific regions of interest (color coded in early and late tailbud embryos that express GCaMP6 throughout the body). **(B)** Cross-correlograms include (among others) the temporal relationship between signals in the cerebral ganglion and in muscle (maroon trace) and between signals in the caudal ganglion and muscle (blue trace). The time lag shift in these traces (in seconds, *s*) indicates that at the early tailbud stage Ca2+ signals in the tail muscle cells precedes that in either ganglion, whereas at the late tailbud stage the sequence is reversed. Modified from Tolstenkov et al. (2022), Figure 2.

not arise until the end of a tail movement (Okawa et al., 2020). This led Okawa et al. (2020) to postulate a sensory feedback loop that activates the central neurons once a tail movement is completed. An alternative explanation is that the cyclic nature of these phenomena is driven by an intrinsic clock that is independent of feedback signals. Of interest here is the observation by Tolstenkov et al. (2022) that the neurally driven Ca2+ signals have the same regularity as the earlier muscle-driven signals. One might expect that signals driven by sensory input would lose regularity and rather relate more to the vagaries of environmental conditions.

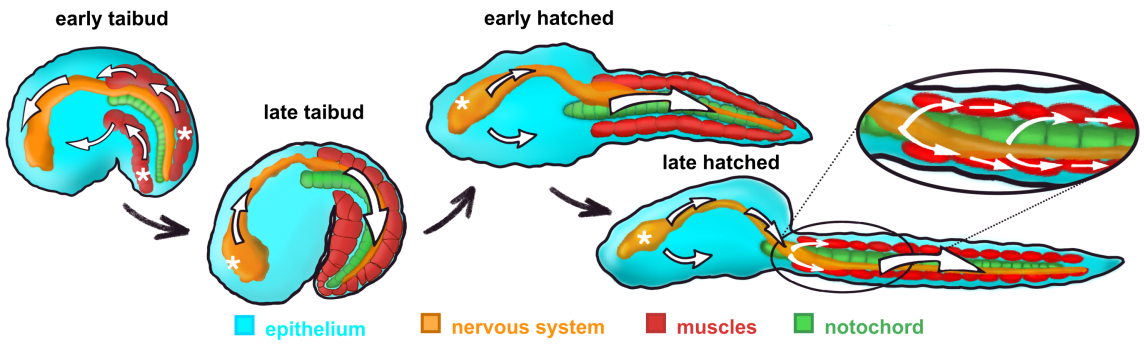

FIGURE 6
Diagrammatic illustration of the change in intercellular Ca2+ signal origin (white asterisks) and trajectory (white arrows) during post-gastrulation development in *Oikopleura dioica*. From Tolstenkov et al. (2022).

Calcium signals in the epidermis/epithelium

In both *Ciona* and *Oikopleura*, Ca2+ signals arise in the epidermis and epithelium, respectively, once these are established as definitive tissues (Akahoshi et al., 2017; Tolstenkov et al., 2022). Initially, signals in presumptive epidermis/epithelium are driven by the muscle lineage origin, but at about the time muscle signals begin to be driven by the CNS, the epidermal/epithelial signals begin to follow their own separate temporal pattern. At first haphazard, in separated individual cells, the signals eventually organize into a wave that typically starts in the head/trunk region and then travels caudally, often spreading into the notochord after reaching the tip of the tail. The function of these signals is unclear.

Conclusion

Calcium signaling in tunicates, as in other animal groups, plays a key role in a variety of developmental processes. From oocyte maturation to polyspermy block at fertilization, to the differentiation of specific cell types, in particular muscle cells, tunicates share calcium-dependent mechanisms that appear to be conserved throughout much of the chordate radiation. The evolutionary significance of other aspects of calcium signaling that have been characterized in tunicates deserves a more comprehensive assessment – both between different tunicate classes and between tunicates and vertebrates. Of note is the muscle lineage origin of whole embryo Ca2+ signals, clearly demonstrated in the appendicularian *Oikopleura dioica*, and its transition to neurally driven signals mediated by neuromuscular synaptic transmission. The role of gap junctions in coordinating the muscle lineage-driven whole embryo signals should be investigated in other tunicate species and compared to vertebrates. The same holds for the way this transitions to more tissue-specific signals, presumably through the regulation of tissue-specific connexin expression. The nature and underlying mechanisms of the pacemakers that drive Ca2+ signals, both in the single oocyte and in the multicellular embryo, need to be elucidated in more detail, again in a comparative context. As the embryo matures, the fate of the clock(s) that drive(s) intercellular Ca2+ signals needs to be determined, as the nervous system gains primacy in directing muscle activity, and other tissues and organs attain their specific functions. Of particular interest is the function of the primitive movements triggered by intrinsic waves of intercellular Ca2+ signals, as the forerunner of more complex, goal-directed movement repertoires that are engaged by sensory inputs. In all of these questions, tunicates – with their small larval size, low cell number, and rapid development - are well positioned to contribute insight into the developmental and evolutionary significance of calcium signaling in the chordate lineage.

Author contributions

JG: Writing – original draft, Writing – review & editing. OT: Writing – review & editing. YM: Writing – review & editing.

Funding

The author(s) declare financial support was received for the research, authorship, and/or publication of this article. Norwegian Research Council provided funding for salaries and research through grant number 234817.

Conflict of interest

The authors declare that the research was conducted in the absence of any commercial or financial relationships that could be construed as a potential conflict of interest.

Publisher's note

References

Abdul-Wajid, S., Morales-Diaz, H., Khairallah, S. M., and Smith, W. C. (2015). T-type calcium channel regulation of neural tube closure and EphrinA/EPHA expression. *Cell Rep.* 13, 829–839. doi: 10.1016/j.celrep.2015.09.035

Akahoshi, T., Hotta, K., and Oka, K. (2017). Characterization of calcium transients during early embryogenesis in ascidians Ciona robusta (Ciona intestinalis type A) and Ciona savignyi. *Dev. Biol.* 431, 205–214. doi: 10.1016/j.ydbio.2017.09.019

Albrieux, M., Lee, H. C., and Villaz, M. (1998). Calcium signaling by cyclic ADP-ribose, NAADP, and inositol trisphosphate are involved in distinct functions in ascidian oocytes. *J. Biol. Chem.* 273, 14566–14574. doi: 10.1074/jbc.273.23.14566

Albrieux, M., Sardet, C., and Villaz, M. (1997). The two intracellular Ca2+ release channels, ryanodine receptor and inositol 1,4,5-trisphosphate receptor, play different roles during fertilization in ascidians. *Dev. Biol.* 189, 174–185. doi: 10.1006/dbio.1997.8674

Albrieux, M., and Villaz, M. (2000). Bilateral asymmetry of the inositol trisphosphate-mediated calcium signaling in two-cell ascidian embryos. *Biol. Cell.* 92, 277–284. doi: 10.1016/S0248-4900(00)01066-2

Arnoult, C., and Villaz, M. (1994). Differential developmental fates of the two calcium currents in early embryos of the ascidian *Ciona intestinalis*. *J. Membr. Biol.* 137, 127–135. doi: 10.1007/BF00233482

Block, M. L., and Moody, W. J. (1987). Changes in sodium, calcium and potassium currents during early embryonic development of the ascidian Boltenia villosa. *J. Physiol.* 393, 619–634. doi: 10.1113/jphysiol.1987.sp016844

Bosma, M. M., and Moody, W. J. (1990). Macroscopic and single-channel studies of two Ca^{2+} channel types in oocytes of the ascidian *Ciona intestinalis*. *J. Membr Biol.* 114, 231–243. doi: 10.1007/BF01869217

Brownlee, C., and Dale, B. (1990). Temporal and spatial correlation of fertilization current, Ca2+ waves and cytoplasmic contraction in eggs of Ciona intestinalis. *Proc. R Soc. Lond B* 239, 321–328. doi: 10.1098/rspb.1990.0019

Carroll, M., Levasseur, M., Wood, C., Whitaker, M., Jones, K. T., and McDougall, A. (2003). Exploring the mechanism of action of the sperm-triggered calcium-wave pacemaker in ascidian zygotes. *J. Cell Sci.* 116, 4997–5004. doi: 10.1242/jcs.00846

Carvacho, I., Piesche, M., Maier, T. J., and Machaca, K. (2018). Ion channel function during oocyte maturation and fertilization. *Front Cell Dev. Biol.* 6, 63. doi: 10.3389/fcell.2018.00063

Chen, J., Xia, L., Bruchas, M. R., and Solnica-Krezel, L. (2017). Imaging early embryonic calcium activity with GCaMP6s transgenic zebrafish. *Dev. Biol.* 430, 385–396. doi: 10.1016/j.ydbio.2017.03.010

Cheung, C. Y., Webb, S. E., Love, D. R., and Miller, A. L. (2011). Visualization, characterization and modulation of calcium signaling during the development of slow muscle cells in intact zebrafish embryos. *Int. J. Dev. Biol.* 55, 153–174. doi: 10.1387/ijdb.103160cc

Christodoulou, N., and Skourides, P. A. A. (2015). Cell-autonomous Ca2+ flashes elicit pulsed contractions of an apical actin network to drive apical constriction during neural tube closure. *Cell Rep.* 13, 2189–2202. doi: 10.1016/j.celrep.2015.11.017

Chuang, C. F., VanHoven, M. K., Fetter, R. D., Verselis, V. K., and Bargmann, C. I. (2007). An innexin-dependent cell network establishes left-right neuronal asymmetry in C. elegans. *Cell* 129, 787–799. doi: 10.1016/j.cell.2007.02.052

Clapham, D. E. (2007). Calcium signaling. *Cell* 131, 1047–1058. doi: 10.1016/j.cell.2007.11.028

Coombs, J. L., Villaz, M., and Moody, W. J. (1992). Changes in voltage-dependent ion currents during meiosis and first mitosis in eggs of an ascidian. *Dev. Biol.* 153, 272–282. doi: 10.1016/0012-1606(92)90112-T

Créton, R., Kreiling, J. A., and Jaffe, L. F. (2000). Presence and roles of calcium gradients along the dorsal-ventral axis in Drosophila embryos. *Dev. Biol.* 217, 375–385. doi: 10.1006/dbio.1999.9542

Créton, R., Speksnijder, J. E., and Jaffe, L. F. (1998). Patterns of free calcium in zebrafish embryos. *J. Cell Sci.* 111, 1613–1622. doi: 10.1242/jcs.111.12.1613

Cuomo, A., Silvestre, F., De Santis, R., and Tosti, E. (2006). Ca2+ and Na+ current patterns during oocyte maturation, fertilization, and early developmental stages of *Ciona intestinalis*. *Mol. Reprod. Dev.* 73, 501–511. doi: 10.1002/mrd.20404

Dale, B., and DeFelice, L. J. (1984). Sperm-activated channels in ascidian oocytes. *Dev. Biol.* 101, 235–239. doi: 10.1016/0012-1606(84)90135-0

Dale, B., Talevi, R., and DeFelice, L. J. (1991). L- type Ca 2+ currents in ascidian eggs. *Exp. Cell Res.* 192, 302–306. doi: 10.1016/0014-4827(91)90190-6

Dale, B., Wilding, M., Coppola, G., and Tosti, E. (2010). How do spermatozoa activate oocytes? *Reprod. BioMed. Online.* 21, 1–3. doi: 10.1016/j.rbmo.2010.02.015

Delsuc, F., Brinkmann, H., Chourrout, D., and Philippe, H. (2006). Tunicates and not cephalochordates are the closest living relatives of vertebrates. *Nature* 439, 965–968. doi: 10.1038/nature04336

Delsuc, F., Philippe, H., Tsagkogeorga, G., Simion, P., Tilak, M. K., Turon, X., et al. (2018). A phylogenomic framework and timescale for comparative studies of tunicates. *BMC Biol.* 16, 39. doi: 10.1186/s12915-018-0499-2

Delsuc, F., Tsagkogeorga, G., Lartillot, N., and Philippe, H. (2008). Additional molecular support for the new chordate phylogeny. *Genesis* 46, 592–604. doi: 10.1002/dvg.v46:11

de Melo Reis, R. A., Freitas, H. R., and de Mello, F. G. (2020). Cell calcium imaging as a reliable method to study neuron–glial circuits. *Front. Neurosci.* 14, 569361. doi: 10.3389/fnins.2020.569361

Dumollard, R., McDougall, A., Rouvière, C., and Sardet, C. (2004). Fertilisation calcium signals in the ascidian egg. *Biol. Cell.* 96, 29–36. doi: 10.1016/j.biolcel.2003.11.002

Ferrari, M. B., and Spitzer, N. C. (1999). Calcium signaling in the developing *Xenopus* myotome. *Dev. Biol.* 213, 269–282. doi: 10.1006/dbio.1999.9387

Galione, A. (2019). NAADP receptors. *Cold Spring Harb. Perspect. Biol.* 11, a035071. doi: 10.1101/cshperspect.a035071

Gallo, A., Russo, G. L., and Tosti, E. (2013). T-type Ca2+ current activity during oocyte growth and maturation in the ascidian Styela plicata. *PLoS One* 8, e54604. doi: 10.1371/journal.pone.0054604

Gilland, E., Miller, A. L., Karplus, E., Baker, R., and Webb, S. E. (1999). Imaging of multicellular large-scale rhythmic calcium waves during zebrafish gastrulation. *Proc. Natl. Acad. Sci. U.S.A.* 96, 157–161. doi: 10.1073/pnas.96.1.157

Goudeau, H., Depresle, Y., Rosa, A., and Goudeau, M. (1994). Evidence by a voltage-clamp study of an electrically mediated block to polyspermy in the egg of the ascidian *Phallusia mammillata*. *Dev. Biol.* 166, 489–501. doi: 10.1006/dbio.1994.1332

Goudeau, M., and Goudeau, H. (1993). In the egg of the ascidian Phallusia mammillata, removal of external Ca2+ modifies the fertilization potential, induces polyspermy, and blocks the resumption of meiosis. *Dev. Biol.* 160, 165–177. doi: 10.1006/dbio.1993.1295

Guse, A. H. (2023). Enzymology of Ca2+-mobilizing second messengers derived from NAD: from NAD glycohydrolases to (Dual) NADPH oxidases. *Cells* 12, 675. doi: 10.3390/cells12040675

Hackley, C., Mulholland, E., Kim, G. J., Newman-Smith, E., and Smith, W. C. (2013). A transiently expressed connexin is essential for anterior neural plate development in Ciona intestinalis. *Development* 140, 147–155. doi: 10.1242/dev.084681

Hirano, T., and Takahashi, K. (1984). Comparison of properties of calcium channels between the differentiated 1 cell embryo and the egg cell of ascidians. *J. Physiol. (Lond)* 347, 301–325. doi: 10.1113/jphysiol.1984.sp015067

Holland, L. (2016). Tunicates. *Curr. Biol.* 26, R146–R152. doi: 10.1016/j.cub.2015.12.024

Jaffe, L. F., and Nuccitelli, R. (1974). An ultrasensitive vibrating probe for measuring steady extracellular currents. *J. Cell. Biol.* 63, 614–628. doi: 10.1083/jcb.63.2.614

Kettunen, P. (2020). Calcium imaging in the Zebrafish. *Adv. Exp. Med. Biol.* 1131, 901–942. doi: 10.1007/978-3-030-12457-1_36

Kim, U. H. (2022). Roles of cADPR and NAADP in pancreatic beta cell signaling. *Cell Calcium* 103, 102562. doi: 10.1016/j.ceca.2022.102562

Kreiling, J. A., Balantac, Z. L., Crawford, A. R., Ren, Y., Toure, J., Zchut, S., et al. (2008). Suppression of the endoplasmic reticulum calcium pump during zebrafish gastrulation affects left-right asymmetry of the heart and brain. *Mech. Dev.* 125, 396–410. doi: 10.1016/j.mod.2008.02.004

Lambert, C. C. (2011). Signaling pathways in ascidian oocyte maturation: the roles of cAMP/Epac, intracellular calcium levels, and calmodulin kinase in regulating GVBD. *Mol. Reprod. Dev.* 78, 726–733. doi: 10.1002/mrd.v78.10/11

Lambert, C. C., Gonzales, G. P., and Miller, K. M. (1994). Independent initiation of calcium dependent glycosidase release and cortical contractions during the activation of ascidian eggs: (Ascidian, Ryanodine, Thimerosal, Thapsigargin, N-acetylglucosaminidase). *Dev. Growth Differ* 36, 133–139. doi: 10.1111/j.1440-169X.1994.00133.x

Leclerc, C., Webb, S. E., Daguzan, C., Moreau, M., and Miller, A. L. (2000). Imaging patterns of calcium transients during neural induction in *Xenopus laevis* embryos. *J. Cell Sci.* 113, 3519–3529. doi: 10.1242/jcs.113.19.3519

Levasseur, M., Carroll, M., Jones, K. T., and McDougall, A. (2007). A novel mechanism controls the Ca2+ oscillations triggered by activation of ascidian eggs and has an absolute requirement for Cdk1 activity. *J. Cell Sci.* 120, 1763–1771. doi: 10.1242/jcs.003012

Levasseur, M., Dumollard, R., Chambon, J. P., Hebras, C., Sinclair, M., Whitaker, M., et al. (2013). Release from meiotic arrest in ascidian eggs requires the activity of two phosphatases but not CaMKII. *Development* 140, 4583–4593. doi: 10.1242/dev.096578

Levasseur, M., and McDougall, A. (2000). Sperm-induced calcium oscillations at fertilisation in ascidians are controlled by cyclin B1-dependent kinase activity. *Development* 127, 631–641. doi: 10.1242/dev.127.3.631

Matsubara, S., Shiraishi, A., Osugi, T., Kawada, T., and Satake, H. (2019). The regulation of oocyte maturation and ovulation in the closest sister group of vertebrates. *eLife* 8, e49062. doi: 10.7554/eLife.49062.035

Matsuo, M., Onuma, T. A., Omotezako, T., and Nishida, H. (2020). Protein phosphatase 2A is essential to maintain meiotic arrest, and to prevent Ca2+ burst at spawning and eventual parthenogenesis in the larvacean *Oikopleura dioica*. *Dev. Biol.* 460, 155–163. doi: 10.1016/j.ydbio.2019.12.005

McDougall, A., and Levasseur, M. (1998). Sperm-triggered calcium oscillations during meiosis in ascidian oocytes first pause, restart, then stop: correlations with cell cycle kinase activity. *Development* 125, 4451–4459. doi: 10.1242/dev.125.22.4451

McDougall, A., and Sardet, C. (1995). Function and characteristics of repetitive calcium waves associated with meiosis. *Curr. Biol.* 5, 318–328. doi: 10.1016/s0960-9822(95)00062-5

McDougall, A., Chenevert, J., and Dumollard, R. (2012). Cell-cycle control in oocytes and during early embryonic cleavage cycles in Ascidians. *Int. Rev. Cell Mol. Biol.* 297, 235–264. doi: 10.1016/B978-0-12-394308-8.00006-6

McDougall, A., Sardet, C., and Lambert, C. C. (1995). Different calcium-dependent pathways control fertilisation-triggered glycoside release and the cortical contraction in ascidian eggs is followed by regular bursts whose initiation relocates to a focal point within the ER. *Zygote* 3, 251–258. doi: 10.1017/S0967199400002641

Mikhaleva, Y., Tolstenkov, O., and Glover, J. C. (2019). Gap junction-dependent coordination of intercellular calcium signalling in the developing appendicularian tunicate *Oikopleura dioica*. *Dev. Biol.* 450, 9–22. doi: 10.1016/j.ydbio.2019.03.006

Moody, W. J., and Bosma, M. M. (1989). A nonselective cation channel activated by membrane deformation in oocytes of the ascidian *Boltenia villosa*. *J. Membr. Biol.* 107, 179–188. doi: 10.1007/BF01871723

Moreau, M., Leclerc, C., Gualandris-Parisot, L., and Duprat, A. M. (1994). Increased internal Ca2+ mediates neural induction in the amphibian embryo. *PNAS* 91, 12639–12643. doi: 10.1073/pnas.91.26.12639

Nakajo, K., Chen, L., and Okamura, Y. (1999). Cross-coupling between voltage-dependent Ca2+ channels and ryanodine receptors in developing ascidian muscle blastomeres. *J. Physiol.* 515, 695–710. doi: 10.1111/j.1469-7793.1999.695ab.x

Nixon, V. L., McDougall, A., and Jones, K. T. (2000). Ca 2+ oscillations and the cell cycle at fertilisation of mammalian and ascidian eggs. *Biol. Cell* 92, 187–196. doi: 10.1016/S0248-4900(00)01068-6

Nuccitelli, R. (1987). The wave of activation current in the egg of the medaka fish. *Dev. Biol.* 122, 522–534. doi: 10.1016/0012-1606(87)90316-2

Nugues, C., Helassa, N., and Haynes, L. P. (2022). Mitosis, focus on calcium. *Front. Physiol.* 13, 951979. doi: 10.3389/fphys.2022.951979

Ohtsuka, Y., and Okamura, Y. (2007). Voltage-dependent calcium influx mediates maturation of myofibril arrangement in ascidian larval muscle. *Dev. Biol.* 301, 361–373. doi: 10.1016/j.ydbio.2006.08.013

Okawa, N., Shimai, K., Ohnishi, K., Ohkura, M., Nakai, J., Horie, T., et al. (2020). Cellular identity and Ca(2+) signaling activity of the non-reproductive GnRH system in the Ciona intestinalis type A (Ciona robusta) larva. *Sci Rep.* 10, 18590. doi: 10.1038/s41598-020-75344-7

Onuma, T. A., Hayashi, M., Gyoja, F., Kishi, K., Wang, K., and Nishida, H. (2020). A chordate species lacking Nodal utilizes calcium oscillation and Bmp for left–right patterning. *PNAS* 117, 4188–4198. doi: 10.1073/pnas.1916858117

Paredes, R. M., Etzler, J. C., Watts, L. T., Zheng, W., and Lechleiter, J. D. (2008). Chemical calcium indicators. *Methods* 46, 143–151. doi: 10.1016/j.ymeth.2008.09.025

Prudent, J., Popgeorgiev, N., Bonneau, B., Thibaut, J., Gadet, R., Lopez, J., et al. (2013). Bcl-wav and the mitochondrial calcium uniporter drive gastrula morphogenesis in zebrafish. *Nat. Commun.* 4, 2330. doi: 10.1038/ncomms3330

Ridgway, E. B., Gilkey, J. C., and Jaffe, L. F. (1977). Free calcium increases explosively in activating medaka eggs. *PNAS* 74, 623–627. doi: 10.1073/pnas.74.2.623

Runft, L. L., and Jaffe, L. A. (2000). Sperm extract injection into ascidian eggs signals Ca(2+) release by the same pathway as fertilization. *Development* 127, 3227–3236. doi: 10.1242/dev.127.15.3227

Runft, L. L., Jaffe, L. A., and Mehlmann, L. M. (2002). Egg activation at fertilization: where it all begins. *Dev. Biol.* 245, 237–254. doi: 10.1006/dbio.2002.0600

Shah, K. R., Guan, X., and Yan, J. (2022). Diversity of two-pore channels and the accessory NAADP receptors in intracellular Ca(2+) signaling. *Cell Calcium* 104, 102594. doi: 10.1016/j.ceca.2022.102594

Shemesh, O. A., Linghu, C., Piatkevich, K. D., Goodwin, D., Celiker, O. T., Gritton, H. J., et al. (2020). Precision calcium imaging of dense neural populations via a cell-body-targeted calcium indicator. *Neuron* 107, 470–486.e11. doi: 10.1016/j.neuron.2020.05.029

Silvestre, F., Cuomo, A., and Tosti, E. (2009). Ion current activity and molecules modulating maturation and growth stages of ascidian (Ci*ona intestinalis*) oocytes. *Mol. Reprod. Dev.* 76, 1084–1093. doi: 10.1002/mrd.v76:11

Simoncini, L., Block, M. L., and Moody, W. J. (1988). Lineage-specific development of calcium currents during embryogenesis. *Science* 242, 1572–1575. doi: 10.1126/science.2849207

Slusarski, D. C., and Pelegri, F. (2007). Calcium signaling in vertebrate embryonic patterning and morphogenesis. *Dev. Biol.* 307, 1–13. doi: 10.1016/j.ydbio.2007.04.043

Smedley, M. J., and Stanisstreet, M. (1985). Calcium and neurulation in mammalian embryos. *J. Embryol. Exp. Morphol.* 89, 1–14. doi: 10.1242/dev.89.1.1

Søviknes, A. M., Chourrout, D., and Glover, J. C. (2007). Development of the caudal nerve cord, motoneurons, and muscle innervation in the appendicularian urochordate *Oikopleura dioica*. *J. Comp. Neurol.* 503, 224–243. doi: 10.1002/cne.v503:2

Speksnijder, J. E. (1992). The repetitive calcium waves in the fertilized ascidian egg are initiated near the vegetal pole by a cortical pacemaker. *Dev. Biol.* 153, 259–271. doi: 10.1016/0012-1606(92)90111-S

Speksnijder, J. E., Corson, D. W., Sardet, C., and Jaffe, L. F. (1989). Free calcium pulses following fertilization in the ascidian egg. *Dev. Biol.* 135, 182–190. doi: 10.1016/0012-1606(89)90168-1

Speksnijder, J. E., Sardet, C., and Jaffe, L. F. (1990). Periodic calcium waves cross ascidian eggs after fertilization. *Dev. Biol.* 142, 246–249. doi: 10.1016/0012-1606(90)90168-I

Steinhardt, R., Zucker, R., and Schatten, G. (1977). Intracellular calcium release at fertilization in the sea urchin egg. *Dev. Biol.* 58, 185–196. doi: 10.1016/0012-1606(77)90084-7

Stricker, S. A. (1999). Comparative biology of calcium signaling during fertilization and egg activation in animals. *Dev. Biol.* 211, 157–176. doi: 10.1006/dbio.1999.9340

Tolstenkov, O., Mikhaleva, Y., and Glover, J. C. (2022). Post-gastrulation transition from whole-body to tissue-specific intercellular calcium signaling in the appendicularian tunicate *Oikopleura dioica*. *Dev. Biol.* 492, 37–46. doi: 10.1016/j.ydbio.2022.09.004

Tosti, E., Gallo, A., and Silvestre, F. (2011). Ion currents involved in oocyte maturation, fertilization and early developmental stages of the ascidian *Ciona intestinalis*. *Mol. Reprod. Dev.* 78, 854–860. doi: 10.1002/mrd.v78.10/11

Tsuruwaka, Y., Shimada, E., Tsutsui, K., and Ogawa, T. (2017). Ca2+ dynamics in zebrafish morphogenesis. *PeerJ* 5, e2894. doi: 10.7717/peerj.2894

Wallingford, J. B., Ewald, A. J., Harland, R. M., and Fraser, S. E. (2001). Calcium signaling during convergent extension in *Xenopus*. *Curr. Biol.* 11, 652–661. doi: 10.1016/S0960-9822(01)00201-9

Webb, S. E., Cheung, C. C., Chan, C. M., Love, D. R., and Miller, A. L. (2012). Application of complementary luminescent and fluorescent imaging techniques to visualize nuclear and cytoplasmic Ca^{2+} signalling during the in *vivo* differentiation of slow muscle cells in zebrafish embryos under normal and dystrophic conditions. *Clin. Exp. Pharmacol. Physiol.* 39, 78–86. doi: 10.1111/j.1440-1681.2011.05582.x

Webb, S. E., and Miller, A. L. (2011). Visualization of Ca^{2}+ signaling during embryonic skeletal muscle formation in vertebrates. *Cold Spring Harb. Perspect. Biol.* 3, a004325. doi: 10.1101/cshperspect.a004325

Webb, S. E., and Miller, A. L. (2003). Calcium signalling during embryonic development. *Nat. Rev. Mol. Cell Biol.* 4, 539–551. doi: 10.1038/nrm1149

Webb, S. E., Moreau, M., Leclerc, C., and Miller, A. L. (2005). Calcium transients and neural induction in vertebrates. *Cell Calcium* 37, 375–385. doi: 10.1016/j.ceca.2005.01.005

Whitaker, M. (2006). Calcium at fertilization and in early development. *Physiol. Rev.* 86, 25–88. doi: 10.1152/physrev.00023.2005

Whitaker, M. (2008). Calcium signaling in early embryos. *Phil. Trans. R. Soc B* 363, 1401–1418. doi: 10.1098/rstb.2008.2259

Wilding, M., Marino, M., Monfrecola, V., and Dale, B. (2000). Meiosis-associated calcium waves in ascidian oocytes are correlated with the position of the male centrosome. *Zygote* 8, 285–293. doi: 10.1017/S0967199400001088

Zhang, J., Campbell, R. E., Ting, A. Y., and Tsien, R. Y. (2002). Creating new fluorescent probes for cell biology. *Nat. Rev. Mol. Cell. Biol.* 3, 906–918. doi: 10.1038/nrm976

Frontiers in
Ecology and Evolution

Ecological and evolutionary research into our natural and anthropogenic world

This multidisciplinary journal covers the spectrum of ecological and evolutionary inquiry. It provides insights into our natural and anthropogenic world, and how it can best be managed.

Discover the latest Research Topics

See more →

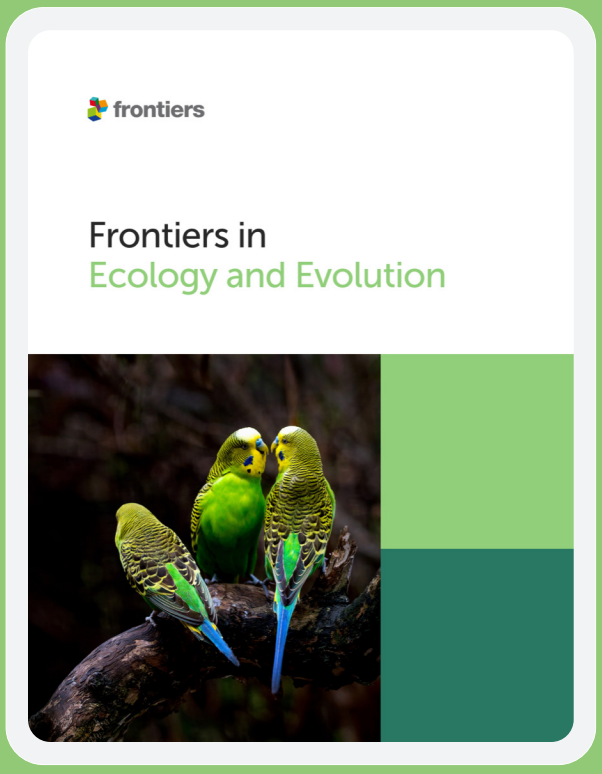

Frontiers

Avenue du Tribunal-Fédéral 34
1005 Lausanne, Switzerland
frontiersin.org

Contact us

+41 (0)21 510 17 00
frontiersin.org/about/contact